PRECISE SYNTHESIS OF SOFT MATERIALS WITH TUNABLE PROPERTIES VIA

POLYMERIZATIONS BASED ON STEREOSELECTIVE OLEFIN METATHESIS

A Dissertation

by

TING-WEI HSU

Submitted to the Graduate and Professional School of
Texas A&M University
in partial fulfillment of the requirements for the degree of

DOCTOR OF PHILOSOPHY

Chair of Committee,	Quentin Michaudel
Committee Members,	David C. Powers
	Lei Fang
	Jaime C. Grunlan
Head of Department,	Simon W. North

August 2023

Major Subject: Chemistry

ABSTRACT

Polymerizations based on olefin metathesis have enabled the synthesis of a large variety of olefin-containing polymers. While numerous studies have shown that the stereochemistry of the alkenes in the polymer backbone has a notable impact on the physical properties of the polymer, the synthesis of stereodefined polymers via olefin metathesis remains a great challenge. Most metathesis catalysts operate under thermodynamic control, which generally favor *E* (*trans*) linkages with the main chain connected on opposite sides of the alkenes. Therefore, the properties of polymers with high-*cis* content are comparatively underexplored due to a scarcity of synthetic methods to access these structures.

Within these polymers, poly(*p*-phenylene vinylene)s (PPVs), consisting of alternating phenylene and vinylene groups in conjugation, are of special interest. Indeed, the *cis*/*trans* configuration of the olefins in the PPV backbone significantly affect its physical properties including optical behavior and solubility. Interestingly, one-way photoisomerization can readily transform olefins in the PPVs backbone from the *cis* to the *trans* configuration, rendering PPVs light-responsive. In chapter II and III, we discuss a unique strategy to access all-*cis* PPVs with living characteristics capitalizing on the polymerization of paracyclophane diene monomers via stereoretentive ring-opening metathesis polymerization (ROMP). Investigation of the kinetics of the polymerization and its living characters is highlighted. Finally, applications to the synthesis of photoresponsive diblock copolymers is presented with an eye towards the construction of intricate, well-defined, and light-responsive polymeric architectures.

While stereoretentive ROMP is as a powerful tool to access *cis* polymer, the monomer scope is mostly limited to highly strained structures, such as norbornenes and paracyclophane dienes. Additionally, typical ROMP monomers, for example derived from norbornene or cyclooctene, lead to polymers that are challenging to degrade. To overcome these limitations, the development of stereoselective acyclic diene metathesis (ADMET) polymerizations using two families of stereoselective Ru catalysts to deliver a variety of *cis* polyalkenamers is presented in chapter IV and V. The influence of olefin geometry on the thermal and mechanical properties of the synthesized polymers was investigated through a variety of analytical techniques.

DEDICATION

Dedicated to my family for unconditionally supporting my dreams,

and to all my friends and teachers for their company.

ACKNOWLEDGEMENTS

CONTRIBUTORS AND FUNDING SOURCES

Contributors

This work was supervised by a dissertation committee consisting of my advisor Professor Quentin Michaudel, Professor David C. Powers and Professor Lei Fang of the Department of Chemistry, and Professor Jaime C. Grunlan of the Department of Mechanical Engineering.

In **Chapter II**, this work is described in an article that I co-authored with our previous post doc Cheoljae Kim and my advisor Quentin Michaudel.[1] Quentin and Cheoljae laid out the concept and goals of this research project. Cheoljae optimized the monomer synthesis of **1a–c** based on the literature and attempted some preliminary polymerizations. After his departure, I carried out the key stereoretentive polymerization which is the core of this paper. I solely completed the remaining part of this work. The manuscript was co-written by Quentin and me and the Supplementary Information by me.

In **Chapter III**, this work is described in an article that I co-authored with Samuel J. Kempel and my advisor Quentin Michaudel.[2] Quentin and I laid out the concept and goals of this research project, and then I synthesized the monomer and carried out polymerizations and photoisomerizations. Sam performed the measurements for the fluorescence quantum yields of all polymers. The manuscript was co-written by Quentin, Sam and me and the Supplementary Information by Sam and me.

In **Chapter IV**, this work is described in an article that I co-authored with Samuel J. Kempel, Alyssa P. Felix Thayne, and my advisor Quentin Michaudel.[3] Quentin, Sam, and I laid out the concept and goals of this research project, and then I developed the

polymerization set-up and procedure. I developed the synthesis of the aromatic ester, sulfite, and ether monomers, while Sam developed the synthesis of the carbonate monomer. Alyssa helped with the syntheses of monomers and polymerizations. Together, we carried out the polymerizations of all monomers and collected all the data. I optimized the hydrolysis procedure and determined the usage of NMR deconvolution to calculate *cis*/*trans* ratio. The manuscript was co-written by Quentin, Sam and me and the Supplementary Information by Sam and me.

In **Chapter V**, this work is described in an article that I co-authored with Samuel J. Kempel, Jake L. Nicholson, and my advisor Quentin Michaudel.[4] Quentin, Sam, and I laid out the concept and goals of this research project. Sam carried out the optimization of polymerization of carbonate monomer and synthesized unsaturated cyclometalated Ru catalyst (**Ru-4c**). Jake developed the synthesis of halogenated and alcohol monomers. I developed the synthesis of siloxane monomers and the purging method for volatile substrates. Sam, Jake and I cooperated to perform all the polymerizations and collected the thermograms results (TGA and DSC) together. I developed the synthesis of triblock copolymer and perform nanoindentation measurement. The manuscript was co-written by Quentin, Samuel, Jake, and me and the Supplementary Information by Samuel, Jake and me.

NOMENCLATURE

Ac	Acetyl
APCI	Atmospheric-pressure chemical ionization
C	Concentration
calc'd	Calculated (for mass spectrometry analysis)
C_6D_6	Deuterated benzene
$CDCl_3$	Deuterated chloroform
$CHCl_3$	Chloroform
CH_2Cl_2	Dichloromethane
Cy	Cyclohexyl
DCC	*N,N'*-Dicyclohexylcarbodiimide
DCM	Dichloromethane
DIPP	2,6-Diisopropylphenyl
DLS	Dynamic light scattering
DMAP	4-Dimethylaminopyridine
DMF	Dimethylformamide
DMSO	Dimethylsulfoxide
Đ	Dispersity
DP	Degree of polymerization
DSC	Differential scanning calorimetry
ESI	Electrospray ionization
Et	Ethyl

Et$_2$O	Ethyl ether
hν	Light
HRMS	High-resolution mass spectrometry
^{i}Pr	Isopropyl
IR	Infrared
k	Rate constant
L	Ligand
Me	Methyl
Mes	Mestyl
M_n	Number-average molar mass
M_w	Weight-average molar mass
n	Refractive index of the solvent
^{n}Bu	n-butyl
^{n}Hex	n-hexyl
NBS	N-Bromosuccinimide
NCS	N-Chlorosuccinimide
NHC	N-heterocyclic carbene
NMR	Nuclear magnetic resonance
OEH	2-ethylhexyloxy
Ph	Phenyl
PhMe	Toluene
ppm	Parts per million

PPV	Poly(phenylene vinylene)
rt	Room temperature
PPV	Poly(phenylene vinylene)
RPM	Revolutions per minute
SEC	Size exclusion chromatography
TCB	1,2,4-trichlorobenzene
Temp	Temperature
TGA	Thermogravimetric analysis
THF	Tetrahydrofuran
TLC	Thin-layer chromatography
T_c	Crystallization temperature
T_d	Decomposition temperature
T_m	Melting temperature
T_g	Glass transition temperature
Tf	Triflate
TMS	Trimethylsilyl
Ts	Tosyl
UV-vis	Ultraviolet-visible
Φ_{PL}	Fluorescence quantum yield
λ_{ex}	Excitation wavelength
δ	Chemical shift

TABLE OF CONTENTS

xvi

LIST OF FIGURES

xviii

LIST OF TABLES

CHAPTER I

INTRODUCTION

The spatial arrangement of repeating units in polymers strongly impacts their physical properties. Controlling tacticity and *cis/trans* configurations along the polymer chains is therefore crucial to embed soft materials with desirable properties.[5] However, this remains an unmet challenge for most families of polymers, which hampers the precise synthesis of well-defined polymers.

Tacticity refers to the regularity in the arrangement of the pendant groups in repeating units within a polymer chain, more precisely of adjacent chiral centers. The investigation of the influence of tacticity on polymer properties has been ongoing for decades. Polypropylene (PP), for example, exhibits distinct thermal and mechanical behaviors in its atactic (*a*PP) and isotactic (*i*PP) forms (Figure I-1).[6] *a*PP is a soft, amorphous, and rubbery material, while *i*PP is a hard thermoplastic with a high degree of crystallinity and a melt transition.[6] Similarly, polystyrene (PS), another widely-used plastic, showcases different properties based on its tacticity. *a*PS, the most common form
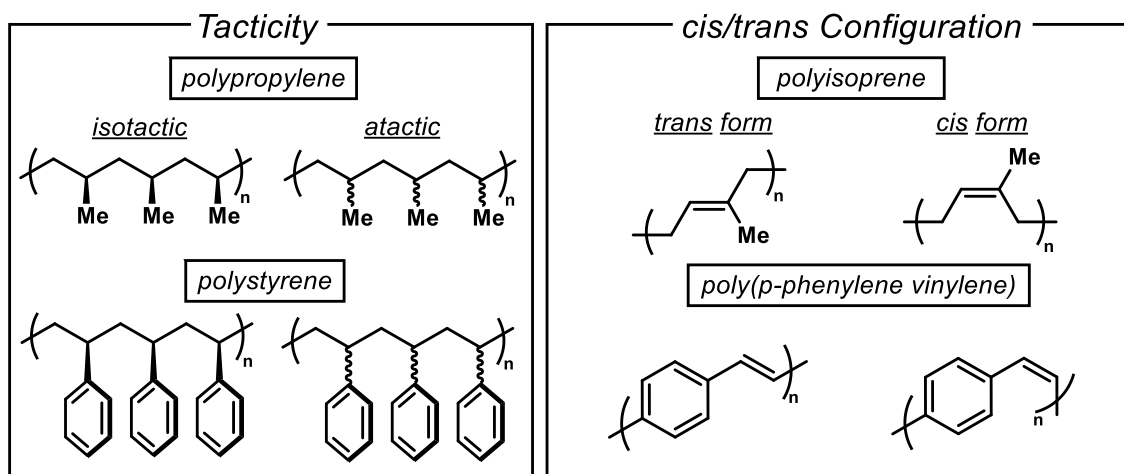
Figure I-1 Influence of stereochemistry on the properties of polymers.

1

produced commercially, is amorphous, but *i*PS showcases semi-crystalline characteristics.[7]

Likewise, the configuration of repeating olefin also considerably influences the properties of alkene-containing polymers. For example, *cis*-polyisoprene (natural rubber) exhibits a flexible texture and is used as an elastic material found in latex gloves,[8,9] while *trans*-polyisoprene (gutta-percha) is relatively stiff and was once used in the manufacturing of golf balls.[10] Extensive catalyst optimization has enabled access to all-*trans* and all-*cis* polyisoprene, and to polymers with compositions in between through coordination-insertion polymerization.[11] However, this method is mostly limited to 1,3-diene monomers and exhibits poor functional group tolerance. Therefore, the need for complementary methods that can control olefin configuration on various polymers is no longer negligible. Alkene-containing conjugated polymer is another notable example, such as poly(*p*-phenylene vinylene)s (PPVs), which have been found to exhibit significant differences in electronic, optical, and physical properties based on their *cis* and *trans* content.[12,13] Though the importance of alkene configuration is clearly apparent in these examples, synthetic methods that provide control over *cis*/*trans* stereochemistry within the polymer backbone remain scarce, and the impact of alkene orientation on polymer properties is understudied compared to that of tacticity. Polymerizations based on olefin metathesis are attractive to access alkene-containing polymers because of their tunability and robustness. However, such polymerization typically favors the formation of *E*-configurated alkenes through thermodynamic control. Indeed, the mechanism of olefin metathesis, first proposed by Chauvin,[14] entails a [2+2] cycloaddition between a metal

2

alkylidene and an alkene, followed by a retro [2+2] cycloaddition of the resulting

metallocyclobutane to generate a new carbon-carbon double bond. The reversibility of

these steps tends to favor the formation of the most stable product (typically the *E* (*trans*)

form), regardless of potential differences in the free-energy landscape for each pathway.

This phenomenon makes it arduous to synthesize high-*cis* polymers through conventional

olefin-metathesis polymerizations. To overcome this limitation of olefin metathesis,

several Mo-, W- and Ru-based olefin metathesis catalysts have been successfully

developed to achieve stereoselectivity through a kinetic pathway, which leads to products

with predictable *Z* (*cis*) or *E* (*trans*) configuration.[15] In particular, two families of Ru-

catalysts coined *Z*-selective (e.g. **Ru-4**) and stereoretentive (e.g. **Ru-5** and **Ru-6**), first

reported by Gubbs[16,17] and by Hoveyda[18-20] respectively, have exhibited great *cis*

selectivities toward olefin metathesis (Figure I-2).   Typical Ru-based catalysts bearing
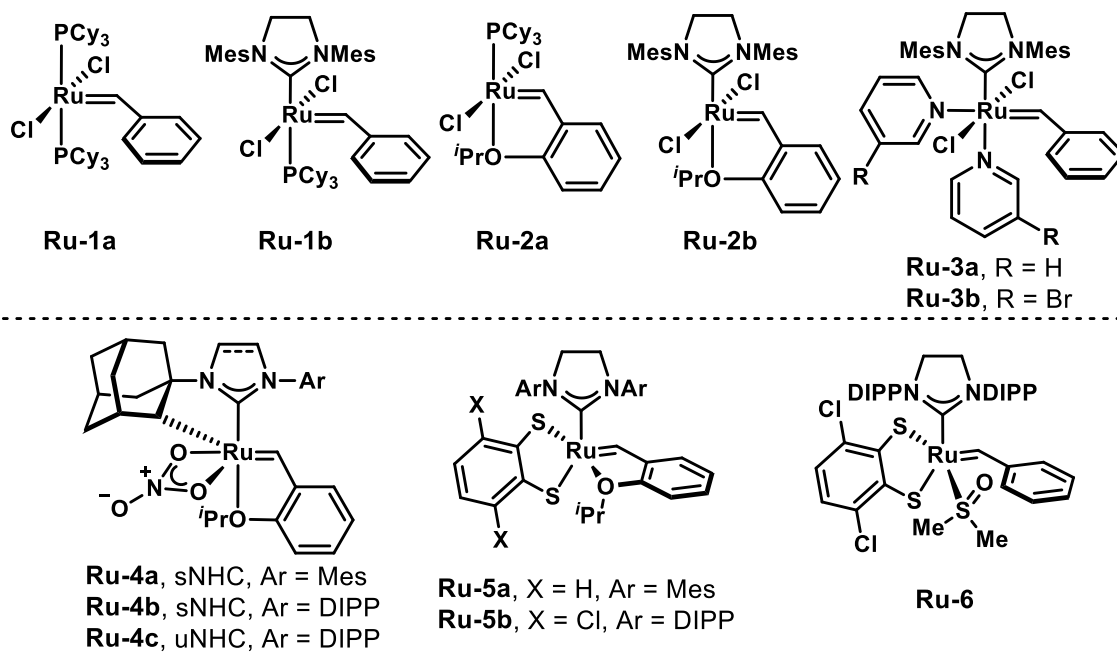
Figure I-2 Typical (**Ru-1**–**Ru-3**) and stereoselective (**Ru-4**–**Ru-6**) Ru-based catalyst.

two chloride ligands (**Ru-1–3**) favor *trans* products because of the formation of a metallocyclobutane on the opposite side of the metal center from the NHC ligand (bottom-bound pathway, intermediate **I**), where the R_1 and R_2 substituents are prone to have *anti* orientation that minimizes the dipole moment (Figure I-3). To favor the *cis* configuration, Grubbs[21] and Hoveyda,[22] respectively, shown that formation of intermediate **II** with the metallacyclobutane on the equatorial plane is essential since the presence of a bulky NHC ligand forces all the substituents away from it and favors *cis* selectivity. However, this scenario is unfavored with typical Grubbs catalysts because of the large dipole moment and significant electron repulsion between the halide anions. The replacement of the chloride with a bidentate ligand (see **III**, Figure I-3) favors this so-called side-bound
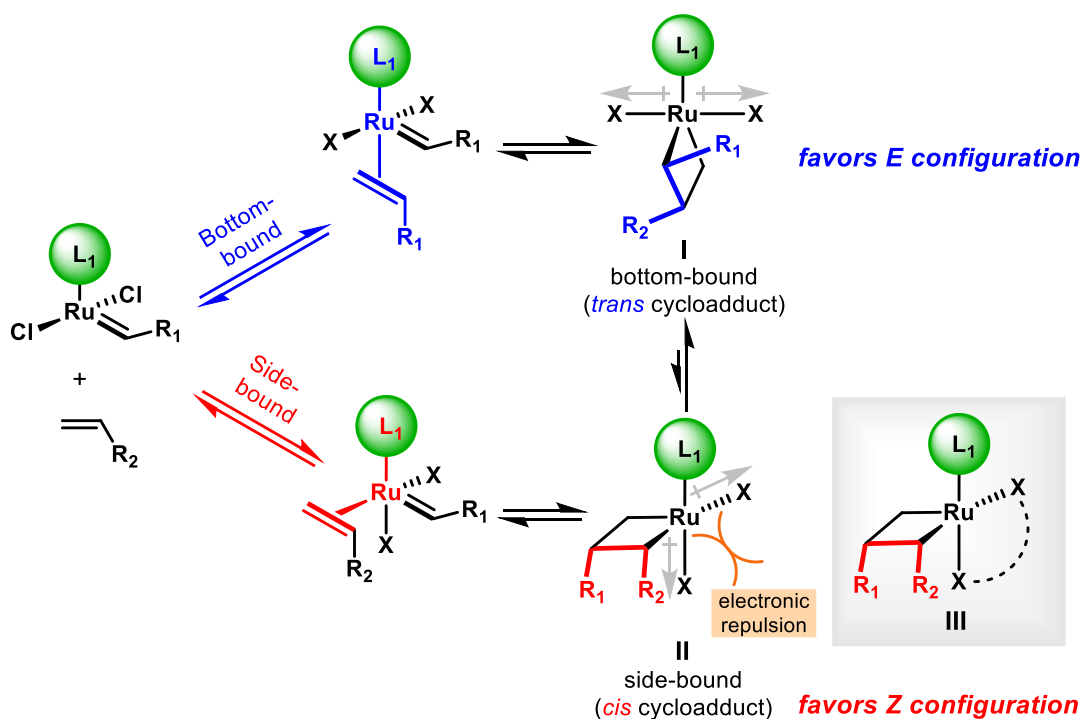
Figure I-3 Different olefin approach to the ruthenium alkylidene leading to diastereo-meric ruthenacyclobutanes.

mechanism, which delivers the desired *Z* configuration. Indeed, the experimental and computational results suggest that both of the cyclometalated structures (*Z*-selective)[21] and the dithiolate structure (stereoretentive)[23] are prone to undergo side-bound pathway rather than bottom-bound and deliver *cis* selectivity. While operating a similar mechanism, the *Z*-selective and stereoretentive catalysts have distinct characteristics. The former delivers the *Z* olefin irrespective of the stereochemistry of the starting olefin, while the latter retains the stereochemistry of the olefin throughout the olefin metathesis process (Figure I-4). In the case of the *Z*-selective catalyst, the steric hindrance of the substituents on the NHC ligand forces the metallacyclobutane substituents away from the NHC, favoring the *Z* pathway over the *E* pathway (Figure I-4, path 1).[21] Conversely, stereoretentive catalysts preserve the alkene configuration of the starting material during the metathesis process.
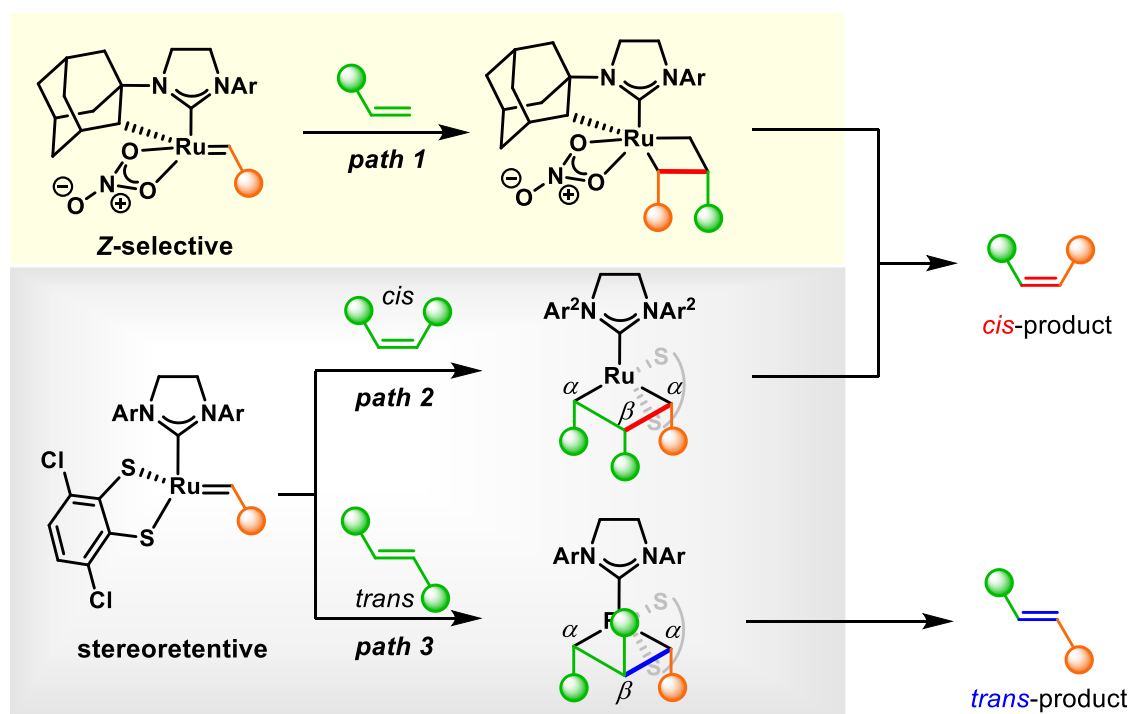
Figure I-4 *Z*-selective olefin metathesis (yellow box) versus stereoretentive olefin metathesis (grey box).

This retention is primarily attributed to the side-bound mechanism originated by the *cis*-chelating catechothiolate ligand and the different steric hindrance from the NHC to the two α positions of the metallocyclobutane and to the β position. This "open pocket" above β position is key to this stereoretention by allowing the substituents to point toward or away from the NHC. When a *cis* olefin reacts with stereoretentive catalyst, the resulting ruthenacycle is characterized by substituents pointing away from the NHC ligand (Figure I-4, path 2). In contrast, when the catalyst reacts with a *trans* alkene, the resulting metallocyclobutane intermediate exhibits one substituent positioned away from the NHC ligand at the α position due to steric hindrance from the NHC. The substituent at the β position, which is further from the NHC, is oriented toward this large ligand, leading to the formation of a *trans* product (Figure 2, path 3). This model, proposed by Pederson and Grubbs[22] and supported by computational studies by Houk and Liu[23], contributes to the understanding of the observed stereoretention.
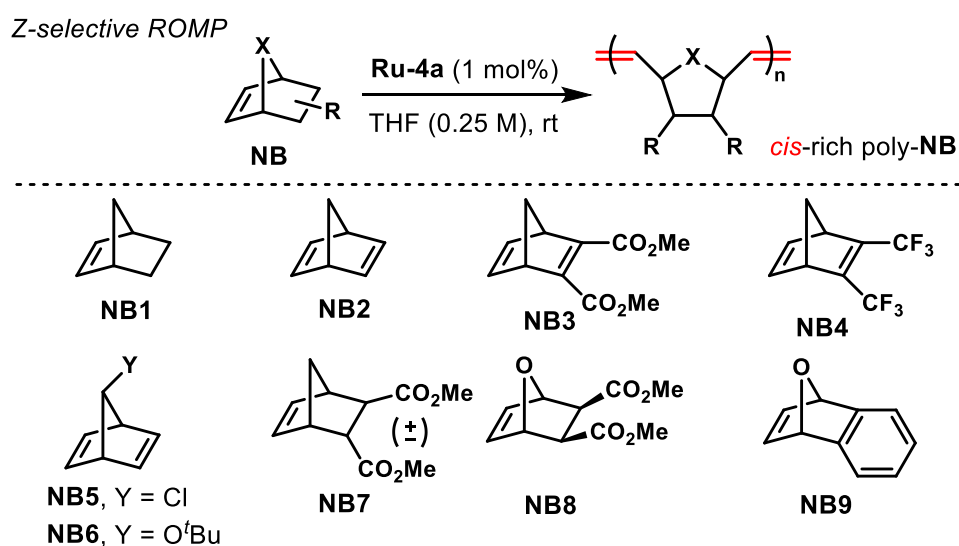
Figure I-5 Examples of *Z*-selective ROMP of norbornene derivatives using cyclometalated Ru catalysts (**Ru-4a**).

Despite early successes in the synthesis of small molecules with these catalysts, polymerizations capitalizing on these catalysts remain uncommon comparatively to those using typical Grubbs catalysts.[15] It has been shown to deliver good *cis* selectivity in the ROMP of norbornene derivatives using **Ru-4a** (Figure I-5a).[24] Hoveyda demonstrated stereoretentive ROMP of norbornene and cyclooctadiene to afford high- to all-*cis* polymers using a dithiolate Ru catalyst (**Ru-5a**) (Figure I-6).[18] The Choi group later disclosed a stereoretentive ROMP of norbornene and *endo*-tricyclo[4.2.2.02,5]deca-3,9-diene derivatives using **Ru-5b** to access *cis* polymers. They observed a better sheer resistance ability of *cis* polymer than that of *trans* one, demonstrating the dependence of
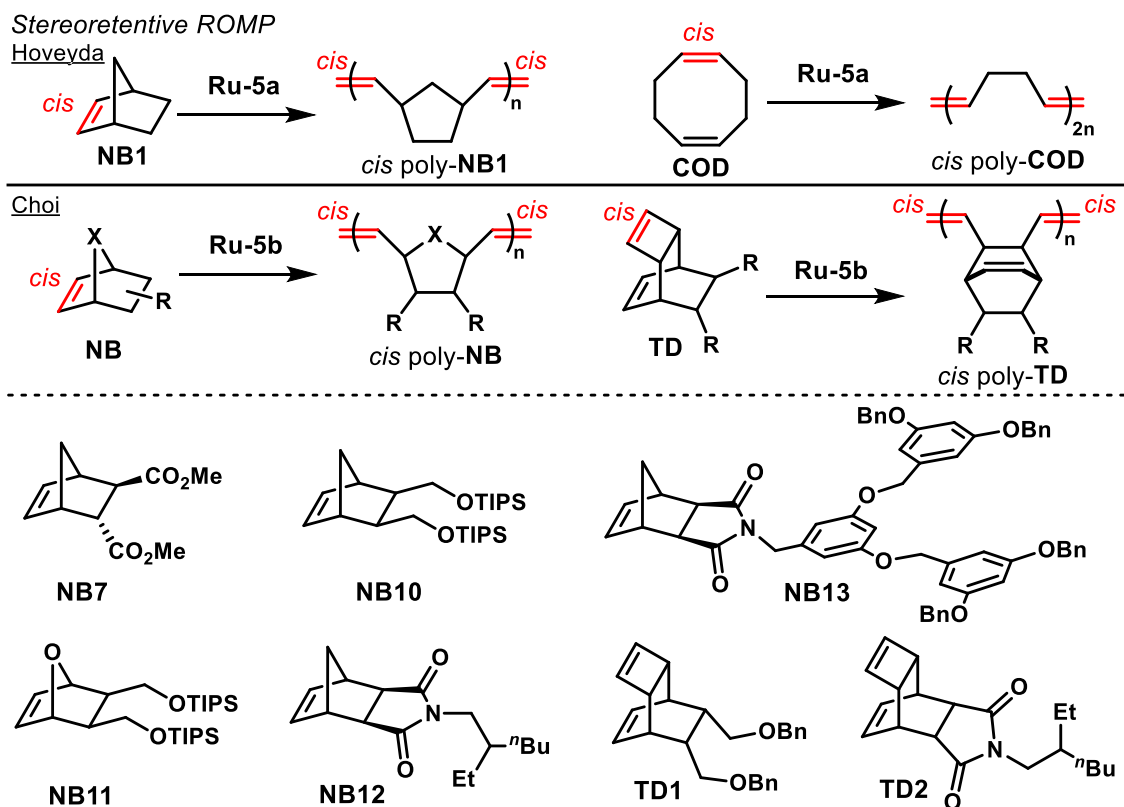
Figure I-6 Examples of stereoretentive ROMP using dithiolate Ru catalysts (**Ru-5a** and **Ru-5b**).

7

polymer properties on the configuration of the repeating alkene (Figure I-6).[25] All these examples demonstrate the versatility of these catalysts and their potential for the design of soft materials with tailored properties.

To leverage the extraordinary selectivity and reactivity of these stereoselective Ru catalysts, we aim to develop stereoselective olefin metathesis polymerizations for the synthesis of complex polymers with precise stereochemistry and to investigate the impact of stereochemistry on polymer properties. Ultimately, this innovative approach will provide an efficient strategy to tailor polymer materials by controlling the *cis* and *trans* content within the polymer backbone.

CHAPTER II

STEREORETENTIVE RING-OPENING METATHESIS POLYMERIZATION TO

ACCESS ALL-*cis* POLY(*p*-PHENYLENE VINYLENE)S WITH LIVING

CHARACTERISTICS[*]

II.1 Introduction

Despite decades of study into the poly(*p*-phenylenevinylene) (PPV) family of
conjugated polymers (Figure II-1a), methods for the precise control of each stilbenoid
olefin configuration remain scarce.[26] Indeed, the *cis* or *trans* (*Z* or *E*) configuration of the
olefins dramatically affects the physical and chemical properties of the material. *cis*-Rich
PPVs are characterized by a twisted and coiled polymer chain, whereas *trans*-rich PPVs
possess a rodlike structure which increases $\pi-\pi$ interactions and packing. As a result, *cis*
alkenes tend to decrease the effective conjugation length of the polymer but increase its
solubility.[12,13] PPV was used to make the first organic light-emitting diode (OLED)[27] and
was one of the components blended into the first "bulk heterojunction" solar cells.[28] The
relative stability of PPV and its desirable semiconducting properties (i.e., band gap in the
visible range) have motivated numerous academic and industrial research groups to
explore its optoelectronic properties.[29] This effort led to many robust syntheses of PPVs,
including controlled polymerizations, with high molar masses (M_n),[30,31] but few allow
precise control over the configuration of the repeating olefins. Additionally, oneway[32]

---

photochemical isomerization rapidly transforms *cis* into *trans* linkages. This clean photoisomerization has been exploited by Katayama and co-workers to pattern PPVs, capitalizing on the difference in solubility between cis and trans congeners,[33] and by Choi and co-workers to prepare semiconducting nanofibers via controlled self-assembly.[34,35] In an effort to harness the full potential of PPVs as stimuli-responsive materials, we report herein the synthesis of all-*cis* PPVs with living characteristics in homopolymers and block copolymers. Syntheses of all-*cis* PPVs are far scarcer than those of all-*trans* PPVs. Indeed, Wittig,[36] Horner−Wadsworth−Emmons,[37] or Knoevenagel[38] polycondensations either lead to an uncontrolled *cis*/*trans* ratio or favor *trans* olefins. Radical or anionic polymerization of *p*-quinodimethane during the Gilch process also favors the more stable *trans* linkage.[30,31] In 2005, Katayama, Ozawa, and co-workers reported a stereospecific Suzuki−Miyaura polymerization that affords all-*cis* PPVs with low molar mass, but selectivities up to 99:1 using linear monomers with preinstalled *Z*-stereochemistry.[33,39] In a different approach, Swager and co-workers synthesized all-*cis* PPVs via postpolymerization reduction of poly(phenylene ethynylene)s (PPEs) with stoichiometric titanium isopropoxide and isopropyl magnesium chloride (Figure II-1b).[40] Both routes afforded impressive stereoselectivity, but are based on uncontrolled chain-growth polymerization, which limits their applications. Our strategy to access all-*cis* PPVs with living characteristics relied on the polymerization of [2.2] paracyclophane-1,9-diene
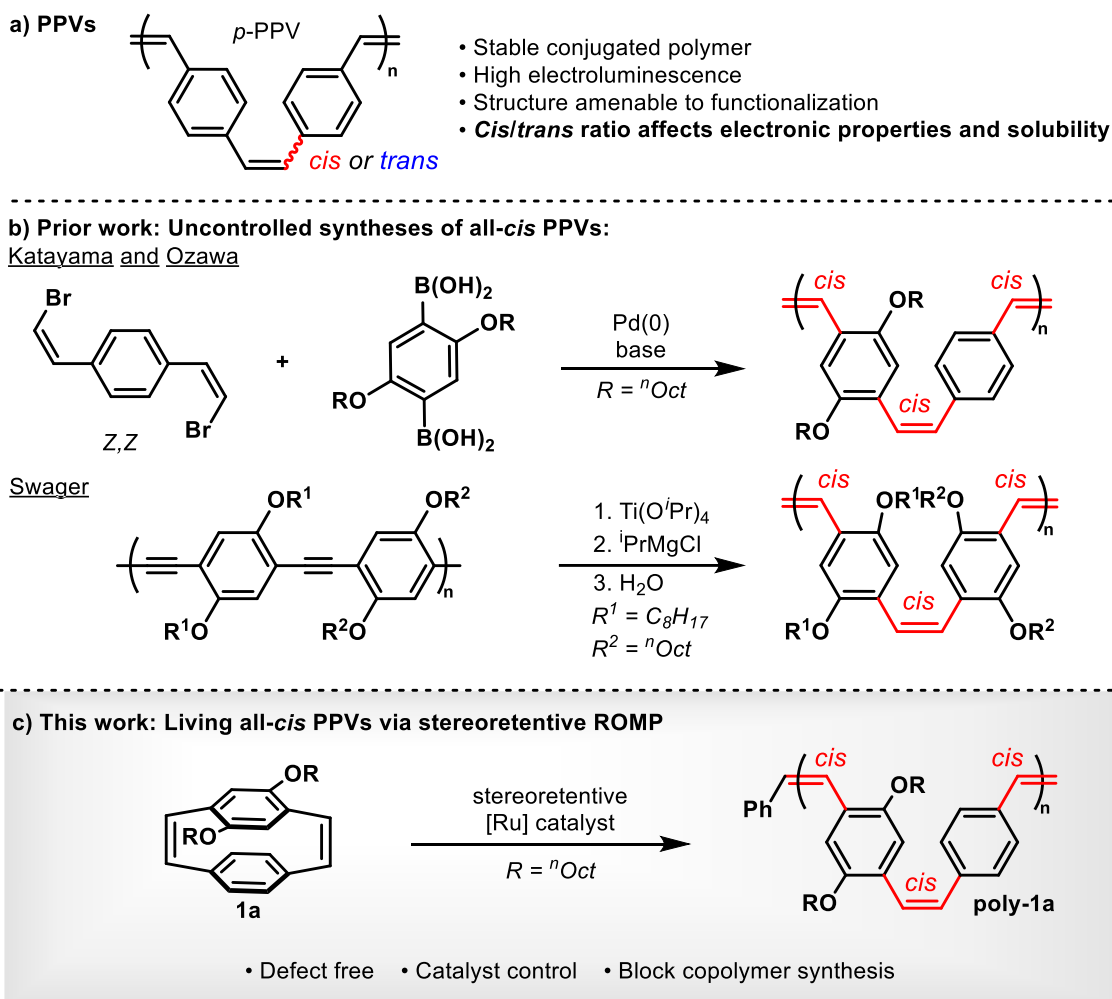
Figure II-1. a) General structure of poly(*p*-phenylene vinylene)s (PPVs). b) The only two examples of uncontrolled synthesis of all-*cis* PPVs. c) A stereoretentive ROMP strategy en route to all-*cis* PPVs with living characteristics.

monomers (Figure II-1c, **1a**) via ringopening metathesis polymerization (ROMP). Early studies from Turner demonstrated that these strained alkene monomers could undergo efficient ROMP, leading to PPVs with alternating *cis* and *trans* linkages using Grubbs' second generation catalyst (**Ru-1b**) (see Figure 2 for catalyst structures).[41-43] The *trans* alkenes are postulated to arise from isomerization driven by the catalyst during ROMP. We hypothesized that either *Z*-selective (**Ru-4a**)[44] or stereoretentive (**Ru-6**)[18-20]

Monomers:
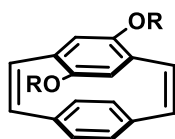
1a

R = *ⁿOct*
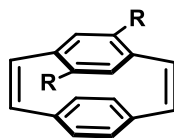
1b

R = *ⁿOct*
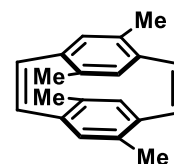
1c

Catalysts:
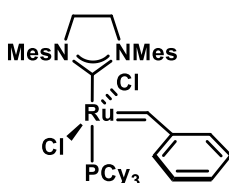
Ru-1b
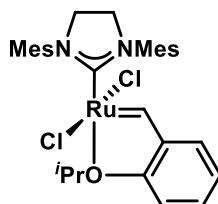
Ru-2b
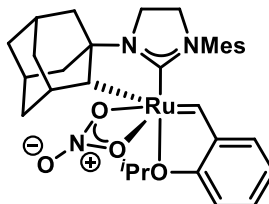
Ru-4a
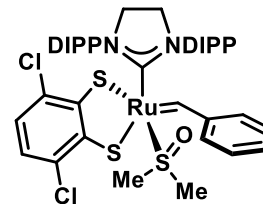
Ru-6

Figure II-2. Paracyclophane diene monomers **1a–c** and olefin metathesis catalysts used for the initial screening.

metathesis catalysts could allow for the controlled preparation of all-*cis* PPVs with predictable high M_n's, low *Đ*'s, and little to no *trans* defects. While *Z*-selective catalyst **Ru-4a** has been applied to polymerize a variety of norbornene derivatives,[24] stereoretentive dithiolate-chelated Ru catalysts such as **Ru-5** or **Ru-6** have seldomly been used for ROMP. Only norbornene,[18,45] cyclooctadiene,[18] and norbornadiene[46] have been polymerized with this new generation of catalysts that enables retention of the alkene stereochemistry during metathesis.[25,47,48] Importantly, perfect *cis* control in the ROMP process was targeted since any postpolymerization isomerization would lead to all-*trans* PPVs.[49-51]

II.2 Results and Discussion

II.2.1 Catalyst Screening for Selectivity

Olefin metathesis catalysts **Ru-1b**, **Ru-2b**, **Ru-4a** and **Ru-6** were selected for the initial screening, and [2.2] paracyclophane-1,9-diene monomers **1a−c** were synthesized using literature procedures (Figure II-2).[42,52] While monomers **1a** and **1b** successfully polymerized with all catalysts, **1c** only afforded small polymers with **Ru-1b** and **Ru-2b**, and did not polymerize with **Ru-4a**, which was ascribed to increased steric hindrance around the alkenes when both rings are substituted. In contrast to poly-**1a**, determination of the stereoselectivity by ^{1}H NMR spectroscopy in poly-**1b** was complicated by the overlap of the key signals (see the Experiment Detail section). The determination of catalyst stereocontrol was therefore achieved by examining the ratio of *cis* and *trans* linkages in polymers obtained with these catalysts and monomer **1a** using ^{1}H NMR spectroscopy (Figure II-3).[33] In THF at 60 °C, Grubbs' second generation (**Ru-1b**)
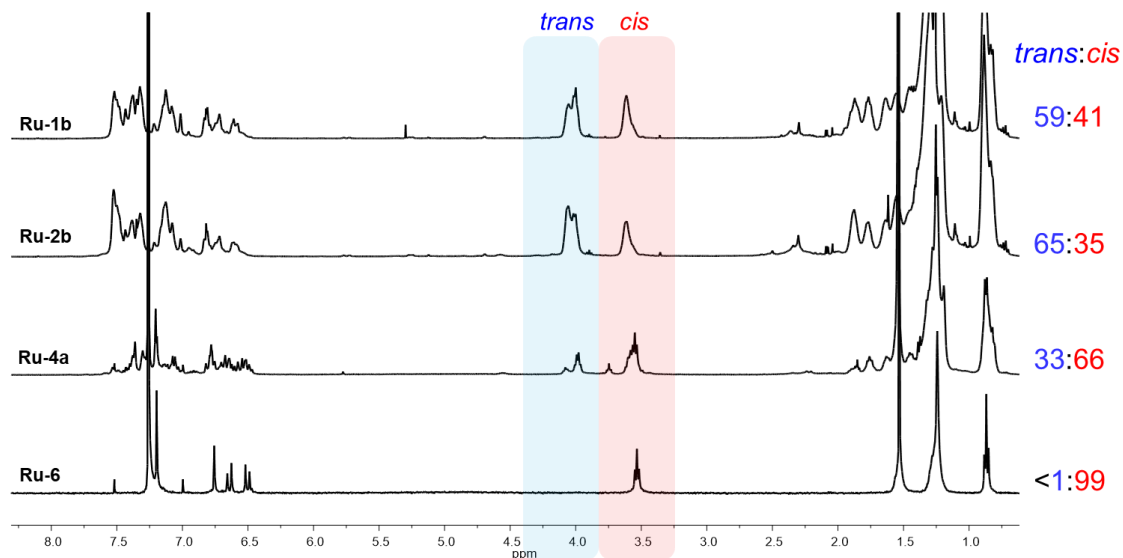
Figure II-3. ^{1}H NMR comparison of *p*-PPV poly-**1a** synthesized with catalysts in THF at 60 °C in the dark for 24 h.

afforded a *p*-PPV with a 59:41 ratio in favor of the *trans* alkenes. The deviation from the expected 1:1 ratio might be due to thermal isomerization under these conditions. Hoveyda−Grubbs' second generation (**Ru-2b**) delivered a similar result with a ratio that is even more skewed toward *trans* alkenes (65:35). As hypothesized, switching to the commercially available *Z*-selective catalyst **Ru-4a** inversed that ratio, with 66% of the olefins being *cis*-configured. To our delight, complete *cis* selectivity (>99:1) was observed using stereoretentive catalyst **Ru-6** synthesized by Materia Inc.[53] Following ROMP with **Ru-6**, no *trans* linkages could be detected in poly-**1a** within the limits of sensitivity of ^{1}H NMR spectroscopy. The reaction conditions using **Ru-6** were then optimized in order to furnish PPVs with living characteristics using **Ru-6**. Polymerizations were kept in the dark to avoid photoisomerization and were conducted in the glovebox because **Ru-6** proved to be sensitive to oxygen in solution. Maintaining a reaction temperature of 40 °C in THF not only delivered exquisite control of the configuration of all alkenes in the backbone, but also allowed for the preparation of PPVs with predictable M_n's up to 13.1 kg/mol and low *Đ*'s by varying the ratio of monomer **1a** to catalyst **Ru-6** (Table II-1).

Table II-1. ROMP of **1a** Catalyzed by **Ru-6**

Entry[a]	1a:Ru-6 ratio	1a conversion	M_n^{theo} (kg/mol)	M_n^{exp} (kg/mol)	*Đ*
1	10:1	100%	4.6	5.4	1.43
2	20:1	100%	9.2	9.6	1.51
3	30:1	100%	13.8	14.3	1.52

[a]**1a** (0.05 mmol) was polymerized with **Ru-6** at 40 °C in THF in the dark and under nitrogen for 4 h. M_n's and *Đ*'s were determined by SEC (THF) using polystyrene standards (RI detection).

II.2.2 Kinetics Study of Stereoretentive ROMP

As expected for controlled polymerization, a linear relationship between M_n and

monomer conversion was observed by monitoring the polymerization of **1a**, and dispersity
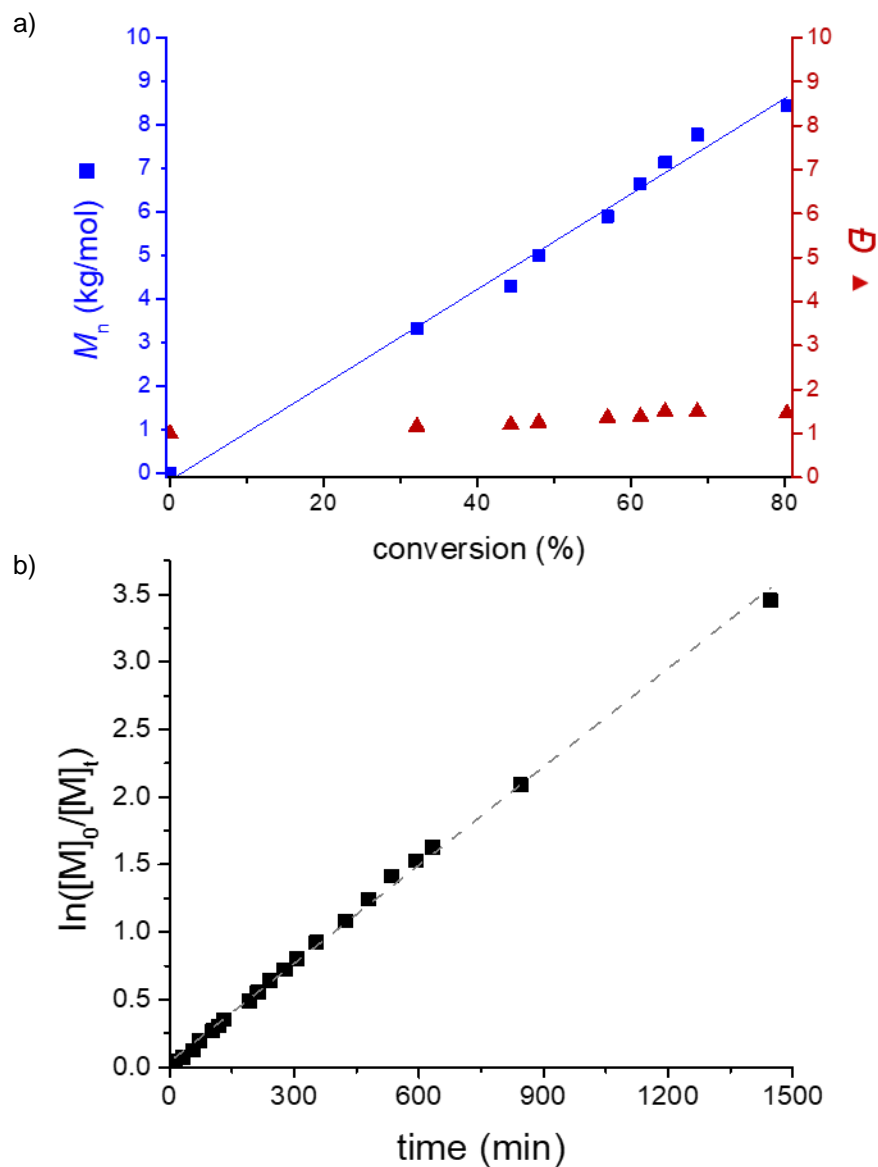
Figure II-4. Polymerization of **1a** with catalyst **Ru-6**: a) M_n and *Đ* vs conversion. b) Determination of the rate of propagation ($R^2 = 0.99795$). Kinetic studies were performed at room temperature to slow down the propagation and to allow for the collection of data points over a convenient length of time.

values remained around 1.1 throughout the ROMP (Figure II-4a). Notably, full conversion can be reached without loss of control over the molar mass distribution. The living character of the polymerization process was confirmed by a first-order consumption of monomer **1a** as illustrated by the linear association between $\ln([M_0]/[M_t])$ and time (Figure II-4b). The slope of this linear plot provided the apparent rate constant of propagation, $k_p^{app} = 0.00243$ min^{-1}. The rate of initiation was too high to be calculated by NMR spectroscopy, since all of catalyst **Ru-6** had reacted with **1a** before the first spectrum could be collected. This extremely fast initiation at room temperature is undoubtedly key to the observed control over M_n and constitutes a notable difference with the Grubbs' catalysts previously used with [2.2] paracyclophane-1,9-diene monomers.[54,55]

II.2.3 Diblock Copolymer with All-cis PPV Segment via Chain Extension

By contrast to the prior syntheses of all-*cis* PPVs,[33,40] the living behavior of the ROMP process enables functionalization of the chain-end of all-*cis* poly-**1a**, as well as chain-extension to access multiblock copolymers. In order to investigate the responsiveness of all-*cis* PPV poly-**1a** to light within intricate polymeric architecture, block copolymers containing a block of **1a** and a block of *exo*-norbornene-imide **2**[56,57]
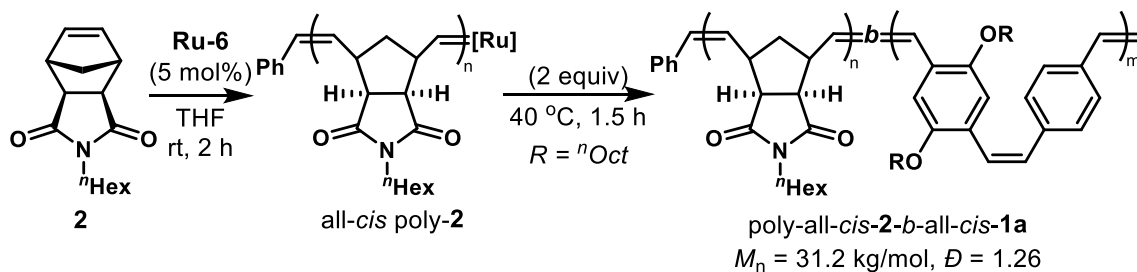
Figure II-5. Synthesis of all-*cis* poly-**2** and poly-all-*cis*-**2**-*b*-all-*cis*-**1a** via chain extension.

16

were prepared. The excellent chain-end fidelity observed with the stereoretentive ROMP allowed for the synthesis to start with either block (Figure II-19−23). However, chain extension of poly-**2** with **1a** helped increase the size of the PPV segment despite its intrinsically low solubility (Figure II-5). In line with the stereoretentive ROMP of norbornene reported by Hoveyda and co-workers,[18] only *cis* linkages were identified in poly-**2** by NMR spectroscopy.

II.2.4 Light-Responsive Behavior of All-cis PPV

With poly-all-*cis*-**2**-*b*-all-*cis*-**1a** in hand, photoisomerization of this construct was investigated. Irradiation with UV light (365 nm) for 30 min triggered clean isomerization of the PPV block from all-*cis* to all-*trans* as shown by ^{1}H NMR and UV−visible absorption spectroscopies (Figure II-6). Careful inspection of the ^{1}H NMR spectra showed that the block based on **2** remained unchanged during the isomerization, which highlights the mildness and blockselectivity of the process. Analysis of the particle size by dynamic light scattering was complicated by potential aggregation of poly-all-*cis*-**2**-*b*-all-*cis*-**1a**. A marked increase of the hydrodynamic radius was nonetheless observed after photoisomerization consistent with a coil-to-rod transition (Figure II-31). As expected, the solubility of the resulting polymer was lower, as poly-all-*cis*-**2**-*b*-all-*trans*-**1a** started to precipitate out of the THF solution during irradiation. In summary, we have demonstrated that the exquisite stereoselectivity afforded by dithiolate-chelated Ru metathesis catalysts is not limited to common norbornene-based monomers. Catalyst **Ru-6** allows the efficient and stereoretentive ROMP of unusual [2.2] paracyclophane-1,9-diene monomer **1a**, which provides access to well-defined and functionalizable all-*cis* PPVs. This approach does not

17

require the preparation of stereodefined linear alkenes or harsh conditions using stoichiometric metal reagents and, thus, could deliver all-*cis* PPVs based on a variety of paracyclophane-type monomers.[58-60] The optimized conditions allowed for a controlled chain-growth process resulting in polymers with predicable M_n and narrow $Đ$ values. The high-chain fidelity was harnessed to prepare block copolymers that can be isomerized with UV light. We anticipate that the efficiency and practicality of the photoisomerization combined with the universality of ROMP will allow the synthesis of all-*cis* PPVs embedded in complex polymeric architectures and will allow one to exploit the full potential of PPV as stimuli-responsive materials.
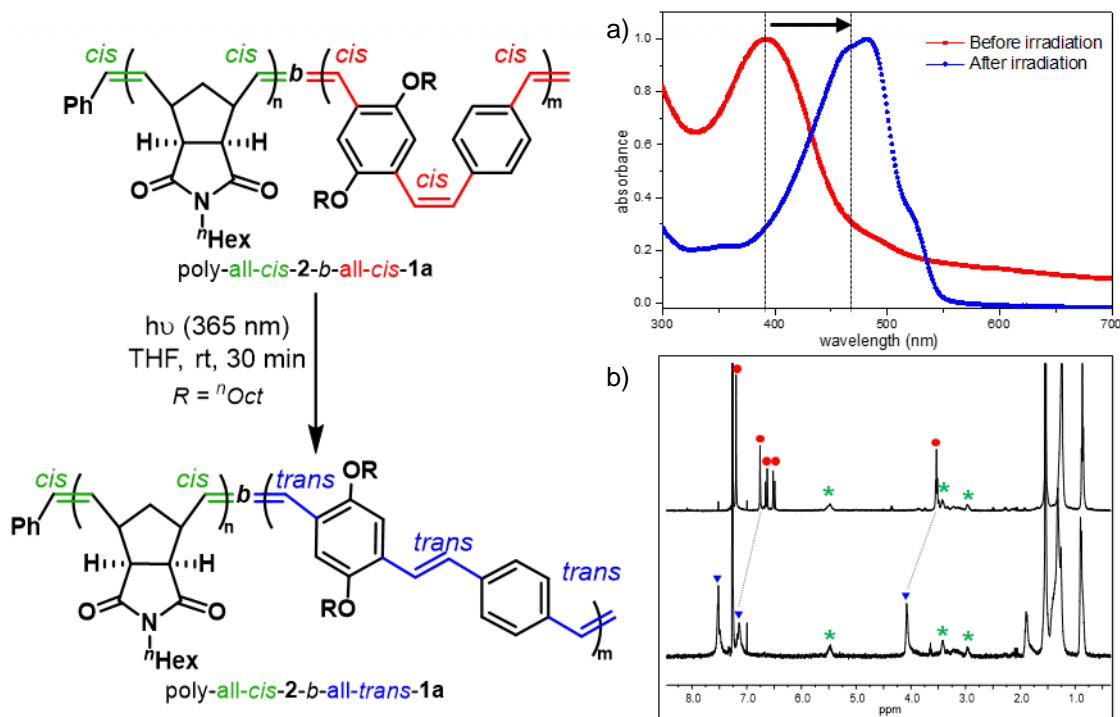
Figure II-6. Photoisomerization poly-all-*cis*-**2**-*b*-all-*cis*-**1a**: a) UV-visible absorption spectroscopy before and after UV light (365 nm) irradiation. b) ^{1}H-NMR spectra. Characteristic peaks are indicated as follows: all-*cis* poly-**1a** block (red spheres), all-*trans* poly-**1a** block (blue triangles), all-*cis* poly-**2** block (green asterisk).

II.3 Experimental Details

II.3.1 General Reagent Information

All reactions were carried out under an inert nitrogen atmosphere with dry solvents under anhydrous conditions unless otherwise stated. Dry dichloromethane (DCM), diethyl ether (Et$_2$O), tetrahydrofuran (THF), toluene (PhMe) were obtained by passing the previously degassed solvents through activated alumina columns. Synthesis of polymers using stereoretentive ruthenium catalyst was carried out in a nitrogen-filled glove box (SG1800/750TS-F, VIGOR). Reagents were purchased at the highest commercial quality and used without further purification, unless otherwise stated. Yields refer to chromatographically and spectroscopically (^{1}H NMR) homogeneous material, unless otherwise stated. Reactions were monitored by thin layer chromatography (TLC) carried out on 250 μm SiliCycle SiliaPlate™ silica plates (F254), using UV light as the visualizing agent. Flash silica gel chromatography was performed using SiliCycle SiliaFlash® Irregular Silica Gel (60 Å, particle size 40–63 μm). Polymers were isolated after precipitation using an Eppendorf 5804 centrifuge.

II.3.2 General Analytical Information

All polymer samples were analyzed using a Tosoh EcoSec HLC 8320GPC system with a TSKgel SuperHM-M column and a TSKgel SuperH-RC column at a flow rate of 0.40 mL/min at 40 °C. THF stabilized with BHT was used as the eluent and all number-average molecular weights (M_n), weight-average molecular weights (M_w), and dispersities ($Đ$) for polymers were calculated from refractive index and UV

chromatograms against TSKgel polystyrene standards. NMR spectra were recorded on Bruker Avance Neo 400 instruments and were calibrated using residual undeuterated solvent as an internal reference (CHCl$_3$ @ 7.26 ppm ^{1}H-NMR, 77.16 ppm ^{13}C-NMR; THF @ 3.58 ppm ^{1}H-NMR). The following abbreviations were used to explain NMR peak multiplicities: s = singlet, d = doublet, t = triplet, q = quartet, m = multiplet, br = broad. UV/vis spectra were obtained by Shimadzu UV-2600 UV-visible spectrophotometer and fluorescence spectra were obtained by Horiba FluorEssenceTM fluorescence spectrometer. Dynamic light scattering (DLS) was performed using a Malvern Zetasizer Nano ZS instrument. Atmospheric pressure chemical ionization mass spectrometry (APCI-MS) experiment was performed using a Thermo Scientific Q Exactive Focus. Sample was injected into a 10 µL loop and methanol was used as a mobile phase at a flow rate of 300 µL/min. The Q Exactive Focus APCI source was operated in full MS in positive mode. The mass resolution was tuned to 70000 FWHM at m/z 200. The discharge current was set at 5 µA, and the sheath gas and auxiliary gas flow rates were set to 30 and 0 arbitrary units, respectively and the auxiliary gas temperature was set to 250 ^{o}C. The transfer capillary temperature was held at 250 ^{o}C and the S-Lens RF level was set at 50 v. Exactive Series 2.11 /Xcalibur 4.02.47 software was used for data acquisition and processing.

II.3.3 Monomer Synthesis
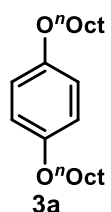
Monomers **1a** and **1b** were synthesized according to literature procedures (Scheme II-2).[52] The preparation of monomer **1c** was adapted from the synthesis of a tetraoctyl analog (Scheme II-2) and the exact structure of **1c** was assigned by NMR comparison to that of this analog.[52]

Scheme II-1 Synthesis of Monomers **1a** and **1b**
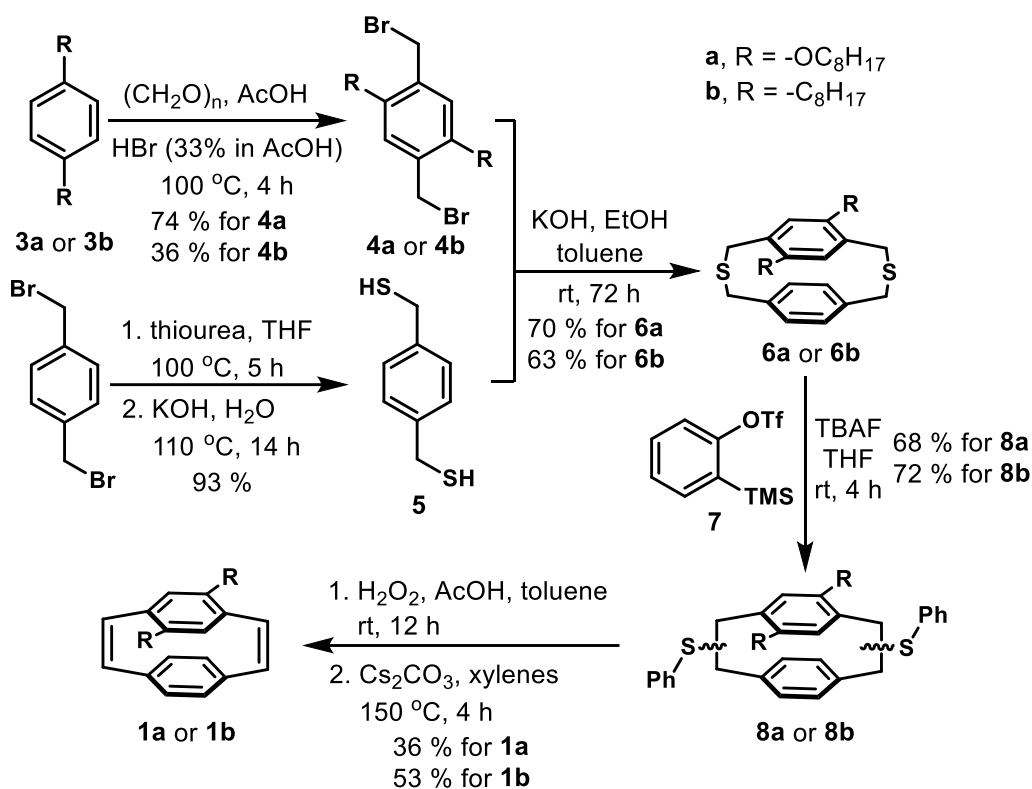
Scheme II-2 Synthesis of Monomer **1c**
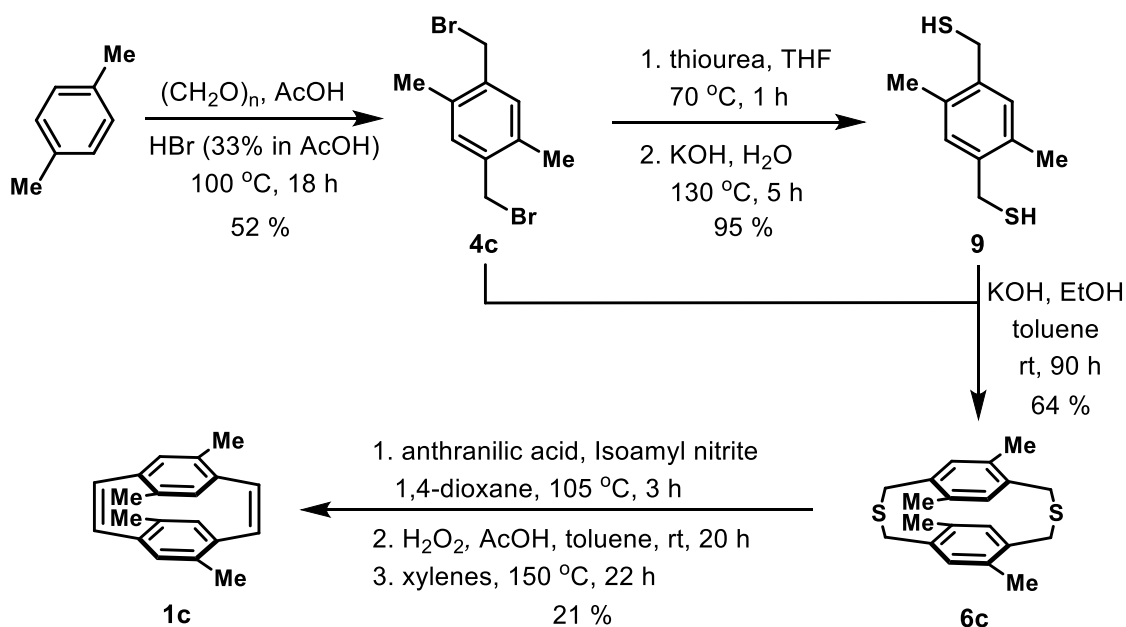
1,4-Di(octyloxy)benzene 3a. *p*-Hydroquinone (11.0 g, 100 mmol, 1.0 equiv) was dissolved in EtOH (110 mL), then KOH (85 wt%, 15.8 g, 240 mmol, 2.4 equiv) was added to the mixture. After stirring the solution for 20 min at room temperature, *n*-octyl bromide (41.5 mL, 240 mmol, 2.4 equiv) was slowly added into the reaction mixture at room temperature. The solution was stirred overnight at 80 °C. The reaction mixture was filtered through a filter paper and the residues were washed with DCM (3 × 50 mL). The filtrate was concentrated *in vacuo*. The residues were dissolved in DCM (100 mL) then the organic solution was washed with water (3 × 50 mL). The organic phase was dried with MgSO$_4$ and the solvent was removed *in vacuo*. The solid residues were dissolved in the minimum amount of DCM and recrystallized by addition of MeOH. Compound **3a** was isolated as a white solid (29.5 g, 88.3 mmol, 88%).

22

The spectroscopic data for this compound were identical to those reported in the literature.[61]

^{1}H NMR (400 MHz, CDCl$_3$) δ 6.82 (s, 4 H), 3.89 (t, J = 6.6 Hz, 4 H), 1.80–1.69 (m, 4 H), 1.49–1.38 (m, 4 H), 1.38–1.24 (m, 16 H), 0.88 (t, J = 6.9 Hz, 6 H) ppm.
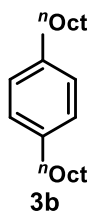
^{n}Oct   **1,4-Dioctylbenzene 3b**. Magnesium powder (9.19 g, 378 mmol, 3.2 equiv) was added in a flame-dried 250 mL 3-neck-round bottom flask adapted with **^{n}Oct** condenser. The whole glassware setup was placed under vacuum and then **3b** backfilled with nitrogen. Under nitrogen, THF (120 mL) was added into the flask, followed by dropwise addition of *n*-octyl bromide (63.6 mL, 368 mmol, 3.1 equiv) into the reaction mixture. The reaction mixture was stirred at 50 °C for 2 h. 1,4-dichlorobenzene (17.6 g, 120 mmol, 1.0 equiv) and 1,3-bis(diphenylphosphino)propane nickel chloride (325 mg, 0.60 mmol, 5 mol%) were added into a 500 mL flask. The flask was placed under vacuum and then backfilled with nitrogen. Under nitrogen, THF (240 mL) was added into the flask and cooled to 0 °C, then the generated Grignard reagent was transferred via a canula into the reaction mixture at 0 °C. The reaction was stirred for 2 h at 0 °C, then the reaction mixture was stirred at room temperature for 16 h. The reaction was quenched with a saturated aq. NH$_4$Cl at 0 °C. The solvent was removed *in vacuo*. The residues were filtered through a filter paper and washed with diethyl ether (3 × 10 mL). The filtrate was diluted with DCM (250 mL) and washed with water (3 × 100 mL). The organic phase was dried over MgSO$_4$ and the solvent was removed *in vacuo*. Compound

3b was isolated after column chromatography (SiO$_2$, hexanes) as a clear oil (32.6 g, 108 mmol, 90%).

The spectroscopic data for this compound were identical to those reported in the literature.[52]

^{1}H NMR (400 MHz, CDCl$_3$) δ 7.08 (s, 4 H), 2.56 (t, J = 7.8 Hz, 4 H), 1.59 (quin., J = 7.4 Hz, 4 H), 1.35–1.23 (m, 20 H), 0.88 (t, J = 6.9 Hz, 6 H) ppm.
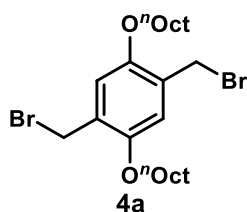
1,4-Bis(bromomethyl)-2,5-di(octyloxy)benzene 4a. 1,4-Di(octyloxy)benzene (16.7 g, 50.0 mmol, 1.0 equiv) and paraformaldehyde (6.00 g, 200 mmol, 4.0 equiv) were added to a round-bottom flask, then a solution of HBr (30 wt% in acetic acid, 30 mL) was added slowly. A condenser was adapted onto the flask and the reaction mixture was stirred at 120 °C for 4 h. Once cooled to room temperature, the mixture was poured into water (250 mL) at 0 °C. The precipitated solid was filtered and washed with water several times. The solid residues were then washed with MeOH (3 × 20 mL), and compound **4a** was isolated in as a white solid (19.21 g, 36.9 mmol, 74%).

The spectroscopic data for this compound were identical to those reported in the literature.[62]

^{1}H NMR (400 MHz, CDCl$_3$) δ 6.85 (s, 2 H), 4.52 (s, 4 H), 3.98 (t, J = 6.4 Hz, 4 H), 1.86–1.75 (m, 4 H), 1.53–1.45 (m, 4 H), 1.40–1.26 (m, 16 H), 0.89 (t, J = 6.7 Hz, 6 H) ppm.
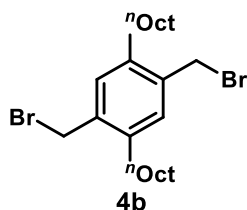
1,4-Bis(bromomethyl)-2,5-dioctylbenzene **4b**. 1,4-Dioctylbenzene (32.6 g, 108 mmol, 1.0 equiv) and paraformaldehyde (13.0 g, 432 mmol, 4.0 equiv) were placed in a 250 mL round-bottom flask, and then a solution of HBr (30 wt% in acetic acid, 75 mL) was added to the reaction mixture slowly. A condenser was adapted onto the flask and the reaction mixture was stirred at 120 °C for 5 days. Once cooled to room temperature, the mixture was poured into water (250 mL) at 0 °C. The precipitated solid was filtered and washed with water several times. The solid residues were dissolved in DCM (200 mL). The DCM solution was extracted with saturated aq. $NaHCO_3$ (3 × 100 mL), then the organic layer was dried over $MgSO_4$. The solvent was removed *in vacuo*. The residues were dissolved in a minimum amount of DCM, then the product was recrystallized by adding MeOH. Solvent was removed by filtration, and **4b** was isolated as a white solid (19.2 g, 39.2 mmol, 36%).

The spectroscopic data for this compound were identical to those reported in the literature.[52]

^{1}H NMR (400 MHz, CDCl$_3$) δ 7.14 (s, 2 H), 4.49 (s, 4 H), 2.66 (t, J = 8.0 Hz, 4 H), 1.63 (quin., J = 7.6 Hz, 4 H), 1.44–1.25 (m, 2 H), 0.89 (t, J = 6.8 Hz, 6 H) ppm.
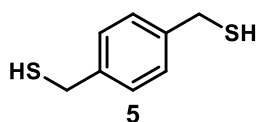
1,4-Bis(thiolatomethyl)benzene 5. 1,4-bis(bromomethyl)benzene (15.0 g, 56.8 mmol, 1.0 equiv) and thiourea (10.4 g, 136 mmol, 2.4 equiv) were dissolved in EtOH (200 mL). The solution was stirred for 5 h at 80 °C. The suspension was cooled to room temperature and the solvent was removed *in vacuo*.

KOH (85 wt%, 15.0 g, 227 mmol, 4.0 equiv) and deoxygenated water (350 mL) were added to the crude product. The reaction mixture was stirred at 105 °C for 14 h, then the reaction was cooled to room temperature. The resulting solution was neutralized with aq. H_2SO_4 (50 % *v/v*), and then extracted with diethyl ether (3 × 100 mL). The combined organic layers were washed with brine, and then dried over $MgSO_4$. The solvent was removed *in vacuo*. The resulting solid was dissolved in a minimum amount of DCM and recrystallized by slowly transferring into MeOH. **5** was isolated as as a white solid (8.95 g, 52.6 mmol, 93 %).

The spectroscopic data for this compound were identical to those reported in the literature.[52]

^{1}H NMR (400 MHz, CDCl$_3$) δ 7.28 (s, 4 H), 3.73 (d, *J* = 7.5 Hz, 4 H), 1.75 (t, *J* = 7.5 Hz, 2 H) ppm.
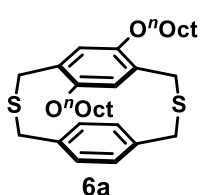
4,7-Dioctyloxy-2,11-dithia[3,3]-paracyclophane 6a. Using two syringe-pumps, a solution of **4a** (10.41 g, 20.0 mmol, 1.0 equiv) in toluene (190 mL) and a solution of **5** (3.41 g, 20.0 mmol, 1.0 equiv) in toluene (190 mL) were added dropwise concomitantly into a solution of KOH (85 wt%, 3.96 g, 60.0 mmol, 3.0 equiv) in EtOH (950 mL) for a period of 72 h under nitrogen at room temperature. After stirring for an additional 6 h, the volatiles were removed *in vacuo*, and the residues were extracted with DCM (3 × 150 mL). The combined organic layers were dried over $MgSO_4$, and then the solvent was removed *in vacuo*. Column

chromatography (SiO$_2$, 80:20, hexanes:DCM) provided **6a** as a clear oil (7.37 g, 13.9 mmol, 70%).

The spectroscopic data for this compound were identical to those reported in the literature.[63]

^{1}H NMR (400 MHz, CDCl$_3$) δ 6.96 (dd, J = 7.9, 1.5 Hz, 2 H), 6.88 (dd, J = 7.9, 1.6 Hz, 2 H), 6.42 (s, 2 H), 4.27 (d, J = 18.7 Hz, 2 H), 3.80 (dt, J = 9.0, 6.5 Hz, 2 H), 3.68–3.72 (m, 6 H), 3.34 (d, J = 14.7 Hz, 2 H), 1.89–1.77 (m, 4 H), 1.62–1.51 (m, 4 H), 1.46–1.29 (m, 16 H), 0.91 (t, J = 6.9 Hz, 6 H) ppm.
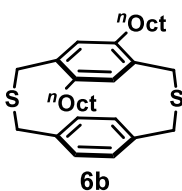
4,7-Dioctyl-2,11-dithia[3,3]-paracyclophane 6b. Using two syringe-pumps, a solution of **4b** (9.75 g, 20.0 mmol, 1.0 equiv) in toluene (190 mL) and a solution of **5** (3.40 g, 20.0 mmol, 1.0 equiv) in toluene (190 mL) were added dropwise concomitantly into a solution of KOH (85 wt%, 3.96 g, 60.0 mmol, 3.0 equiv) in EtOH (950 mL) for a period of 72 h under nitrogen atmosphere at room temperature. After stirring for an additional 6 h, the volatiles were removed *in vacuo*, and the residue was extracted with DCM (3 × 150 mL). The combined organic layers were dried over MgSO$_4$, and then the solvent was removed *in vacuo*. Column chromatography (SiO$_2$, 90:10 hexanes:DCM) provided **6b** as a clear oil (6.24 g, 12.6 mmol, 63%).

The spectroscopic data for this compound were identical to those reported in the literature.[52]

^{1}H NMR (400 MHz, CDCl$_3$) δ 6.96 (dd, J = 7.9, 1.6 Hz, 2 H), 6.85 (dd, J = 8.0, 1.5 Hz, 2 H), 6.64 (s, 2 H), 3.92 (d, J = 14.7 Hz, 2 H), 3.80 (dd, J = 21.2, 15.1 Hz, 4 H), 3.62 (d, J = 14.7 Hz, 2 H), 2.71 (ddd, J = 14.5, 9.0, 5.8 Hz, 2 H), 2.42 (ddd, J = 14.1, 9.4, 6.6 Hz, 2 H), 1.52–1.40 (m, 4 H), 1.37–1.24 (m, 20 H), 0.89 (t, J = 6.8 Hz, 6 H) ppm.
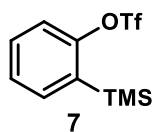
2-(trimethylsilyl)phenyl trifluoromethanesulfonate (**7**). Benzyne precursor **7** was prepared according to a procedure reported by Turner.[52] Bromophenol (6.7 mL, 63.5 mmol, 1.0 equiv) and HMDS (20 mL, 95.9 mmol, 1.5 equiv) were dissolved in THF (20 mL). The reaction mixture was stirred for 4 h at 80 °C and cooled to room temperature. The solvent and unreacted HMDS were removed *in vacuo*. The resulting intermediate (2.45 g, 10 mmol, 1.0 equiv) was dissolved in THF (15 mL) and the solution was cooled to –78 °C. *n*-BuLi (2.5 M in hexane, 4.8 mL, 12 mmol, 1.2 equiv) was added dropwise to the reaction mixture at –78 °C. After stirring for 40 min at –78 °C, Tf$_2$O was added dropwise to the reaction mixture. After stirring for another 40 min at –78 °C, the reaction mixture was warmed to room temperature and stirred for an additional 20 min. The reaction was quenched with cold saturated aq. NaHCO$_3$, and the reaction mixture was extracted with ether (3 × 30 mL). The combined organic layers were dried over MgSO$_4$, and the solvent was removed *in vacuo*. Column chromatography (SiO$_2$, hexanes) afforded **7** as a clear oil (2.50 g, 8.38 mmol, 84%).

The spectroscopic data for this compound were identical to those reported in the literature.[52]

^{1}H NMR (400 MHz, CDCl$_3$) δ 7.54 (dd, J = 7.5, 1.9 Hz, 1 H), 7.44 (ddd, J = 8.3, 7.3, 1.9 Hz, 1 H), 7.38–7.31 (m, 2 H), 0.37 (s, 9 H) ppm.
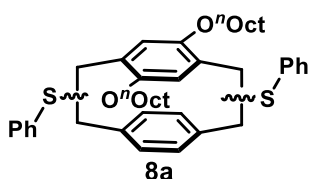
Dithiaparacyclophane Isomers 8a. **6a** (7.37 g, 13.9 mmol, 1.0 equiv) and 2-(trimethylsilyl)phenyl trifluoromethanesulfonate (**7**) (8.1 mL, 33.4 mmol, 2.4 equiv) were dissolved in THF (250 mL). A solution of TBAF (1.0 M in THF, 42.0 mL, 42.0 mmol, 3.0 equiv) was added dropwise to the solution for a period of 4 h under nitrogen at room temperature. After stirring for an additional hour at room temperature, the solvent was removed *in vacuo*. Column chromatography (SiO$_2$, 90:10 hexanes:DCM) afforded **8a** as a mixture of regio- and diastereoisomers (6.46 g, 9.49 mmol, 68%).

The spectroscopic data for this compound were identical to those reported in the literature.[63]

^{1}H NMR (400 MHz, CDCl$_3$) characteristic peaks: δ 7.57–7.51 (m), 7.47–7.37 (m), 7.32–7.28 (m), 7.24–7.16 (m), 7.16–7.07 (m), 6.92–6.73 (m), 6.49–6.44 (m), 6.42–6.34 (m), 6.27 (s), 6.25 (s), 6.12 (s), 6.10 (s), 5.98 (s), 5.91 (d, J = 11.46 Hz), 5.73 (s), 5.52 (s), 5.41–5.31 (m), 4.89–4.78 (m), 4.66–4.60 (m), 4.00–3.57 (m), 3.42 (dd, J = 13.9, 5.2 Hz), 3.17 (dd, J = 13.9, 10.1 Hz), 2.74 (dd, 13.8, 4.7 Hz), 2.65–2.54 (m), 2.44–2.24 (m), 1.96–1.72 (m), 1.59–1.47 (m), 1.48–1.27 (m), 0.94–0.87 (m) ppm.
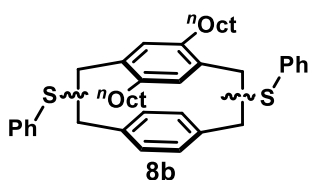
Dithiaparacyclophane Isomers S5b. **6b** (6.24 g, 12.6 mmol, 1.0 equiv) and 2-(trimethylsilyl)phenyl trifluoromethanesulfonate (**7**) (7.34 mL, 30.2 mmol, 2.4 equiv) were dissolved in THF (250 mL). A solution of TBAF (1.0M in THF, 37.8 mL, 37.8 mmol, 3.0 equiv) was added dropwise to the solution for a period of 4 h under nitrogen at room temperature. After stirring for an additional hour at room temperature, the solvent was removed *in vacuo*. Column chromatography (SiO$_2$, 90:10 hexanes:DCM) afforded **6b** as a mixture of regio- and diastereoisomers (5.87 g, 9.05 mmol, 72%).

The spectroscopic data for this compound were identical to those reported in the literature.[52]

^{1}H NMR (400 MHz, CDCl$_3$) characteristic peaks: δ 7.57–7.38 (m), 7.25–7.17 (m), 7.15–7.09 (m), 6.95–6.90 (m), 6.90–6.85 (m), 6.80–6.73 (m), 6.73–6.59 (m), 6.52–6.47 (m), 6.43–6.37 (m), 6.25 (s), 6.17 (s), 6.09 (t, *J* = 8.80 Hz), 5.92 (s), 5.07 (dd, *J* = 9.6, 4.1 Hz), 4.91 (dd, *J* = 9.1, 6.5 Hz), 4.79–4.67 (m), 3.92–3.82 (m), 3.75–3.62 (m), 3.44–3.35 (m), 3.15 (dd, *J* = 14.16, 4.38 Hz), 3.07–2.95 (m), 2.90–2.78 (m), 2.74–2.64 (m), 2.61–2.43 (m), 2.37–2.13 (m), 1.51–1.14 (m), 0.93–0.84 (m) ppm.
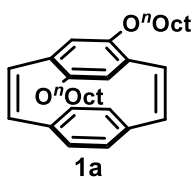
Monomer **1a**. Isomers **8a** (6.43 g, 9.43 mmol, 1.0 equiv) were dissolved in a mixture of toluene (120 mL) and acetic acid (60 mL). The solution was cooled to 0 °C and H$_2$O$_2$ (30 wt% aqueous solution, 2.4 mL) was added dropwise into the reaction mixture over a period of 30 min. After stirring for an additional 20 h at room temperature, the solution was diluted with DCM (200mL) and

washed with brine (3×100mL). The organic layer was dried over MgSO₄, and the solvent was removed *in vacuo* to obtain the crude intermediate as a pale yellow oil. The oxidized intermediate was dissolved in xylenes (200 mL). Cs_2CO_3 (13.12 g, 40.3 mmol, 4.3 equiv) was added to the reaction mixture. After stirring for 4 h at 150 °C, the solution was cooled to room temperature, diluted with DCM (300 mL), and carefully washed with aq. HCl (1 M, 3×100 mL). The aqueous layer was extracted with DCM (300 mL) and the combined organic layers were dried over MgSO₄, and the solvent was removed *in vacuo*. Column chromatography (SiO_2, 80:20 hexanes:DCM) provided monomer **1a** as a pale yellow semisolid (1.57 g, 3.41 mmol, 36%).

The spectroscopic data for this compound were identical to those reported in the literature.[63]

^{1}H NMR (400 MHz, CDCl₃) δ 7.11 (d, *J* = 10.2 Hz, 2 H), 6.90 (d, *J* = 10.2 Hz, 2 H), 6.81 (dd, *J* = 8.1, 1.1 Hz, 2 H), 6.48 (dd, *J* = 8.0, 1.2 Hz, 2 H), 5.78 (s, 2 H), 3.77 (ddt, *J* = 24.3, 9.3, 6.6 Hz, 4 H), 1.78–1.65 (m, 4 H), 1.51–1.39 (m, 4 H), 1.37–1.26 (m, 16 H), 0.89 (t, *J* = 6.9 Hz, 6 H) ppm.
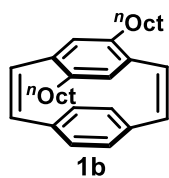
Monomer **1b**. Isomers **8b** (5.87 g, 9.05 mmol, 1.0 equiv) were dissolved in a mixture of toluene (120 mL) and acetic acid (60 mL). The solution was cooled to 0 °C and H_2O_2 (30 wt% aqueous solution, 2.3 mL) was added dropwise into the reaction mixture over a period of 30 min. After stirring for an additional 20 h at room temperature, the solution was diluted with DCM (200mL) and

washed with brine (3×100 mL). The organic layer was dried over $MgSO_4$, and the solvent was removed *in vacuo* to obtain the crude intermediate as a pale yellow oil.

The oxidized intermediate was dissolved in xylenes (200 mL). Cs_2CO_3 (11.7 g, 35.9 mmol, 4.0 equiv) was added to the reaction mixture. After stirring for 4 h at 150 °C, the solution was cooled to room temperature, diluted with DCM (300 mL), and carefully washed with aq. HCl (1 M, 3×100 mL). The aqueous layer was extracted with DCM (300 mL) and the combined organic layer were dried over $MgSO_4$, and the solvent was removed *in vacuo*. Column chromatography (SiO_2, hexanes) provided monomer **1b** as a clear oil (2.05 g, 4.78 mmol, 53%).

The spectroscopic data for this compound were identical to those reported in the literature.[52]

^{1}H NMR (400 MHz, $CDCl_3$) δ 7.06 (dd, J = 17.6, 10.4 Hz, 4 H), 6.71 (dd, J = 8.0, 1.7 Hz, 2 H), 6.42 (dd, J = 8.0, 1.6 Hz, 2 H), 6.10 (s, 2 H), 2.54 (dt, J = 13.8, 7.7 Hz, 2 H), 2.28–2.17 (m, 2 H), 1.45–1.35 (m, 4 H), 1.31–1.22 (m, 20 H), 0.87 (t, J = 6.8 Hz, 6 H) ppm.
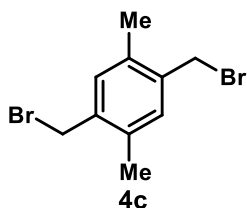
1,4-Bis(bromomethyl)-2,5-dimethylbenzene 4c. *p*-xylene (6.2 mL, 50.0 mmol, 1.0 equiv) and paraformaldehyde (3.30 g, 110 mmol, 2.2 equiv) was added into a round-bottom flask, then a solution of HBr (30 wt% in acetic acid, 29 mL) was added into the reaction mixture. After set-up condenser, the reaction mixture was refluxed for 18 h. After cooled to room temperature, the reaction was poured into water (250 mL) at 0 °C. The generated solid was filtered by washing with water. The solid residue was then recrystallized with DCM

by using dry ice/acetone bath, and compound **S1c** was isolated as a white solid (7.62 g, 26.1 mmol, 52%).

The spectroscopic data for this compound were identical to those reported in the literature.[64]

^{1}H NMR (400 MHz, CDCl$_3$) δ 7.14 (s, 2 H), 4.47 (s, 4 H), 2.37 (s, 6 H) ppm.
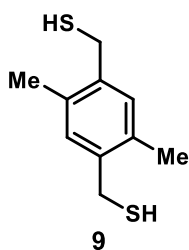
1,4-Bis(thiolatomethyl)-2,5-dimethylbenzene 9. **4c** (3.21 g, 11.0 mmol, 1.0 equiv) and thiourea (2.01 g, 26.4 mmol, 2.4 equiv) were stirred at 70 °C in THF (150 mL) for one hour. The suspension was cooled to room temperature and the solvent was removed *in vacuo*. KOH (85 wt%, 2.18 g, 33.0 mmol, 3.0 equiv) and deoxygenated water (110 mL) were added to the crude product. The reaction mixture was stirred at 130 °C for 5 h, and then the reaction was cooled to room temperature. The solution was neutralized with aq. H$_2$SO$_4$ (50 % *v/v*), and then extracted with DCM (3 × 100 mL). The combined organic layers were washed with brine (100 mL), and then dried over MgSO$_4$. The solvent was removed *in vacuo* to obtain compound **9** as a white solid (2.07 g, 10.5 mmol, 95 %).

The spectroscopic data for this compound were identical to those reported in the literature.[65]

^{1}H NMR (400 MHz, CDCl$_3$) δ 7.03 (s, 2 H), 3.69 (d, *J* = 7.2 Hz, 4 H), 2.34 (s, 6 H) ppm.
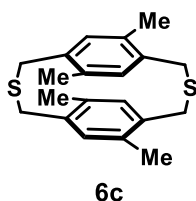
Dithiaparacyclophane isomers 6c. Using two syringe-pumps, a solution of **4c** (2.84 g, 9.7 mmol, 1.0 equiv) in toluene (100 mL) and a solution of **9** (1.93 g, 9.7 mmol, 1.0 equiv) in toluene (100 mL) were added dropwise concomitantly into a solution of KOH (85 wt%, 1.93 g, 29.2 mmol, 3.0 equiv) in EtOH (500 mL) for a period of 90 h under nitrogen at room temperature. After stirring for an additional 6 h, the solvents were removed *in vacuo*. The residues were dissolved in DCM (150 mL) and water (50 mL) was added. The organic layer was separated and the aqueous layer was extracted with DCM (3 × 150 mL). The combined organic layers were dried over MgSO₄ and the solvent was removed *in vacuo*. Column chromatography (SiO₂, 80:20 to 50:50 hexanes:DCM) provided **6c** as a mixture of isomers (2.06 g, 6.3 mmol, 64%).

^{1}H NMR (400 MHz, CDCl₃) characteristic peaks of the major isomer: δ 6.83 (s, 4 H), 3.77 (d, *J* = 14.8 Hz, 4 H), 3.63 (d, *J* = 14.8 Hz, 4 H), 2.21 (s, 12 H) ppm.
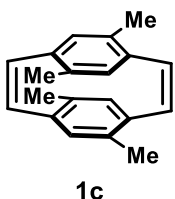
Monomer 1c. The mixed isomers **6c** (1.72 g, 5.24 mmol, 1.0 equiv) and anthranilic acid (2.51 g, 18.3 mmol, 3.5 equiv) were dissolved in 1,4-dioxane (130 mL). Isoamyl nitrite (4.2 mL, 31.4 mmol, 6.0 equiv) was added dropwise to the solution for a period of 15 min under nitrogen at 105 °C in the dark. After stirring for an additional 3 h at 105 °C, the solvent was removed *in vacuo*. Column chromatography (SiO₂, 80:20 hexanes:DCM) provided a mixture of regio- and diastereoisomers (1.07 g) that was used as is for the next steps.

^{1}H NMR (400 MHz, CDCl$_3$) selected peaks: δ 7.44–7.35 (m), 7.30–7.18 (m), 7.18–7.11(m), 4.84 (td, J = 9.7, 5.3 Hz), 3.44–3.30 (m), 2.15 (s), 2.10 (s), 2.05 (s), 1.99 (s) ppm.

The mixed isomers (1.02 g, 2.12 mmol, 1.0 equiv) were dissolved in a mixture of toluene (30 mL) and acetic acid (15 mL), then the solution was cooled to 0 °C. H$_2$O$_2$ (30 wt% aqueous solution, 0.50 mL) was added dropwise to the reaction mixture for a period of 30 min at 0 °C. The mixture was warmed to room temperature and stirred for an additional 20 h. The resulting solution was washed with brine (100 mL) and the aqueous layer was extracted with DCM (100 mL). The combined organic layers were dried over MgSO$_4$, and the solvent was removed *in vacuo* to obtain the crude intermediate as a white solid.

The oxidized intermediate was dissolved in xylenes (50 mL). After stirring for 22 h at 150 °C, the solution was cooled to room temperature, diluted with DCM (150 mL), and carefully washed with aq. HCl (1 M, 50 mL). The aqueous layer was extracted with DCM (150 mL) and the combined organic layer were dried over MgSO$_4$, and the solvent was removed *in vacuo*. The combined organic layers were dried over MgSO$_4$, and the solvent was removed *in vacuo*. Column chromatography (SiO$_2$, hexanes) and recrystallization provided the major isomer (> 90%), monomer **1c,** as a white solid (293 mg, 1.12 mmol, 21%).

^{1}H NMR (400 MHz, CDCl$_3$) δ 6.91 (s, 4 H), 6.39 (s, 4 H), 1.99 (s, 12 H) ppm.

^{13}C NMR (101 MHz, CDCl$_3$) δ 137.8, 134.7, 134.5, 129.0, 19.3 ppm.

HRMS-ESI: calc'd. for C$_{20}$H$_{21}$ [M+H]$^+$ 261.1638, found 261.1633.

II.3.4 Catalyst Screen to Obtain All-cis PPV with Perfect Stereoselectivity

In a nitrogen-filled glove box, the catalyst (2.5 mmol, 5 mol%, **Ru-1b, Ru-2b, Ru-4a** or **Ru-6**) was weighed and transfer to a sample vial with a stir bar. The vial was taken out of the glovebox. A deoxygenated solution of monomer **1a–c** (50 mmol) in anhydrous THF (1 mL) was transferred into the vial containing the catalyst (**Ru-1b, Ru-2b, Ru-4a** or **Ru-6**). The mixture was placed into a preheated oil bath at 60 °C and stirred for 24 h in the dark. Once cooled to room temperature, the reaction was quenched with ethyl vinyl ether (0.1 mL) and stirred for an additional 30 min at room temperature. The polymer was precipitated upon addition of methanol and the solid was isolated by
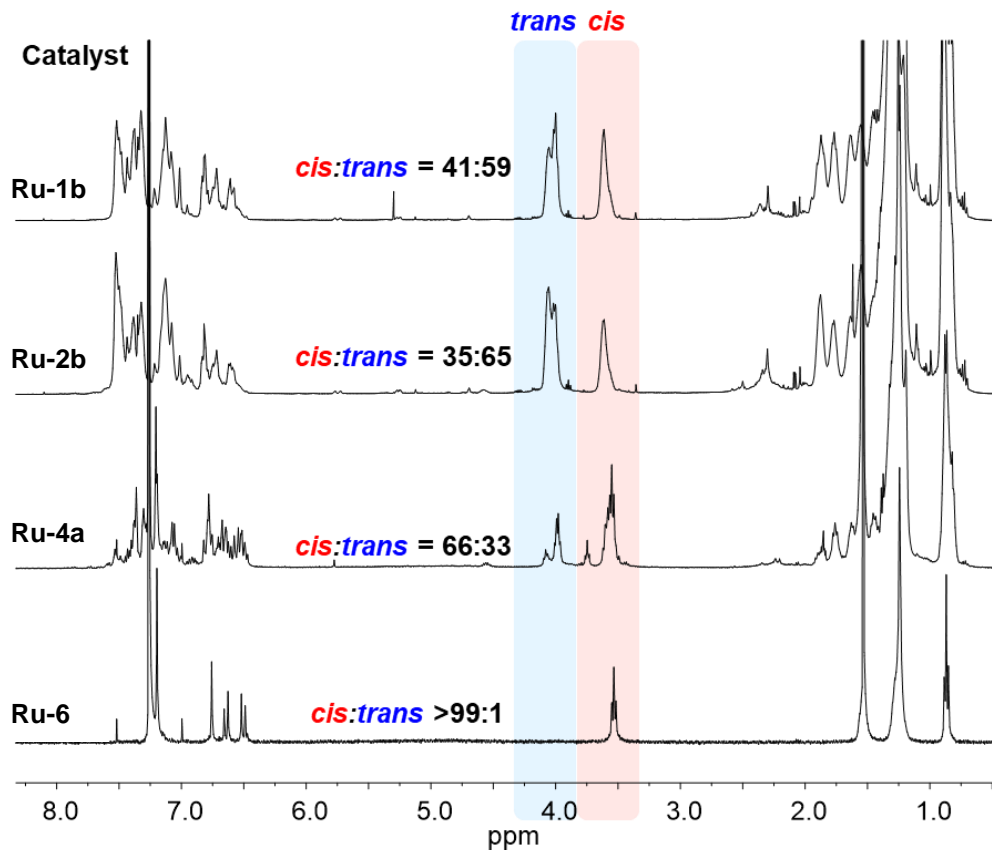
Figure II-7. ^{1}H NMR comparison of *p*-PPV poly-**1a** synthesized with catalysts in THF at 60 °C in the dark for 24 h.

centrifugation and decantation. The resulting polymer was dried under high vacuum. The polymers were stored in vials wrapped with aluminum foil and kept away from light. ^{1}H NMR analysis was used to determine the ratio of *cis* and *trans* alkenes within poly-**1a** (Figure II-7). A similar analysis with poly-**1b** was hindered by the overlap of characteristic peaks (Figure II-8). Finally, only oligomers could be obtained with monomer **1c** or no polymers at all (Table II-2).
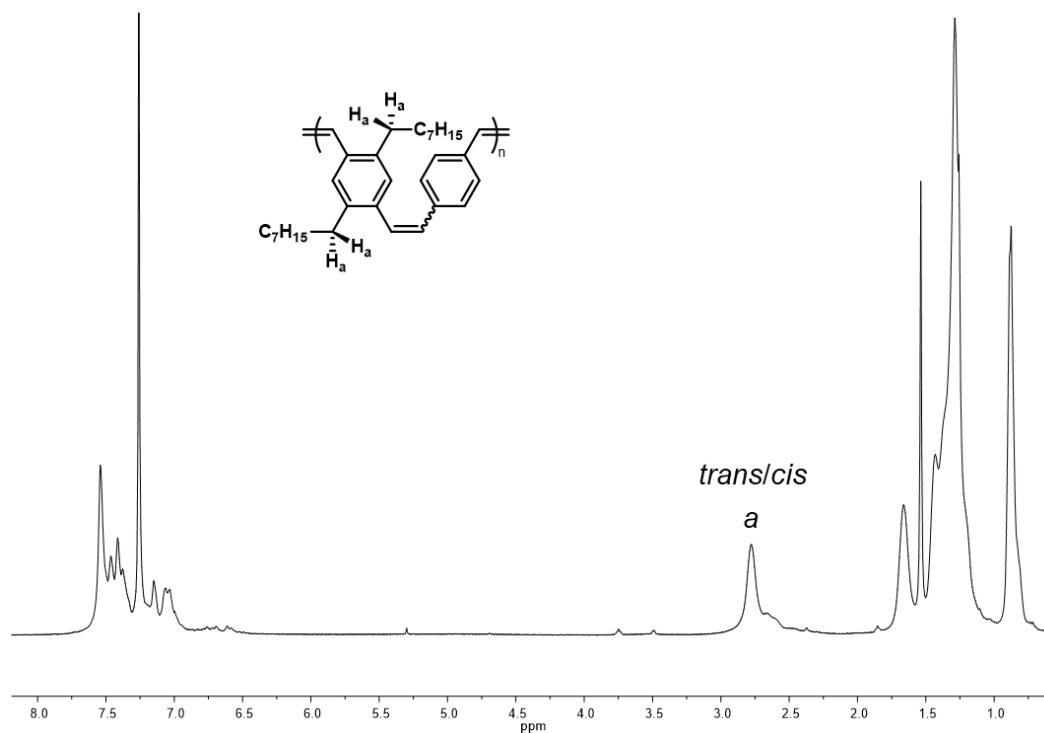
Figure II-8. ^{1}H NMR (400 MHz, CDCl$_3$) spectrum of poly-**1b** using catalyst **Ru-1b** showed an overlap between peaks characteristic of *trans* and *cis* configurations (protons Ha).

Table II-2. ROMP Attempts of Monomer **1c** with Catalysts **Ru-1b**, **Ru-2b** and **Ru-4a**

Catalyst	temperature (°C)	M_n (kg/mol)	$Đ$
Ru-1b	60	1.2	1.68
Ru-2b	60	1.6	1.65
Ru-4a	60	—	—

M_n's and $Đ$'s were determined by SEC (THF) using polystyrene standards (RI detection).

SEC analysis revealed that only oligomers were obtained with **Ru-1b** and **Ru-2b** and that polymerization did not take place with **Ru-4a**.

Table II-3. Solvent Screen for The Polymerization of **1a** with Catalyst **Ru-6**

Solvent	M_n^{exp} (kg/mol)	M_n^{theo} (kg/mol)	$Đ$	*cis*:*trans* ratio
CHCl$_3$	2.9	9.3	1.35	>99:1
THF	8.7	9.3	1.73	>99:1
chlorobenzene	3.3	9.3	1.68	>99:1
o-dichlorobenzene	3.3	9.3	1.59	>99:1

All reactions were conducted at 60 °C for 24 h. M_n's and $Đ$'s were determined by SEC (THF) using polystyrene standards (RI detection).

II.3.5 General Procedure for Stereoretentive ROMP with catalyst ***Ru-6***

In a nitrogen-filled glove box, a solution of ruthenium catalyst **Ru-6** (2.5mM) in deoxygenated THF (1.0 mL) was added into a reaction vial containing monomer **1a** or **2** (50 μmol) and a stir bar. The vial was hermetically sealed with a cap and parafilm and taken out of the glovebox. The mixture was stirred at room temperature for 5 minutes and placed into a preheated oil bath at 40 °C for 2 h in the dark. Once cooled to room temperature, the reaction was quenched with ethyl vinyl ether (0.1 mL) and stirred for an

additional 30 min at room temperature. The solution was diluted to 1.5 mg/mL with THF, filtered, and then injected to GPC instrument directly. The remaining polymer was precipitated upon addition of methanol and the solid was isolated by centrifugation and decantation. The resulting polymer was dried under high vacuum. The polymers were stored in vials wrapped with aluminum foil and kept away from light.

Synthesis of all-*cis* poly-**1a**
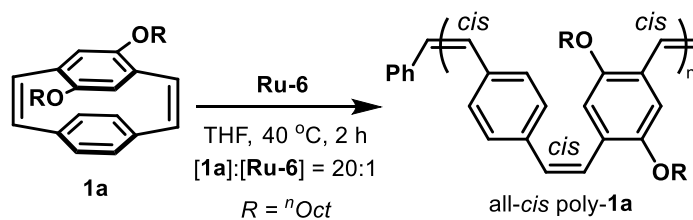
All-*cis* **poly-1a**:

^{1}H NMR (400 MHz, CDCl$_3$) δ 7.20 (s, 4 H), 6.76 (s, 2 H), 6.64 (d, J = 12.3 Hz, 2 H), 6.50 (d, J = 12.3 Hz, 2 H), 3.53 (t, J = 6.5 Hz, 4 H), 1.33–1.20 (m, 24 H), 0.87 (t, J = 6.6 Hz, 6 H) ppm.

^{13}C NMR: (100 MHz, CDCl$_3$) δ 150.3, 136.4, 128.8, 126.4, 125.5, 114.1, 69.0, 32.0, 29.4, 29.4, 29.3, 26.1, 22.8, 14.3 ppm.

The spectroscopic data for this polymer were identical to those reported by Ozawa and coworkers.[33]
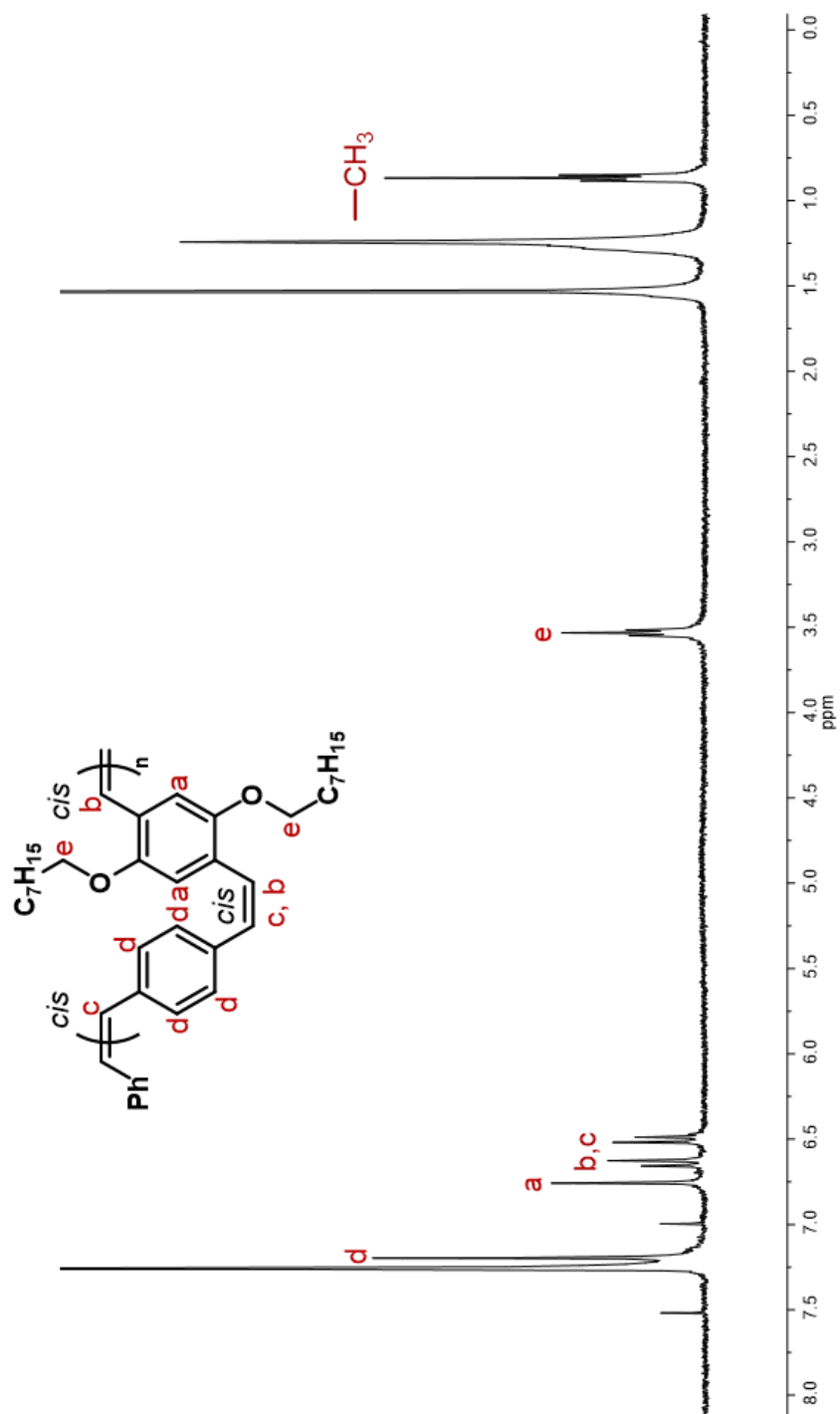
Figure II-9. ^{1}H NMR (400 MHz, CDCl$_3$) spectrum of all-*cis* poly-**1a**.
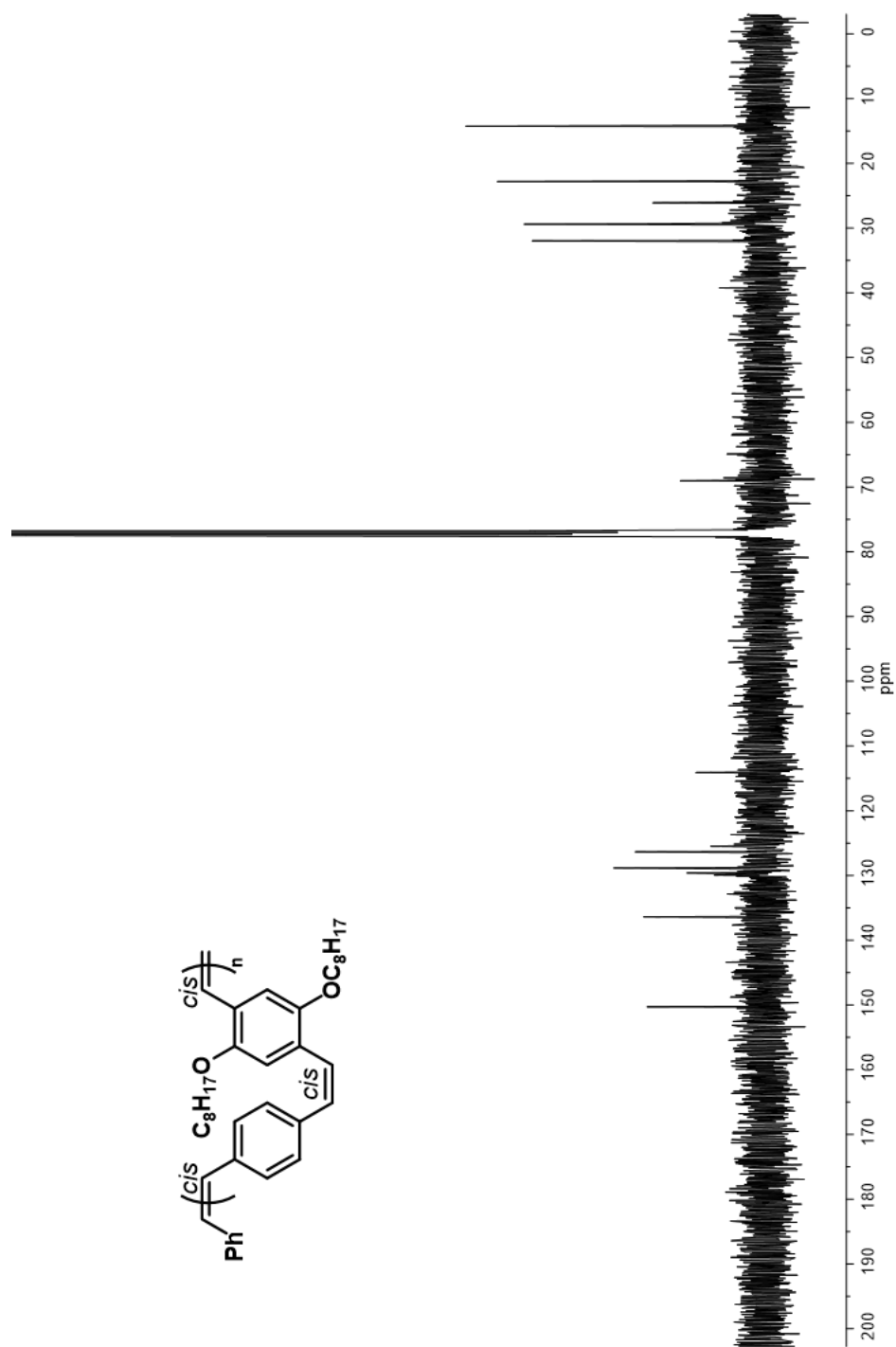
Figure II-10. ^{13}C NMR (101 MHz, CDCl$_3$) spectrum of all-*cis* poly-**1a**.
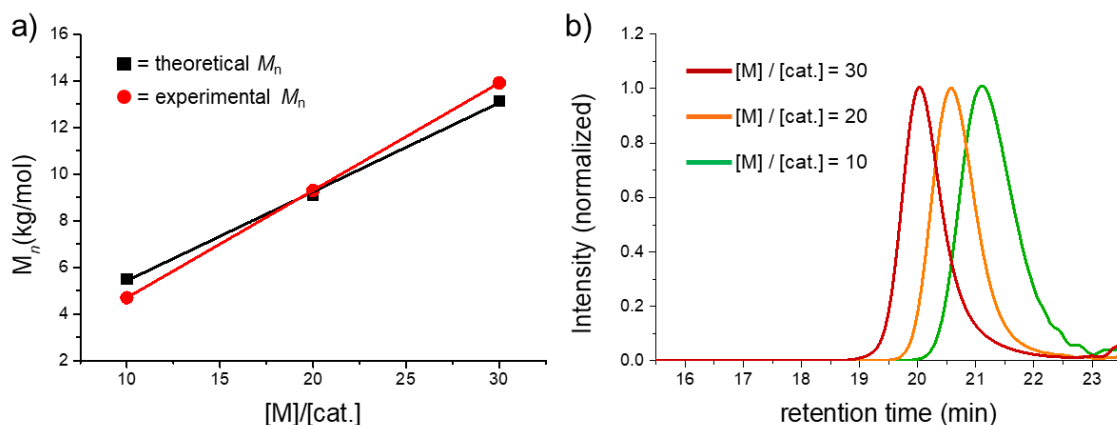
Figure II-11. a) Dependence of the molecular weight (M_n) of all-*cis* poly-**1a** on the ratio **1a**:**Ru-6**. b) GPC traces for three different ratios **1a**:**Ru-6** (THF, RI detection).

Synthesis of all-*cis* poly-**2**
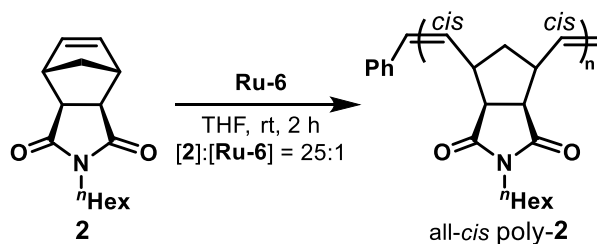
All-*cis* **poly-2**:

^{1}H NMR (400 MHz, CDCl$_3$,) δ 5.58–5.40 (m, 2 H), 3.47–3.37 (m, 2 H), 3.32–2.97 (m, 4 H), 2.27–2.05 (m, 1 H), 1.72–1.58 (m, 1 H), 1.58–1.45 (m, 2 H), 1.33–1.19 (m, 6 H), 0.92–0.79 (m, 3 H) ppm.

^{13}C NMR (100 MHz, CDCl$_3$) δ 178.4, 133.3, 52.6, 41.9, 39.0, 38.9, 31.5, 27.8, 26.7, 26.6, 22.7, 14.2 ppm.

The peaks assignment for this polymer is in agreement with the literature.[25]
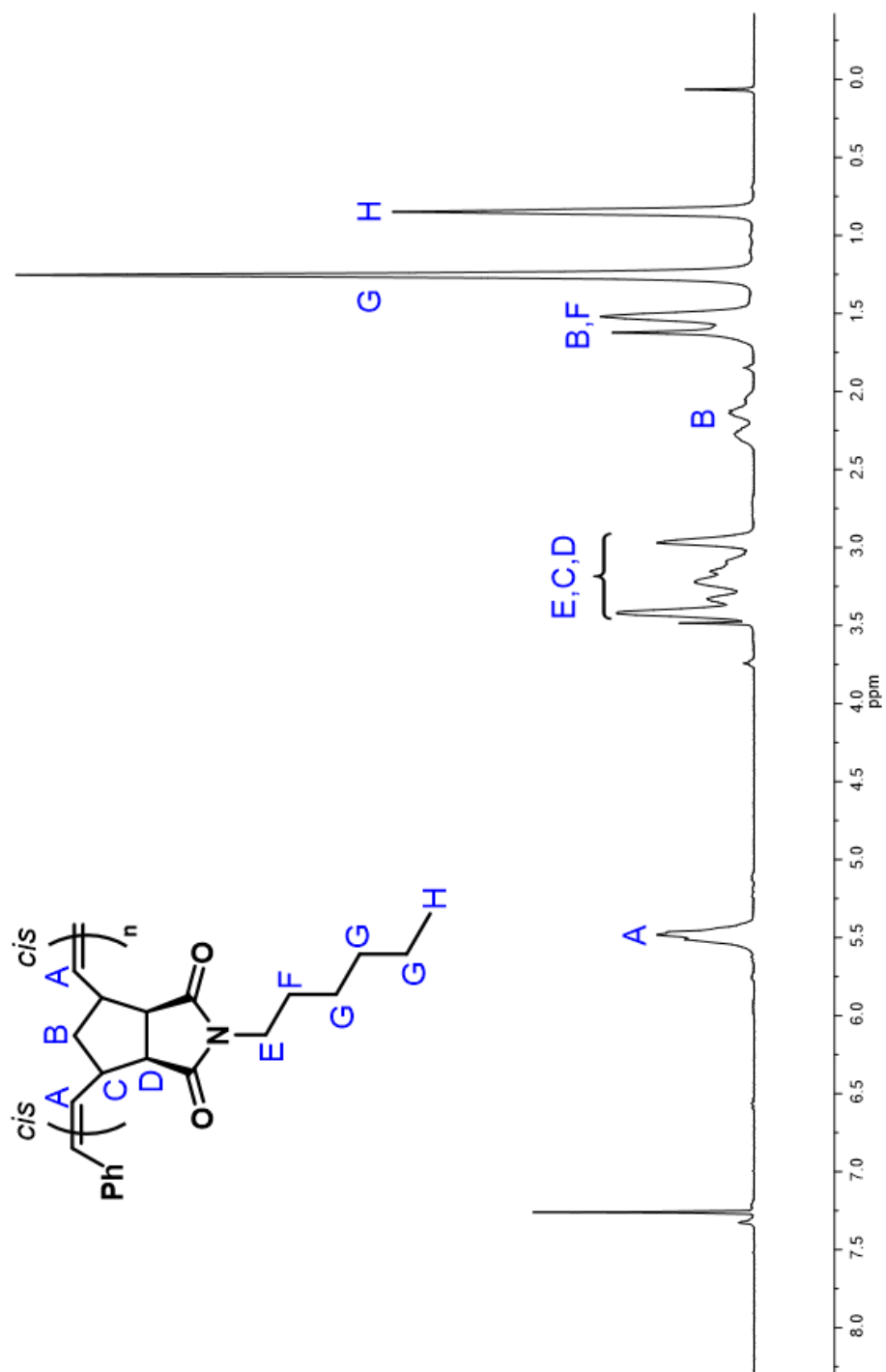
Figure II-12. ^{1}H NMR (400 MHz, CDCl$_3$) spectrum of all-*cis* poly-**2**.
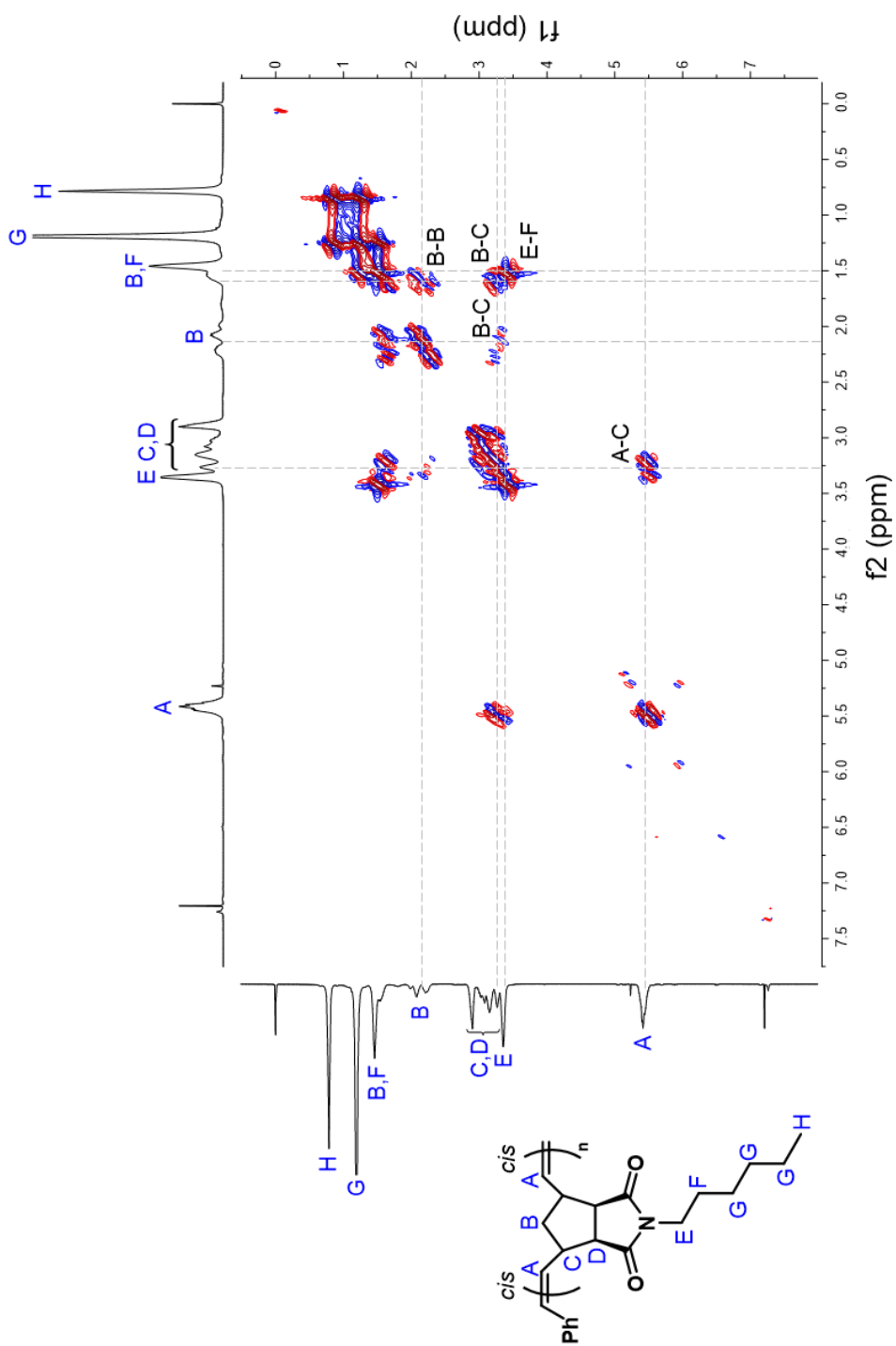
Figure II-13. COSY spectrum of all-*cis* poly-**2**.
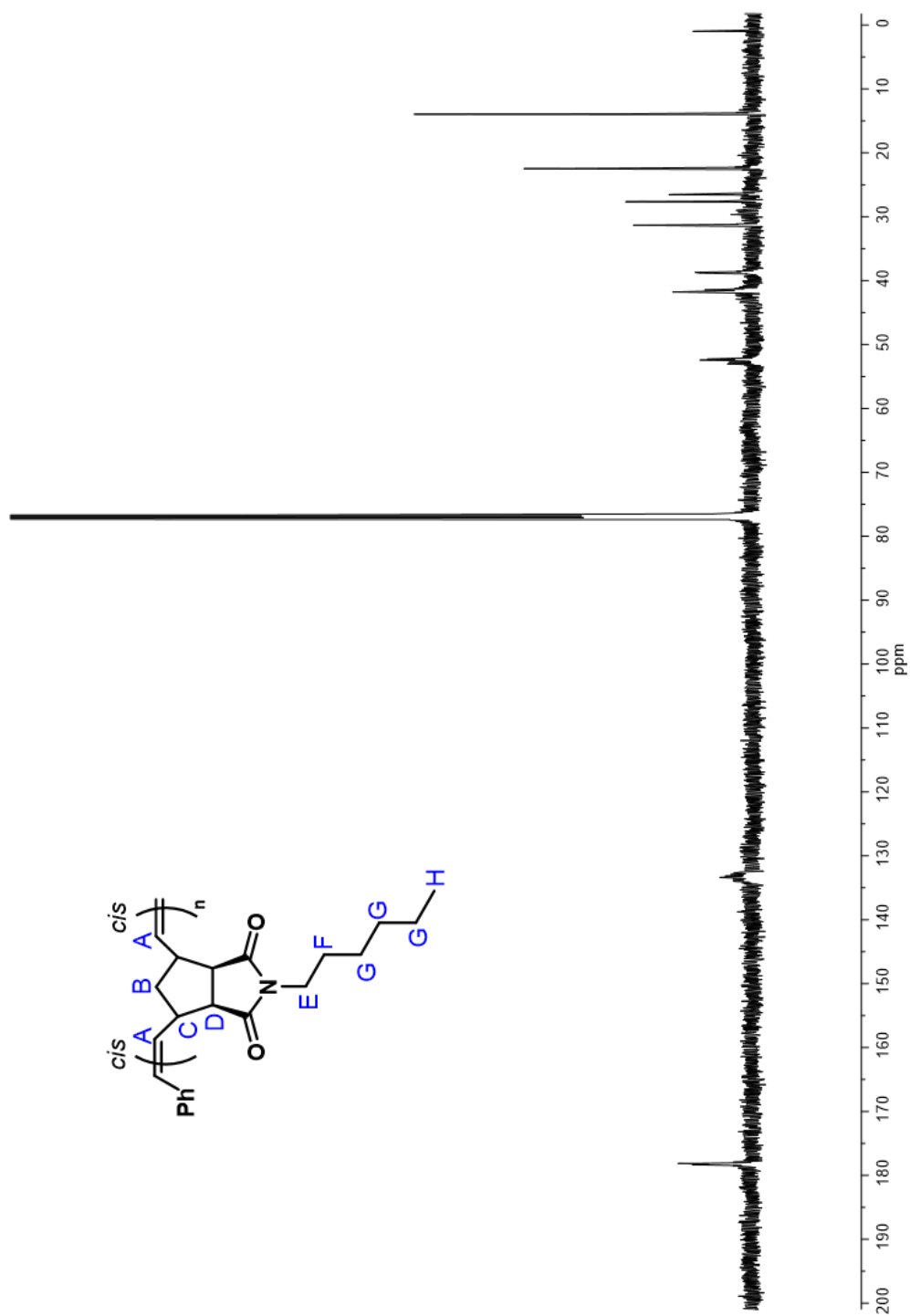
Figure II-14. ^{13}C NMR (101 MHz, CDCl$_3$) spectrum of all-*cis* poly-**2**.
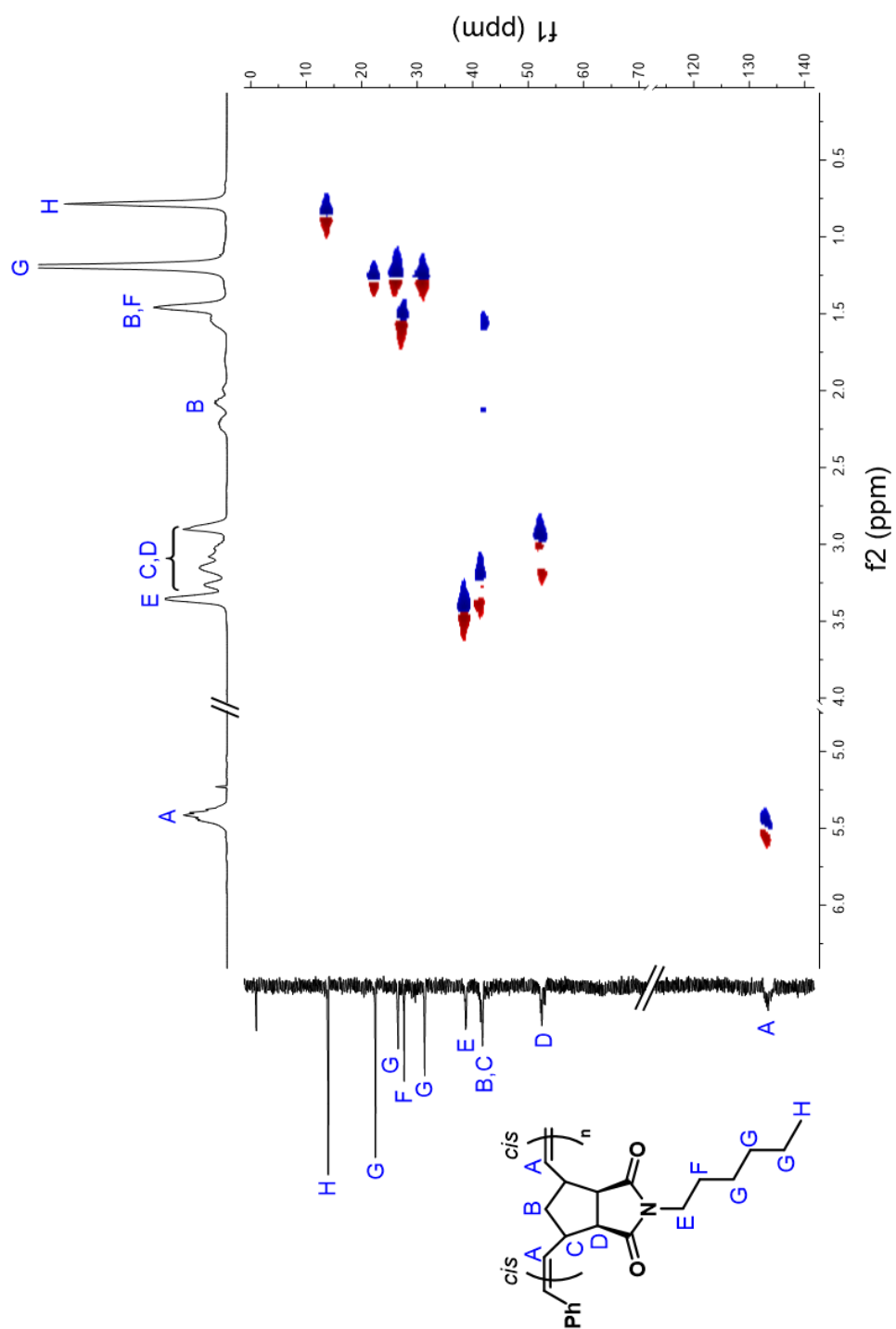
Figure II-15. HSQC spectrum of all-*cis* poly-**2**.

46
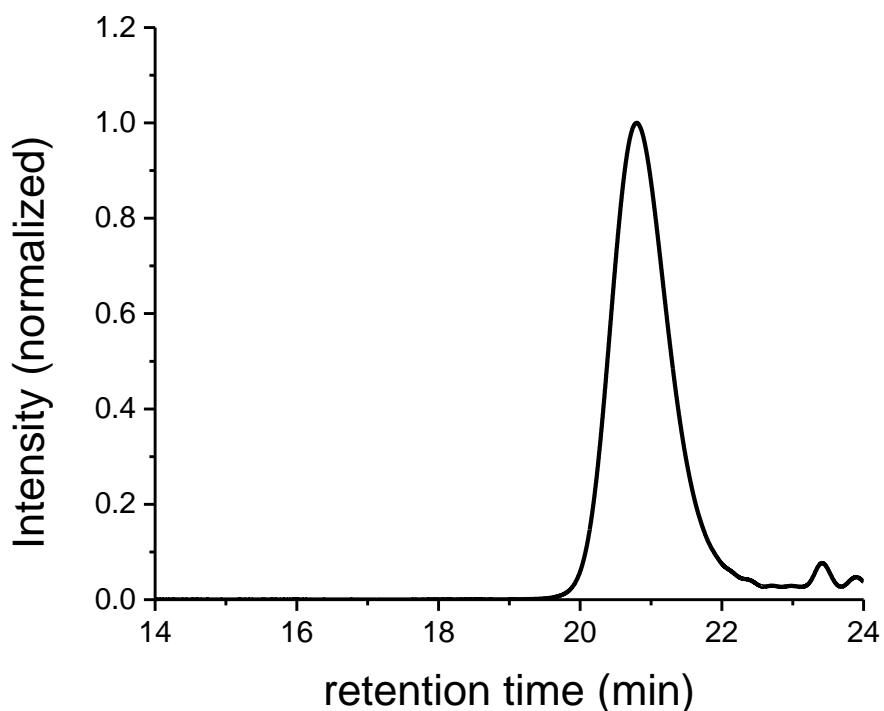
Figure II-16. GPC trace of all-*cis* poly-**2**.

*II.3.6 Study of the Kinetics of the Stereoretentive ROMP Using Monomer **1a** and Catalyst*

***Ru-6** (Figure II-4)*

In a nitrogen-filled glove box, a solution of ruthenium catalyst **Ru-6** (0.6 mM) in deoxygenated THF (2.5 mL) was added into a reaction vial containing monomer **1a** (38.4 μmol) a stir bar. The mixture was stirred at room temperature and aliquots were sampled from the reaction solution over time. Each aliquot was quenched with ethyl vinyl ether (0.05 mL) and stirred for an additional 30 min at room temperature. The molecular weight (M_n) and dispersity values ($Đ$) were determined by SEC analysis for each aliquot, and the monomer conversion was monitored by ^{1}H NMR.

The investigation of the rates of initiation and propagation

A solution of **1a** (46.7 μmol) and **Ru-6** (0.9 mM) in d_8-THF (1.5 mL) was prepared in a nitrogen-filled glovebox and transferred into a J. Young tube kept at room temperature without stirring. Activation of catalyst **Ru-6** and conversion of **1a** were monitored by ^{1}H NMR. It was found that all catalyst **Ru-6** was activated by the time the first NMR spectrum could be collected (Figure II-17). In order to determinate the rate of propagation, the ratio of the dioctyloxy aromatic protons of monomer **1a** (5.77 ppm in d_8-THF) to the dioctyloxy aromatic protons of polymer **poly-1a** (6.80 ppm in d_8-THF) was measured to access the conversion of **1a**.

$$-\frac{d[M]}{dt} = k_p^{app}[M_t] \qquad (1)$$
$$k_p^{app} = k_p[C_t] \qquad (2)$$
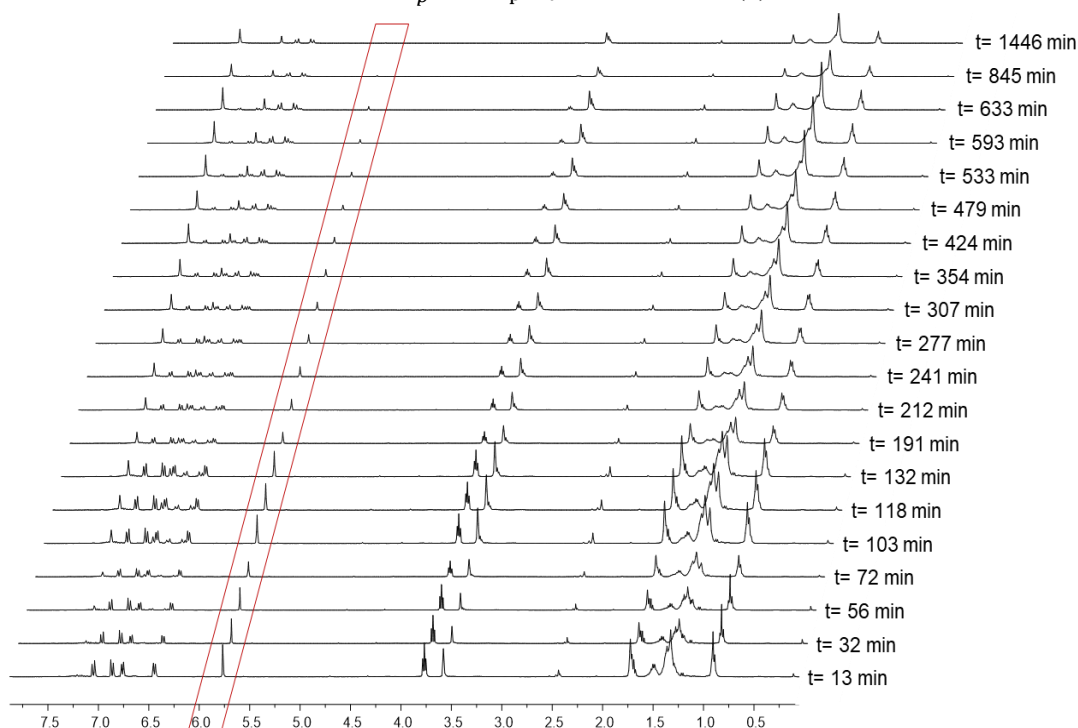
Figure II-17 Monitoring the polymerization of **1a** with catalyst **Ru-6** over time using ^{1}H NMR (400 MHz, d_8-THF) analysis.
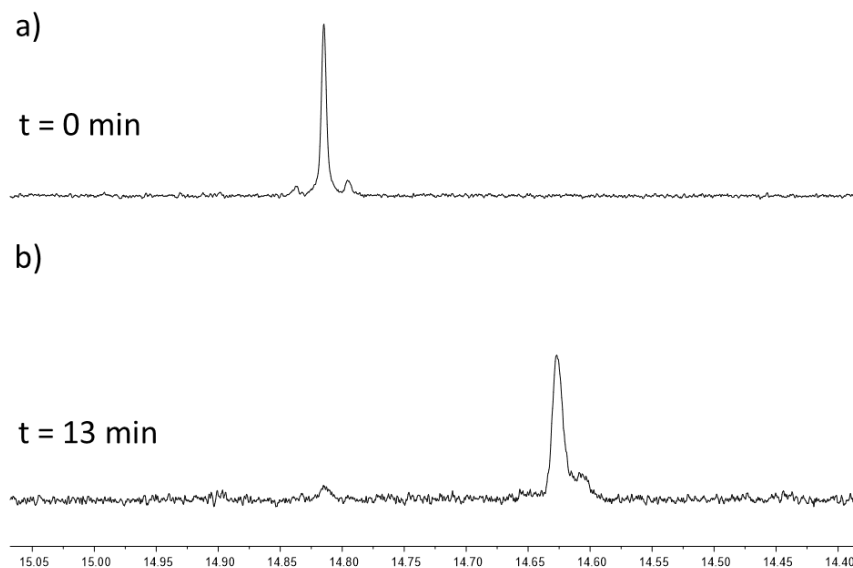
Figure II-18. ^{1}H NMR signals corresponding to the Ru-alkylidene proton for a) catalyst **Ru-6** before activation with **1a** and b) catalyst **Ru-6** after activation with **1a**.

II.3.7 Synthesis of Block Copolymers
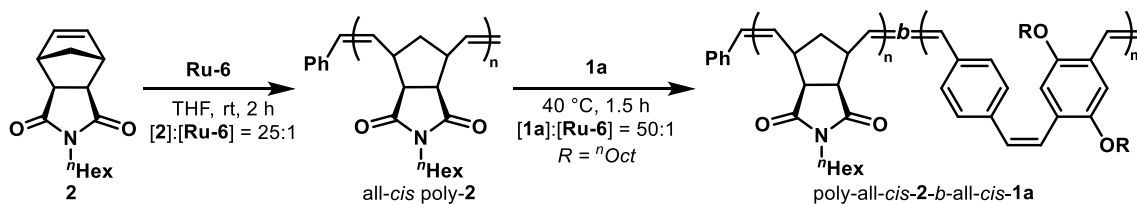
poly-all-*cis*-2-*b*-all-*cis*-1a

poly-all-*cis*-**2**-*b*-all-*cis*-**1a**. In a nitrogen filled glove box, a solution of ruthenium catalyst **Ru-6** in deoxygenated THF (3 mM) was added into a reaction vial charged with monomer **2** and a stir bar. The reaction was stirred in the glovebox at room temperature for 2 h until full monomer conversion was reached. The mixture was then transferred to another reaction vial charged with monomer **1a** and a stir bar. The vial was hermetically sealed

with a cap and parafilm and taken out of the glovebox. The mixture was stirred at room temperature for 5 min and placed into a preheated oil bath at 40 °C for 1.5 h in the dark. Once cooled to room temperature, the reaction was quenched by ethyl vinyl ether (0.1 mL) and stirred for an additional 30 min at room temperature. The solution was diluted to 1.5 mg/mL with THF, filtered, and then injected to GPC instrument directly. The remaining polymer was precipitated upon addition of methanol and the solid was isolated by centrifugation and decantation. The resulting polymer was dried under high vacuum. The polymers were stored in vials wrapped with foil and kept away from light.

^{1}H NMR (400 MHz, CDCl$_3$) δ 7.20 (s, 4 H), 6.76 (s, 2 H), 6.64 (d, J = 12.3 Hz, 2 H), 6.50 (d, J = 12.3 Hz, 2 H), δ 5.59–5.39 (m, 2 H), 3.53 (t, J = 6.5 Hz, 4 H), 3.47–3.37 (m, 2 H), 3.37–2.89 (m, 4 H), 2.34–2.02 (m, 1 H), 1.33–1.20 (m, 30 H), 0.90–0.82 (m, 9 H) ppm.

^{13}C NMR (101 MHz, CDCl$_3$) δ 178.5, 178.4, 178.2, 150.3, 136.4, 133.5, 129.6, 128.8, 126.4, 125.5, 114.1, 69.0, 52.6, 52.4, 41.9, 41.6, 39.0, 38.9, 32.0, 31.5, 29.4, 29.4, 27.8, 26.7, 26.6, 26.1, 22.8, 22.6, 14.2, 14.1 ppm.
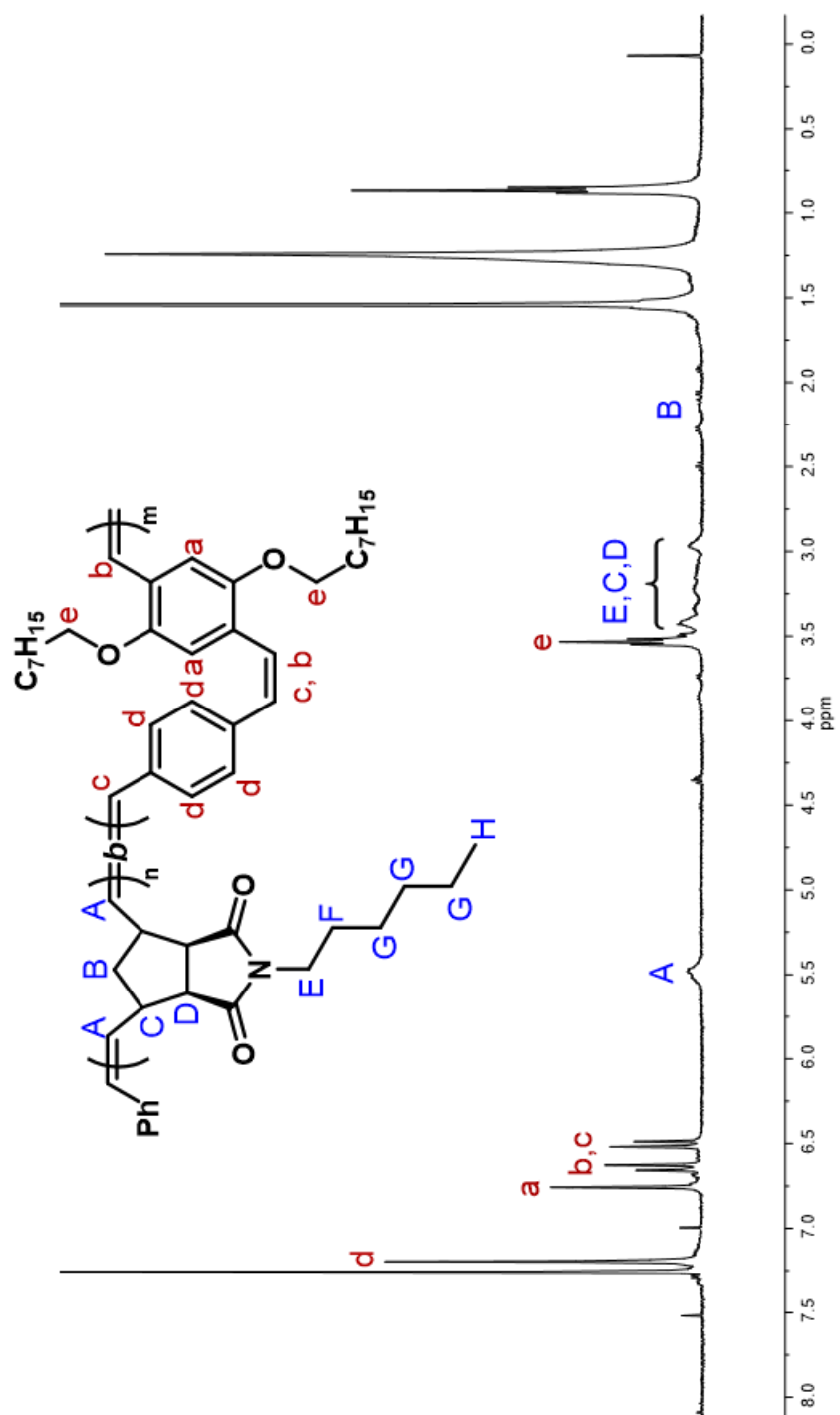
Figure II-19. ^{1}H NMR (400 MHz, CDCl$_3$) spectrum of poly-all-*cis*-**2**-*b*-all-*cis*-**1a**.

51
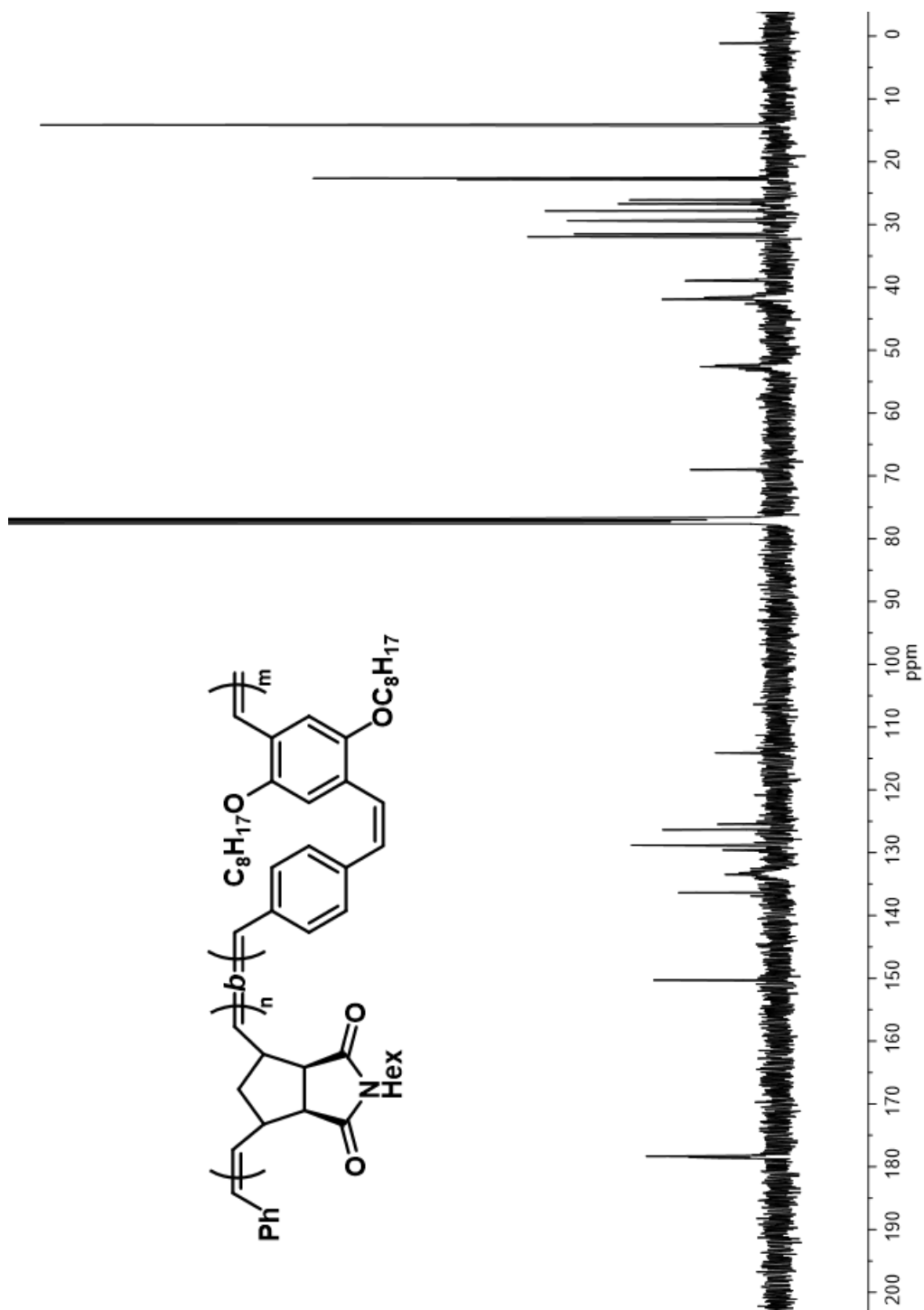
Figure II-20. ^{13}C NMR (101 MHz, CDCl$_3$) spectrum of poly-all-*cis*-**2**-*b*-all-*cis*-**1a**.
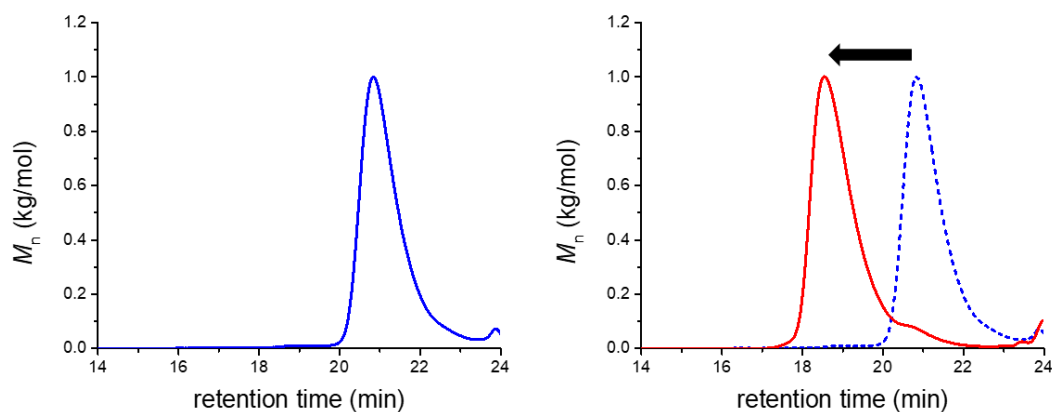
Figure II-21. GPC traces of all-*cis* poly-**2** (blue) and poly-all-*cis*-**2**-*b*-all-*cis*-**1a** (red) after chain extension.

poly-all-*cis*-1a-*b*-all-*cis*-2
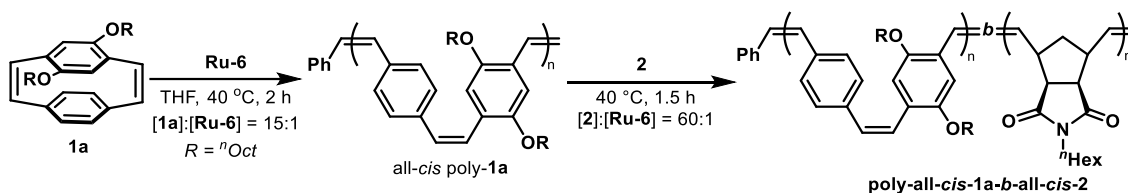
poly-all-*cis*-**2**-*b*-all-*cis*-**1a**. In a nitrogen filled glove box, a solution of ruthenium catalyst **Ru-6** in deoxygenated THF (3 mM) was added into a reaction vial charged with monomer **1a** and a stir bar. The vial was hermetically sealed with a cap and parafilm and taken out of the glovebox. The mixture was stirred at room temperature for 5 minutes and placed into a preheated oil bath at 40 °C for 2 h in the dark. The vial was then taken into the glovebox, and the mixture was transferred to another reaction vial charged with monomer **2** and a stir bar. The vial was hermetically sealed with a cap and parafilm and taken out of the glovebox. The mixture was stirred at room temperature for 5 min and placed into a preheated oil bath at 40 °C for 1.5 h in the dark. Once cooled to room temperature, the reaction was quenched by ethyl vinyl ether (0.1 mL) and stirred for an additional 30 min

53

at room temperature. The solution was diluted to 1.5 mg/mL with THF, filtered, and then injected to GPC instrument directly. The remaining polymer was precipitated upon addition of methanol and the solid was isolated by centrifugation and decantation. The resulting polymer was dried under high vacuum. The polymers were stored in vials wrapped with foil and kept away from light.

^{1}H NMR (400 MHz, CDCl$_3$) δ 7.20 (s, 4 H), 6.76 (s, 2 H), 6.66 (d, J = 12.3 Hz, 2 H), 6.52 (d, J = 12.3 Hz, 2 H), δ 5.59–5.39 (m, 17 H), 3.53 (t, J = 6.5 Hz, 4H), 3.48–3.37 (m, 17H), 3.37–3.05 (m, 24 H), 3.02–2.89 (m, 10 H), 2.36–2.01 (m, 8 H), 1.33–1.20 (m, 86 H), 0.91–0.81 (m, 37 H) ppm.
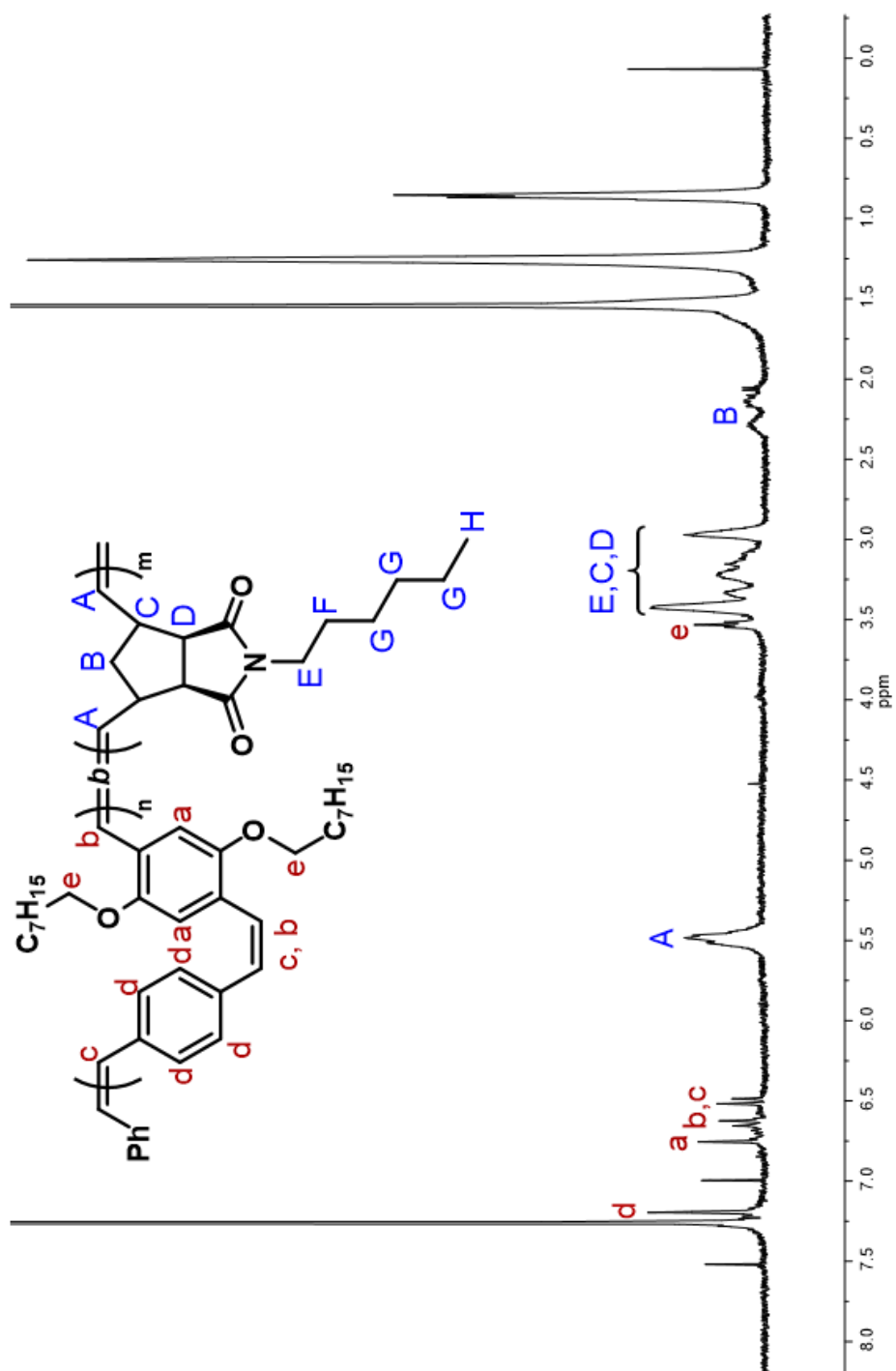
Figure II-22. ^{1}H NMR (400 MHz, CDCl$_3$) spectrum of poly-all-*cis*-**1a**-b-all-*cis*-**2**.
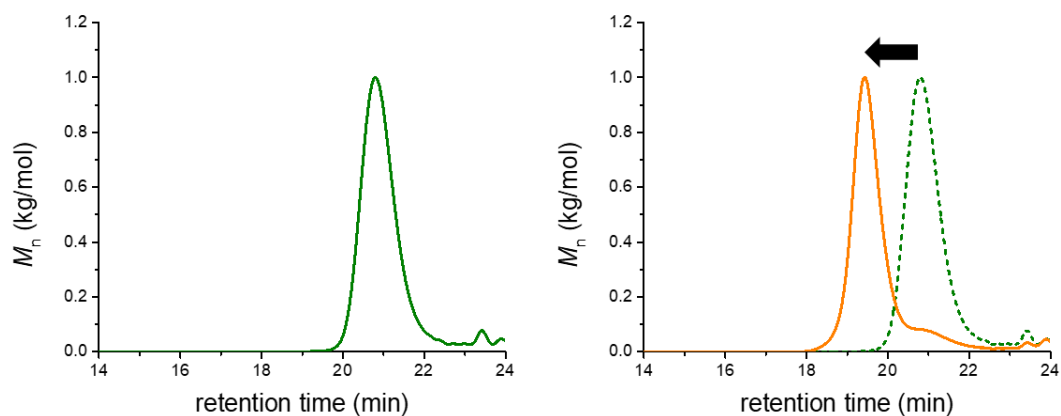
Figure II-23. GPC traces of all-*cis* poly-**1a** (green) and poly-all-*cis*-**1a**-*b*-all-*cis*-**2** (orange) after chain extension.

Table II-4. Molecular Weights and Dispersity Values for The Diblock Copolymers Poly-all-*cis*-**2**-*b*-all-*cis*-**1a** and Poly-all-*cis*-**1a**-*b*-all-*cis*-**2**

Block copolymer	n, m	1st block M_n^{theo} (kg/mol)	1st block M_n^{exp} (kg/mol)	Đ	diblok M_n^{theo} (kg/mol)	diblock M_n^{exp} (kg/mol)	Đ
2-*b*-**1a**	25, 50	6.3	6.3	1.16	29.3	31.2	1.26
1a-*b*-**2**	15, 60	7.0	7.3	1.13	21.8	19.5	1.17

M_n's and Đ's were determined by SEC (THF) using polystyrene standards (RI detection).

II.3.8 cis *to* trans *Photoisomerization*

Solutions of homo- or diblock copolymers in THF (0.1 mg/mL) were irradiated by using two 365 nm UV lamps at room temperature for 30 min. After irradiation, aliquots were taken and diluted with THF to 0.2 μg/mL for UV measurement, to 1 μg/mL for fluorescence measurement. No dilution was used for DLS measurement (0.1 mg/mL).
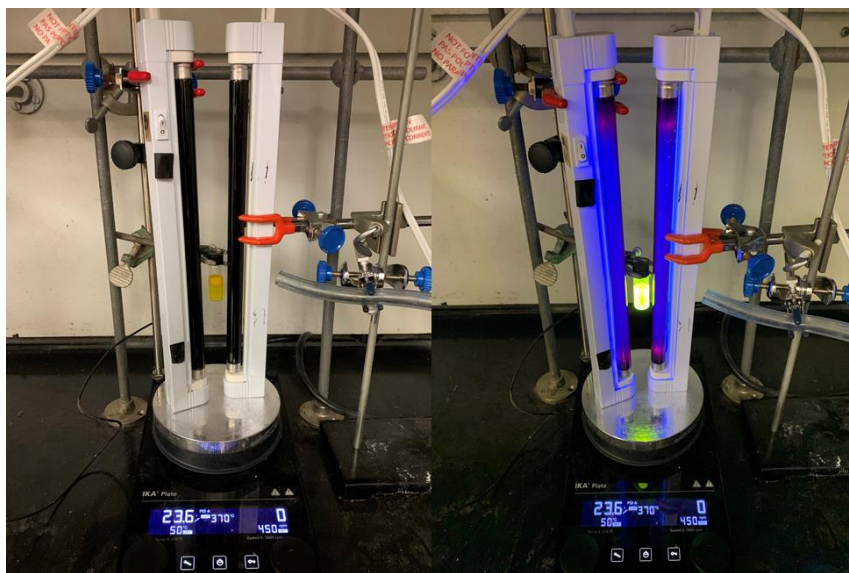
Figure II-24. Set-up of photoisomerization experiments (two 365 nm UV lamps and air flow for cooling).

Homopolymer isomerization

All-*cis* poly-**1a** to all-*trans* poly-**1a**:
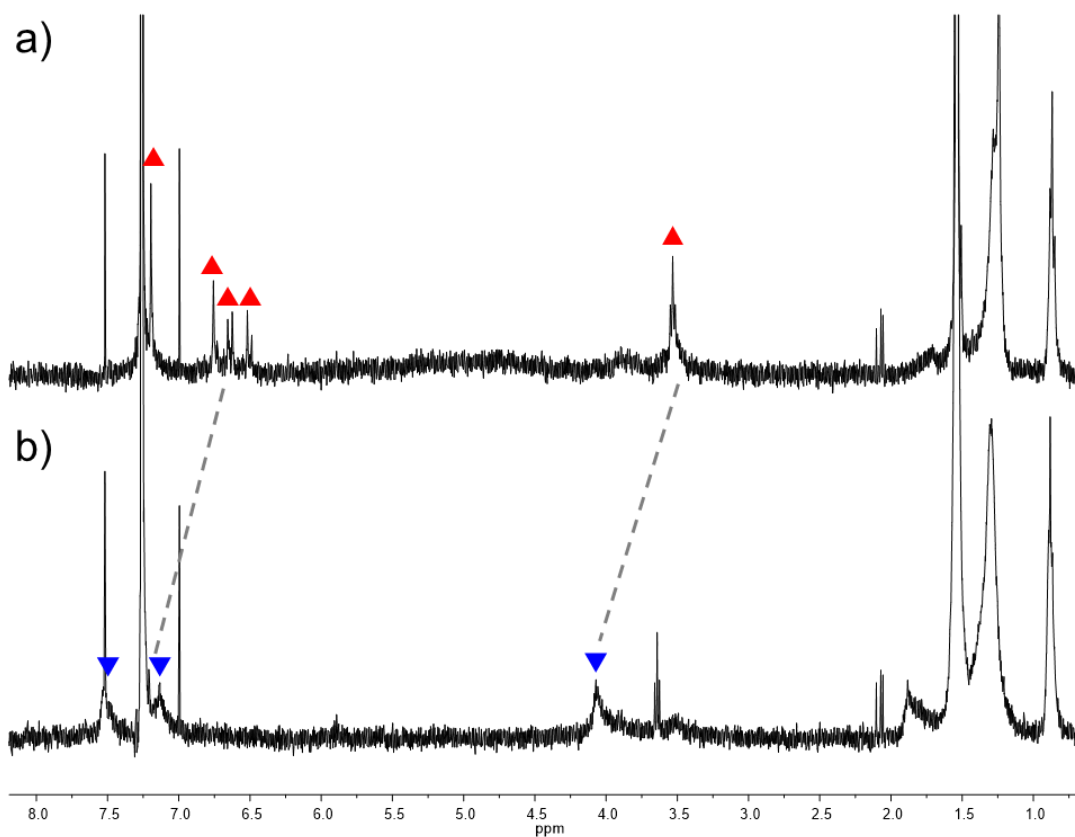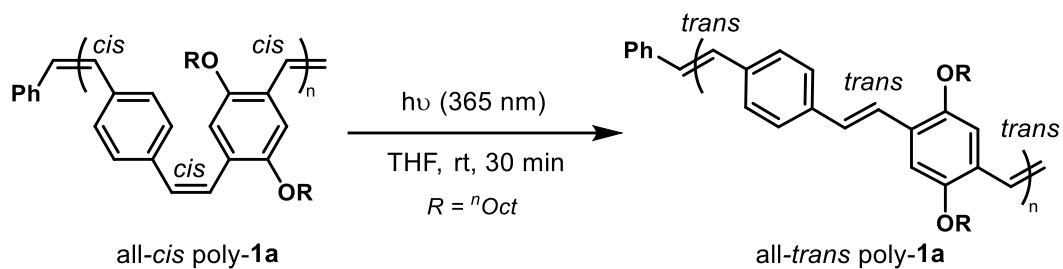
Figure II-25. ^{1}H NMR (400 MHz, CDCl$_3$) spectra of a) all-*cis* poly-**1a**; b) all-*trans* poly-**1a** after irradiation.
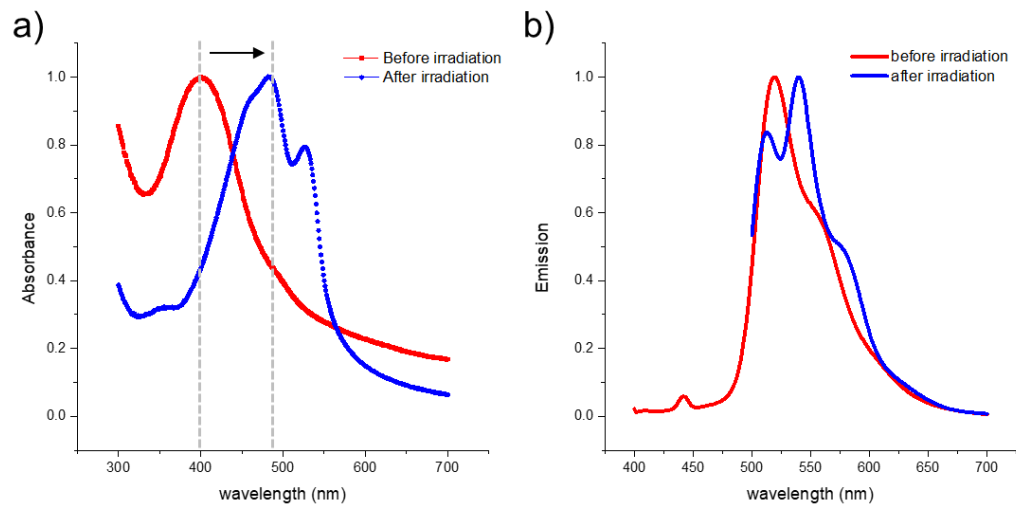
Figure II-26. a) UV spectra of all-*cis* poly-**1a** (red) and all-*trans* poly-**1a** (blue) after irradiation. b) Fluorescence spectra of all-*cis* poly-**1a** (red) and all-*trans* poly-**1a** (blue) after irradiation.

Diblock copolymer isomerization

Poly-all-*cis*-**2**-*b*-all-*cis*-**1a** to poly-all-*cis*-**2**-*b*-all-*trans*-**1a**:
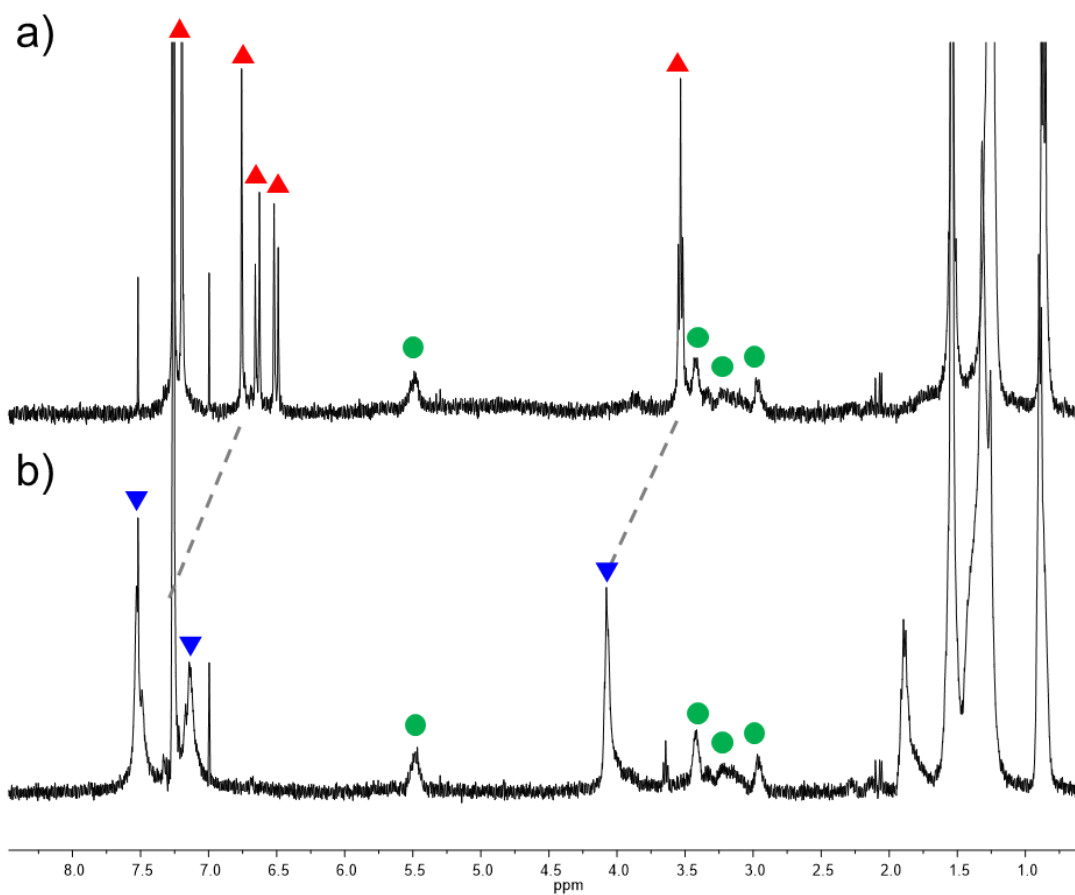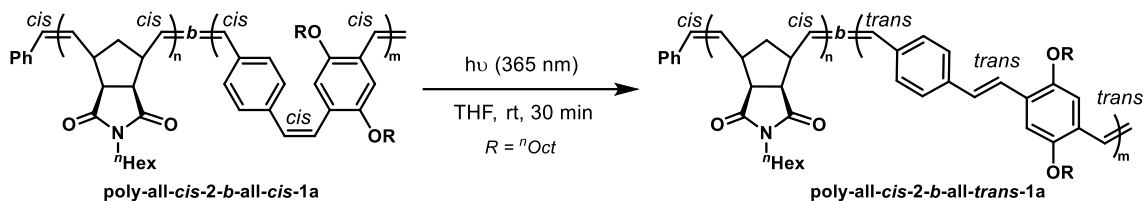
Figure II-27. ^{1}H NMR (400 MHz, CDCl$_3$) spectra of a) poly-all-*cis*-**2**-*b*-all-*cis*-**1a**; b) poly-all-*cis*-**2**-*b*-all-*trans*-**1a** after irradiation.

60
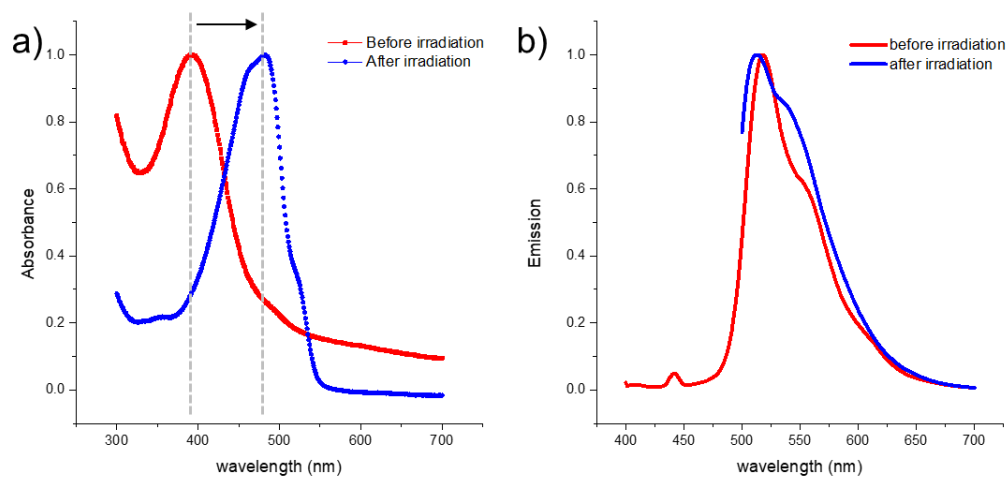
Figure II-28. a) UV spectra of poly-all-*cis*-**2**-*b*-all-*cis*-**1a** (red) and poly-all-*cis*-**2**-*b*-all-*trans*-**1a** (blue) after irradiation. b) Fluorescence spectra of poly-all-*cis*-**2**-*b*-all-*cis*-**1a** (red) and poly-all-*cis*-**2**-*b*-all-*trans*-**1a** (blue) after irradiation.

Poly-all-*cis*-**1a**-*b*-all-*cis*-**2** to Poly-all-*trans*-**1a**-*b*-all-*cis*-**2**:
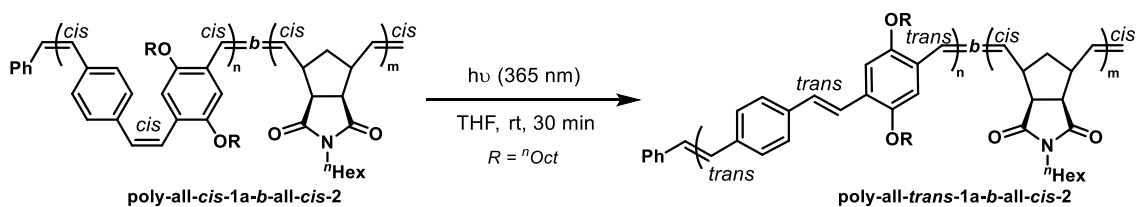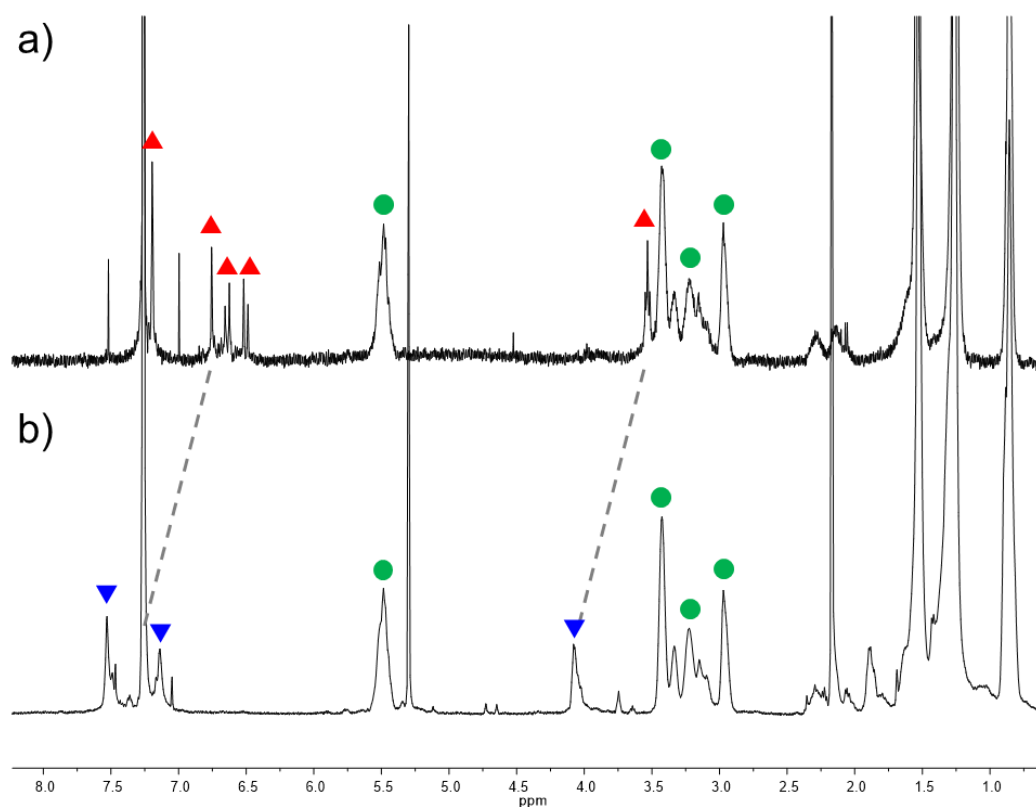
Figure II-29. ^{1}H NMR (400 MHz, CDCl$_3$) spectra of a) poly-all-*cis*-**1a**-*b*-all-*cis*-**2**; b) poly-all-*trans*-**1a**-*b*-all-*cis*-**2** after irradiation.
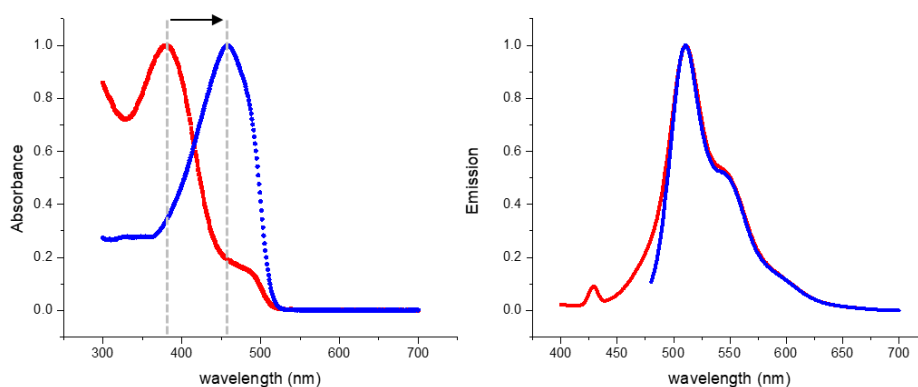
Figure II-30. a) UV spectra of poly-all-*cis*-**1a**-*b*-all-*cis*-**2** (red) and poly-all-*trans*-**1a**-*b*-all-*cis*-**2** (blue) after irradiation. b) Fluorescence spectra of poly-all-*cis*-**1a**-*b*-all-*cis*-**2** (red) and poly-all-*trans*-**1a**-*b*-all-*cis*-**2** (blue) after irradiation.

	Z-average (nm) before	Z-average (nm) after
Homopolymer Poly-**1a**	630	5504
Diblock copolymer Poly-**2**-*b*-**1a**	407	1034
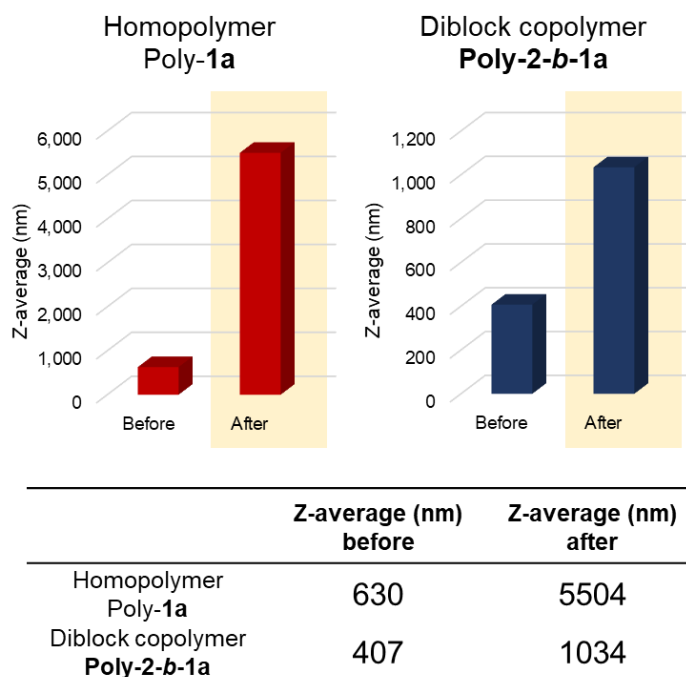
Figure II-31. Dynamic light scattering (DLS) showed an increase of the polymeric particle size after photoisomerization of the PPV block from all-*cis* to all-*trans*.
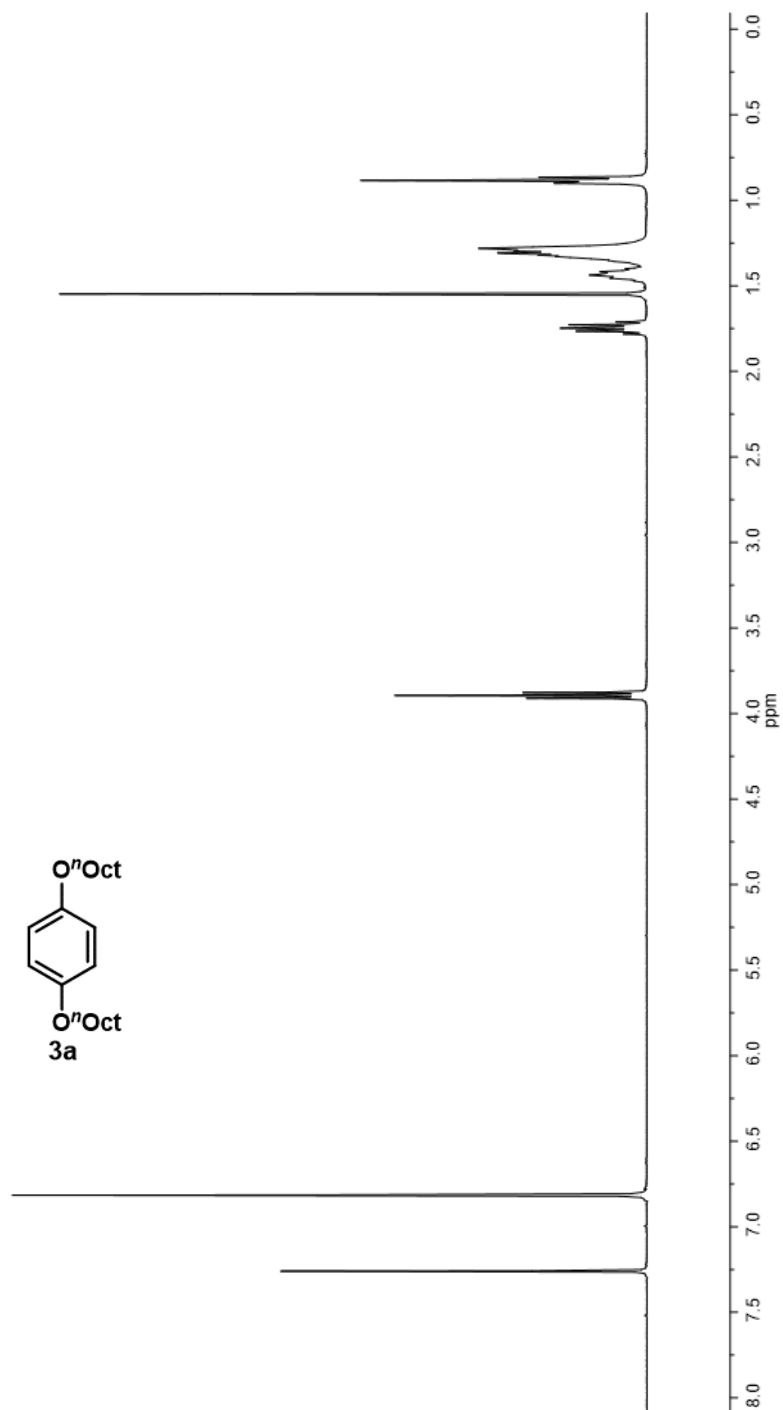
Figure II-32. ^{1}H NMR (400 MHz, CDCl$_3$) spectrum of compound **3a**.
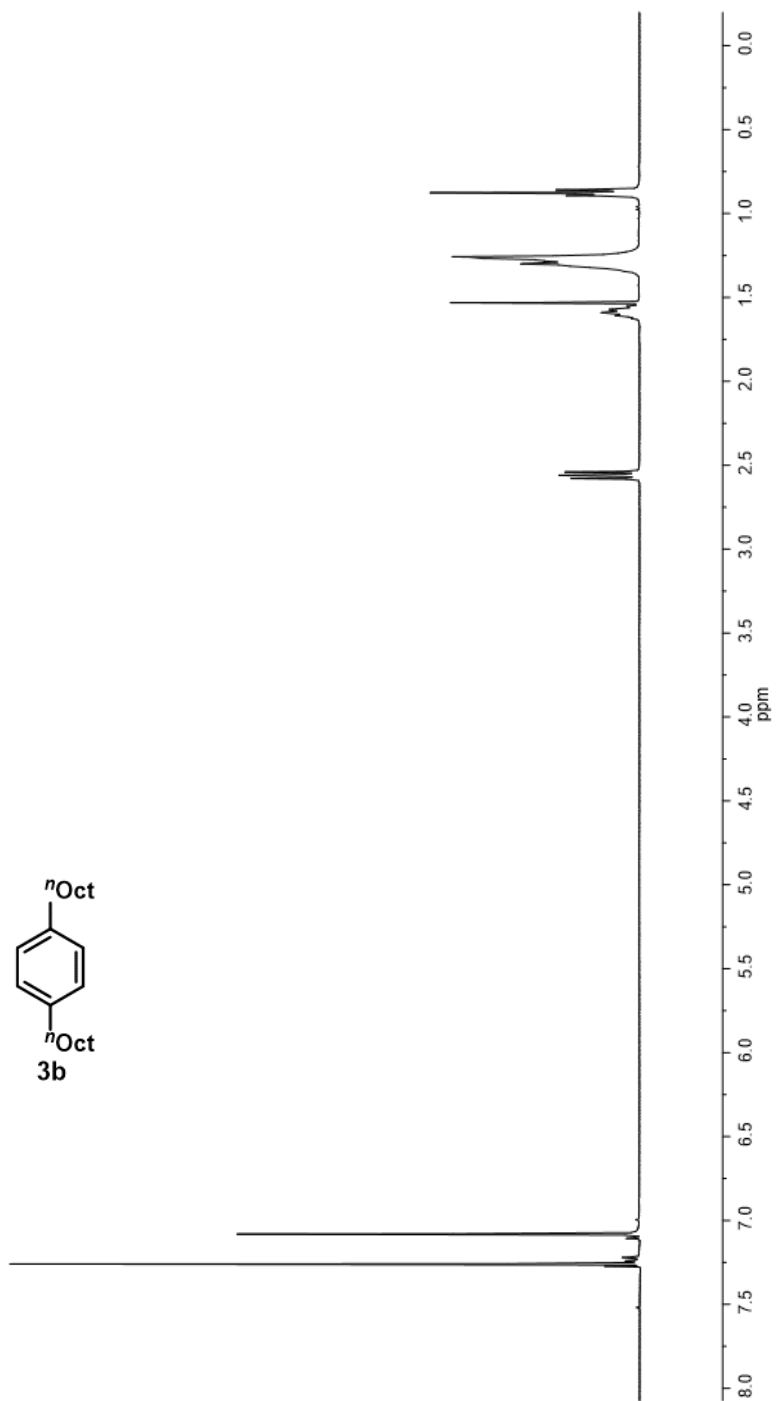
Figure II-33. ^{1}H NMR (400 MHz, CDCl$_3$) spectrum of compound **3b**.
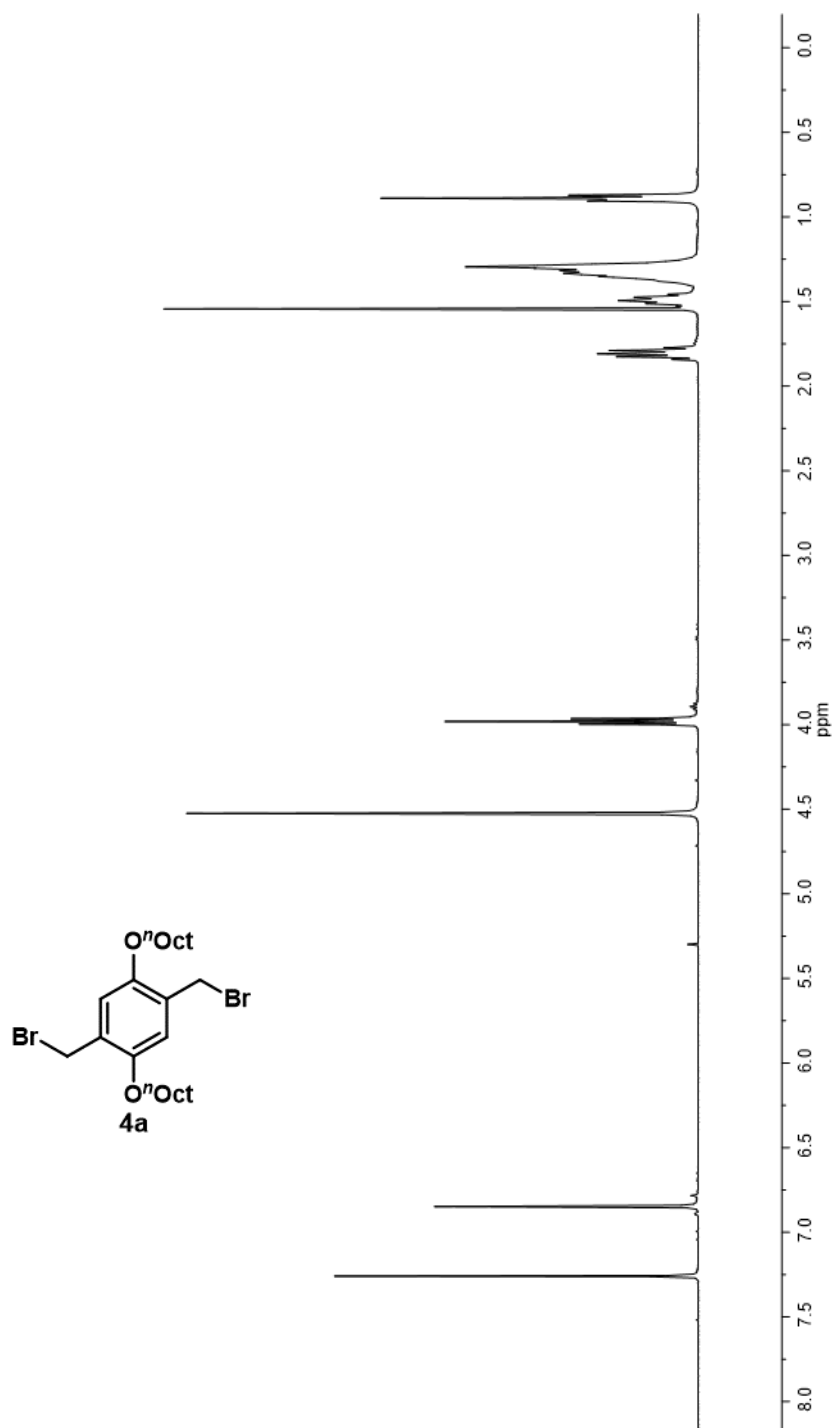
Figure II-34. ^{1}H NMR (400 MHz, CDCl$_3$) spectrum of compound **4a**.
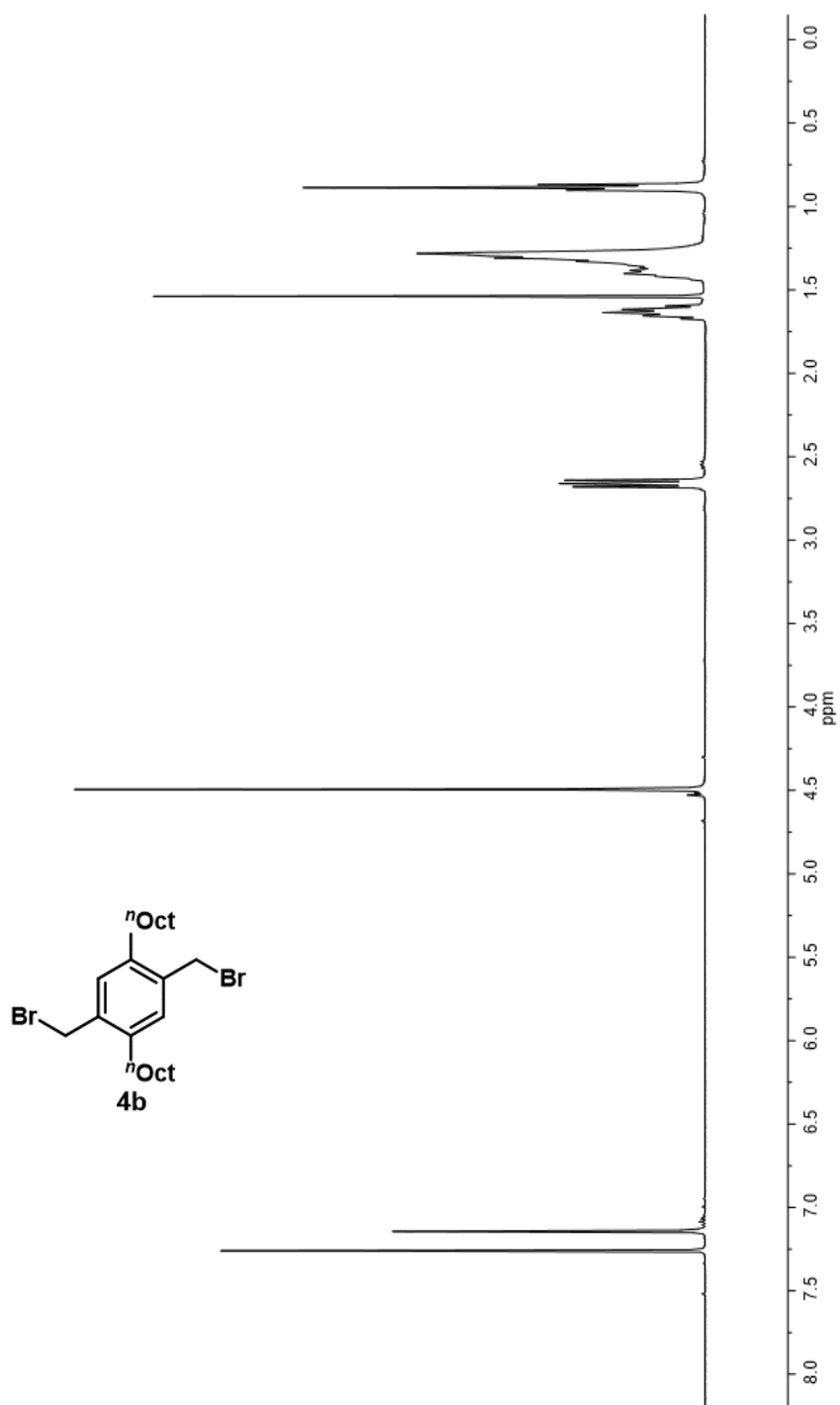
Figure II-35. ^{1}H NMR (400 MHz, CDCl$_3$) spectrum of compound **4b.**

67
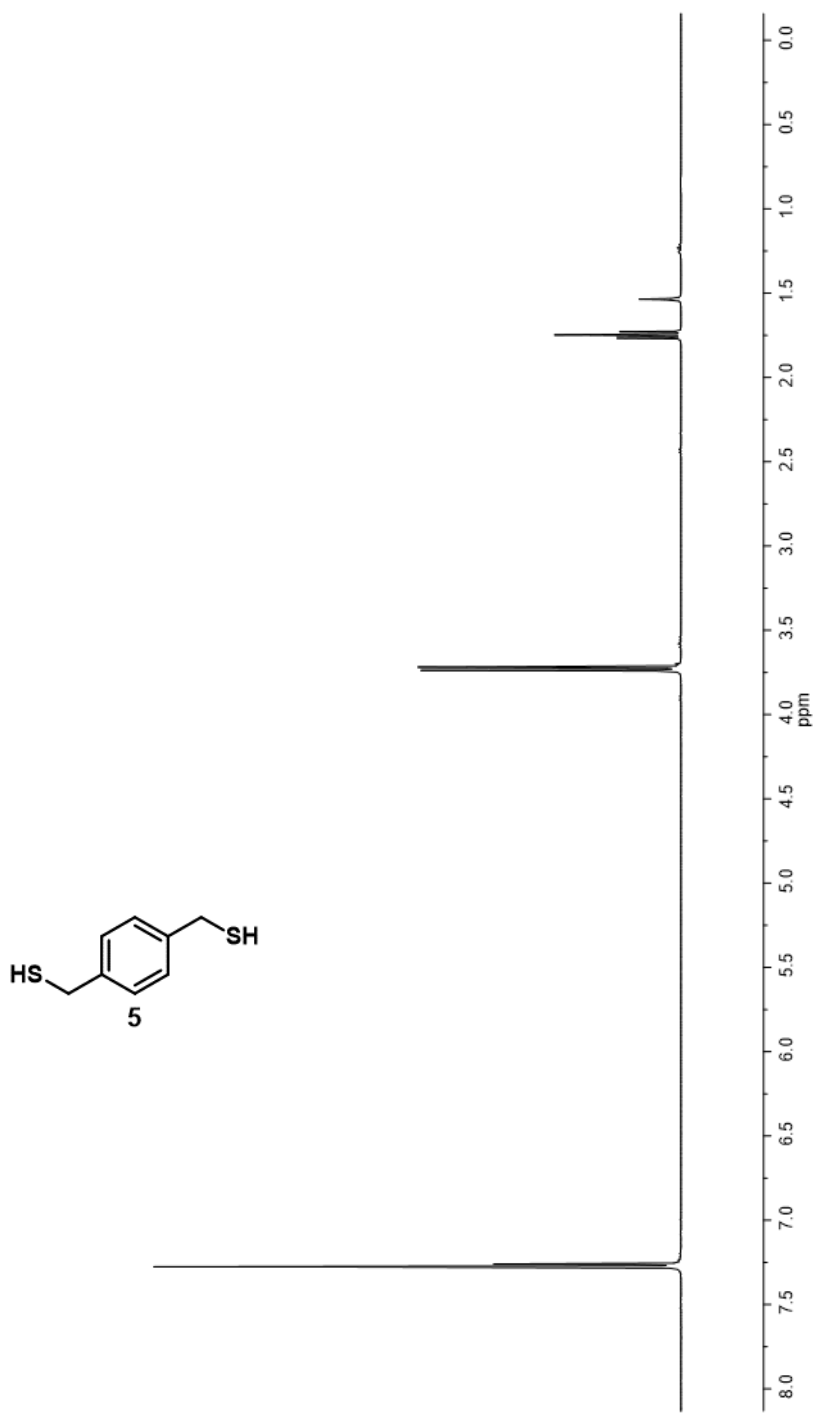
Figure II-36. ^{1}H NMR (400 MHz, CDCl$_3$) spectrum of compound **5**.
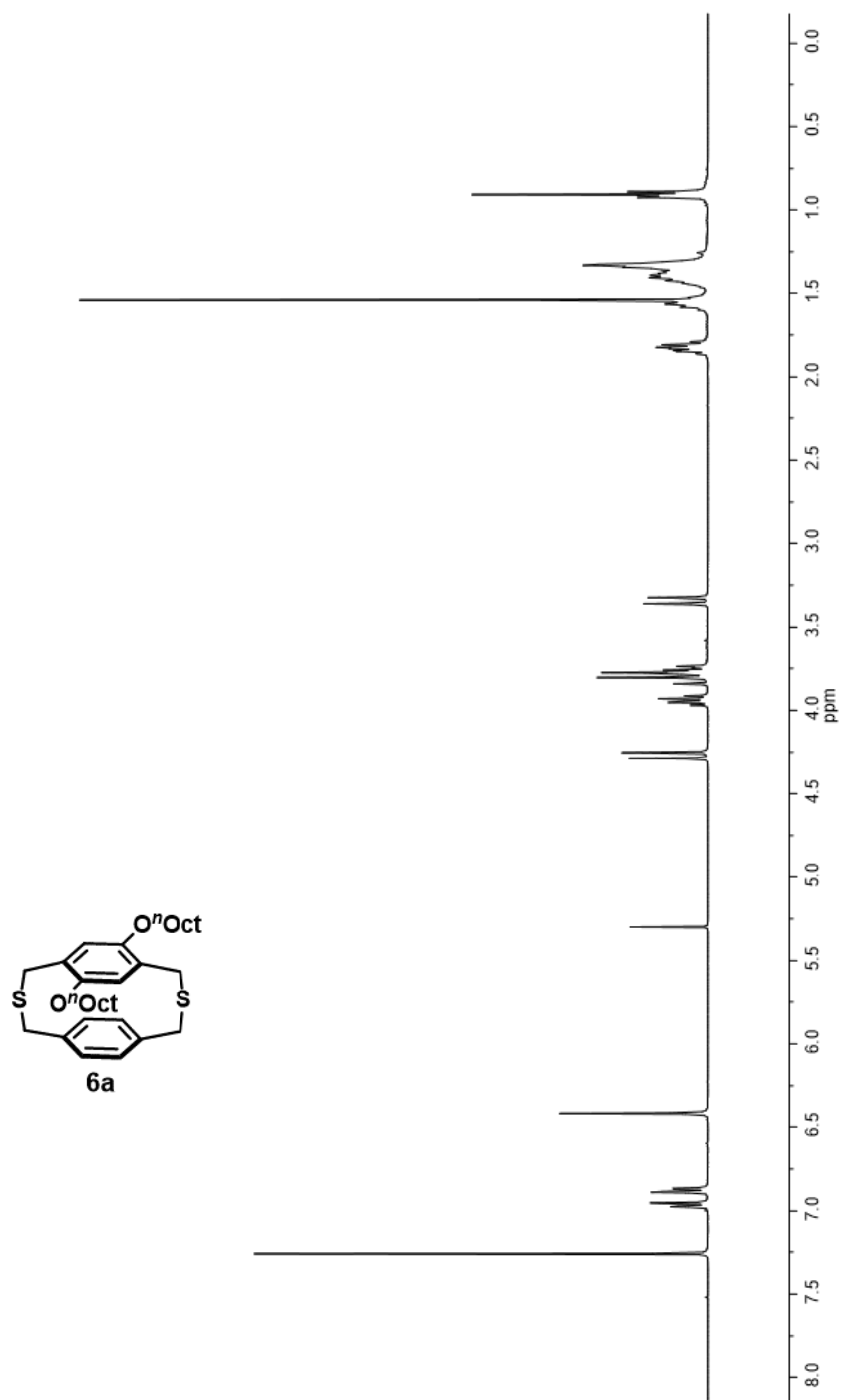
Figure II-37. ^{1}H NMR (400 MHz, CDCl$_3$) spectrum of compound **6a**.
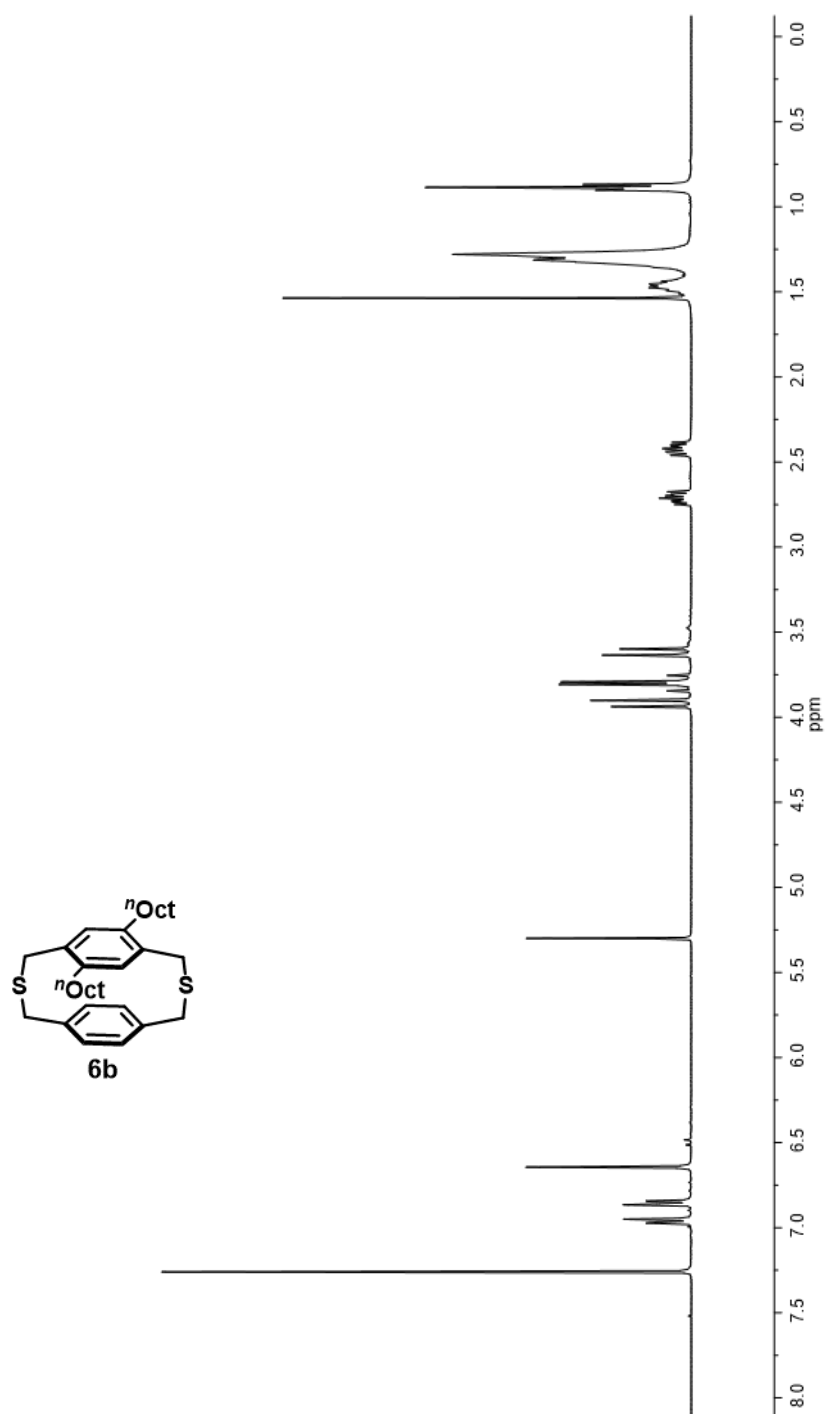
Figure II-38. ^{1}H NMR (400 MHz, CDCl$_3$) spectrum of compound **6b**.
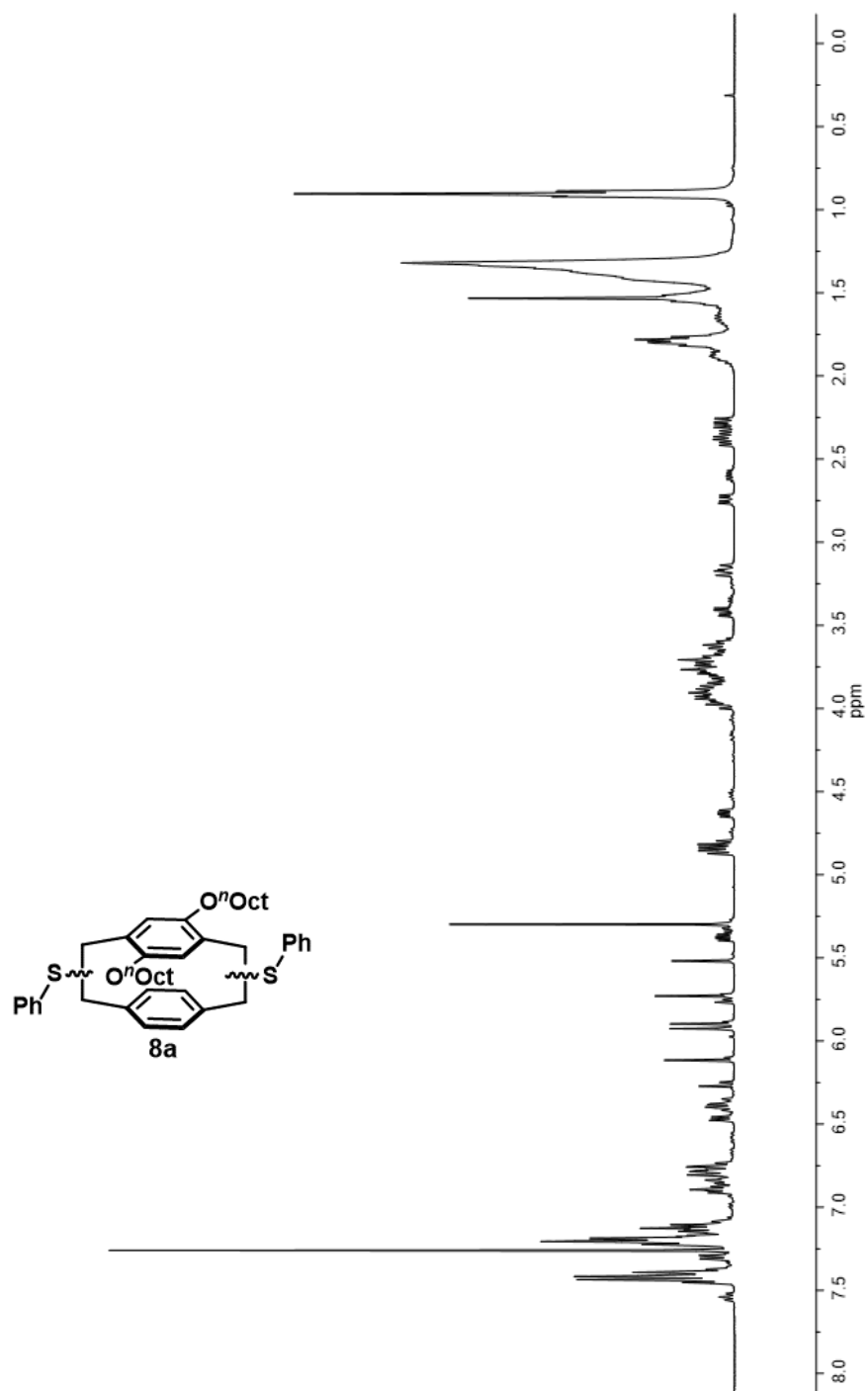
Figure II-39. ^{1}H NMR (400 MHz, CDCl$_3$) spectrum of compound **8a.**
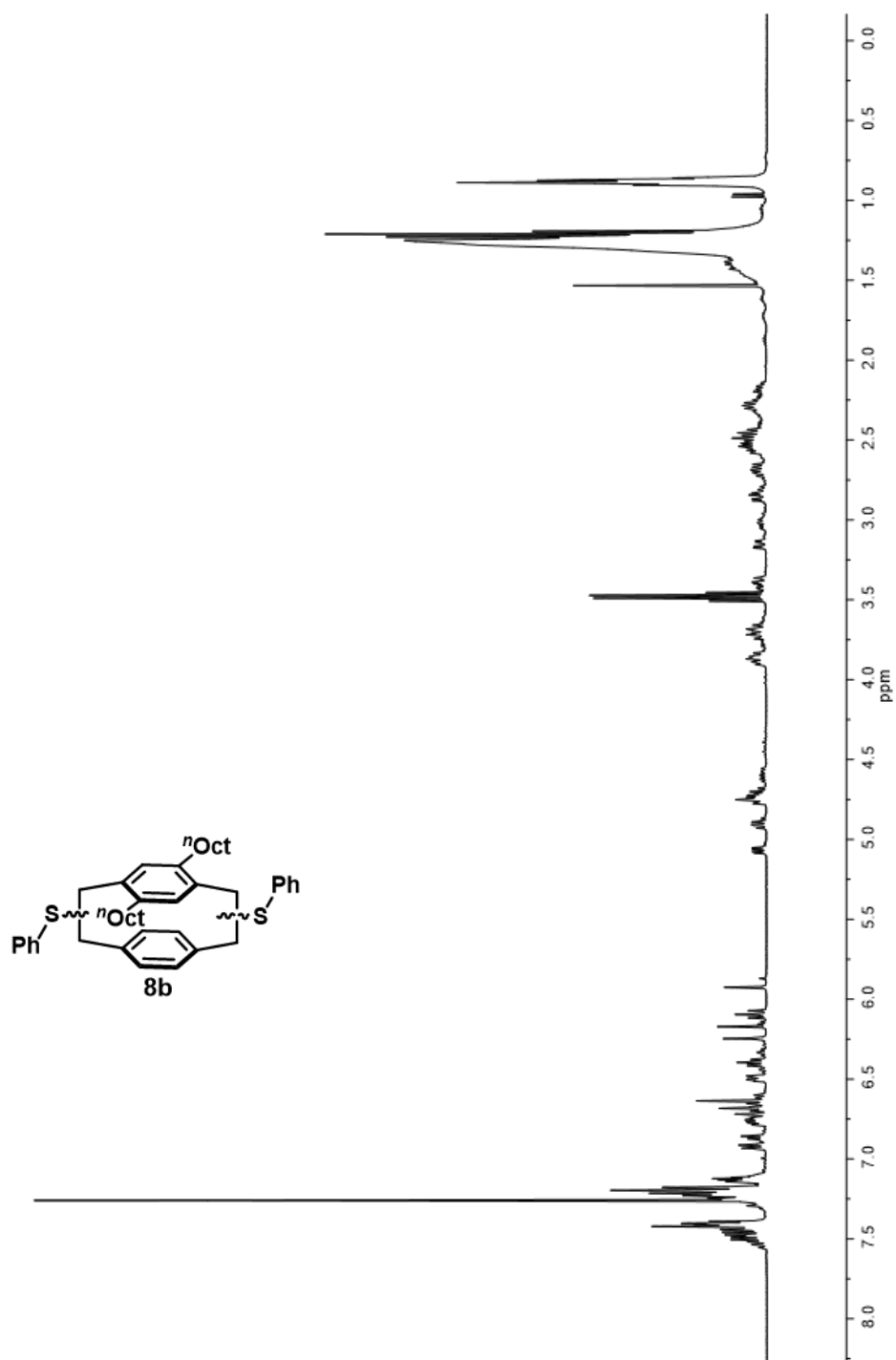
Figure II-40. ^{1}H NMR (400 MHz, CDCl$_3$) spectrum of compound **8b.**
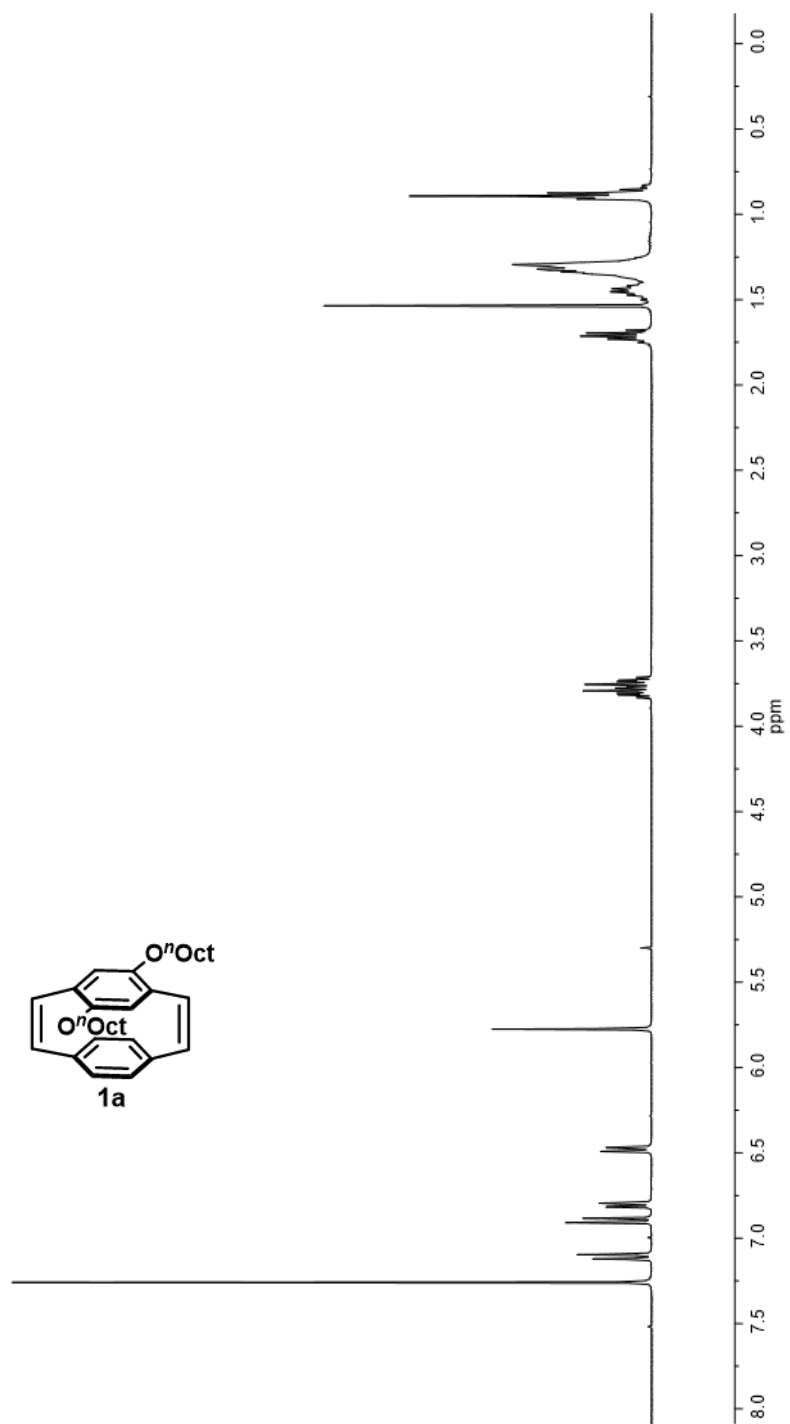
Figure II-41. ^{1}H NMR (400 MHz, CDCl$_3$) spectrum of monomer **1a.**
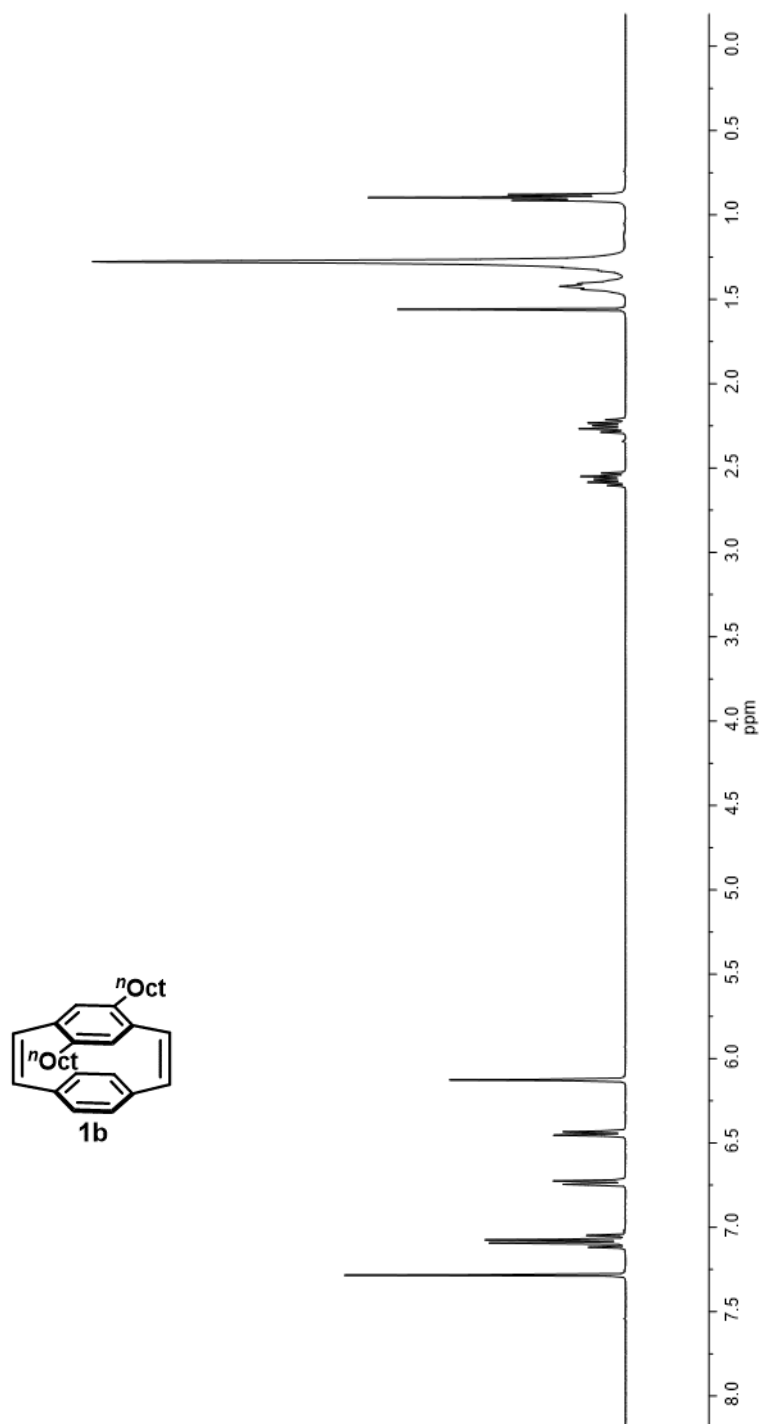
Figure II-42. ^{1}H NMR (400 MHz, CDCl$_3$) spectrum of monomer **1b.**

74
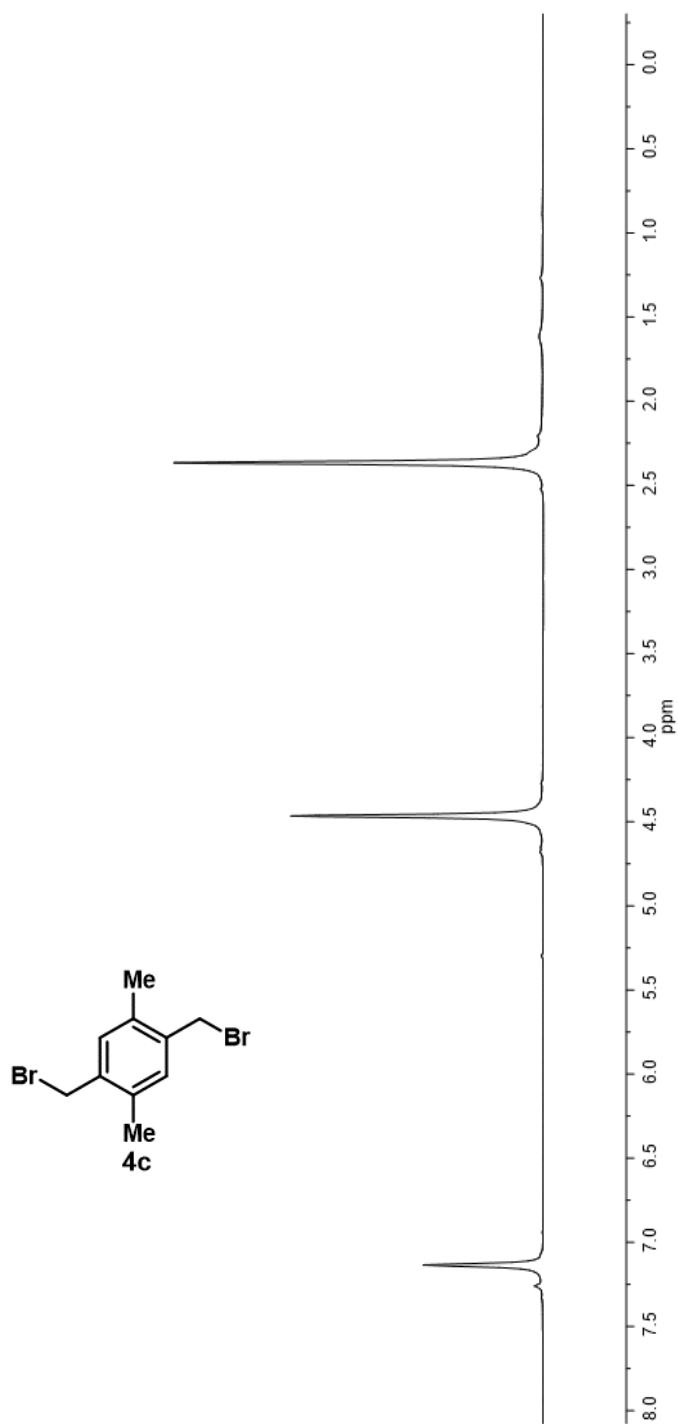
Figure II-43. ^{1}H NMR (400 MHz, CDCl$_3$) spectrum of compound **4c**.
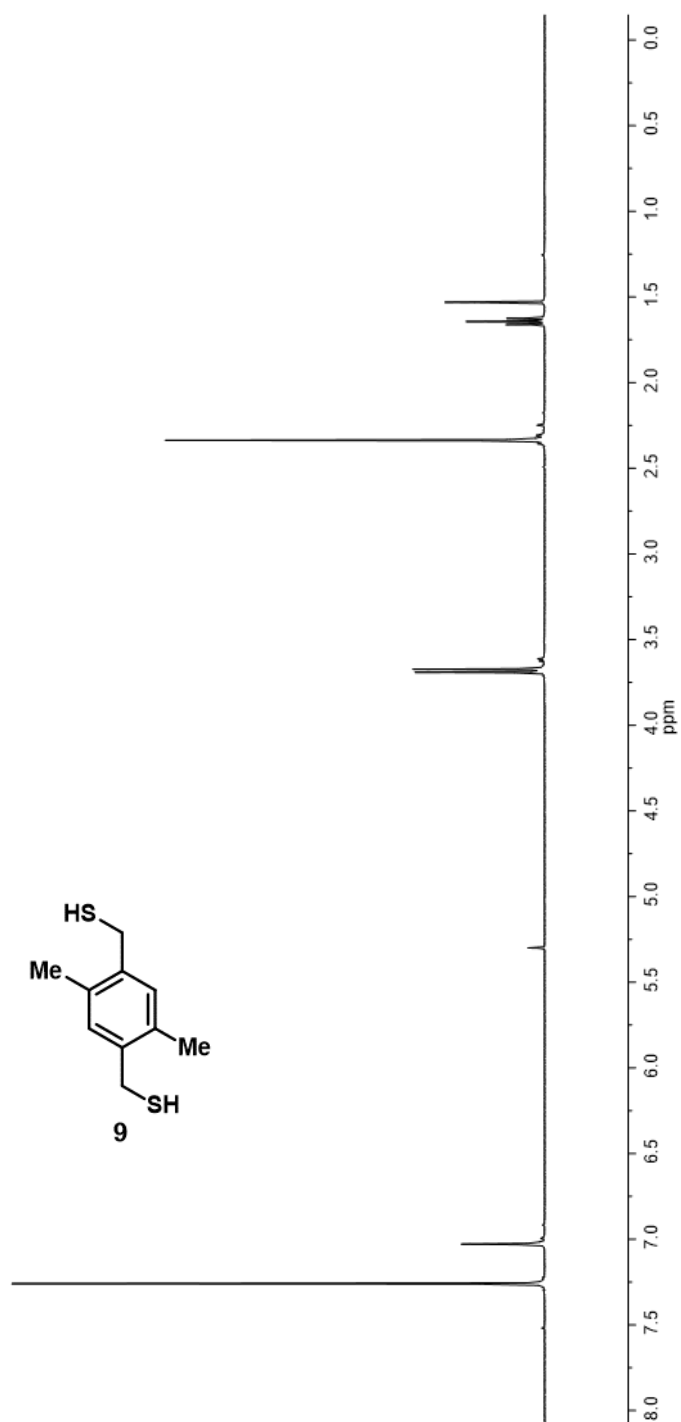
Figure II-44. ^{1}H NMR (400 MHz, CDCl$_3$) spectrum of compound **9**.
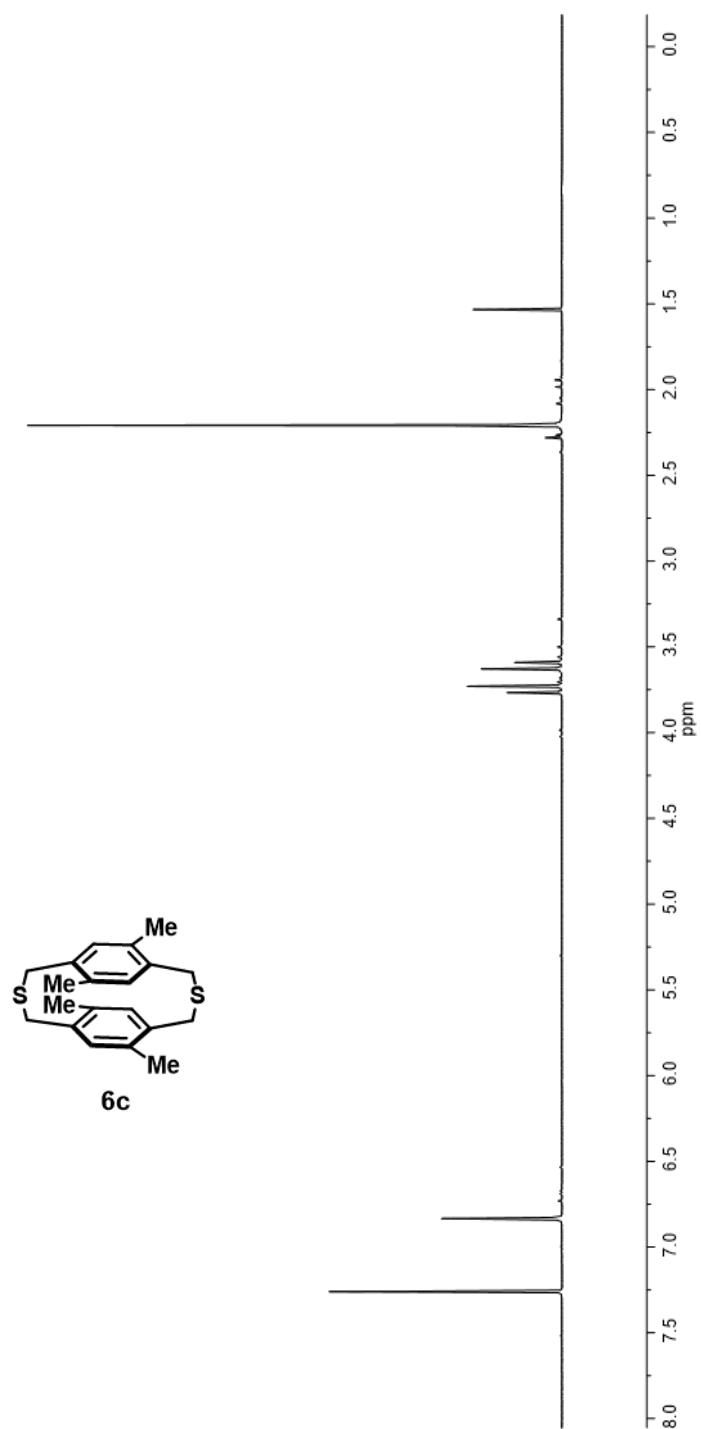
Figure II-45. ^{1}H NMR (400 MHz, CDCl$_3$) spectrum of compound **6c**.
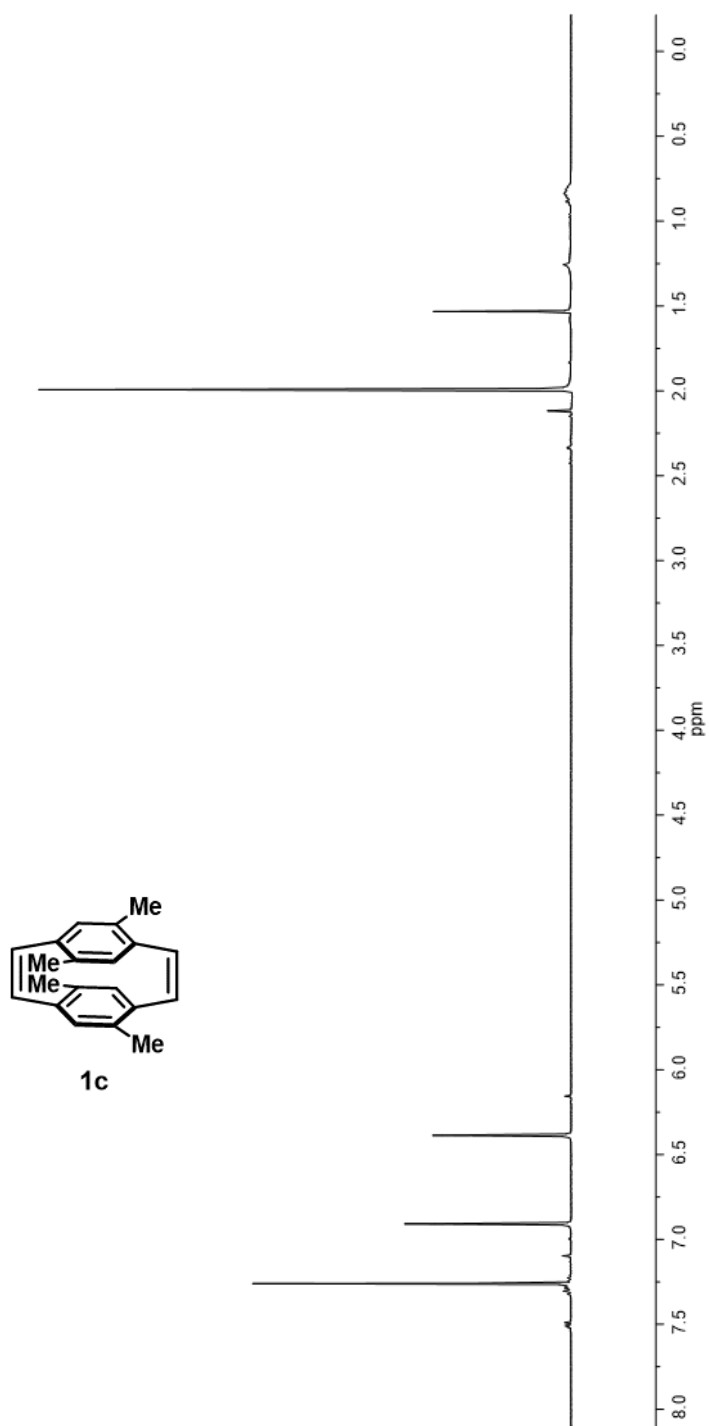
Figure II-46. ^{1}H NMR (400 MHz, CDCl$_3$) spectrum of monomer **1c**.
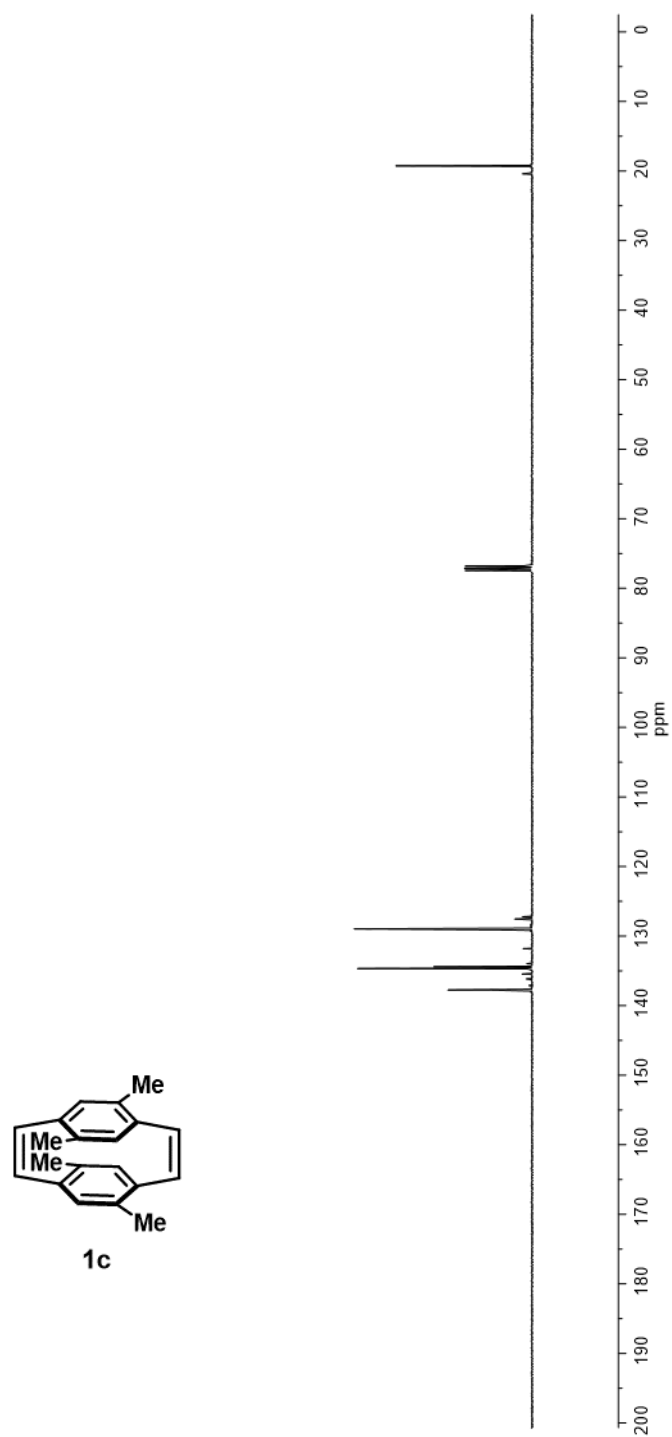
Figure 41. ^{13}C NMR (101 MHz, CDCl$_3$) spectrum of monomer **1c.**

CHAPTER III

ALL-*cis* POLY(*p*-PHENYLENE VINYLENE)S WITH HIGH MOLAR MASSES AND

FAST PHOTOISOMERIZATION RATES OBTAINED THROUGH

STEREORETENTIVE RING-OPENING METATHESIS POLYMERIZATION OF

[2,2]PARACYCLOPHANE DIENES WITH VARIOUS ARYL SUBSTITUENTS[*]

III.1 Introduction

Herein, we report the synthesis of all-*cis* poly(*p*-phenylene vinylene)s (PPVs) with living characteristics and high degrees of polymerization (DP up to 236) and molar masses (M_n up to 108.8 kg/mol) via stereoretentive ring-opening metathesis polymerization (ROMP).[18,25,46] Characterization of the influence of the aryl substituents on the UV–visible light absorption and emission, in addition to the photoisomerization kinetics, is disclosed. PPVs comprise a common family of conjugated polymers whose properties have been studied in the context of light-emitting materials as well as photovoltaics.[27,28,66] Characterized by alternating alkene and aryl rings, PPVs are stable to oxidation relative to other conjugated polymers such as polyacetylenes.[67] Their attractive semi-conducting properties can be tuned through structural modification of either the aryl substituents or the stereochemistry of the alkenes. The *cis* or *trans* (*Z* or *E*) configuration of these stilbenoid double bonds indeed dictates several key parameters including chain conformation, overall polymer morphology, and solubility.[12,13] For example, prior studies

---

showed that a predominance of *cis* junctions results in twisted and coiled polymer chains, whereas *trans*-rich PPVs exhibit a rod-like structure with increased π–π interactions and stronger packing between chains. This increased aggregation imbues *trans*-rich PPVs with poorer solubility in organic solvents relative to its *cis*-rich congener. However, *trans*-rich PPVs possess a longer effective conjugation length, leading to more narrow optical band gaps compared to *cis*-rich PPVs.[12,13] As a result, PPVs with the most desirable optical
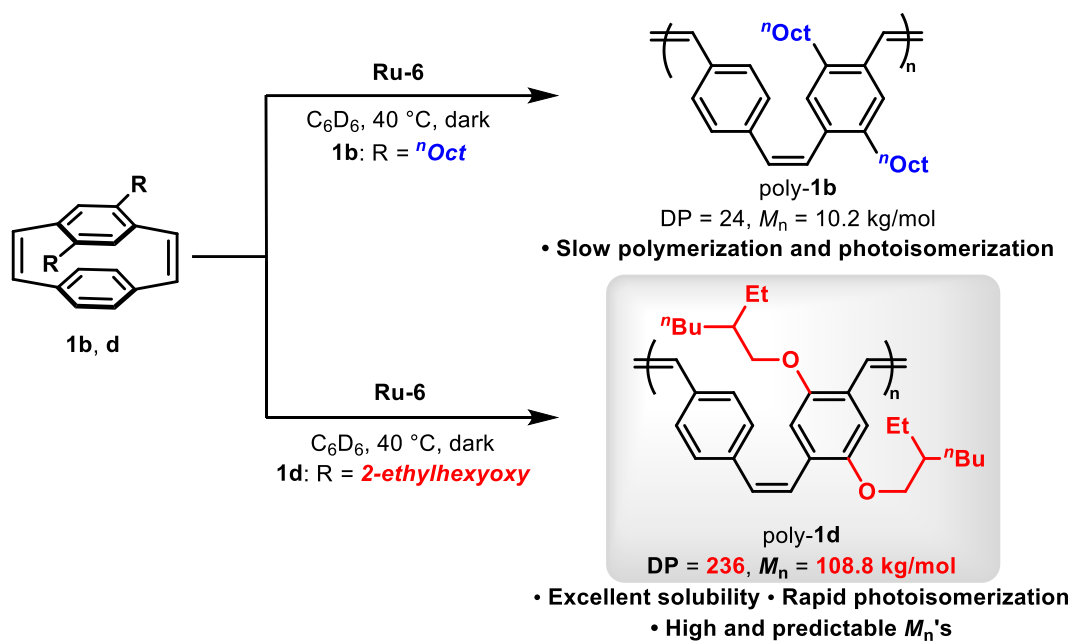
Figure III-1. Modifications of the monomer substituents allowed the synthesis of poly-**1d** with predictable DPs up to 236 (M_n = 108.8 kg/mol) and fast *cis*-to-*trans* isomerization mediated by UV light.

properties are also the most challenging to process. Along with *cis* and *trans* alkene content, the molar mass is another critical parameter for modulating the morphology of PPV thin films.[68,69] Interestingly, *cis* junctions in PPVs can be isomerized upon photochemical stimulation. This *cis*-to-*trans* isomerization therefore appears as an attractive strategy to efficiently synthesize and process all-*trans* PPVs with high molar

masses via the intermediacy of the all-*cis* congeners. Elegant demonstrations of the feasibility of this approach have been reported by several groups with applications including patterning and self-assembly of diblock copolymers.[33-35] While many methods have been invented for the preparation of PPVs,[26,30] accessing such materials with predictable, high molar masses, living chain ends, and perfect *cis* stereochemistry throughout the macromolecule remains a grand challenge. Polycondensations such as the Wittig,[36] Horner-Wadsworth-Emmons,[37] and Knoevenagel[38] methods as well as radical and anionic routes like the Gilch protocol[26,30,31] provide polymers with primarily *trans* alkene linkages and little to no control over molar mass distribution. The scarce early examples of approaches toward all-*cis* PPVs similarly did not afford control over this key parameter: A stereoretentive Suzuki-Miyaura polycondensation reported by Ozawa and coworkers formed all-*cis* PPV with a high dispersity and a low molar mass (M_n = 4.7 kg/mol, $Đ$ = 1.92),[33] while the *cis*-selective reduction of a poly(phenylene ethynylene) (PPE) by Swager and coworkers delivered the PPV with a higher M_n(61 kg/mol) but with a broad dispersity ($Đ$ =4.0).[40] Inspired by prior work on the ROMP of [2.2]para-cyclophane diene monomers leading to PPVs with alternating *cis* and *trans* alkenes,[41,55,59,70,71] we later reported the synthesis of all-*cis* poly-**1a** using a stereoretentive ROMP catalyst (**Ru-6**).[1,72] Owing to the living characteristics of this process, polymers with predictable molar masses up to 13.1 kg/mol and narrow dispersities were obtained. Additionally, excellent chain-end fidelity permitted the preparation of diblock copolymers, whose PPV segment could be selectively isomerized with UV light.

However, despite being more soluble than their all-*trans* counterparts, all-*cis* PPVs were shown to aggregate in solution through dynamic light scattering over time. This prompted us to study the influence of the aryl substituents of the [2.2]paracyclophane diene monomer over the stereoretentive ROMP process, as well as their impact on optical properties and solubility. To this end, [2.2]paracyclophane dienes **1b** and **1d** were synthesized to serve as monomers. **1b** was anticipated to showcase a similar steric environment around the alkene as **1a**, but different electronic features. Furthermore, the polymerization of **1b** with Grubbs' second generation catalyst was observed to be faster than with alkoxide-substituted monomers and could be conducted at lower temperatures.[43] In contrast, **1d** should have a very similar electronic behavior as **1a**, but branched alkyl chains have been shown to provide increased solubility when appended onto conjugated polymers, relative to linear alkyl chains.[73,74] This increased solubility might help mitigate the loss of control at higher molar masses, which would allow the preparation of PPVs with high molar masses. In this work, we disclose the stereoretentive ROMP of **1b** and **1d**, which afforded all-*cis* poly-**1b** and all-*cis* poly-**1d** (Figure III-1), both with good control over M_n. Notably, all-*cis* poly-**1d** could be isolated with unprecedently high molar masses, potentially due to an increase in solubility in organic solvents. Spectroscopical characterization of these polymers and kinetics of the isomerization were also investigated.

III.2 Results and Discussion

III.2.1 Stereoretentive ROMP of [2.2]Paracyclophane Dienes *1b* and *1d*

1b and **1d** were prepared following established synthetic routes,[42,52] and subjected to catalyst **Ru-6** in various solvents at 40 °C and in the dark to avoid premature isomerization of any *cis* double bonds (Table 1).

Table III-1 Optimization of The Stereoretentive ROMP of **1b** and **1d** with **Ru-6**
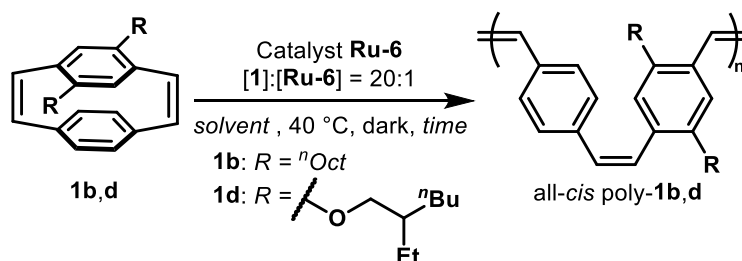
Entry[a]	Monomer	Solvent	Time (h)	Conv. (%)	M_n^{theor} (kg/mol)	M_n^{exp} (kg/mol)	Đ
1	1b	C_6D_6	48	>99	8.7	10.2	1.22
2		THF	48	>99	8.7	10.9	1.08
3		CH_2Cl_2	48	>99	8.7	11.5	1.15
4	1d	C_6D_6	12	>99	9.3	10.9	1.05
5		THF	12	>99	9.3	11.9	1.11
6		CH_2Cl_2	12	>99	9.3	9.9	1.16

[a]**1b** and **1d** (0.050 mmol) were polymerized with **Ru-6** at 40 °C in the dark and under nitrogen. M_n's and Đ's were determined by SEC (THF) using polystyrene standards (RI detection).

Polymerizations of **1b** and **1d** in C_6D_6, THF, and CH_2Cl_2 all led to good agreement between theoretical and experimental M_n's at full conversion as established by size

exclusion chromatography (SEC). THF was found to provide the narrowest dispersity for monomer **1b** ($Đ = 1.08$, Table III-1, entry 2), but C_6D_6 provided the smallest value for **1d** ($Đ = 1.08$, Table III-1, entry 4). All molar masses determined experimentally were slightly higher than the expected values, which was ascribed to the difference in hydrodynamic volume between PPVs and the polystyrene standards. For the purpose of monitoring the polymerization via ^{1}H NMR, C_6D_6 was subsequently used for the remainder of this study. Notably, in addition to the slightly broader distribution, **1b** also required a considerably longer reaction time to attain full conversion. While complete consumption of the monomer took place within 12 h with **1d** (Table III-1, entries 4–6), it took over 48 h with **1b** (Table III-1, entries 1–3). Interestingly, the slow formation of poly-**1b** compared to alkoxy-substituted poly-**1d** with **Ru-6** differs from previous reports with common Grubbs' catalysts, which displayed the opposite reactivity trend with substituted [2.2]paracyclophane dienes.[43] In our previous report, polymers up to ~13 kg/mol (DP ~ 30) could be prepared with monomer **1a** with experimental M_n's similar to the predicted values and with narrow dispersities.[1] Attempts to increase the DP of poly-**1a** by further raising the monomer-to-catalyst ratio were met with moderate success.

Table III-2 Synthesis of All-*cis* PPVs with Tunable Molar Masses
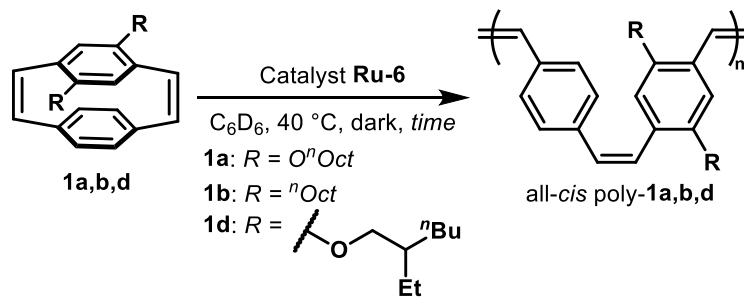
Entry[a]	Monomer	Time (h)	[1]:[Ru-6][b] Ratio	Conv. (%)	M_n^{theor} (kg/mol)	M_n^{exp} (kg/mol)	Đ
1	1a	12	20:1	>99	9.3	10.8	1.18
2		12	60:1	>99	27.7	34.5	1.32
3		24	100:1	>99	46.2	53.1[c]	1.75
4		48	200:1	>99	92.1	49.2[c]	1.67
5	1b	48	20:1	>99	8.7	10.2	1.22
6		48	60:1	91	25.7	20.4	1.06
7	1d	12	20:1	>99	9.3	10.9	1.05
8		12	60:1	>99	27.7	34.7	1.18
9		24	100:1	>99	46.2	43.2	1.13
10		48	200:1	94	92.1	108.8	1.54

[a]1a, 1b and 1d was polymerized with Ru-6 at 40 °C in C_6D_6 in the dark and under nitrogen. M_n's and Đ's were determined by SEC (THF) using polystyrene standards (RI detection).[b]Concentration of Ru-6 was kept constant (C = 2.9 mM). [c]Poor solubility of poly-1a precluded precise measurement of M_n and Đ.

When the ratio of 1a to Ru-6 was increased to 60:1 or 100:1 (Table III-2, entries 2 and 3), the dispersity rose to 1.32 and 1.75, respectively. At an even higher ratio (e.g., 200:1, Table III-2, entry 4), the measured M_n was considerably smaller than the expected value (49.2 vs. 92.1 kg/mol) with a Đ of 1.67. Of note, the investigation of the molar mass distribution of poly-1a at high M_n was complicated by its lack of solubility in organic solvents including THF. The longer chains of the distribution were indeed likely lost during the filtration process prior to SEC analysis. The slow polymerization rates observed with 1b rendered the synthesis of poly-1b with high M_n's challenging as well. When targeting a DP of 60 with 1b, only 91% conversion was observed after 48 h (Table III-2, entry 6) in contrast to the polymerization of 1a that reached full conversion in 12 h in

otherwise identical reaction conditions (Table III-2, entry 2). Remarkably, switching from *n*-octyloxy substituents in **1a** to the branched 2-ethylhexyloxy side chains in **1d** allowed the polymerization to proceed in a living manner with a variety of monomer-to-catalyst ratios. Manipulation of this ratio enabled the preparation of all-*cis* PPVs with a wide window of molar masses. Ratios of 60:1 and 100:1 afforded polymers with M_n's in close agreement with theoretical values and narrow dispersities ($Đ = 1.18$ and 1.13, Table III-2, entries 8 and 9). All polymerizations reached full conversion except when targeting a DP of 200, which stalled around 94% conversion (Table III-2, entry 10) and displayed an increased dispersity ($Đ = 1.54$). Nonetheless, these conditions delivered poly-**1d** with a M_n of 108.8 kg/mol (DP = 236) thereby demonstrating that this method provides access to PPVs of unparalleled lengths while maintaining living characteristics.[26,30] Further optimization of the reaction conditions and/or monomer structure will likely be necessary to further increase the size of PPVs while retaining control over the molar mass distribution. As seen with other polymers,[73,74] the increased branching of the 2-ethylhexyloxy substituents likely decreased aggregation between chains relative to poly-**1a**, which potentially helped in achieving the high degree of control observed at high molar masses. The improvement in solubility can also be observed visually with all-*cis* poly-**1d** ($M_n = 10.9$ kg/mol) forming a clear solution (C = 1 mg/ml) compared to the turbid solution obtained with all-*cis* poly-**1a** of similar molar mass ($M_n = 9.8$ kg/mol, C = 1 mg/ml) (Figure III-2).

The stereoselectivity of the ROMP of monomers **1b** and **1d** was investigated through ^{1}H and ^{13}C NMR spectroscopical analysis of the resulting polymers. NOESY and
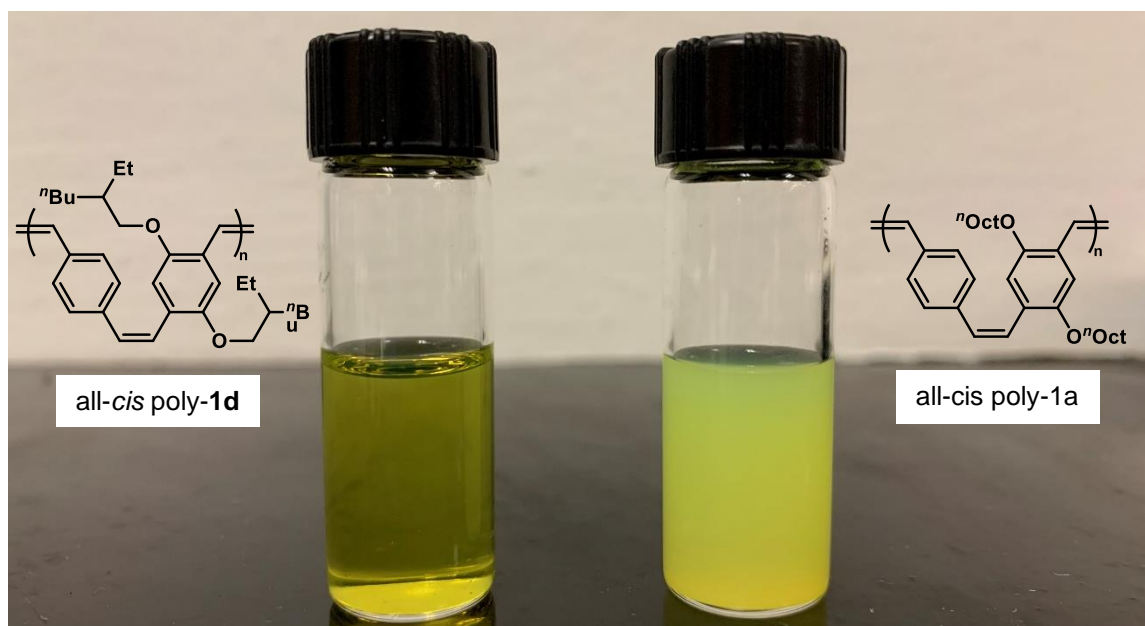
Figure III-2. All-*cis* poly-**1d** exhibits a significantly improved solubility over all-*cis* poly-**1a** in THF (C = 1 mg/mL).

HSQC experiments were also recorded to unambiguously assign characteristic peaks present in the spectra of both nuclei (Figures III-15–22). Comparison of the NMR spectra of synthesized poly-**1b** and poly-**1d** to the reported spectra of polymers with identical composition but containing mixtures of *cis* and *trans* alkenes[42,43] revealed an exquisite control over the stereochemistry of the alkene linkages during the stereoretentive ROMP.[75] Indeed, all-*cis* poly-**1b** and poly-**1d** were formed with no *trans* defects within the limits of detection of ^{1}H NMR.

Finally, exhaustive isomerization of all *cis* olefins was performed using UV light (365 nm, Figure III-3), which allowed the isolation of all-*trans* congeners and subsequent NMR comparison (Figure III-4). ^{1}H NMR spectra of all-*trans* poly-**1b** and poly-**1c** showcased characteristic peaks (indicated with blue triangles in Figure III-4) with higher chemical shifts relative to the corresponding protons in all-*cis* poly-**1b** and poly-**1d**
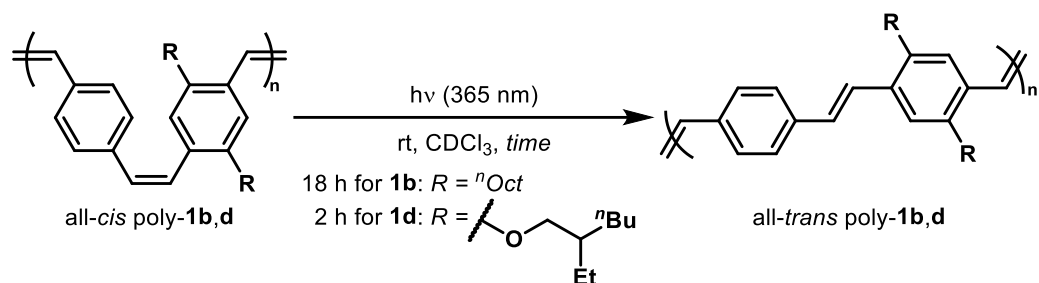
Figure III-3. UV light-promoted isomerization of all-*cis* poly-**1b** and poly-**1d**.

(indicated with red triangles). This trend is common for alkyl and alkoxy-substituted PPVs.[1,33] For example, the benzylic methylene protons at C5 in all-*cis* poly-**1b** result in a multiplet at 2.48–2.38 ppm, upfield from the same protons in all-*trans* poly-**1b** (2.70–2.85 ppm) (Figure III-4a). The aromatic protons at C1 and C4 and vinylic protons at C2 andC3 in all-*cis* poly-**1b** are found at 7.00–6.95 ppm and 6.75and 6.65 ppm, respectively, whereas the aromatic and vinylic peaks of all-*trans* poly-**1b** are all above 7 ppm. Similarly, the signal corresponding to the methylene protons at C5 is found at 3.40 ppm in all-*cis* poly-**1d** and 3.98 ppm in *trans* poly-**1d** (Figure III-4b). The aromatic and vinylic protons in all-*cis* poly-**1d** are well resolved, giving four separate signals at 7.21, 6.75, 6.64, and 6.48 ppm corresponding to the protons at C4, C1, C2, and C3 respectively. On the other hand, the same protons in all-*trans* poly-**1d** appear as two broad, overlapping signals at 7.53 and 7.15 ppm.

89
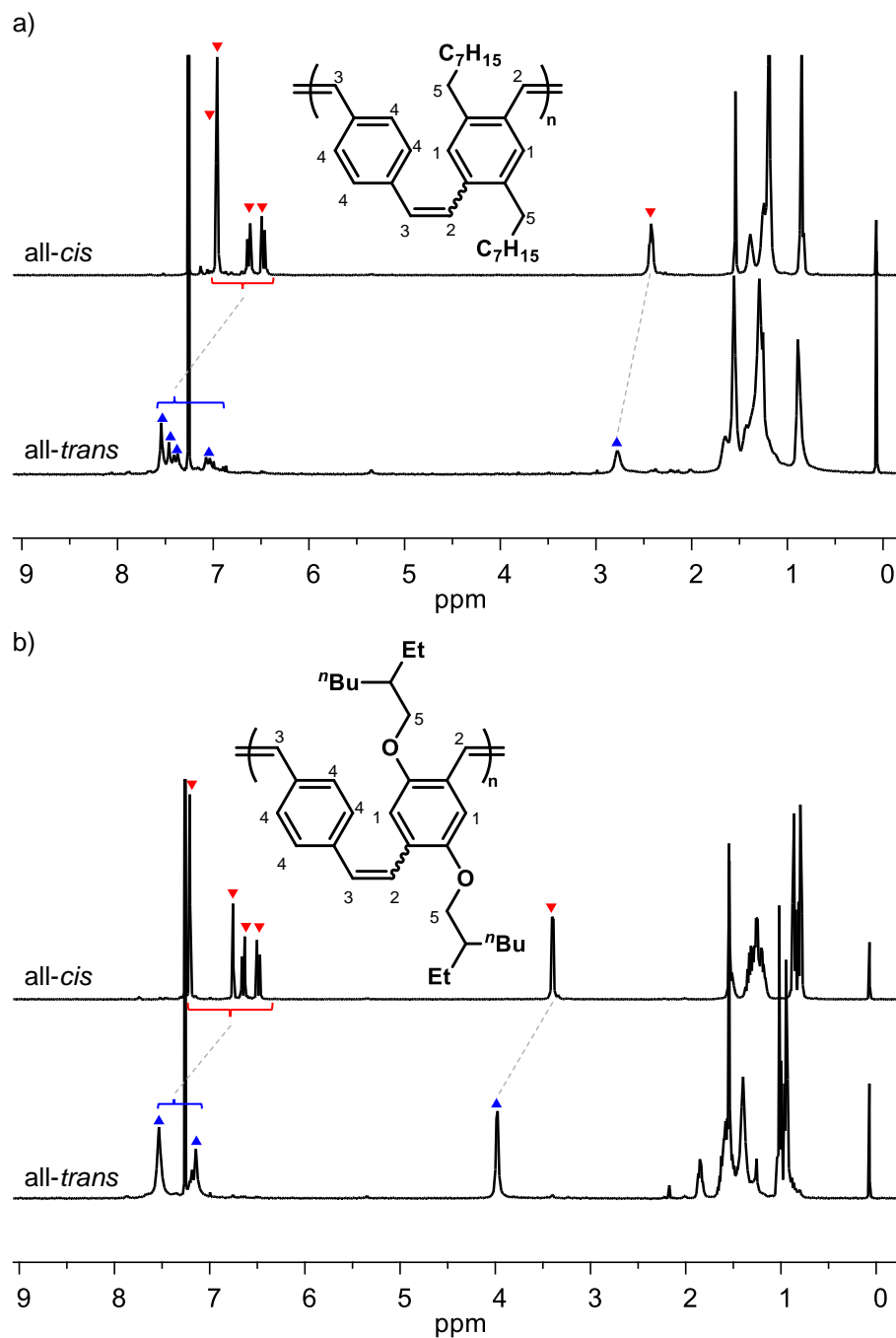
Figure III-4. a) ^{1}H NMR of all-*cis* (top) and all-*trans* (bottom) poly-**1b**. b) ^{1}H NMR of all-*cis* (top) and all-*trans* (bottom) poly-**1d**. NMRs in Figure III-4 were taken in a sealed J-Young tube in degassed CDCl$_3$ under N$_2$ without purification in order to carefully monitor the isomerization process.

In addition to changes in ^{1}H NMR spectra, isomerization of PPVs led to an apparent increase in molar masses measured by SEC caused by the larger hydrodynamic radius of the all-*trans* congeners (Table III-3), which is consistent with prior studies.[43] For example, the molar mass of all-*cis* poly-**1d** was 11.3 kg/mol and that of all-*trans* poly-**1d** was 23.6 kg/mol after photoisomerization (Table III-3, entries 5 and 6).

Table III-3 Molar Masses and Quantum Yields of All-*cis* and All-*trans* PPVs

Entry	Polymer	*cis:trans*	M_n^{exp} [kg/mol]	Đ	Φ_{PL}
1	all-*cis* poly-**1a**	>99:1	10.8	1.18	0.28
2	all-*trans* poly-**1a**	<1:99	$-^a$	$-^a$	0.53
3	all-*cis* poly-**1b**	>99:1	9.4	1.14	0.32
4	all-*trans* poly-**1b**	<1:99	15.2	1.20	0.58
5	all-*cis* poly-**1d**	>99:1	11.3	1.11	0.33
6	all-*trans* poly-**1d**	<1:99	23.6	1.33	0.53

$^a M_n$ and Đ values could not be determined by SEC due to the insolubility of all-*trans* poly-**1a** in THF.

III.2.2 Optical Properties of Synthesized All-cis PPVs

The absorption and emission spectra of all-*cis* poly-**1b** and poly-**1d** were measured in THF (Figure III-5). As shown in Figure III-5, the more electron-rich all-*cis* poly-**1d** exhibited a red shifted absorption (λ_{max} = 389 nm) relative to all-*cis* poly-**1b** (λ_{max} = 334 nm). Furthermore, the emission spectra of both polymers depicted in Figure III-5 reveal a similar red shift when comparing all-*cis* poly-**1b** (λ_{max} = 483 nm) and all-*cis* poly-**1d** (λ_{max} = 517 nm). Upon full photoisomerization, both all-*trans* poly-**1b** and poly-**1d** displayed strong red shifts in both absorption and luminescence as a consequence of the increased

conjugation length observed in all-*trans* PPVs (Figure III-5).[12,13] For poly-**1b**, the maximum absorbance for the all-*trans* form was measured at 427 nm, while all-*trans* poly-**1d** exhibited a similar red shift in absorbance (λ_{max} = 469 nm) from the all-*cis* form.
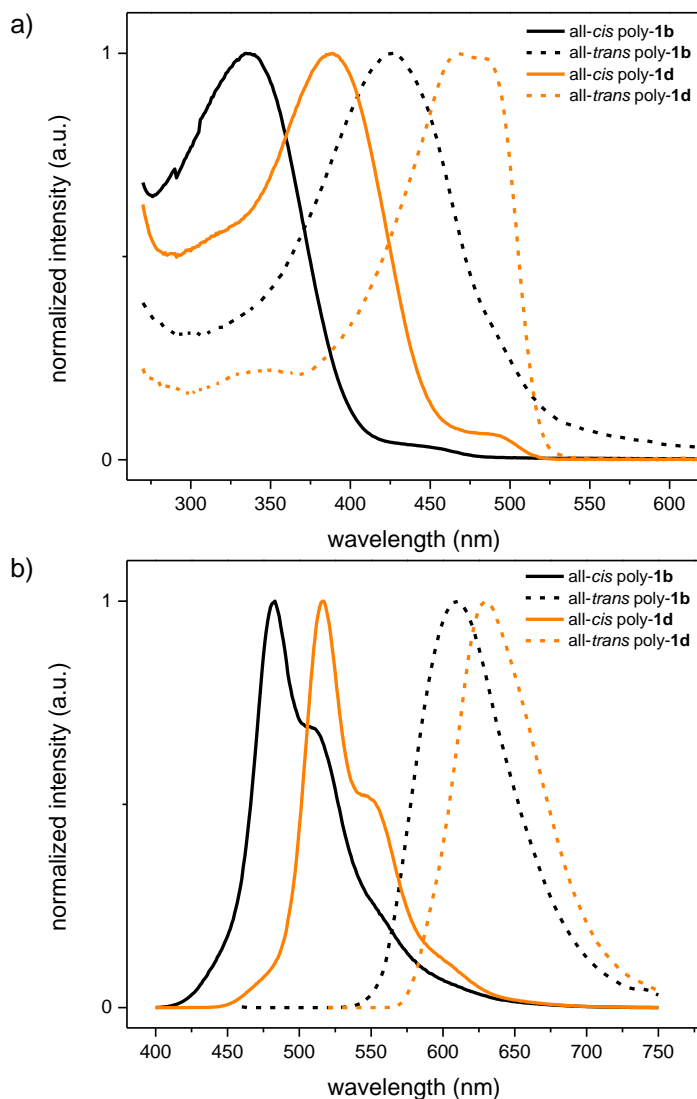
Figure III-5. a) UV-visible and b) emission spectra of all-*cis* poly-**1b** (black curve, solid), all-*trans* poly-**1b** (black curve, dotted), all-*cis* poly-**1d** (orange curve, solid), and all-*trans* poly-**1d** (orange curve, dotted).

The complete isomerization of all-*cis* poly-**1** to their all-*trans* counterparts also resulted in a stark increase in quantum yields of photoluminescence (Φ_{PL}, Table III-3). In order to use
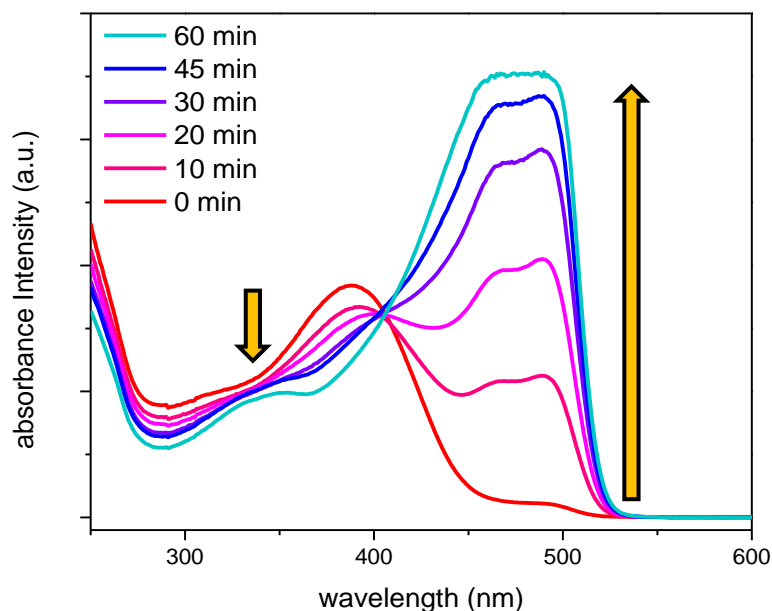
Figure III-6. Photoisomerization of poly-**1d** monitored by UV-visible spectra.

these polymers for patterning[33] or self-assembly,[35] fast isomerization of the *cis* alkenes is desirable, which prompted us to investigate the rate of photoisomerization. The evolution of the absorbance in the UV-visible range was monitored during the photoisomerization of poly-**1d** (Figure III-6). Fast isomerization took place within the first 10 min and complete disappearance of the signal at 389 nm was observed after 60 min, indicating full isomerization to the all-*trans* polymer.

In order to gain more insights on the kinetics of isomerization of all-*cis* poly-**1b** and all-*cis* poly-**1d**, the photoisomerization process was monitored via ^{1}H NMR spectroscopy in CDCl$_3$ (Figure III-7a). As previously observed in THF, isomerization of all-*cis* poly-**1d** also proceeded rapidly in CDCl$_3$, reaching 95% conversion within 60 min (C = 4 mg/ml). This rate of isomerization is similar to that of poly-**1a** (Figure III-8).[1] In contrast, all-*cis* poly-**1b** containing octyl substituents did not reach 80% isomerization of

cis alkenes until 140 min. Interestingly, the photoisomerization of both poly-**1b** and poly-**1d** was found to follow a first-order behavior (Figure III-7b), which is consistent with the kinetics of isomerization of PPVs induced by sonication,[76] as well as with the kinetics observed in photoisomerization of discrete stilbenoid and azobenzene groups.[77-79] Remarkably, all-*trans* poly-**1d** (M_n = 10.9 kg/mol) was found to be soluble in a variety of
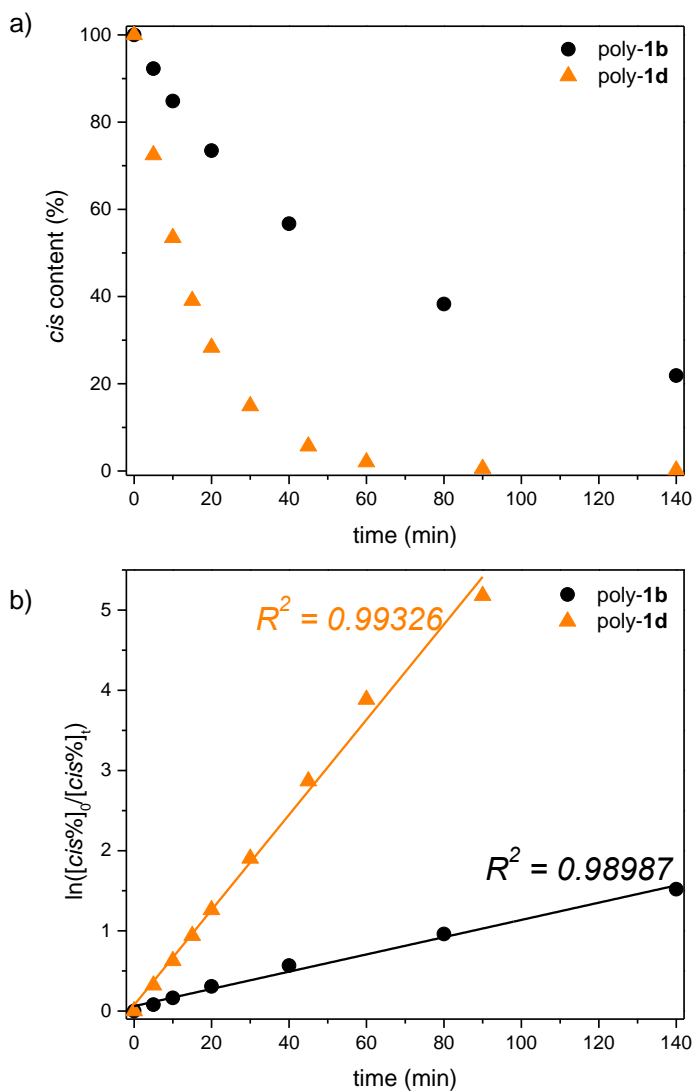
Figure III-7. a) Evolution of the *cis* content in poly-**1b** and poly-**1d** during the isomerization process. b) The photoisomerization of poly-**1b** and poly-**1d** follows a first-order behavior.

94

organic solvents (THF, C_6D_6, CH_2Cl_2, and $CDCl_3$), in contrast to all-*trans* poly-**1a** and poly-**1b** of similar molar masses, which precipitated during isomerization.

III.3 Conclusion

We developed a synthesis of PPVs with living characteristics and unprecedented molar masses (M_n's up to 108.8 kg/mol), capitalizing on the perfect stereocontrol afforded by **Ru-6** in the stereoretentive polymerization of [2,2] paracyclophane dienes. These high DPs were likely attainable because of the increased solubility provided by both the *cis* olefins and the 2-ethylhexyloxy side chains. This study provides another example of the advantageous use of branched side-chains to increase the solubility of conjugated polymers, relative to their linear counterparts.[73,74] Indeed, poly-**1a** is markedly less soluble than poly-**1d** despite having the same atomic composition. Additionally, all-*cis* poly-**1d** could be fully isomerized to all-*trans* poly-**1d** in 2 h in THF or $CDCl_3$. On the other hand, deleting the oxygen from the side chains with octyl monomer **1b** resulted in lower rates of both polymerization and photoisomerization relative to **1a** and **1d**. We anticipate that this study should help the design of processable materials containing long all-*trans* PPVs chains, whose length have been shown to critically impact the morphology of PPVs in thin films.[68,69]

III.4 Experimental Procedures and Data

III. 4.1 General Reagent Information

Monomers **1b** and **1d** were synthesized according to literature procedures.[42,52] Reagents were purchased at the highest commercial quality and used directly without further purification, unless otherwise stated. Dry dichloromethane (CH_2Cl_2), and tetrahydrofuran (THF) were obtained by passing the previously degassed solvents through activated alumina columns. C_6D_6 and $CDCl_3$ was purchased from Cambridge Isotope Laboratories, Inc. and degassed via "freeze-pump-thaw" before being placed in the glovebox. The synthesis of polymers using the stereoretentive catalyst was conducted in a nitrogen-filled glove box (SG1800/750TS-F, VIGOR). Polymers were isolated after precipitation using an Eppendorf 5804 centrifuge.

III.4.2 General Analytical Information

^1H and ^{13}C NMR spectra were recorded on Bruker Avance Neo 400 and Bruker Avance 500 instruments and were calibrated using residual undeuterated solvent as an internal reference ($CHCl_3$ @ 7.26 ppm ^1H-NMR, 77.16 ppm ^{13}C-NMR; C_6H_6 @ 7.16 ppm ^1H-NMR). The following abbreviations were used to explain NMR peak multiplicities: s = singlet, d = doublet, t = triplet, q = quartet, m = multiplet, br = broad.

All polymer samples were analyzed using a Tosoh EcoSec HLC 8320GPC system with a TSKgel SuperHM-M column and a TSKgel SuperH-RC column at a flow rate of 0.40 mL/min at 40 °C. THF stabilized with BHT was used as the eluent and all number-average molecular weights (M_n), weight-average molecular weights (M_w), and dispersities ($Đ$) for

polymers were calculated from refractive index and UV chromatograms against TSKgel polystyrene standards.

UV-vis spectra were recorded on a Shimadzu UV-2600 UV-visible spectrophotometer and fluorescence spectra were recorded on a Horiba FluorEssenceTM fluorescence spectrometer.

III.4.3 General Procedures

Solvent Screen for the Stereoretentive ROMP

In a nitrogen-filled glove box, a solution of ruthenium catalyst **Ru-6** (0.0025 mmol, 8.3 mM) in deoxygenated solvent (0.3 mL) was added into a reaction vial containing monomer **1b** or **1d** (0.050 mmol) and a stir bar. The mixture was stirred outside of the glovebox at room temperature for 5 min and placed into a preheated water bath at 40 ℃ in the dark for 48 h (**1b**) or 12 h (**1d**). Once cooled to room temperature, the reaction was quenched with ethyl vinyl ether (0.05 mL) and stirred for an additional 10 min at that temperature. The solution was diluted to ~4.0 mg/mL with THF, filtered, and then used for SEC analysis directly. The remaining polymer was precipitated upon addition of methanol and the solid was isolated by centrifugation and decantation. The resulting polymer was dried under high vacuum. The polymers were stored in vials wrapped with aluminum foil and kept away from light.

*III.4.4 Polymerization of **1d** Targeting Various DPs*

In a nitrogen-filled glove box, a solution of ruthenium catalyst **Ru-6** (1.0 mg, 0.0012 mmol, C = 2.9 mM) and monomer **1d** in deoxygenated C_6D_6 (0.4 mL) was added into a J. Young NMR tube. The NMR tube was sealed with a screw cap and taken out of the glove box where it was placed in a water bath set to 40 °C. The reaction progress was monitored by ^{1}H NMR. Once full conversion was reached, the reaction was cooled to room temperature and quenched with ethyl vinyl ether (0.05 mL) and stirred for an additional 10 min at room temperature. The solution was diluted to ~4.0 mg/mL with THF, filtered, and then used for SEC analysis directly. The remaining polymer was precipitated upon addition of methanol and the solid was isolated by centrifugation and decantation. The resulting polymer was dried under high vacuum. The polymers were stored in vials wrapped with aluminum foil and kept away from light.

*III.4.5 UV-visible absorption spectroscopy of poly-**1d** during* cis *to* trans *photoisomerization*

A solution of all-*cis* poly-**1d** in THF (4 mg/mL) was irradiated using two 365 nm UV lamps at room temperature. To monitor the absorbance of poly-**1d** over time, aliquots were taken and diluted with THF to 0.2 μg/mL for UV measurement.
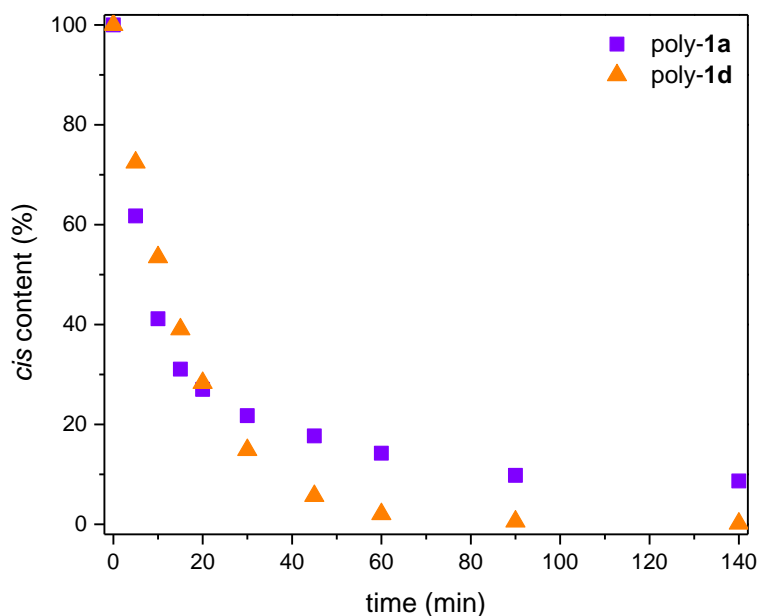
Figure III-8 Decrease in %*cis* alkenes in poly-**1a** and poly-**1d** over time during photoisomerization.

III.4.6 Kinetics Studies of cis *to* trans *Photoisomerization via ^{1}H NMR*

Solutions of all-*cis* poly-**1b** and all-*cis* poly-**1d** in CDCl$_3$ (4 mg/mL) were irradiated using two 365 nm UV lamps at room temperature while the *cis* content was monitored by ^{1}H NMR until full conversion.

*III.4.7 Determination of Quantum Yield of Fluorescence for All-*cis *and All-*trans *Poly-*1a*,*

*Poly-*1b*, and Poly-*1d*

Quantum yields of fluorescence were measured in dilute solutions of all-*cis* poly-**1a**, poly-**1b**, and poly-**1d** and all-*trans* poly-**1a**, poly-**1b**, and poly-**1d** in THF (*n* = 1.407) against either fluorescein (λ$_{ex}$ = 470 nm) in aq. NaOH (C = 0.1 M, Φ = 0.91, *n* = 1.33) for

all-*trans* poly-**1a** and all-*trans* poly-**1d** or quinine sulfate (λ_{ex} = 370 nm for all-*cis* poly-**1a**, all-*cis* poly-**1d**, and all-*trans* poly-**1b**; λ_{ex} = 340 nm for all-*cis* poly-**1b**) in aq. H_2SO_4 (C = 0.1 M, Φ = 0.52, n = 1.33). All absorbance measurements were taken on a Shimadzu UV-2502PC UV-vis spectrophotometer and kept below 0.03 to prevent reabsorption during fluorescence. Fluorescence measurements were collected on a PTI QuantaMaster spectrofluorometer (slit width = 2.5 nm). Fluorescence quantum yields were calculated based on the gradients (slope) of the plot of integrated emission versus absorbance at the λ_{ex} using the following the equation:[80]

$$\Phi_{sample} = \Phi_{standard} \times \left(\frac{Gradient_{sample}}{Gradient_{standard}}\right) \times \left(\frac{n_{sample}}{n_{standard}}\right)^2 \tag{1}$$
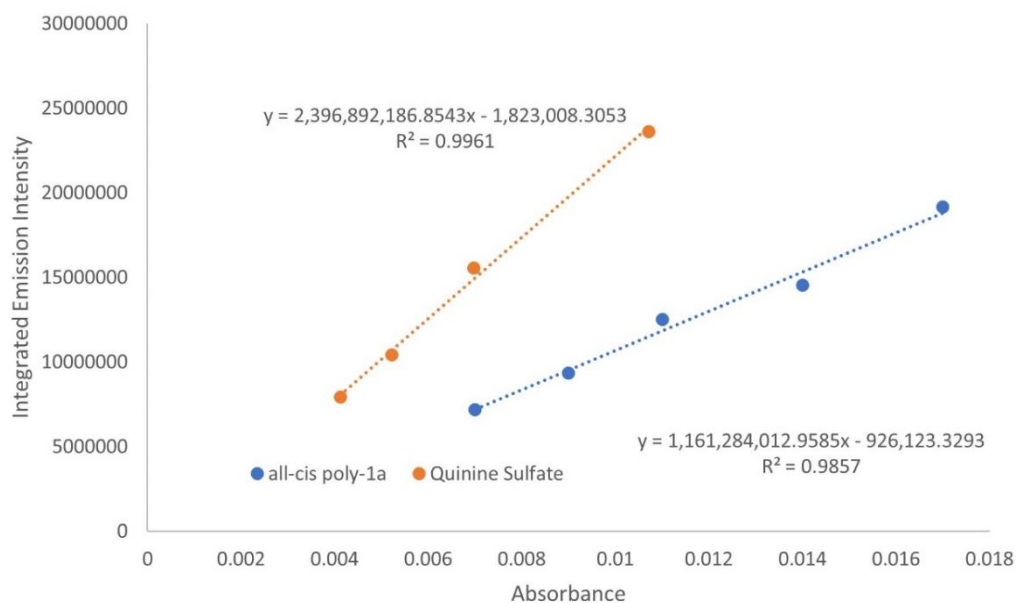
Figure III-9 Plot of integrated emission intensity vs. absorbance for all-*cis* poly-**1a** and quinine sulfate (λex = 370 nm)
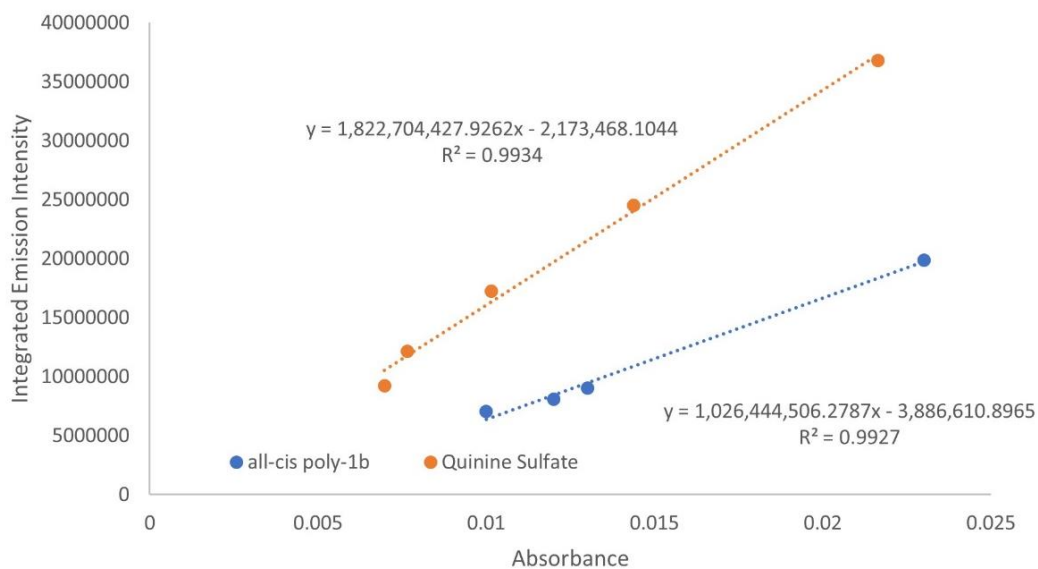
Figure III-10 Plot of integrated emission intensity vs. absorbance for all-*cis* poly-**1b** and quinine sulfate (λex = 340 nm)
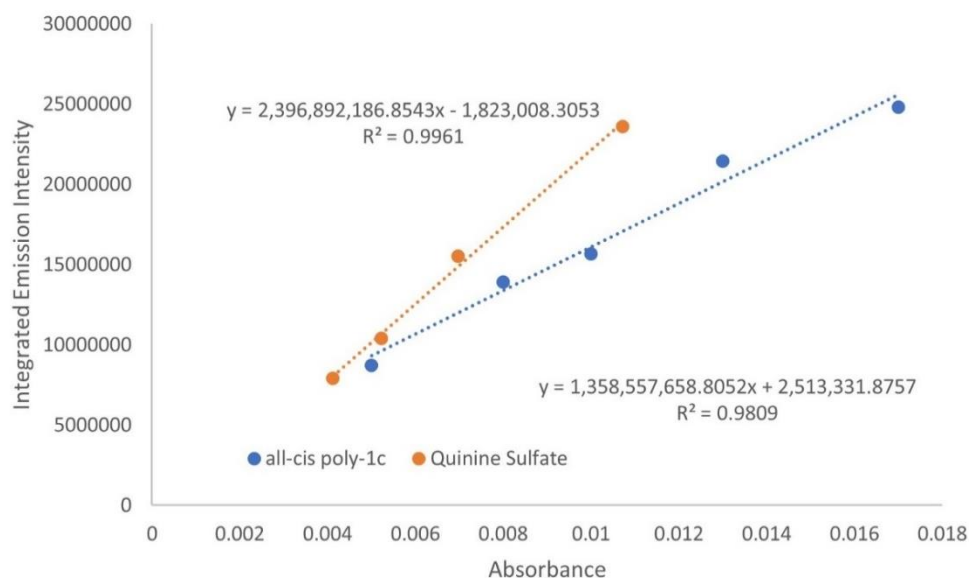
Figure III-11 Plot of integrated emission intensity vs. absorbance for all-*cis* poly-**1d** and quinine sulfate (λ_{ex} = 370 nm)
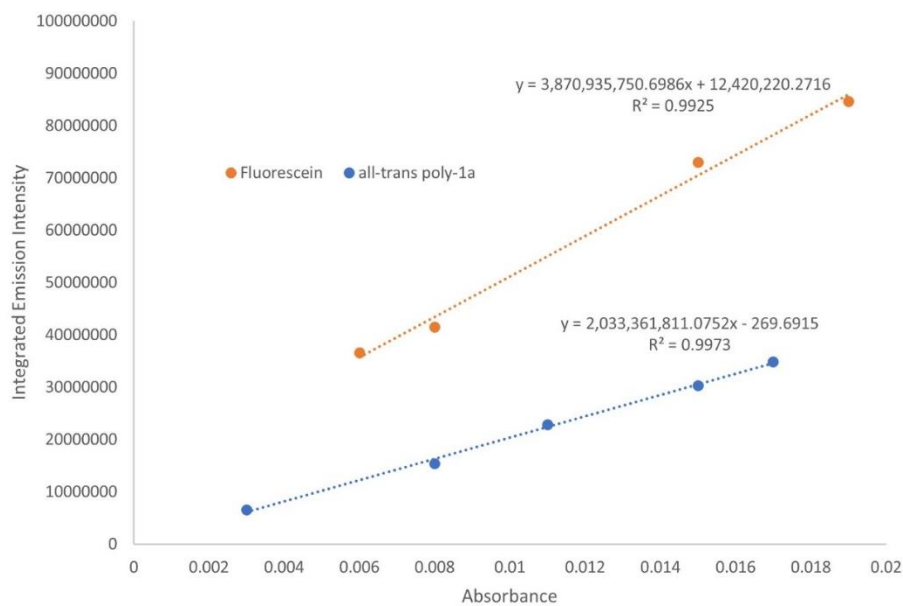
Figure III-12 Plot of integrated emission intensity vs. absorbance for all-*trans* poly-**1a** and fluorescein (λ_{ex} = 470 nm)
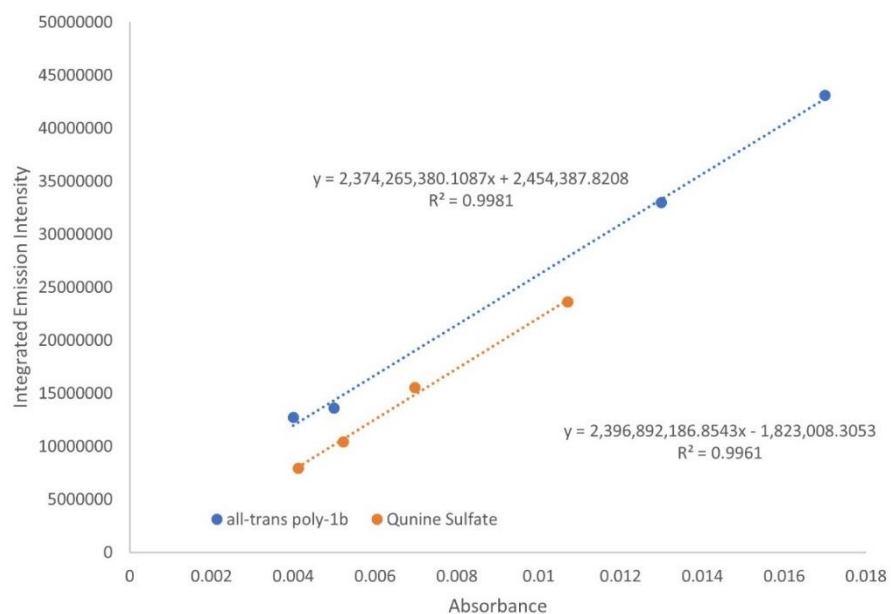
Figure III-13 Plot of integrated emission intensity vs. absorbance for all-*trans* poly-**1b** and quinine sulfate (λ_{ex} = 370 nm)
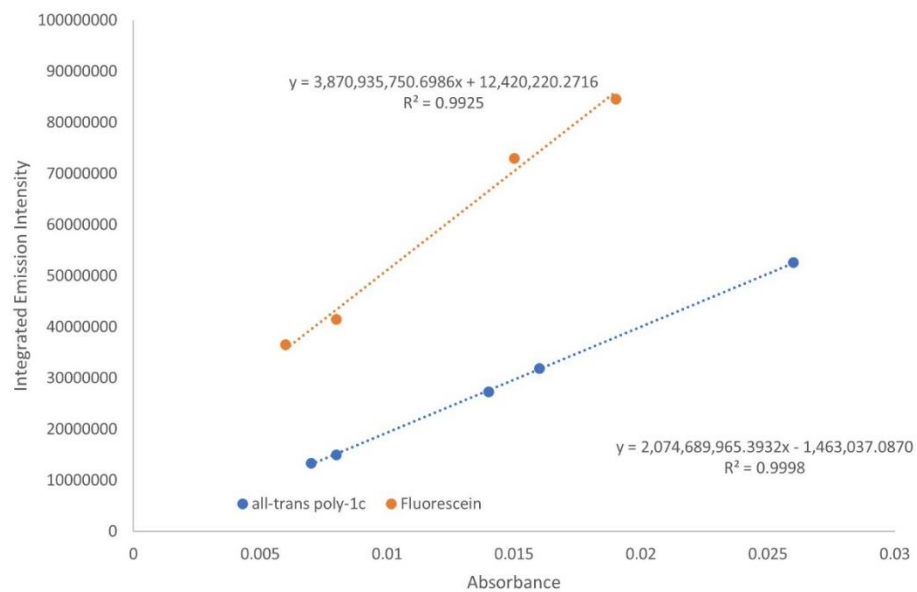
Figure III-14 Plot of integrated emission intensity vs. absorbance for all-*trans* poly-**1d** and fluorescein (λ_{ex} = 470 nm)

*III.4.8 Spectroscopic Data for Poly-**1b** and Poly-**1d***

All-*cis* poly-**1b**

^{1}H NMR (500 MHz, CDCl$_3$) δ 7.00–6.95 (m, 6 H), 6.63 (d, *J* = 12.2 Hz, 2 H), 6.48 (d, *J* = 12.2 Hz, 2 H), 2.48–2.38 (m, 4 H), 1.39 (s, 4 H), 1.32–1.13 (m, 20 H), 0.85 (t, *J* = 6.9 Hz, 6 H) ppm.

^{13}C NMR (126 MHz, CDCl$_3$) δ 138.2, 135.8, 135.6, 130.0, 130.2, 129.4, 128.7, 33.1, 31.9, 30.7, 29.5, 29.3, 22.7, 14.1 ppm.

All-*trans* poly-**1b**

^{1}H NMR (500 MHz, CDCl$_3$) δ 7.55–7.25 (m, 7 H), 7.10–6.85 (m, 3 H), 2.85–2.50 (m, 4 H), 1.65–1.54 (m, 4 H). The spectroscopic data for this polymer were identical to those reported in the literature.[52]

All-*cis* poly-**1d**

^{1}H NMR (500 MHz, CDCl$_3$) δ 7.21 (s, 4 H), 6.75 (s, 2 H), 6.65 (d, *J* = 12.3 Hz, 2 H), 6.49 (d, *J* = 12.3 Hz, 2 H), 3.40 (d, *J* = 5.7 Hz, 4 H), 1.13–1.40 (m, 18 H), 0.86 (t, *J* = 7.2 Hz, 6 H), 0.80 (t, *J* = 7.2 Hz, 6 H) ppm.

^{13}C NMR (126 MHz, CDCl$_3$) δ 150.3, 136.4, 129.3, 128.7, 126.1, 125.3, 113.8, 71.2, 39.3, 30.5, 28.9, 23.9, 23.0, 14.1, 11.0 ppm.

All-*trans* poly-**1d**

^{1}H NMR (500 MHz, CDCl$_3$) δ 7.63–7.43 (m, 6 H), 7.24–7.00 (m, 4 H), 4.05–3.91 (m, 4 H), 1.90–1.80 (m, 2 H), 1.72–1.28 (m, 16 H), 1.05–0.92 (m, 12 H) ppm. The spectroscopic data for this polymer were identical to those reported in the literature.[42]

III.4.9 Nuclear Magnetic Resonance Spectra
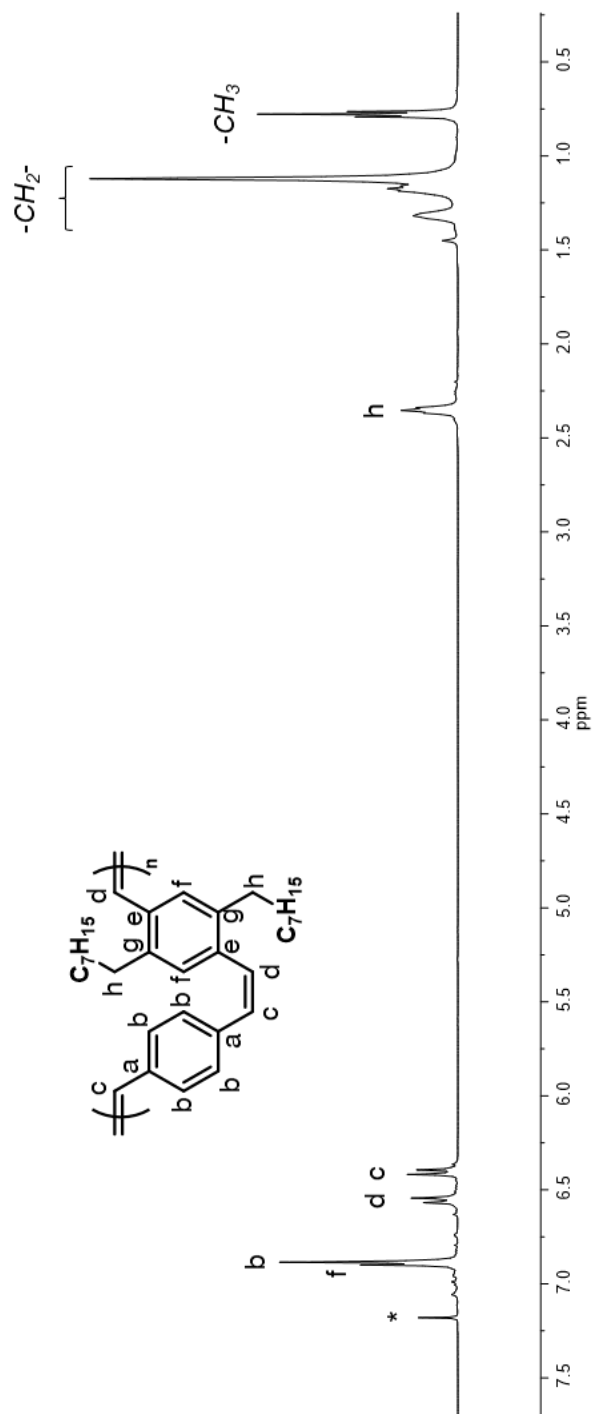
Figure III-15 ^{1}H NMR (500 MHz, CDCl$_3$) spectrum of all-*cis* poly-**1b.**
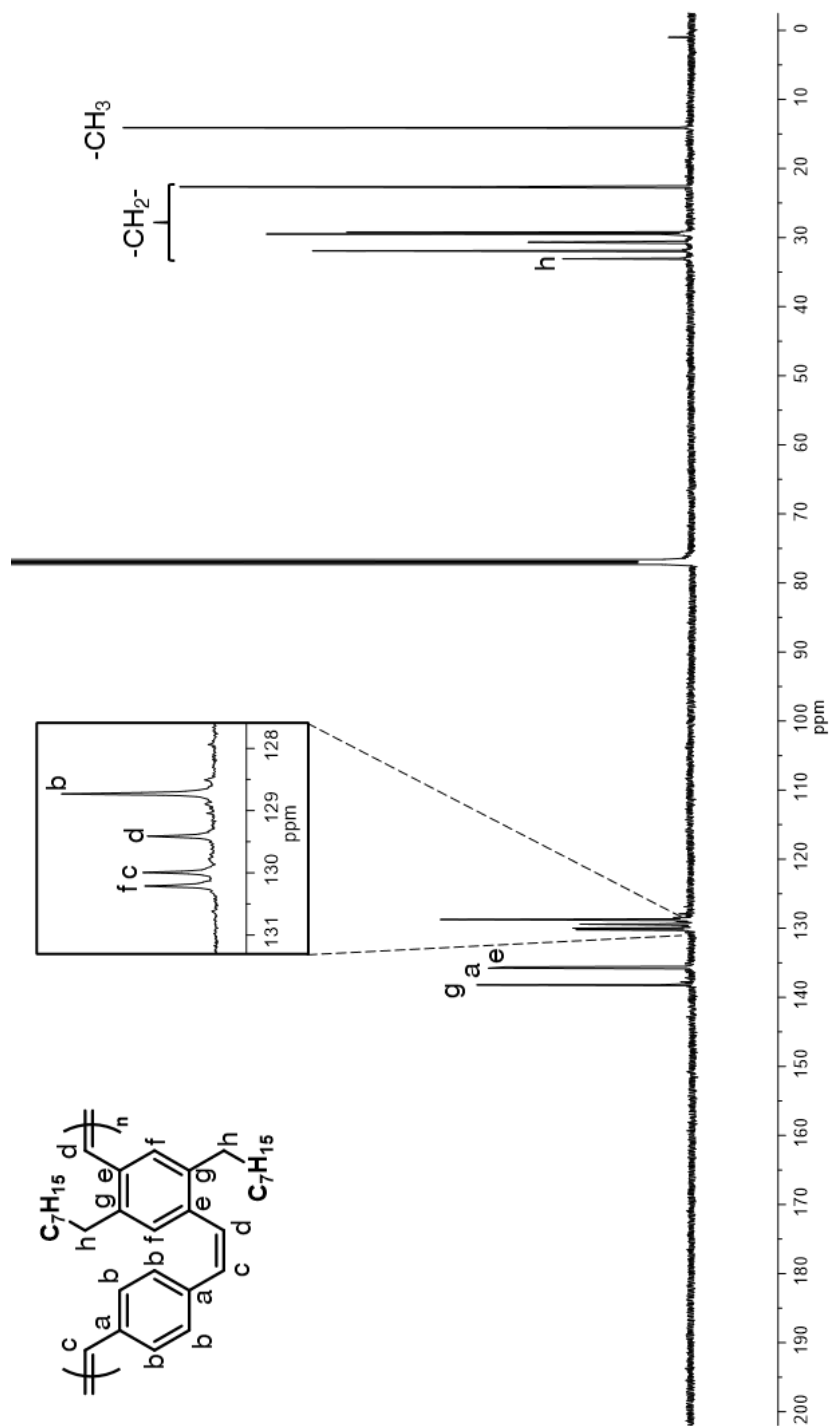
Figure III-16 ^{13}C NMR (126 MHz, CDCl$_3$) spectrum of all-*cis* poly-**1b.**
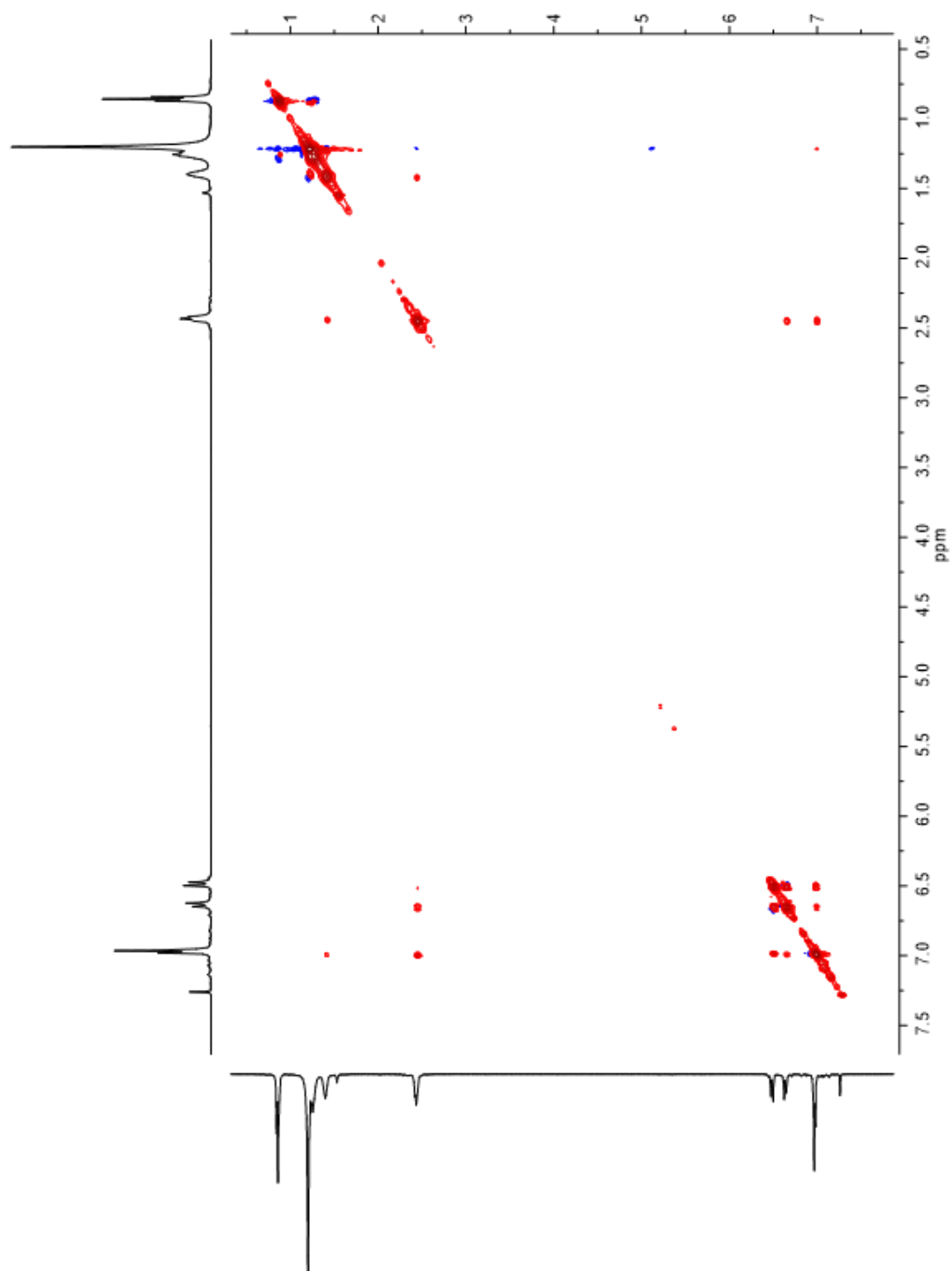
Figure III-17 NOESY spectrum of all-*cis* poly-**1b.**
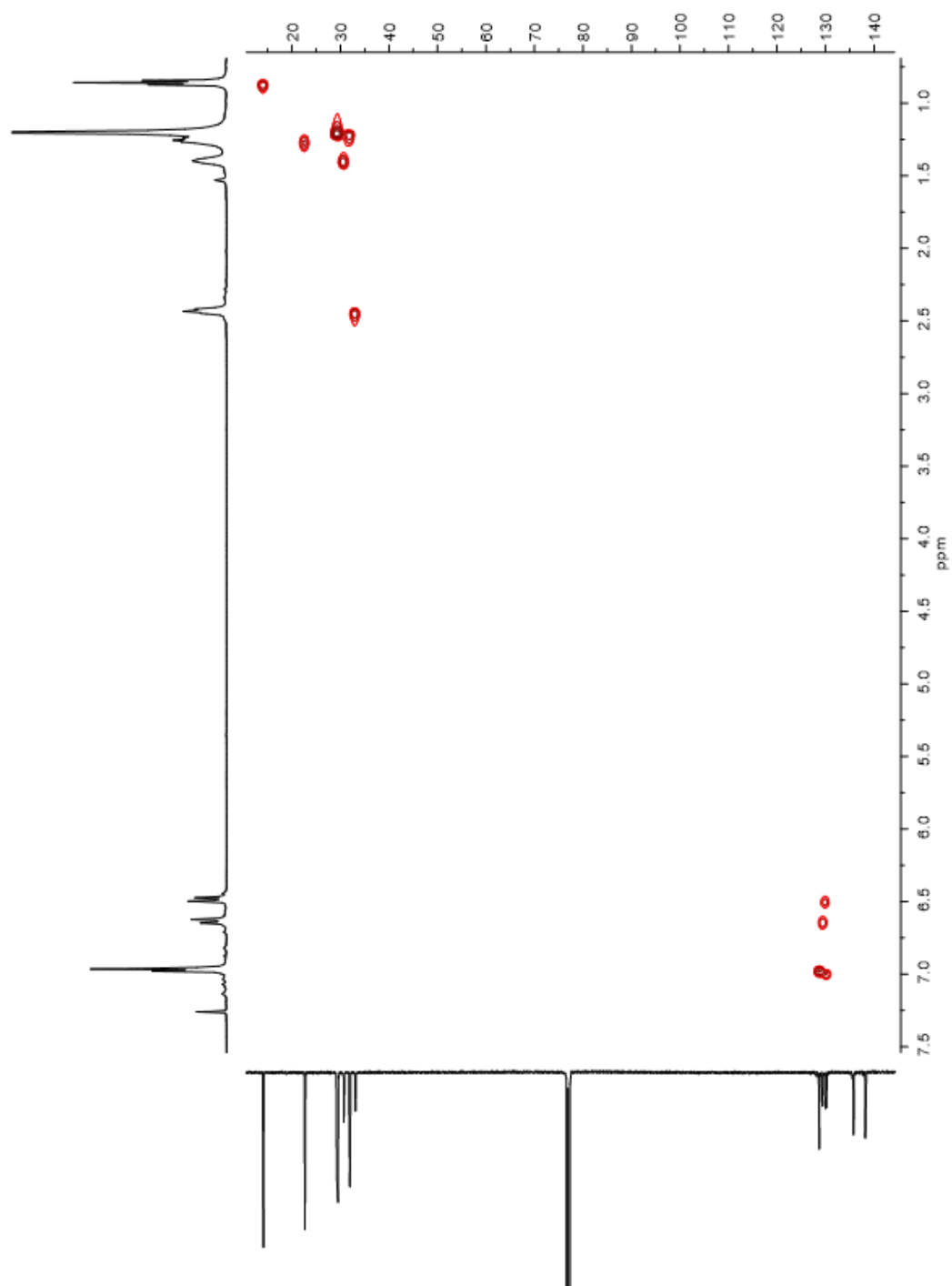
Figure III-18 HSQC spectrum of all-*cis* poly-**1b.**
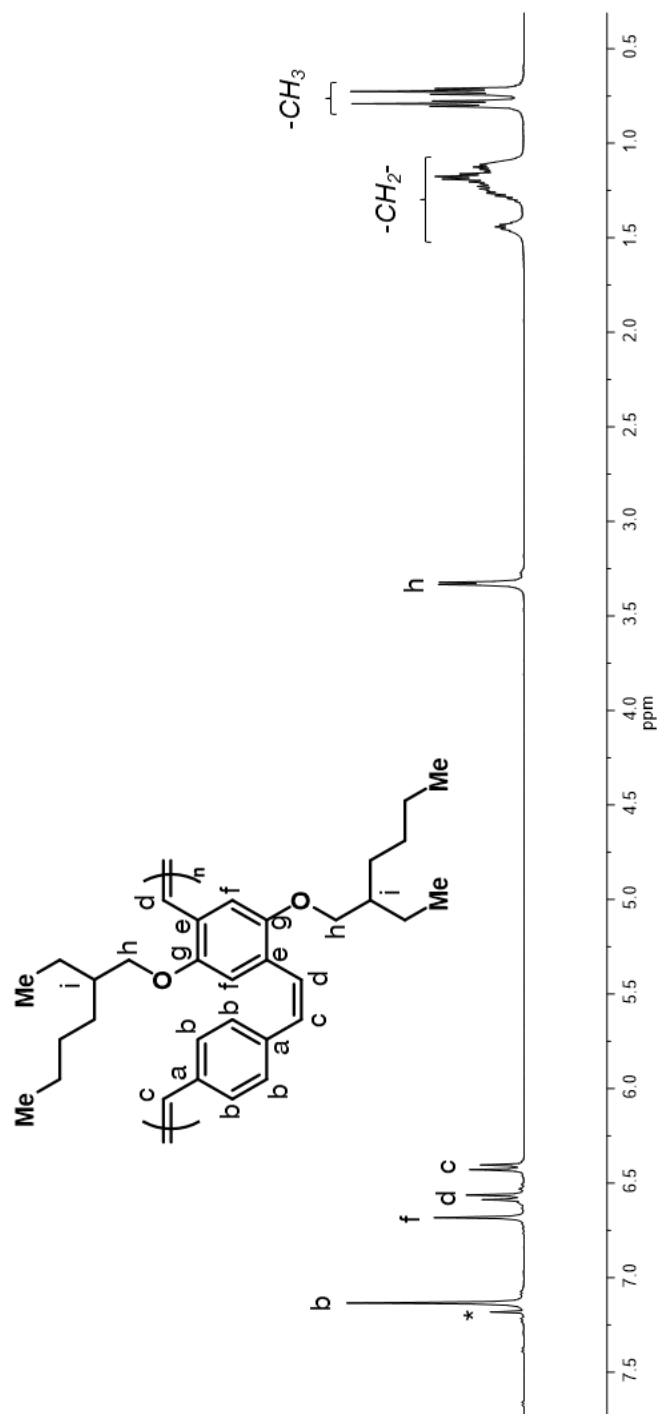
Figure III-19 ^{1}H NMR (500 MHz, CDCl$_3$) spectrum of all-*cis* poly-**1d.**
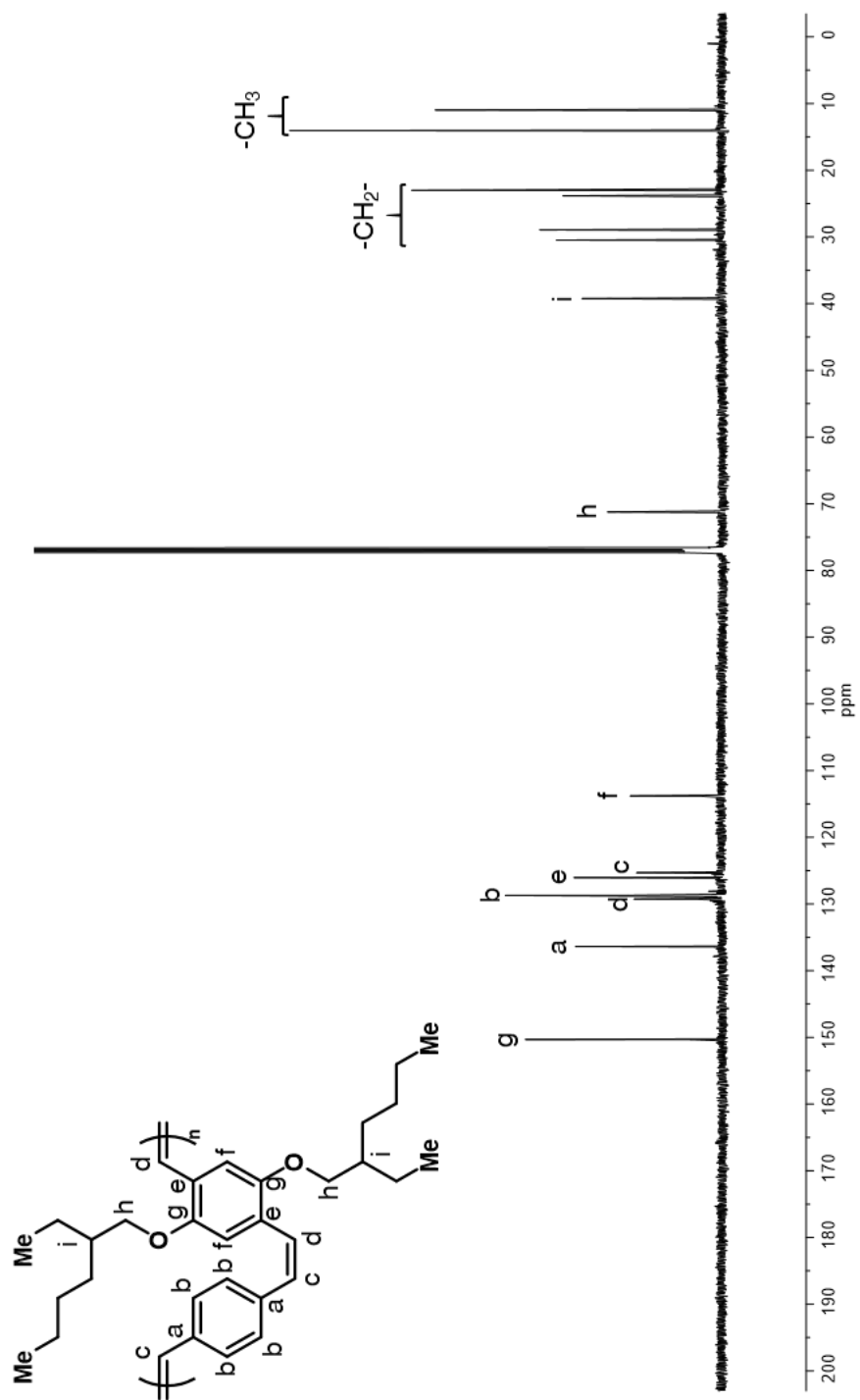
Figure III-20 ^{13}C NMR (126 MHz, CDCl$_3$) spectrum of all-*cis* poly-**1d.**
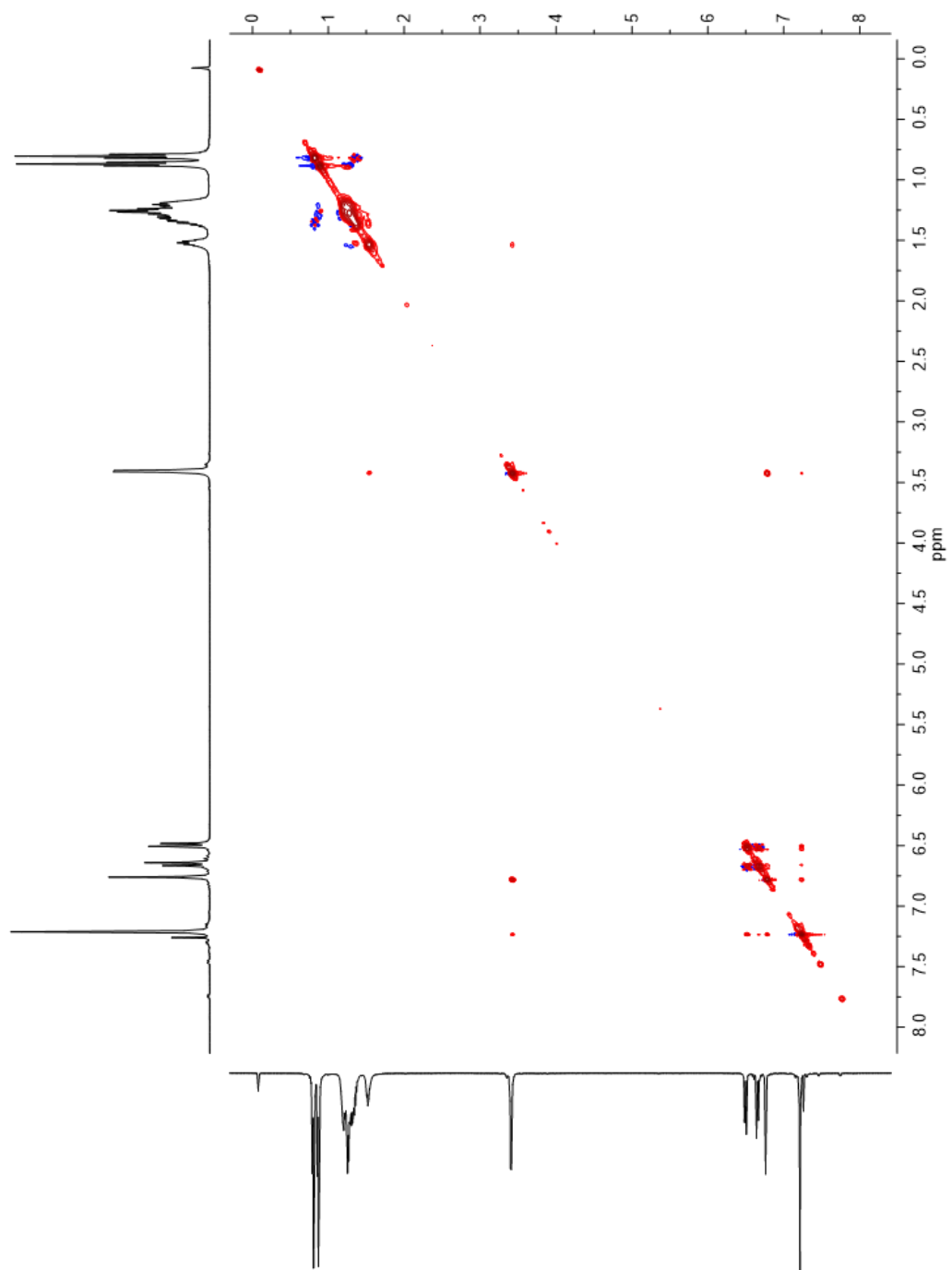
Figure III-21 NOESY spectrum of all-*cis* poly-**1d.**
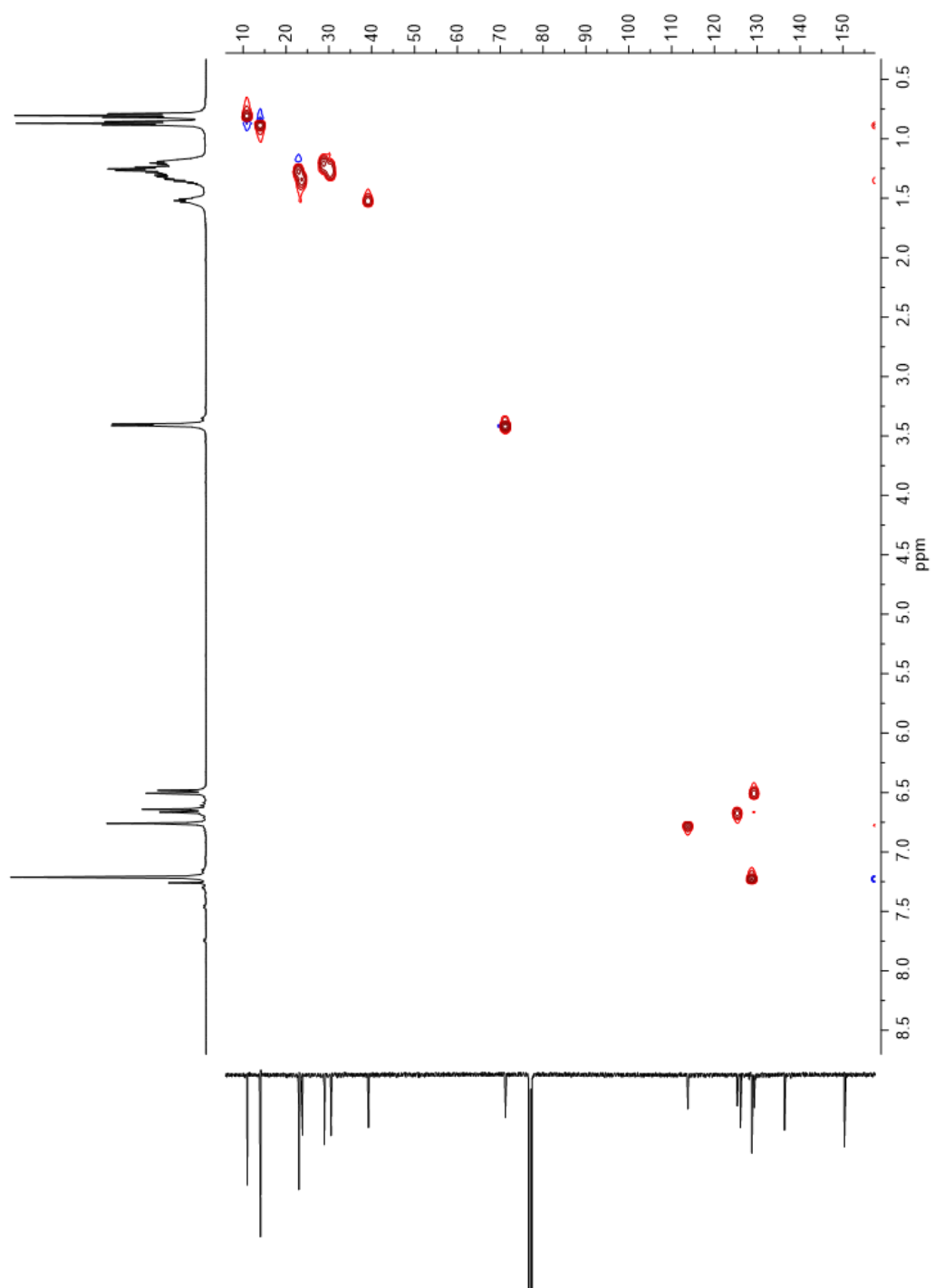
Figure III-22 HSQC spectrum of all-*cis* poly-**1d.**

CHAPTER IV

STEREOCONTROLLED ACYCLIC DIENE METATHESIS POLYMERIZATION[*]

IV.1 Introduction

Perhaps best exemplified by the numerous modifications of the venerable Wittig and Horner–Wadsworth–Emmons reactions, controlling the stereochemistry of alkenes in organic molecules has motivated the development of a myriad of synthetic methods.[81] Indeed, the configuration of alkenes dramatically impacts the shape, properties and reactivity of compounds. Interestingly, despite the importance of this structural parameter on the thermal and mechanical properties of polymeric materials,[5] few polymerizations allow the practitioner to precisely dictate the *cis*:*trans* ratio within macromolecules and these processes are limited to a narrow scope of monomers.[11,82-84] Among the classic examples illustrating the influence of alkene geometry over material properties, *trans*-polyisoprene (gutta percha) is a hard, brittle semi-crystalline material, once used in the manufacturing of golf balls,[10] while the more amorphous *cis*-polyisoprene is an elastic material found in latex gloves.[8,9] Ring-opening metathesis polymerization (ROMP) and acyclic diene metathesis (ADMET) polymerization are among the most powerful methods to access unsaturated polymers but typically afford *cis*/*trans* mixtures or *trans*-rich linkages dictated by the thermodynamic stability of the products.[19] The recent introduction of stereoselective Mo, W and Ru catalysts has paved the way for kinetic control of the olefin metathesis process, overcoming the product preference for *trans* alkenes.[15,18,24,85-89]

While careful catalyst design has afforded impressive *cis* selectivity in a variety of transformations based on olefin metathesis, only a limited number of polymers have been synthesized through stereoselective processes, all through ROMP. For example, dithiolate Ru carbenes uniquely preserve the configuration of the starting olefin throughout the metathesis process.[20,22,90] Hoveyda and co-workers demonstrated that ROMP of norbornene or cyclooctadiene with this family of stereoretentive catalysts leads to exquisite *cis* selectivity along the polymer backbone.[18] Choi and co-workers expanded the scope of norbornene-type monomers for stereoretentive ROMP (ref.[25]) and reported that the shear stability of the resulting all-*cis* polymers was greatly enhanced relative to that of their all-*trans* counterparts. Later, we harnessed the reactivity of this family of catalysts in combination with [2.2]paracyclophane diene monomers to synthesize all-*cis* poly(*p*-phenylene vinylene)s (PPVs) with living characteristics and unusually high molar masses.[1,2] While these examples of stereoretentive ROMP afforded extremely precise polymeric structures (narrow molar mass distributions, perfect *cis* stereoselectivity and so on), the ROMP process typically requires highly strained monomers, thereby narrowing the scope of accessible polymers. Further, these scarce examples only afforded strict *cis* selectivity. In this Article, we report the implementation of stereoretentive olefin metathesis into the ADMET process as a versatile method to access all-*cis* polyalkenamers. Additionally, careful optimization of the reaction conditions provided stereocontrol over the proportion of *cis* and *trans* alkenes throughout the polymer backbone. Several families of alkene-containing polymers were synthesized with

114

predictable *cis*:*trans* ratios from 20:80 to >99:1, providing a valuable strategy to tune the thermal properties of several types of polymers.

One of the major advantages of ADMET over other polymerizations based on olefin metathesis is the simplicity and ubiquity of the monomer structure characterized by the presence of two terminal alkenes. These α,ω-dienes are polymerized following a step-growth mechanism, where removal of ethylene gas is the thermodynamic driving force (Figure IV-1a).[91,92] Pioneered by Wagener and co-workers,[93] ADMET polymerization has been employed to synthesize an impressive variety of polymers including polyethylene with precise alkyl branching,[94] ionic polymers[95] and conjugated polymers, albeit with high *trans* alkene content.[96] Developing a stereoselective ADMET would therefore open the door to a cornucopia of stereodefined polymers for a variety of applications, but several pitfalls were identified at the outset of this work. Since ADMET polymerization relies on
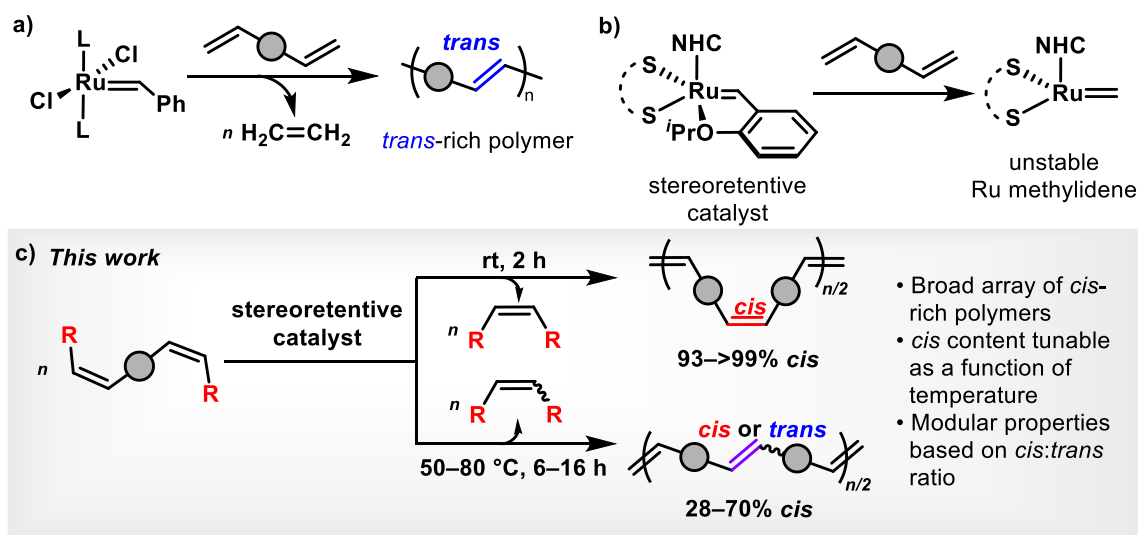
Figure IV-1. Design of stereocontrolled ADMET. a) Typical ADMET polymerizations favor high trans alkene content. b) Dithiolate Ru catalysts lead to highly unstable Ru methylidenes with terminal diene monomers. c) Design of a stereocontrolled ADMET modulated by the reaction temperature.

115

iterative couplings between terminal dienes that are neither *cis* nor *trans*, typical ADMET monomers preclude the stereoretentive mechanism of dithiolate Ru catalysts. Additionally, the Ru methylidene intermediate generated upon reaction of the dithiolate carbene with a terminal alkene is known to readily decompose (Figure IV-1b). This is likely due to a 1,2-shift of the anionic sulfide ligand.[86] Hoveyda and co-workers reported an elegant strategy to circumvent the premature deactivation of the catalyst in the cross metathesis of terminal alkenes through in situ methylene capping with gaseous *cis*-but-2-
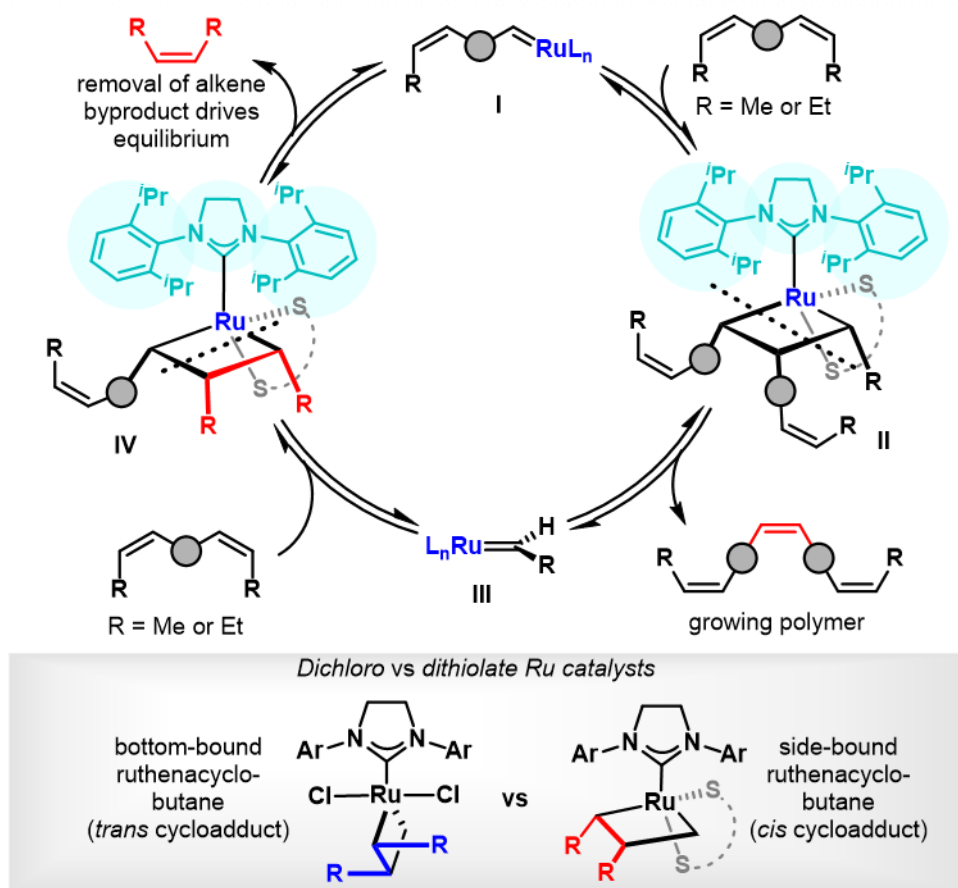
Figure IV-2 Proposed stereoretentive ADMET cycle (the initial reaction between the Ru precatalyst and the monomer was omitted for clarity) through side-bound approach with dithiolate Ru catalysts instead of bottom-bound olefin approach with dichloro Ru catalysts.

ene.[97] However, this approach is not compatible with ADMET, which requires constant removal of volatile alkene by-products to drive the step-growth process. We envisioned that synthesizing capped monomers with pre-installed *cis* geometry would obviate both catalyst decomposition and the need for *cis*-but-2-ene, as well as allow the desired stereoretention (Figure IV-1c). While non-terminal dienes have previously been polymerized using ADMET (ref.[98]), the retention of alkene configuration of the monomer was not observed with Grubbs' second generation catalyst. The proposed mechanistic cycle of a stereoretentive ADMET is outlined in Figure IV-2. The [2 + 2] cycloaddition of carbene intermediate **I** with a capped monomer or a growing polymer would afford ruthenacyclobutane **II** and subsequent cycloreversion would lead to the formation of stabilized Ru ethylidene (R = Me) or propylidene (R = Et) intermediate **III**. In contrast to the bottom-bound approach typically observed with dichloro Ru carbenes, the dithiolate ligand is known to enforce a side-bound approach of the monomer with the alkene substituents pointing away from the bulky aryl groups of the *N*-heterocyclic carbene (NHC) ligand (Figure IV-2).[90] Following cycloreversion, Ru-ethylidene/propylidene **III** would further react with another capped alkene (from a monomer or a growing polymer) to form ruthenacycle **IV**, whose cycloreversion would regenerate a reactive Ru carbene (**I**) and expel volatile *cis*-but-2-ene (R = Me) or *cis*-hex-3-ene (R = Et). Removal of either by-product would drive all equilibria towards a productive cycle.

IV.2 Results and Discussion

IV.2.1 Development of a Stereocontrolled ADMET Process

Capitalizing on the inexpensive and readily available *cis*-hex-4-en-1-ol and *cis*-oct-5-en-1-ol, a variety of monomers were synthesized in one or two steps in high yields (see Figure IV-3 and 'General procedure A' to 'General Procedure E' in the Experimental Detail section).[99-102] These two groups of monomers (**10**–**13** and **14**–**17**) were selected to interrogate the tolerance of dithiolate catalysts to polar monomers containing Lewis basic functional groups, as well as the effect of increasing the size of the capping group (Et versus Me) on the polymerization.

As a benchmark of *cis*/*trans* selectivity, terminal diene **23** was polymerized under standard ADMET conditions using **Ru-1a** (Figure IV-3) in 1,2,4-trichlorobenzene at 50 °C under high vacuum (~100 mtorr) for 16 h. The resulting polymer, poly-**10** (M_n = 13.1 kg/mol, $Đ$ = 2.61, where $Đ$ is the dispersity), was isolated with 23% *cis* content as established by ^{1}H NMR (Table IV-1, entry 1 and Figure IV-11). As expected, the polymerization of **23** with dithiolate catalysts **Ru-6** and **Ru-5b** (Fig. 2b) did not afford any polymers (Table IV-1, entries 2 and 3). Switching to methyl-capped monomer **10** did not result in any increase of *cis* content with **Ru-1a** (Table IV-1, entries 4 and 5) nor with **Ru-1b** (Table IV-1, entry 6). Of note, increasing the temperature with **Ru-1a** allowed the production of poly-**3** with higher molar masses but did not significantly affect the *cis* content. By contrast, methyl-capped monomer **10** in combination with **Ru-6** afforded
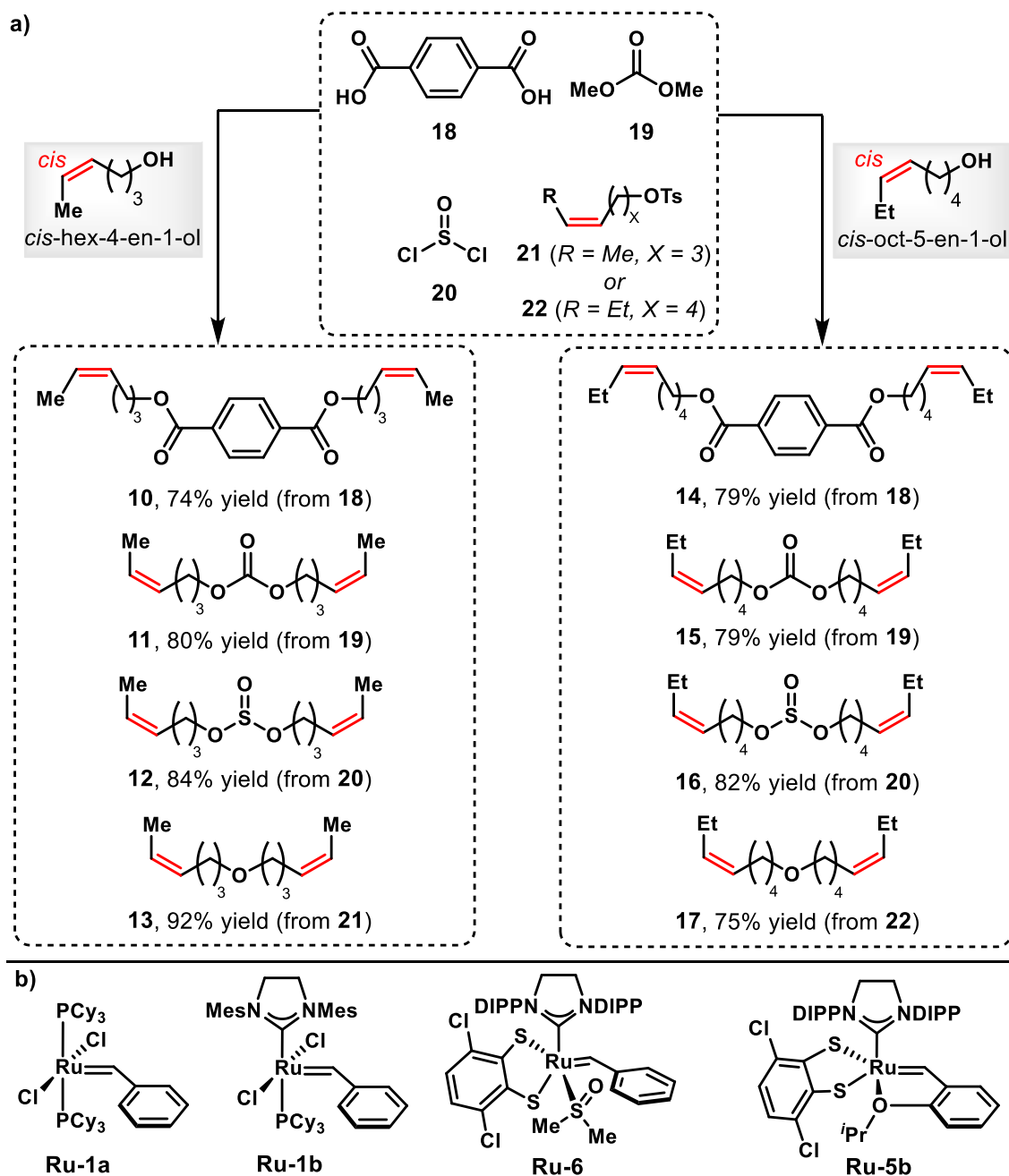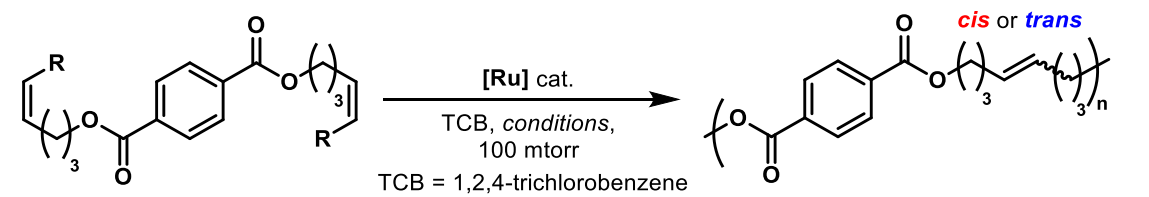
Figure IV-3. Monomers and Ru catalysts. a) Readily accessible methyl- and ethyl-capped *cis,cis*-monomers from commercially available reagents. b) Catalysts screened in stereocontrolled ADMET.

poly-**10** with 54% *cis* content (Table IV-1, entry 7). Interestingly, when the reaction time

was decreased to 4 or 2 h, the molar masses of poly-**10** did not significantly decrease

(M_n = 12.6 and 11.8 kg/mol, respectively), but the *cis* selectivity improved to 62 and 73%

(Table 1, entries 8 and 9), respectively.

Table IV-1 Optimization of Stereoretentive ADMET with Dithiolate Ru Catalysts

entry	monomer	[Ru] (mol%)	Temperature (°C)	Time (h)	M_n (kg/mol)[a]	Đ[b]	cis (%)[c]
1	23	**Ru-1a** (5)	50	16	13.1	2.61	23
2	23	**Ru-6** (5)	50	16	—	—	—
3	23	**Ru-5b** (5)	50	16	—	—	—
4	10	**Ru-1a** (5)	50	16	4.3	1.50	29
5	10	**Ru-1a** (5)	80	16	11.8	2.76	26
6	10	**Ru-1b** (5)	50	16	13.4	2.00	21
7	10	**Ru-6** (5)	50	16	13.1	2.13	54
8	10	**Ru-6** (5)	50	4	12.6	1.74	62
9	10	**Ru-6** (5)	50	2	11.8	1.81	73
10	10	**Ru-6** (0.5)	23	2	13.5	1.88	>99
11	10	**Ru-5b** (0.5)	23	2	13.0	1.75	>99
12	10 (95% *cis*)	**Ru-6** (0.5)	23	2	7.7	1.63	>99

[a]M_n determined through size exclusion chromatography (SEC) in THF against polystyrene standards (RI detection). [b]M_w/M_n. [c]Calculated using ^{1}H NMR analysis.

To our delight, running the polymerization at room temperature to further increase

kinetic control over the polymerization and at lower catalyst loading (0.5 mol%) afforded

perfect cis selectivity (M_n = 13.5 kg/mol, Đ = 1.88, Table IV-1, entry 10). The low catalyst

loading permitted by the high reactivity of **Ru-6** is promising for large-scale applications. Notably, **Ru-5b** furnished an all-*cis* polymer of similar size (M_n = 13.0 kg/mol, $Đ$ = 1.75) when subjected to the same conditions (Table IV-1, entry 11). This is consistent with the step-growth mechanism in Figure IV-2 in which only the activation of the precatalyst differs between **Ru-6** and **Ru-5b**.

Finally, the tolerance to trans impurities in the monomer batch was probed. Indeed, trans alkenes are known to react more slowly with stereoretentive dithiolate catalysts than

a) Polyalkenamers from Methyl-Capped Monomers

poly-**10**
[a]26% *cis*,
M_n = 11.8 kg/mol, $Đ$ = 2.76
[b]99% *cis*,
M_n = 13.5 kg/mol, $Đ$ = 1.88

poly-**11**
[a]24% *cis*,
M_n = 10.0 kg/mol, $Đ$ = 1.55
[b]99% *cis*,
M_n = 8.2 kg/mol, $Đ$ = 1.50

poly-**12**
[a]16% *cis*,
M_n = 10.1 kg/mol, $Đ$ = 1.41
[b]99% *cis*,
M_n = 12.0 kg/mol, $Đ$ = 1.67

poly-**13**
[a]19% *cis*,
M_n = 8.2 kg/mol, $Đ$ = 1.42
[b]99% *cis*,
M_n = 9.2 kg/mol, $Đ$ = 1.31

b) Polyalkenamers from Ethyl-Capped Monomers

poly-**14**
[a]22% *cis*,
M_n = 7.8 kg/mol, $Đ$ = 1.97
[b]94% *cis*,
M_n = 15.9 kg/mol, $Đ$ = 1.87

poly-**15**
[a]22% *cis*,
M_n = 7.5 kg/mol, $Đ$ = 1.46
[b]99% *cis*,
M_n = 7.2 kg/mol, $Đ$ = 1.40

poly-**16**
[a]12% *cis*,
M_n = 6.8 kg/mol, $Đ$ = 1.33
[b]99% *cis*,
M_n = 10.1 kg/mol, $Đ$ = 1.43

poly-**17**
[a]20% *cis*,
M_n = 5.7 kg/mol, $Đ$ = 1.25
[b]93% *cis*,
M_n = 14.0 kg/mol, $Đ$ = 1.62

Figure IV-4. Polymer scope of stereocontrolled ADMET. a) Polymers from methyl-capped monomers (poly-**10**–poly-**13**). b) Polymers from ethyl-capped monomers (poly-**14**–poly-**17**).

121

the *cis* congeners due to the steric clash between one substituent of the ruthenacycle and the NHC ligand.[22] This would potentially allow the use of less expensive, stereochemically impure monomers. Impressively, polymerization of 95% *cis* **10** led to poly-**10** with >99% *cis* content and a slightly diminished molar mass (M_n = 7.7 kg/mol, $Đ$ = 1.63, Table IV-1, entry 12). This finding should open the door to the synthesis of a variety of monomers through diverse synthetic routes (for example, hydrogenation of alkynes with Lindlar's catalyst, Wittig olefination and so on) without the need for perfect diastereoselectivities. Under optimized conditions (Figure IV-4), all-*cis* poly-**11**, poly-**12** and poly-**13** were also obtained from monomers **11**, **12** and **13**, respectively, showing the excellent functional group tolerance of stereoretentive ADMET (Figure IV-4a). These ADMET conditions are also milder compared to those of traditional ADMET processes that are generally conducted at higher temperatures for several hours or even days. After determining
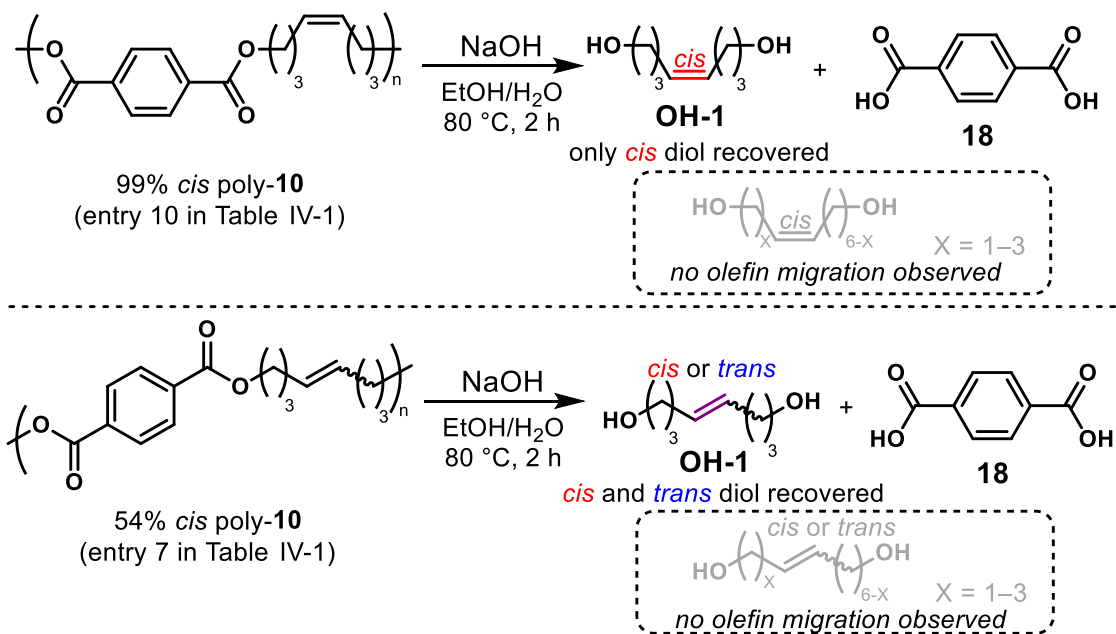
Figure IV-5 Hydrolysis of poly-**3** (99% *cis* from Table IV-1, entry 10 and 54% *cis* from Table IV-1, entry 7) indicates that olefin migration does not take place with **Ru-6.**

122

suitable conditions for the polymerization of methyl-capped monomers, the ethyl-capped monomers were found to only require moderate increases in reaction time (4 instead of 2 h) and catalyst loading (1–2 mol% instead of 0.5 mol%) to access similarly sized all-*cis* polymers, poly-**14**–poly-**17** (Figure IV-4b and Table IV-6–9). The ability to use different capping groups with similarly high cis selectivity should broaden the scope of monomers for the stereoretentive ADMET. The lower *cis*-selectivity observed at 50 °C with **Ru-6** prompted an investigation of temperature modulation as a means to dictate the content of *cis* and *trans* olefins in polyalkenamers. Decreasing amounts of *cis* olefins (from ~70 to ~30%) were obtained when the ADMET polymerization was performed at 50 or 80 °C for increased reaction times (6–16 h) (Figure IV-6 and Table IV-2–9). Olefin isomerization has been reported in ADMET processes with Ru metathesis catalysts containing an NHC ligand such as **Ru-1b**. Several mechanisms have been postulated for this isomerization, including those involving a Ru–H species and metal allyl complexes derived from
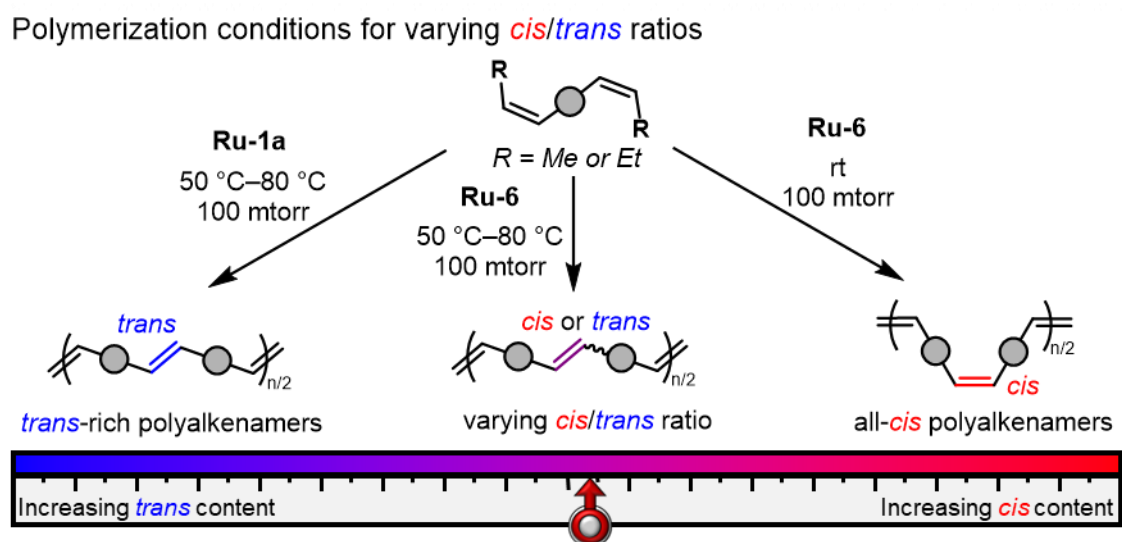
Figure IV-6. Preparation of polyalkenamers with different *cis*/*trans* content via ADMET using different reaction conditions.

123

decomposed catalyst.[103-105] Notably, these pathways generally lead to concomitant alkene migration, which was indeed observed using **Ru-1b** (Figure IV-12).

However, hydrolysis of poly-**10** revealed that olefin migration does not take place with stereoretentive **Ru-6**, neither at room temperature, nor at higher temperatures (Figure IV-5). Hydrolytic degradation of *cis*-rich poly-**10**, poly-**11**, poly-**12**, poly-**14**, poly-**15** and poly-**16** under basic conditions cleanly delivered the *cis* isomer of oct-4-ene-1,8-diol (**OH-1**) or dec-5-ene-1,10-diol (**OH-2**). While the exact mechanism of isomerization remains unclear, modulation of the *cis*/*trans* content without olefin migration was successfully performed with all monomers, thereby providing access to a library of polyalkenamers with tailored backbone geometries from single building blocks. Importantly, the lack of olefin migration engenders more reproducible polymer properties.[106] All polymers were soluble in several organic solvents including dichloromethane, chloroform and tetrahydrofuran. This should facilitate the processability of these materials that are structurally analogous to industrially relevant polymers.

IV.2.2 Study of the Influence of Alkene Stereochemistry over Thermal Behaviour of the Macromolecules

The thermal properties of the synthesized polyalkenamers with varying *cis*/*trans* ratios were analysed using thermogravimetric analysis (TGA) and differential scanning calorimetry (DSC) (see Figure IV-7 for selected polymers and also 'Thermal Characterization' in the Experimental Detail section). While the range of molar masses (~7–25 kg/mol) resulting from the ADMET step-growth process renders the

deconvolution of the impact of olefin stereochemistry challenging in some cases, comparison of polyalkenamers of similar sizes revealed enhanced stability with an increase in *cis* content (Figure IV-7a–c). For poly-**14** with 94% *cis* double bonds ($M_n = 15.9$ kg/mol), a decomposition temperature (T_d) recorded at 5% mass loss was observed at 361 °C compared to 357 °C for 62% *cis* ($M_n = 23.1$/kg mol) and 330 °C for 31% *cis* ($M_n = 19.0$ kg/mol) (Figure IV-7a). The T_d of poly-**15** decreased by 46 °C when going from 99% *cis* to 16% *cis* for almost identical molar masses (Figure IV-7b). Poly-**17** exhibited a T_d of 390 °C for the 93% *cis* polymer ($M_n = 14.0$ kg /mol) as opposed to 374 °C for a 67% *cis* polymer ($M_n = 16.9$ kg/mol, Figure IV-7c). Analogously, all other synthesized polyalkenamers had thermal stabilities that varied with *cis* content (Table

Figure IV-7. Relationship between polymer stereochemistry and thermal properties. TGA thermograms of a) poly-**14**, b) poly-**15**, and c) poly-**17**. DSC thermograms of d) poly-**14**, e) poly-**15**, and f) poly-**17**.

125

IV-10–17). DSC revealed a clear influence of *cis*-alkene content on thermal transitions as shown in the thermograms in Figure IV-7d–f. This is in line with reports by Buchard and co-workers[107] and Dove and Becker and co-workers.[82,108] In addition to small variations of glass transition temperature (T_g), striking differences in crystalline behaviour were observed. For example, *cis*-rich poly-**14**, poly-**15** and poly-**17** appeared amorphous using DSC, while the same polyalkenamers with a majority of *trans* olefins exhibited both a melting (T_m) and a crystallization temperature (T_c). Poly-**14** with only 31 and 21% *cis* olefins showed T_m values of 67 and 86 °C, respectively (Figure IV-7d). The only sample of poly-**15** to present a T_m (38 °C) contained only 16% *cis* linkages (Figure IV-7e). Meanwhile, all other samples of poly-**15** had no observable thermal transitions. Poly-**17** showcased the most diverse thermal profile as a function of alkene stereochemistry. No thermal transitions could be detected with the 93 and 67% *cis* forms, but T_m and T_c values were measured for samples with decreased *cis* content (38 and 20%) (Figure IV-7f). DSC analysis of the two *trans*-rich poly-**17** samples revealed sharp melting transitions with T_m values of −6 °C (20% *cis*) and −19 °C (38% *cis*). Other synthesized polyalkenamers such as poly-**16** showed amorphous characteristics regardless of *cis* content with no thermal transitions detected in the DSC (Figure IV-29). While the nature of the polar groups and the number of methylenes in the repeating unit clearly impact the phase transitions of the polyalkenamers, controlling the geometry of alkenes throughout the backbone provides an additional handle to tune the thermal properties of a variety of polymers.

IV.3 Conclusion

Control over the molecular structure and physical properties of polyalkenamers—including polyesters, polycarbonates, polysulfites and polyethers—has been achieved through stereocontrolled ADMET. This method uses methyl- or ethyl-capped diene monomers to impart both the stereochemical information and catalyst stability critical to the polymerization process. Over 99% *cis* selectivity was achieved for a variety of polymers including unsaturated polyesters, polycarbonates, polysulfites and polyethers, which is a testament to the versatility of this method. The high reactivity of stereoselective dithiolate Ru catalysts towards *cis* monomers led to a low catalyst loading (0.5 mol%), rapid reaction at room temperature (2–4 h) and tolerance towards *trans* monomer impurities, which are all attractive features for large-scale implementation. Stereoretention during the polymerization process was found to be sensitive to the reaction conditions. This provided a functional handle to modulate the ratio of *cis*:*trans* alkene units within the polymer backbone. This stereocontrol was harnessed to produce a variety of polyalkenamers with predictable *cis*:*trans* ratios from 20:80 to >99:1 and to study the influence of alkene geometry over the thermal properties of the macromolecules. Increased thermal stability was generally correlated to increased *cis* olefin content and thermal transitions such as T_g, T_m and T_c were greatly affected by the stereochemistry of the alkenes in the backbone. Of note, polyesters, polycarbonates and polysulfites were prepared and exhibited tunable phase transition temperatures and efficient depolymerization via hydrolysis. This process provides a practical and efficient handle to control material properties for a large variety of olefin-containing polymers. Therefore,

this method aligns well with the polymer field's pursuit of precise macromolecular structures for soft materials with designable properties and functionality.[109]

IV.4 Experimental Procedures and Data

IV.4.1 General Reagent Information

All reactions were carried out under an inert nitrogen atmosphere with dry solvents under anhydrous conditions unless otherwise stated. Dry dichloromethane (DCM), diethyl ether (Et$_2$O), tetrahydrofuran (THF), toluene (PhMe) were obtained by passing the previously degassed solvents through activated alumina columns. Anhydrous 1,2,4-trichlorobenzene (TCB) was purchased from Sigma Aldrich and used without further purification and degassed via "freeze-pump-thaw" before being brought into a nitrogen-filled glove box. Syntheses of polymers using stereoretentive ruthenium catalysts were carried out in a nitrogen-filled glove box (SG1800/750TS-F, VIGOR). Reagents were purchased at the highest commercial quality and used without further purification, unless otherwise stated. For example, *cis*-hex-4-en-1-ol was purchased from TCI (>95% purity, $8.17/g, 2022) and *cis*-oct-5-en-1-ol was purchased from Sigma Aldrich (≥ 97% purity, $0.84/g, 2022). Yields refer to chromatographically and spectroscopically (^{1}H NMR) homogeneous material, unless otherwise stated. Reactions were monitored by thin layer chromatography (TLC) carried out on 250 μm SiliCycle SiliaPlate™ silica plates (F254), using UV light as the visualizing agent and a solution of KMnO$_4$ and heat as a developing agent. Flash silica gel chromatography was performed using SiliCycle SiliaFlash®

Irregular Silica Gel (60 Å, particle size 40–063 μm). Polymers were isolated after precipitation using an Eppendorf 5804 centrifuge.

IV.4.2 General Analytic Information

All polymer samples were analyzed using a Tosoh EcoSec HLC 8320GPC system with a TSKgel SuperHM-M column and a TSKgel SuperH-RC column at a flow rate of 0.40 mL/min at 40 °C. THF stabilized with BHT was used as the eluent and all number-average molecular weights (M_n), weight-average molecular weights (M_w), and dispersities ($Đ$) for polymers were calculated from refractive index and UV chromatograms against TSKgel polystyrene standards. NMR spectra were recorded on Bruker Avance Neo 400 instruments and were calibrated using residual undeuterated solvent as an internal reference (CHCl$_3$ @ 7.26 ppm ^{1}H-NMR, 77.16 ppm ^{13}C-NMR). The following abbreviations were used to explain NMR peak multiplicities: s = singlet, d = doublet, dd = doublet of doublets, t = triplet, q = quartet, p = pentet, m = multiplet, br = broad. Thermogravimetric analysis (TGA) was performed on a TA Instruments TGA 5500 Thermogravimetric Analyzer. Differential scanning calorimetry (DSC) was performed using a TA instrument DSC 2500. FT-IR spectra were acquired using an Agilent Cary 630 FT-IR in the ATR mode. High-resolution mass spectra (HRMS) were recorded on an Agilent LC/MSD TOF mass spectrometer by Atmospheric pressure chemical ionization (APCI) or electrospray ionization (ESI).

Thermogravimetric analysis (TGA)

Samples were weighed on to a platinum sample pan (2–3 mg). Samples were heated at 20 °C/min to 100 °C, followed by an isothermal period of 1 minute, and then heated at 10 °C/min to 600 °C under nitrogen.

Differential scanning calorimetry (DSC)

Samples (around 2–6 mg) were heated to 150–200 °C at 10 °C/min, followed by an isothermal period of 5 minutes. The samples were then cooled to −70 °C at 10 °C/min, followed by an isothermal period of 5 minutes. This process was repeated three times. For poly-**11** and poly-**15**, a slower heating rate of 5 °C/min was used.

IV.4.3 Monomer Synthesis
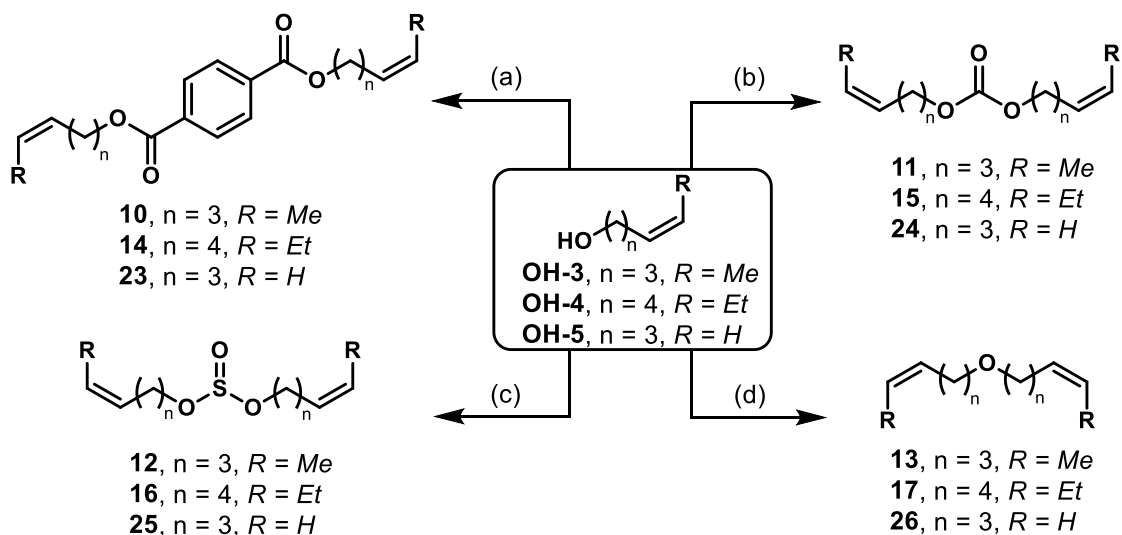
Figure IV-8 Monomer syntheses from commercially available unsaturated alcohols **OH-3–5**. (a) terephthalic acid (**18**), DCC, DMAP, DCM, rt, 24 h; (b) dimethylcarbonate (**19**), NaOH, Hexanes, 95 °C, 7–14 h; (c) thionyl chloride (**20**), Et3N, DCM, 2 h, 0 °C to rt; (d) 1) TsCl, pyridine, DCM, rt, 2 h; 2) R–OH (**OH-3–5**), NaH, DMF, 0 °C to rt, 14 h.

General procedure A: synthesis of aromatic diester monomers

Terephthalic acid **18** (1 equiv), DCC (2.1 equiv), and DMAP (0.1 equiv) were weighed into a flame-dried round bottom flask equipped with a stir bar. The flask was evacuated and backfilled with N_2 three times. Anhydrous DCM (concentration of terephthalic acid: $C = 0.1$ M) was added to the flask, followed by dropwise addition of unsaturated alcohol **OH-3**, **OH-4**, or **OH-5** (1 equiv). The mixture was stirred at room temperature for 24 h. The reaction mixture was then filtered through a pad of celite (~ 2 cm) and the volatiles were removed *in vacuo*. Column chromatography (SiO$_2$, 1:1 hexane:DCM to 100% DCM) afforded the desired ester as a clear oil.

cis,cis-Monomer **10**

10
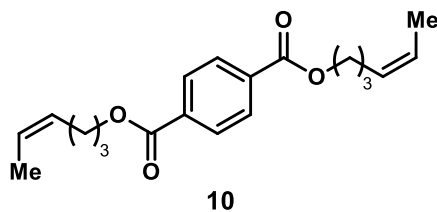
Synthesized following **general procedure A** using *cis*-hex-4-en-1-ol (**OH-3**) (35.9 mmol), terephthalic acid (**18**) (17.1 mmol), DCC (39.4 mmol), and DMAP (1.7 mmol). Yield: 4.1 g, 12.4 mmol, 74%.

^{1}H NMR (400 MHz, CDCl$_3$) δ 8.11 (s, 4 H), 5.57–5.37 (m, 4 H), 4.38–4.32 (t, *J* = 6.5 Hz, 4 H), 2.26–2.18 (q, *J* = 7.2 Hz, 4 H), 1.90–1.81 (p, *J* = 6.7 Hz, 4 H), 1.64–1.59 (dd, *J* = 1.5 Hz, 5.2 Hz, 6 H) ppm.

^{13}C NMR (101 MHz, CDCl$_3$) δ 166.0, 134.3, 129.6, 129.1, 125.3, 65.0, 28.6, 23.4, 12.9 ppm.

HRMS-APCI: calc'd. for C$_{20}$H$_{27}$O$_4$ [M+H]$^+$ 331.1904, found 331.1901.

cis,cis-Monomer **14**

14
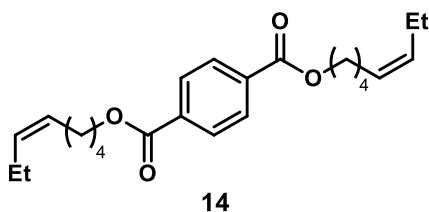
Synthesized following **general procedure A** using *cis*-oct-5-en-1-ol (**OH-4**) (13.3 mmol), terephthalic acid (**18**) (6.0 mmol), DCC (12.2 mmol), and DMAP (0.6 mmol). Yield 1.7 g, 4.7 mmol, 79%.

^{1}H NMR (400 MHz, CDCl$_3$) δ 8.09 (s, 4 H), 5.44–5.30 (m, 4 H), 4.35 (t, *J* = 6.6 Hz, 4 H), 2.14–2.01 (m, 8 H), 1.83–1.76 (m, 4 H), 1.55–1.48 (m, 4 H), 0.96 (t, *J* = 7.5 Hz, 6 H) ppm.

^{13}C NMR (101 MHz, CDCl$_3$) δ 165.9, 134.2, 132.3, 129.5, 128.4, 65.4, 28.2, 26.6, 26.1, 20.5, 14.3 ppm.

HRMS-APCI: calc'd. for C$_{24}$H$_{35}$O$_4$ [M+H]$^+$ 387.2530, found 387.2530.

Monomer **23**

23
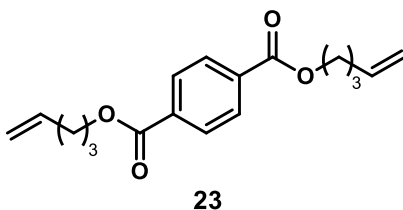
Synthesized following **general procedure A** using pent-4-en-1-ol (**OH-5**) (11.6 mmol), terephthalic acid (**18**) (5.8 mmol), DCC (14.5 mmol), and DMAP (0.6 mmol). Yield: 1.1 g, 3.5 mmol, 60%.

The spectroscopic data for this compound were identical to those reported in the literature.[99]

^{1}H NMR (400 MHz, CDCl$_3$) δ 8.10 (s, 4 H), 5.92–5.78 (m, 2 H), 5.13–4.98 (m, 4 H), 4.39–4.34 (t, *J* = 6.6 Hz, 4 H), 2.27–2.19 (q, *J* = 7.1 Hz, 4 H), 1.95–1.84 (p, *J* = 6.7 Hz, 4 H) ppm.

General procedure B: synthesis of carbonate monomers

General procedure B was adapted from the literature.[110] NaOH (0.05 equiv) was weighed into a flame-dried 25 mL round bottom flask equipped with a stir bar. The flask was then fitted with a Dean-Stark apparatus and a condenser. Distilled H$_2$O (7 mL) was then added to the Dean-Stark apparatus and degassed under vacuum for 10 min. Hexanes were degassed by vigorous purging with Ar and added to the Dean-Stark until the apparatus was filled to the point of spilling over into the collection flask. Degassed hexanes (concentration of dimethyl carbonate: C =1 M) were then added to the flask followed by dimethyl carbonate **19** (0.5 equiv) and the unsaturated alcohol **OH-3**–**5** (1.0 equiv). The reaction was then lowered into an oil bath at 95 °C and wrapped with aluminum foil. After 1 h, another equivalent of unsaturated alcohol was added and heating continued for 13 h. The round bottom flask was then allowed to cool to room temperature, hexanes were removed *in vacuo*, and the contents were subjected to column chromatography (SiO$_2$, 5:95 EtOAc:hexanes, visualized by KMnO$_4$ stain), which afforded the unsaturated carbonate as a clear oil.

cis,*cis*-Monomer **11**
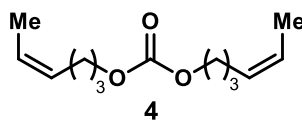
Synthesized following **general procedure B** using *cis*-hex-4-en-1-ol (**OH-3**) (40.0 mmol), dimethyl carbonate (**19**) (10.0 mmol), and NaOH (1.0 mmol) Yield: 1.8 g, 8.0 mmol, 80%.

^{1}H NMR (400 MHz, CDCl$_3$) δ 5.55–5.32 (m, 4 H), 4.13 (t, J = 6.7 Hz, 4 H), 2.18–2.10 (q, J = 7.4 Hz, 4 H), 1.78–1.69 (p, J = 6.7 Hz, 4 H), 1.62–1.58 (dd, J = 5.0 Hz, 1.7 Hz, 6 H) ppm.

^{13}C NMR (101 MHz, CDCl$_3$) δ 155.7, 129.2, 125.4, 67.7, 28.8, 23.3, 13.0 ppm.

HRMS-APCI: calc'd. for C$_{13}$H$_{22}$O$_3$ [M+H]$^+$ 227.1642, found 227.1641.

cis,*cis*-Monomer **15**
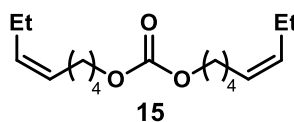
Synthesized following **general procedure B** using *cis*-oct-5-en-1-ol (**OH-4**) (31.0 mmol), dimethyl carbonate (**19**) (7.8 mmol), NaOH (0.8 mmol). Yield 1.7 g, 6.2 mmol, 79%.

^{1}H NMR (400 MHz, CDCl$_3$) δ 5.48–5.19 (m, 4 H), 4.13 (t, J = 6.7 Hz, 4 H), 2.13–1.94 (m, 8 H), 1.76–1.61 (m, 4 H), 1.51–1.37 (m, 4 H), 0.95 (t, J = 7.5 Hz, 6 H) ppm.

^{13}C NMR (101 MHz, CDCl$_3$) δ 155.4, 132.2, 128.4, 67.9, 28.2, 26.6, 25.8, 20.5, 14.3 ppm.

HRMS-+ESI: calc'd. for C$_{17}$H$_{30}$O$_3$ [M+H]$^+$ 283.2268, found 283.2267.

Monomer **24**

24
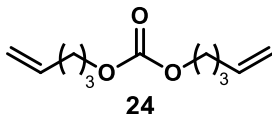
Synthesized following **general procedure B** using pent-4-en-1-ol (**OH-5**) (12.0 mmol), dimethyl carbonate (**19**) (2.9 mmol), and NaOH (0.3 mmol) Yield: 345.0 mg, 1.7 mmol, 60%.

The spectroscopic data for this compound were identical to those reported in the literature.[100]

^{1}H NMR (400 MHz, CDCl$_3$) δ 5.89–5.72 (m, 2 H), 5.09–4.96 (m, 4 H), 4.14 (t, J = 6.6 Hz, 4 H), 2.19–2.10 (q, J = 7.4 Hz, 4 H), 1.82–1.73 (p, J = 6.6 Hz, 4 H) ppm.

General procedure C: synthesis of sulfite monomers

General procedure C was based on a literature procedure.[102] To a flame dried round-bottom flask, anhydrous DCM (0.6 M), unsaturated alcohol **OH-3**, **OH-4**, or **OH-5** (2 equiv), and Et$_3$N (2 equiv) were added. The flask was cooled to 0 °C with an ice/water bath and thionyl chloride **20** (1 equiv) was added dropwise. After addition of thionyl chloride, the turbid solution was removed from the ice/water bath and allowed to warm slowly to room temperature. After stirring the reaction for 2 h, the unsaturated alcohol was fully consumed as determined by TLC analysis (1:1 Hexanes:DCM, visualized by KMnO$_4$ stain). The mixture was then washed with distilled H$_2$O. The aqueous layer was then extracted with DCM. The combined organic layers were then washed with brine and

subsequently dried over sodium sulfate. The volatiles were then removed *in vacuo*, leaving a yellow oil that was subjected to column chromatography (SiO$_2$, 1:1 hexanes: DCM). The desired product was isolated as a clear oil.

cis,cis-Monomer **12**
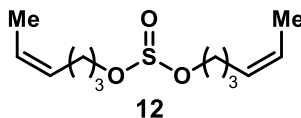
Synthesized following **general procedure C** using *cis*-hex-4-en-1-ol (**OH-3**) (20.0 mmol), Et$_3$N (20.0 mmol), and thionyl chloride (**20**) (10.0 mmol). Yield: 2.1 g, 8.4 mmol, 84% yield.

^{1}H NMR (400 MHz, CDCl$_3$) δ 5.56–5.46 (m, 2 H), 5.40–5.31 (m, 2 H), 4.08–3.89 (m, 4 H), 2.19–2.11 (q, *J* = 7.1 Hz, 4 H), 1.78–1.70 (p, *J* = 6.6 Hz, 4 H), 1.63–1.59 (dd, *J* = 6.7 Hz, 1.7 Hz, 6 H) ppm.

^{13}C NMR (101 MHz, CDCl$_3$) δ 128.7, 125.2, 61.7, 29.3, 23.0, 12.8 ppm.

HRMS-APCI: calc'd. for C$_{12}$H$_{22}$O$_3$S$_1$ [M+H]$^+$ 247.1362, found 247.1362.

cis,cis-Monomer **16**
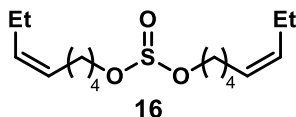
Synthesized following **general procedure C** using *cis*-oct-5-en-1-ol (**OH-4**) (6.6 mmol), Et$_3$N (6.6 mmol), and thionyl chloride (**20**) (3.3 mmol). Yield: 0.8 g, 2.7 mmol, 82% yield.

^{1}H NMR (400 MHz, CDCl$_3$) δ 5.50–5.21 (m, 4 H), 4.05–3.89 (m, 4 H), 2.09–1.99 (m, 8 H), 1.72–1.64 (m, 4 H), 1.48–1.40 (m, 4 H), 0.95 (t, *J* = 7.5 Hz, 6 H).

^{13}C NMR (101 MHz, CDCl$_3$) δ 132.3, 128.2, 62.1, 29.0, 26.5, 25.8, 20.5, 14.3 ppm.

HRMS-ESI: calc'd. for C$_{16}$H$_{31}$O$_3$S [M+H]$^+$ 303.1988, found 303.1987.

Monomer **25**

25
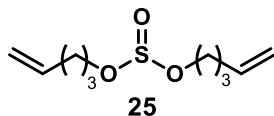
Synthesized following **general procedure C** using pent-4-en-1-ol (**OH-5**) (11.6 mmol), Et$_3$N (11.6 mmol), and thionyl chloride (**20**) (5.8 mmol). Yield: 0.7 g, 3.3 mmol, 56% yield.

The spectroscopic data for this compound were identical to those reported in the literature.[102]

^{1}H NMR (400 MHz, CDCl$_3$) δ 5.85–5.73 (m, 2 H), 5.09–4.98 (m, 4 H), 4.08–3.90 (m, 4 H), 2.20–2.12 (m, 4 H), 1.82–1.74 (m, 4 H) ppm.

General procedure D: synthesis of tosylate intermediates

General procedure D was based on a literature procedure.[111] In a flame-dried round bottom flask equipped with a stir bar, tosyl chloride (1.1 equiv) and DMAP (0.1 equiv) were added. The contents were evacuated and backfilled with N$_2$ three times. Anhydrous DCM (alcohol concentration: C = 0.4 M) was then added to the flask under an atmosphere of N$_2$. Unsaturated alcohol **OH-3**, **OH-4**, or **OH-5** (1 equiv) was added dropwise, followed by anhydrous Et$_3$N (2.3 equiv). After stirring reaction (between 90–120 minutes as monitored by TLC) at room temperature, the contents were washed with distilled H$_2$O

three times and brine once. The organic layer was dried over sodium sulfate and the volatiles were removed *in vacuo*. Purification via column chromatography (SiO$_2$, 2:1 hexanes: DCM) afforded the desired tosylate compound as a clear oil.

cis-Tosylate **21**

21
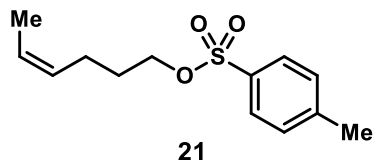
Synthesized following **general procedure D** using *cis*-hex-4-en-1-ol (**OH-3**) (10.0 mmol), tosyl chloride (11.0 mmol), DMAP (1.0 mmol), and Et$_3$N (23.0 mmol). Yield: 2.4 g, 9.4 mmol, 94%.

^{1}H NMR (400 MHz, CDCl$_3$) δ 7.79 (d, J = 8.3 Hz, 2 H), 7.34 (d, J = 8.1 Hz, 2 H), 5.51–5.42 (m, 1 H), 5.29–5.21 (m, 1H), 4.06–4.01 (t, J = 6.4 Hz, 2 H), 2.45 (s, 3 H) 2.11–2.03 (q, J = 7.3 Hz, 2 H), 1.74–1.66 (p, J = 6.5 Hz, 2 H), 1.57–1.53 (dd, J = 6.8, 1.6 Hz, 3 H) ppm.

^{13}C NMR (101 MHz, CDCl$_3$) δ 144.8, 133.4, 129.9, 128.4, 128.0, 125.7, 70.2, 28.8, 22.8, 21.8, 12.8 ppm.

HRMS-ESI: calc'd. for C$_{13}$H$_{18}$O$_3$S$_1$ [M+Na]$^+$ 277.0869, found 277.0872.

cis-Tosylate **22**

22
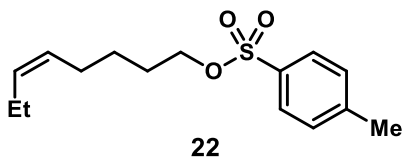
Synthesized following **general procedure D** using *cis*-oct-5-en-1-ol (**OH-4**) (13.3 mmol), tosyl chloride (14.6 mmol), DMAP (1.3 mmol), and Et$_3$N (17.2 mmol). Yield: 2.8 g, 9.9 mmol, 75%.

^{1}H NMR (400 MHz, CDCl$_3$) δ 7.79 (d, *J* = 8.3 Hz, 2 H), 7.34 (d, *J* = 8.1 Hz, 2 H), 5.36–5.17 (m, 2 H), 4.02 (t, *J* = 6.5 Hz, 2 H), 2.45 (s, 3 H), 1.98 (m, 4 H), 1.72–1.59 (m, 2 H), 1.44–1.32 (m, 2 H), 0.93 (t, *J* = 7.5 Hz, 3 H).

^{13}C NMR (101 MHz, CDCl$_3$) δ 144.6, 133.2, 132.4, 129.8, 128.0, 127.9, 70.5, 28.3, 26.2, 25.3, 21.6, 20.5, 14.3 ppm.

HRMS-ESI: calc'd. for C$_{15}$H$_{22}$O$_3$S$_1$ [M+Na]$^+$ 305.1182, found 305.1188.

Tosylate **27**

27
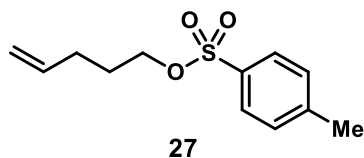
Synthesized following **general procedure D** using pent-4-en-1-ol (**OH-5**) (5.8 mmol), tosyl chloride (6.4 mmol), DMAP (0.58 mmol), and Et$_3$N (13.3 mmol). Yield: 1.4 g, 5.5 mmol, 98%.

The spectroscopic data for this compound were identical to those reported in the literature.[112]

^{1}H NMR (400 MHz, CDCl$_3$) δ 7.79 (d, *J* = 8.3 Hz, 2 H), 7.35 (d, *J* = 8.0 Hz, 2 H), 5.75–5.63 (m, 1H), 4.99–4.96 (m, 1H), 4.95–4.92 (m, 1H), 4.06–4.01 (t, *J* = 6.4 Hz, 2 H), 2.45 (s, 3 H) 2.12–2.05 (q, *J* = 7.0 Hz, 2 H), 1.78–1.70 (p, *J* = 6.4 Hz, 2 H) ppm.

General procedure E: synthesis of ether monomers

General procedure E was modified from a literature procedure.[113] A flame-dried reaction flask was charged with unsaturated tosylate **21**, **22**, or **27** (1 equiv), which was then dissolved in anhydrous DMF (C = 0.3 M) under Ar. Sodium hydride (1.2 equiv, 60% dispersion in mineral oil) was added to the round bottom flask, which was subsequently cooled to 0 °C in an ice/water bath. Unsaturated alcohol **OH-3**, **OH-4**, or **OH-5** (1.2 equiv) was added dropwise to the flask under Ar. After complete addition, the round bottom flask was allowed to slowly warm to room temperature and the mixture were stirred overnight. The yellow-orange solution was further diluted in ether and washed three times with a saturated ammonium chloride solution and once with brine. The organic layer was then dried over sodium sulfate and the solvent was removed *in vacuo*. Purification via column chromatography (SiO$_2$, hexanes) afforded the desired monomer as a clear oil.

cis,*cis*-Monomer **13**
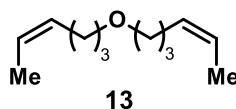
Synthesized following **general procedure E** using tosylate **21** (10.0 mmol), *cis*-hex-4-en-1-ol (**OH-3**) (12.0 mmol), and sodium hydride (60% dispersion in mineral oil) (12.0 mmol). Yield: 1.7 g, 9.2 mmol, 92%.

^{1}H NMR (400 MHz, CDCl$_3$) δ 5.52–5.33 (m, 4 H), 3.45–3.36 (t, *J* = 6.6 Hz, 4 H), 2.17–2.06 (q, *J* = 7.1 Hz, 4 H), 1.68–1.58 (m, 10 H) ppm.

^{13}C NMR (101 MHz, CDCl$_3$) δ 130.1, 124.4, 70.4, 29.7, 23.6, 12.9 ppm.

HRMS-APCI: calc'd. for C$_{12}$H$_{23}$O$_1$ [M+H]$^+$ 183.1743, found 183.1744.

cis,*cis*-Monomer **17**
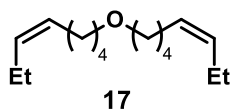
Synthesized following **general procedure E** using tosylate **22** (9.7 mmol), *cis*-oct-5-en-1-ol (**OH-4**) (10.2 mmol), and sodium hydride (60% dispersion in mineral oil) (12.7 mmol). Yield: 1.7 g, 7.3 mmol, 75%.

^{1}H NMR (400 MHz, CDCl$_3$) δ 5.55–5.16 (m, 4 H), 3.40 (t, *J* = 6.6 Hz, 4 H), 2.12–1.92 (m, 8 H), 1.62–1.54 (m, 4 H), 1.44–1.36 (m, 4 H), 0.95 (t, *J* = 7.5 Hz, 6 H) ppm.

^{13}C NMR (101 MHz, CDCl$_3$) δ 131.8, 128.9, 70.8, 29.4, 26.9, 26.3, 20.5, 14.3 ppm.

HRMS-APCI: calc'd. for C$_{16}$H$_{31}$O$_1$ [M+H]$^+$ 239.2369, found 239.2369.

Monomer **26**
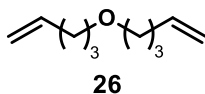
Synthesized following **general procedure E** using compound **27** (5.8 mmol), pent-4-en-1-ol (**OH-5**) (6.9 mmol), and sodium hydride (60% dispersion in mineral oil) (6.9 mmol). Yield: 568.0 mg, 3.7 mmol, 64%.

The spectroscopic data for this compound were identical to those reported in the literature.[114]

^{1}H NMR (400 MHz, CDCl$_3$) δ 5.88–5.76 (m, 2 H), 5.06–4.93 (m, 4 H), 3.43–3.39 (t, *J* = 6.5 Hz, 4 H), 2.16–2.08 (q, *J* = 7.1 Hz, 4 H), 1.71–1.63 (p, *J* = 6.5 Hz, 4 H) ppm.

IV.4.4 General Polymerization Procedure for Ester, Carbonate, Sulfite, and Ether Monomers

An oven-dried vial was charged with a Ru catalyst (**Ru-1a**, **Ru-1b**, **Ru-5b** or **Ru-6**) and dissolved in 1,2,4-trichlorobenzene (0.1 mL) in an N_2-filled glovebox. The solution of catalyst was added to another vial containing the pre-weighed monomer (0.1–1.0 mmol). The reaction mixture was then transferred by a syringe to a Schlenk flask equipped with a stir bar and a red rubber septum wrapped with electrical tape. The flask was then removed from the glovebox and attached to a high vacuum manifold where the contents of the flask were put under vacuum (~100 mTorr) and the reaction was allowed to stir until completion at room temperature or into an oil bath preheated at the desired temperature. After the reaction was complete, the flask was placed under static vacuum and ethyl vinyl ether (50 µL) was added at room temperature and the mixture was stirred for an additional 5 minutes. The polymer was then precipitated with ice-cold methanol and isolated via centrifugation (8500 rpm, 10 minutes). The polymers were then dried under high vacuum for 16–24 h. Conversions of monomers were determined by ^{1}H NMR spectra of the crude reaction mixture and the *cis* content was quantified by deconvolution of *cis* and *trans* olefin peaks in the ^{1}H NMR spectra (demonstrated with *cis/trans* poly-**10** in Figure IV-11). Molar masses and dispersity were characterized by size exclusion chromatography. The configuration of olefins on polymers was further confirmed by the isolation of corresponding *cis* or *trans* diols (**OH-1** or **OH-2**) via basic hydrolysis of the polymer (poly-**10**–**12** and poly-**14**–**16**) (procedure described in **Hydrolysis** section) or IR spectra (poly-**13** and poly-**17**).

Table IV-2 Optimization of Stereoretentive ADMET Polymerization of Monomers **10** and **23**

10: R = Me
23: R = H

TCB = 1,2,4-trichlorobenzene

poly-**10**
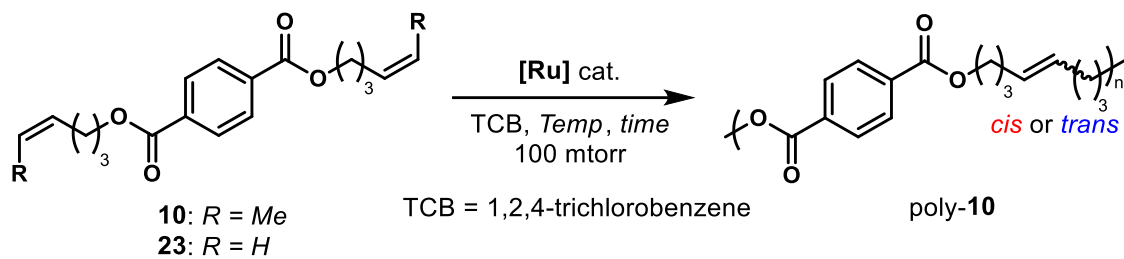
entry	monomer	cat. (mol%)	T (°C)	time (h)	M_n (kg/mol)	Đ	cis%
1	23	**Ru-1a** (5.0)	50	16	13.1	2.61	23
2	23	**Ru-6** (5.0)	50	16	—	—	—
3	23	**Ru-5b** (5.0)	50	16	—	—	—
4	10	**Ru-1a** (5.0)	50	16	4.3	1.50	29
5	10	**Ru-1a** (5.0)	80	16	11.8	2.76	26
6	10	**Ru-1b** (5.0)	50	16	13.4	2.00	21
7	10	**Ru-6** (5.0)	80	16	15.7	2.41	52
8	10	**Ru-6** (5.0)	50	16	13.1	2.13	54
9	10	**Ru-6** (5.0)	50	8	17.2	1.84	54
10	10	Ru-6 (5.0)	50	4	12.6	1.74	62
11	10	**Ru-6** (5.0)	50	2	11.8	1.81	73
12	10	**Ru-6** (0.5)	23	2	13.5	1.88	>99
13	10	**Ru-5b** (0.5)	23	2	13.0	1.75	>99

14	10	**Ru-6** (5.0)	50	1	8.1	1.62	84
15	10	**Ru-6** (5.0)	50	0.5	9.3	1.79	79
16	*trans*-**10**	**Ru-6** (5.0)	23	2	—	—	—
17	23	**Ru-1a** (5.0)	23	2	2.0	1.14	40
18	10	**Ru-1a** (5.0)	23	2	—	—	—
19	10	**Ru-6** (0.1)	23	2	10.5	1.59	>99
20[a]	10	**Ru-6** (0.5)	23	2	4.0	1.68	>99

[a]Polymerization ran in bulk conditions with no TCB.

cis-rich poly-**10** (entry 12)

^{1}H NMR (400 MHz, CDCl$_3$) δ 8.05 (s, 4 H), 5.46 (t, J = 4.7 Hz, 2 H), 4.31 (t, J = 6.6 Hz, 4 H), 2.21 (dd, J = 12.7, 7.1 Hz, 4 H), 1.91–1.76 (m, 4 H) ppm.

^{13}C NMR (101 MHz, CDCl$_3$) δ 165.7, 134.0, 129.4, 129.4, 64.8, 28.5, 23.6 ppm.
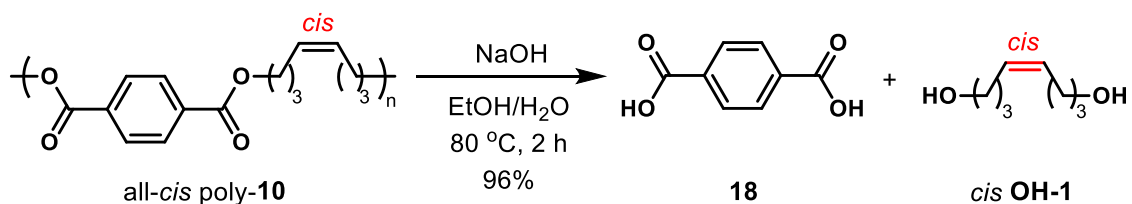
Olefin configuration was further characterized by the isolation of *cis*-oct-4-ene-1,8-diol (*cis* **OH-1**) via basic hydrolysis of the polymer in 96% yield (procedure described in **Hydrolysis** section, Figure IV-12). The *cis* content of the isolated diol was found to be consistent with the *cis* content in the starting polymer.

144

trans-rich poly-**10** (entry 5)

The spectroscopic data for this compound were identical to those reported in the literature.[99]

^{1}H NMR (400 MHz, CDCl$_3$) δ 8.09–8.05 (m, 4 H), 5.51–5.45 (m, 2 H), 4.35–4.31 (t, *J* = 6.7 Hz, 4 H), 2.21–2.14 (m, 4 H), 1.87–1.80 (m, 4 H) ppm.

^{13}C NMR (101 MHz, CDCl$_3$) δ 165.8, 134.1, 129.9, 129.5, 64.8, 28.9, 28.4, 23.6 ppm.
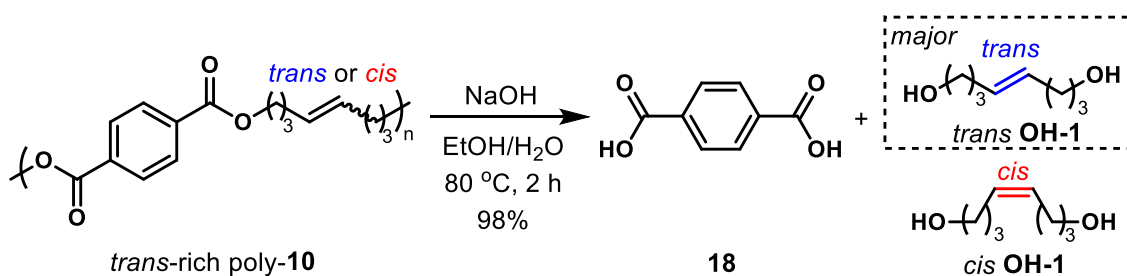
Olefin configuration was further characterized by the isolation of *cis/trans*-oct-4-ene-1,8-diol (*cis/trans* **OH-1**) through basic hydrolysis of the polymer in 98% yield (procedure described in **Hydrolysis** section, Figure IV-12). The *cis* content of the isolated diol was found to be consistent with the *cis* content in the starting polymer.

Table IV-3 Polymerization of **11** and **24** to Access Various *cis/trans* Ratios
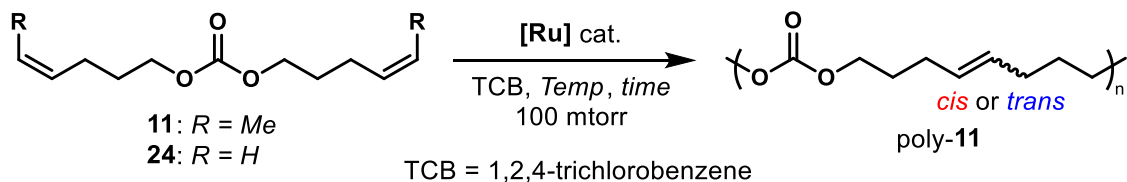
entry	monomer	cat (mol%)	T (°C)	time (h)	conv. (%)	M_n (kg/mol)	Đ	*cis%*
1	**11**	**Ru-6** (0.5)	23	2	100	8.2	1.50	99

145

2	**11**	**Ru-6** (0.5)	80	6	100	12.2	1.80	62
3	**11**	**Ru-6** (0.5)	60	6	100	12.2	1.80	45
4	**11**	**Ru-1a** (1.0)	55	16	100	10.0	1.55	24
5	**24**	**Ru-1a** (1.0)	55	16	100	21.9	1.97	19

cis-rich poly-**11** (entry 1)

^{1}H NMR (400 MHz, CDCl$_3$) δ 5.38–5.28 (m, 2 H), 4.11–4.00 (t, J = 6.8 Hz, 4 H), 2.11–1.96 (m, 4 H), 1.71–1.61 (p, J = 6.7 Hz, 4 H) ppm.

^{13}C NMR (101 MHz, CDCl$_3$) δ 155.4, 129.4, 67.4, 28.6, 23.4 ppm.
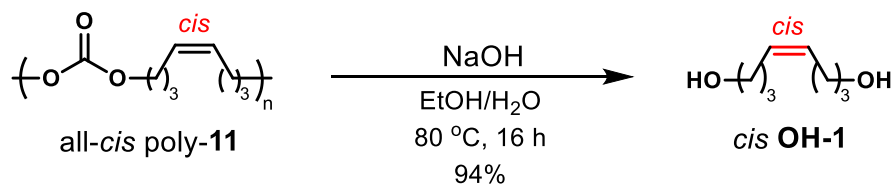
all-*cis* poly-**11** → (NaOH, EtOH/H$_2$O, 80 °C, 16 h, 94%) → *cis* **OH-1**

Olefin configuration was further characterized by the isolation of *cis*-oct-4-ene-1,8-diol (*cis* **OH-1**) via basic hydrolysis of the polymer in 94% yield (procedure described in **Hydrolysis** section, Figure IV-12). The *cis* content of the isolated diol was found to be consistent with the *cis* content in the starting polymer.

trans-rich poly-**11** (entry 5)

The spectroscopic data for this compound were identical to those reported in the literature.[100]

^{1}H NMR (400 MHz, CDCl$_3$) δ 5.43–5.31 (m, 2 H), 4.13–4.05 (t, J = 6.9 Hz, 4 H), 2.14–1.95 (m, 4 H), 1.77–1.64 (p, J = 6.8 Hz, 4 H) ppm.

^{13}C NMR (101 MHz, CDCl$_3$) δ 155.4, 130.0, 129.4, 67.4, 28.7, 28.6, 23.5 ppm.
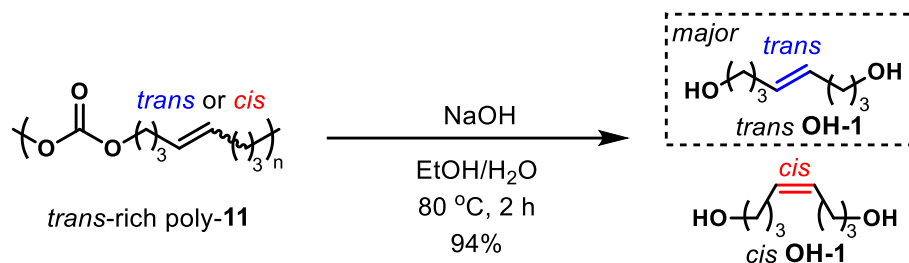
Olefin configuration was further characterized by the isolation of *cis/trans*-oct-4-ene-1,8-diol (*cis/trans* **OH-1**) through basic hydrolysis of the polymer in 94% yield (procudure described in **Hydrolysis** section, Figure IV-12). The *cis* content of the isolated diol was found to be consistent with the *cis* content in the starting polymer.

Table IV-4 Polymerization of **12** and **25** to Access Various *cis/trans* Ratios
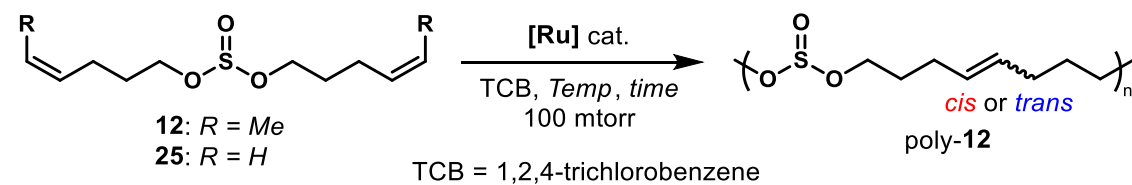
entry	monomer	cat. (mol%)	T (ºC)	time (h)	conv. (%)	M_n (kg/mol)	Đ	cis%
1	**12**	**Ru-6** (0.5)	23	2	100	12.0	1.67	99
2	**12**	**Ru-6** (5.0)	50	4	100	11.0	1.69	73
3	**12**	**Ru-6** (5.0)	80	16	100	10.9	1.55	55

147

| 4 | **12** | **Ru-1a** (2.0) | 80 | 16 | 100 | 10.1 | 1.41 | 16 |
| 5 | **25** | **Ru-1a** (3.0) | 50 | 24 | 100 | 8.7 | 1.55 | 21 |

cis-rich poly-**12** (entry 1)

^{1}H NMR (400 MHz, CDCl$_3$) δ 5.39 (t, J = 4.7 Hz, 2 H), 4.06–3.88 (m, 4 H), 2.14 (m, 4 H), 1.82–1.67 (m, 4 H) ppm.

^{13}C NMR (101 MHz, CDCl$_3$) δ 129.3, 61.6, 29.4, 23.4 ppm.

Olefin configuration was further characterized by the isolation of *cis*-oct-4-ene-1,8-diol (*cis* **OH-1**) via basic hydrolysis of the polymer in 94% yield (procedure described in **Hydrolysis** section, Figure IV-12). The *cis* content of the isolated diol was found to be consistent with the *cis* content in the starting polymer.

trans-rich poly-**12** (entry 5)

The spectroscopic data for this compound were identical to those reported in the literature.[102]

^{1}H NMR (400 MHz, CDCl$_3$) δ 5.44–5.38 (m, 2 H), 4.06–3.88 (m, 4 H), 2.16–2.07 (m, 4 H), 1.76–1.70 (m, 4 H) ppm.

^{13}C NMR (101 MHz, CDCl$_3$) δ 129.8, 61.6, 29.2, 28.6 ppm.

Olefin configuration was further characterized by the isolation of *cis/trans*-oct-4-ene-1,8-diol (*cis/trans* **OH-1**) through basic hydrolysis of the polymer in 94% yield (procedure described in **Hydrolysis** section, Figure IV-12). The *cis* content of the isolated diol was found to be consistent with the *cis* content in the starting polymer.

Table IV-5 Polymerization of **13** and **26** to Access Various *cis/trans* Ratios

entry	monomer	cat. (mol%)	T (°C)	time (h)	conv. (%)	M_n (kg/mol)	Đ	cis%
1	**13**	**Ru-6** (0.5)	23	2	100	9.2	1.31	99
2	**13**	**Ru-6** (0.5)	50	6	100	23.1	1.95	67
3	**13**	**Ru-6** (0.5)	80	6	100	21.3	2.00	45
4	**13**	**Ru-1a** (1.0)	55	16	100	8.2	1.42	19
5	**26**	**Ru-1a** (1.0)	55	16	100	17.2	1.78	20

149
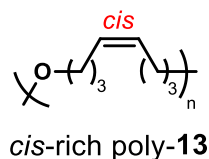
cis-rich poly-**13**

cis-rich poly-**13** (entry 1)

^{1}H NMR (400 MHz, CDCl$_3$) δ 5.42–5.33 (m, 2 H), 3.42–3.35 (t, *J* = 6.7 Hz, 4 H), 2.16–2.00 (m, 4 H), 1.67–1.56 (p, *J* = 6.8 Hz, 4 H) ppm.

^{13}C NMR (101 MHz, CDCl$_3$) δ 129.8, 70.5, 29.9, 23.9 ppm.

Olefin configuration was further characterized by IR spectrum (Figure IV-9).
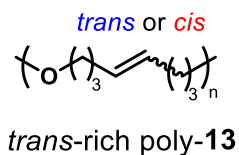
trans-rich poly-**13**

trans-rich poly-**13** (entry 5)

The spectroscopic data for this compound were identical to those reported in the literature.[114]

^{1}H NMR (400 MHz, CDCl$_3$) δ 5.50–5.32 (m, 2 H), 3.42–3.34 (t, *J* = 6.4 Hz, 4 H), 2.12–1.95 (m, 4 H), 1.68–1.56 (t, *J* = 6.3 Hz, 4 H) ppm.

^{13}C NMR (101 MHz, CDCl$_3$) δ 130.2, 129.8, 70.4, 29.7, 23.9 ppm.

Olefin configuration was further characterized by IR spectrum (Figure IV-9).

150
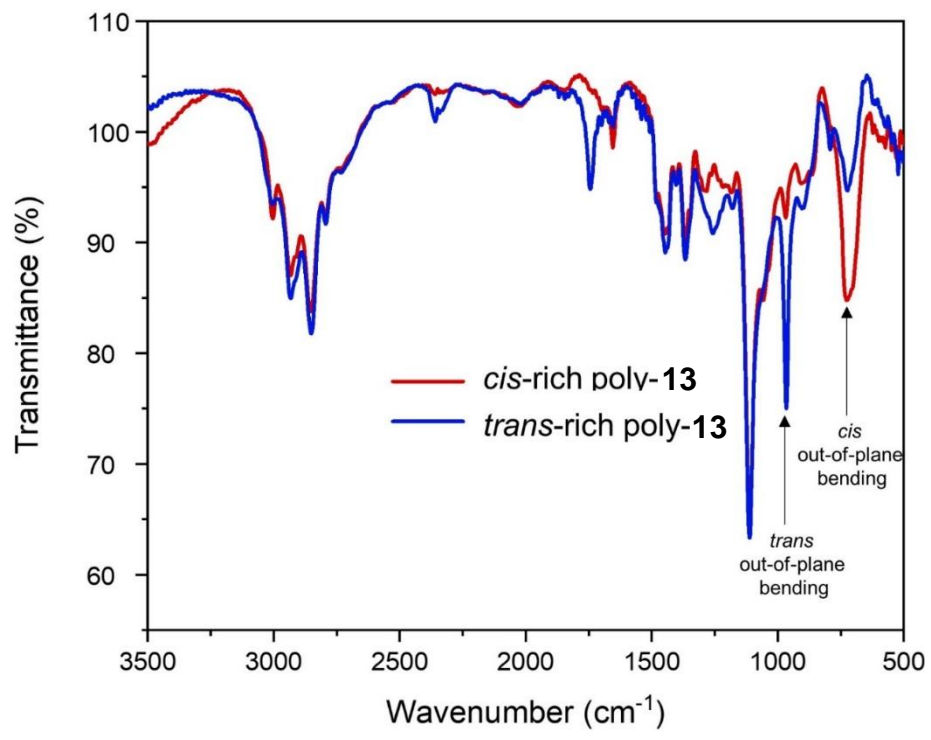
Figure IV-9 IR comparison between *cis*-rich poly-**13** and *trans*-rich poly-**13**.

IV.4.6 ADMET Polymerization of Ethyl-Capped Monomers

Table IV-6 Polymerization of **14** to Access Various *cis/trans* Ratios

entry	cat. (mol%)	T (ºC)	time (h)	conv. (%)	M_n (kg/mol)	Đ	*cis*%
1	**Ru-6** (1)	23	4	100	15.9	1.87	94
2	**Ru-6** (2)	80	6	100	23.1	2.98	62
3	**Ru-6** (2)	80	16	100	19.0	2.08	31
4	**Ru-1a** (2)	80	16	100	7.8	1.97	21

cis-rich poly-**14** (entry 1)

^{1}H NMR (400 MHz, CDCl$_3$) δ 8.08 (s, 4 H), 5.40 (t, *J* = 4.6 Hz, 2 H), 4.33 (t, *J* = 6.6 Hz, 4 H), 2.14–2.09 (m, 4 H), 1.82–1.75 (m, 4 H), 1.55–1.47 (m, 4 H) ppm.

^{13}C NMR (101 MHz, CDCl$_3$) δ 165.8, 134.1, 129.8, 129.5, 65.3, 28.2, 26.8, 26.0 ppm.
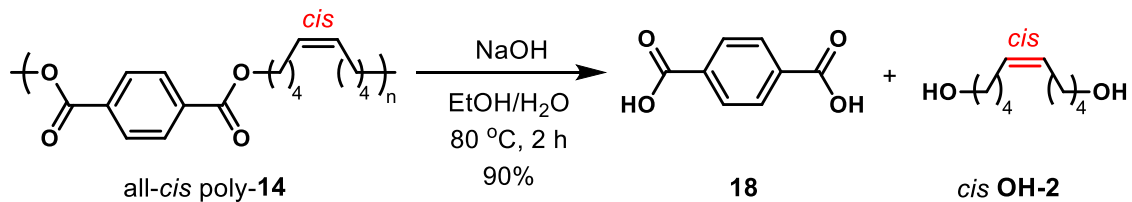
Olefin configuration was further characterized by the isolation of *cis*-dec-5-ene-1,10-diol (*cis* **OH-2**) via basic hydrolysis of the polymer in 90% yield (procedure described in **Hydrolysis** section, Figure IV-13). The *cis* content of the isolated diol was found to be consistent with the starting polymer.

trans-rich poly-**14** (entry 4)

^{1}H NMR (400 MHz, CDCl$_3$) δ 8.08 (s, 4 H), 5.44–5.39 (m, 2 H), 4.33 (t, J = 6.6 Hz, 4 H), 2.14– 2.05 (m, 4 H), 1.81–1.74 (m, 4 H), 1.54–1.47 (m, 4 H) ppm.

^{13}C NMR (101 MHz, CDCl$_3$) δ 165.8, 134.1, 130.3, 129.5, 65.4, 32.1, 28.1, 25.9 ppm.
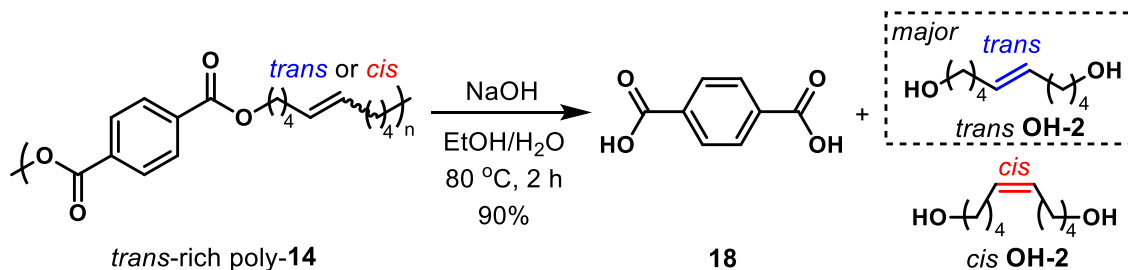
Olefin configuration was further characterized by the isolation of *cis*/*trans*-dec-5-ene-1,10-diol (*cis*/*trans* **OH-2**) via basic hydrolysis of the polymer in 90% yield (procedure described in **Hydrolysis** section, Figure IV-12). The *cis* content of the isolated diol was found to be consistent with the *cis* content in the starting polymer.

Table IV-7 Polymerization of **15** to Access Various *cis*/*trans* Ratios
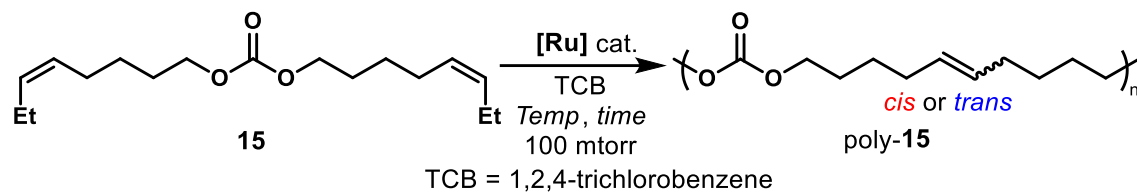
entry	cat. (mol%)	T (°C)	time (h)	conv. (%)	M_n (kg/mol)	Đ	*cis*%
1	**Ru-6** (2)	23	4	100	7.2	1.40	99
2	**Ru-6** (2)	30	4	100	12.5	1.63	73
3	**Ru-6** (2)	55	16	100	19.4	2.24	28
4	**Ru-1a** (2)	55	16	100	7.5	1.46	16

cis-rich poly-**15** (entry 1)

^{1}H NMR (400 MHz, CDCl3) δ 5.40–5.30 (m, 2 H), 4.15–4.08 (t, J = 6.7 Hz, 4 H), 2.11–1.95 (m, 4 H), 1.72–1.62 (p, J = 6.7 Hz, 4 H), 1.47–1.38 (p, J = 7.9 Hz, 4 H) ppm.

^{13}C NMR (100 MHz, CDCl3) δ 155.5, 129.8, 68.0, 28.4, 26.9, 25.9 ppm.
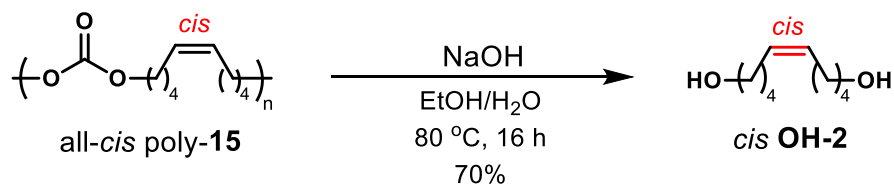
Olefin configuration was further characterized by the isolation of *cis*-dec-5-ene-1,10-diol (*cis* **OH-2**) via basic hydrolysis of the polymer in 70% yield (procedure described in

154

Hydrolysis section, Figure IV-12). The *cis* content of the isolated diol was found to be consistent with the *cis* content in the starting polymer.

trans-rich poly-**15** (entry 4)

^{1}H NMR (400 MHz, CDCl$_3$) δ 5.41–5.30 (m, 2 H), 4.15–4.06 (t, J = 6.6 Hz, 4 H), 2.09–1.92 (m, 4 H), 1.70–1.59 (p, J = 6.3 Hz, 4 H), 1.47–1.36 (p, J = 7.9 Hz, 4 H) ppm.

^{13}C NMR (100 MHz, CDCl$_3$) δ 155.5, 130.3, 129.8, 68.0, 32.2, 28.2, 25.7 ppm.
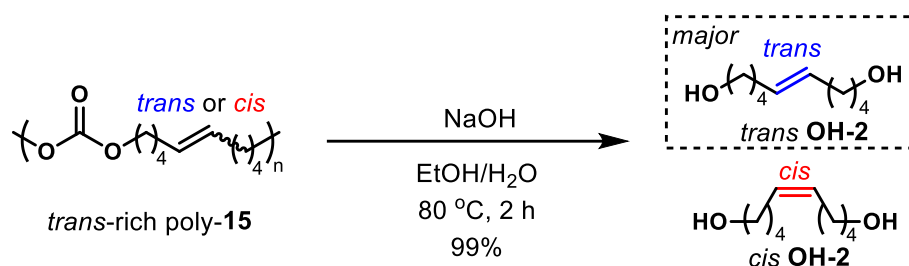
Olefin configuration was further characterized by the isolation of *cis*/*trans*-dec-5-ene-1,10-diol (*cis*/*trans* **OH-2**) via basic hydrolysis of the polymer in 99% yield (procedure described in **Hydrolysis** section, Figure IV-12). The *cis* content of the isolated diol was found to be consistent with the *cis* content in the starting polymer.

155

Table IV-8 Polymerization of **16** to Access Various *cis/trans* Ratios
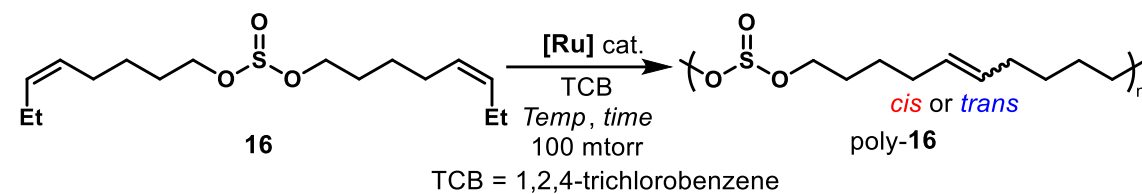
entry	cat. (mol%)	T (ºC)	time (h)	conv. (%)	M_n (kg/mol)	Đ	*cis%*
1	**Ru-6** (1)	23	4	100	10.1	1.43	99
2	**Ru-6** (2)	50	4	100	11.5	1.61	72
3	**Ru-6** (2)	80	16	100	16.8	1.79	48
4	**Ru-1a** (2)	50	16	100	6.8	1.33	12

cis-rich poly-**16** (entry 1)

^{1}H NMR (400 MHz, CDCl$_3$) δ 5.36 (t, *J* = 4.7 Hz, 2 H), 4.07–3.88 (m, 4 H), 2.09–2.04 (m, 4 H), 1.72–1.65 (m, 4 H), 1.48–1.41 (m, 4 H) ppm.

^{13}C NMR (101 MHz, CDCl$_3$) δ 129.7, 62.1, 29.1, 26.7, 25.8 ppm.
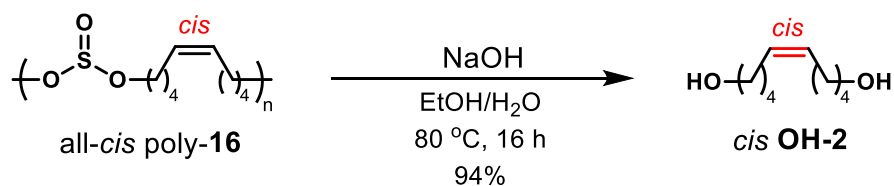
Olefin configuration was further characterized by the isolation of *cis*-dec-5-ene-1,10-diol (*cis* **OH-2**) via basic hydrolysis of the polymer in 94% yield (procedure described in

Hydrolysis section, Figure IV-12). The *cis* content of the isolated diol was found to be consistent with the *cis* content in the starting polymer.

trans-rich poly-**16** (entry 4)

^{1}H NMR (400 MHz, CDCl$_3$) δ 5.40–5.34 (m, 2 H), 4.06–3.88 (m, 4 H), 2.07–1.99 (m, 4 H), 1.70– 1.63 (m, 4 H), 1.48–1.40 (m, 4 H) ppm.

^{13}C NMR (101 MHz, CDCl$_3$) δ 130.2, 62.1, 32.0, 28.9, 25.6 ppm.
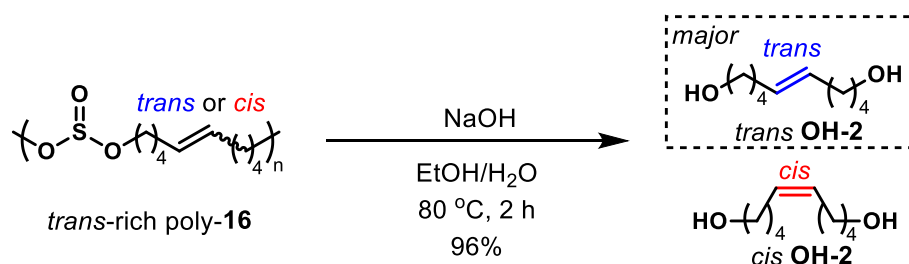
Olefin configuration was further characterized by the isolation of *cis*/*trans*-dec-5-ene-1,10-diol (*cis*/*trans* **OH-2**) via basic hydrolysis of the polymer in 96% yield (procedure described in **Hydrolysis** section, Figure IV-12). The *cis* content of the isolated diol was found to be consistent with the *cis* content in the starting polymer.

**Table IV-9** Polymerization of **17** to Access Various *cis/trans* Ratios

TCB = 1,2,4-trichlorobenzene
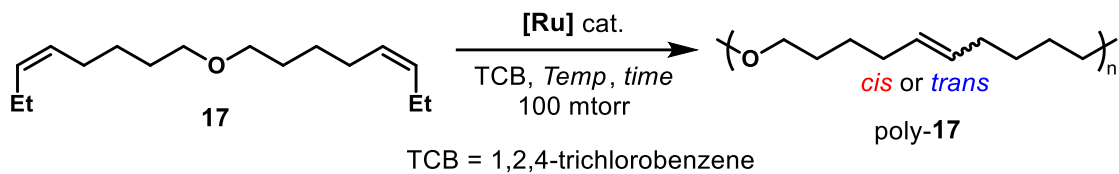
entry	cat. (mol%)	T (ºC)	time (h)	conv. (%)	M_n (kg/mol)	Đ	*cis*%
1	**Ru-6** (1)	23	4	100	14.0	1.62	93
2	**Ru-6** (2)	30	4	100	16.9	1.53	67
3	**Ru-6** (2)	80	6	100	24.7	2.01	38
4	**Ru-6** (2)	80	16	100	24.2	1.97	20
5	**Ru-1a** (2)	80	16	100	5.7	1.25	20
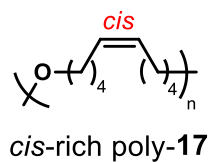
cis-rich poly-**17**

cis-rich poly-**17** (entry 1)

^{1}H NMR (400 MHz, CDCl₃) δ 5.35 (t, *J* = 4.6 Hz, 2 H), 3.39 (t, *J* = 6.6 Hz, 4 H), 2.07–2.02 (m, 4 H), 1.61–1.54 (m, 4 H), 1.43–1.36 (m, 4 H) ppm.

^{13}C NMR (101 MHz, CDCl₃) δ 129.8, 70.8, 29.4, 27.0, 26.3 ppm.

Olefin configuration was further characterized by IR spectrum (Figure IV-10).
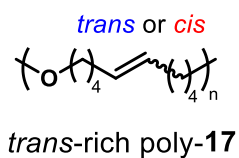
trans-rich poly-**17**

trans-rich poly-**17** (entry 4)

^{1}H NMR (400 MHz, CDCl$_3$) δ 5.40–5.34 (m, 2 H), 3.38 (t, *J* = 6.6 Hz, 4 H), 2.17–1.89 (m, 4 H), 1.66–1.50 (m, 4 H), 1.52–1.19 (m, 4 H) ppm.

^{13}C NMR (101 MHz, CDCl$_3$) δ 130.3, 70.8, 32.4, 29.3, 26.2 ppm.

Olefin configuration was further characterized by IR spectrum (Figure IV-10).
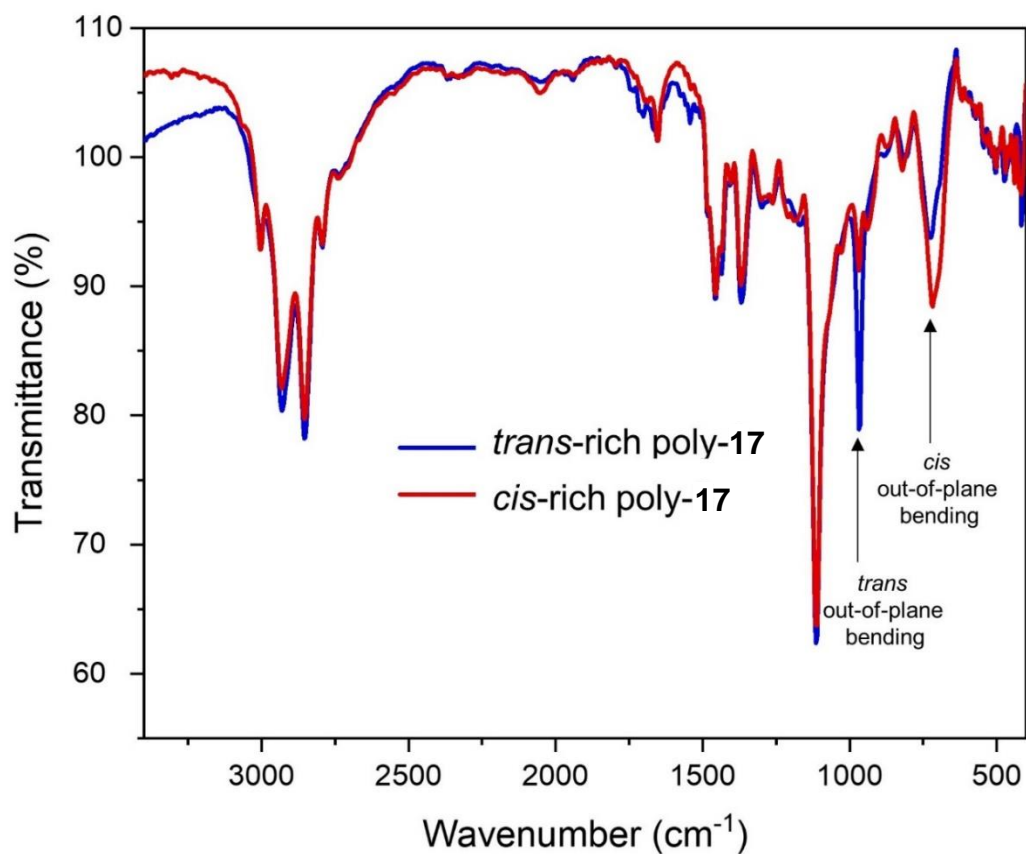
Figure IV-10 IR comparison between *cis*-rich poly-**17** and *trans*-rich poly-**17**.
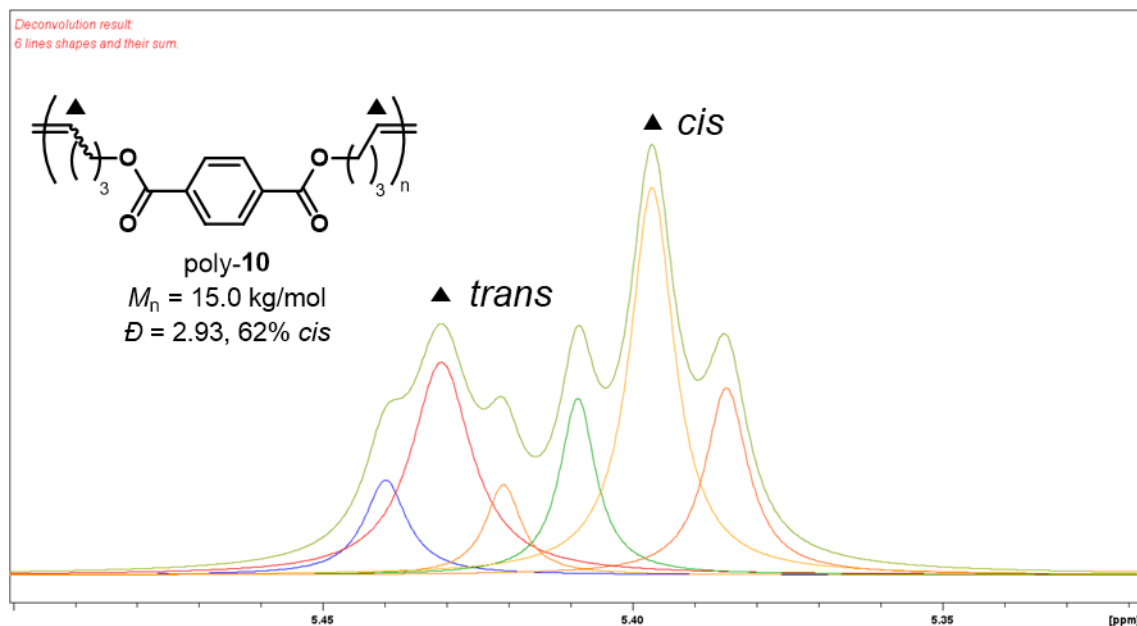
Figure IV-11 Determination of *cis*/*trans* ratio by ^{1}H NMR deconvolution of *cis*/*trans* poly-**10**.

*IV.4.8 Hydrolysis of Poly-**10** and Poly-**14***

Either poly-**10** or poly-**14** (3 mg in each experiment) was placed in a reaction tube equipped with a stir bar, and solution of NaOH (100 mg) in a EtOH:H_2O mixture (1:1, 8 mL) was added to the tube. The polymer suspension was heated to 80 °C for 2 h (16 h for poly-**11** and 40 h for poly-**15**). The reaction was cooled to room temperature and diluted with dichloromethane (10 mL). The organic layer was washed with H_2O (5 mL), dried over sodium sulfate, and then the solvent was removed *in vacuo* affording diol **OH-1** (from poly-**10**) or diol **OH-2** (from poly-**14**). The aqueous layer was acidified with 3M aq. HCl and then extracted with dichloromethane twice. The combined organic fraction was dried over sodium sulfate and concentrated *in vacuo* to obtain terephthalic acid (**18**).
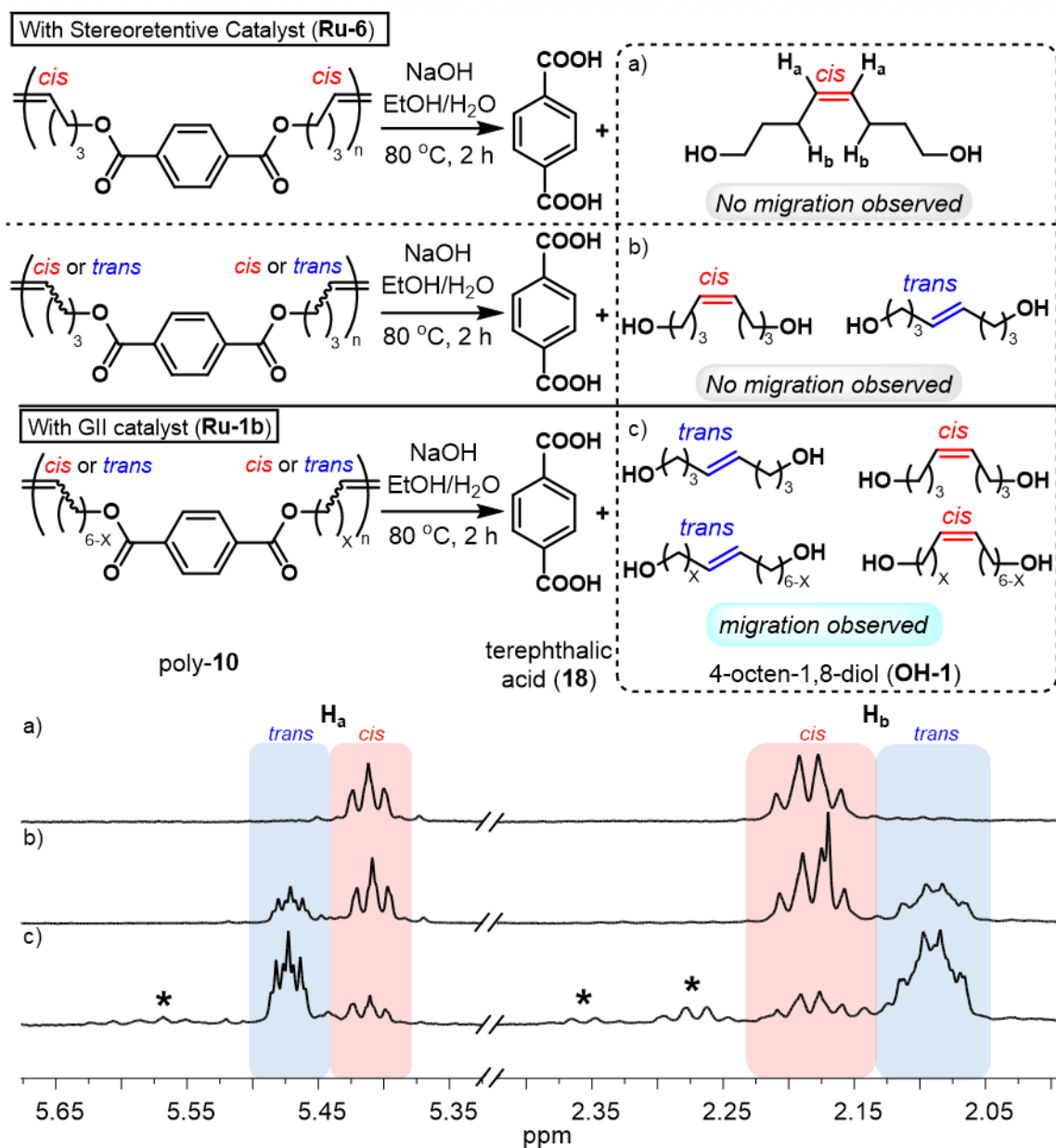
Figure IV-12 Basic hydrolysis of poly-**10** with different *cis* content prepared from **Ru-6** or **Ru-1b** (asterisk (*) designates signals assigned as other isomers of diol species caused by olefin migration).

cis-oct-4-ene-1,8-diol (*cis* **OH-1**)

The spectroscopic data for this compound were identical to those reported in the literature.[115]

^{1}H NMR (400 MHz, CDCl$_3$) δ 5.41 (t, *J* = 4.6 Hz, 2 H), 3.66 (t, *J* = 6.2 Hz, 4 H), 2.18 (dd, *J* = 12.8, 7.1 Hz, 4 H), 1.68–1.60 (m, 4 H) ppm.
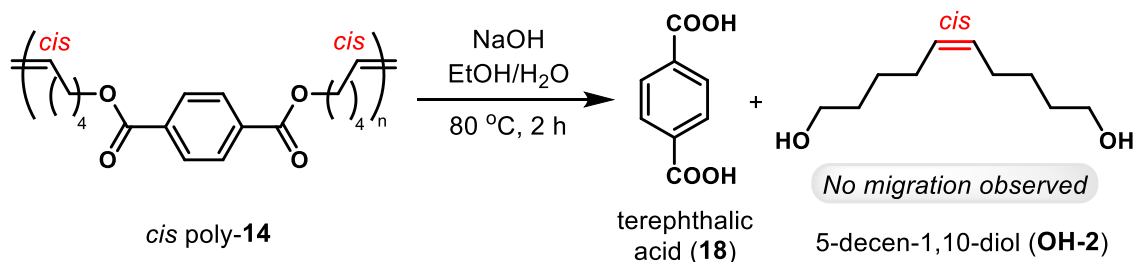
Figure IV-13 Basic hydrolysis of *cis*-rich poly-**14** to terephthalic acid (**18**) and 5-decen-1,10-diol (**OH-2**).

cis-dec-5-ene-1,10-diol (*cis* **OH-2**)

The spectroscopic data for this compound were identical to those reported in the literature.[116]

^{1}H NMR (400 MHz, CDCl$_3$) δ 5.38 (t, *J* = 4.6 Hz, 2 H), 3.65 (t, *J* = 6.6 Hz, 4 H), 2.09–2.04 (m, 4 H), 1.61–1.55 (m, 4 H), 1.47–1.41 (m, 4 H) ppm.

163
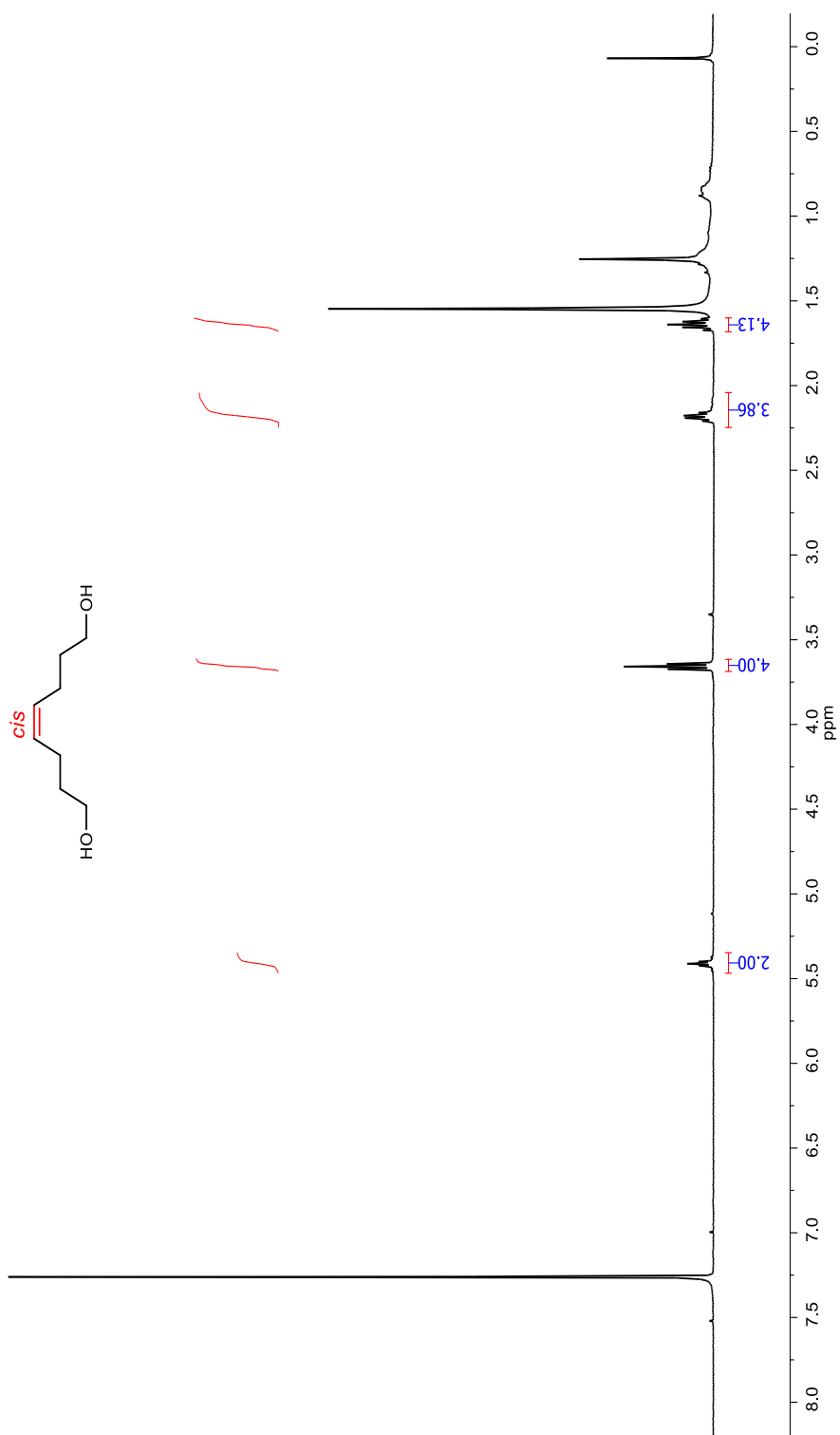
Figure IV-14 ^{1}H NMR (400 MHz, CDCl$_3$) spectrum of compound *cis* **OH-1**.
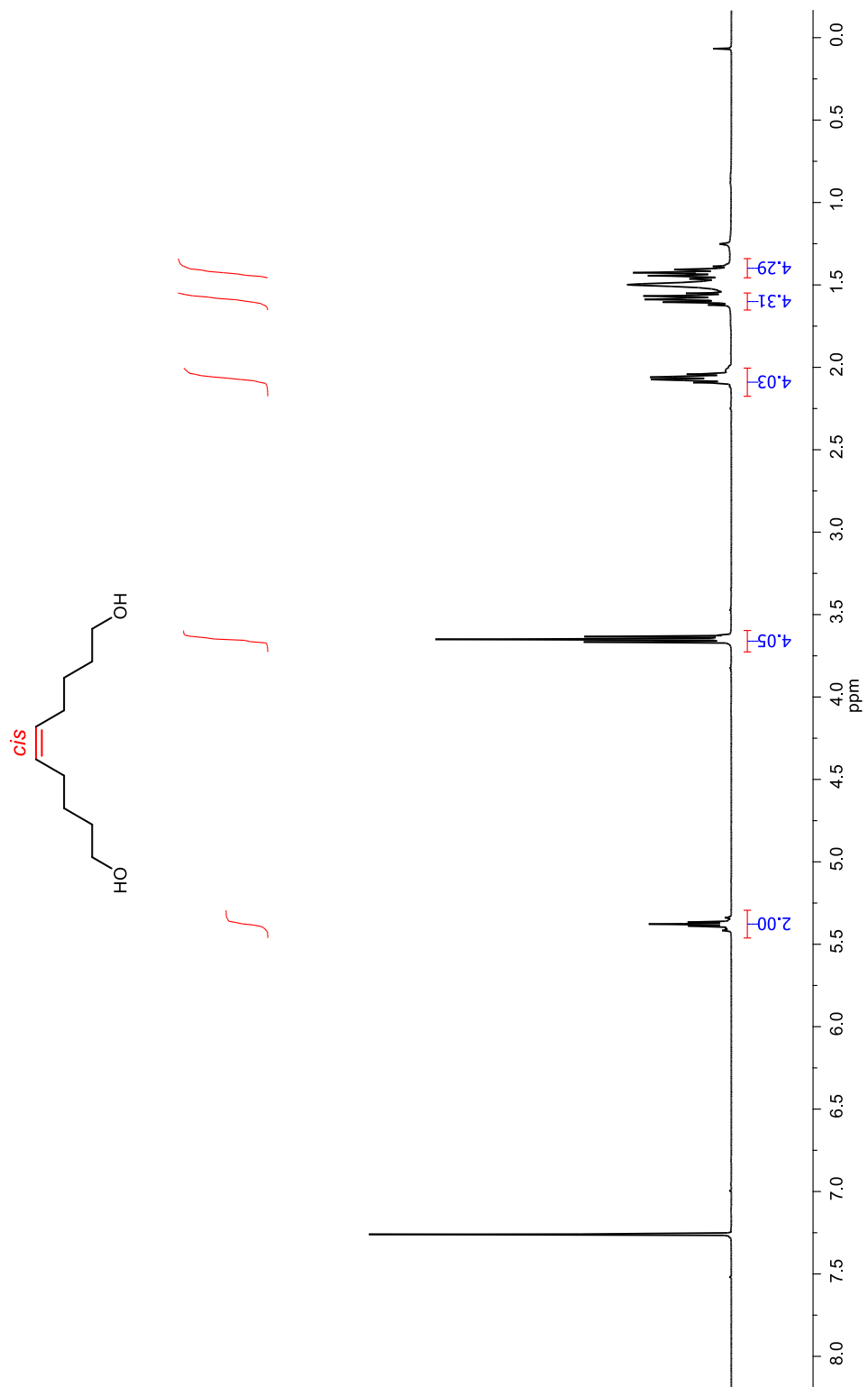
Figure IV-15 ^{1}H NMR (400 MHz, CDCl$_3$) spectrum of compound *cis* **OH-2**.

IV.4.9 Thermal Characterization
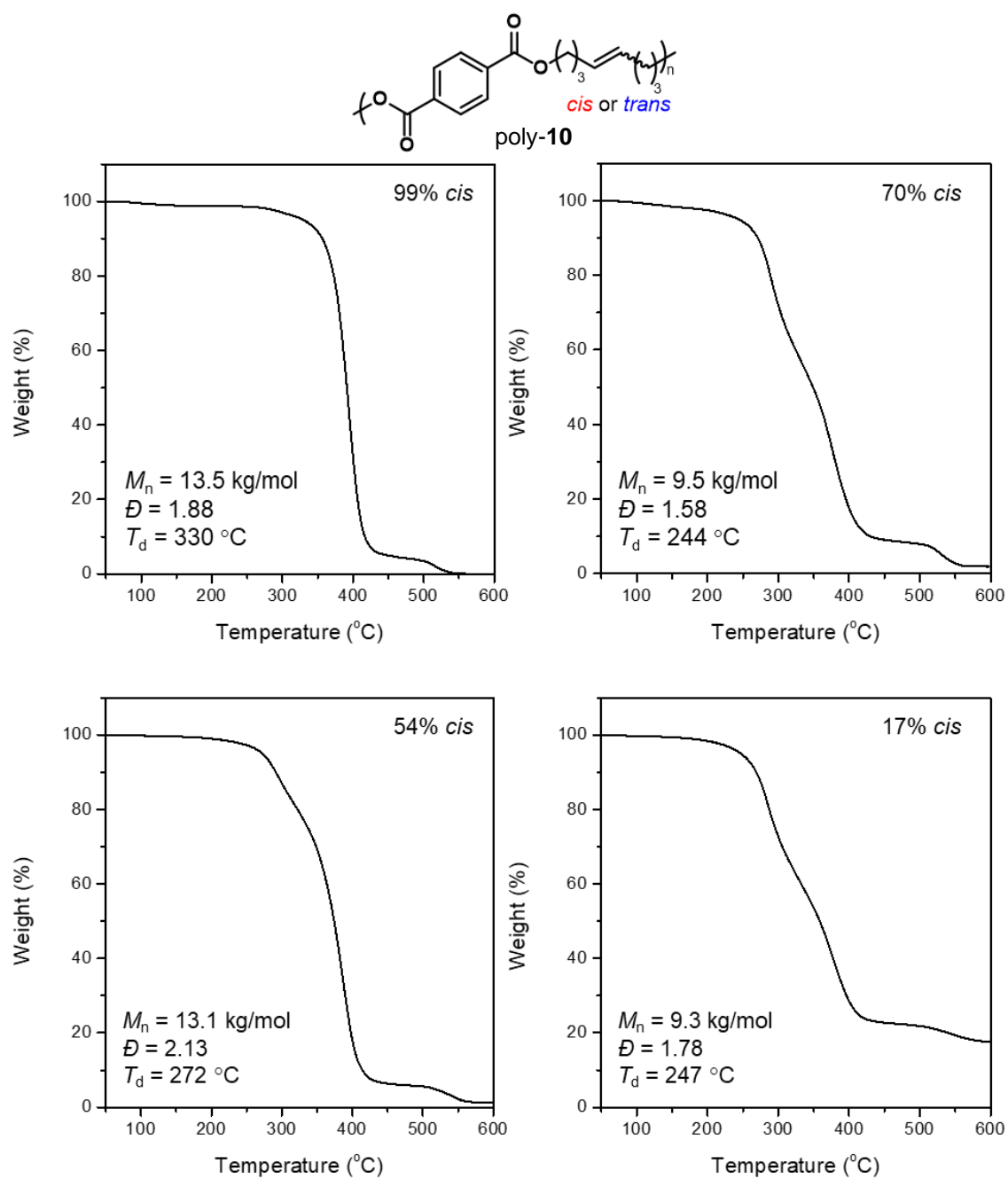
Figure IV-16 TGA thermograms of poly-**10** with 99%, 70%, 54% and 17% *cis* content.
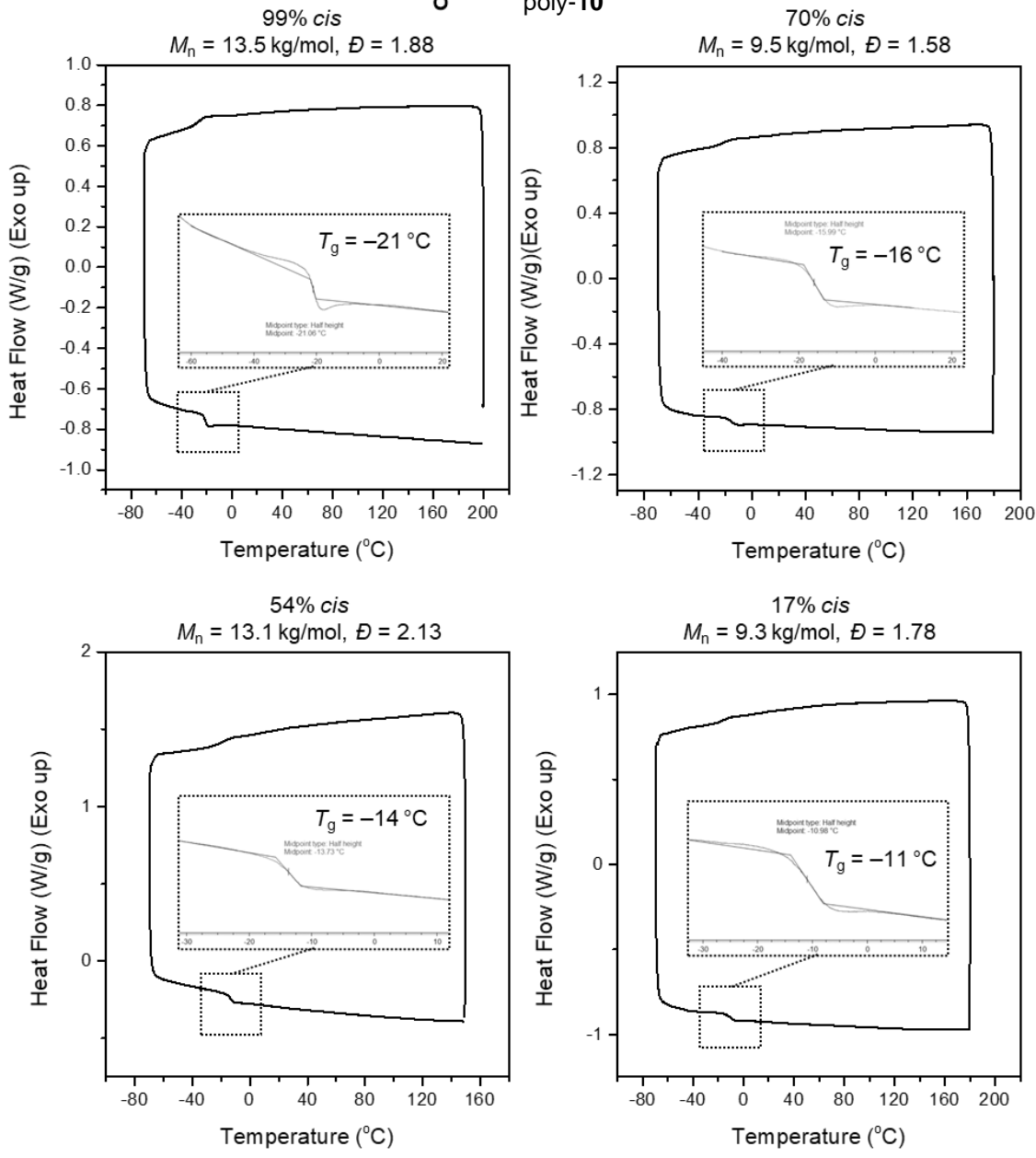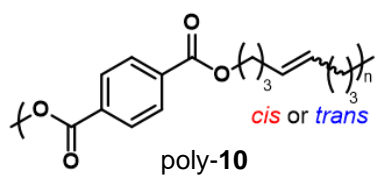
Figure IV-17 DSC thermograms of poly-**10** with 99%, 70%, 54% and 17% *cis* content.

Table IV-10 Thermal Properties of Poly-**10** with Varied *cis* Content

entry	*cis* content (%)	M_n (kg/mol)	M_w (kg/mol)	Đ	T_d (°C)	T_g (°C)	T_m (°C)	T_c (°C)
1	99	13.5	25.4	1.88	330	–21	—	—
2	70	9.5	15.0	1.58	244	–16	—	—
3	54	13.1	27.9	2.13	272	–14	—	—
4	17	9.3	16.6	1.78	247	–11	—	—
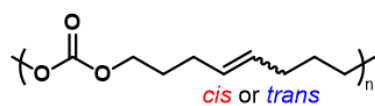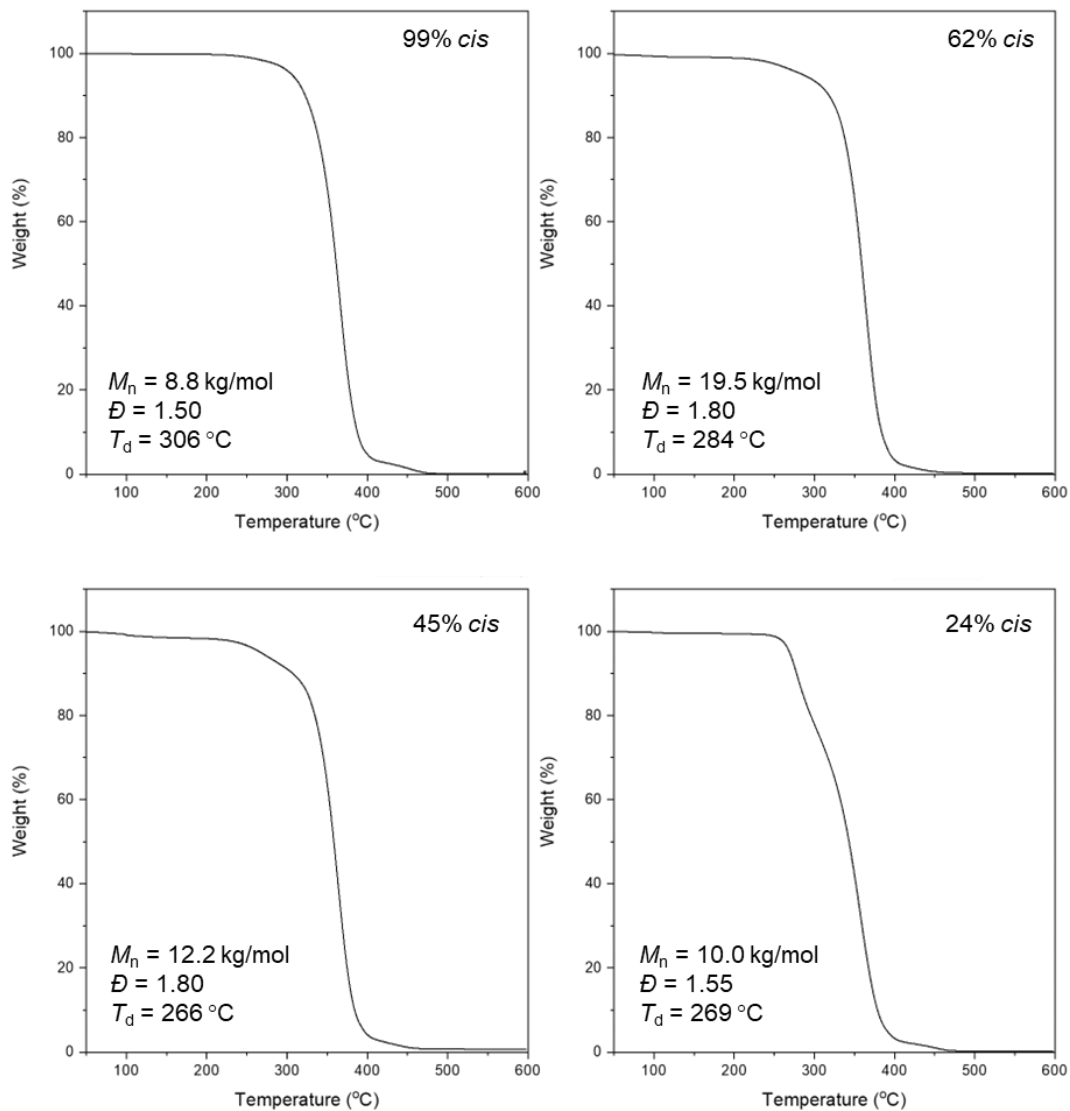
Figure IV-18 TGA thermograms of poly-**11** with 99%, 62%, 45% and 24% *cis* content.
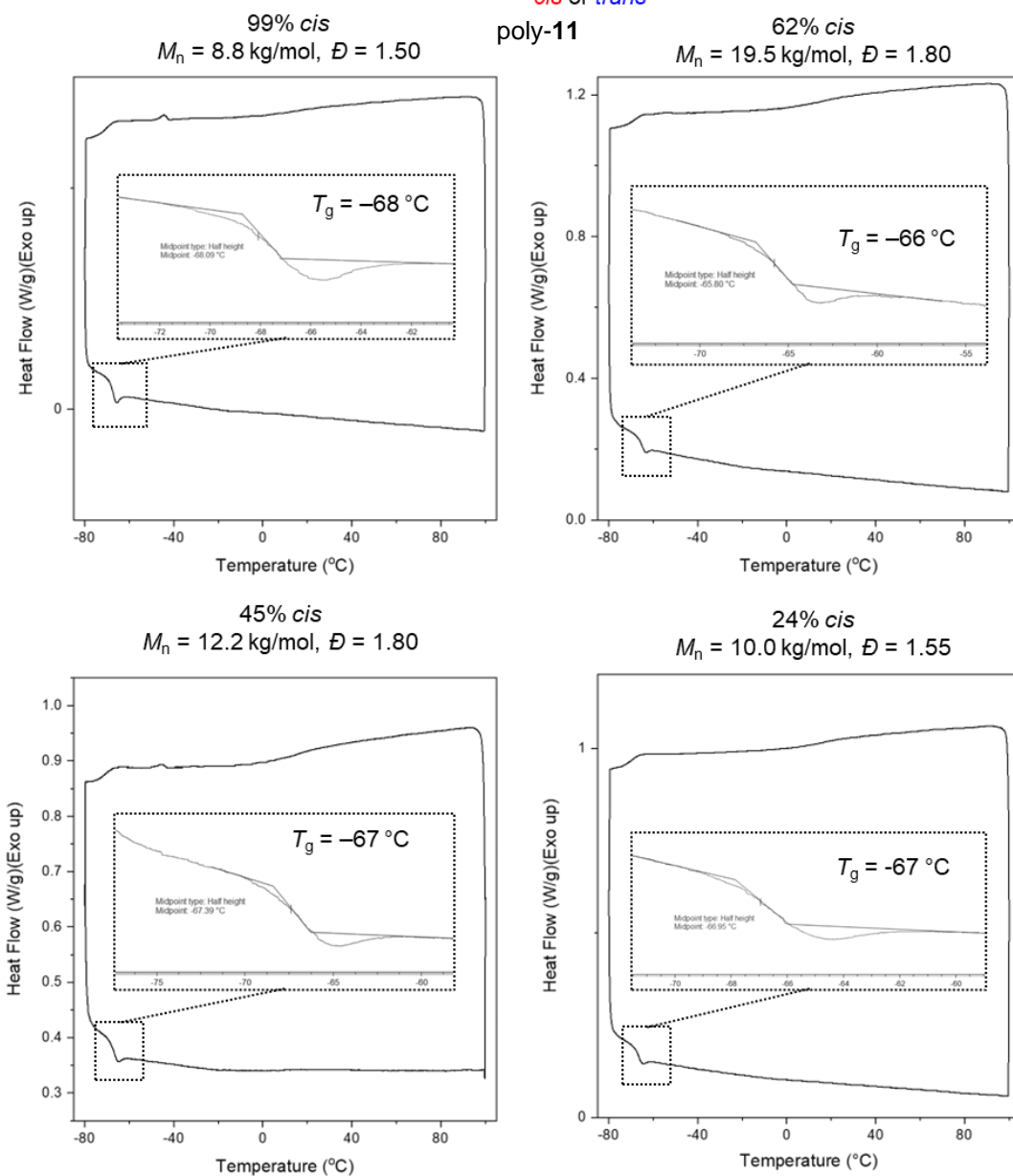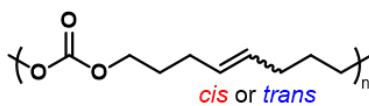
Figure IV-19 DSC thermograms of poly-**11** with 99%, 62%, 45% and 24% *cis* content.

Table IV-11 Thermal Properties of Poly-**11** with Varied *cis* Content

entry	*cis* content (%)	M_n (kg/mol)	M_w (kg/mol)	$Đ$	T_d (°C)	T_g (°C)	T_m (°C)	T_c (°C)
1	99	8.8	12.2	1.50	306	–68	—	—
2	62	19.5	35.0	1.80	284	–66	—	—
3	45	12.2	22.0	1.80	266	–67	—	—
4	24	10.0	15.2	1.55	269	–67	—	—
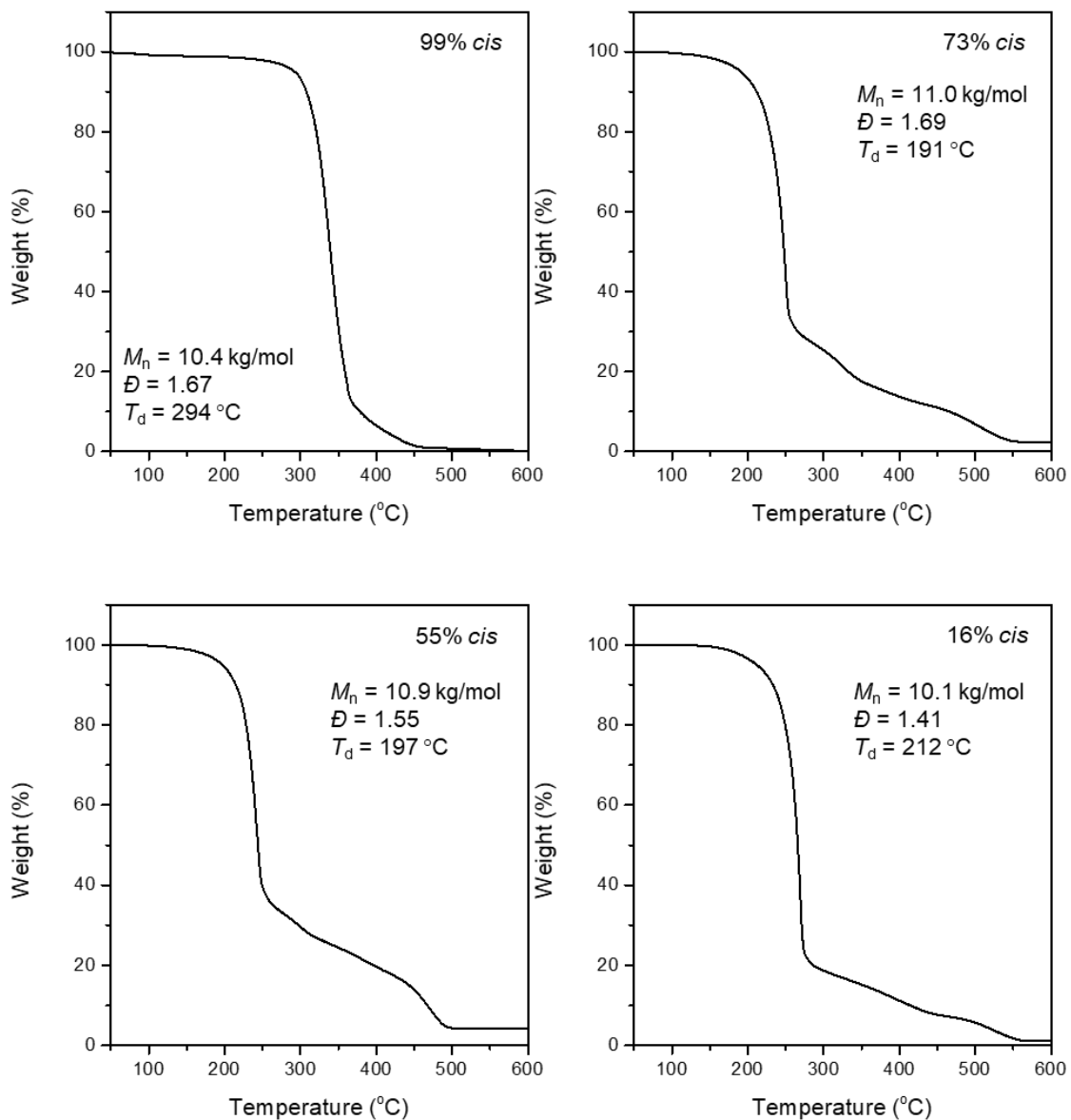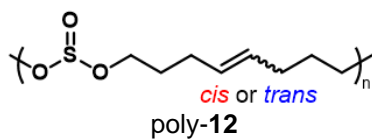
Figure IV-20 TGA thermograms of poly-**12** with 99%, 73%, 55% and 16% *cis* content.
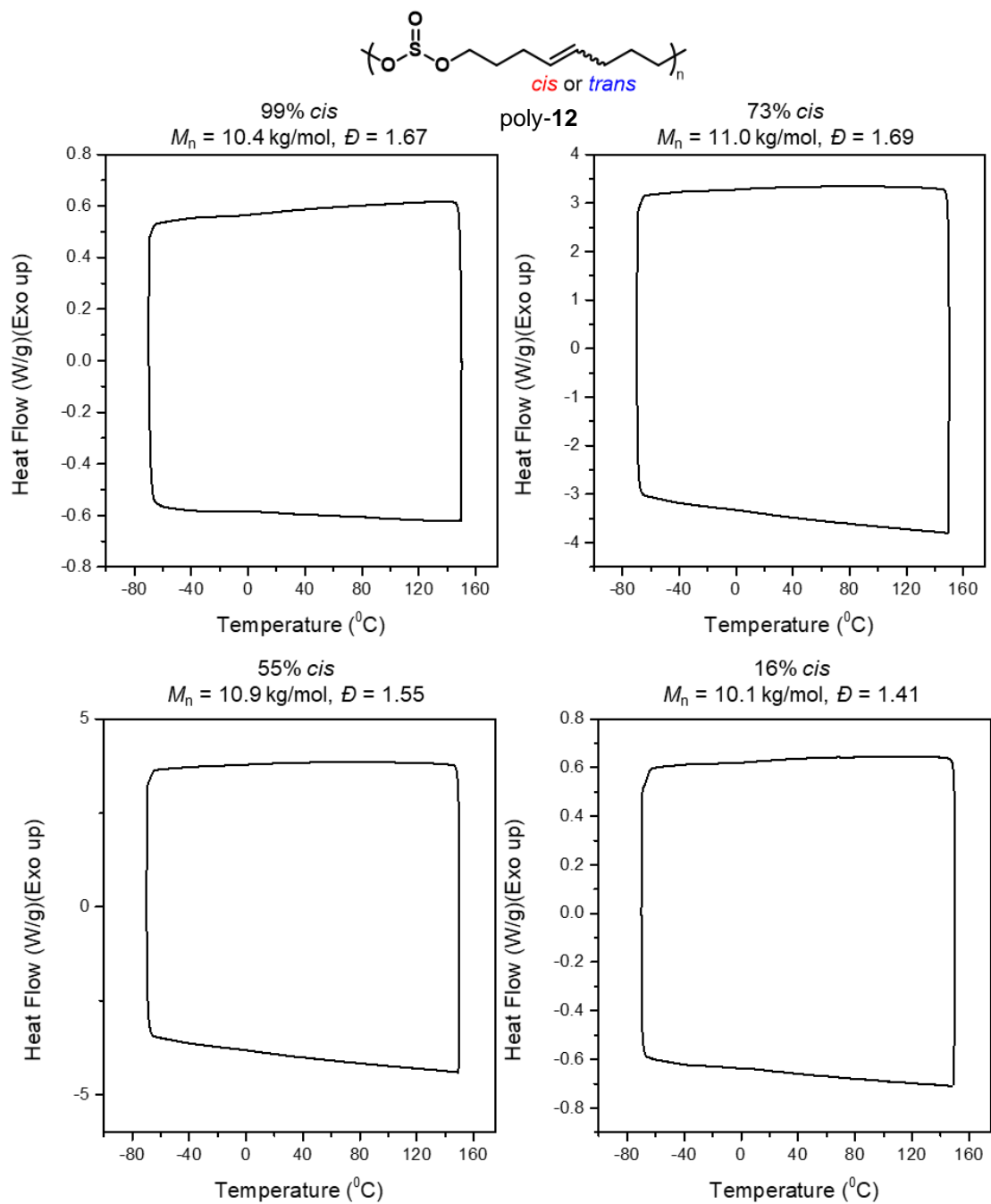
Figure IV-21 DSC thermograms of poly-**12** with 99%, 73%, 55% and 16% *cis* content.

Table IV-12 Thermal Properties of Poly-**12** with Varied *cis* Content

entry	*cis* content (%)	M_n (kg/mol)	M_w (kg/mol)	Đ	T_d (°C)	T_g (°C)	T_m (°C)	T_c (°C)
1	99	12.0	17.4	1.67	294	—	—	—
2	73	11.0	18.6	1.69	191	—	—	—
3	55	10.9	16.9	1.55	197	—	—	—
4	16	10.1	14.2	1.41	212	—	—	—
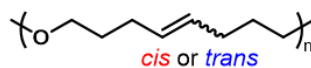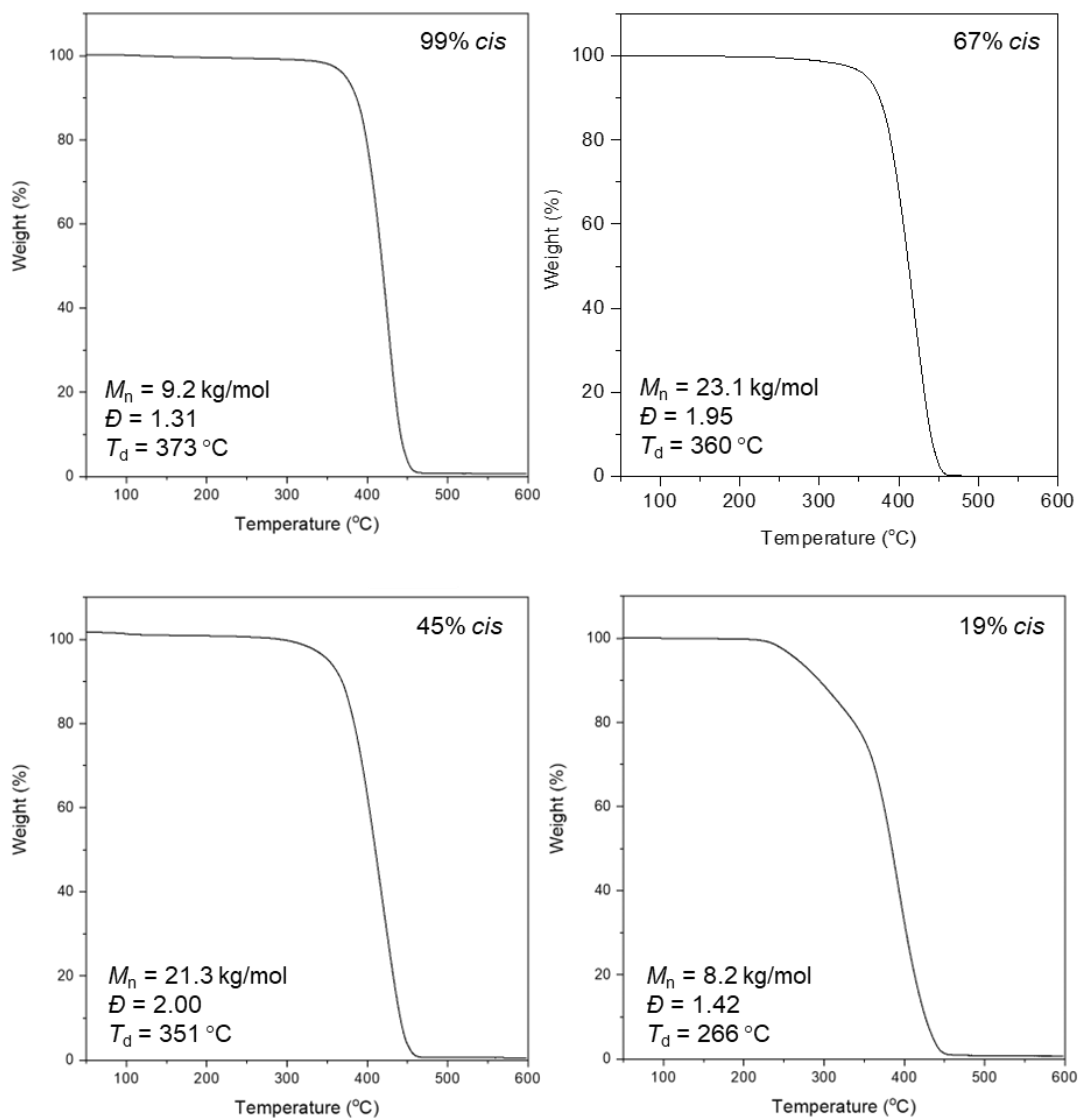
Figure IV-22 TGA thermograms of poly-**13** with 99%, 67%, 45% and 19% *cis* content.
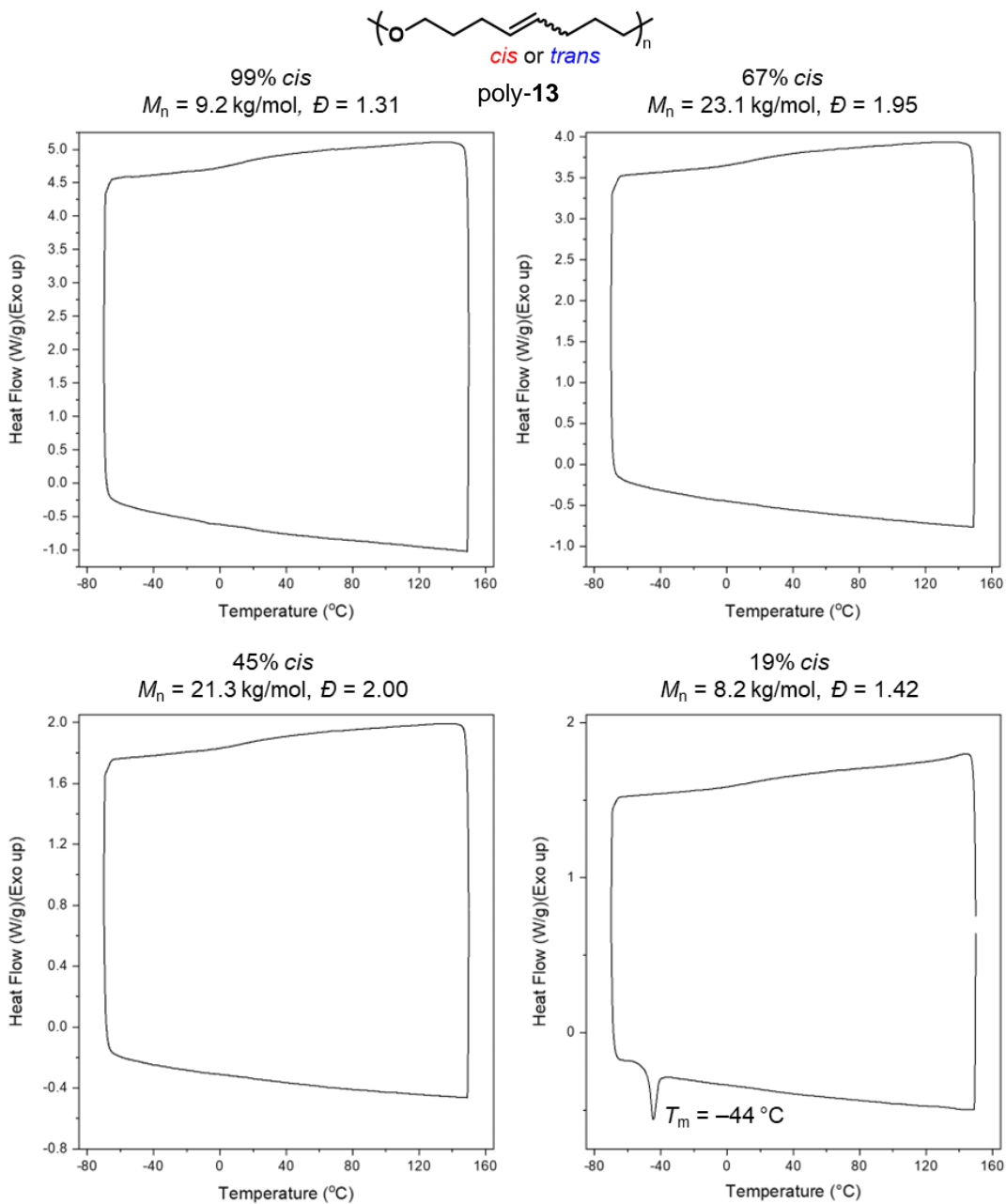
Figure IV-23 DSC thermograms of poly-**13** with 99%, 67%, 45% and 19% *cis* content.

Table IV-13 Thermal Properties of Poly-**13** with Varied *cis* Content

entry	*cis* content (%)	M_n (kg/mol)	M_w (kg/mol)	$Đ$	T_d (°C)	T_g (°C)	T_m (°C)	T_c (°C)
1	99	9.2	12.0	1.31	373	—	—	—
2	67	23.1	45.0	1.95	360	—	—	—
3	45	21.3	42.5	2.00	351	—	—	—
4	19	8.2	11.7	1.42	266	—	–44	—
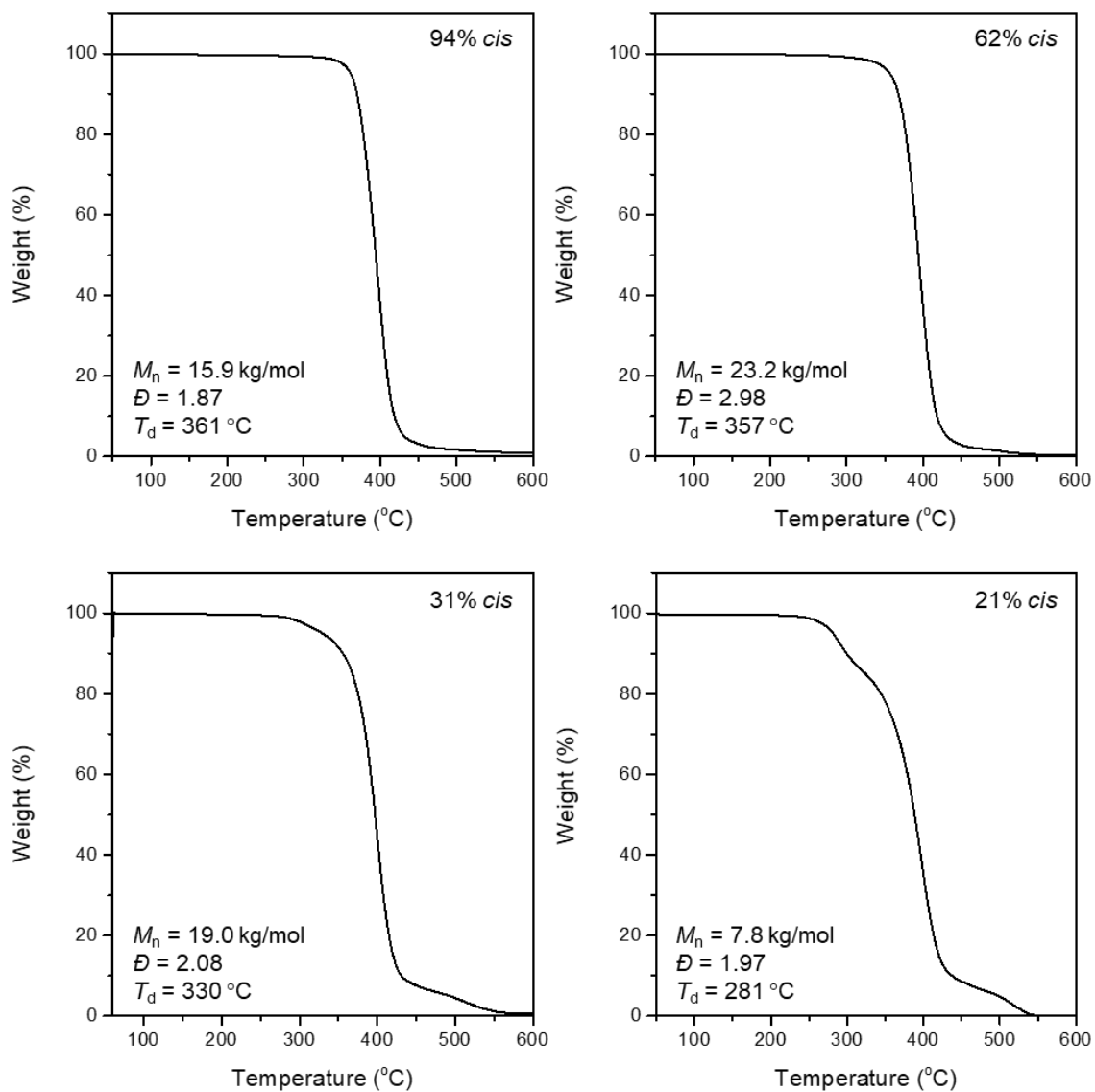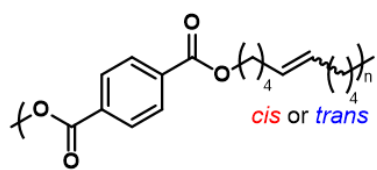
Figure IV-24 TGA thermograms of poly-**14** with 94%, 62%, 31% and 21% *cis* content.
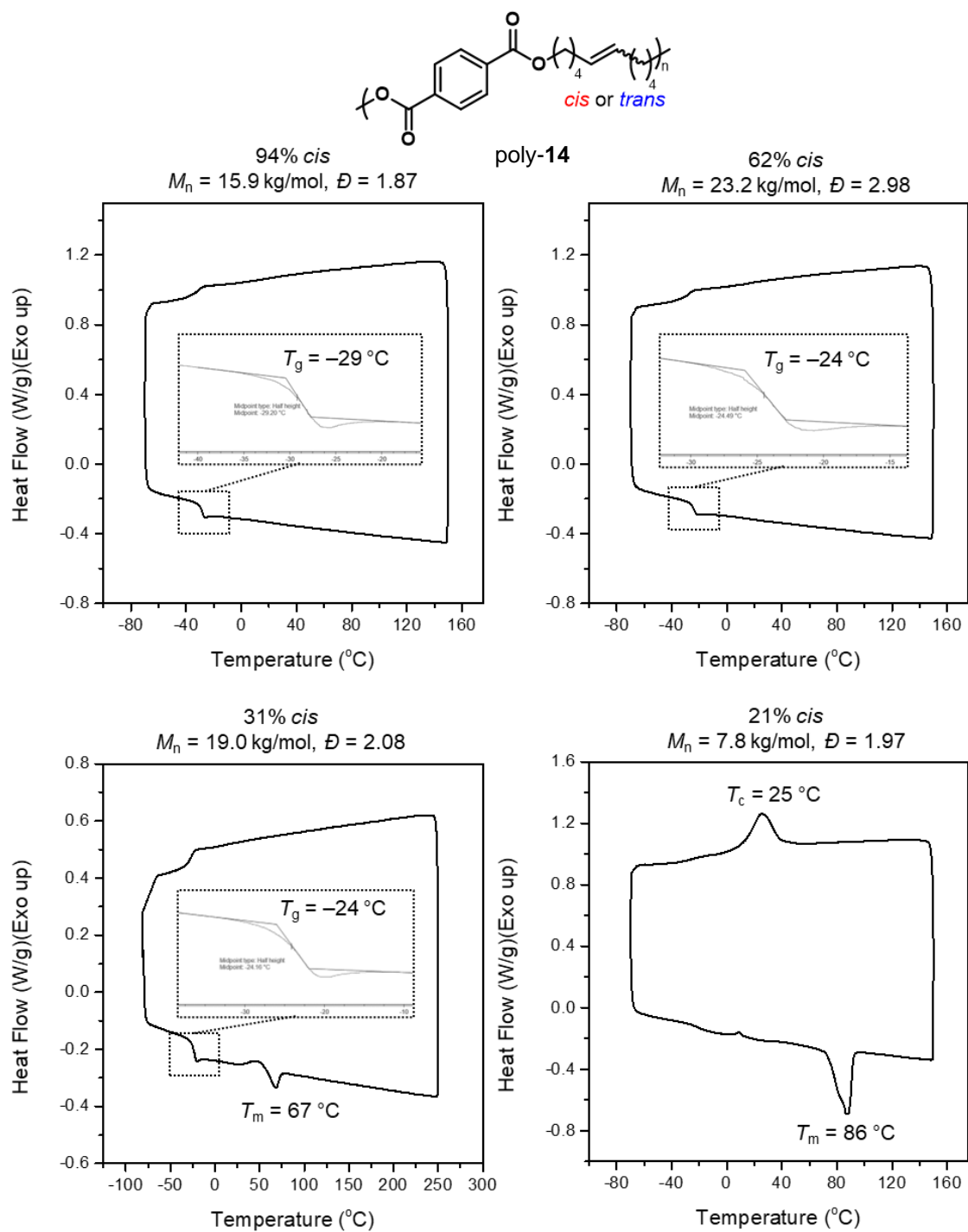
Figure IV-25 DSC thermograms of poly-**14** with 94%, 62%, 31% and 21% *cis* content.

Table IV-14 Thermal Properties of Poly-**14** with Varied *cis* Content

entry	*cis* content (%)	M_n (kg/mol)	M_w (kg/mol)	$Đ$	T_d (°C)	T_g (°C)	T_m (°C)	T_c (°C)
1	94	15.9	29.7	1.87	361	–29	—	—
2	62	23.2	69.1	2.98	357	–24	—	—
3	31	19.0	39.5	2.08	330	–24	67	—
4	21	7.8	15.4	1.97	281	—	86	25
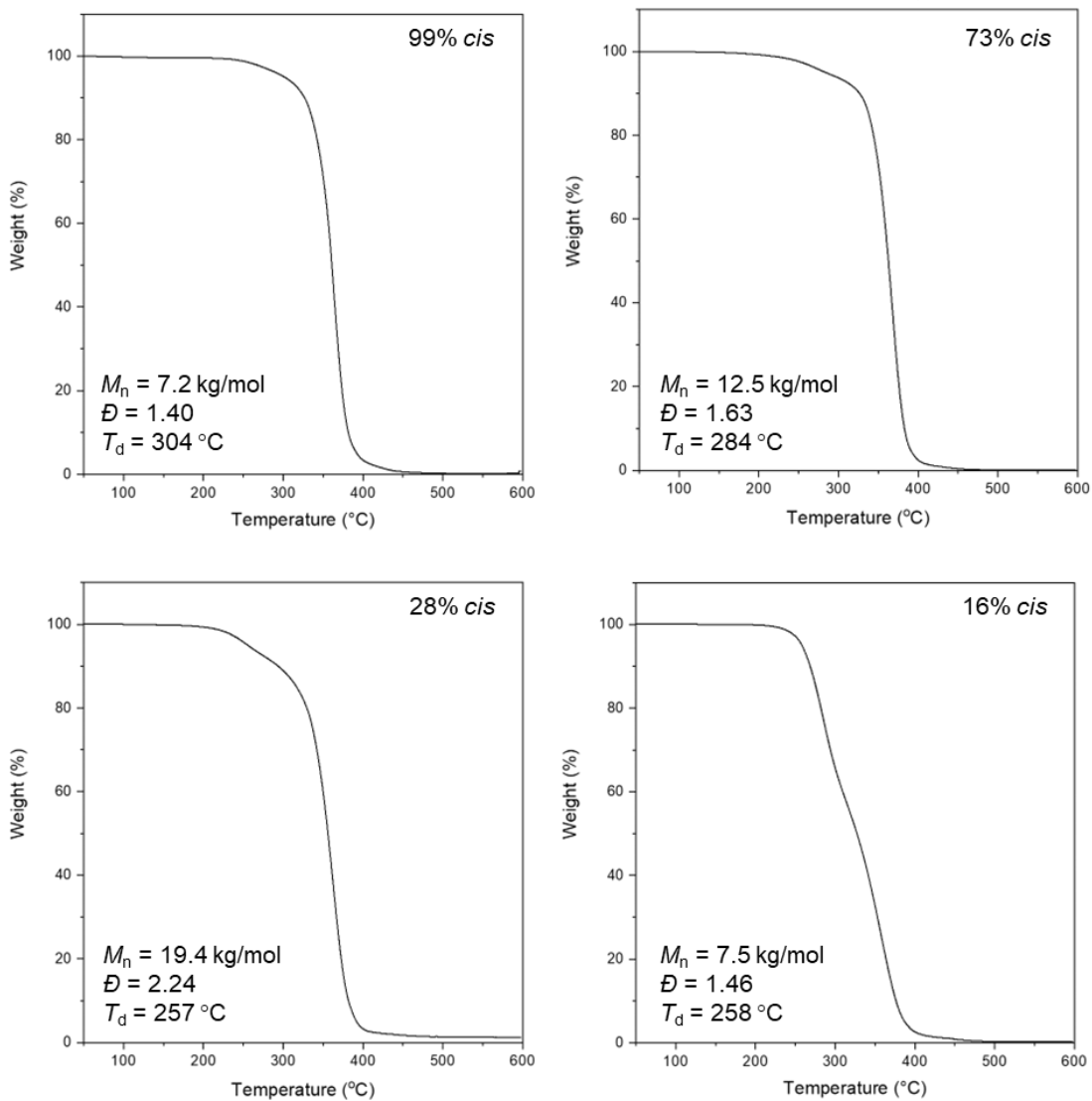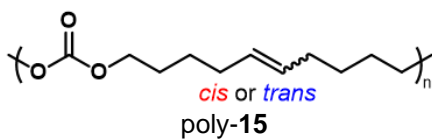
Figure IV-26 TGA thermograms of poly-**15** with 99%, 73%, 28% and 16% *cis* content.
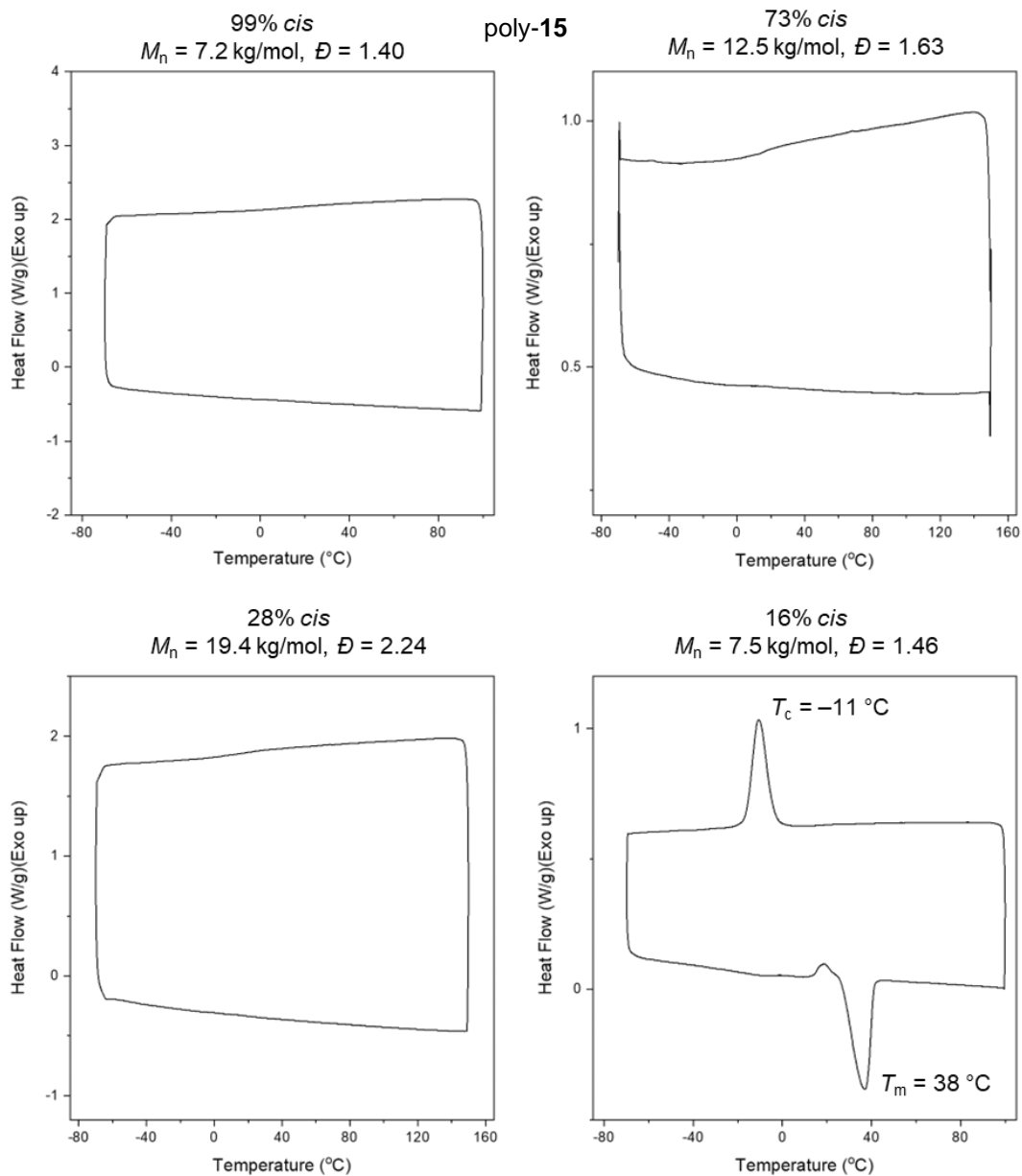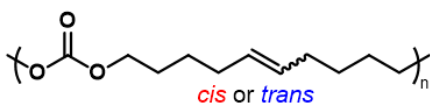
Figure IV-27 DSC thermograms of poly-**15** with 99%, 73%, 28% and 16% *cis* content.

Table IV-15 Thermal Properties of poly-**15** with Varied *cis* Content

entry	*cis* content (%)	M_n (kg/mol)	M_w (kg/mol)	Đ	T_d (°C)	T_g (°C)	T_m (°C)	T_c (°C)
1	99	7.2	10.1	1.40	304	—	—	—
2	73	12.5	20.4	1.63	284	—	—	—
3	28	19.4	43.5	2.24	257	—	—	—
4	16	7.5	10.9	1.46	258	—	38	−11
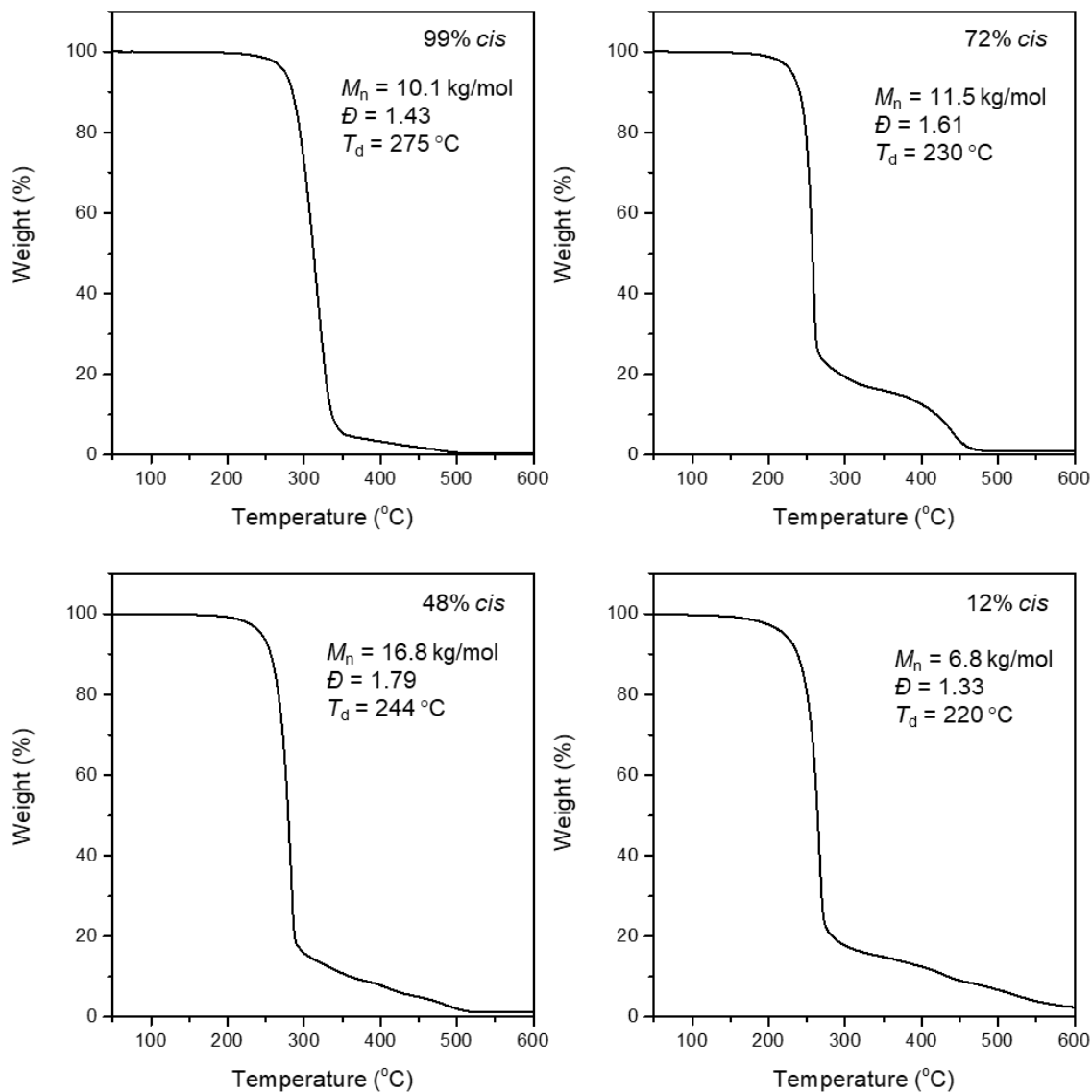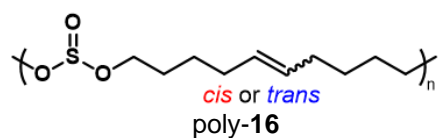
Figure IV-28 TGA thermograms of poly-**16** with 99%, 72%, 48% and 12% *cis* content.
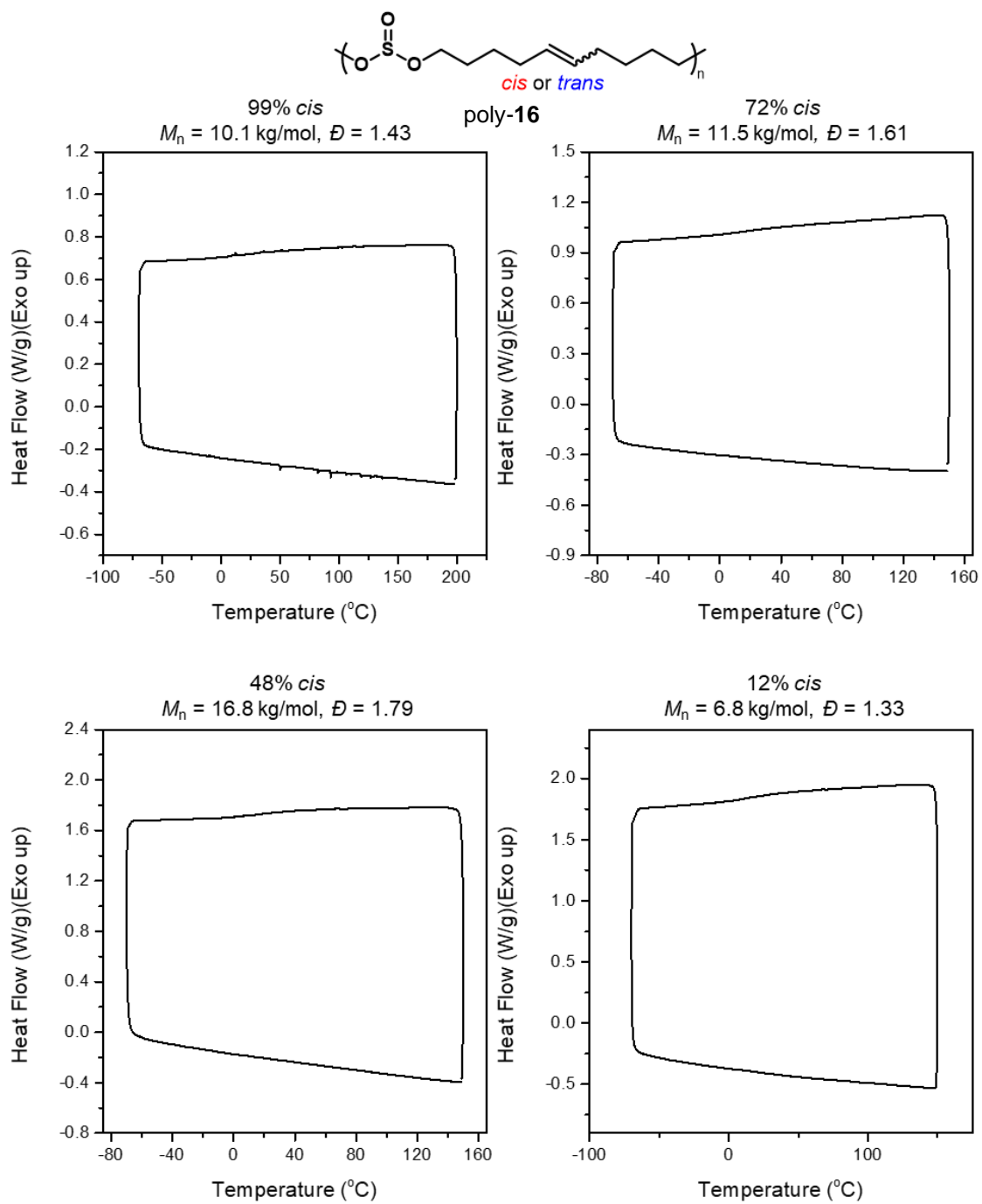
Figure IV-29 DSC thermograms of poly-**16** with 99%, 72%, 48% and 12% *cis* content.

Table IV-16 Thermal Properties of Poly-**16** with Varied *cis* Content

entry	*cis* content (%)	M_n (kg/mol)	M_w (kg/mol)	Đ	T_d (°C)	T_g (°C)	T_m (°C)	T_c (°C)
1	99	10.1	14.4	1.43	275	—	—	—
2	72	11.5	18.5	1.61	230	—	—	—
3	48	16.8	30.1	1.79	244	—	—	—
4	12	6.8	9.0	1.33	220	—	—	—
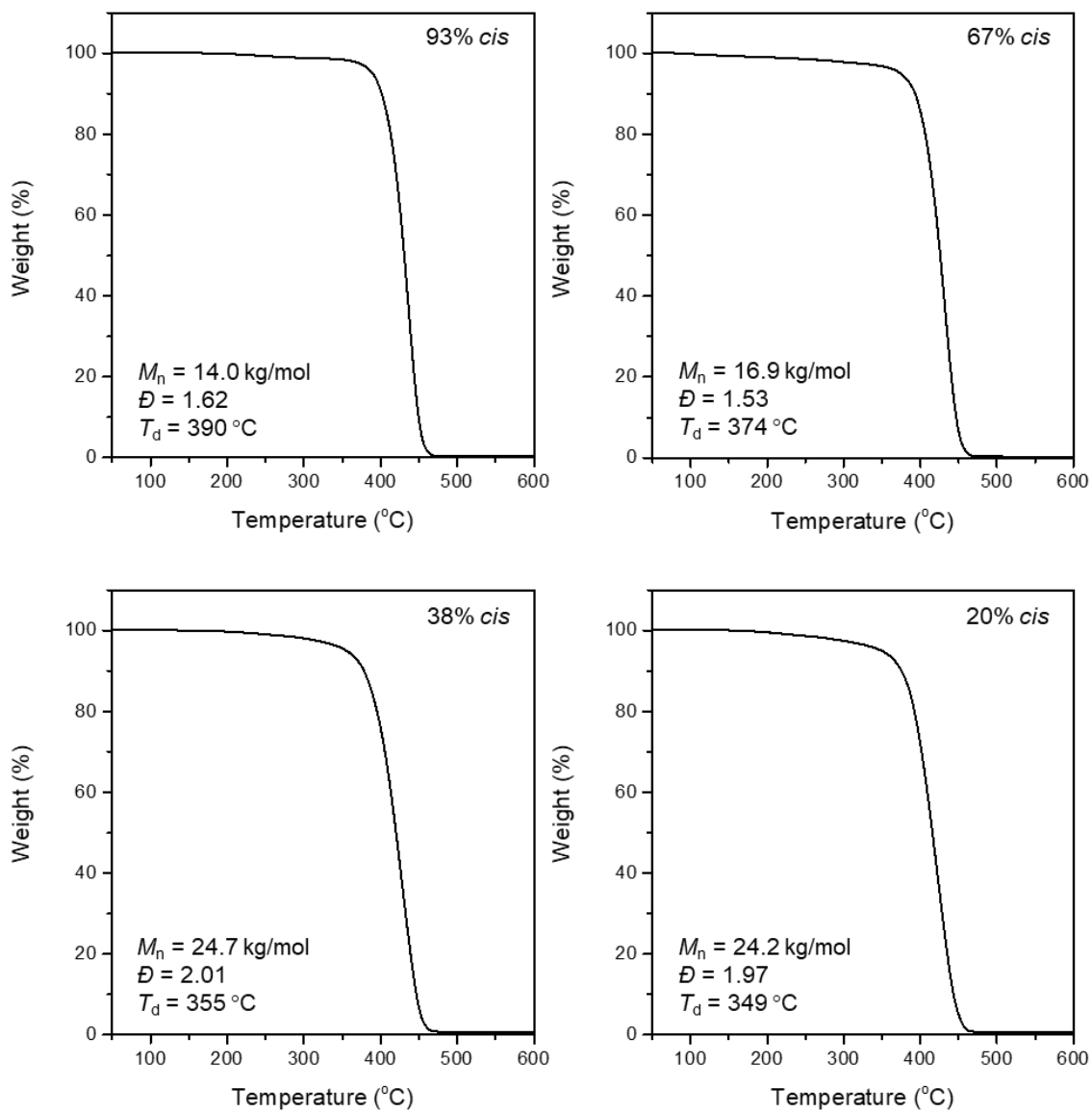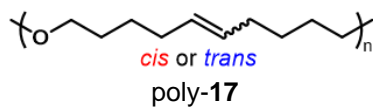
Figure IV-30 TGA thermograms of poly-**17** with 93%, 67%, 38% and 20% *cis* content.
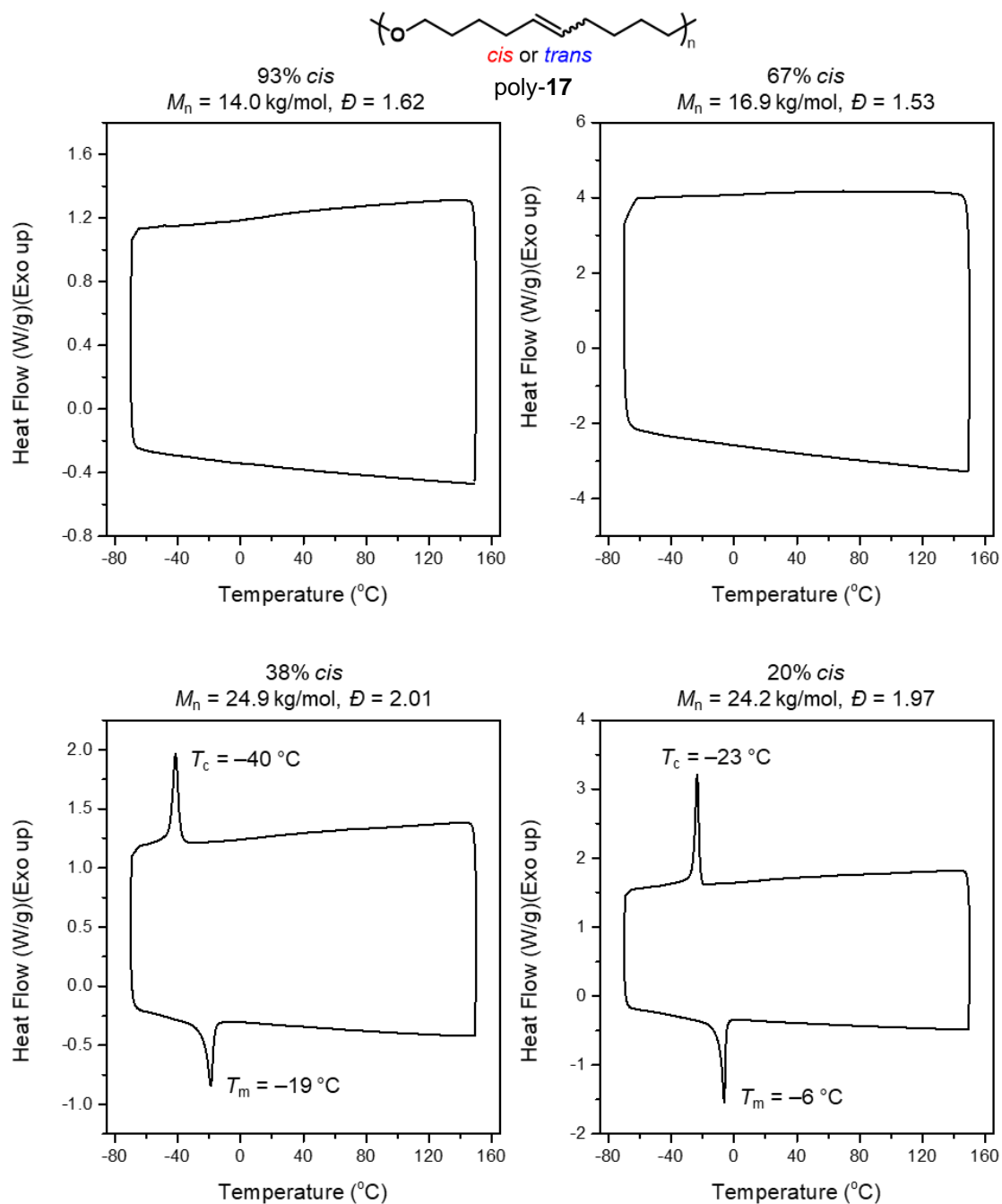
Figure IV-31 DSC thermograms of poly-**17** with 93%, 67%, 38% and 20% *cis* content.

Table IV-17 Thermal Properties of Poly-**17** with Varied *cis* Content

entry	*cis* content (%)	M_n (kg/mol)	M_w (kg/mol)	Đ	T_d (°C)	T_g (°C)	T_m (°C)	T_c (°C)
1	93	14.0	22.7	1.62	390	—	—	—
2	67	16.9	25.9	1.53	374	—	—	—
3	38	24.9	49.6	2.01	355	—	−19	−40
4	20	24.2	47.7	1.97	349	—	−6	−23

IV.4.10 NMR Spectra of Synthesized Intermediates, Monomers and Polymers
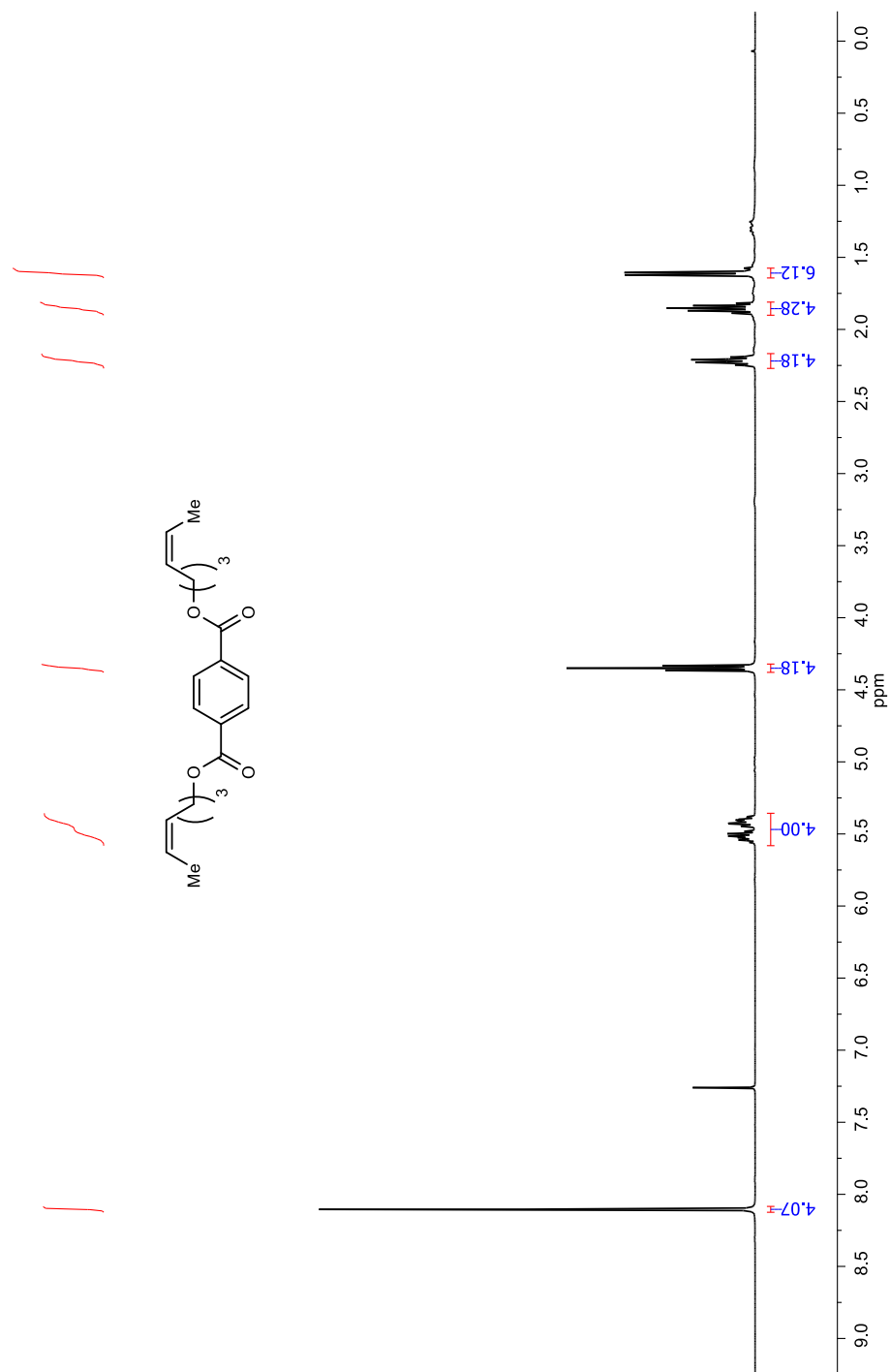
Figure IV-32 ^{1}H NMR (400 MHz, CDCl₃) spectrum of compound **10**.
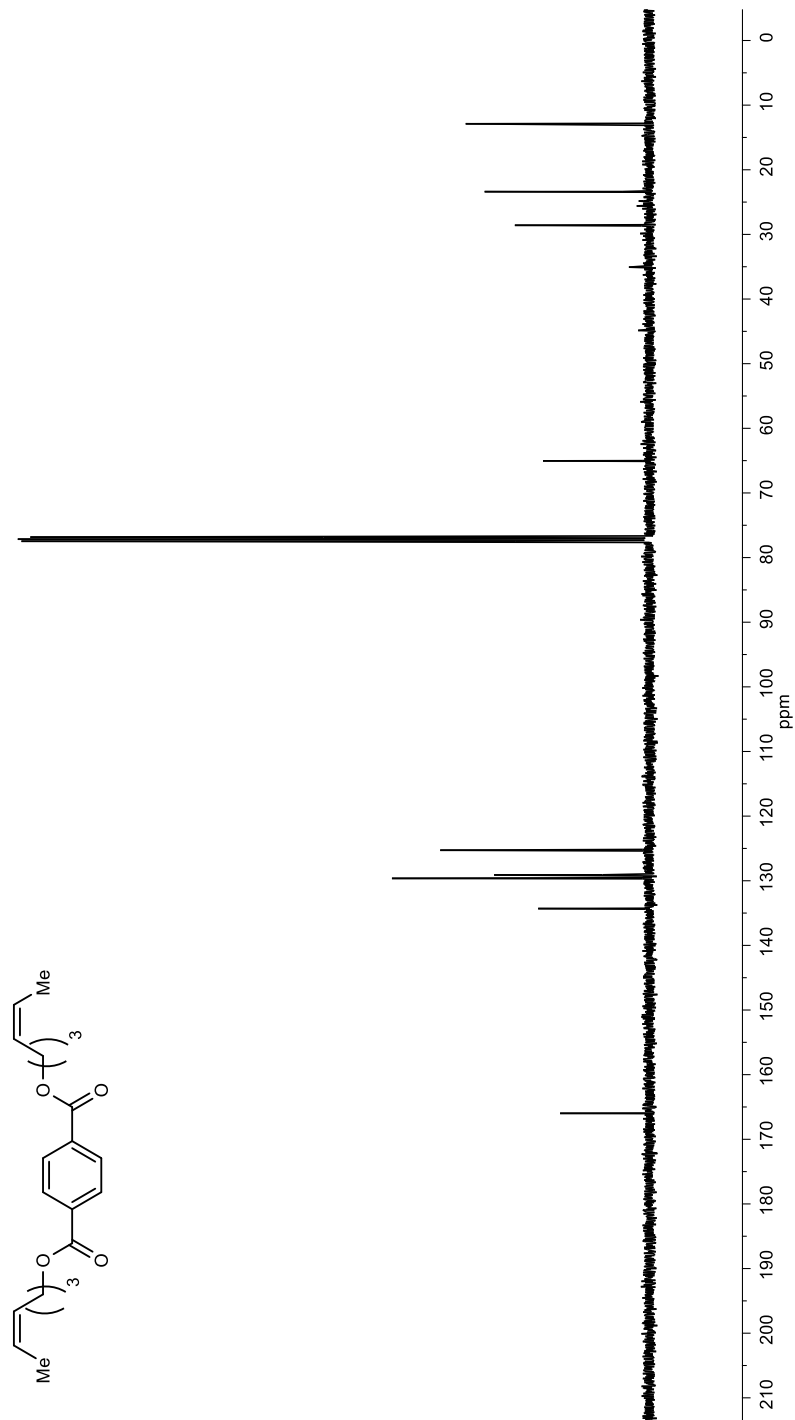
Figure IV-33 ^{13}C NMR (101 MHz, CDCl$_3$) spectrum of compound **10**.
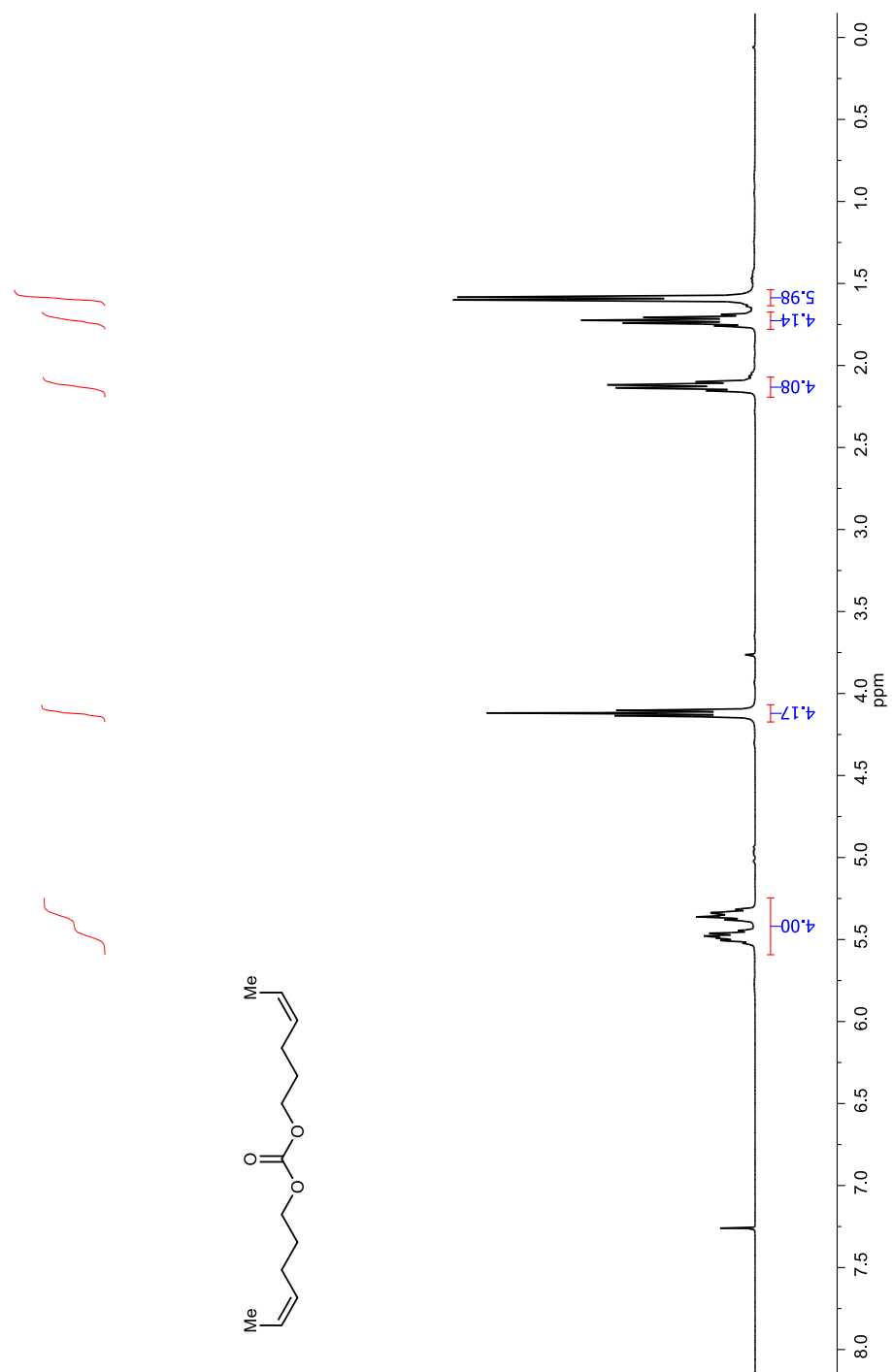
Figure IV-34 ^{1}H NMR (400 MHz, CDCl$_3$) spectrum of compound **11**.
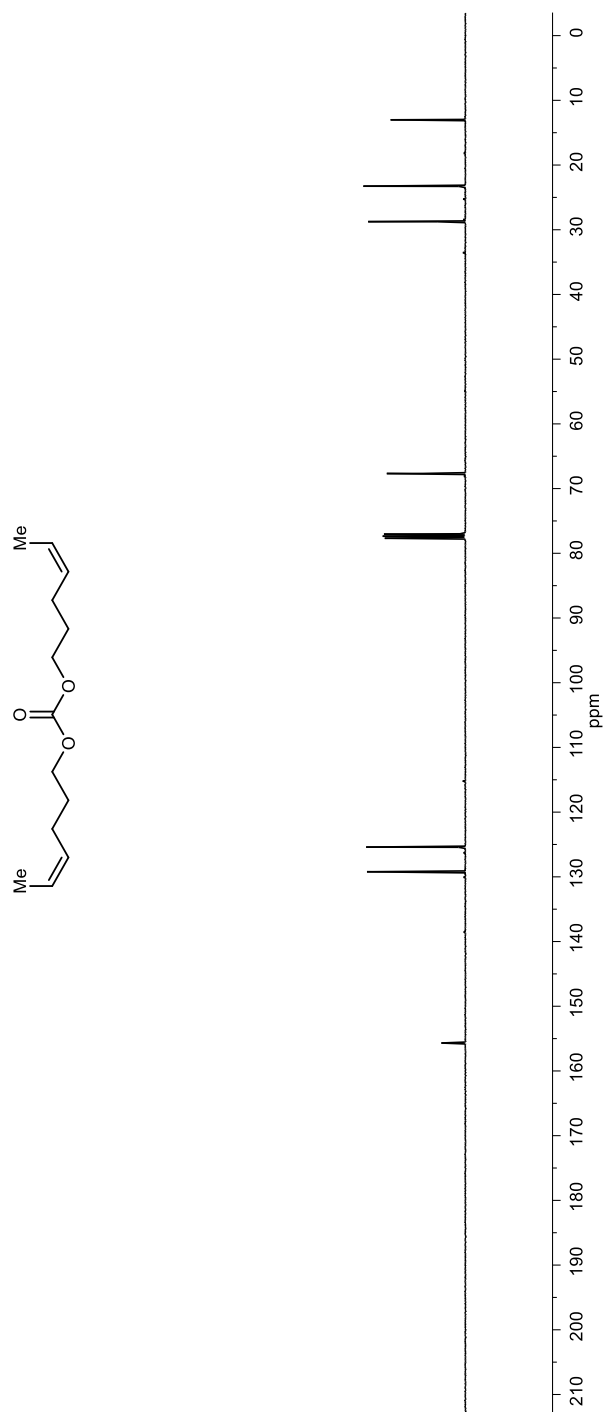
Figure IV-35 ^{13}C NMR (101 MHz, CDCl$_3$) spectrum of compound **11**.
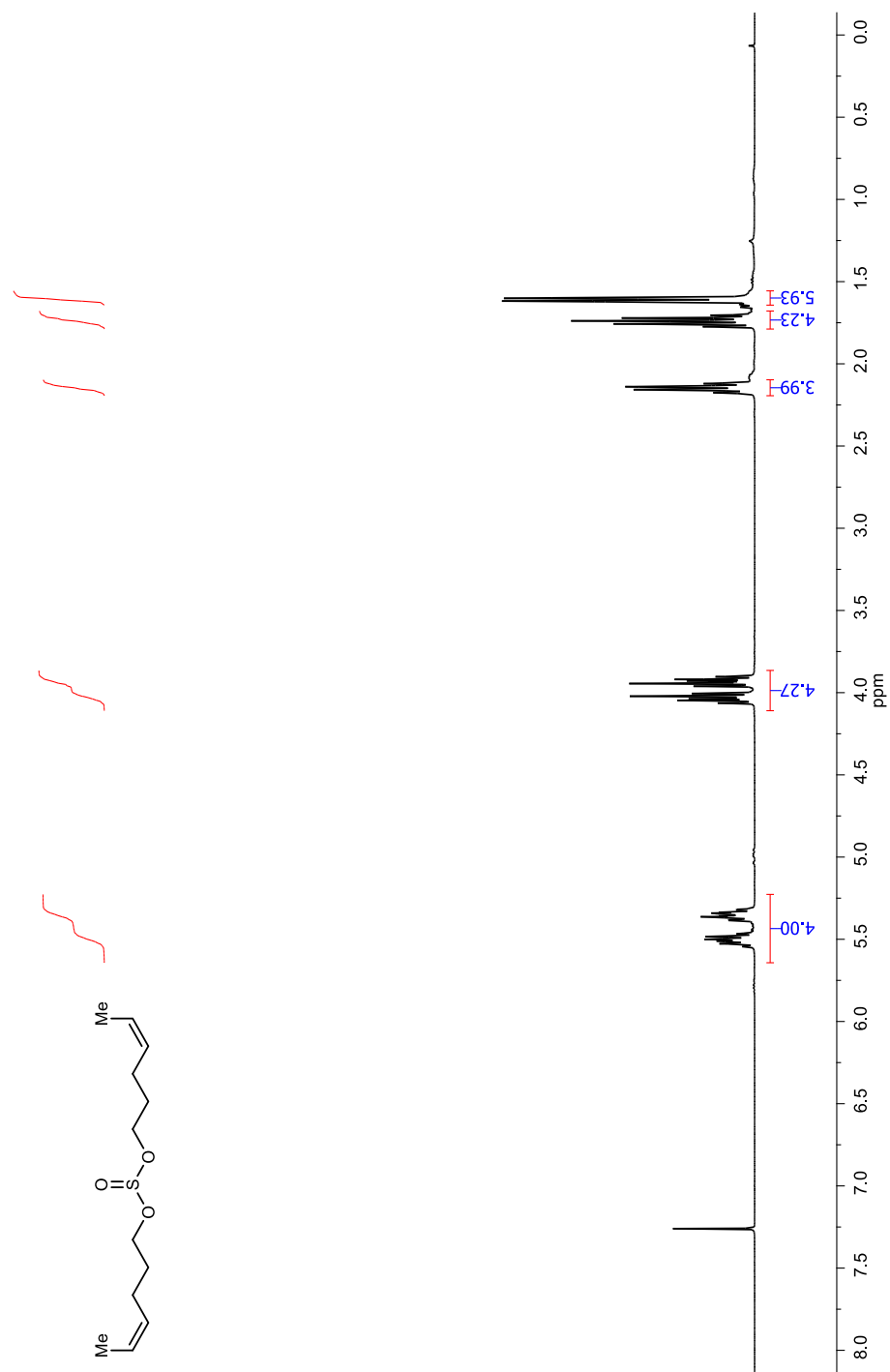
Figure IV-36 ^{1}H NMR (400 MHz, CDCl$_3$) spectrum of compound **12**.
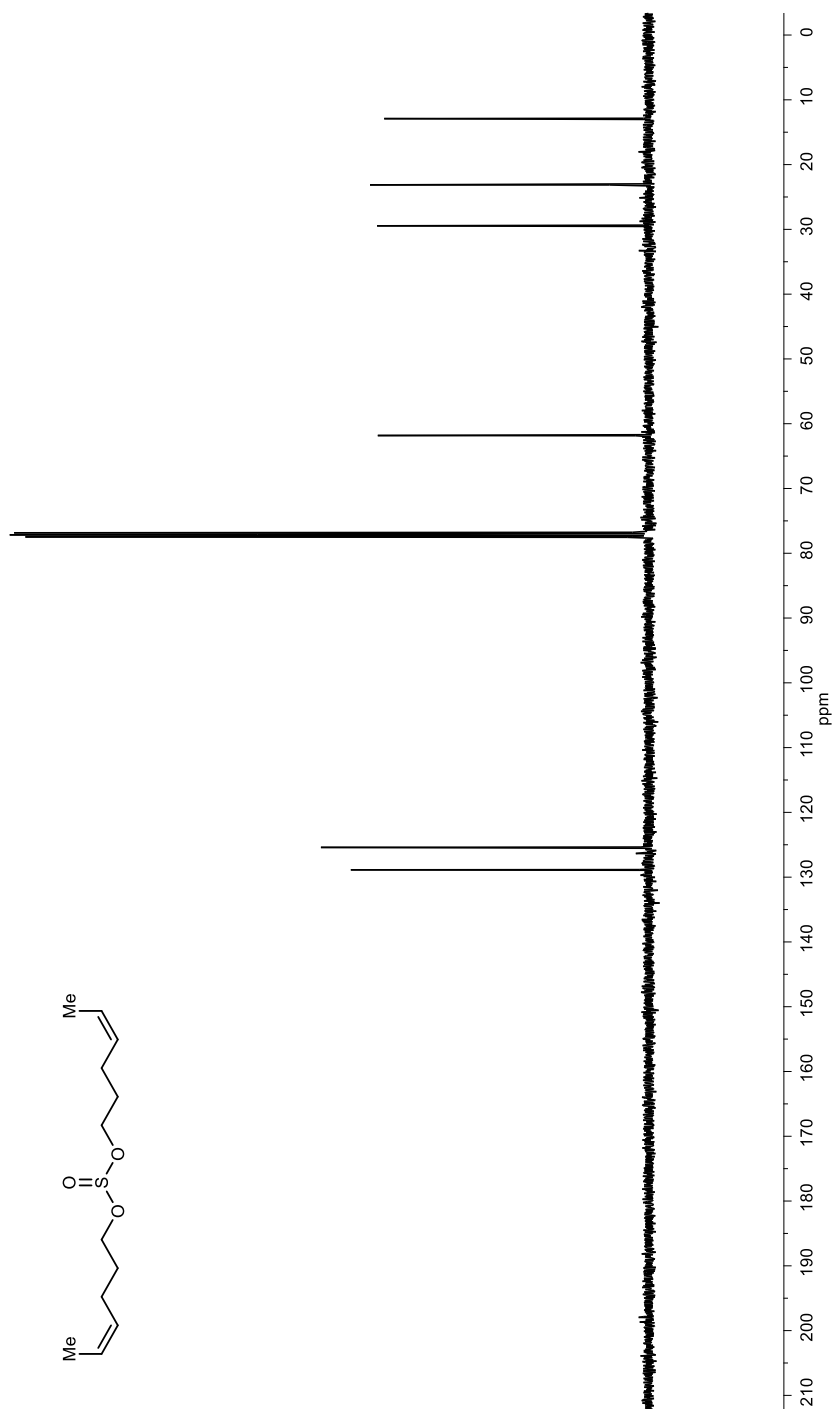
Figure IV-37 ^{13}C NMR (101 MHz, CDCl$_3$) spectrum of compound **12**.
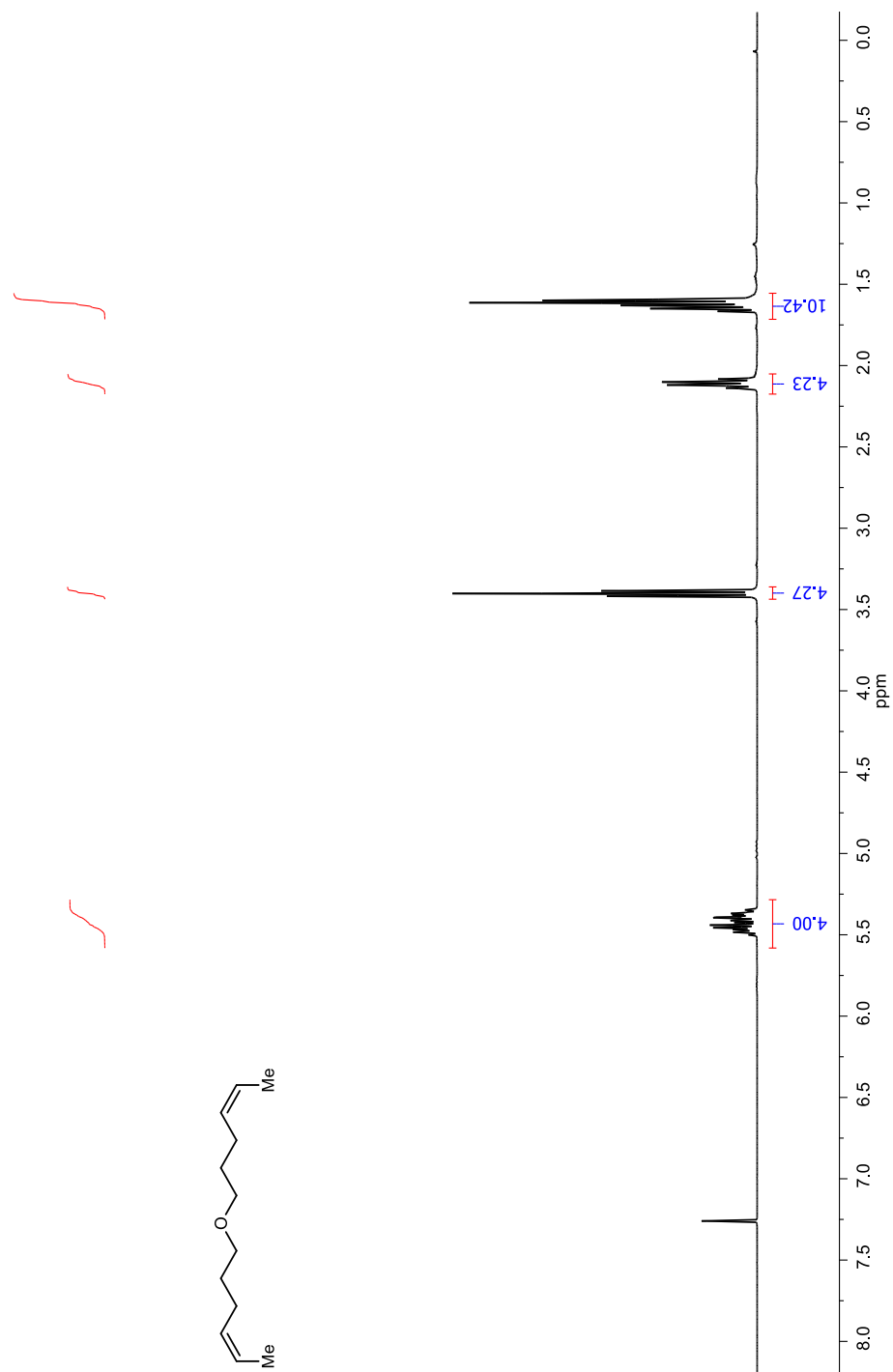
Figure IV-38 ^{1}H NMR (400 MHz, CDCl$_3$) spectrum of compound **13**.

Figure IV-39 ^{13}C NMR (101 MHz, CDCl₃) spectrum of compound **13**.

197
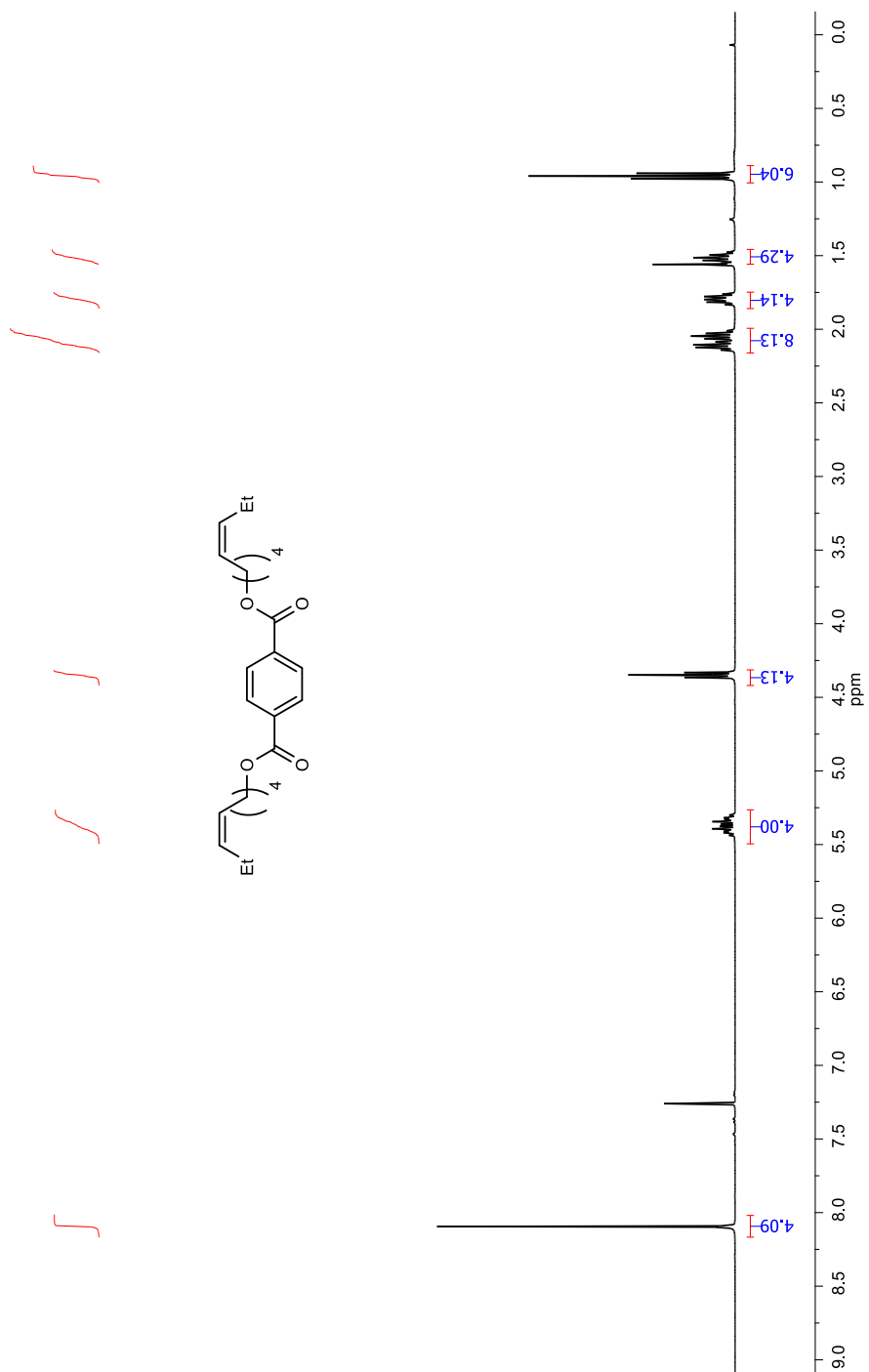
Figure IV-40 ^{1}H NMR (400 MHz, CDCl$_3$) spectrum of compound **14**.
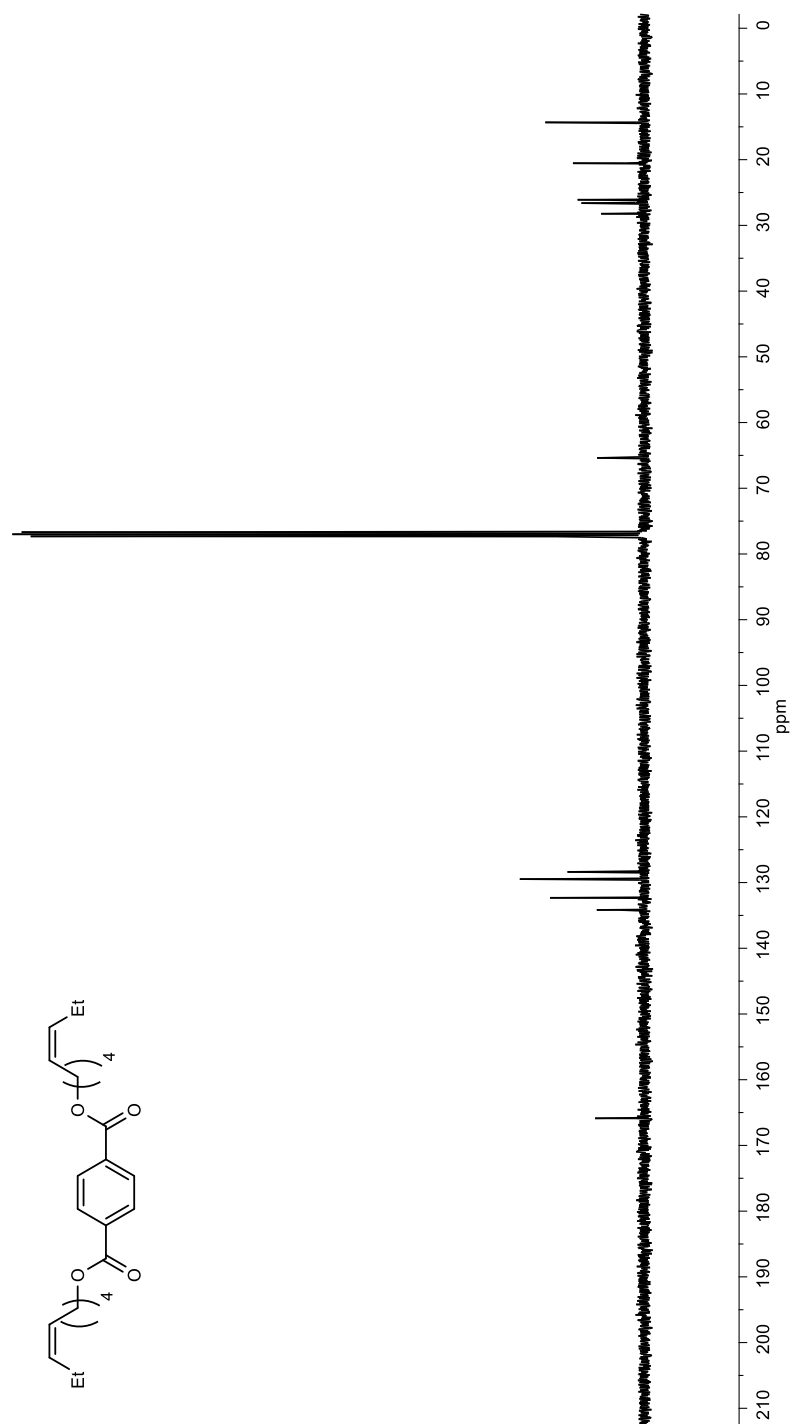
Figure IV-41 ^{13}C NMR (101 MHz, CDCl$_3$) spectrum of compound **14**.
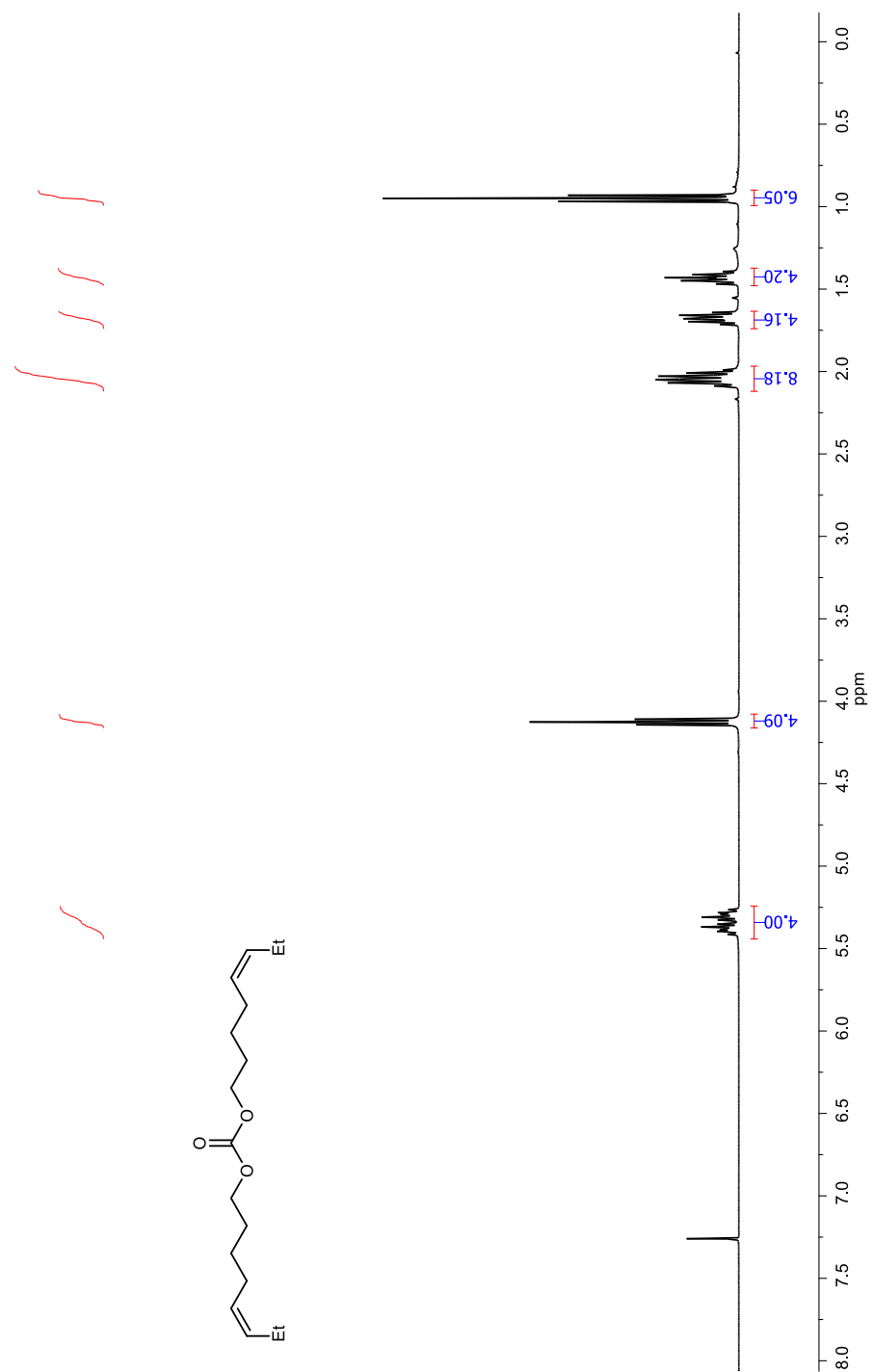
Figure IV-42 ^{1}H NMR (400 MHz, CDCl$_3$) spectrum of compound **15**.

Figure IV-43 ^{13}C NMR (101 MHz, CDCl$_3$) spectrum of compound **15**.
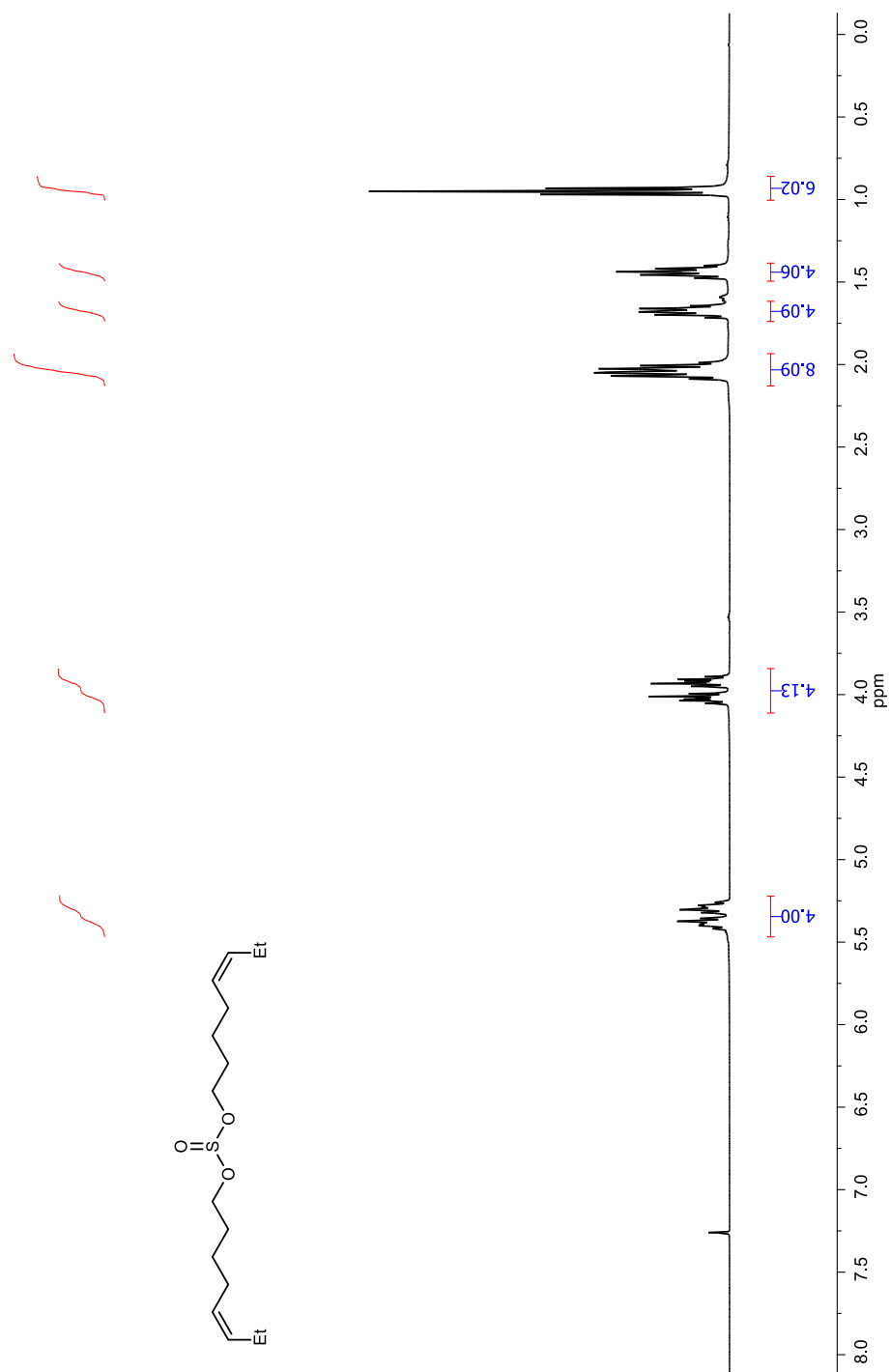
Figure IV-44 ^{1}H NMR (400 MHz, CDCl$_3$) spectrum of compound **16**.
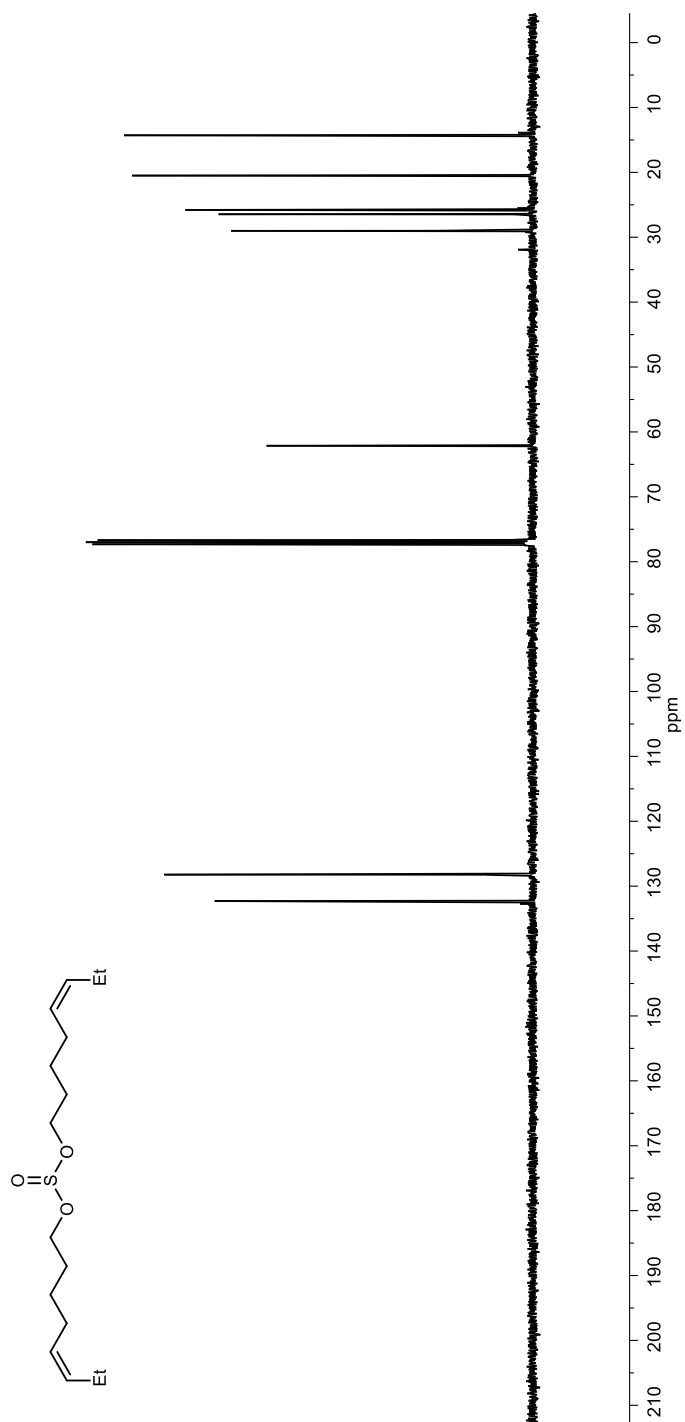
Figure IV-45 ^{13}C NMR (101 MHz, CDCl$_3$) spectrum of compound **16**.
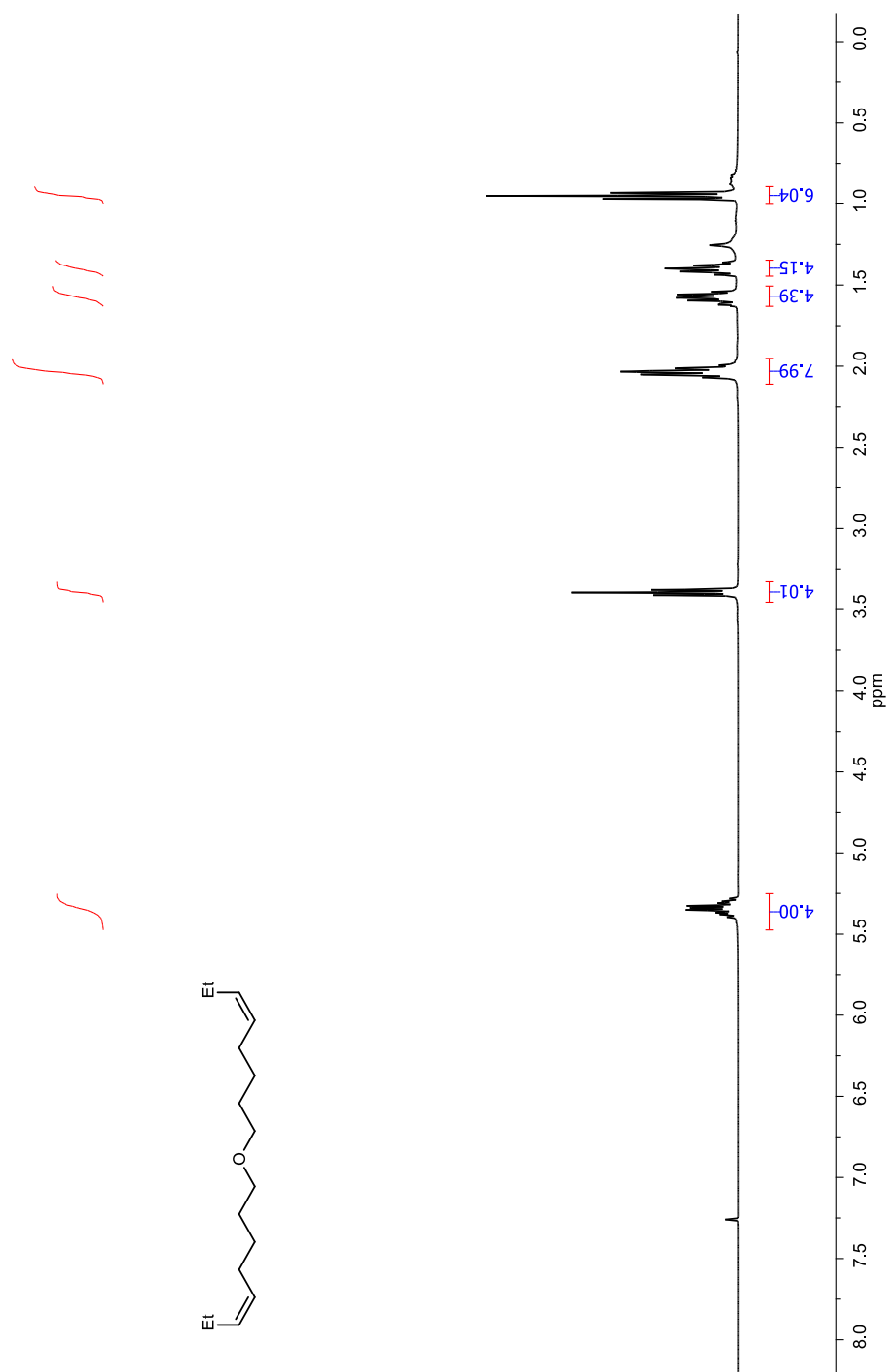
Figure IV-46 ^{1}H NMR (400 MHz, CDCl$_3$) spectrum of compound **17**.
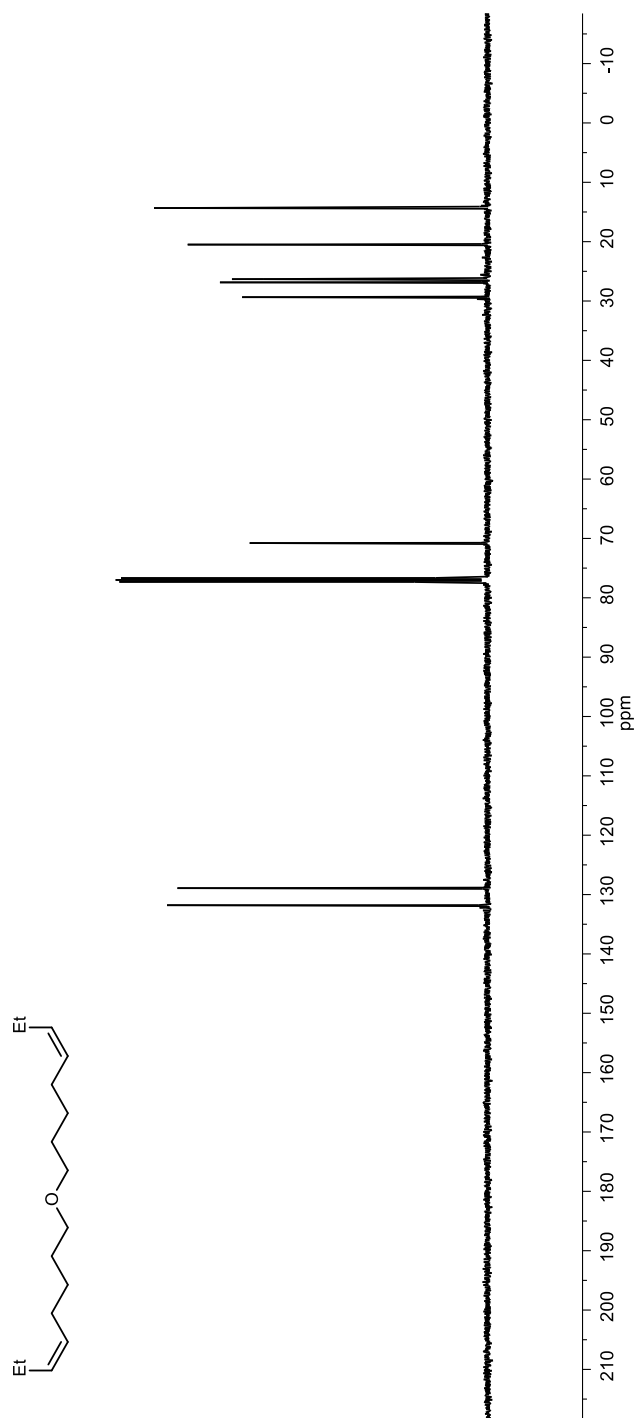
Figure IV-47 ^{13}C NMR (101 MHz, CDCl$_3$) spectrum of compound **17**.
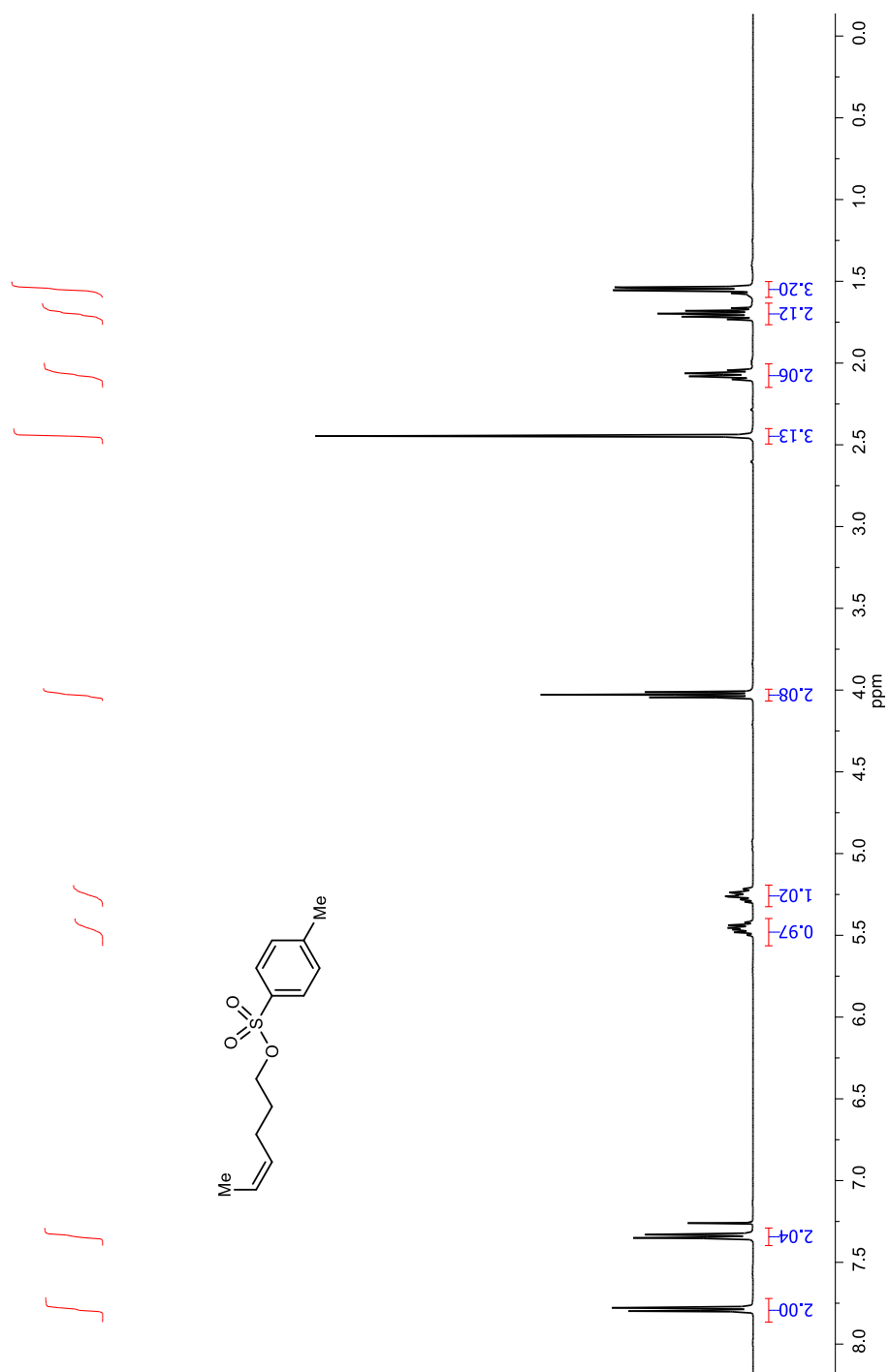
Figure IV-48 ^{1}H NMR (400 MHz, CDCl$_3$) spectrum of compound **21**.
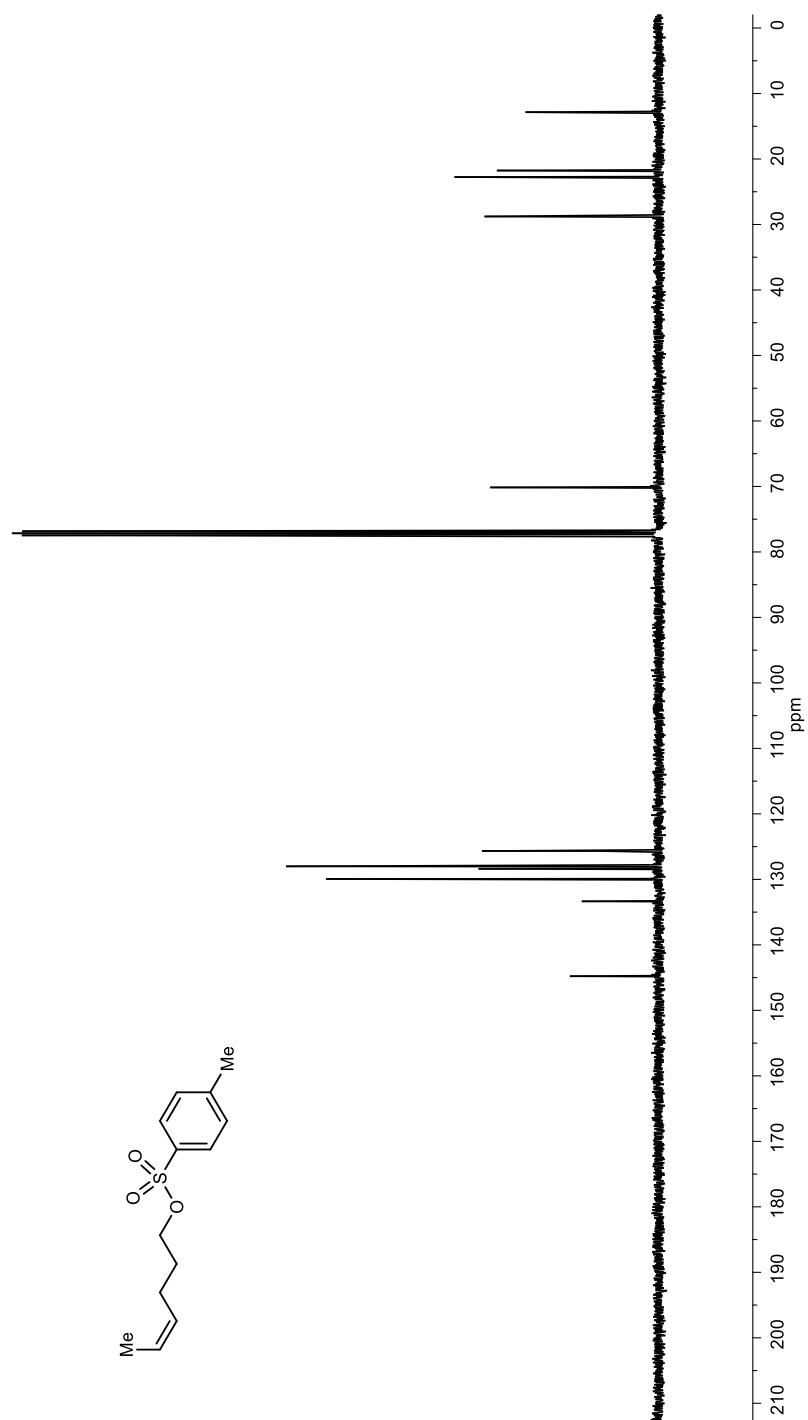
Figure IV-49 ^{13}C NMR (101 MHz, CDCl$_3$) spectrum of compound **21**.
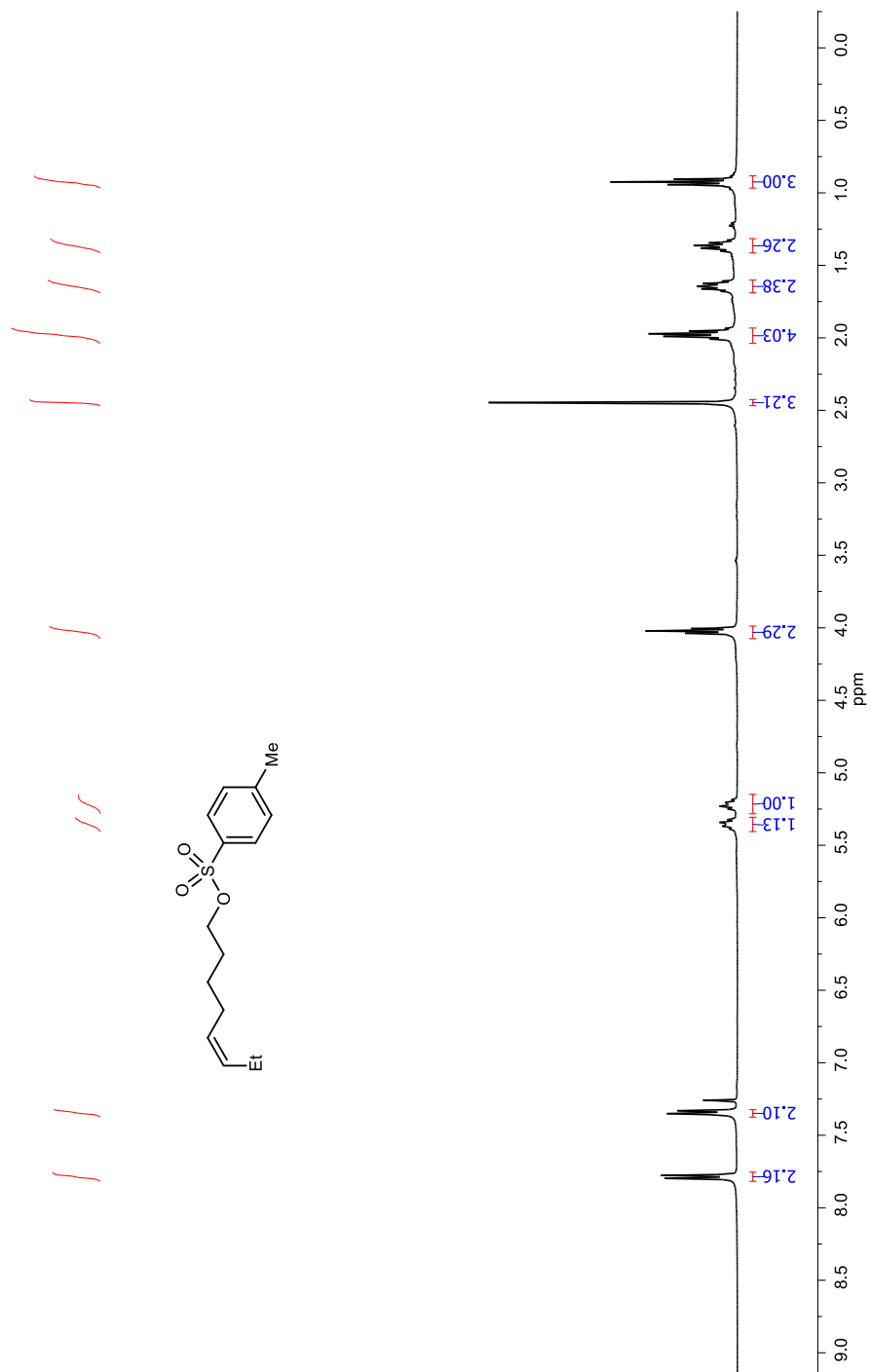
Figure IV-50 ^{1}H NMR (400 MHz, CDCl$_3$) spectrum of compound **22**.
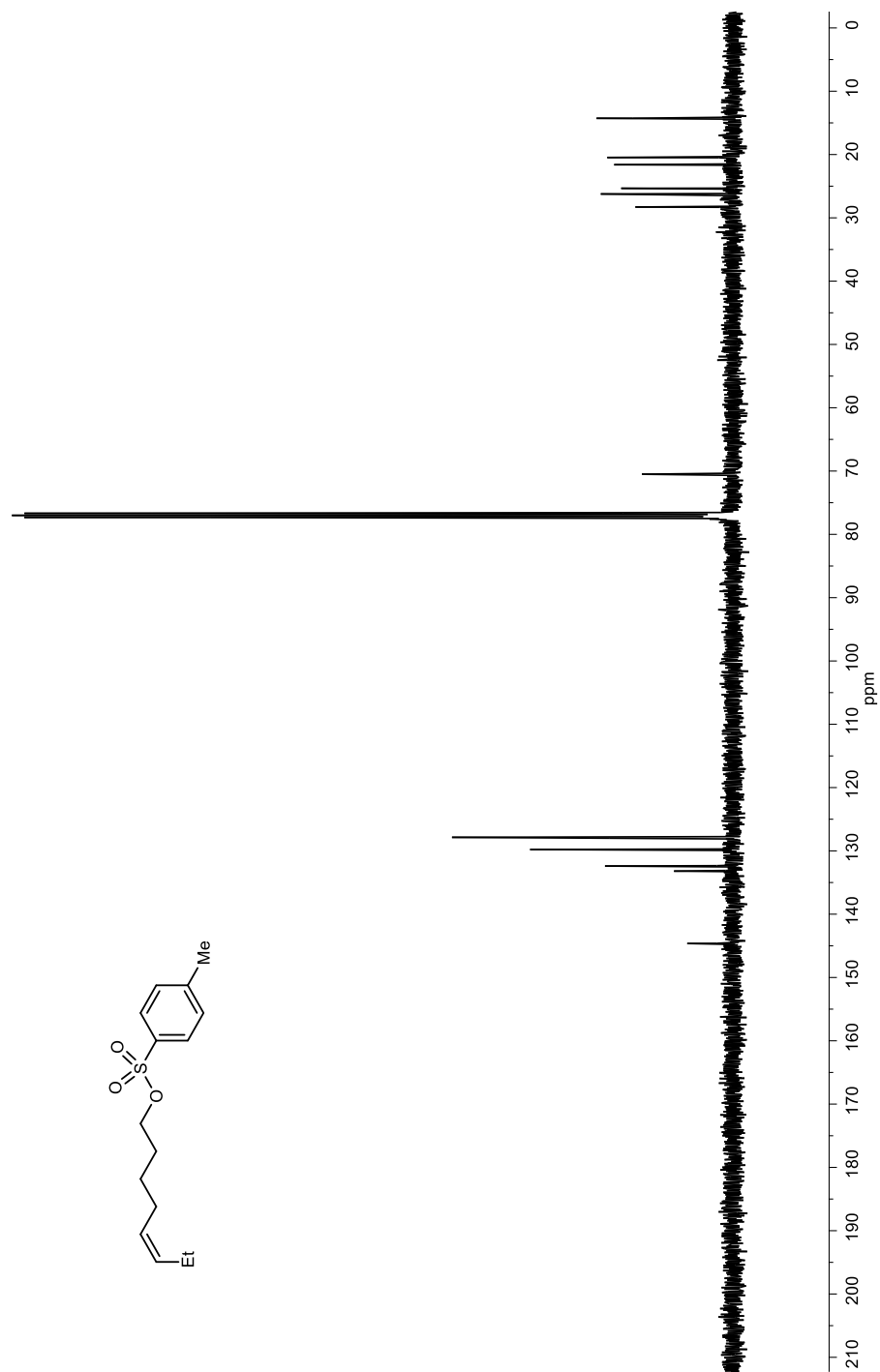
Figure IV-51 ^{13}C NMR (101 MHz, CDCl$_3$) spectrum of compound **22**.
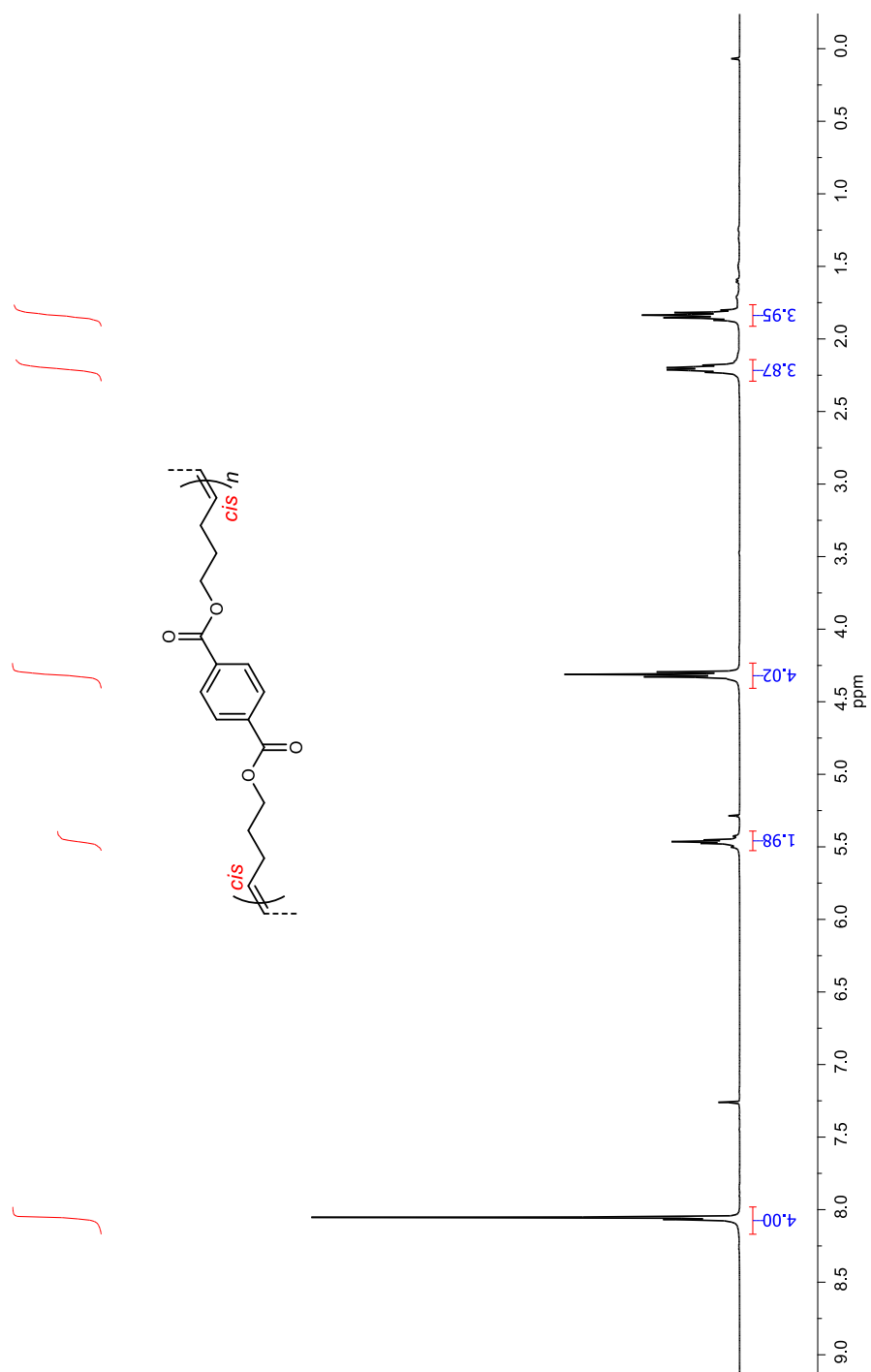
Figure IV-52 ^{1}H NMR (400 MHz, CDCl$_3$) spectrum of *cis*-rich poly-**10**.
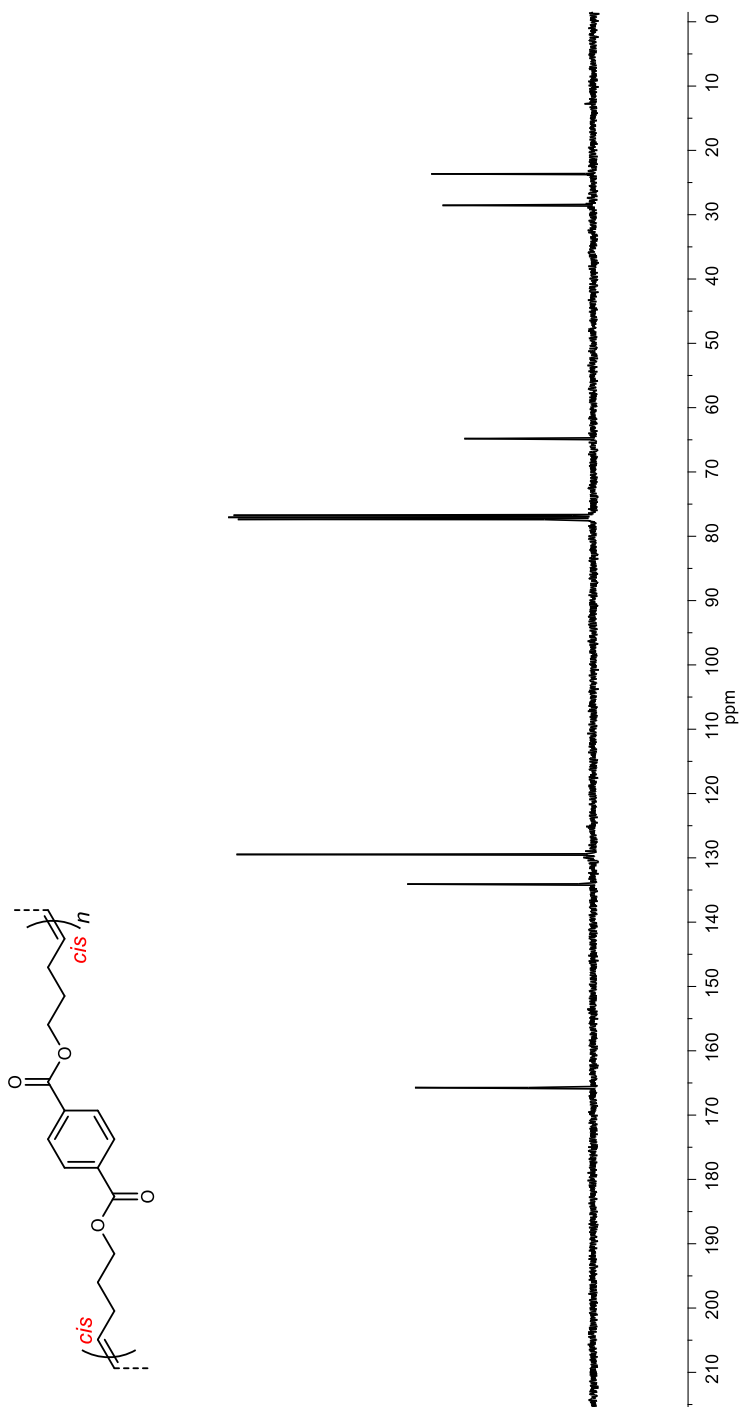
Figure IV-53 ^{13}C NMR (101 MHz, CDCl$_3$) spectrum of *cis*-rich poly-**10**.
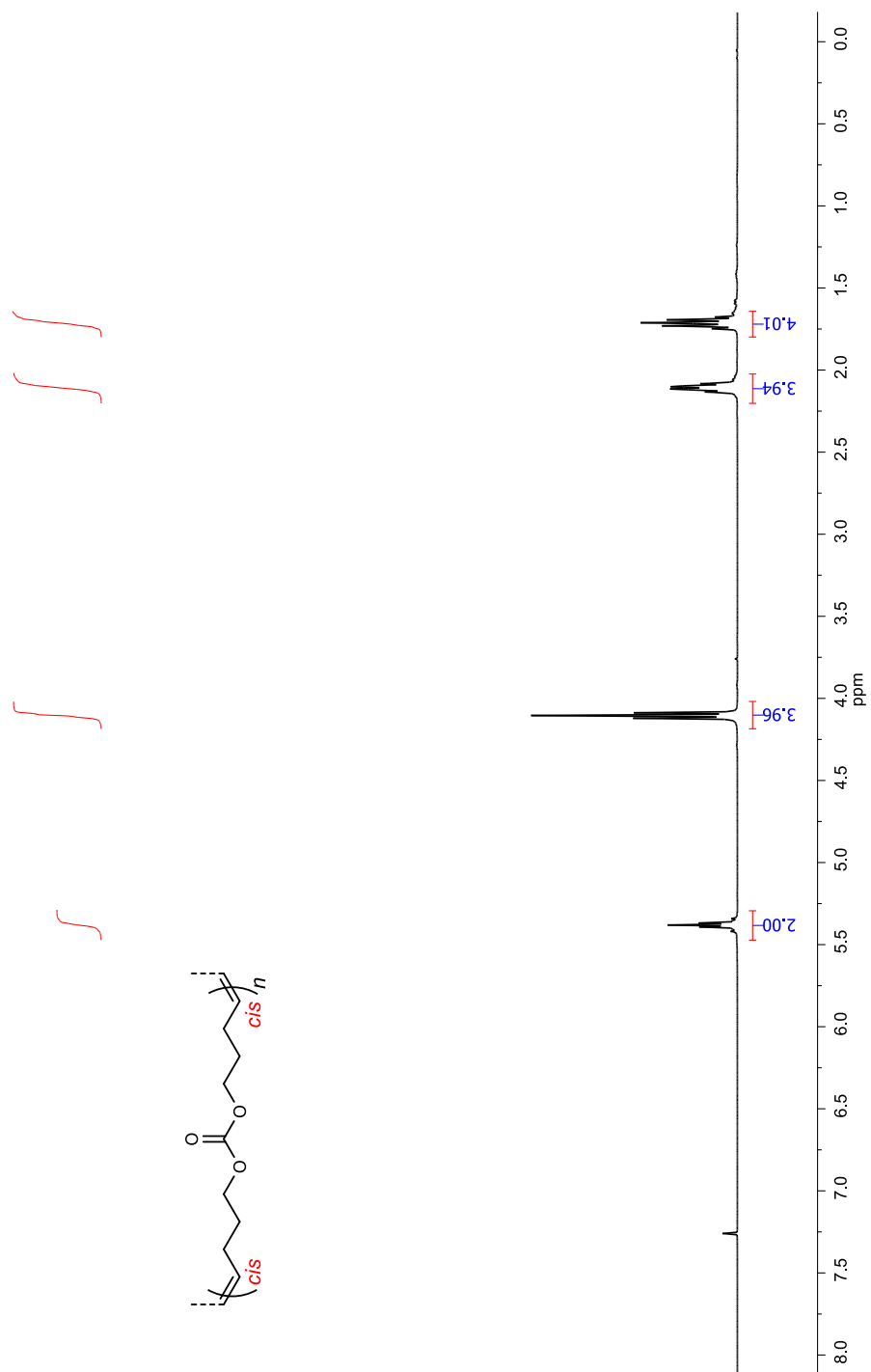
Figure IV-54 ^{1}H NMR (400 MHz, CDCl$_3$) spectrum of *cis*-rich poly-**11**.
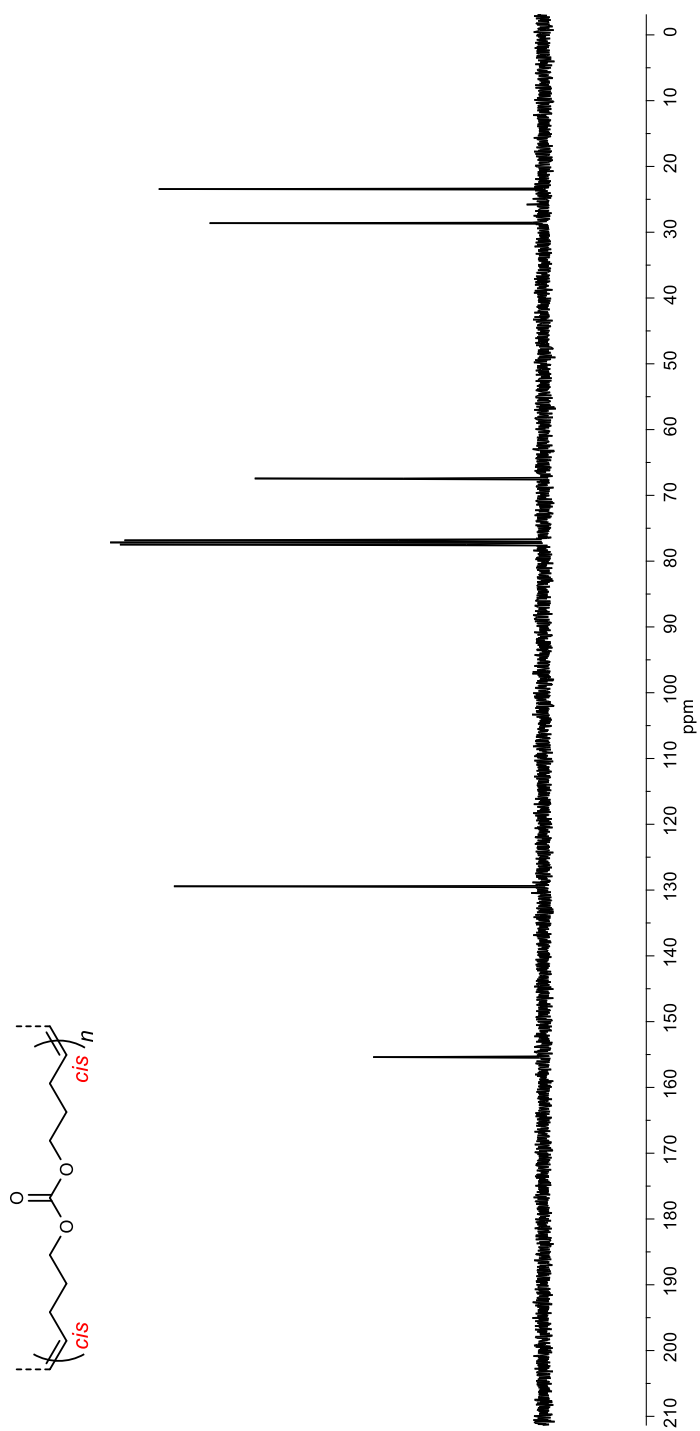
Figure IV-55 ^{13}C NMR (101 MHz, CDCl₃) spectrum of *cis*-rich poly-**11**.
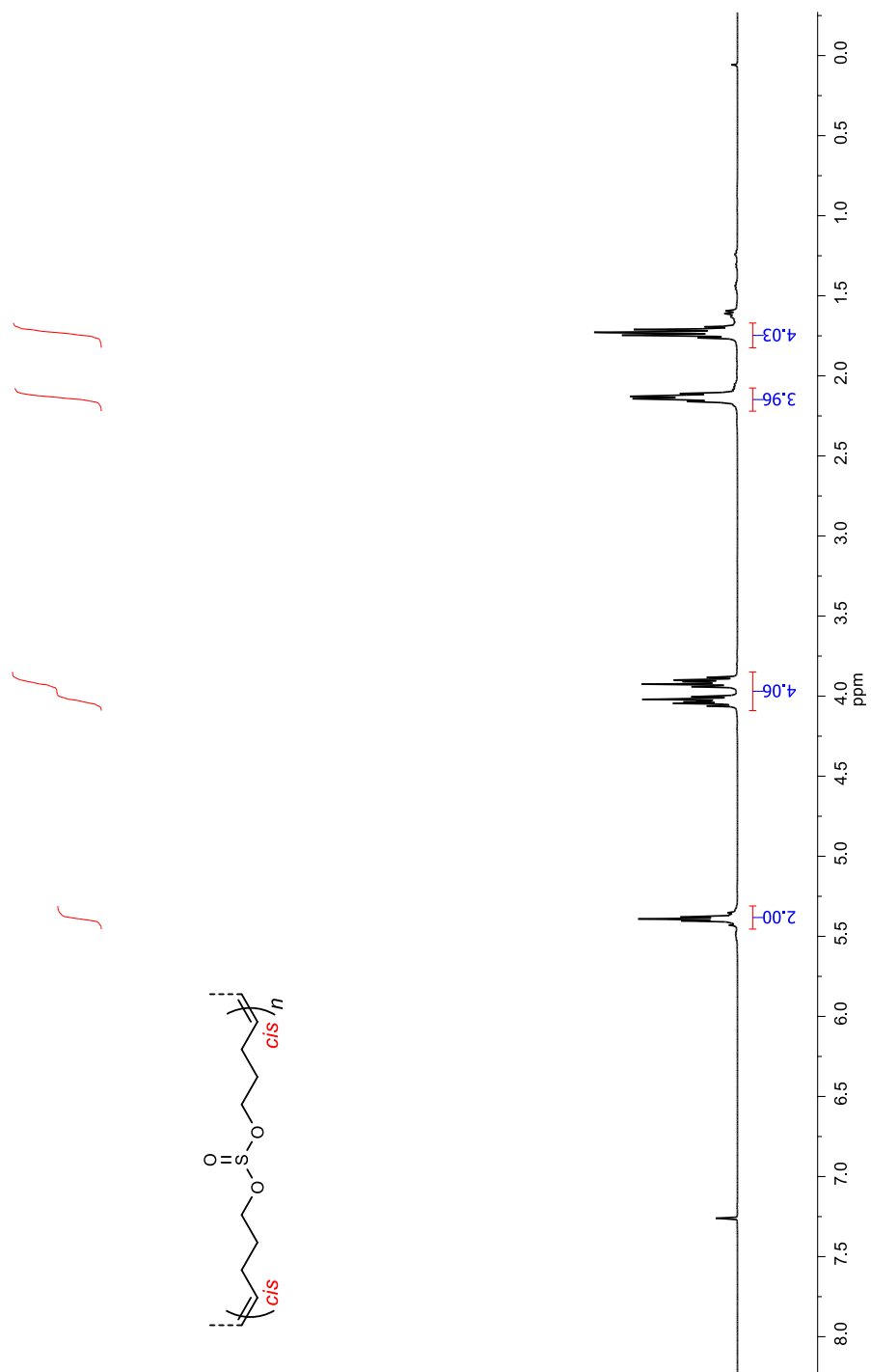
Figure IV-56 ^{1}H NMR (400 MHz, CDCl$_3$) spectrum of *cis*-rich poly-**12**.

214
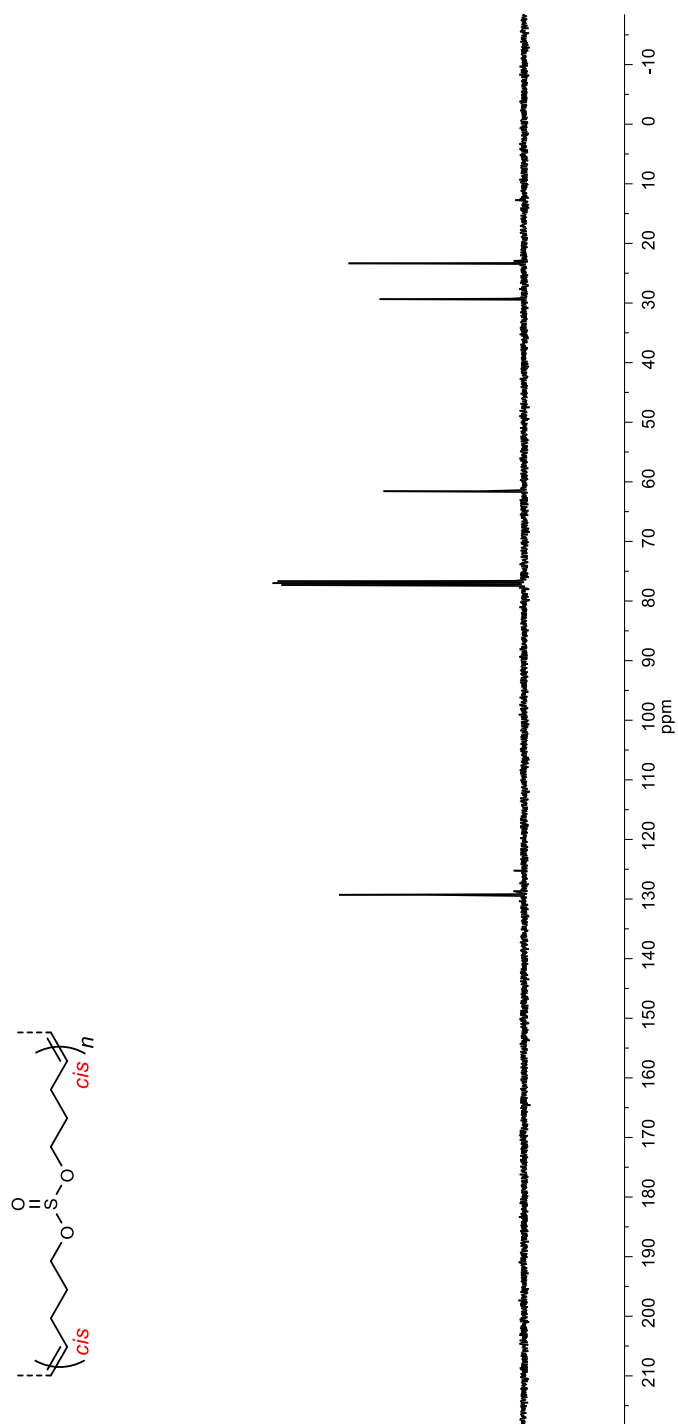
Figure IV-57 ¹³C NMR (101 MHz, CDCl₃) spectrum of *cis*-rich poly-**12**.

215
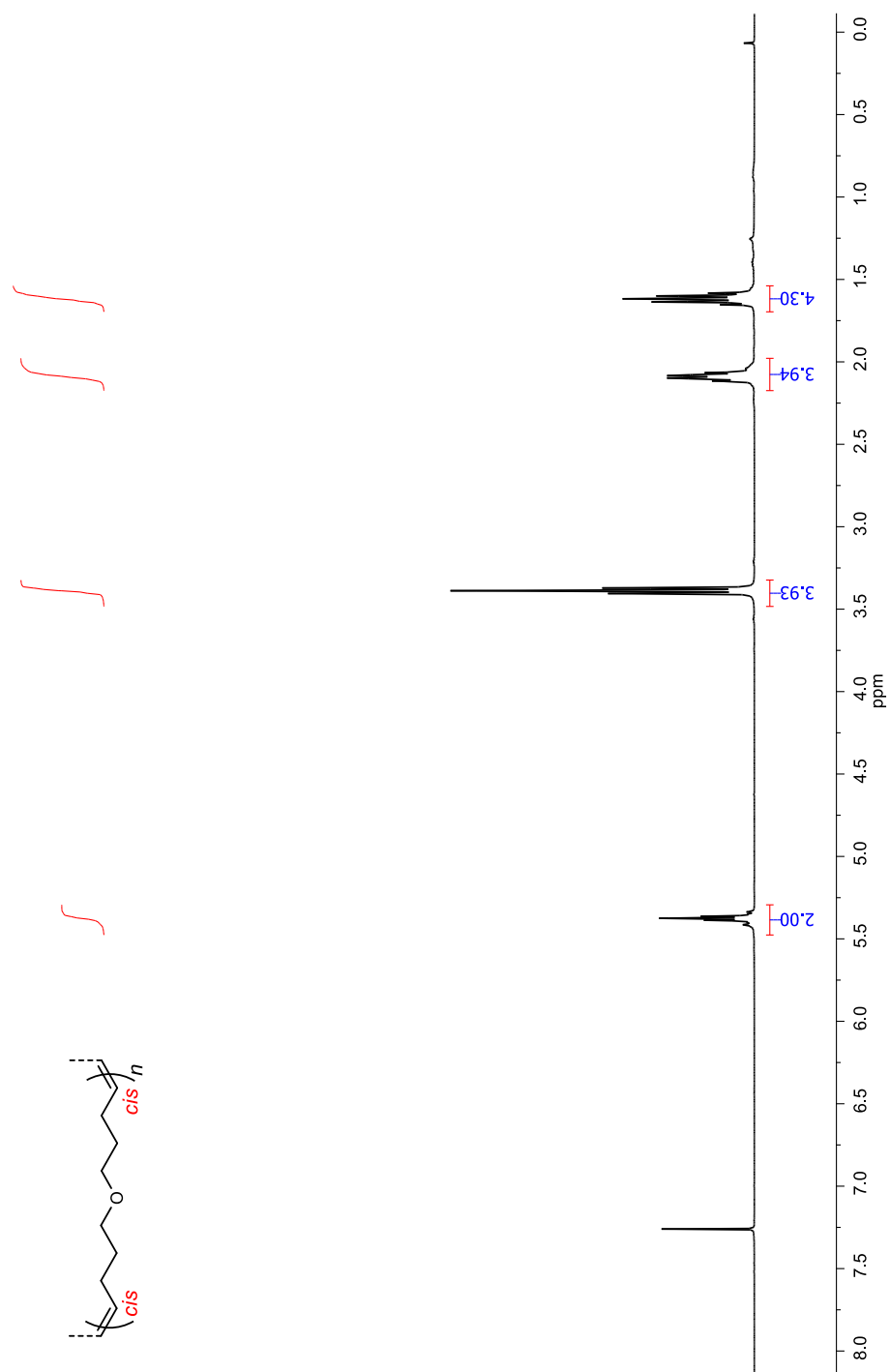
Figure IV-58 ^{1}H NMR (400 MHz, CDCl$_3$) spectrum of *cis*-rich poly-**13**.
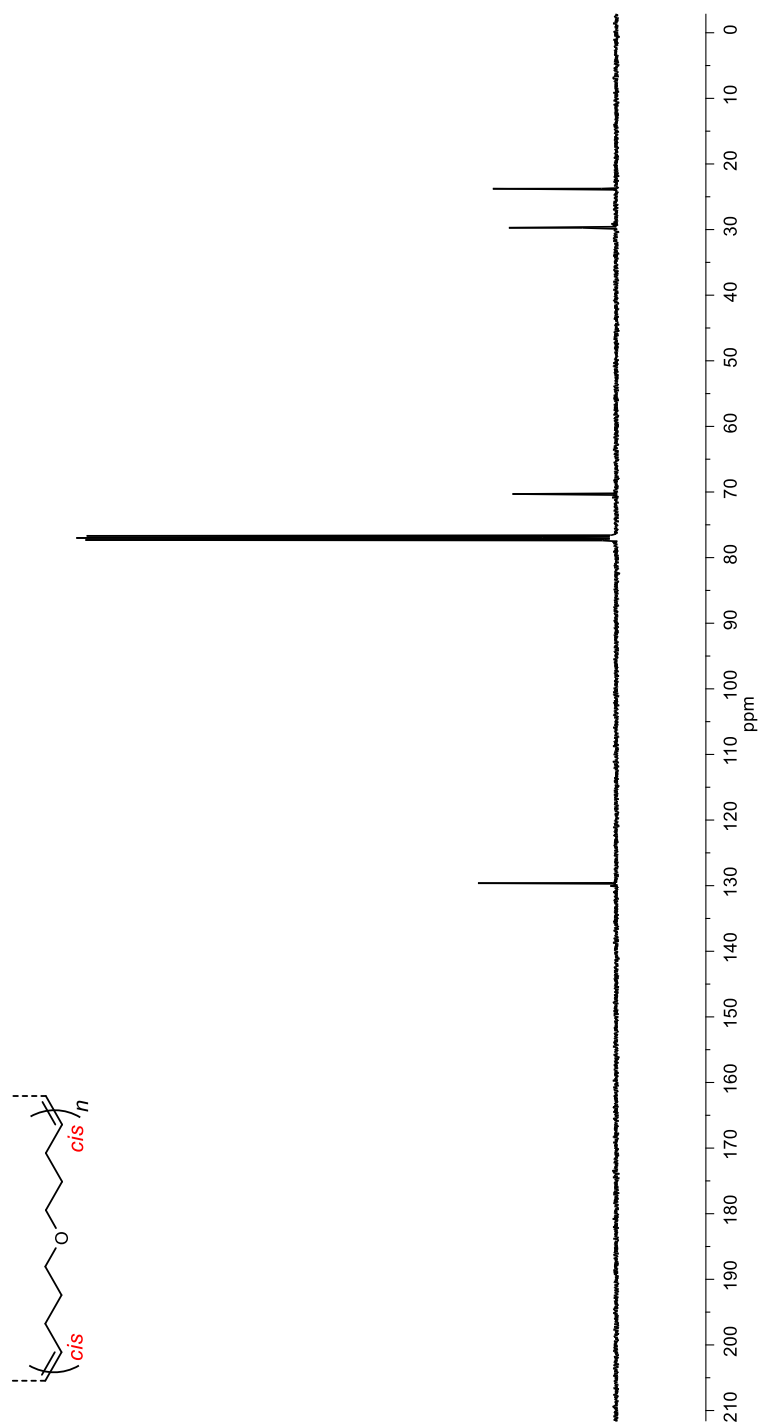
Figure IV-59 ^{13}C NMR (101 MHz, CDCl$_3$) spectrum of *cis*-rich poly-**13**.
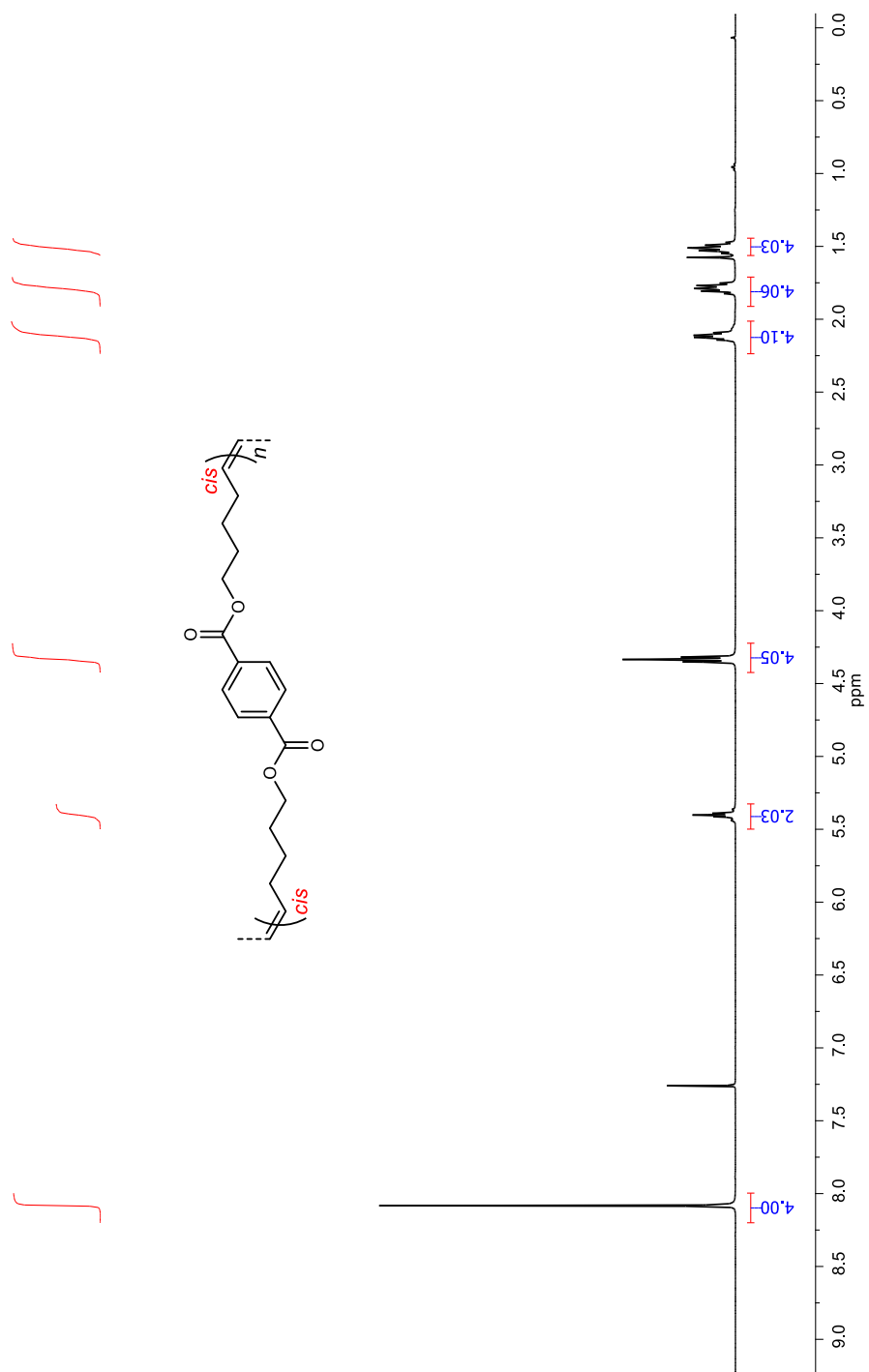
Figure IV-60 ^{1}H NMR (400 MHz, CDCl$_3$) spectrum of *cis*-rich poly-**14**.
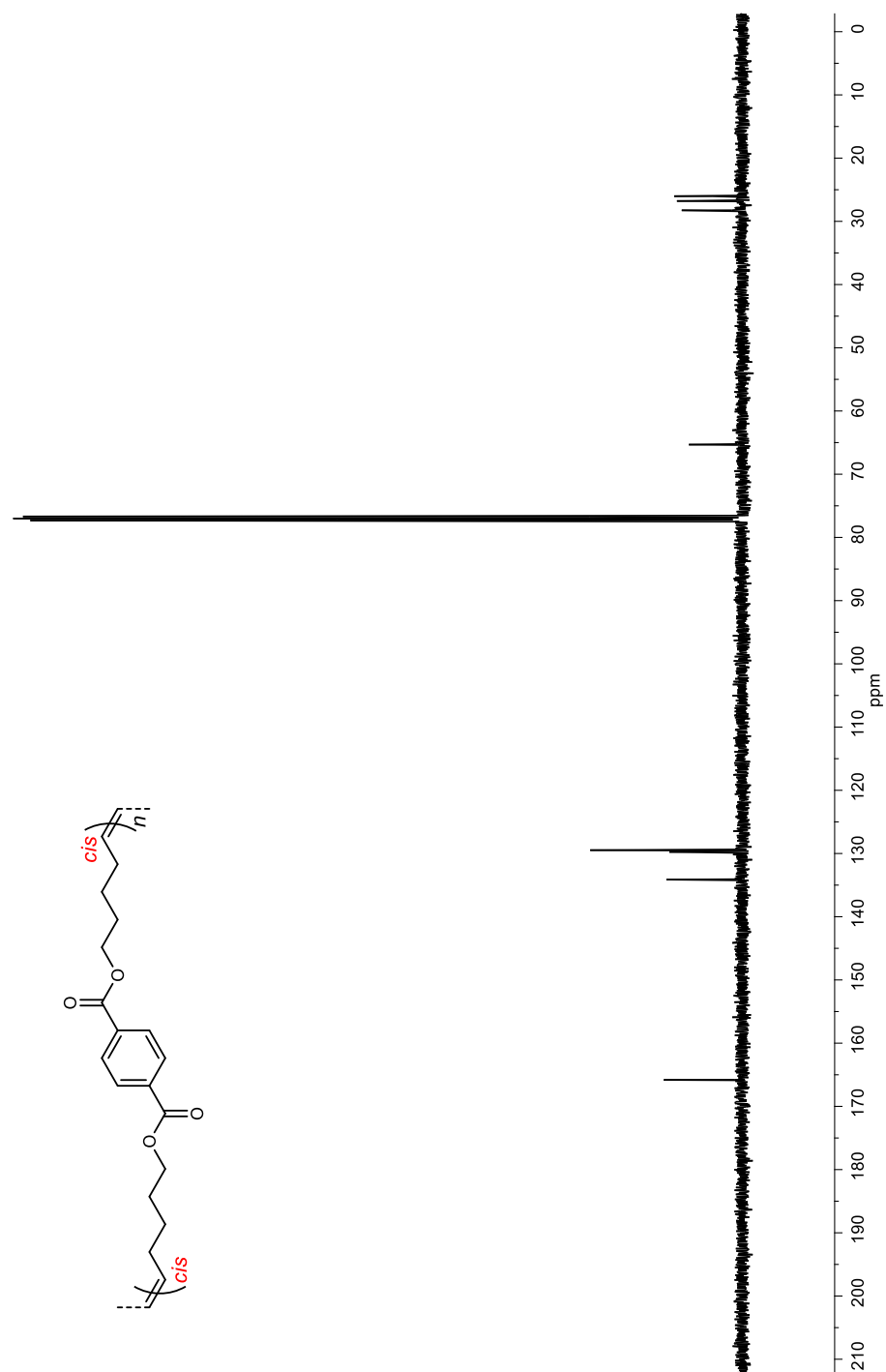
Figure IV-61 ^{13}C NMR (101 MHz, CDCl$_3$) spectrum of *cis*-rich poly-**14**.
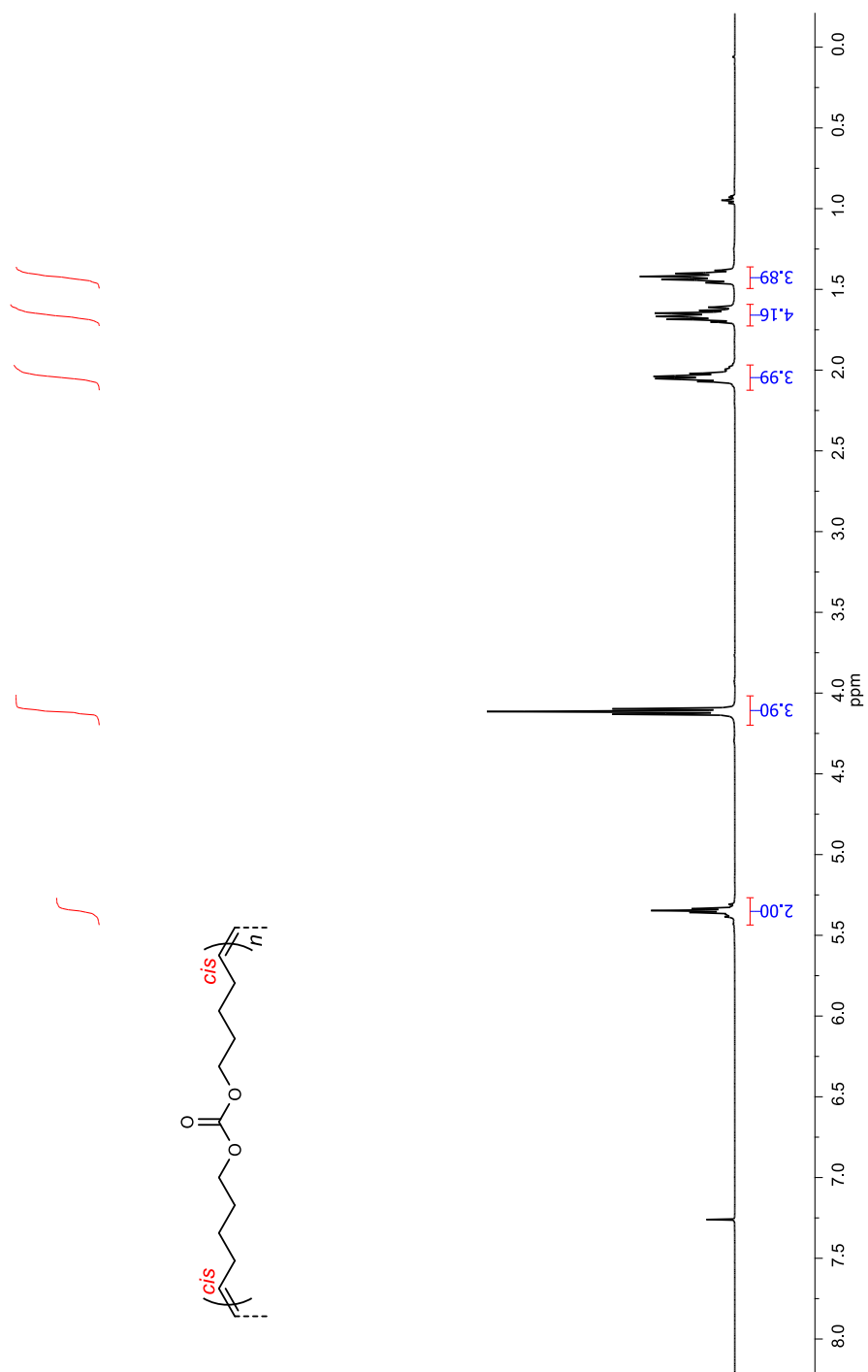
Figure IV-62 ^{1}H NMR (400 MHz, CDCl$_3$) spectrum of *cis*-rich poly-**15**.
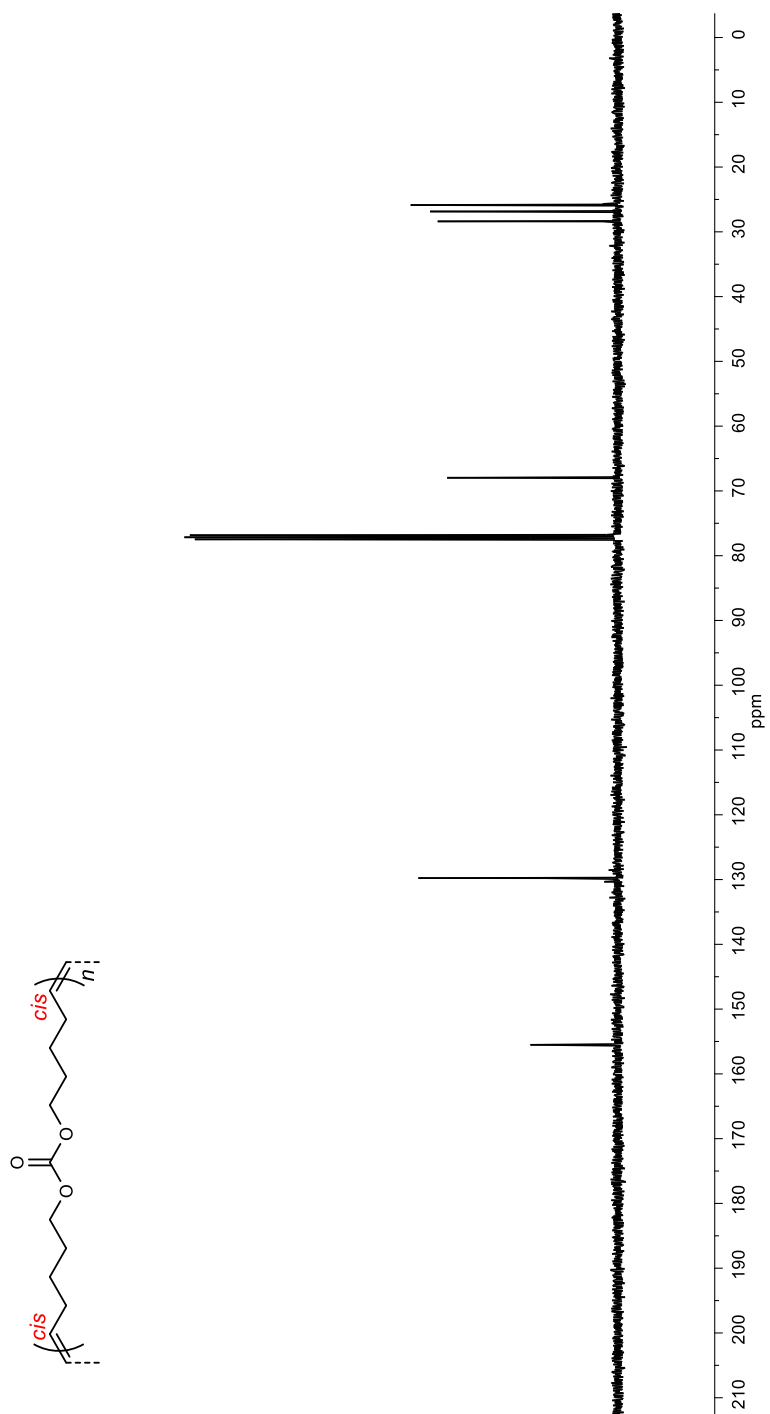
Figure IV-63 ^{13}C NMR (101 MHz, CDCl₃) spectrum of *cis*-rich poly-**15**.
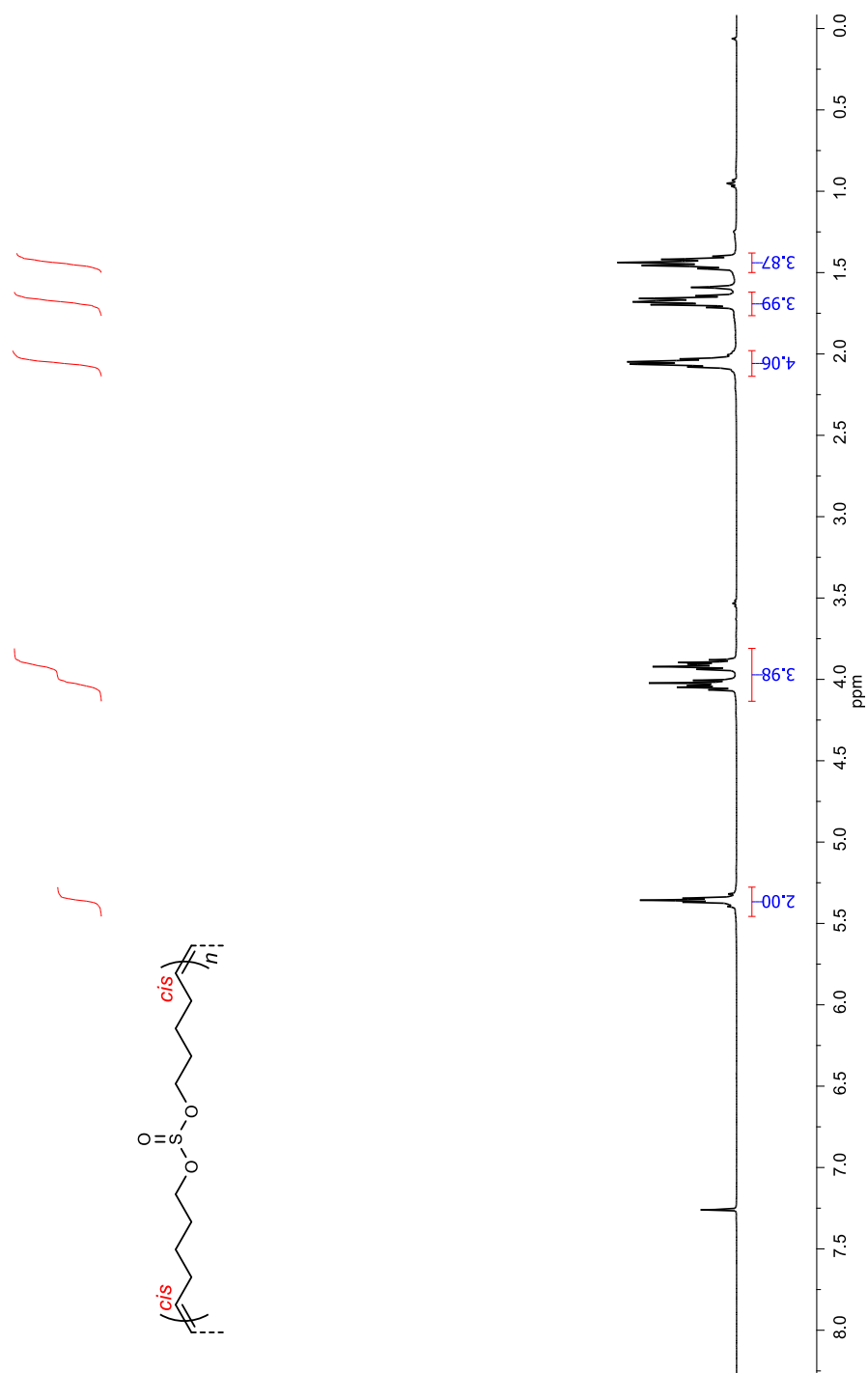
Figure IV-64 ^{1}H NMR (400 MHz, CDCl$_3$) spectrum of *cis*-rich poly-**16**.
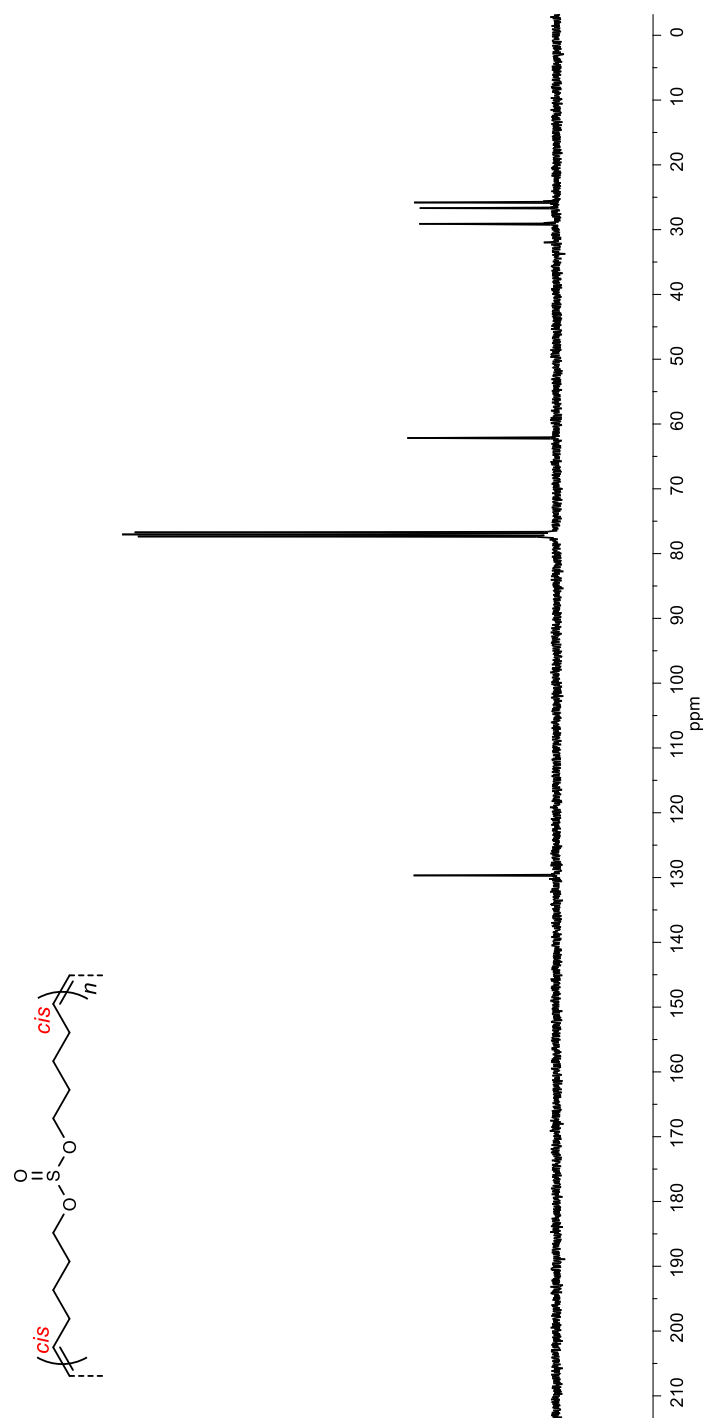
Figure IV-65 ^{13}C NMR (101 MHz, CDCl$_3$) spectrum of *cis*-rich poly-**16**.
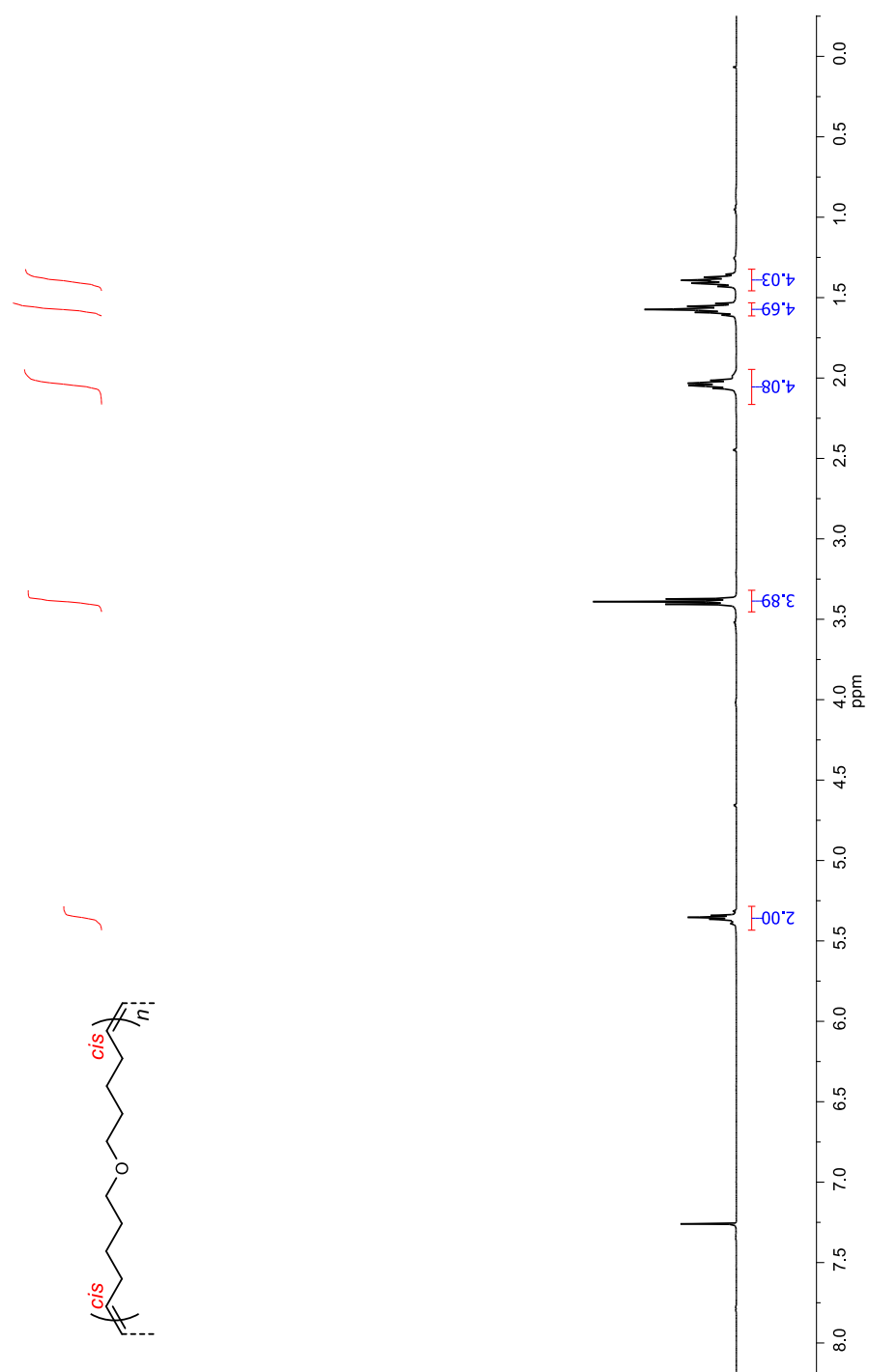
Figure IV-66 ^{1}H NMR (400 MHz, CDCl$_3$) spectrum *cis*-rich poly-**17**.
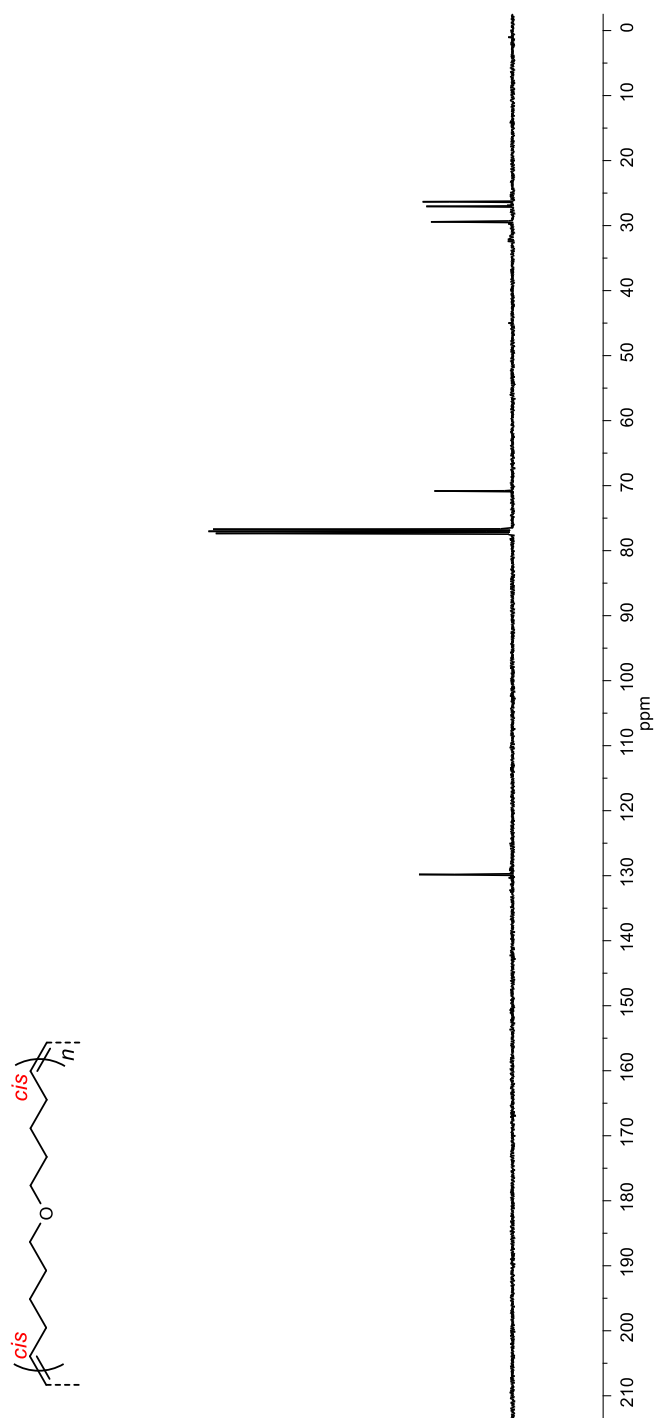
Figure IV-67 ^{13}C NMR (101 MHz, CDCl₃) spectrum of *cis*-rich poly-**17**.

CHAPTER V

cis-SELECTIVE ACYCLIC DIENE METATHESIS POLYMERIZATION OF α,ω-

DIENES[*]

V.1 Introduction

The development of stereoselective methods to access olefin-containing macromolecules with precise geometries remains a grand synthetic challenge despite the documented dependence of the properties of such soft materials on *cis/trans* stereochemistry.[5] For example, *cis* polyisoprene (PI) is an elastic soft material, while *trans* PI is a hard, brittle material.[9] Homogeneous and heterogeneous catalysts have been developed for the coordination-insertion polymerization of 1,3-dienes with selective formation of either *trans* or *cis* linkages, but these catalytic systems are notoriously intolerant to polar functional groups and can lead to the formation of vinyl defects through competitive 1,2-insertions.[11] Recently, several elegant approaches have been implemented to deliver polymers with predictable *cis*:*trans* contents either through thiol-yne click chemistry[82,84,117] or via a metal-free ring-opening metathesis polymerization (ROMP) mediated by light.[83] However, the scope of these processes is limited, and high *cis* contents are generally more challenging to access because of thermodynamic penalties. Monomers containing a spectator *cis* olefin have been used to circumvent this issue,[107,108,118] but undesired isomerization can erode the stereochemistry of the macromolecules.[119,120]

Polymerizations based on olefin metathesis such as acyclic diene metathesis (ADMET)[91,121] and ROMP[122] represent a promising and versatile strategy to access a diverse pool of stereodefined polyalkenamers because of the robustness, functional-group tolerance, and structural diversity of metathesis catalysts.[89,123] Specifically designed W or Mo alkylidenes were found to overcome the thermodynamic preference of ROMP and to deliver high *cis*-selectivity mostly with non-polar monomers via kinetic control.[15,85] The recent development of Z-selective[16,17,24,124-126] and stereoretentive[18,20,22] Ru catalysts has allowed the expansion of the scope of *cis*-selective ROMP processes.[1,2,25,72] Interestingly, while ADMET is a powerful tool for the precise synthesis of polymers,[94,95] control over the stereochemistry of the repeating alkenes has long escaped this versatile polymerization.

ADMET typically delivers polymers with a predominance of *trans* alkenes with Grubbs and Hoveyda-Grubbs dichloro Ru catalysts (Scheme V-1).[91,120] We recently leveraged the exquisite stereoretention afforded by dithiolate Ru-catalysts to produce a variety of all-*cis* polyalkenamers using *cis*,*cis*-diene monomers (Scheme 1b).[3] However, this method required the synthesis of monomers with preinstalled *cis*,*cis* stereochemistry and utilized air-sensitive Ru carbenes.[86]

Herein, we report a *cis*-selective ADMET process capitalizing on robust cyclometalated Ru-carbenes (Scheme 1c), which afforded a broad array of polyalkenamers with *cis* content up to >99% from readily accessible α,ω-dienes containing various functional groups. This diversity-oriented polymerization allowed the study of the influence of olefin stereochemistry over the thermal properties of these

materials. Finally, an ABA triblock copolymer was prepared to demonstrate that mechanical properties can be modulated through modification of the stereochemistry of the middle block.

Scheme V-1 Typical ADMET vs Stereoretentive and *cis*-Selective Processes

a) ADMET with Dichloro Ru Catalysts
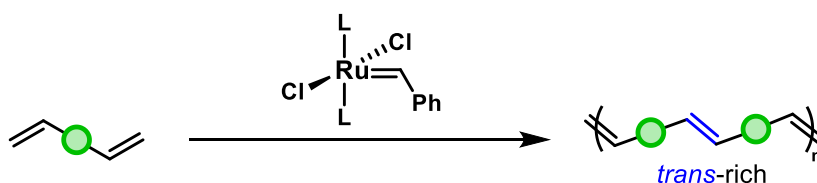
✓ α,ω-diene monomers   ✗ favors t*rans*-rich polymers

b) Stereoretentive ADMET with Dithiolate Catalysts
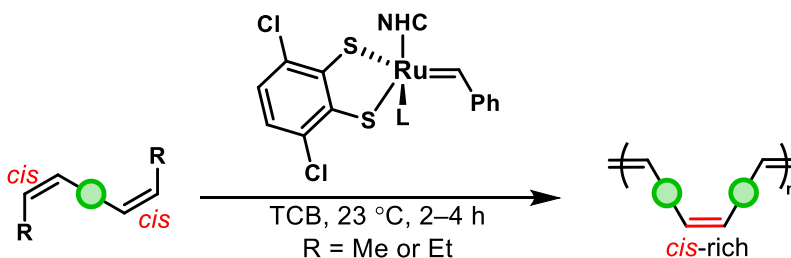
✗ preinstalled *cis,cis*-diene required   ✓ excellent stereoretention

c) *cis*-Selective ADMET with Cyclometalated Ru Catalysts
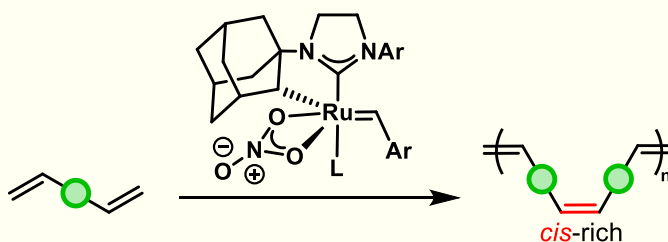
✓ readily available α,ω-diene monomers   ✓ diversity-oriented polymerization

✓ up to 99% *cis* selectivity   ✓ measurable impact on polymer properties

228

V.2 Results and Discussion

V.2.1 Development of a cis-*Selective ADMET Process Using Cyclometalated Ru Catalyst*

ADMET is a polycondensation involving iterative cross-metathesis reactions between α,ω-dienes (Scheme V-2). To drive this fully reversible process toward high molar masses, continuous removal of ethylene is required. We hypothesized that using catalysts allowing kinetic control, including cyclometalated **Ru-4**[17,127] or dithiolate **Ru-6**[52] (Table V-1), would thwart the thermodynamic selectivity and lead to a *cis*-selective ADMET if a robust catalyst capable of maintaining high *cis*-selectivity over time could be identified.

Scheme V-2 Development of a *cis*-Selective ADMET Process through Kinetic Control
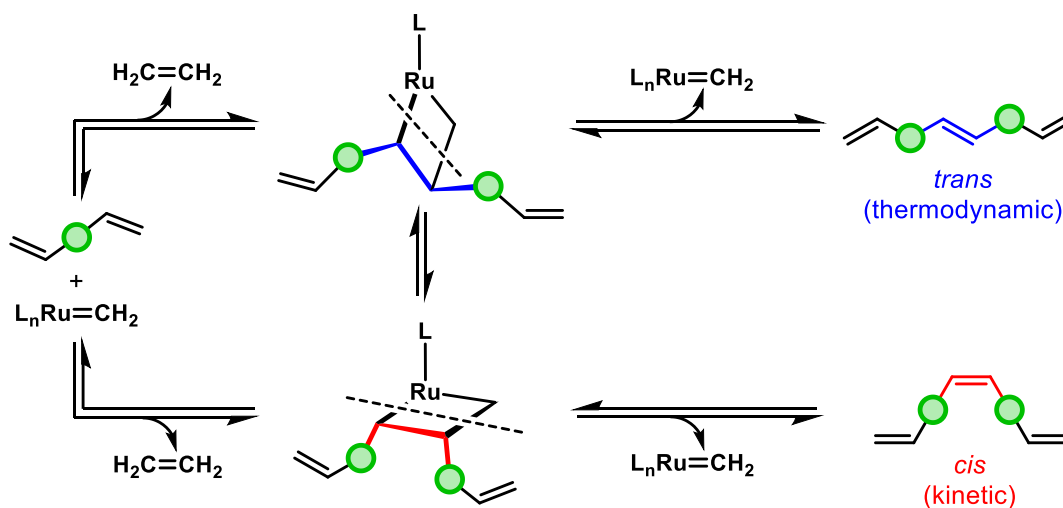
Table V-1 Optimization of *cis*-Selective ADMET
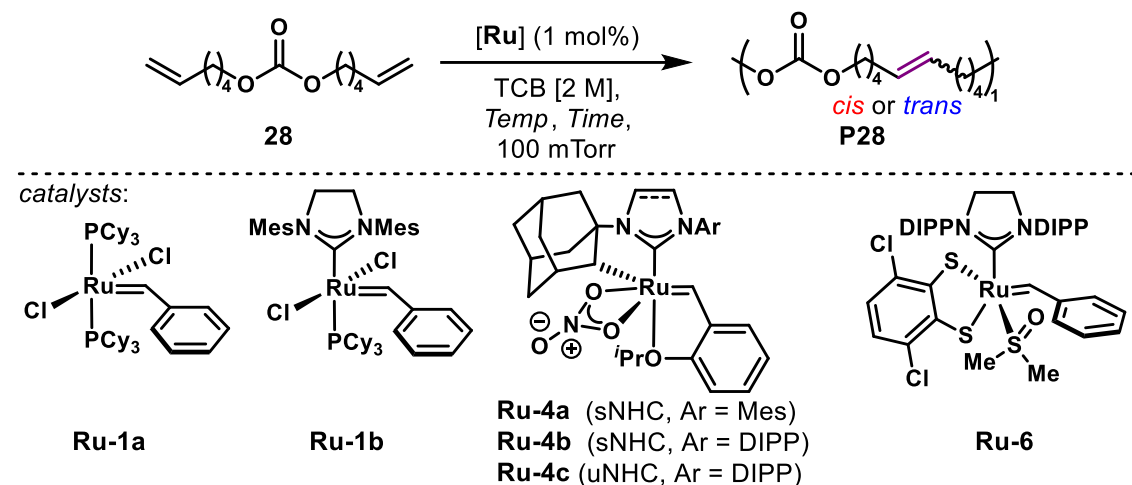
entry	catalyst	temp (°C)	M_n (kg/mol)^a	Đ	*cis* (%)^b
1	**Ru-1a**	80	27.9	1.75	14
2	**Ru-1b**	80	25.6	1.89	9
3	**Ru-4a**	80	17.7	1.73	18
4	**Ru-4b**	80	28.7	2.99	38
5	**Ru-4b**	40	13.5	1.75	97
6	**Ru-4b**	23	9.8	1.67	99
7^c	**Ru-4b**	23	9.9	1.47	99
8^c	**Ru-4a**	23	11.2	1.61	80
9^c	**Ru-4c**	23	6.8	1.52	89
10^{c,d}	**Ru-6**	23	—	—	—

sNHC = saturated NHC; uNHC = unsaturated NHC; DIPP = 2,6-diisopropylphenyl; Mes = 2,4,6-trimethylphenyl. ^{a}Determined through size exclusion chromatography (SEC) in THF against polystyrene standards. ^{b}Determined via ^{1}H NMR analysis. ^{c}Reaction performed at a concentration of 5 M. ^{d}4 h instead of 16 h.

Carbonate monomer **28** was selected at the onset of the investigation to favor ADMET over the competing ring-closing metathesis. As a benchmark, monomer **28** was exposed to typical ADMET conditions using dichloro **Ru-1a** and **Ru-1b**. Upon reaction with **Ru-1a** at 80 °C in 1,2,4-trichlorobenzene (TCB) under vacuum (100 mTorr), polymer **P28** was formed with only 14% *cis* double bonds (Table V-1, entry 1). Polymerization with **Ru-1b** delivered **P28** with a similarly low *cis* content (9%) (Table V-1, entry 2). Surprisingly, commercially available *cis*-selective catalyst **Ru-4a** only marginally improved the *cis* content to 18% (Table V-1, entry 3). Based on the unique geometry of the ruthenacycle imparted by the nitrato and adamantane ligand,[21,125] we hypothesized that increasing the steric hindrance of the aryl substituent of the NHC (DIPP vs Mes) might improve the stereoselectivity. Pleasingly, switching to **Ru-4b**, which was first reported by Grubbs,[124] more than doubled the *cis* selectivity to 38% (Table V-1, entry 4). To further favor kinetic control and minimize potential unselective secondary metathesis events, the reaction temperature was lowered to 40 °C, which led to 97% *cis* content (Table V-1, entry 5). Decreasing the temperature further to 23 °C led to the isolation of an all-*cis* **P28** (>99% *cis*) within the limit of detection of ^{1}H NMR (Table V-1, entry 6). While a decrease in molar masses was observed at lower temperature, respectable degrees of polymerization (DP ~ 50–70) and molar masses (M_n = 9.8 and 13.5 kg/mol) were obtained for **P28** exhibiting 97–99% *cis* alkenes (Table V-1, entries 5 and 6).
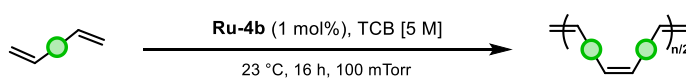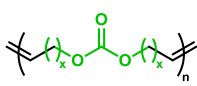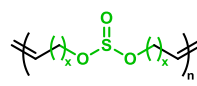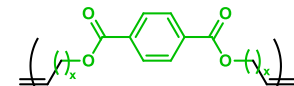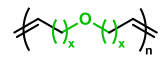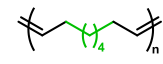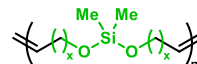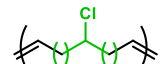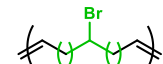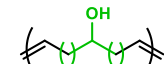
Performing the polymerization at higher concentration (C = 5 M) did not increase M_n (Table V-1, entry 7), while attempts to run the reaction in the bulk only delivered small oligomers (Table V-3). The importance of the DIPP substituent on *cis*-selectivity was

further demonstrated by using **Ru-4a** in the optimal reaction conditions, which resulted in only 80% *cis* **P28** (Table V-1, entry 8). Unsaturated variant **Ru-4c**,[127] showcased slightly lower stereoselectivity (89% *cis*) and molar masses (6.8 kg/mol) (Table V-1, entry 9). Finally, stereoretentive catalyst **Ru-6** led to unproductive ADMET presumably because of the rapid degradation of the unstable dithiolate Ru methylidene intermediate (Table V-1, entry 10).[3,86] Further investigation into the solvent concentration, temperature, time, and catalyst loading did not produce polymers with higher molar masses (Table V-3).

V.2.2 Scope of the cis-*Selective ADMET Polymerization*

With these optimized conditions in hand, we investigated the scope of the polymerization (Table V-2). Polycarbonate **P28**, polysulfite **P29**, and polyether **P31** were all isolated with 99% *cis* content, while polyester **P30** was formed with slightly diminished

Table V-2 Substrate Scope for *cis*-Selective ADMET

P28 (x = 4): **99% cis**, M_n = 12.0 kg/mol, Đ = 1.60
P24 (x = 3): **99% cis**, M_n = 9.1 kg/mol, Đ = 1.38

P29 (x = 4): **99% cis**, M_n = 8.4 kg/mol, Đ = 1.42
P25 (x = 3): **99% cis**, M_n = 9.5 kg/mol, Đ = 1.56

P30 (x = 4): **91% cis**, M_n = 8.3 kg/mol, Đ = 1.52
P23 (x = 3): **99% cis**, M_n = 5.0 kg/mol, Đ = 1.69

P31 (x = 4): **99% cis**, M_n = 10.0 kg/mol, Đ = 1.49
P26 (x = 3): **99% cis**, M_n = 10.6 kg/mol, Đ = 1.35

P32[a] **99% cis**, M_n = 8.5 kg/mol, Đ = 1.80

P33 (x = 4): **99% cis**, M_n = 10.3 kg/mol, Đ = 1.45
P34 (x = 3): **99% cis**, M_n = 17.6 kg/mol, Đ = 1.29

P35 (x = 4): **92% cis**, M_n = 7.3 kg/mol, Đ = 1.64
P36 (x = 3): **97% cis**, M_n = 7.2 kg/mol, Đ = 1.56

P37 (x = 4): **85% cis**, M_n = 7.8 kg/mol, Đ = 1.76
P38 (x = 3): **90% cis**, M_n = 6.8 kg/mol, Đ = 1.65

P39 (x = 4): **97% cis**, M_n = 4.8 kg/mol, Đ = 1.47
P40 (x = 3): **96% cis**, M_n = 2.4 kg/mol, Đ = 1.40

[a]N_2 purging instead of vacuum; C = 2 M instead of 5 M.

cis content (91% *cis*). Reducing the number of methylene spacers between the alkene and the functional group did not negatively affect the stereoselectivity (**P23–26**). Commercially available deca-1,9-diene (**32**) was transformed into all-*cis* polyoctenamer **P32**,[128] the *cis*-variant of industrially-produced vestenamer.[129] To further explore the functional group tolerance of the *cis*-selective ADMET, polysiloxanes which are common in coatings, ceramics, and dynamic covalent networks,[130,131] were targeted. Polysiloxanes **P33** and **P34** were isolated from monomers **33** and **34** with exquisite *cis* selectivity and M_n's up to 17.6 kg/mol. Halogenated monomers **35,36** and **37,38** were tolerated albeit with a slight decrease in *cis* selectivity, which is nonetheless in stark contrast to the typical ADMET polymerization of **35,36** and **37,38** with dichloro Ru carbenes.[132] These halogenated polymers might be amenable to post-polymerization functionalization for the precise synthesis of additional polymer classes.[133,134] Interestingly, alcohol monomers **39** and **40** were polymerized with high *cis* selectivity (93 and 96%), but in lower molar masses, which was ascribed to potential poisoning of the Ru catalyst. Overall, all monomers could be purchased or synthesized without tedious purifications, which is a notable advantage of the *cis*-selective ADMET. Additionally, **Ru-4b** was not found to be sensitive to oxidative degradation in contrast to dithiolate Ru catalysts (e.g **Ru-6**, Table V-4).[135]

V.2.3 Study of the Influence of Alkene Stereochemistry over Thermal Behavior of the Macromolecules

The development of a versatile *cis*-selective ADMET allowed us to probe the impact of *cis/trans* stereochemistry over the thermal properties of about 30 polyalkenamers. *trans*-Rich variants of **P23**–**26** and **P28**–**40** (>70% *trans*) were synthesized using **Ru-1a** (Supporting Information) and compared to the *cis*-rich polymers synthesized with **Ru-4b**. The thermal stability of the polymers was tested through thermogravimetric analysis (TGA, Figure V-1a). Interestingly, *cis*-rich polyalkenamers were found to have higher T_d's in almost all cases with the exception of **P32** and **P33**. The increased thermal stability is especially marked for polyesters ($\Delta T_d = 36$ °C for **P23**) and polycarbonates ($\Delta T_d = 36$ °C for **P28** and 61 °C for **P24**). The thermal properties were further investigated through differential scanning calorimetry (DSC). A general trend was also observed for the glass- transition temperatures (T_g's). All polyalkenamers with an observable T_g within the scanned temperature range exhibited a lower T_g for the *cis* congener relative to the *trans* one (Figure V-1b). Finally, only a few polyalkenamers presented a melting transition (Figure V-1c). While **P32** was characterized by a melting temperature (T_m) in both *cis*-rich ($T_m = 32$ °C) and *trans*-rich forms ($T_m = 24$ °C), **P28**, **P30** and **P31** only had a T_m when trans linkages were predominant throughout the backbone. Semi-crystallinity is known to increase with the *trans* content in poly(1,3-diene)s, but inconsistent trends have been observed between stereochemistry and semicrystallinity with other families including polycarbonates[3,107] and polynorbornene.[83,136] ADMET offers a unique opportunity to generate libraries of both

234

trans-rich and *cis*-rich polyalkenamers upon the choice of catalyst and to interrogate the complex relationship between precise molecular structure and material properties.
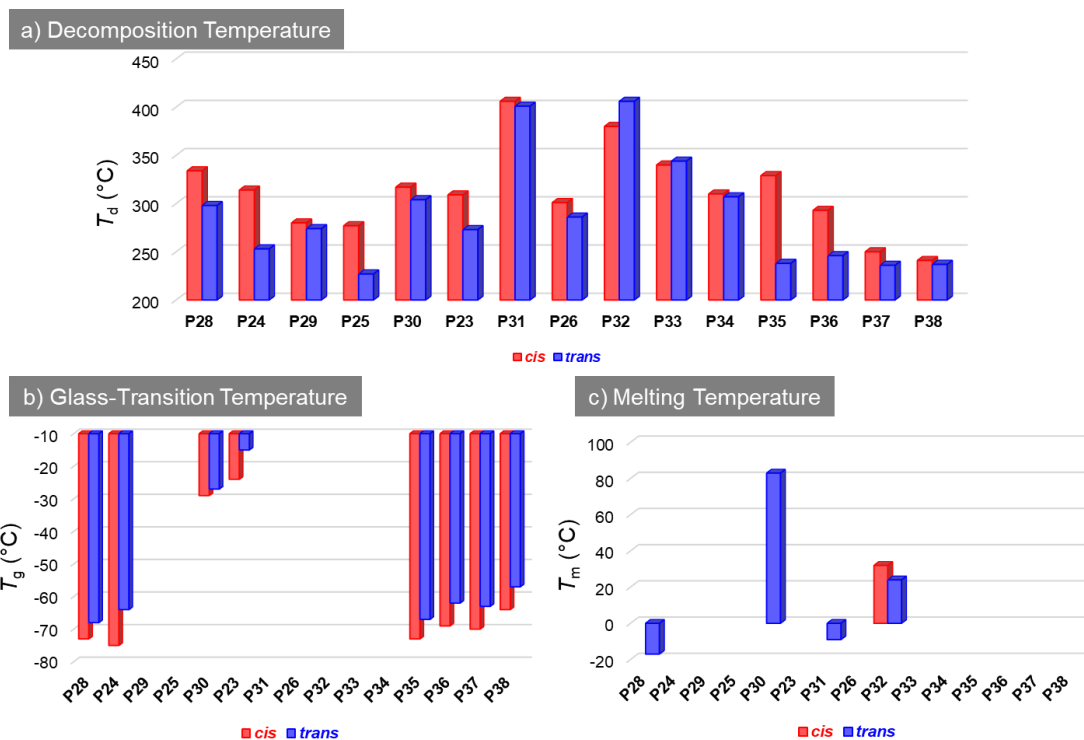
Figure V-1 Bar graphs comparing the influence of stereochemistry on (a) T_d (5% weight loss), (b) T_g, and (c) T_m.

V.2.4 Triblock Copolymers with Tunable Properties Based on Olefin Geometry

Polyalkenamers are commonly incorporated into industrial block copolymers to obtain thermoplastic elastomers (TPE),[5] but very few studies have investigated the effect of *cis/trans* configuration.[137] We sought to build an ABA triblock copolymer using **P32** as middle block and poly(lactic acid) (PLA) as end blocks. As a biosourced and biodegradable polymer, PLA is an attractive, yet brittle, material,[138] whose toughness can be improved by incorporation of a rubbery middle block.[139] Building upon a polymerization-depolymerization ADMET strategy initially reported by Wagener with

235

Figure V-2 (a) Synthesis of *cis* triblock copolymer **P42**-*b*-**P32**_{*cis*}-*b*-**P42**. (b) Thermal properties and (c) reduced Young's modulus (E_r) of *cis*/*trans* triblocks and homopolymer **P42**.

Ru-1a,[140] telechelic **P32**_{*cis*}-**OAc** was synthesized using monomer **32** in the presence of **Ru-4b** and acetate reagent **41** (Figure V-2). Optimized conditions provided quantitative capping of both chain ends as shown by NMR. Subsequent basic hydrolysis cleanly delivered macromolecular diol **P32**_{*cis*}-**OH** (M_n = 3.3 kg/mol, 99% *cis*) with no change in M_n compared to the acetoxy precursor. Meanwhile, **P32**_{*trans*}-**OH** (M_n = 3.1 kg/mol, 89% *trans*) was prepared similarly using **Ru-1a**. Chain extension of telechelic macroinitiators **P32**_{*cis*}-**OH** and **P32**_{*trans*}-**OH** using D,L-lactide (**42**) and triazabicyclodecene (TBD) as

236

catalyst efficiently provided ABA triblock copolymers **P42**-*b*-**P32**-*b*-**P42** with either a *cis*-

or *trans*-rich middle **P32** block, but similar molar mass distributions. TGA and DSC

analysis revealed interesting trends (Figure V-2b). Both triblocks displayed higher T_d's

than that of homopolymer **P42**, the *cis*-triblock being highest (278 °C) which is consistent

with our previous observations. Incorporation of a *cis* middle block also led to the starkest

decrease in T_g (32 °C vs 44 °C for the *trans* and 49 °C for **P42**). Finally, only the *trans*-

triblock showcased crystallinity, which is in line with previous literature reports.[139]

Nanoindentation was subsequently used to determine the hardness (Figure V-47) and

reduced Young's modulus (E_r) of all three polymers from the unloading segments of the

load-displacement curves (Figure V-46) using the standard Oliver and Pharr analysis.[141]

As expected based on prior studies,[139] both triblock architectures had a decreased E_r

compared to **P42** (4.7 GPa, Figure V-2c). The *cis* triblock exhibited a lower E_r (3.0 GPa)

than the *trans* congener (3.4 GPa), which indicates that the stiffness of the rubbery block

can be finely tuned as a function of its stereochemistry.

V.3 Conclusion

In summary, we have developed a *cis*-selective ADMET polymerization of readily

available and inexpensive α,ω-dienes. Up to 99% *cis* selectivity was obtained for most

monomers through exquisite kinetic control of the olefin metathesis process enabled by a

robust cyclometalated Ru catalyst (**Ru-4b**) at room temperature. This diversity-oriented

polymerization allowed us to compare the thermal properties of a variety of *cis*-rich

polyalkenamers containing different polar functional groups with their *trans*-rich

congeners. High *cis*-content was found to correlate with increased thermal stability, a lower glass transition temperature, and typically amorphous behavior. Moreover, an ABA triblock copolymer with PLA as end blocks and polyoctenamer as a rubbery middle segment was synthesized. Nanoindentation measurements revealed that the *cis* stereochemistry led to a greater decrease in stiffness when compared to the *trans*-triblock. Overall, this study provides both insights in stereoselective catalysis for polymerization and a general method for the modulation of thermal and mechanical properties of soft materials including TPE via control of the *cis*/*trans* stereochemistry throughout the main chain.

V.4 Experimental Procedures and Data

V.4.1 General Reagent Information

All reactions were carried out under an inert nitrogen atmosphere with dry solvents under anhydrous conditions unless otherwise stated. Dry dichloromethane (DCM), tetrahydrofuran (THF), *N*,*N*-dimethylformamide (DMF) and toluene (PhMe) were obtained by passing the previously degassed solvents through activated alumina columns. Anhydrous 1,2,4-trichlorobenzene (TCB) was purchased from Sigma Aldrich and used without further purification and degassed via "freeze-pump-thaw" before being brought into a nitrogen-filled glove box. All polymerizations using ruthenium catalysts were set up in a nitrogen-filled glove box (SG1800/750TS-F, VIGOR). Reagents were purchased at the highest commercial quality and used without further purification, unless otherwise stated. For example, hex-5-en-1-ol (97%), 6-bromohex-1-ene (97%), deca-1,9-diene (**32**)

(98%) and 5-bromopent-1-ene (98%) were purchased from Oakwood Chemical and Pent-4-en-1-ol (97%) and TBD (97%) were purchased from Combi-blocks. D,L-Lactide (97%) was purchased from Combi-blocks and recrystallized from ethyl acetate prior to use. Monomers **23**–**26** were prepared following our previously published procedures. [3] Catalysts **Ru-1a**, **Ru-1b**, and **Ru-4a** were purchased from Sigma-Aldrich and used without further purification. Catalyst **Ru-4b** and **Ru-6** were generously donated by Umicore. Catalyst **Ru-4c** was prepared following a literature procedure. [127] Yields refer to chromatographically and spectroscopically (^{1}H NMR) homogeneous material, unless otherwise stated. Reactions were monitored by thin layer chromatography (TLC) carried out on 250 μm SiliCycle SiliaPlate™ silica plates (F254), using UV light as the visualizing agent and a solution of $KMnO_4$ and heat as a developing agent. Flash silica gel chromatography was performed using SiliCycle SiliaFlash® Irregular Silica Gel (60 Å, particle size 40–63 μm). Polymers were isolated after precipitation using an Eppendorf 5804 centrifuge.

V.4.2 General Analytical Information

All polymer samples were analyzed using a Tosoh EcoSec HLC 8320GPC system with a TSKgel SuperHM-M column and a TSKgel SuperH-RC column at a flow rate of 0.40 mL/min at 40 °C. THF stabilized with BHT was used as the eluent and all number-average molecular weights (M_n), weight-average molecular weights (M_w), and dispersities ($Đ$) for polymers were calculated from refractive index and UV chromatograms against TSKgel polystyrene standards. NMR spectra were recorded on Bruker Avance Neo 400 or Bruker

Avance 500 instruments and were calibrated using residual undeuterated solvent as an internal reference (CHCl$_3$ @ 7.26 ppm ^{1}H-NMR, 77.16 ppm ^{13}C-NMR). The following abbreviations were used to explain NMR peak multiplicities: s = singlet, d = doublet, dd = doublet of doublets, t = triplet, q = quartet, p = pentet, m = multiplet, br = broad. Thermogravimetric analysis (TGA) was performed on a TA Instruments TGA 5500 Thermogravimetric Analyzer. Differential scanning calorimetry (DSC) was performed using a TA instrument DSC 2500. High-resolution mass spectra (HRMS) were recorded on an Agilent LC/MSD TOF mass spectrometer by Atmospheric pressure chemical ionization (APCI), electrospray ionization (ESI), or Thermo Scientific DSQ II GC-MS by electron ionization (EI). Nanoindentation experiments were performed on a Hysitron TI 950 Triboindenter equipped with a diamond Berkovich indenter tip. The tip shape was calibrated to a fused quartz standard using the Oliver and Pharr methodology prior to testing.[141]

Thermogravimetric analysis (TGA)

Samples were weighed on to a platinum sample pan. Samples were heated at 20 °C/min to 100 °C, followed by an isothermal period of 1 minute, and then heated at 10 °C/min to 600 °C under nitrogen.

Differential scanning calorimetry (DSC)

Samples (around 2–6 mg) were heated to 180 °C at 10 °C/min (150 °C for **P28**), followed by an isothermal period of 5 min. The samples were then cooled to −80 °C at 10 °C/min,

followed by an isothermal period of 5 min. This process was repeated two times. Thermograms taken from the third heating/cooling cycle.

Nanoindentation

Samples for nanoindentation experiments were prepared by drop-casting a solution of 30 mg of polymer in 0.1 ml DCM onto a 1 cm square glass plate. The samples were left at room temperature for 4 h then annealed at 80 °C under vacuum for 4 h, at room temperature under vacuum for 16 h, and then affixed onto steel pucks with epoxy. 5 x 5 Arrays of indentations with 20 µm spacing between neighboring indents were performed. All indents were load-controlled with a maximum applied load of 6000 µN, a loading and holding time of 10 s, and an unloading time of 2 s. The hardness (H) and reduced modulus (E_r) were then calculated from the unloading segments of the load-displacement curves using the standard Oliver and Pharr analysis.[141]

V.4.3 Monomer Synthesis

Monomer **28**
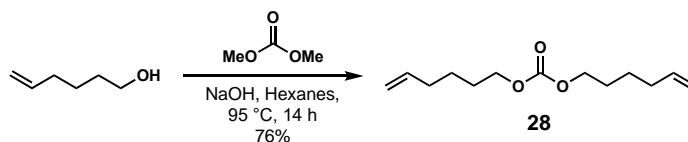
Synthesis adapted from a literature procedure.[3] Dimethyl carbonate (1.07 g, 1.0 mL, 11.9 mmol, 1 equiv), hexanes (12 mL), 5-hexen-1-ol (2.38 g, 2.85 mL, 23.8 mmol, 2 equiv) and NaOH (48 mg, 1.1 mmol, 0.1 equiv) were combined in a round bottom flask under air. The round bottom flask was fitted with a Dean-Stark apparatus. Water was added to

fill up half of the volume of the Dean-Stark, followed by hexanes for the remainder of the volume. The Dean Stark was then fitted with a waterless condenser. The round bottom flask was lowered into an oil bath preheated to 95 °C. After stirring for 1 h, an additional batch of 5-hexen-1-ol (2.38 g, 2.85 mL, 23.8 mmol, 2 equiv) was added after cooling the reaction to room temperature. The round bottom flask was again lowered into the oil bath and allowed to stir overnight (14 h). The reaction was allowed to cool to room temperature. The reaction mixture was transferred to a separatory funnel where it was washed with water (3 x 10 mL). The organic portion was dried over $MgSO_4$, filtered, and the solvent was removed *in vacuo*. The resulting oil was purified through column chromatography (SiO_2; hexanes to 6:4 hexanes:DCM). The product was visualized with a $KMnO_4$ stain. Removal of solvent and subsequent drying on the high vacuum line provided the product as a clear oil. Yield: 2.04 g, 76%.

The spectroscopic data for this compound were identical to those reported in the literature.[100]

^{1}H NMR (400 MHz, $CDCl_3$) δ 5.86–5.72 (m, 2 H), 5.07–4.91 (m, 4 H), 4.13 (t, J = 6.7 Hz, 4 H), 2.09 (q, J = 7.1 Hz, 4 H), 1.69 (p, J = 6.7 Hz, 7.2 Hz, 4 H), 1.48 (p, J = 7.7 Hz, 7.5 Hz, 4 H) ppm.

HRMS-APCI: calc'd. for $C_{13}H_{23}O_3$ [M+H]$^+$ 227.1639, found 227.1642.

Monomer **29**
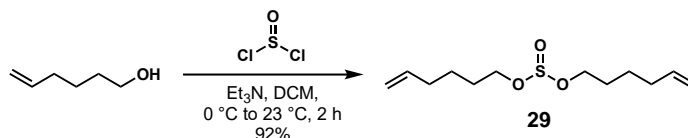
Synthesis adapted from a literature procedure.[3] 5-hexen-1-ol (1.0 g, 1.2 mL, 10 mmol, 2 equiv), Et$_3$N (1.0 g, 1.4 mL, 10 mmol, 2 equiv), and DCM (17 mL) were combined in a flame-dried round-bottom flask equipped with a stir bar under N$_2$. The flask was cooled in an ice/water bath and thionyl chloride (595 mg, 0.36 mL, 5 mmol, 1 equiv) was added dropwise. After complete addition, the flask was allowed to warm to room temperature and was monitored by TLC until completion (2 h). The reaction was then quenched with water (20 mL). The organic layer was extracted with additional DCM (20 mL) and the organic layer was then washed with brine (20 mL). The organic layer was then separated and dried over sodium sulfate. The organic solvent was then removed *in vacuo* and the oil was purified through column chromatography (SiO$_2$, 1:1 hexanes:DCM) to give the product as a clear oil (1.1 g, 92%).

^{1}H NMR (500 MHz, CDCl$_3$) δ 5.85–5.72 (m, 2 H), 5.06–4.93 (m, 4 H), 4.08–3.87 (m, 4 H), 2.13–2.04 (q, *J* = 7.0 Hz, 4 H), 1.74–1.65 (m, 4 H), 1.54–1.44 (m, 4 H) ppm.

^{13}C NMR (125 MHz, CDCl$_3$) δ 138.2, 115.0, 62.2, 33.2, 29.0, 25.1 ppm.

HRMS-APCI: calc'd. for C$_{12}$H$_{22}$O$_3$S [M+H]$^+$ 247.1362, found 247.1359.

Monomer **30**
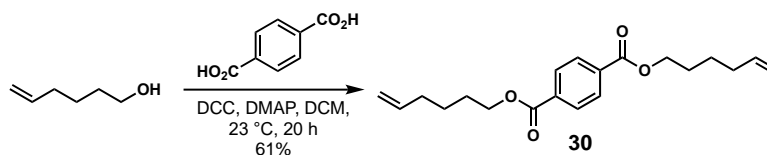
Synthesis adapted from a literature procedure.[3] Terephthalic acid (829 mg, 4.97 mmol, 1 equiv), DCC (2.06 g, 9.98 mmol, 2 equiv), DMAP (122 mg, 1.0 mmol, 0.2 equiv), and DCM (40 mL) were combined in a round bottom flask equipped with a stir bar under air. 5-hexen-1-ol (1.0 g, 1.2 mL, 9.98 mmol, 2 equiv) was added dropwise to the stirring solution and upon complete addition, the reaction was stirred for 20 h at room temperature. Afterwards, the resulting white suspension was filtered through a pad of celite. The solvent was removed *in vacuo*, and the resulting oil was purified through column chromatography (SiO$_2$, 1:1 hexanes:DCM to 100% DCM). The pure product was obtained as a clear oil. Yield: 1.01 g, 61%

The spectroscopic data for this compound were identical to those reported in the literature.[99]

^{1}H NMR (400 MHz, CDCl$_3$) δ 8.10 (s, 4 h), 5.89–5.76 (m, 2 H), 5.08–4.94 (m, 4 H), 4.35 (t, *J* = 6.7 Hz, 4 H), 2.18–2.10 (q, *J* = 7.1 Hz, 4 H), 1.81 (p, *J* = 6.7 Hz, 7.0 Hz, 4 H), 1.56 (p, *J* = 7.7 Hz, 7.6 Hz, 4 H) ppm.

HRMS-APCI: calc'd. for C$_{20}$H$_{26}$O$_4$ [M+H]$^+$ 331.1904, found 331.1897.

Compound **43**
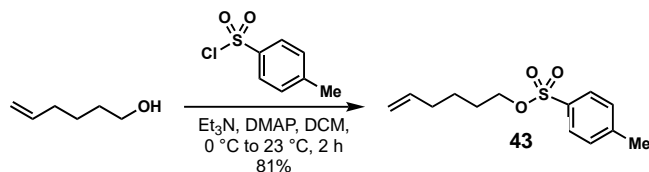
Synthesis adapted from a literature procedure.[3] Tosyl chloride (2.1 g, 11 mmol, 1.1 equiv) freshly recrystallized from benzene and DMAP (122 mg, 1 mmol, 0.1 equiv) were weighed into a flame-dried round-bottom flask equipped with a stir bar and the flask was subsequently subjected to vacuum on a Schlenk line followed by an N_2 refill. This process was repeated twice and then dry DCM (25 mL) was added. The solution was cooled to 0 °C in an ice/water bath. Then, 5-hexen-1-ol (1.0 g, 1.2 mL, 10 mmol, 1 equiv) and anhydrous Et_3N (2.3 g, 3.2 mL, 23 mmol, 2.3 equiv) were each added dropwise. After the addition, the flask was allowed to warm to room temperature and the reaction was monitored by TLC until complete consumption of the alcohol (2 h). The reaction was then washed with water (3 x 10 mL) followed by brine (10 mL). The organic layer was dried over $MgSO_4$. After filtering out the $MgSO_4$, the solvent was removed *in vacuo*. The resulting yellow residue was purified through column chromatography (SiO_2, 2:1 hexanes:DCM) to give the product as a clear oil. Yield 2.06 g, 81%

The spectroscopic data for this compound were identical to those reported in the literature.[142]

^{1}H NMR (400 MHz, $CDCl_3$) δ 7.81–7.76 (m, 2 H), 7.37–7.32 (m, 2 H), 5.78–5.65 (m, 1 H), 4.99–4.91 (m, 2 H), 4.03 (t, $J = 6.4$ Hz, 2 H), 2.45 (s, 3 H), 2.04–1.95 (q, $J = 7.0$ Hz, 2 H), 1.69–1.60 (m, 2 H), 1.45–1.36 (m, 2 H) ppm.

Monomer **31**
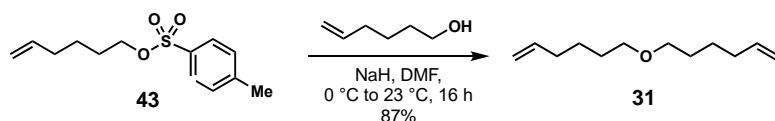
Synthesis adapted from a literature procedure.[3] Compound **43** (2.06 g, 8.1 mmol, 1 equiv) was weighed into a flame-dried round-bottom flask equipped with a stir bar. The flask was then subjected to three vacuum/N_2 cycles. Dry DMF (27 mL) was added to the flask followed by NaH (60% dispersion in mineral oil) (388 mg, 9.7 mmol, 1.2 equiv). The flask was cooled to 0 °C in an ice/water bath. 5-hexen-1-ol (1.0 g, 1.2 mL, 10 mmol, 1.2 equiv) was added slowly to the reaction over 5 min. After addition of 5-hexen-1-ol, the reaction was allowed to warm to room temperature and was stirred for 16 h. Ether (25 mL) was then added to the reaction and the dilute solution was washed with saturated aq. NH_4Cl (3 x 10 mL). The organic layer was then dried over $MgSO_4$. Following the removal of $MgSO_4$, the solvents were removed *in vacuo* and the yellow-orange oil was purified through column chromatography (SiO_2, hexanes) to give the product as a clear oil. Yield: 1.3 g, 87%

The spectroscopic data for this compound were identical to those reported in the literature.[101]

^{1}H NMR (400 MHz, CDCl$_3$) δ 5.88–5.74 (m, 2 H), 5.05–4.91 (m, 4 H), 3.40 (t, *J* = 6.6 Hz, 4 H), 2.11–2.03 (m, 4 H), 1.63–1.54 (m, 4 H), 1.50–1.40 (m, 4 H) ppm.

HRMS-APCI: calc'd. for $C_{12}H_{22}O$ [M+H]$^+$ 183.1741, found 183.1743.

General siloxane monomer procedure

To a flame dried round-bottom flask, imidazole (2.1 equiv) and dry THF (1 M with respect to alcohol) were added. The flask was cooled to 0 °C with an ice/water bath and dichlorodimenthylsilane (1 equiv) was added dropwise. After stirring at room temperature for 1 h, the mixture was cooled to 0 °C and treated with of the unsaturated alcohol (1.0 mL, 2.1 equiv). The cloudy suspension was stirred at room temperature for 16 h and then diluted with 50 mL of hexanes, washed with saturated aq. NH_4Cl (20 mL), water (20 mL) and brine (20 mL). The organic layer was dried over Na_2SO_4 and the solvent was removed *in vacuo* to provide the monomer without further purification.

Monomer **33**
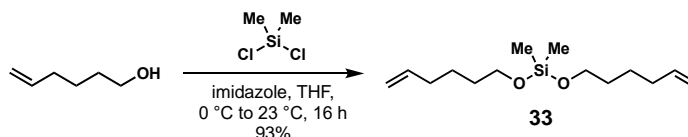
Monomer **33** was synthesized following the General Siloxane Monomer Procedure using 5-hexen-1-ol (1.0 mL, 8.33 mmol), imidazole (8.33 mmol), dichlorodimethylsilane (3.97 mmol, 0.48 mL), and THF (8.0 mL). Product isolated as a colorless oil (0.95 g, 3.70 mmol, 93% yield).

^{1}H NMR (400 MHz, CDCl$_3$) δ 5.87–5.73 (m, 2 H), 5.05–4.88 (m, 4 H), 3.67 (t, J = 6.6 Hz, 4 H), 2.12–2.01 (m, 4 H), 1.63–1.50 (m, 4 H), 1.49–1.36 (m, 4 H), 0.11 (s, 6 H) ppm.

^{13}C NMR (101 MHz, CDCl$_3$) δ 138.9, 114.6, 62.4, 33.6, 32.2, 25.3, –3.1 ppm.

HRMS-APCI: calc'd. for C$_{14}$H$_{28}$O$_2$Si [M+H]$^+$ 257.1931, found 257.1930.

Monomer **34**
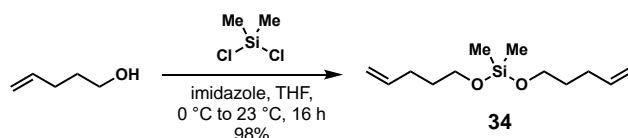
Monomer **34** was synthesized following the General Siloxane Monomer Procedure using 4-penten-1-ol (1.0 mL, 9.68 mmol), imidazole (9.68 mmol), dichlorodimethylsilane (4.61 mmol, 0.56 mL), and THF (9.2 mL). Product isolated as a colorless oil (1.03 g, 4.50 mmol, 98% yield).

^{1}H NMR (400 MHz, CDCl$_3$) δ 5.88–5.74 (m, 2 H), 5.07–4.91 (m, 4 H), 3.68 (t, J = 6.6 Hz, 4 H), 2.15–2.06 (m, 4 H), 1.69–1.60 (m, 4 H), 0.11 (s, 6 H) ppm.

^{13}C NMR (101 MHz, CDCl$_3$) δ 138.4, 114.8, 62.0, 31.8, 30.1, –3.1 ppm.

HRMS-APCI: calc'd. for C$_{12}$H$_{24}$O$_2$Si [M+H]$^+$ 229.1618, found 229.1618.

General halogen monomer procedure

Triphenylphosphine (1.1 equiv) was added to a reaction vial and dissolved in DCM (2.0 M with respect to alcohol). Then, the alcohol (1 equiv) was added to the vial with stirring and the mixture was cooled in an ice water bath to 0 °C. Next, either NCS (1.1 equiv, for **35** and **36**) or NBS (1.1 equiv, for **37** and **38**) was added slowly in portions to the reaction mixture. The reaction was removed from the ice water bath and left to stir at room temperature for 16 h. After removing the solvent *in vacuo*, the reaction was purified using column chromatography (SiO$_2$, pentane) to give the product.

248
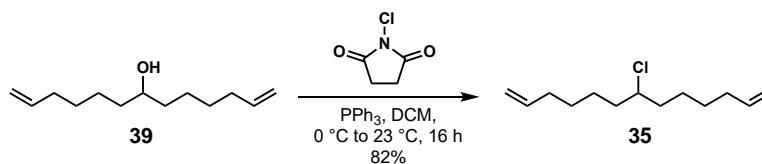
Monomer 35

Monomer **35** was synthesized following the General Halogenation Monomer Procedure using triphenyl phosphine (588 mg, 2.2 mmol, 1.1 equiv), DCM (4.1 mL), alcohol **39** (400 mg, 2.0 mmol, 1 equiv), and NCS (299 mg, 2.2 mmol, 1.1 equiv). Product isolated as clear oil (359 mg, 82%).

^{1}H NMR (400 MHz, CDCl$_3$) δ 5.89–5.77 (m, 2 H), 5.07–4.94 (m, 4 H), 3.95–3.87 (m, 1 H), 2.15–2.04 (m, 4 H), 1.80–1.65 (m, 4 H), 1.65–1.35 (m, 8 H) ppm.

^{13}C NMR (101 MHz, CDCl$_3$) δ 138.9, 114.7, 64.2, 38.5, 33.8, 28.6, 26.1 ppm.

EI: calc'd. for C$_{13}$H$_{23}$Cl [M]$^+$ 214, found 214.

Monomer 36
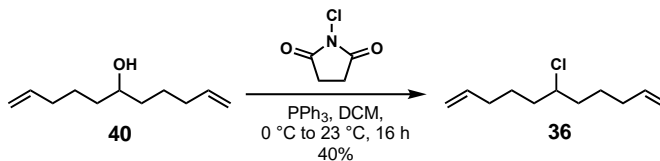
Monomer **36** was synthesized following the General Halogenation Monomer Procedure using triphenyl phosphine (857 mg, 3.3 mmol, 1.1 equiv), DCM (5.9 mL), alcohol **40** (500 mg, 3.0 mmol, 1 equiv), and NCS (436 mg, 3.3 mmol, 1.1 equiv). Product isolated as clear oil (222 mg, 40%).

The spectroscopic data for this compound were identical to those previously reported in the literature.[143]

^{1}H NMR (400 MHz, CDCl$_3$) δ 5.85–5.74 (m, 2 H), 5.06–4.94 (m, 4 H), 3.94–3.86 (m, 1 H), 2.15–2.00 (m, 4 H), 1.80–1.44 (m, 8 H) ppm.

Monomer **37**
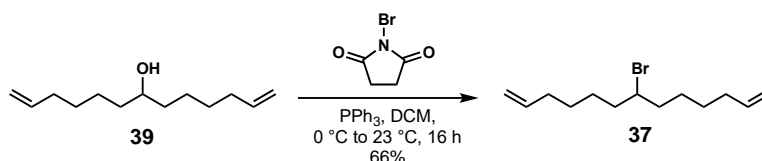
Monomer **37** was synthesized following the General Halogenation Monomer Procedure using triphenyl phosphine (294 mg, 1.1 mmol, 1.1 equiv), DCM (2.0 mL), alcohol **39** (200 mg, 2.0 mmol, 1 equiv), and NBS (199 mg, 1.1 mmol, 1.1 equiv). Product isolated as clear oil (174 mg, 66%).

^{1}H NMR (400 MHz, CDCl$_3$) δ 5.86–5.75 (m, 2 H), 5.00–4.92 (m, 4H), 4.06–3.98 (m, 1 H), 2.11–2.01 (m, 4H), 1.89–1.74 (m, 4H), 1.62–1.32 (m, 8H) ppm.

^{13}C NMR (101 MHz, CDCl$_3$) δ 138.8, 114.7, 58.7, 39.1, 33.7, 28.5, 27.2 ppm.

EI: calc'd. for C$_{13}$H$_{23}$Br [M]$^+$ 258, found 258.

Monomer **38**
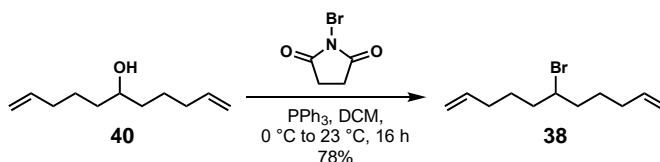
Monomer **38** was synthesized following the General Halogenation Monomer Procedure using triphenyl phosphine (514 mg, 2.0 mmol, 1.1 equiv), DCM (3.6 mL), alcohol **40** (300 mg, 1.8 mmol, 1 equiv), and NBS (349 mg, 2.0 mmol, 1.1 equiv). Product isolated as clear oil (320 mg, 78%).

The spectroscopic data for this compound were identical to those previously reported in the literature.[144]

^{1}H NMR (400 MHz, CDCl$_3$) δ 5.85–5.74 (m, 2 H), 5.06–4.94 (m, 4H), 4.07–3.99 (m, 1 H), 2.16–2.00 (m, 4H), 1.90–1.76 (m, 4H), 1.74–1.45 (m, 4H) ppm.

General alcohol monomer procedure

Synthesis adapted from literature procedure.[145] In a flame-dried 250 mL round bottom flask under N$_2$, a suspension of Mg turnings (2.5 equiv) and iodine (0.05 equiv) in dry THF (0.5 M with respect to the bromoalkene) was prepared. The bromoalkene (2.5 equiv) was then slowly added to the suspension, which was stirred for 45 min at room temperature. The mixture was then cooled to 0 °C in an ice bath, and freshly distilled ethyl formate (1 equiv) was then slowly added to the mixture. After removing the ice bath, the reaction was left to stir at room temperature for 16 h. The reaction was quenched with saturated aq. NH$_4$Cl and extracted with diethyl ether (3 x 20 mL). The combined organics were then washed with water (40 mL), dried with Na$_2$SO$_4$, filtered, and the volatiles were removed *in vacuo*. The product was purified through column chromatography (SiO$_2$, hexanes to 19:1 hexanes:diethyl ether) to give the product as a clear oil.

Monomer 39
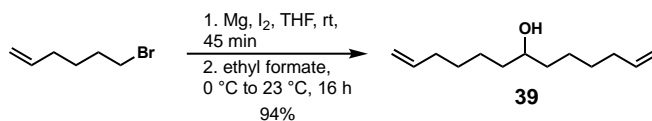
Synthesized following General Alcohol Monomer Procedure using Mg turnings (488 mg, 20.0 mmol, 2.5 equiv), iodine (102 mg, 0.4 mmol, 0.05 equiv), dry THF (40 mL), 6-bromo-1-hexene (2.6 mL, 20.0 mmol, 2.5 equiv), and ethyl formate (0.6 mL, 8.0 mmol, 1 equiv). Yield: 1.3 g, 80%.

^{1}H NMR (400 MHz, CDCl$_3$) δ 5.87–5.75 (m, 2 H), 5.04–4.91 (m, 4 H), 3.63–3.55 (m, 1 H), 2.11–2.02 (m, 4 H), 1.54–1.28 (m, 13 H) ppm.

^{13}C NMR (101 MHz, CDCl$_3$) δ 139.0, 114.5, 72.2, 37.4, 33.9, 29.1, 25.3 ppm.

HRMS-APCI: calc'd. for C$_{13}$H$_{24}$O [M+H]$^+$ 197.1900, found 197.1896.

Monomer 40
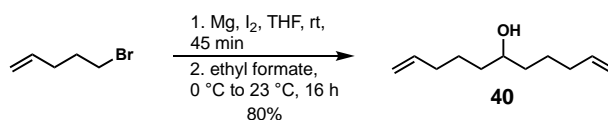
Synthesized following General Alcohol Monomer Procedure using Mg turnings (533 mg, 21.9 mmol, 2.5 equiv), iodine (111 mg, 0.4 mmol, 0.05 equiv), dry THF (43 mL), 5-bromo-1-pentene (2.6 mL, 21.9 mmol, 2.5 equiv), and ethyl formate (0.7 mL, 8.8 mmol, 1 equiv). Yield: 1.4 g, 94%.

The spectroscopic data for this compound were identical to those previously reported in the literature.[145]

^{1}H NMR (400 MHz, CDCl$_3$) δ 5.87–5.74 (m, 2H), 5.05–4.92 (m, 4H), 3.65–3.56 (m, 1H), 2.14–2.00 (m, 4H), 1.60–1.34 (m, 9 H) ppm.

HRMS-APCI: calc'd. for C$_{11}$H$_{20}$O [M+H]$^+$ 169.1587, found 169.1583.

V.4.4 Polymerization Procedures

Optimization of the *cis*-Selective ADMET

In an N$_2$-filled glovebox, a solution of monomer **28** (0.20 mmol, 1 equiv) in TCB (2 – 5 M) was added to another vial containing catalyst (1 – 2 µmol, 0.005 – 0.01 equiv). The solution was then transferred to an oven-dried Schlenk flask through a red rubber septum secured with electrical tape. A Teflon stopper was then fitted into the sidearm. The flask was then removed from the glovebox and the flask was placed under vacuum using a Schlenk line. The flask was then either stirred at room temperature or lowered into a preheated oil bath for the entirety of the reaction time. After the polymerization was finished, the flask was placed under static vacuum and ethyl vinyl ether (~50 µL) was added at room temperature. After stirring for 5 min, the flask was opened to air and an aliquot was removed for NMR analysis. The polymer was dissolved in dichloromethane and precipitated by addition of cold methanol in a centrifuge tube. After centrifugation at 8500 RPM for 10 min, the supernatant was decanted. This process was repeated again and the polymer was dried under vacuum to afford a highly viscous brown oil.
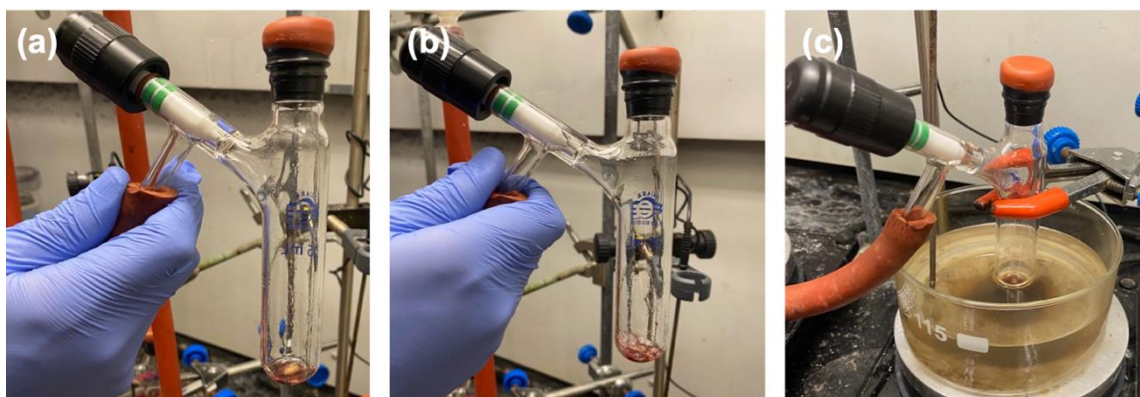
Figure V-3 Typical ADMET reaction setup with **Ru-1a**: (a) Schlenk flask charged with polymerization solution removed from the glovebox and attached to high vacuum line, (b) vacuum applied to the system, and (c) flask lowered into preheated oil bath.

Table V-3 Polymerization Results for **P28**
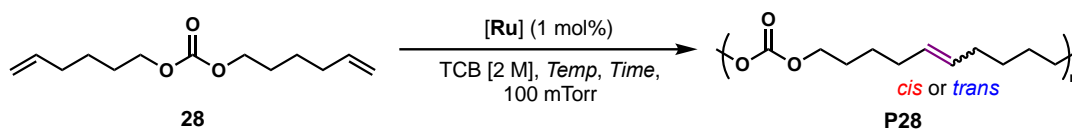
entry	catalyst (mol%)	temp (°C)	t (h)	M_n (kg/mol)	$Đ^a$	cis (%)^b
1	**Ru-1a** (1)	80	16	27.9	1.75	14
2	**Ru-4a** (1)	80	16	17.7	1.73	18
3	**Ru-4b** (1)	80	16	28.7	2.99	38
4	**Ru-4b** (1)	40	16	13.5	1.75	97
5	**Ru-4a** (1)	40	16	15.8	1.83	56
6	**Ru-4b** (1)	23	16	9.8	1.67	99
7	**Ru-4a** (1)	23	16	11.5	1.80	72
8	**Ru-4b** (0.5)	23	16	6.0	1.42	99
9	**Ru-4b** (1)	23	40	12.8	1.58	99

10	**Ru-4b** (1)	23	8	7.3	1.39	99
11	**Ru-4b** (1)	23	6	7.8	1.59	99
12	**Ru-4b** (1)	23	2	5.5	1.30	99
13[c]	**Ru-4b** (1)	23	16	9.9	1.47	99
14[c]	**Ru-4c** (1)	23	16	6.8	1.52	89
15[d,e]	**Ru-4b** (1)	23	16	5.1	1.28	99
16[d,e]	**Ru-4b** (1)	80	16	14.1	1.97	58
17[c,d]	**Ru-6** (2)	23	4	–	–	–

[a]Determined through SEC in THF against polystyrene standards. [b]Calculated using ^{1}H NMR analysis. [c]Polymerization carried out at a concentration of 5 M. [d]Reaction performed on 0.5 mmol scale with respect to the monomer. [e]Polymerization carried out in the bulk.

*V.4.5 Comparison of Oxygen Sensitivity between **Ru-4b** and **Ru-6** in ADMET*

In an N_2-filled glovebox, **Ru-4b** (3.4 mg, 0.05 mmol, 0.01 equiv) and **Ru-6** (2.1 mg, 0.0025 mmol, 0.005 equiv) were weighed into two separate, oven-dried vials equipped with stir bars and dissolved in TCB (0.1 mL). The vials were sealed with a screwcap fitted with a teflon septa. The vials were removed from the glovebox and the septa was pierced with an 18G needle. The vials were then stirred at room temperature (23 °C) for 20 min under air. Next, the catalyst solution was transferred to an oven-dried Schlenk flask under N_2 containing a stir bar and either monomer **28** (113 mg, 0.5 mmol, 1 equiv) for **Ru-4b** or capped monomer **11**[3] (113 mg, 0.5 mmol, 1 equiv) for **Ru-6**. The flask was then placed under vacuum (100 mTorr) and reactions were stirred at room temperature (23 °C) for either 4 h (**Ru-6**) or 16 h (**Ru-4b**). The flask was then placed under

static vacuum and ethyl vinyl ether (~50 µL) was added at room temperature. After stirring for 5 min, the flask was opened to air and an aliquot was removed for NMR analysis. In the attempted polymerization of **11** with **Ru-6**, ^{1}H NMR analysis revealed mostly recovery of the starting material with trace oligomer formation. In the case of the polymerization of **28** with **Ru-4b**, the polymer was dissolved in dichloromethane and precipitated by addition of cold methanol in a centrifuge tube. After centrifugation at 8500 RPM for 10 min, the supernatant was decanted, and the polymer was dried under vacuum to afford a highly viscous brown oil.

Table V-4 Effect of Oxygen on Stereoretentive (**Ru-6**) and *cis*-Selective ADMET (**Ru-4b**)
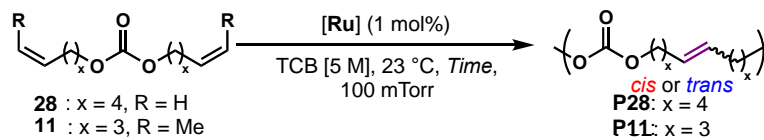
Entry	Monomer	Catalyst (mol%)	t (h)	M_n (kg/mol)	Đ	cis (%)
1	28	**Ru-4b** (1)	16	8.9	1.51	99
2	11	**Ru-6** (0.5)	4	–[a]	–	–

[a]No polymer isolated. Only trace oligomer formation observed in ^{1}H NMR

V.4.6 General cis-*Selective ADMET Polymerization Procedure Using Vacuum (100 mTorr)*

In an N_2 filled glovebox, a solution of monomer (0.50 mmol, 1 equiv) in 0.1 mL of TCB was added to another vial containing **Ru-4b** (3.4 mg, 5.0 µmol, 0.01 equiv). The

solution was then transferred to an oven-dried Schlenk flask through a red rubber septum

secured with electrical tape. A Teflon stopper was then fitted into the sidearm. The flask

was then removed from the glovebox and the flask was placed under vacuum using a

Schlenk line. The flask was then stirred at room temperature for 16 h. After the

polymerization was finished, the flask was placed under static vacuum and ethyl vinyl

ether (~50 μL) was added. After stirring for 5 min, the flask was opened to air and an

aliquot was removed for NMR analysis. The polymerization was then purified through

dissolving the polymer in DCM and precipitating in cold methanol in a centrifuge tube.

After centrifugation at 8500 RPM for 10 min, the methanol was decanted. The polymer

was then dissolved in DCM and reprecipitated in MeOH before undergoing another

centrifugation cycle. After decanting the MeOH, the polymer was dried for 24 h under

vacuum.

Table V-5 Polymerization Results for **P28**

entry	catalyst	temp (°C)	M_n (kg/mol)	Đ	cis (%)
1	**Ru-1a**	80	20.9	1.81	15
2	**Ru-4b**	23	12.0	1.60	99

The spectroscopic data for the *cis*-rich **P28** were identical to those previously reported in

the literature.[3]

cis-rich **P28**: [superscript]1H NMR (400 MHz, CDCl$_3$) δ 5.39–5.28 (m, 2 H), 4.11 (t, *J* = 6.7 Hz, 4 H), 2.11–1.96 (m, 4 H), 1.72–1.60 (m, 4 H), 1.47–1.36 (m, 4 H) ppm.

The spectroscopic data for the *trans*-rich **P28** were identical to those previously reported in the literature.[100]

trans-rich **P28**: [superscript]1H NMR (400 MHz, CDCl$_3$) δ 5.45–5.32 (m, 2 H), 4.12 (t, *J* = 6.7 Hz, 4 H), 2.11–1.95 (m, 4 H), 1.77–1.59 (m, 4 H), 1.48–1.34 (m, 4 H) ppm.

Table V-6 Polymerization Results for **P24**
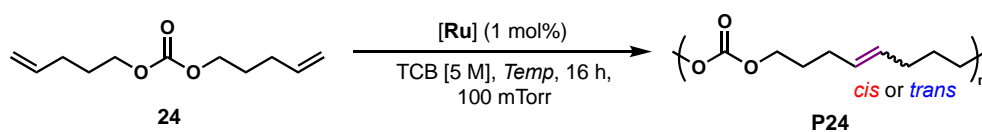
entry	catalyst	temp (°C)	M_n (kg/mol)	Đ	*cis* (%)
1	**Ru-1a**	80	15.7	1.80	17
2	**Ru-4b**	23	9.1	1.39	99

The spectroscopic data for the *cis*-rich **P24** were identical to those previously reported in the literature.[3]

cis-rich **P24**: [superscript]1H NMR (400 MHz, CDCl$_3$) δ 5.44–5.34 (m, 2 H), 4.11 (t, *J* = 6.6 Hz, 4 H), 2.18–2.04 (m, 4 H), 1.78–1.67 (m, 4 H) ppm.

The spectroscopic data for the *trans*-rich **P24** were identical to those previously reported in the literature.[100]

trans-rich **P24**: ^{1}H NMR (400 MHz, CDCl$_3$) δ 5.47–5.36 (m, 2 H), 4.12 (t, *J* = 6.6 Hz, 4 H), 2.18–1.99 (m, 4 H), 1.79–1.67 (m, 4 H) ppm.

Table V-7 Polymerization Results for **P29**

entry	catalyst	temp (°C)	M_n (kg/mol)	Đ	cis (%)
1	**Ru-1a**	80	18.8	1.77	23
2	**Ru-4b**	23	8.4	1.42	99

The spectroscopic data for the *cis*-rich **P29** were identical to those previously reported in the literature.[3]

cis-rich **P29**: ^{1}H NMR (400 MHz, CDCl$_3$) δ 5.42–5.31 (m, 2 H), 4.09–3.87 (m, 4 H), 2.15–1.99 (m, 4 H), 1.74–1.62 (m, 4 H), 1.50–1.38 (m, 4 H) ppm.

trans-rich **P29**: ^{1}H NMR (400 MHz, CDCl$_3$) δ 5.44–5.30 (m, 2 H), 4.07–3.84 (m, 4 H), 2.09–1.96 (m, 4 H), 1.70–1.60 (m, 4 H), 1.48–1.37 (m, 4 H) ppm.

^{13}C NMR (101 MHz, CDCl$_3$) δ 130.3, 129.7, 62.2, 32.0, 29.2, 29.0, 26.8, 25.9, 25.7 ppm

Table V-8 Polymerization Results for **P25**

entry	catalyst	temp (°C)	M_n (kg/mol)	$Đ$	cis (%)
1	**Ru-1a**	80	9.9	1.67	23
2	**Ru-4b**	23	9.5	1.56	99

The spectroscopic data for the *cis*-rich **P25** were identical to those previously reported in the literature.[3]

cis-rich **P25**: ^{1}H NMR (400 MHz, CDCl$_3$) δ 5.44–5.34 (m, 2 H), 4.10–3.86 (m, 4 H), 2.20–2.08 (m, 4 H), 1.79–1.69 (m, 4 H) ppm.

The spectroscopic data for the *trans*-rich **P25** were identical to those previously reported in the literature.[102]

trans-rich **P25**: ^{1}H NMR (400 MHz, CDCl$_3$) δ 5.46–5.37 (m, 2 H), 4.08–3.86 (m, 4 H), 2.19–2.05 (m, 4 H), 1.78– 1.69 (m, 4 H) ppm.

Table V-9 Polymerization Results for **P30**
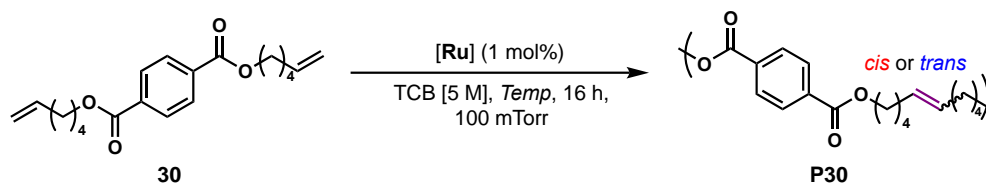
entry	catalyst	temp (°C)	M_n (kg/mol)	$Đ$	cis (%)
1	**Ru-4b**	23	8.3	1.52	91
2	**Ru-1a**	80	7.3	3.28	21

The spectroscopic data for the *cis*-rich **P30** were identical to those previously reported in the literature.[3]

cis-rich **P30**: ^{1}H NMR (400 MHz, CDCl$_3$) δ 8.08 (s, 4H), 5.46–5.34 (m, 2 H), 4.34 (t, J = 6.6 Hz, 4 H), 2.17–2.05 (m, 4 H), 1.84–1.74 (m, 4 H), 1.55–1.46 (m, 4 H) ppm.

The spectroscopic data for the *trans*-rich **P30** were identical to those previously reported in the literature.[99]

trans-rich **P30**: ^{1}H NMR (400 MHz, CDCl$_3$) δ 8.08 (s, 4 H), 5.49–5.36 (m, 2 H), 4.33 (t, J = 6.6 Hz, 4 H), 2.17– 2.03 (m, 4 H), 1.84–1.73 (m, 4 H), 1.56–1.46 (m, 4 H) ppm.

Table V-10 Polymerization Results for **P23**
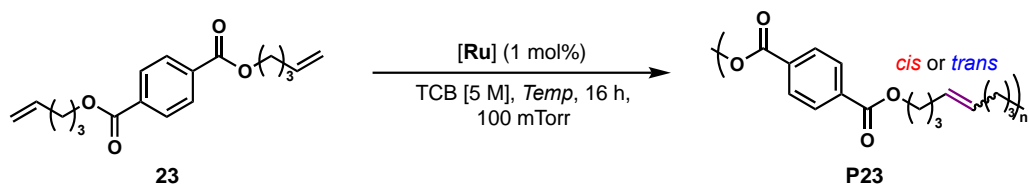
entry	catalyst	temp (°C)	M_n (kg/mol)	Đ	cis (%)
1	**Ru-1a**	80	27.9	1.75	14
2	**Ru-4b**	23	5.0	1.69	99

The spectroscopic data for the *cis*-rich **P23** were identical to those previously reported in the literature.[3]

cis-rich **P23**: ^{1}H NMR (400 MHz, CDCl3) δ 8.08–8.04 (s, 4 H), 5.52–5.41 (m, 2 H), 4.31 (t, J = 6.7 Hz, 4 H), 2.27–2.14 (m, 4 H), 1.89–1.78 (m, 4 H) ppm.

The spectroscopic data for the *trans*-rich **P23** were identical to those previously reported in the literature.[99]

trans-rich **P23**: ^{1}H NMR (400 MHz, CDCl3) δ 8.11–8.05 (m, 4 H), 5.53–5.44 (m, 2 H), 4.38–4.28 (t, J = 6.7 Hz, 4 H), 2.26–2.12 (m, 4 H), 1.90–1.79 (m, 4 H) ppm.

Table V-11 Polymerization Results for **P31**
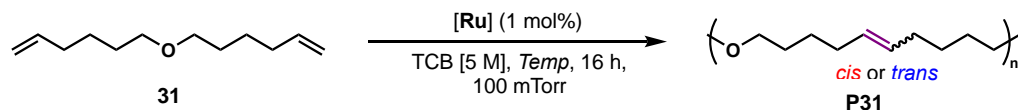
entry	catalyst	temp (°C)	M_n (kg/mol)	Đ	cis (%)
1	**Ru-1a**	80	26.5	1.55	18
2	**Ru-4b**	23	10.0	1.49	99

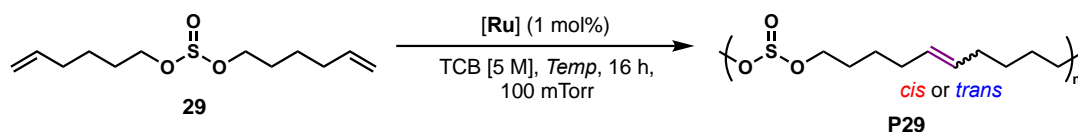The spectroscopic data for the *cis*-rich **P31** were identical to those previously reported in the literature.[3]

cis-rich **P31**: ^{1}H NMR (400 MHz, CDCl$_3$) δ 5.42–5.29 (m, 2 H), 3.39 (t, J = 6.6 Hz, 4 H), 2.10–1.95 (m, 4 H), 1.61–1.50 (m, 4 H), 1.44–1.34 (m, 4 H) ppm.

The spectroscopic data for the *trans*-rich **P31** were identical to those previously reported in the literature.[101]

trans-rich **P31**: ^{1}H NMR (400 MHz, CDCl$_3$) δ 5.45–5.32 (m, 2 H), 3.38 (t, J = 6.6 Hz, 4 H), 2.09–1.94 (m, 4 H), 1.63–1.48 (m, 4 H), 1.45–1.33 (m, 4 H) ppm.

Table V-12 Polymerization Results for **P26**
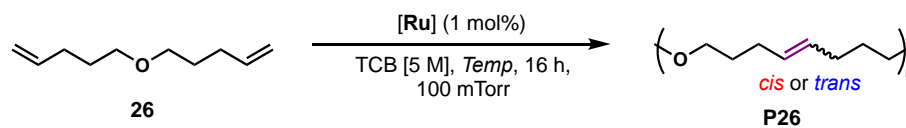
entry	catalyst	temp (°C)	M_n (kg/mol)	Đ	cis (%)
1^a	**Ru-1a**	50^b	22.4	1.61	23
2^a	**Ru-4b**	23	10.6	1.35	99

Reaction performed at a scale of 1 mmol with respect to **26**. [b]Reaction temperature lowered due to the volatility of **26** under vacuum at high temperature.
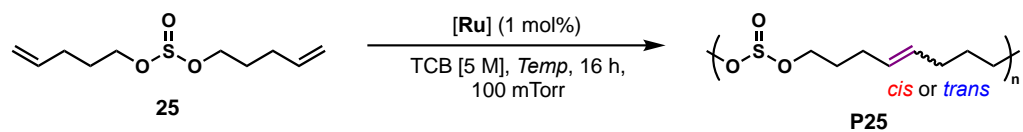
The spectroscopic data for the *cis*-rich **P26** were identical to those previously reported in the literature.[3]

cis-rich **P26**: ^{1}H NMR (400 MHz, CDCl$_3$) δ 5.42–5.29 (m, 2 H), 3.39 (t, *J* = 6.6 Hz, 4 H), 2.10–1.95 (m, 4 H), 1.61–1.50 (m, 4 H), 1.44–1.34 (m, 4 H) ppm.

The spectroscopic data for the *trans*-rich **P26** were identical to those previously reported in the literature.[101]

trans-rich **P26**: ^{1}H NMR (400 MHz, CDCl$_3$) δ 5.45–5.35 (m, 2 H), 3.39 (t, *J* = 6.6 Hz, 4 H), 2.13–1.97 (m, 4 H), 1.67–1.58 (m, 4 H) ppm.

Table V-13 Polymerization Results for **P33**
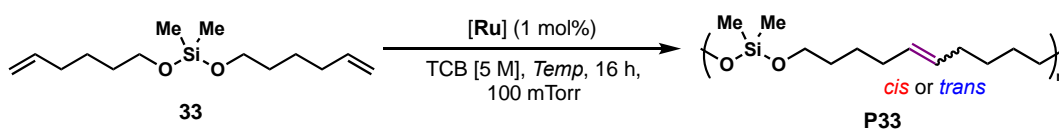
entry	catalyst	temp (°C)	M_n (kg/mol)	Đ	*cis* (%)
1	**Ru-1a**	80	19.1	2.02	13
2	**Ru-4b**	23	10.3	1.45	99

cis-rich **P33**: ^{1}H NMR (400 MHz, CDCl$_3$) δ 5.42–5.30 (m, 2 H), 3.67 (t, J = 6.6 Hz, 4 H), 2.10–1.95 (m, 4 H), 1.61–1.50 (m, 4 H), 1.44–1.33 (m, 4 H), 0.11 (s, 6 H) ppm.

^{13}C NMR (101 MHz, CDCl$_3$) δ 129.9, 62.6, 32.4, 27.1, 26.1, –3.0 ppm.

Basic hydrolysis of *cis*-rich **P33** delivered the corresponding *cis*-dec-5-ene-1,10-diol.
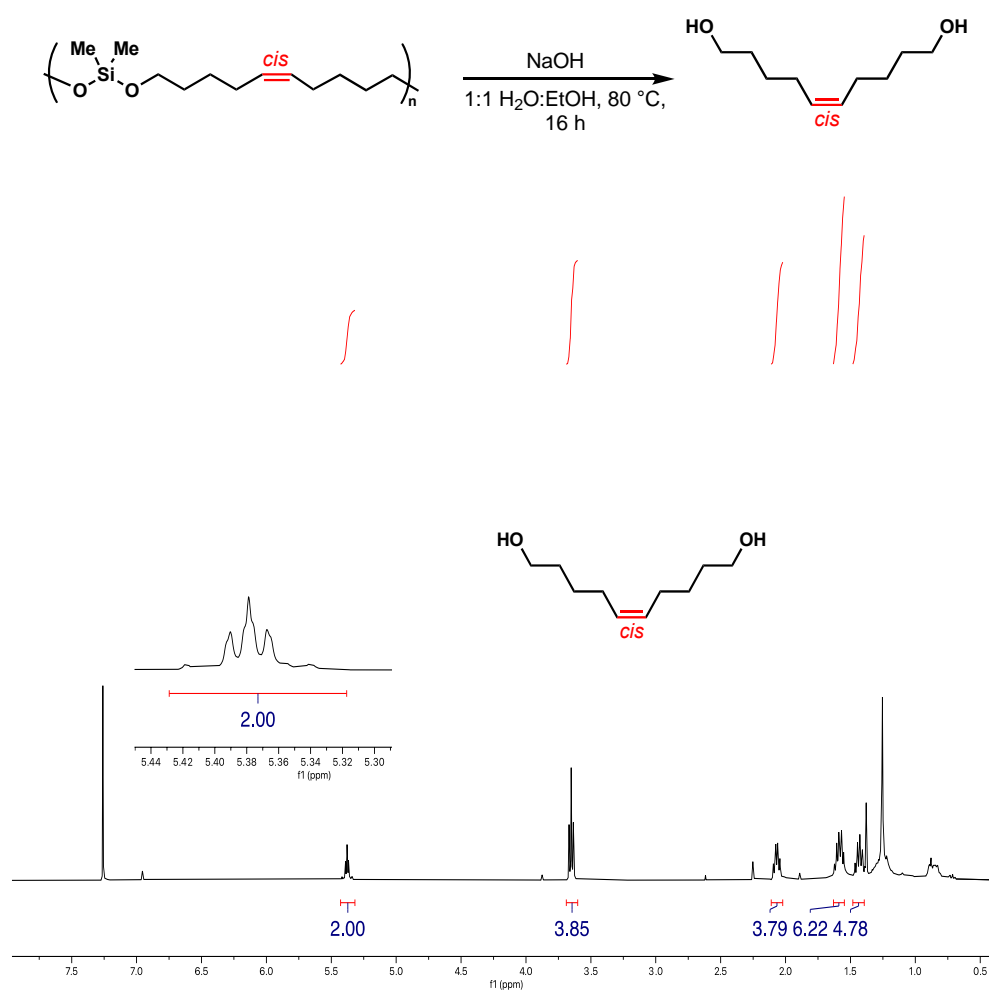
Figure V-4 ^{1}H NMR (400 MHz) of dec-5-ene-1,10-diol obtained from hydrolysis of *cis* **P33**.

265

trans-rich **P33**: ^{1}H NMR (400 MHz, CDCl$_3$) δ 5.45–5.31 (m, 2 H), 3.66 (t, *J* = 6.6 Hz 4 H), 2.10–1.94 (m, 4 H), 1.64–1.49 (m, 4 H), 1.45–1.31 (m, 4 H), 0.11 (s, 6 H) ppm.

^{13}C NMR (101 MHz, CDCl$_3$) δ 130.3, 62.4, 32.3, 32.1, 25.8, –3.0 ppm

Table V-14 Polymerization Results for **P34**
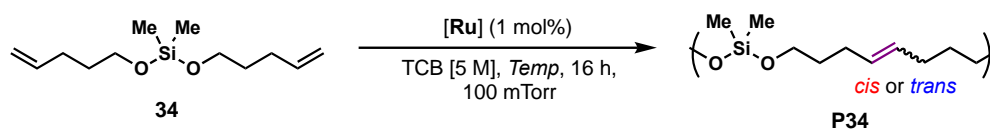
entry	catalyst	temp (°C)	M_n (kg/mol)	Đ	cis (%)
1	**Ru-1a**	80	28.9	1.40	20
2	**Ru-4b**	23	17.6	1.29	99

cis-rich **P34**: ^{1}H NMR (400 MHz, CDCl$_3$) δ 5.45–5.32 (m, 2 H), 3.67 (t, *J* = 6.7 Hz, 4 H), 2.14–2.00 (m, 4 H), 1.67–1.53 (m, 4 H), 0.11 (s, 6 H) ppm.

^{13}C NMR (101 MHz, CDCl$_3$) δ 129.7, 62.1, 32.7, 27.2, 23.6, –3.0 ppm.

Basic hydrolysis of *cis*-rich **P34** delivered the corresponding *cis*-oct-4-ene-1,8-diol.
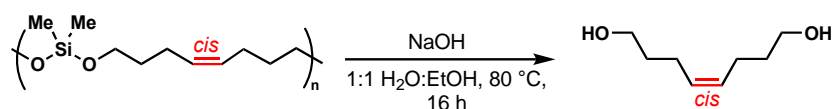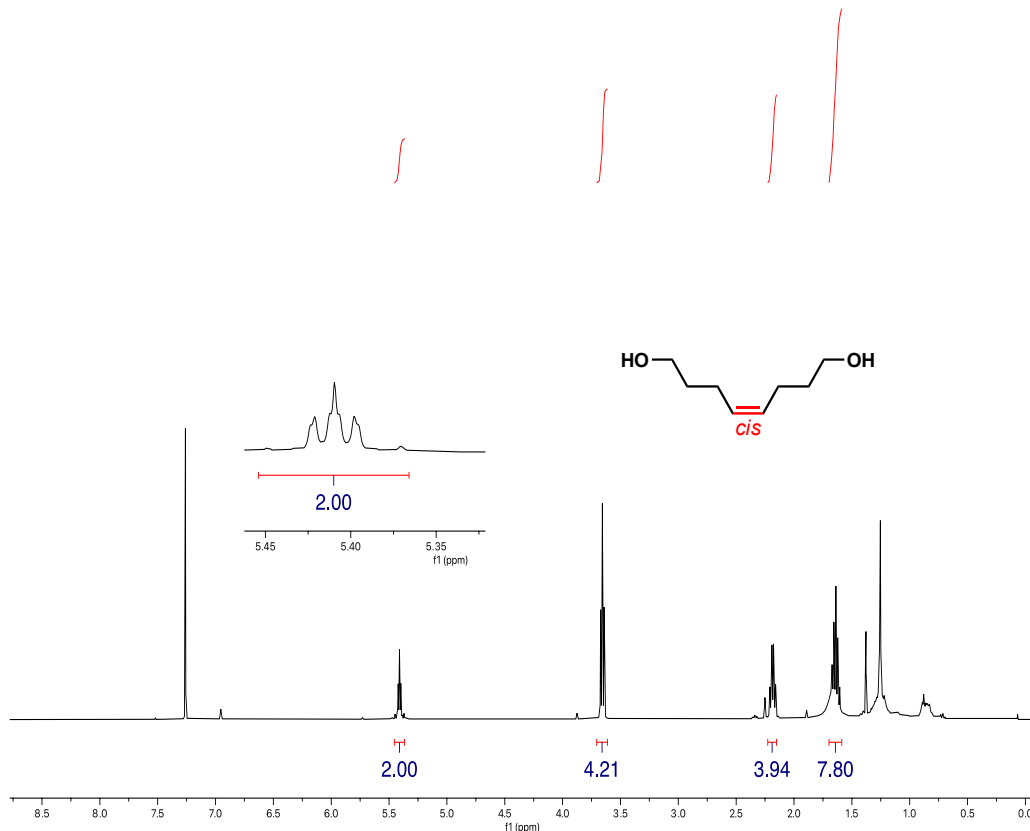
Figure V-5 ^{1}H NMR (400 MHz) of oct-4-ene-1,8-diol obtained from hydrolysis of *cis* **P34**.

trans-rich **P34**: ^{1}H NMR (400 MHz, CDCl$_3$) δ 5.52–5.32 (m, 2 H), 3.66 (t, *J* = 6.7 Hz, 4 H), 2.34–1.95 (m, 4 H), 1.67–1.52 (m, 4 H), 0.11 (s, 6 H) ppm.

^{13}C NMR (101 MHz, CDCl$_3$) δ 130.2, 62.1, 32.7, 32.6, 29.0, –3.0 ppm

Table V-15 Polymerization Results for **P35**
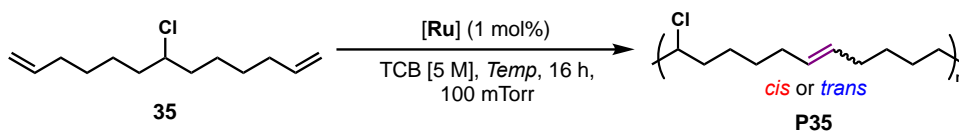
entry	catalyst	temp (°C)	M_n (kg/mol)	Đ	cis (%)
1	**Ru-1a**	40^a	16.2	1.87	19
2	**Ru-4b**	23	7.3	1.64	92

[a]Reaction temperature lowered due to the volatility of **35** under vacuum at high temperature.

cis-rich **P35**: ^{1}H NMR (400 MHz, CDCl₃) δ 5.43–5.31 (m, 2 H), 3.93–3.83 (p, 1 H), 2.10–1.95 (m, 4 H), 1.78–1.63 (m, 4 H), 1.63–1.48 (m, 2 H), 1.48–1.25 (m, 6 H) ppm.

^{13}C NMR (101 MHz, CDCl₃) δ 130.4*, 129.9, 64.3, 38.6, 38.5*, 32.6*, 29.4, 29.3*, 27.3, 26.4, 26.2* ppm.

* = peaks corresponding to the trans signals.

trans-rich **P35**: ^{1}H NMR (400 MHz, CDCl₃): 5.45–5.31 (m, 2 H), 3.93–3.83 (p, 1 H), 2.08–1.93 (m, 4 H), 1.77–1.63 (m, 4 H), 1.61–1.48 (m, 2 H), 1.47–1.24 (m, 6 H) ppm.

^{13}C NMR (101 MHz, CDCl₃): 130.4, 129.9, 64.4, 64.3, 38.6, 38.5, 32.6, 29.4, 29.3, 27.3, 26.4, 26.2 ppm.

Table V-16 Polymerization Results for **P36**
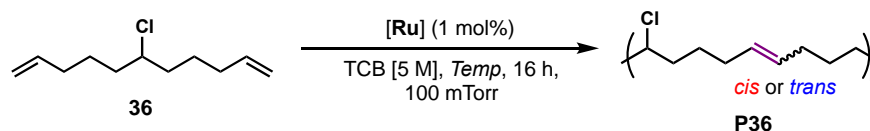
entry	catalyst	temp (°C)	M_n (kg/mol)	Đ	cis (%)
1	**Ru-1a**	40[a]	12.7	1.76	12
2	**Ru-4b**	23	7.2	1.56	97

[a]Reaction temperature lowered due to the volatility of **36** under vacuum at high temperature.

cis-rich **P36**: ^{1}H NMR (400 MHz, CDCl$_3$) δ 5.42–5.32 (m, 2 H), 3.94–3.84 (p, 1 H), 2.13–1.96 (m, 4 H), 1.80–1.66 (m, 4 H), 1.66–1.53 (m, 2 H), 1.53–1.40 (m, 2 H) ppm.

^{13}C NMR (101 MHz, CDCl$_3$) δ 130.4*, 129.9, 64.1, 38.2, 38.1*, 32.2*, 26.8, 26.7, 26.5* ppm.

* = peaks corresponding to the trans signals.

The spectroscopic data for the *trans*-rich **P36** were identical to those previously reported in the literature.[143]

trans-rich **P36**: ^{1}H NMR (400 MHz, CDCl$_3$) δ 5.46–5.32 (m, 2 H), 3.94–3.84 (p, 1 H), 2.13–1.92 (m, 4 H), 1.80–1.66 (m, 4 H), 1.66-1.52 (m, 2 H), 1.52-1.38 (m, 2 H) ppm.

Table V-17 Polymerization Results for **P37**
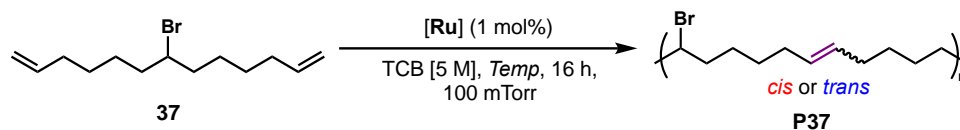
entry	catalyst	temp (°C)	M_n (kg/mol)	Đ	cis (%)
1	**Ru-1a**	40^a	13.4	2.30	9
2	**Ru-4b**	23	7.8	1.76	85

^{a}Reaction temperature lowered due to the volatility of **37** under vacuum at high temperature.

cis-rich **P37**: ^{1}H NMR (400 MHz, CDCl$_3$) δ 5.42–5.32 (m, 2 H), 4.06–3.98 (p, 1 H), 2.11–1.94 (m, 4 H), 1.90–1.73 (m, 4 H), 1.66–1.50 (m, 2 H), 1.50–1.25 (m, 6 H) ppm.

^{13}C NMR (101 MHz, CDCl$_3$) δ 130.4*, 129.9, 58.9, 39.3, 39.2*, 32.5*, 29.3, 29.2*, 27.5, 27.2 ppm.

* = peaks corresponding to the trans signals.

trans-rich **P37**: ^{1}H NMR (400 MHz, CDCl$_3$): 5.46–5.29 (m, 2 H), 4.08–3.97 (p, 1 H), 2.11–1.91 (m, 4 H), 1.90–1.72 (m, 4 H), 1.63–1.48 (m, 2 H), 1.48–1.26 (m, 6 H) ppm.

^{13}C NMR (101 MHz, CDCl$_3$): 130.4, 129.9, 59.0, 58.9, 39.3, 39.2, 32.5, 29.3, 29.2, 27.5, 27.2 ppm.

Table V-18 Polymerization Results for **P38**
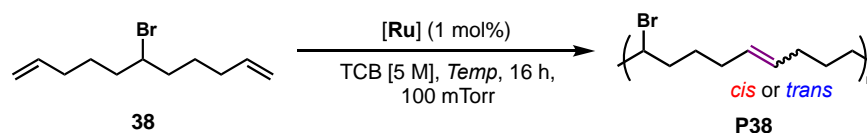
entry	catalyst	temp (°C)	M_n (kg/mol)	Đ	cis (%)
1	**Ru-1**	40^a	8.5	1.96	14
2	**Ru-3b**	23	6.8	1.65	90

[a]Reaction temperature lowered due to the volatility of **38** under vacuum at high temperature.

cis-rich **P38**: ^{1}H NMR (400 MHz, CDCl$_3$) δ 5.45–5.32 (m, 2 H), 4.07–3.97 (p, 1 H), 2.16–1.93 (m, 4 H), 1.90–1.75 (m, 4 H), 1.70–1.55 (m, 2 H), 1.55–1.41 (m, 2 H) ppm.

^{13}C NMR (101 MHz, CDCl$_3$) δ 130.4*, 129.9, 58.6, 58.5, 38.8, 38.7*, 32.1*, 27.7, 27.6*, 26.7 ppm.

* = peaks corresponding to the trans signals.

The spectroscopic data for the *trans*-rich **P38** were identical to those previously reported in the literature.[144]

trans-rich **P38**: ^{1}H NMR (400 MHz, CDCl$_3$) δ 5.45–5.32 (m, 2 H), 4.07–3.97 (p, 1 H), 2.13–1.93 (m, 4 H), 1.89–1.74 (m, 4 H), 1.69–1.55 (m, 2 H), 1.55–1.40 (m, 2 H) ppm.

Table V-19 Polymerization Results for **P39**

271
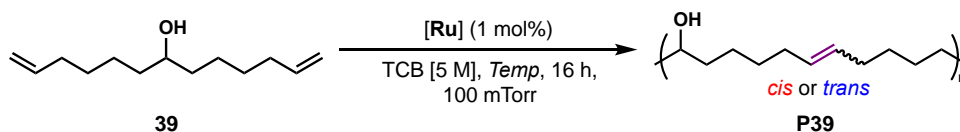
entry	catalyst	temp (°C)	M_n (kg/mol)	Đ	cis (%)
1	**Ru-1a**	80	4.7	1.49	12
2	**Ru-4b**	23	4.8	1.47	93

NOTE: No antisolvent could be identified to purify *cis* and *trans* **P39** through precipitation likely due to their low molar masses.

cis-rich **P39**: ^{1}H NMR (400 MHz, CDCl$_3$): 5.43–5.29 (m, 2H), 3.65–3.49 (br, 1 H), 2.09–1.93 (m, 4H), 1.89–1.68 (br, 1 H), 1.54–1.25 (m, 12 H) ppm.

^{13}C NMR (101 MHz, CDCl$_3$): 130.5*, 130.0, 71.9, 37.5, 37.4*, 32.6*, 29.9, 29.7*, 27.3, 25.4, 25.2* ppm.

* = peaks corresponding to the trans signals.

trans-rich **P39**: ^{1}H NMR (400 MHz, CDCl$_3$): 5.43–5.29 (m, 2 H), 3.65–3.49 (br, 1 H), 2.09–1.93 (m, 4 H), 1.89–1.66 (br, 1 H), 1.65–1.20 (m, 12 H) ppm.

^{13}C NMR (101 MHz, CDCl$_3$): 130.5, 130.0, 71.9, 37.5, 37.4, 32.6, 29.9, 29.7, 27.3, 25.4, 25.2 ppm.

Table V-20 Polymerization Results for **P40**

entry	catalyst	temp (°C)	M_n (kg/mol)	Đ	cis (%)
1	**Ru-4b** (1)	23	2.4	1.40	96
2	**Ru-1a**	80	6.5	1.43	15

NOTE: No antisolvent could be identified to purify *cis* and *trans* **P40** through precipitation likely due to their low molar masses.

cis-rich **P40**: ^{1}H NMR (400 MHz, CDCl$_3$) δ 5.48–5.31 (m, 2 H), 3.65–3.52 (br, 1 H), 2.16–1.94 (m, 4 H), 1.91–1.66 (br, 1 H), 1.63–1.22 (m, 8 H) ppm.

^{13}C NMR (101 MHz, CDCl$_3$): 130.5*, 130.0, 71.7, 71.6, 37.2, 37.0*, 32.6*, 27.3, 25.9, 25.7* ppm.

* = peaks corresponding to the trans signals.

The spectroscopic data for the *trans*-rich **P40** were identical to those previously reported in the literature.[145]

trans-rich **P40**: ^{1}H NMR (400 MHz, CDCl$_3$): 5.48–5.31 (m, 2 H), 3.65–3.52 (br, 1 H), 2.16–1.94 (m, 4 H), 1.91–1.66 (br, 1 H), 1.63–1.22 (m, 8 H) ppm.

V.4.7 cis-*Selective ADMET Polymerization Procedure Using an N$_2$ Flow for Monomer 32*
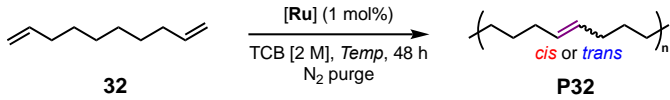
In an N$_2$-filled glovebox, deca-1,9-diene (**32**) (69 mg, 0.5 mmol, 1 equiv.) was weighed into a vial equipped with a stir bar. Then, **Ru-4b** (3.4 mg, 0.005 mmol, 0.01 equiv.) was weighed into a separate vial and dissolved in TCB (0.25 mL). The catalyst solution was taken up in the syringe and ejected back into the vial three times to ensure the catalyst dissolved. The catalyst solution was then transferred to the monomer vial

where the solution was taken up in the syringe and ejected three times. The vial was then capped with a screw cap fitted with a Teflon septa and removed from the box. The vial was taken to a Schlenk line where it was pierced with a 3" 18 G pink needle with a positive N_2 flow until it made contact with the bottom of the vial. An 18 G needle was then pierced through the septa as a bleed needle and the reaction mixture was checked to make sure proper bubbling of N_2 was occurring. The reaction was stirred at 100 rpm at room temperature for 48 h. At this point, 50 µL of ethyl vinyl ether was added to quench the polymerization for 5 minutes. The mixture was then dissolved in the minimum amount of DCM (~ 1 mL) and precipitated in MeOH in a centrifuge tube. The mixture then underwent centrifugation at 8500 rpm for 10 minutes. The MeOH was decanted, the polymer was redissolved in DCM, and precipitated in MeOH again. After a second centrifugation cycle, the MeOH was decanted and **P32** was dried for 24 h under vacuum.

Figure V-6 Purging reaction setup for polymer synthesis with **Ru-4b**.

Table V-21 Polymerization Results for **P32**

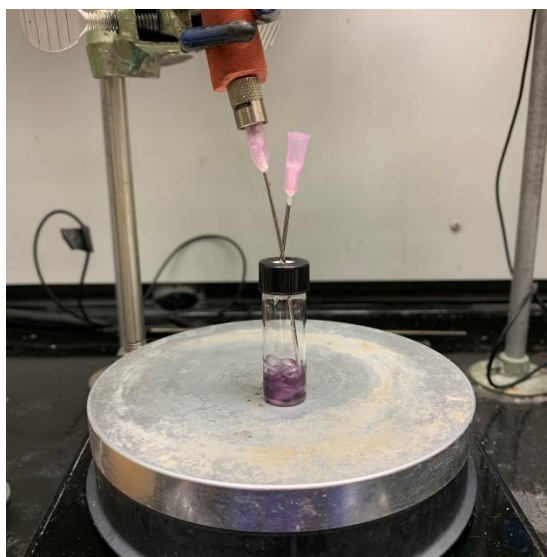| entry	catalyst	temp (°C)	M_n (kg/mol)	$Đ$	cis (%)
1	**Ru-1a**	90	10.2	1.78	16
2	**Ru-4b**	23	8.5	1.80	99

The spectroscopic data for the *cis*-rich **P32** were identical to those previously reported in the literature.[146]

cis-rich **P32**: ^{1}H NMR (400 MHz, CDCl$_3$) δ 5.41–5.28 (m, 2 H), 2.10–1.93 (m, 4 H), 1.40–1.23 (m, 8 H) ppm.

^{13}C NMR (101 MHz, CDCl$_3$) δ 130.0, 29.9, 29.4, 27.4 ppm.

The spectroscopic data for the *trans*-rich **P32** were identical to those previously reported in the literature.[93]

trans-rich **P32**: ^{1}H NMR (400 MHz, CDCl$_3$) δ 5.53–5.27 (m, 2H), 2.06–1.90 (m, 4H), 1.40–1.20 (m, 8H) ppm.

V.4.8 ABA Triblock Copolymer Synthesis

P32_{*cis*}-OAc (99% *cis*)
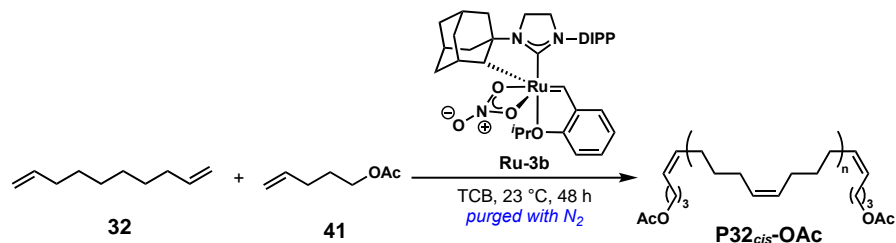
In a nitrogen-filled glove box, an oven-dried vial was charged with **Ru-4b** (5.0 µmol, 0.01 equiv) and TCB (0.25 mL). The solution of catalyst was added to another oven-dried vial containing pre-weighed monomer **32** (0.50 mmol, 1 equiv), acetate reagent **41** (0.10 mmol, 0.2 equiv), and a stir bar. The vial capped with a Teflon cap was then removed from the glove box and stirred for 48 h under a constant nitrogen flow passing through a 3-inch, 18G needle with another 18G bleed needle (Figure V-6). Polymer **P32_{*cis*}-OAc** was then precipitated with ice-cold methanol, isolated via centrifugation (8500 rpm, 10 min), and dried under high vacuum for 16–24 h.

^{1}H NMR (400 MHz, CDCl$_3$) δ 5.35 (t, *J* = 4.7 Hz, 44 H), 4.06 (t, *J* = 6.7 Hz, 4 H), 2.06–1.95 (m, 92 H), 1.32 (d, *J* = 10.4 Hz, 178 H) ppm.

^{13}C NMR (101 MHz, CDCl$_3$) δ 129.9, 29.7, 29.2, 27.2 ppm.

P32_{*trans*}-OAc (89% *trans*)

In a nitrogen-filled glove box, an oven-dried vial was charged with **Ru-1a** (5.0 µmol, 0.01 equiv) and dissolved in TCB (0.25 mL). The solution of catalyst was added to another vial containing the pre-weighed monomer **32** (0.50 mmol, 1 equiv), acetate reagent **41** (0.10

mmol, 0.2 equiv) and a stir bar. The vial capped with a Teflon cap was then removed from the glove box. The reaction was placed in a pre-heated oil bath (90 °C) and stirred for 48 h under a constant nitrogen flow passing through one 3-inch, 18G needle and an 18G bleed needle (Figure V-6). Polymer **P32**$_{trans}$**-OAc** was then precipitated with ice-cold methanol, isolated via centrifugation (8500 rpm, 10 min), and then dried under high vacuum for 16–24 h.

^{1}H NMR (400 MHz, CDCl$_3$) δ 5.44–5.29 (m, 50 H), 4.06 (t, $J = 6.7$ Hz, 4 H), 2.03–1.89 (m, 96 H), 1.38–1.24 (m, 195 H) ppm.

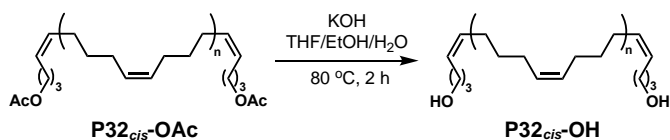^{13}C NMR (101 MHz, CDCl$_3$) δ 130.3, 129.9, 32.6, 29.7, 29.1, 27.2 ppm.

Hydrolysis of **P32**$_{cis}$**-OAc** (99% *cis*) and **P32**$_{trans}$**-OAc** (89% *trans*)

P32$_{cis}$**-OAc** (or **P32**$_{trans}$**-OAc**) (30 mg) was placed in a reaction vial equipped with a stir bar, and solution of KOH (100 mg) in a THF:EtOH:H$_2$O mixture (1:1:1, 6 mL) was added to the vial. The polymer suspension was heated to 80 °C for 2 h. The reaction was cooled to room temperature and diluted with dichloromethane (20 mL). The organic layer was washed with H$_2$O (10 mL), dried over sodium sulfate, and then the solvent was removed *in vacuo* affording **P32**$_{cis}$**-OH** (or **P32**$_{trans}$**-OH**).

^{1}H NMR (400 MHz, CDCl$_3$) δ 5.35 (t, *J* = 4.7 Hz, 50 H), 3.66 (t, *J* = 6.5 Hz, 4 H), 2.09–

1.92 (m, 101 H), 1.39–1.24 (m, 211 H) ppm.

^{13}C NMR (101 MHz, CDCl$_3$) δ 129.9, 29.7, 29.2, 27.2 ppm.

P32*trans***-OH** (89% *trans*)

^{1}H NMR (400 MHz, CDCl$_3$) δ 5.45–5.30 (m, 54 H), 3.65 (t, *J* = 6.3 Hz, 4 H), 2.12–1.87

(m, 110 H), 1.44–1.20 (m, 216 H) ppm.

^{13}C NMR (101 MHz, CDCl$_3$) δ 130.3, 129.9, 32.6, 29.7, 29.6, 29.1, 29.1, 27.2 ppm.

Synthesis of **P42-*b*-P32***cis***-*b*-P42** (99% *cis*) and **P42-*b*-P32***trans***-*b*-P42** (89% *trans*)
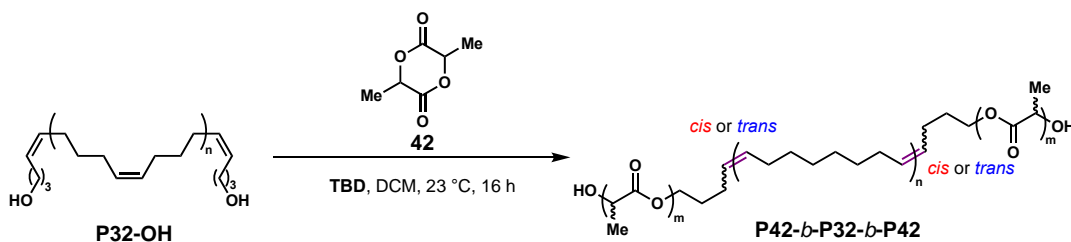
In a nitrogen-filled glove box, D,L-lactide (**42**) (59.2 mg, 411 µmol, 120 equiv) was added

to vial containing anhydrous DCM (0.3 mL). The solution was then transferred to a vial

containing pre-weighed **P32-OH** (3.4 µmol, 1 equiv) and a stir bar. The mixture was

stirred for 5 min followed by rapid addition of a solution of triazabicyclodecene (TBD,

0.376 mg, 2.7 µmol, 0.8 equiv) in anhydrous DCM (0.1 mL) with a syringe. The vial was

then removed from the glovebox, and parafilm was wrapped around the cap to ensure an

optimum seal. The mixture was stirred for 16 h at room temperature, then quenched by

addition of an excess of acetic acid (0.1 mL). The polymer solution was precipitated by addition into methanol, and the solid was isolated by centrifugation and decantation. The resulting ABA triblock copolymer was dried under high vacuum.

P42-*b*-**P32**$_{cis}$-*b*-**P42** (99% *cis*)

^{1}H NMR (400 MHz, CDCl$_3$) δ 5.40–5.29 (m, 44 H), 5.29–5.09 (m, 231 H), 2.11–1.90 (m, 82 H), 1.68–1.47 (m, 736 H), 1.38–1.25 (m, 209 H) ppm.

^{13}C NMR (101 MHz, CDCl$_3$) δ 169.3, 129.9, 69.0, 29.7, 29.2, 27.2, 16.6 ppm.

P42-*b*-**P32**$_{trans}$-*b*-**P42** (89% *trans*)

^{1}H NMR (400 MHz, CDCl$_3$) δ 5.40–5.22 (m, 44 H), 5.20–5.02 (m, 242 H), 2.03–1.81 (m, 83 H), 1.56–1.42 (m, 757 H), 1.32–1.16 (m, 171 H) ppm.

^{13}C NMR (101 MHz, CDCl$_3$) δ 169.4, 130.4, 69.4, 69.1, 32.6, 29.6, 16.7 ppm.
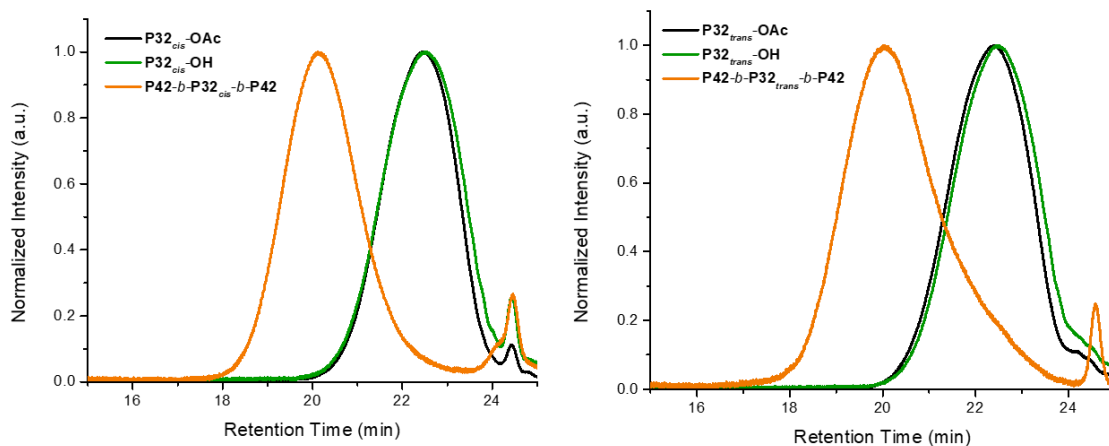
Figure V-7 SEC traces showing formation of **P42**-*b*-**P32**$_{cis}$-*b*-**P42** (left, orange) from **P32**$_{cis}$-**OH** (green) and formation of **P42**-*b*-**P32**$_{trans}$-*b*-**P42** (right, orange) from **P32**$_{trans}$-**OH** (green).

279

V.4.9 NMR Deconvolution

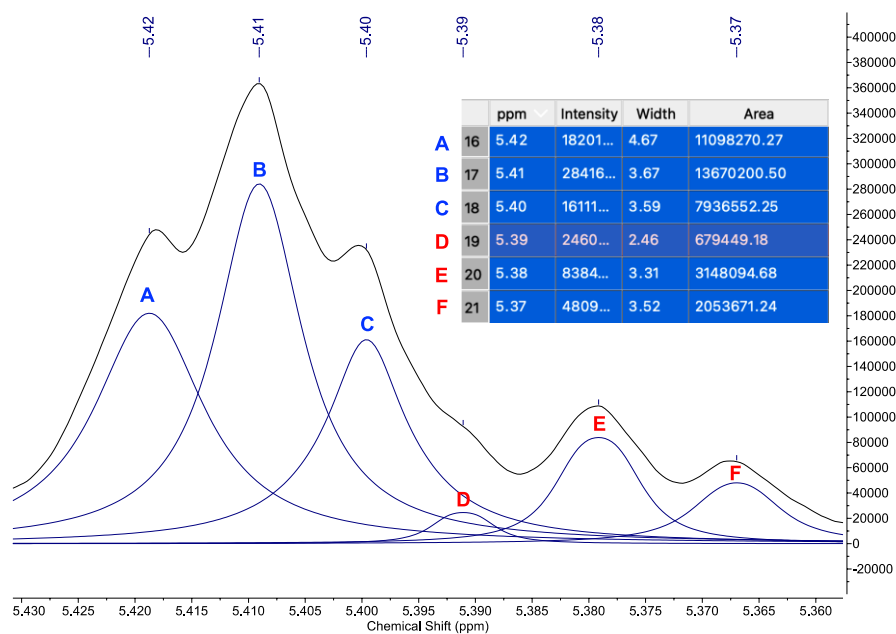Due to overlap in the ^{1}H NMR spectrum between the *cis* and *trans* alkene signals, the built-in MestReNova Global Spectra Deconvolution (GSD) software was used to calculate the cis content. The following equation was used where the letter refers to the area under the specified curve:

$$cis\% = \left[1 - \left(\frac{\sum A:C}{\sum A:F}\right)\right] \times 100 \qquad (1)$$

		ppm	Intensity	Width	Area
A	16	5.42	18201...	4.67	11098270.27
B	17	5.41	28416...	3.67	13670200.50
C	18	5.40	16111...	3.59	7936552.25
D	19	5.39	2460...	2.46	679449.18
E	20	5.38	8384...	3.31	3148094.68
F	21	5.37	4809...	3.52	2053671.24

Figure V-8 ^{1}H NMR spectral deconvolution of **P28** formed by **Ru-1a** at 80 °C (15% *cis*).

V.4.10 Thermal Characterization Data

Table V-22 Summary of DSC and TGA Data

entry	polymer	M_n (kg/mol)	$Đ$	cis (%)	T_d (°C)	T_g (°C)	T_m (°C)	T_c (°C)
1	P28	12.0	1.60	99	334	–73	–	–
2	P28	20.9	1.81	15	298	–68	–17	11
3	P24	9.1	1.38	99	314	–75	–	–
4	P24	15.7	1.80	17	253	–64	–	–
5	P29	8.4	1.42	99	280	–	–	–
6	P29	18.8	1.77	23	274	–	–	–
7	P25	9.5	1.56	99	277	–	–	–
8	P25	9.9	1.67	23	227	–	–	–
9	P30	8.3	1.52	91	317	–29	–	–
10	P30	7.9	2.22	25	304	–27	83	26
11	P23	5.0	1.69	99	309	–24	–	–
12	P23	11.2	3.23	21	273	–15	–	–
13	P31	10.0	1.49	99	406	–	–	–
14	P31	26.5	1.55	18	401	–	–9	–27
15	P26	10.6	1.35	99	301	–	–	–

16	**P26**	22.4	1.61	23	286	–	–	–
17	**P32**	8.5	1.80	99	380	–	32	16
18	**P32**	10.2	1.78	16	406	–	24	12
19	**P32**_{cis}**-OAc**	3.3	1.41	99	349	–	–9	–30, –8
20	**P32**_{trans}**-OAc**	3.6	1.40	11	333	–	–3, 8, 17	–6, 5
21	**P32**_{cis}**-OH**	3.3	1.40	99	247	–	23	–39
22	**P32**_{trans}**-OH**	3.1	1.52	11	295	–	45, 51	36
23	**P42**-*b*- **P32**_{cis}-*b*-**P42**	17.3	1.32	99	278	32	–	–
24	**P42**-*b*- **P32**_{trans}-*b*-**P42**	15.7	1.46	11	273	43	19	–19
19	**P33**	10.3	1.45	99	340	–	–	–
20	**P33**	19.1	2.02	13	344	–	–	–
21	**P34**	17.6	1.29	99	310	–	–	–
22	**P34**	28.9	1.40	20	307	–	–	–
23	**P35**	7.3	1.64	92	329	–73	–	–
24	**P35**	16.2	1.87	19	238	–67	–	–
25	**P36**	7.2	1.56	97	293	–69	–	–
26	**P36**	12.7	1.76	12	246	–62	–	–

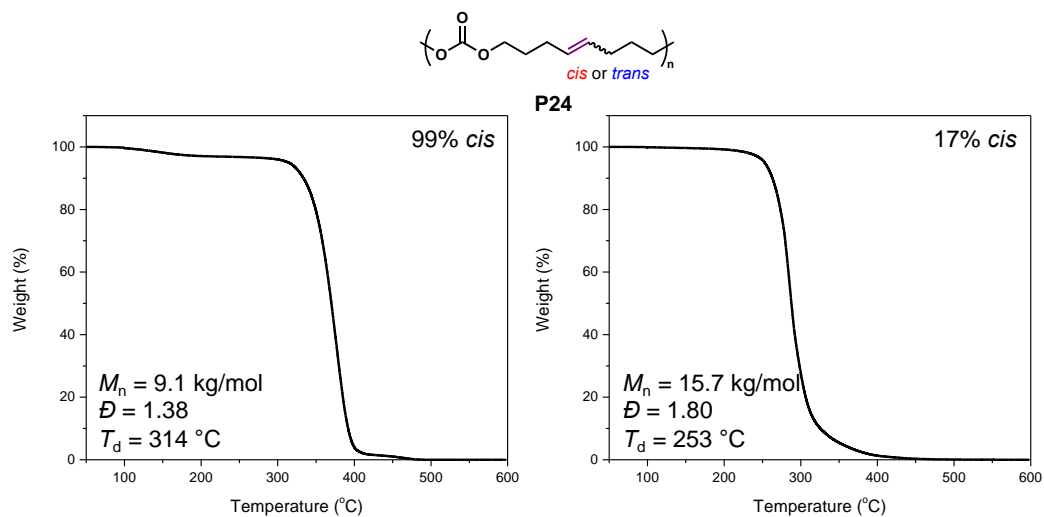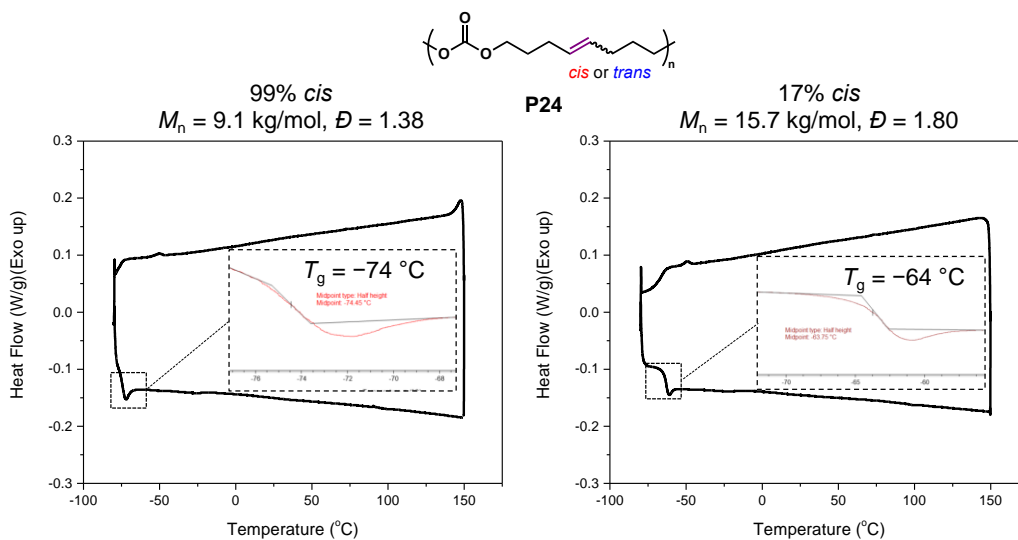| 27	P37	7.8	1.76	85	250	–70	–	–
28	P37	13.4	2.30	9	236	–63	–	–
28	P38	6.8	1.65	90	241	–64	–	–
29	P38	8.5	1.96	14	237	–57	–	–
30	P42	19.9	1.72	–	249	49	–	–
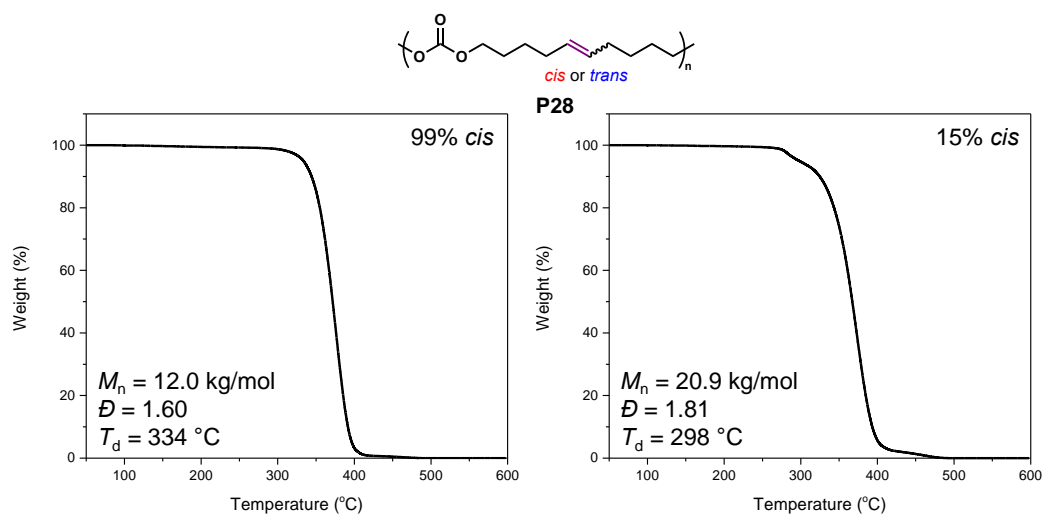
Figure V-9 TGA thermograms of 99% *cis* **P28** (left) and 15% *cis* **P28** (right).
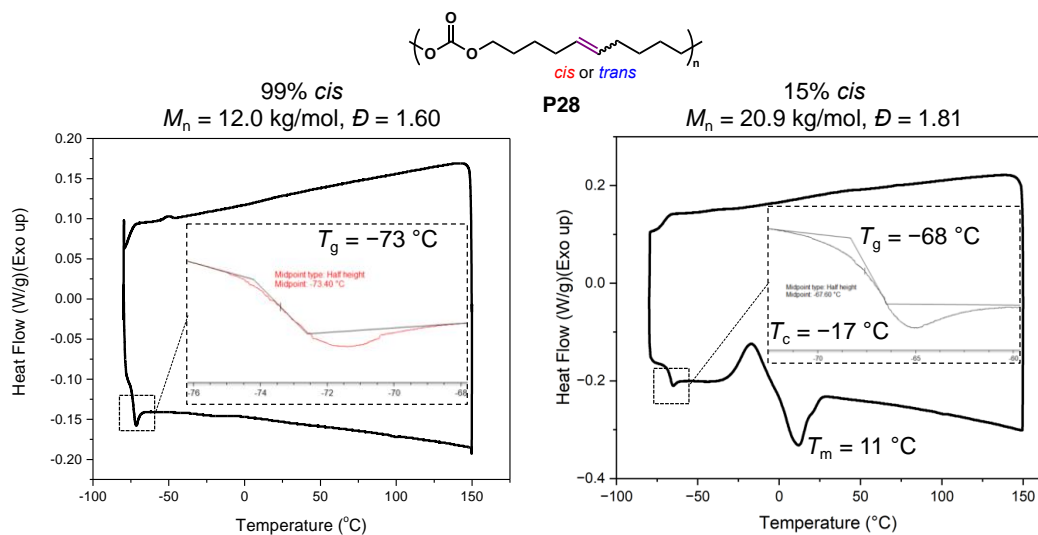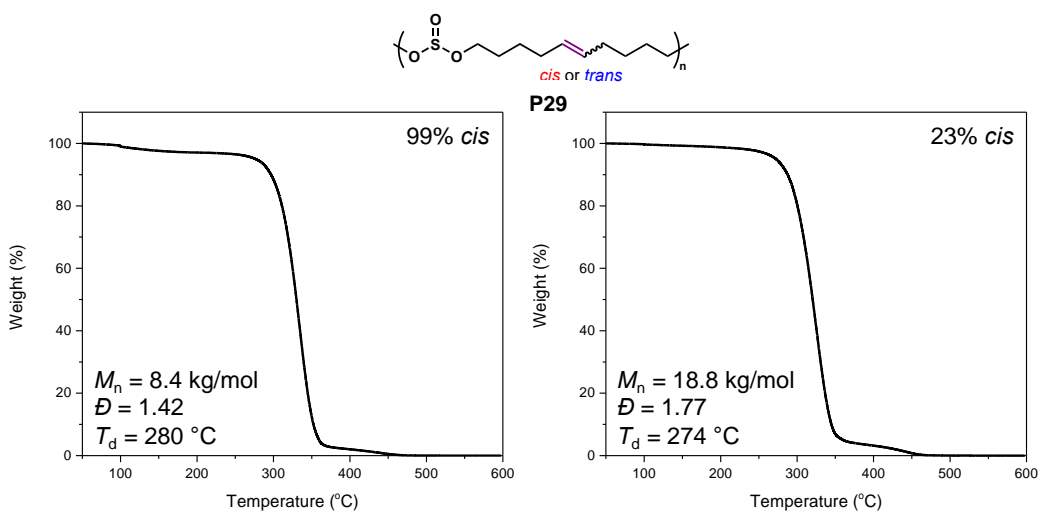
Figure V-10 DSC thermograms of 99% *cis* **P28** (left) and 15% *cis* **P28** (right).
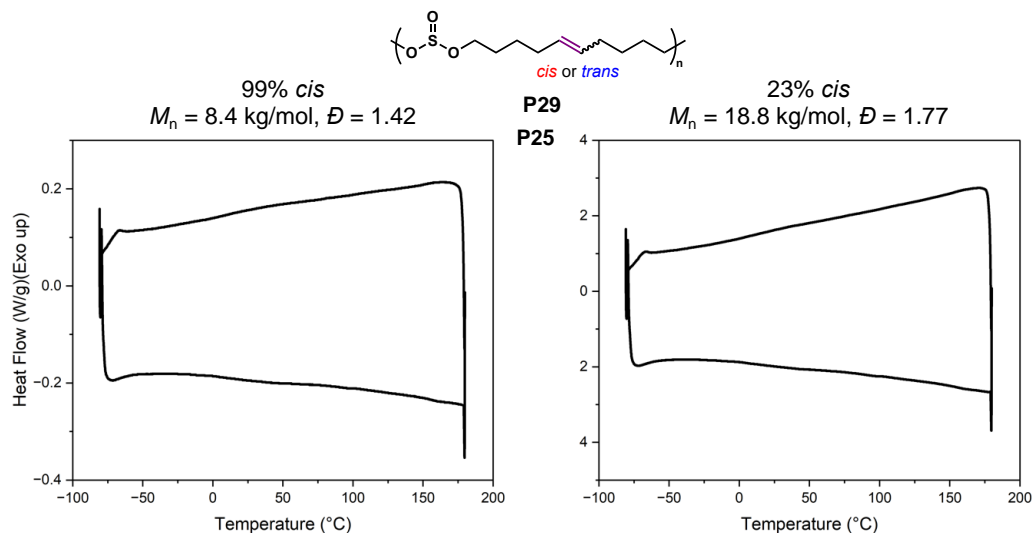

Figure V-11 TGA plots of 99% *cis* **P24** (left) and 17% *cis* **P24** (right).
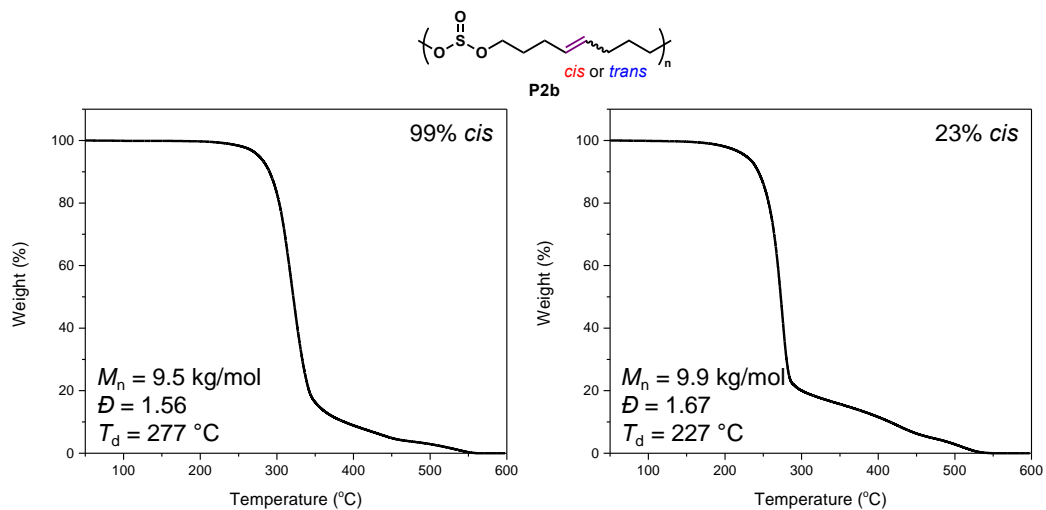
Figure V-12 DSC plots of 99% *cis* **P24** (left) and 17% *cis* **P24** (right).
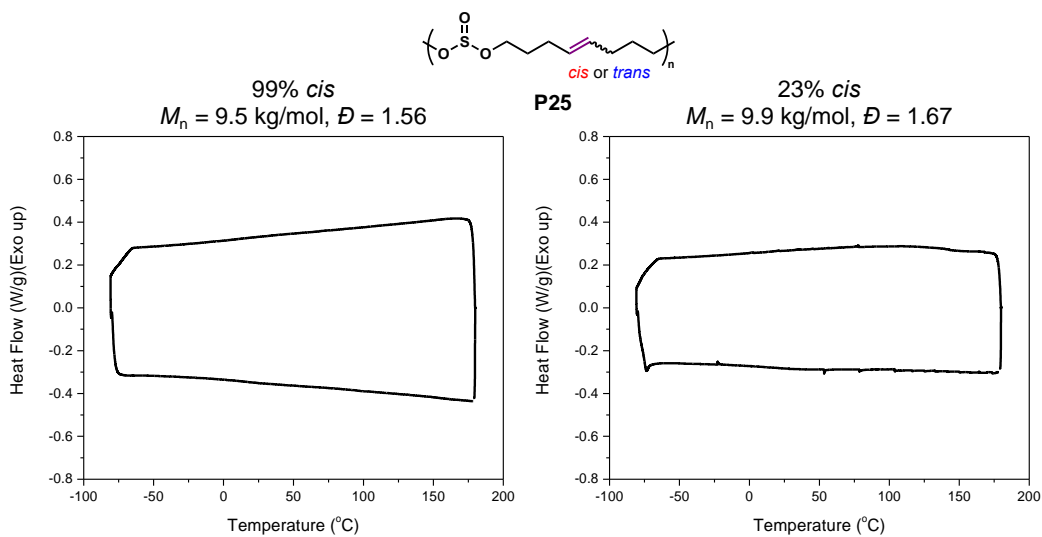

Figure V-13 TGA plots of 99% *cis* **P29** (left) and 23% *cis* **P29** (right).
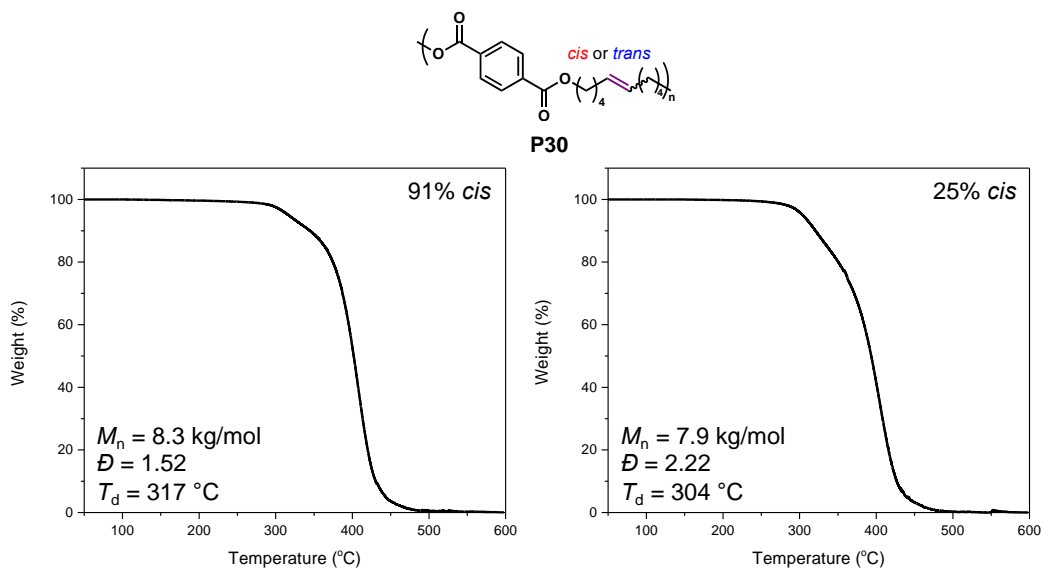
Figure V-14 DSC plots of 99% *cis* **P29** (left) and 23% *cis* **P29** (right).
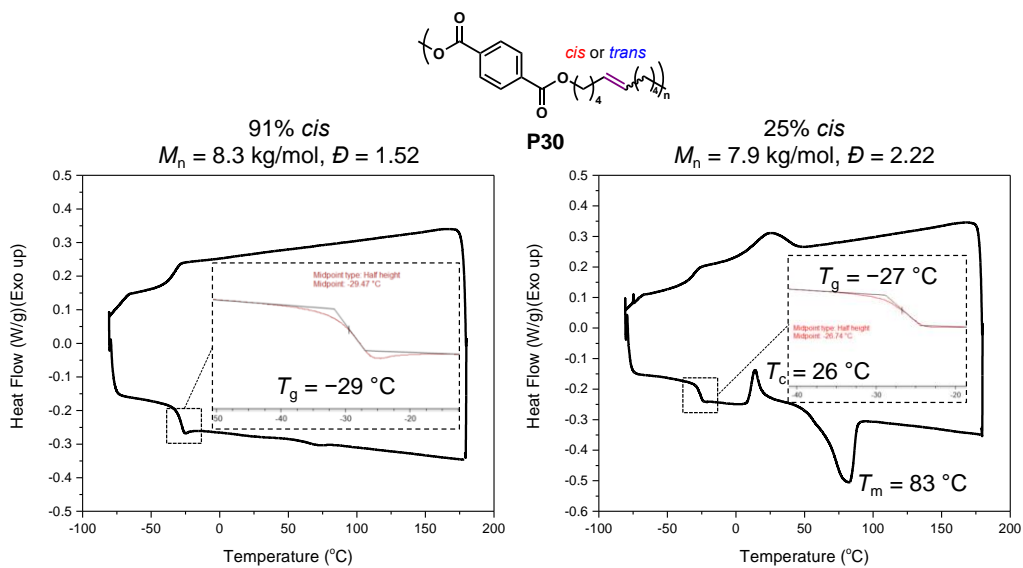

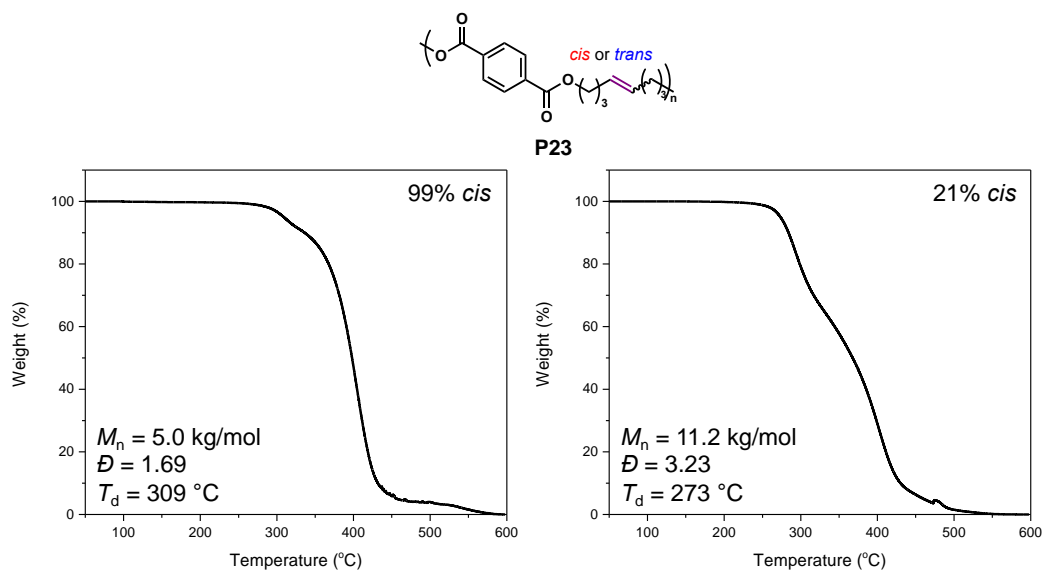**Figure V-15** TGA plots of 99% *cis* **P25** (left) and 23% *cis* **P25** (right).

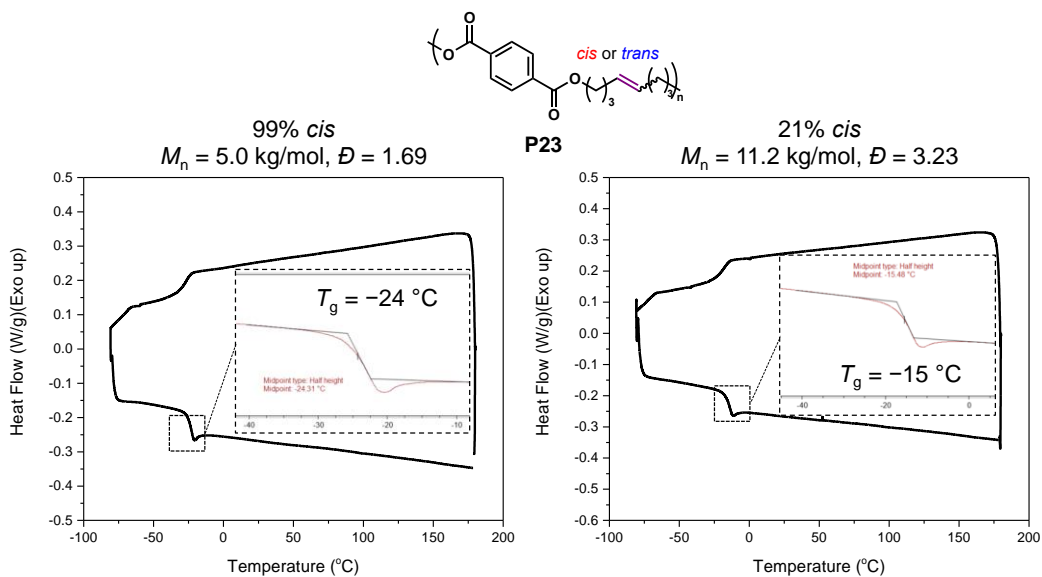**Figure V-16** TGA plots of 99% *cis* **P25** (left) and 23% *cis* **P25** (right).

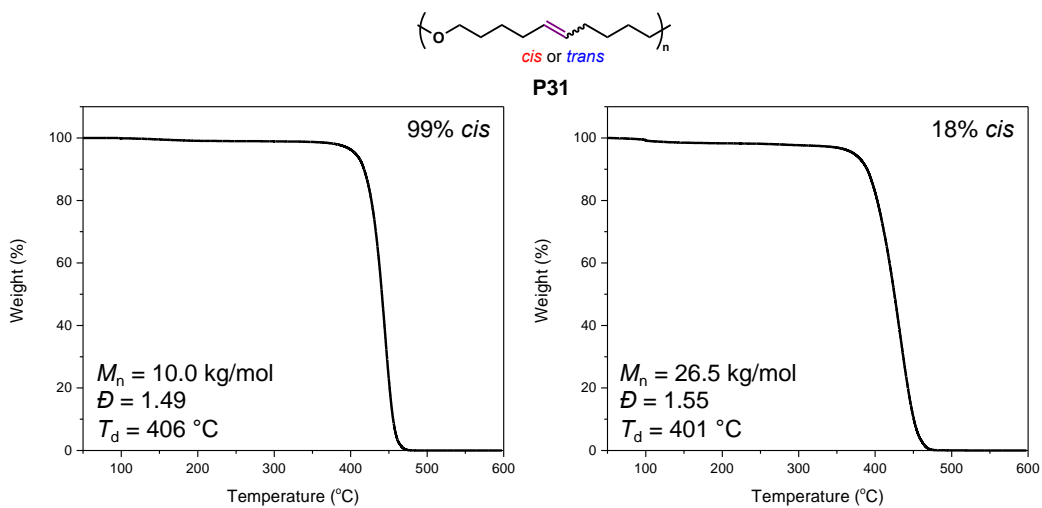**Figure V-17** TGA plots of 91% *cis* **P30** (left) and 25% *cis* **P30** (right).

Figure V-18 DSC plots of 91% *cis* **P30** (left) and 25% *cis* **P30** (right).
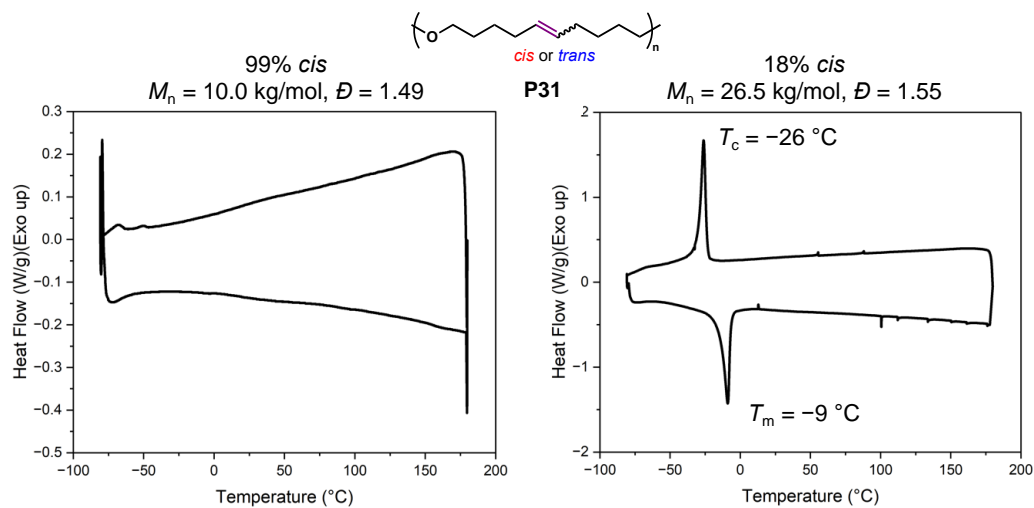

Figure V-19 TGA plots of 99% *cis* **P23** (left) and 21% *cis* **P23** (right).

Figure V-20 DSC plots of 99% *cis* **P23** (left) and 21% *cis* **P23** (right).

Figure V-21 TGA plots of 99% *cis* **P31** (left) and 18% *cis* **P31** (right).

289

99% cis
$M_n = 10.0$ kg/mol, Đ = 1.49

P31

18% cis
$M_n = 26.5$ kg/mol, Đ = 1.55

$T_c = -26$ °C

$T_m = -9$ °C

Figure V-22 DSC plots of 99% *cis* **P31** (left) and 18% *cis* **P31** (right).

P26

99% cis

23% cis

$M_n = 10.6$ kg/mol
Đ = 1.35
$T_d = 301$ °C

$M_n = 22.4$ kg/mol
Đ = 1.61
$T_d = 286$ °C

Figure V-23 TGA plots of 99% *cis* **P26** (left) and 23% *cis* **P26** (right).
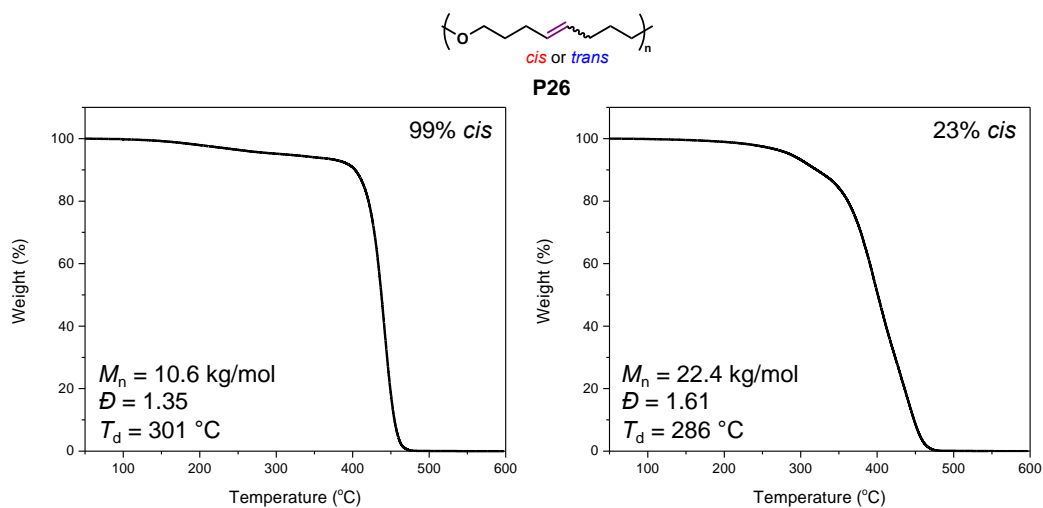
290

Figure V-24 DSC plots of 99% *cis* **P26** (left) and 23% *cis* **P26** (right).
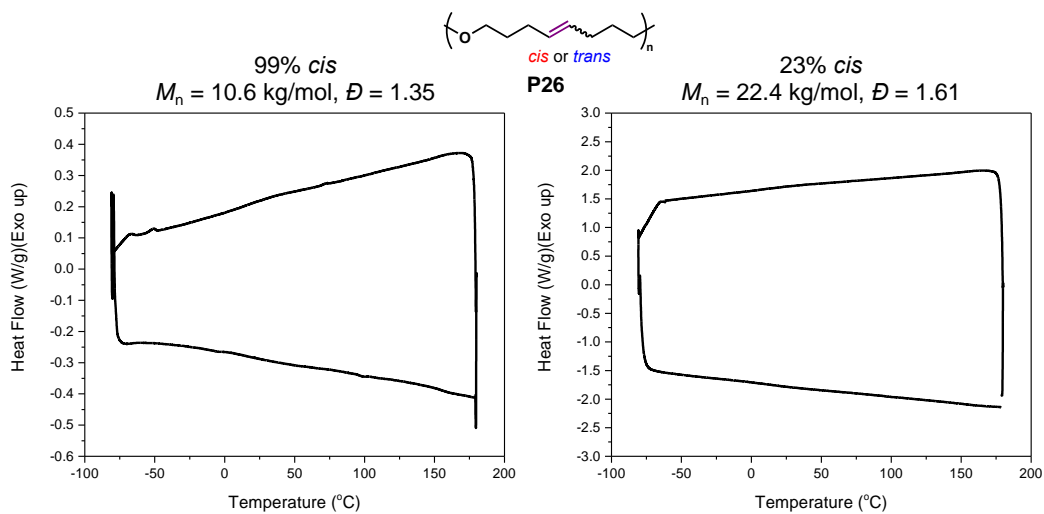

Figure V-25 TGA plots of 99% *cis* **P32** (left) and 16% *cis* **P32** (right).
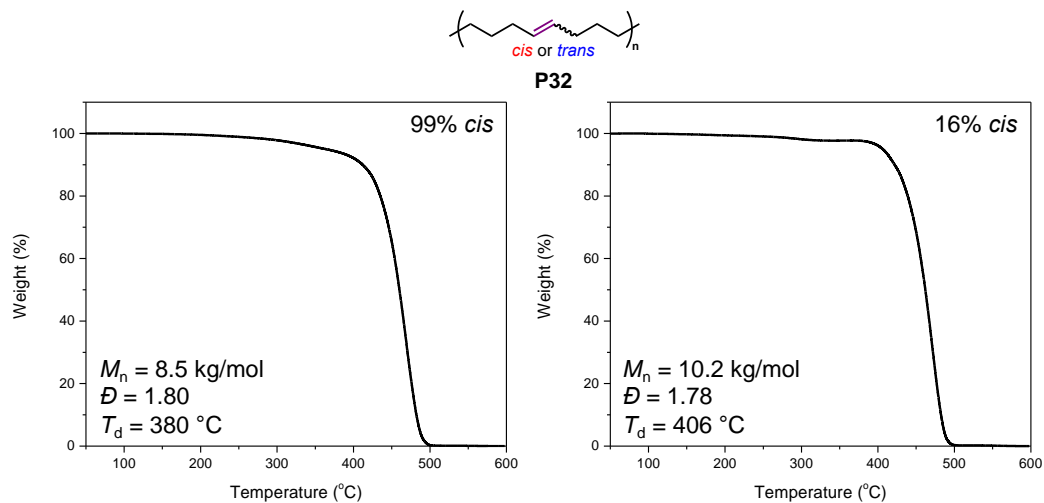
Figure V-26 DSC plots of 99% *cis* **P32** (left) and 16% *cis* **P32** (right).
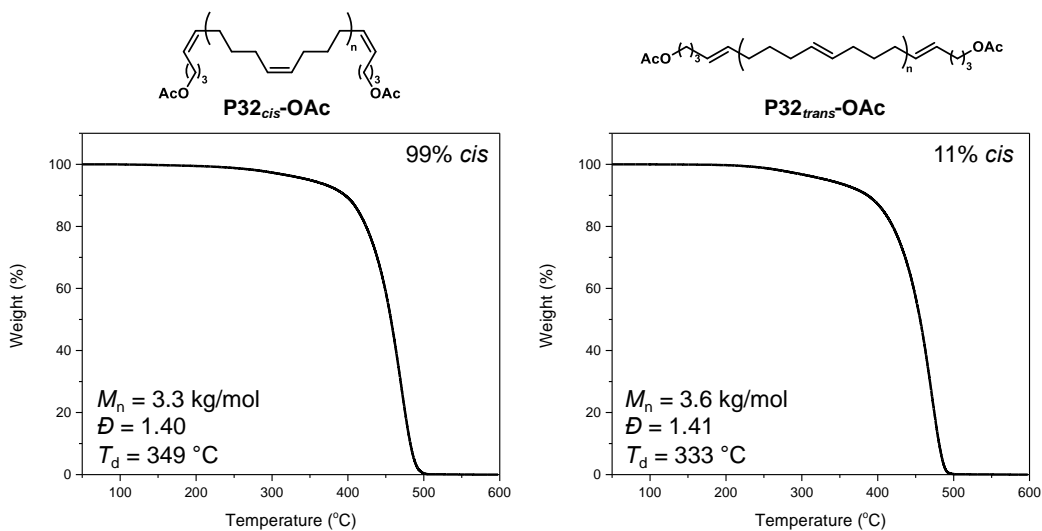
Figure V-27 TGA plots of **P32_*cis*-OAc** (left) and **P32_*trans*-OAc** (right)**.**
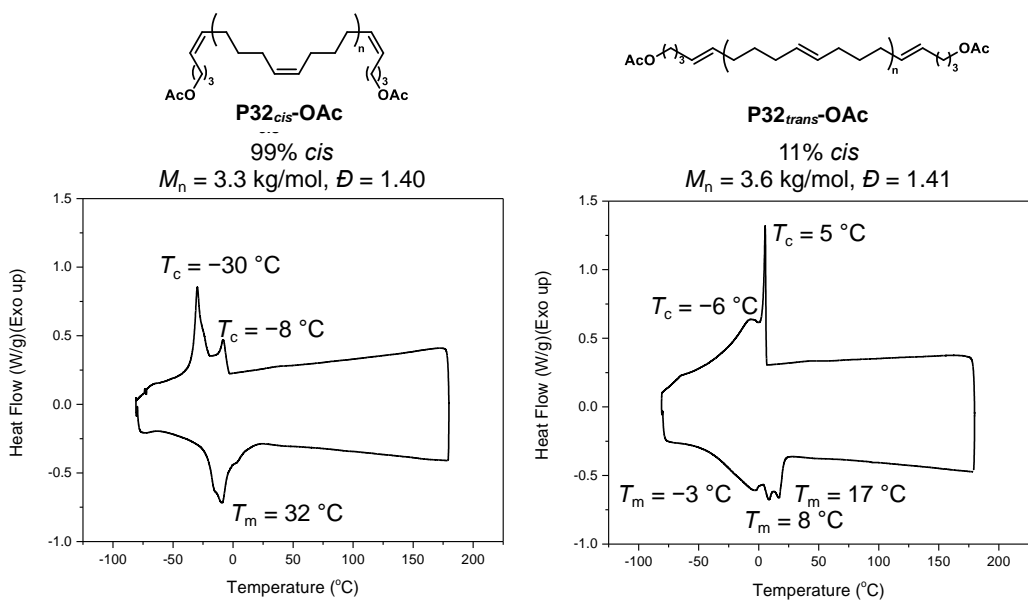
Figure V-28 DSC plots of **P32*cis*-OAc** (left) and **P32*trans*-OAc** (right).
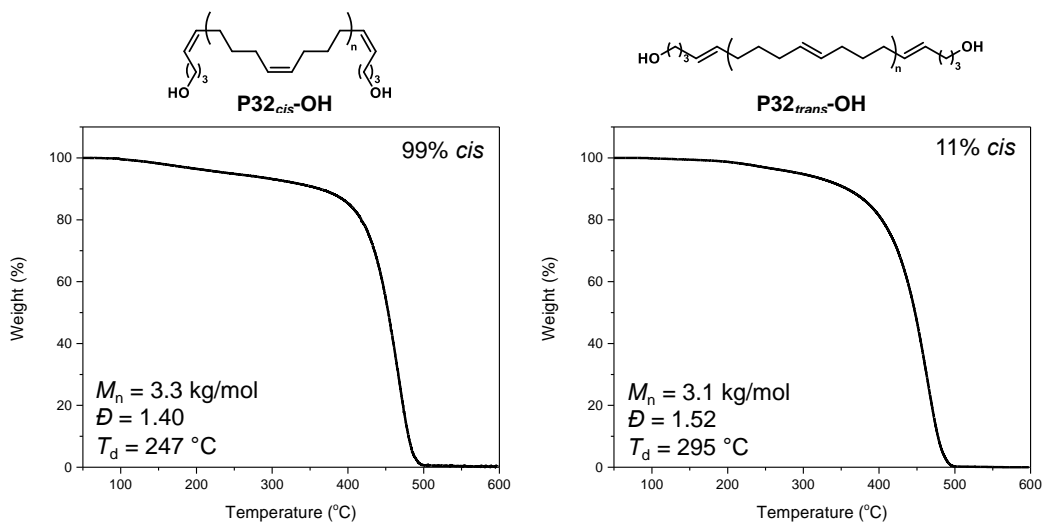
Figure V-29 TGA plots of **P32*cis*-OH** (left) and **P32*trans*-OH** (right).
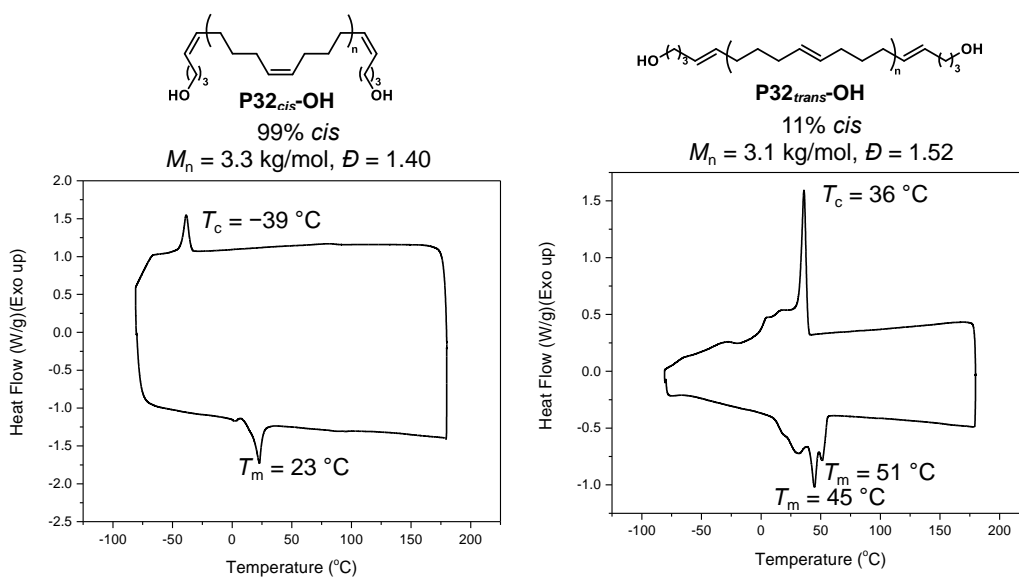
Figure V-30 DSC plots of **P32$_{cis}$-OH** (left) and **P32$_{trans}$-OH** (right).
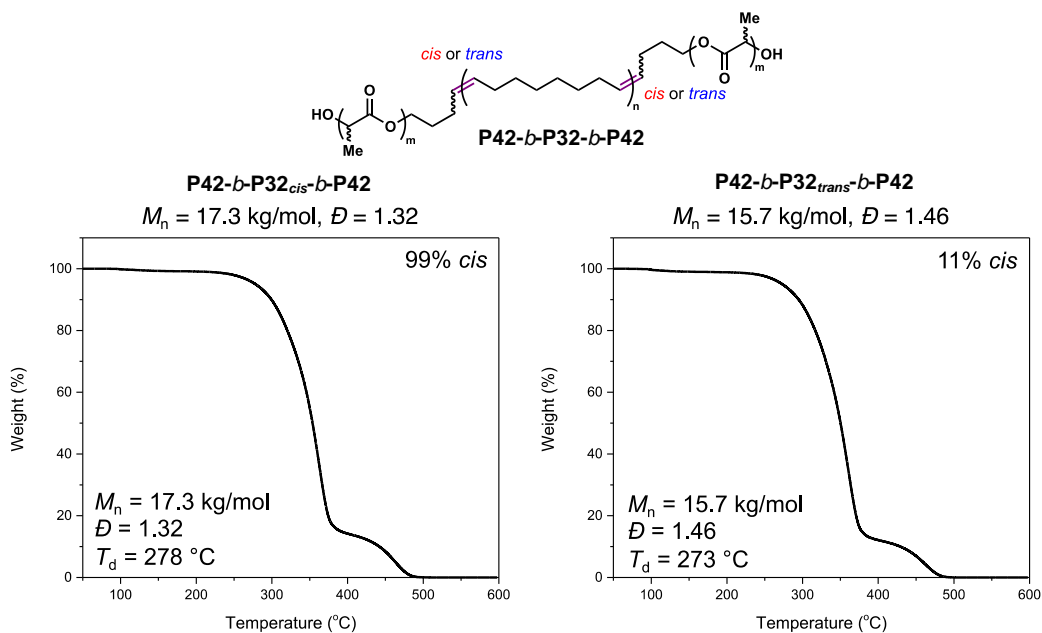
Figure V-31 TGA plots of **P42**-*b*-**P32$_{cis}$**-*b*-**P42** (left) and **P42**-*b*-**P32$_{trans}$**-*b*-**P42** (right).

294
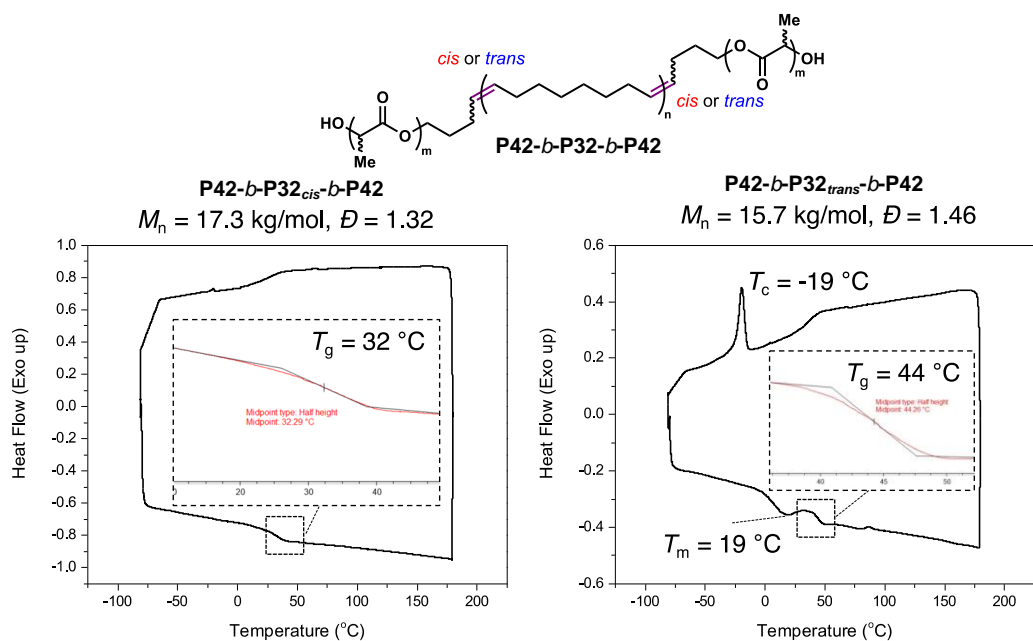
Figure V-32 DSC plots of **P42**-*b*-**P32***cis*-*b*-**P42** (99% *cis*, left) and **P42**-*b*-**P32***trans*-*b*-**P42** (89% *trans*, right).
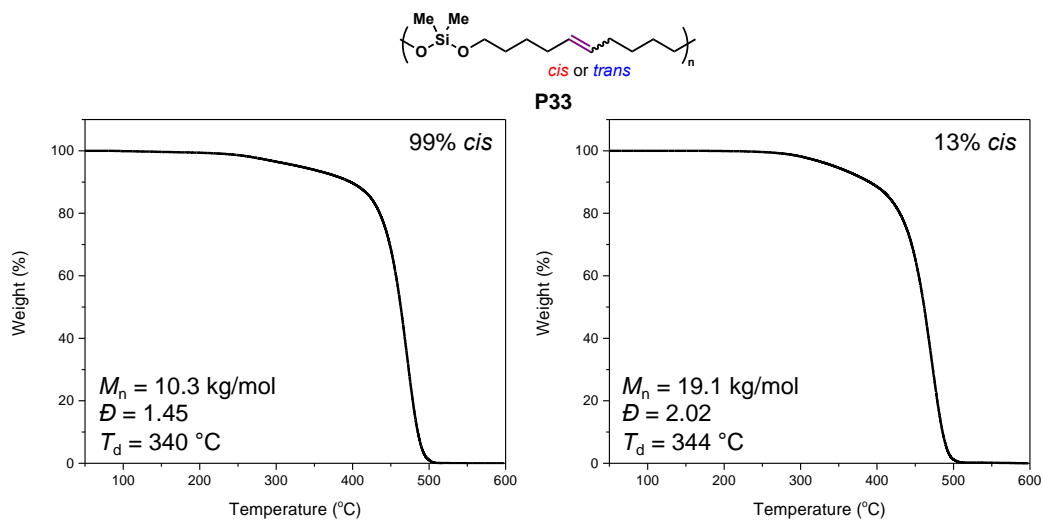
Figure V-33 TGA thermograms of 99% *cis* **P33** (left) and 13% *cis* **P33** (right).
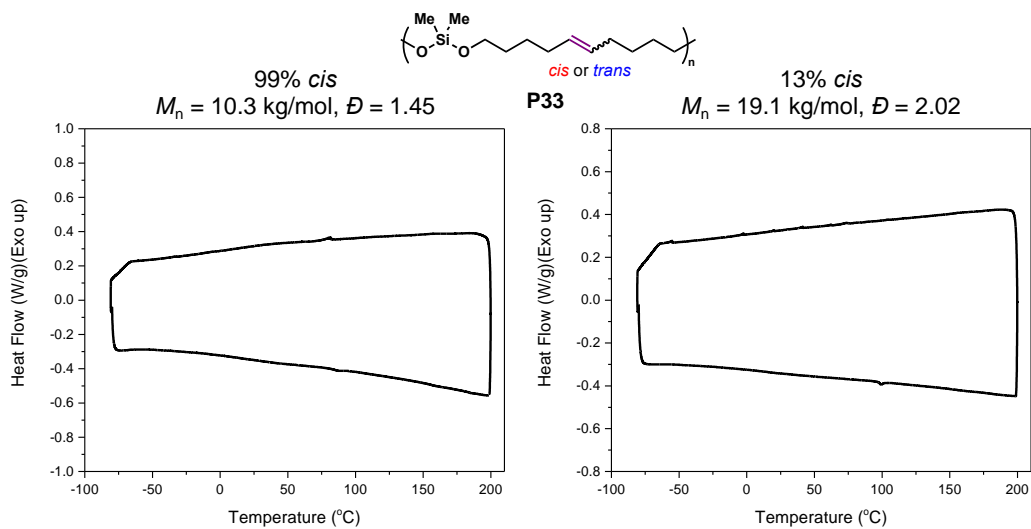
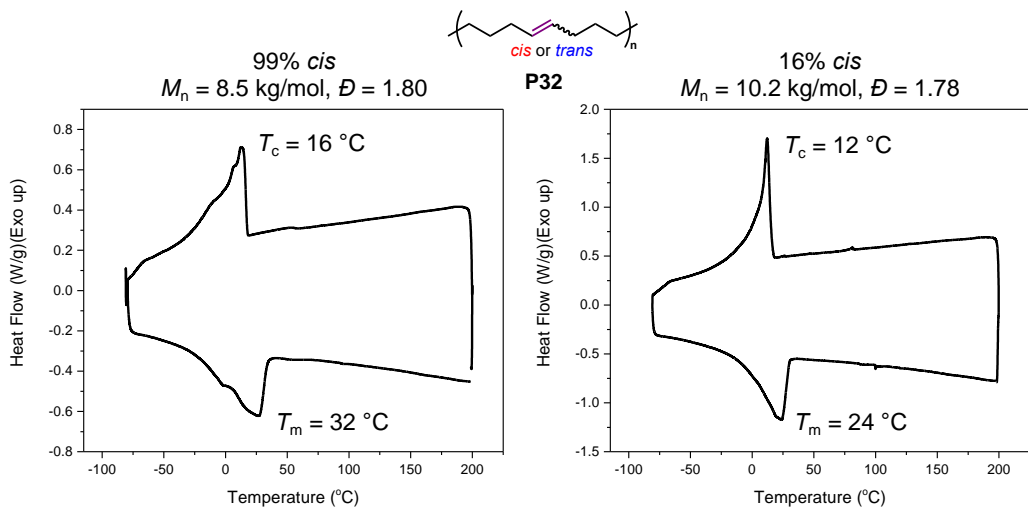**Figure V-34** DSC plots of 99% *cis* **P33** (left) and 13% *cis* **P33** (right).
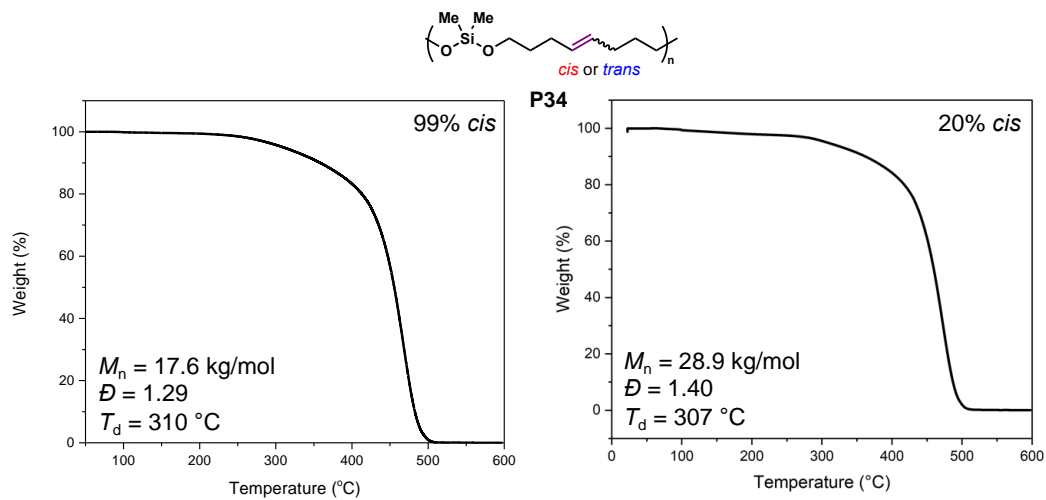
Figure V-35 TGA thermograms of 99% *cis* **P34** (left) and 20% *cis* **P34** (right).
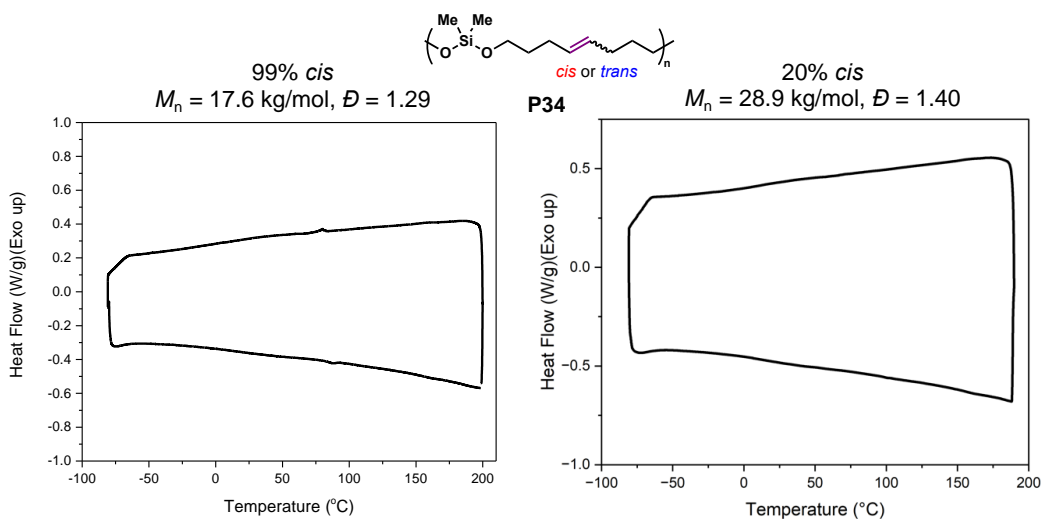
Figure V-36 DSC plots of 99% *cis* **P34** (left) and 20% *cis* **P34** (right).
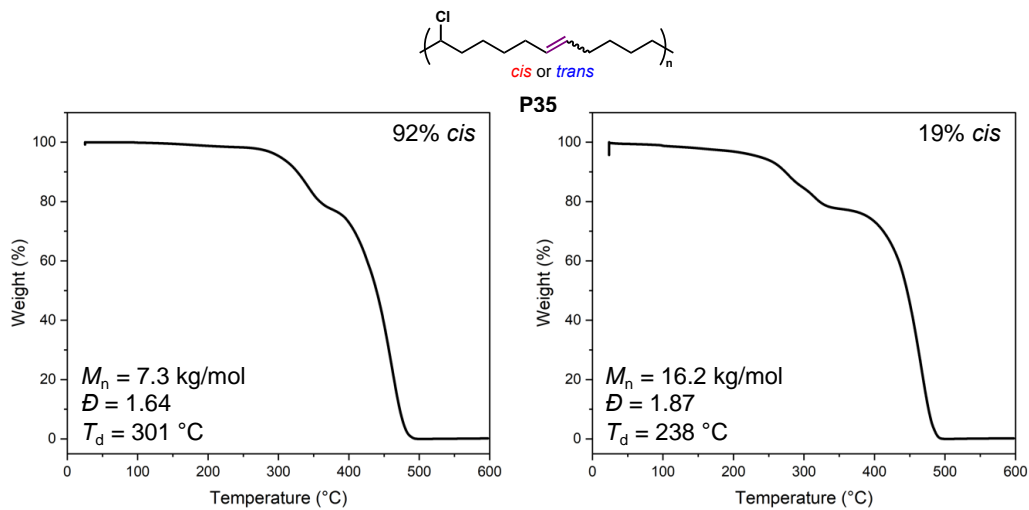
**Figure V-37** TGA thermograms of **P35** with 92% (left) and 19% (right) *cis* content.
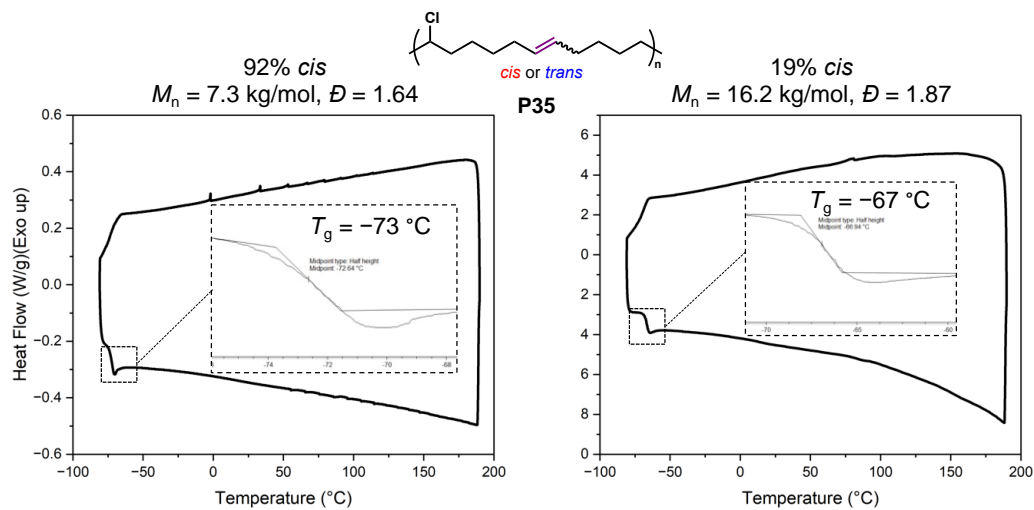
Figure V-38 DSC plots of 99% *cis* **P35** (left) and 19% *cis* **P35** (right).
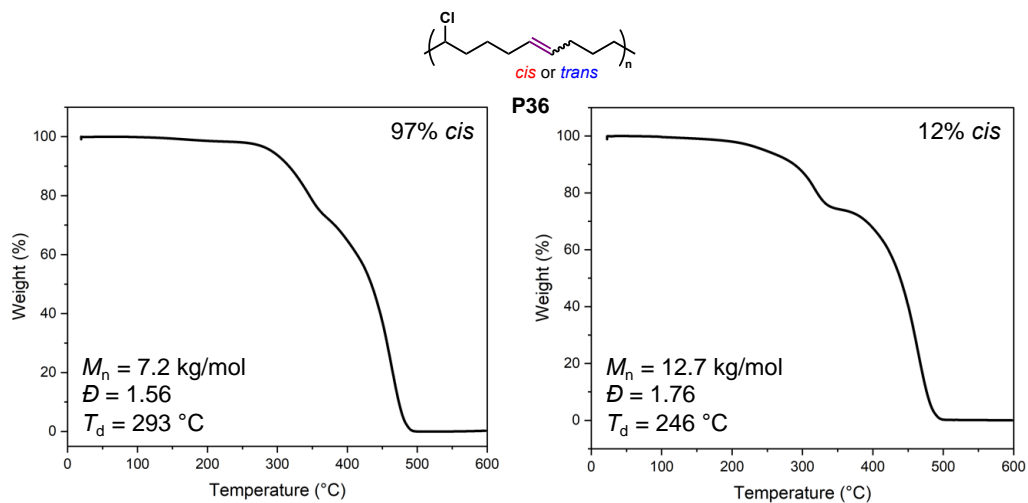
Figure V-39 TGA thermograms of **P36** with 97% (left) and 12% (right) *cis* content.
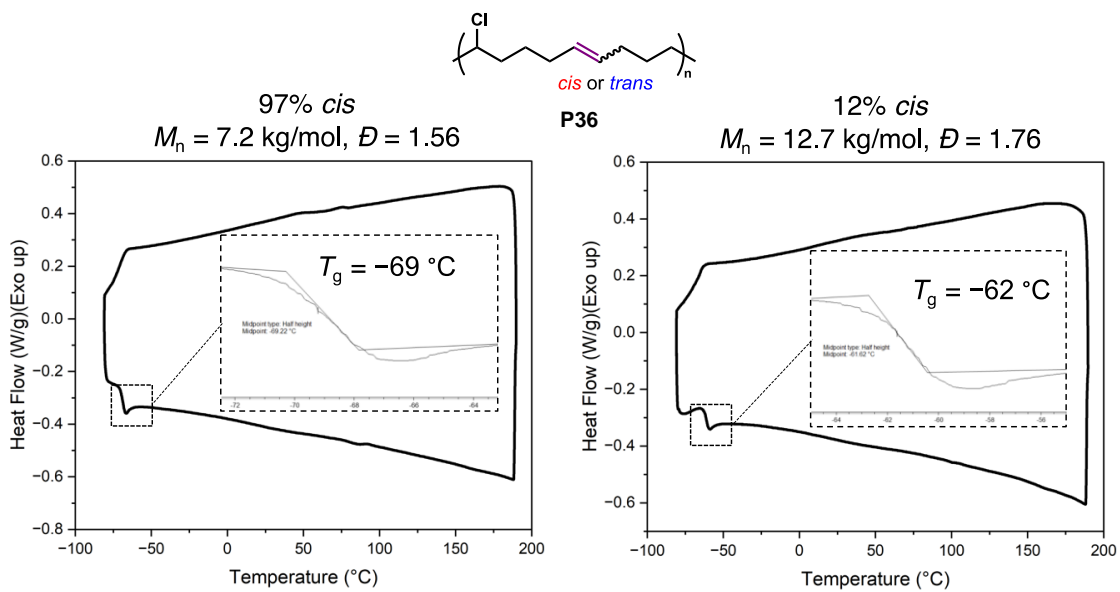
Figure V-40 DSC plots of 97% *cis* **P36** (left) and 12% *cis* **P36** (right).
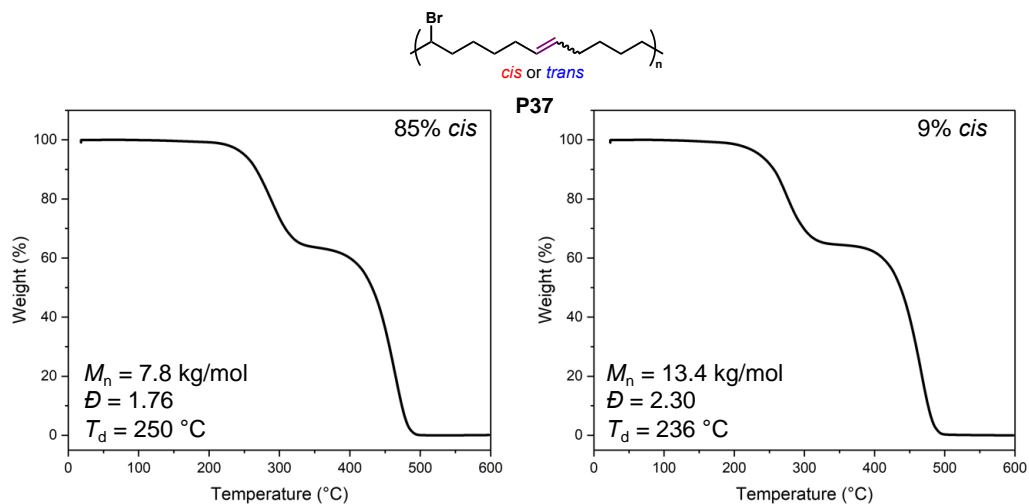
Figure V-41 TGA thermograms of **P37** with 85% (left) and 9% (right) *cis* content.
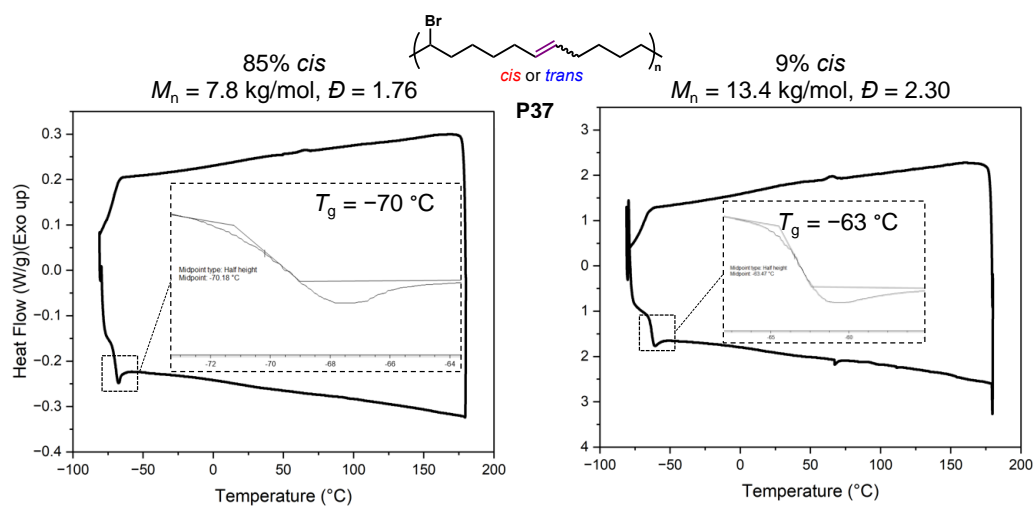
Figure V-42 DSC plots of 85% *cis* **P37** (left) and 9% *cis* **P37** (right).
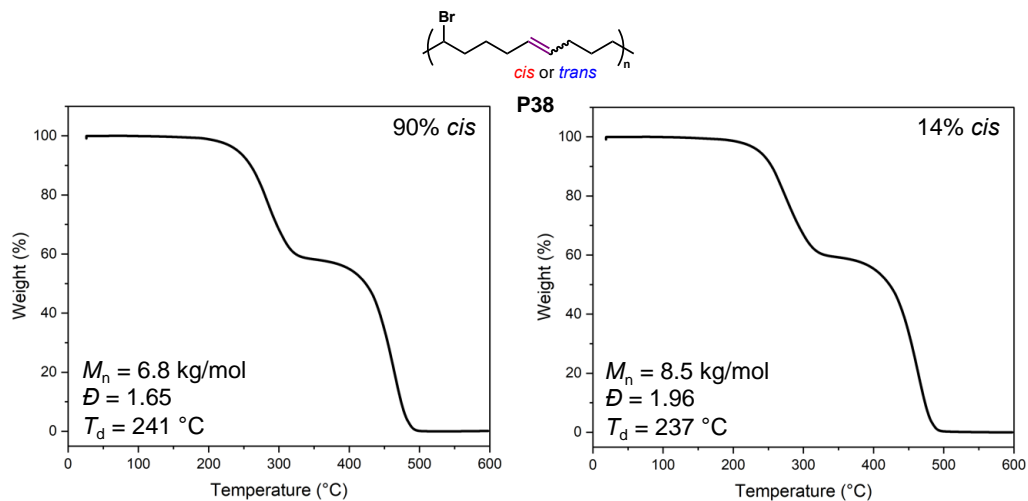
Figure V-43 TGA thermograms of **P38** with 90% (left) and 14% (right) *cis* content.

Figure V-44 DSC thermograms of **P38** with 90% and 14% *cis* content.

Figure V-45 TGA (left) and DSC (right) thermograms of **P42**.
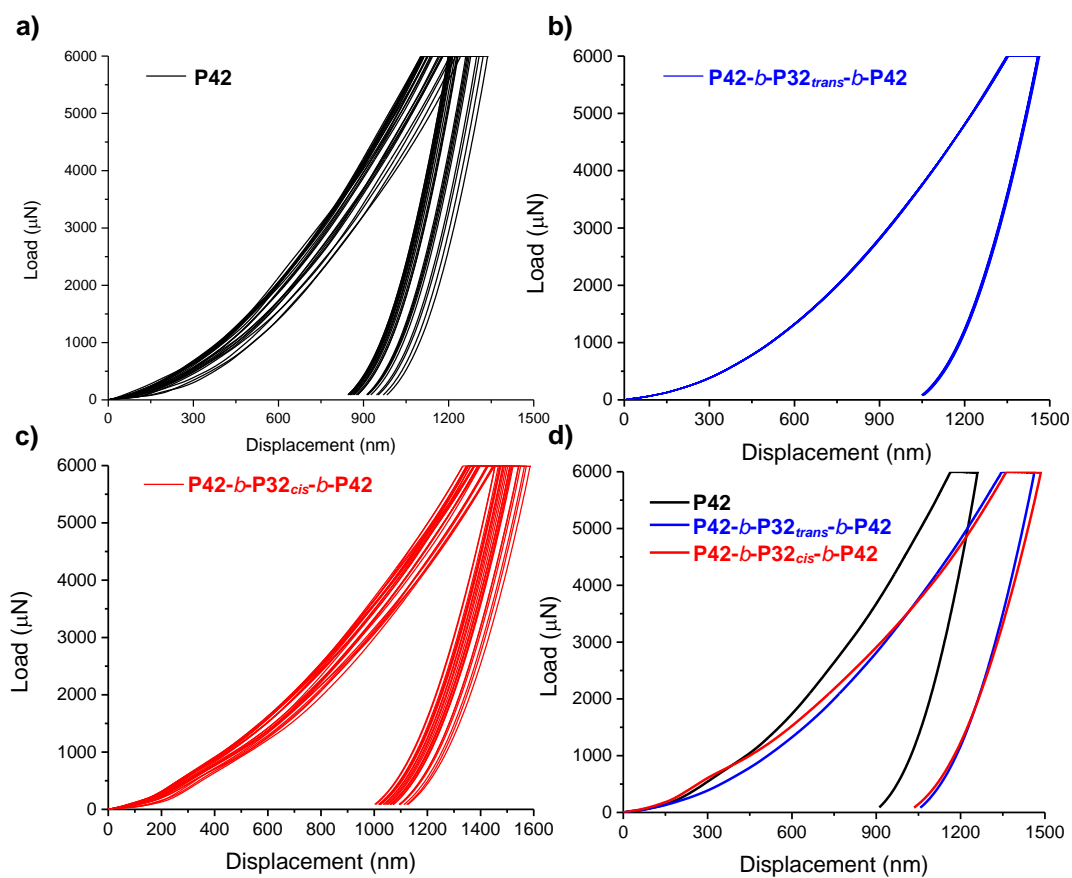
Figure V-46 Load-displacement curves from 25 indents of a) **P42**, b) **P42**-*b*-**P32**$_{trans}$-*b*-**P42**, and c) **P42**-*b*-**P32**$_{cis}$-*b*-**P42** and d) representative comparison of load-displacement curves of polymers from one indent.
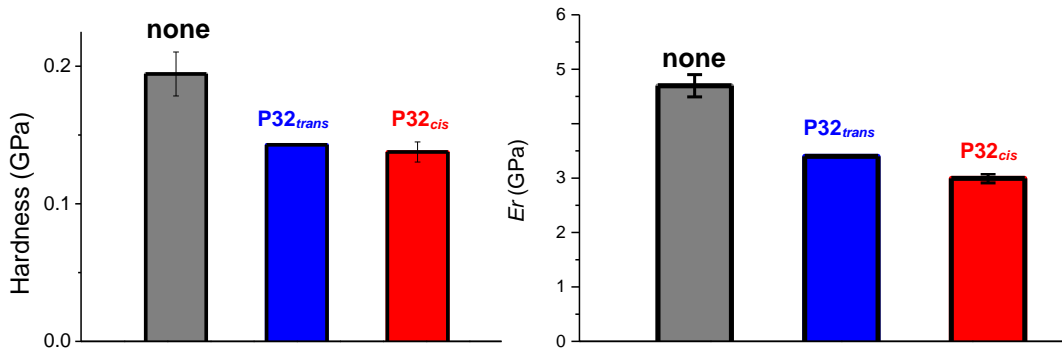
Figure V-47 (Left) Bar graph representing hardness of **P42** (gray, 0.19 ± 0.02 GPA), **P42**-*b*-**P32**$_{trans}$-*b*-**P42** (blue, 0.1429 ± 0.0004 GPA), and **P42**-*b*-**P32**$_{cis}$-*b*-**P42** (red, 0.138 ± 0.007 GPA) and (right) bar graph representing E_r of **P42** (gray, 4.7 ± 0.2 GPA), **P42**-*b*-**P32**$_{trans}$-*b*-**P42** (blue, 3.400 ± 0.007 GPA), and **P42**-*b*-**P32**$_{cis}$-*b*-**P42** (red, 2.99 ± 0.08 GPA).
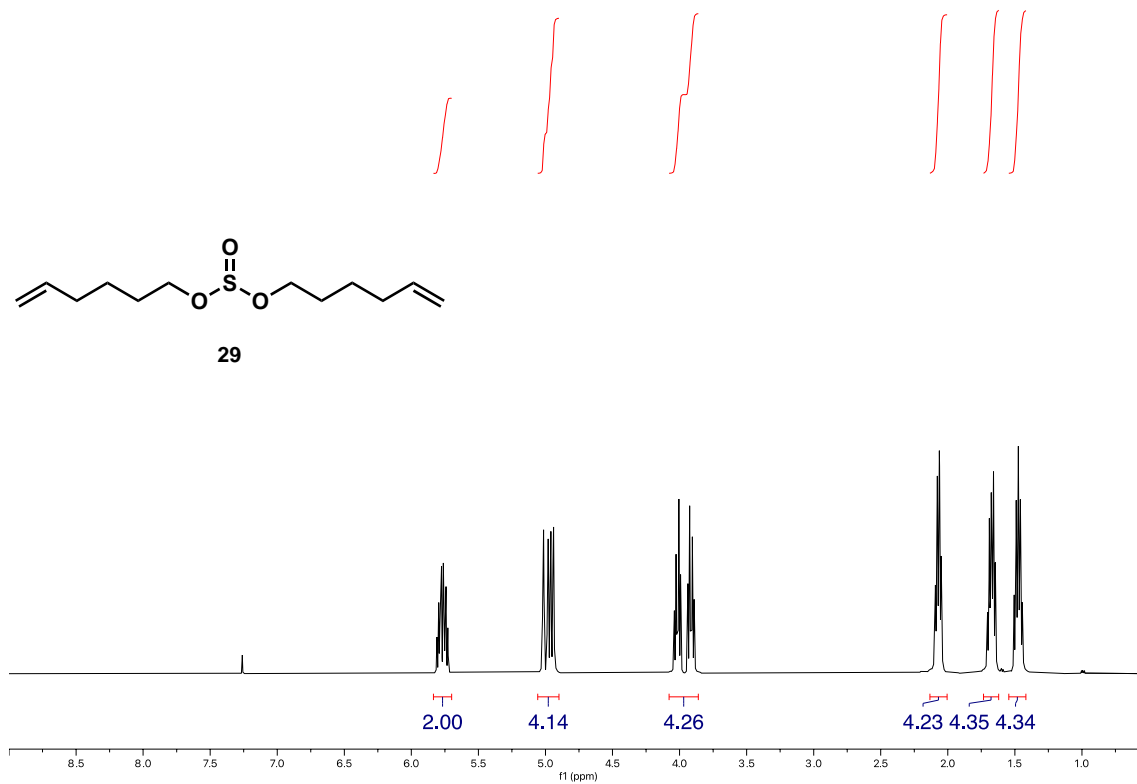
Figure V-48 ^{1}H NMR (500 MHz, CDCl$_3$) spectrum of compound **29**.
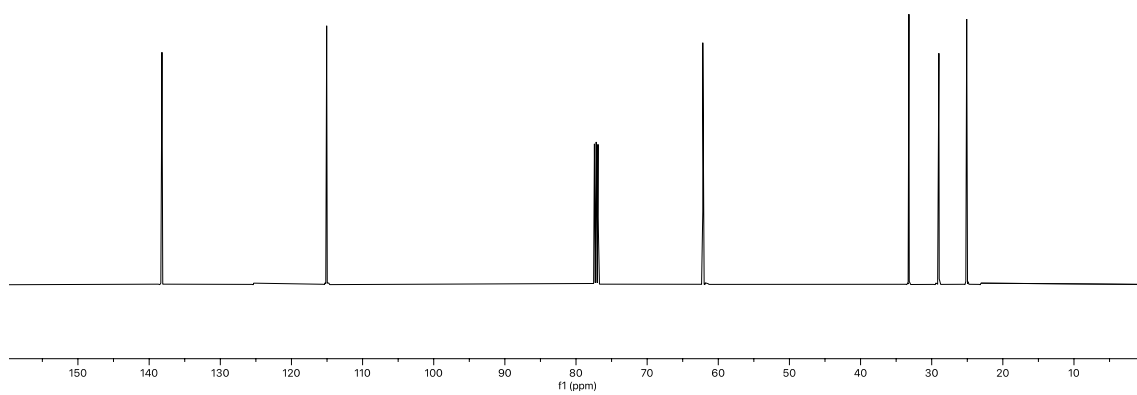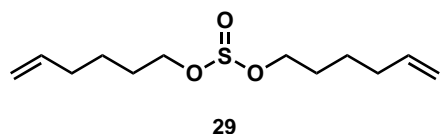
Figure V-49 ^{13}C NMR (125 MHz, CDCl$_3$) spectrum of compound **29**.
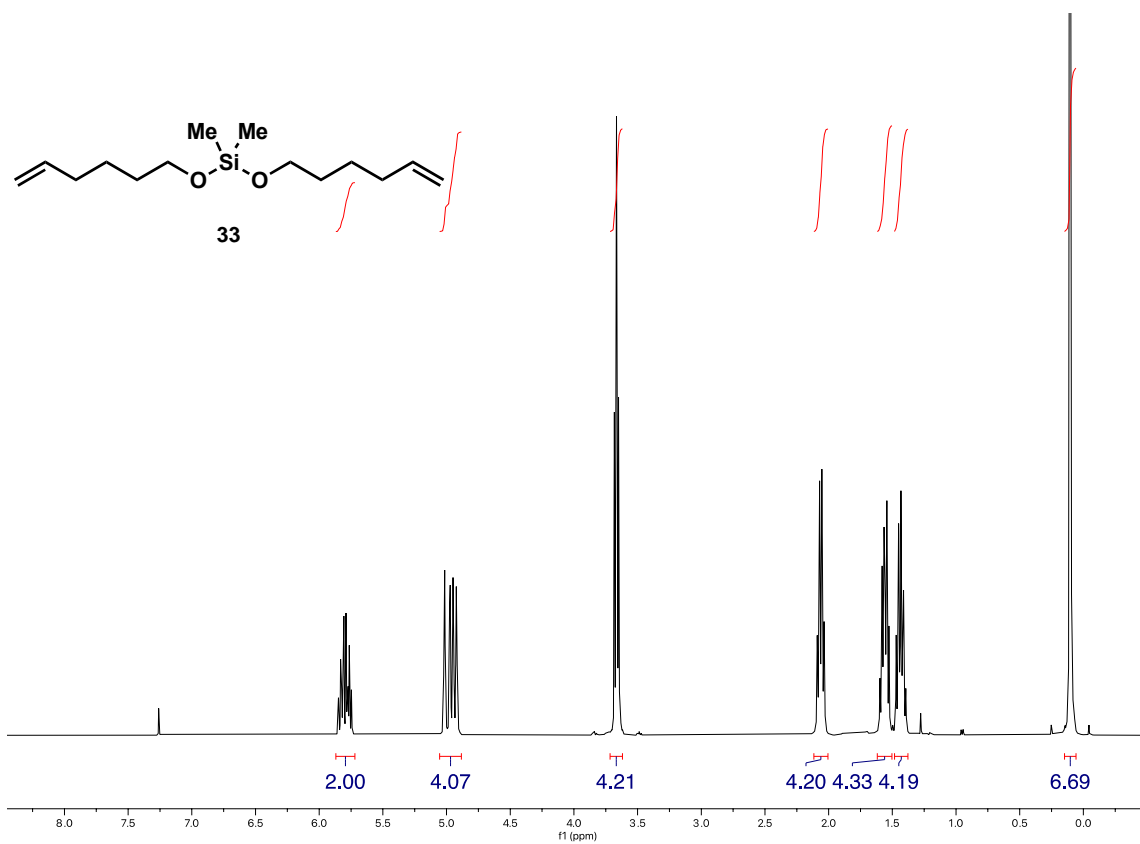
Figure V-50 ^{1}H NMR (400 MHz, CDCl$_3$) spectrum of compound **33**.
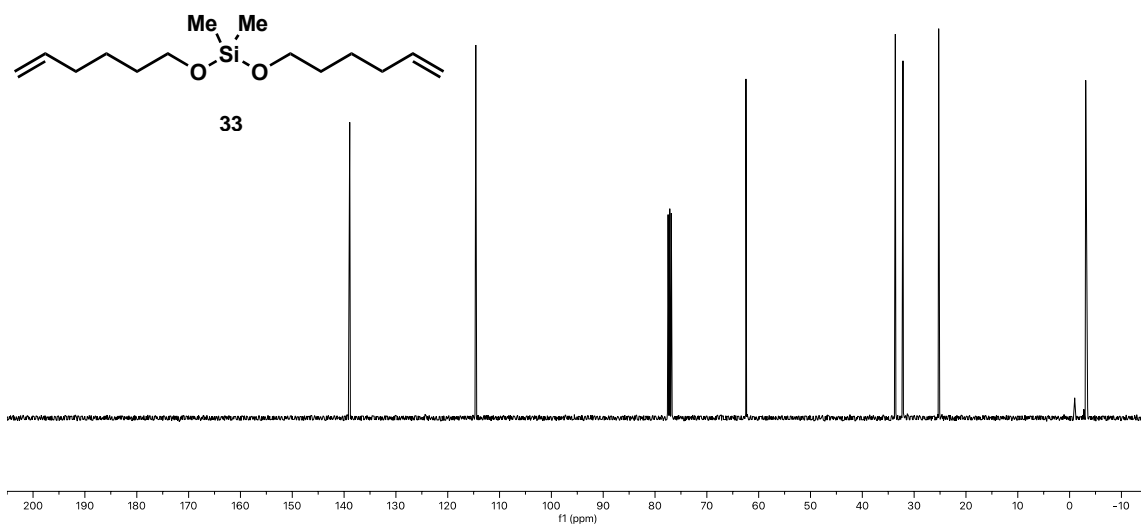
Figure V-51 ^{13}C NMR (101 MHz, CDCl$_3$) spectrum of compound **33**.
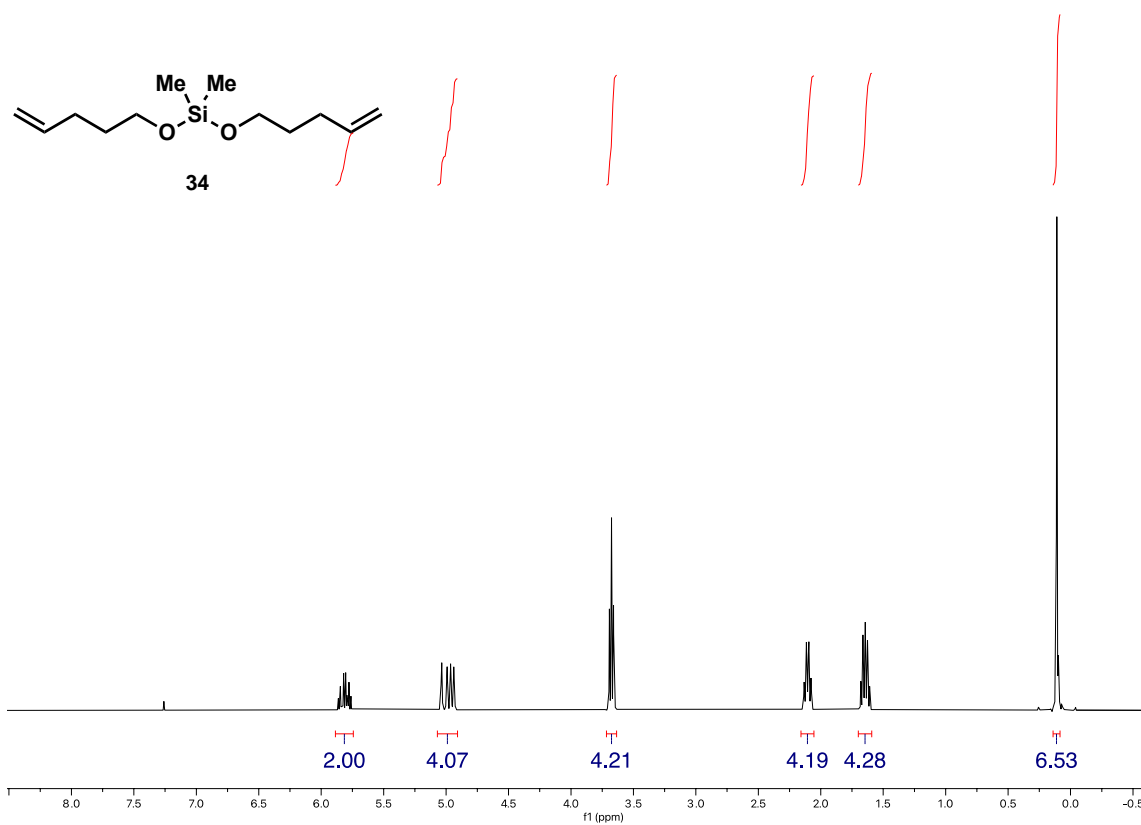
Figure V-52 ^{1}H NMR (400 MHz, CDCl$_3$) spectrum of compound **34**.
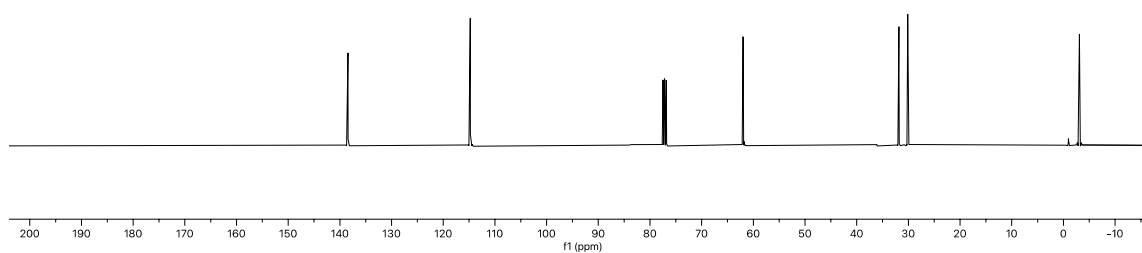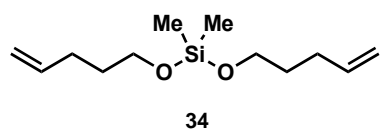
Figure V-53 ^{13}C NMR (101 MHz, CDCl$_3$) spectrum of compound **34**.
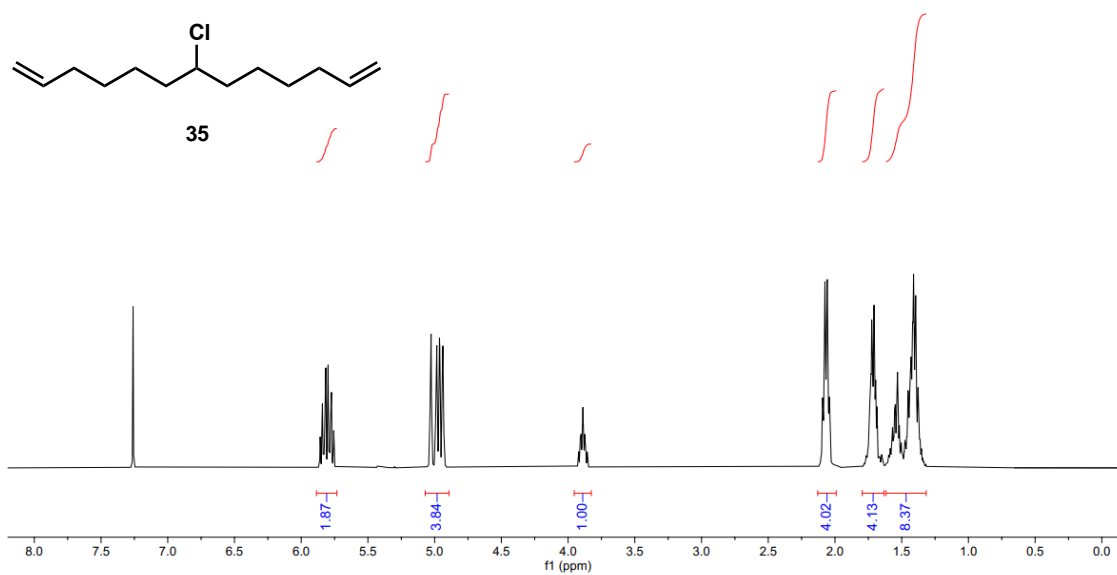
Figure V-54 ^{1}H NMR (400 MHz, CDCl$_3$) spectrum of compound **35**.
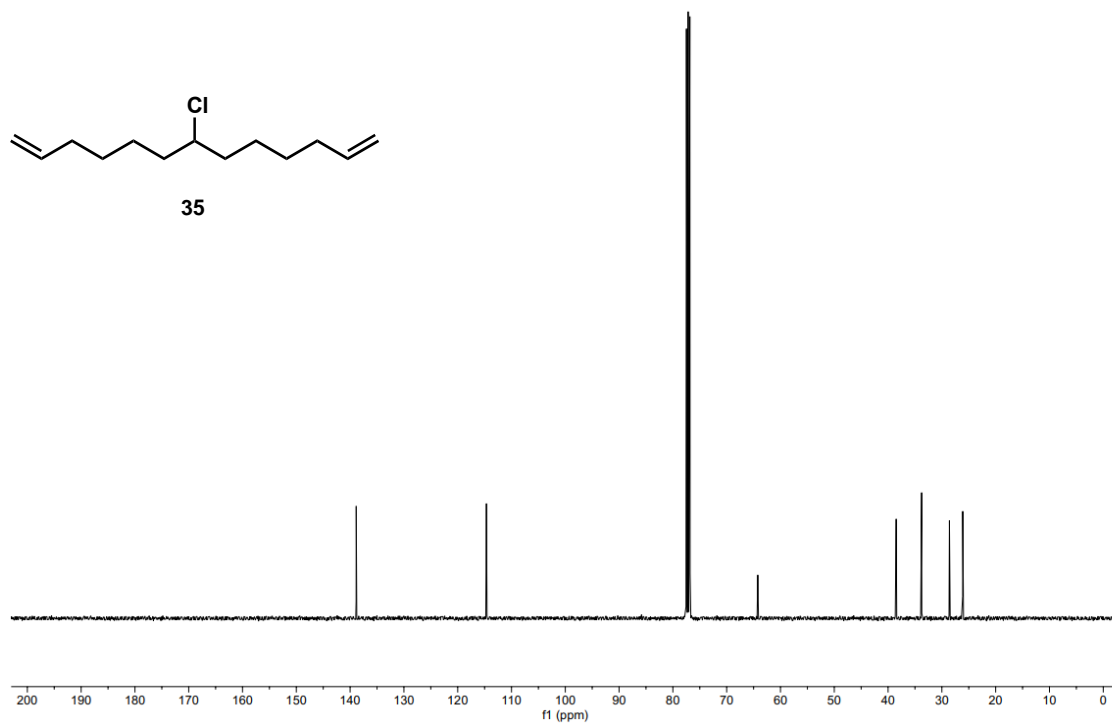
Figure V-55 ^{13}C NMR (101 MHz, CDCl$_3$) spectrum of compound **35**.
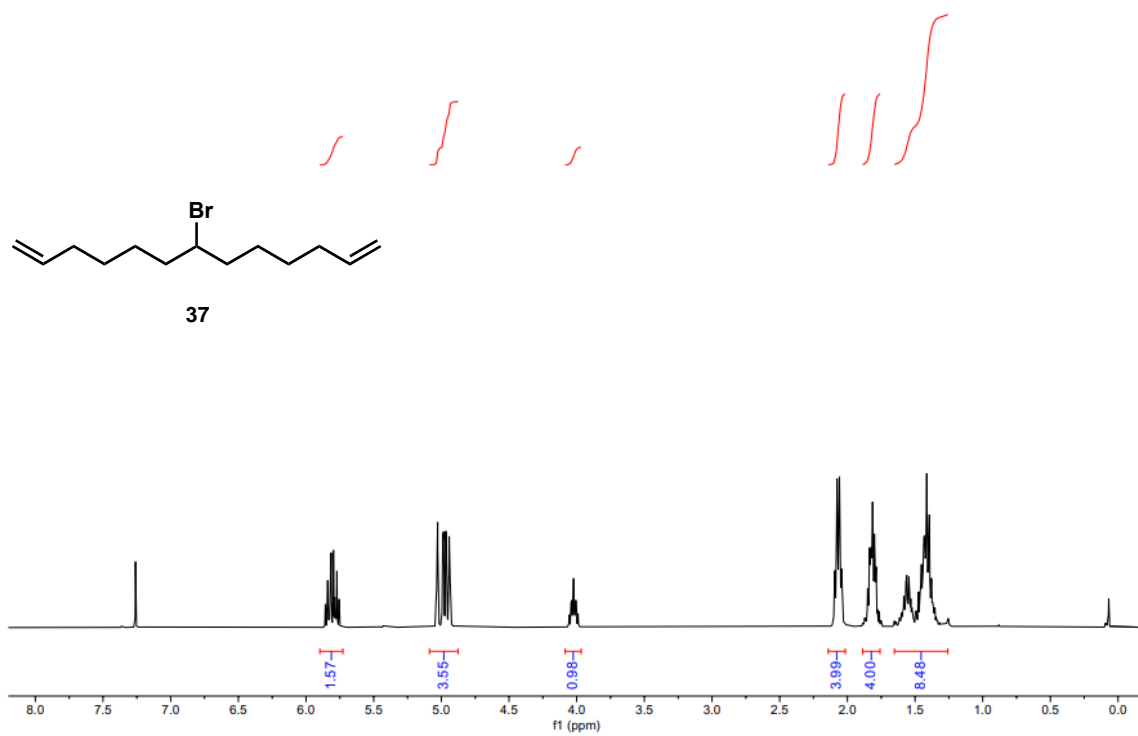
Figure V-56 ^{1}H NMR (400 MHz, CDCl$_3$) spectrum of compound **37**.

Figure V-57 ^{13}C NMR (101 MHz, CDCl$_3$) spectrum of compound **37**.
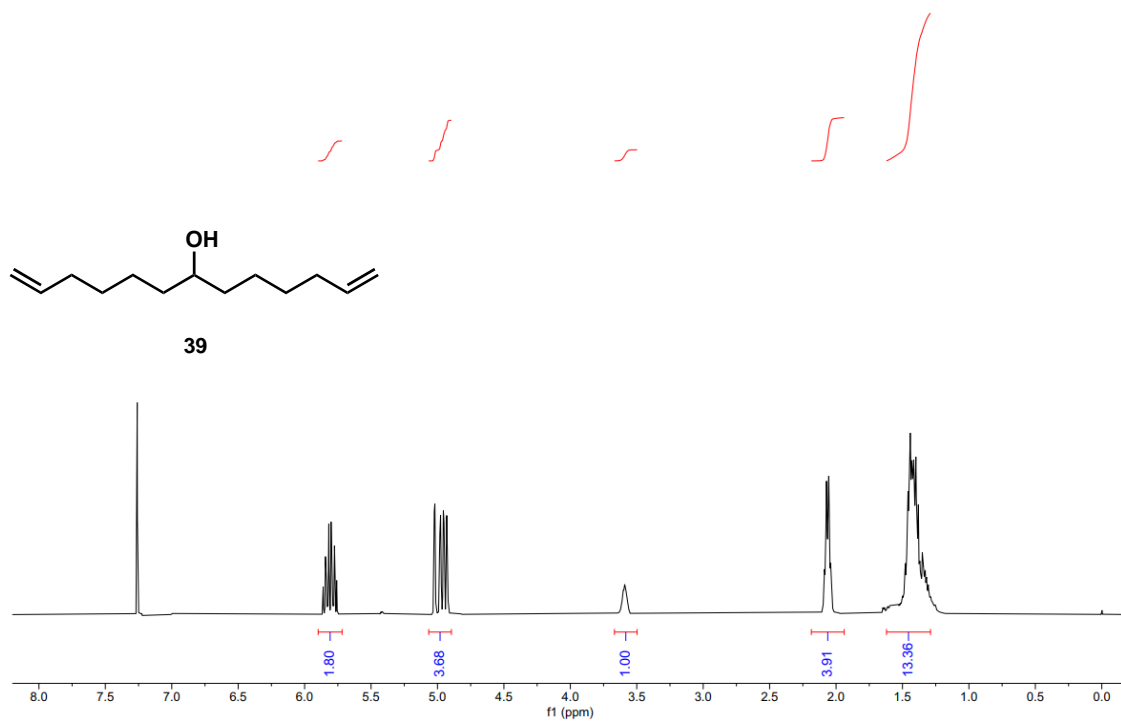
Figure V-58 ^{1}H NMR (400 MHz, CDCl$_3$) spectrum of compound **39**.
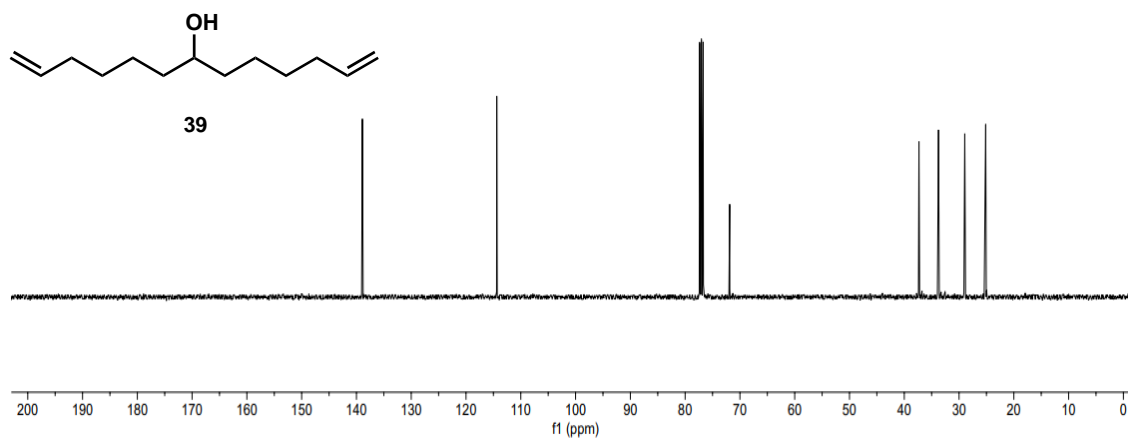
Figure V-59 ^{13}C NMR (101 MHz, CDCl$_3$) spectrum of compound **39**.
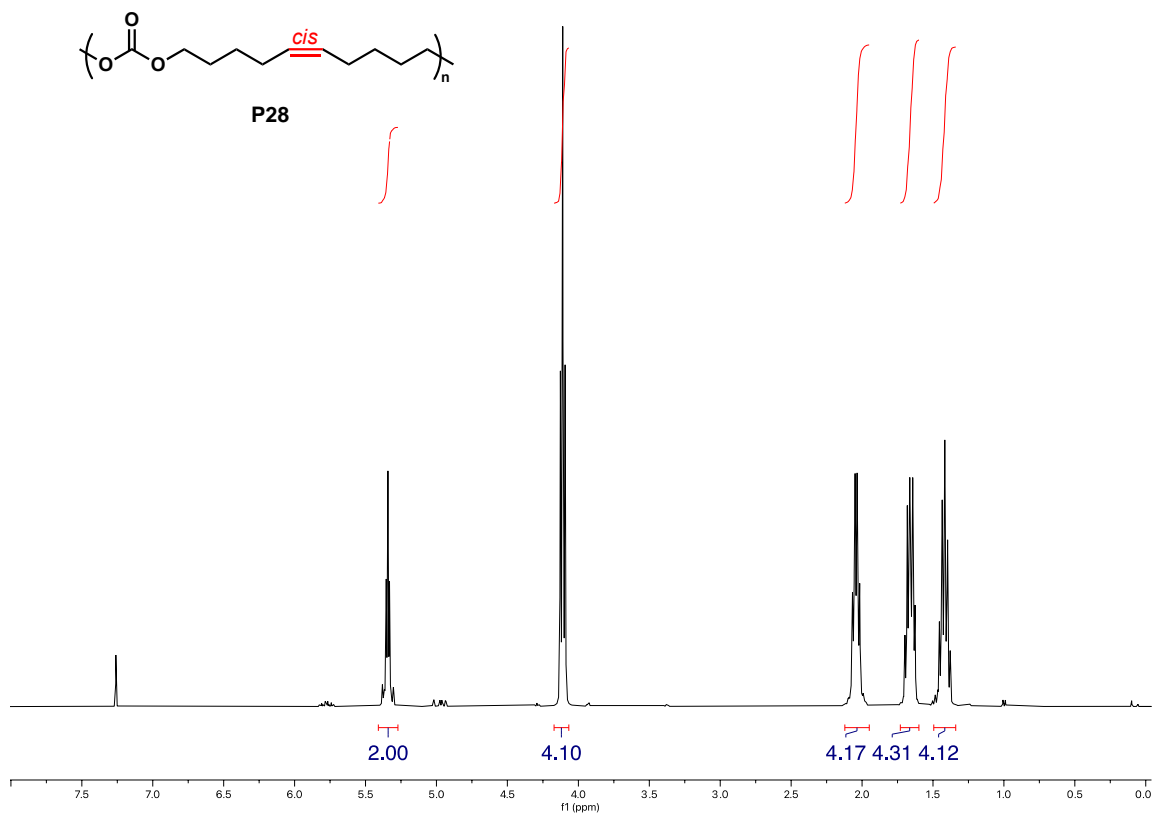
Figure V-60 ^{1}H NMR (400 MHz, CDCl$_3$) spectrum of *cis*-rich **P28**.
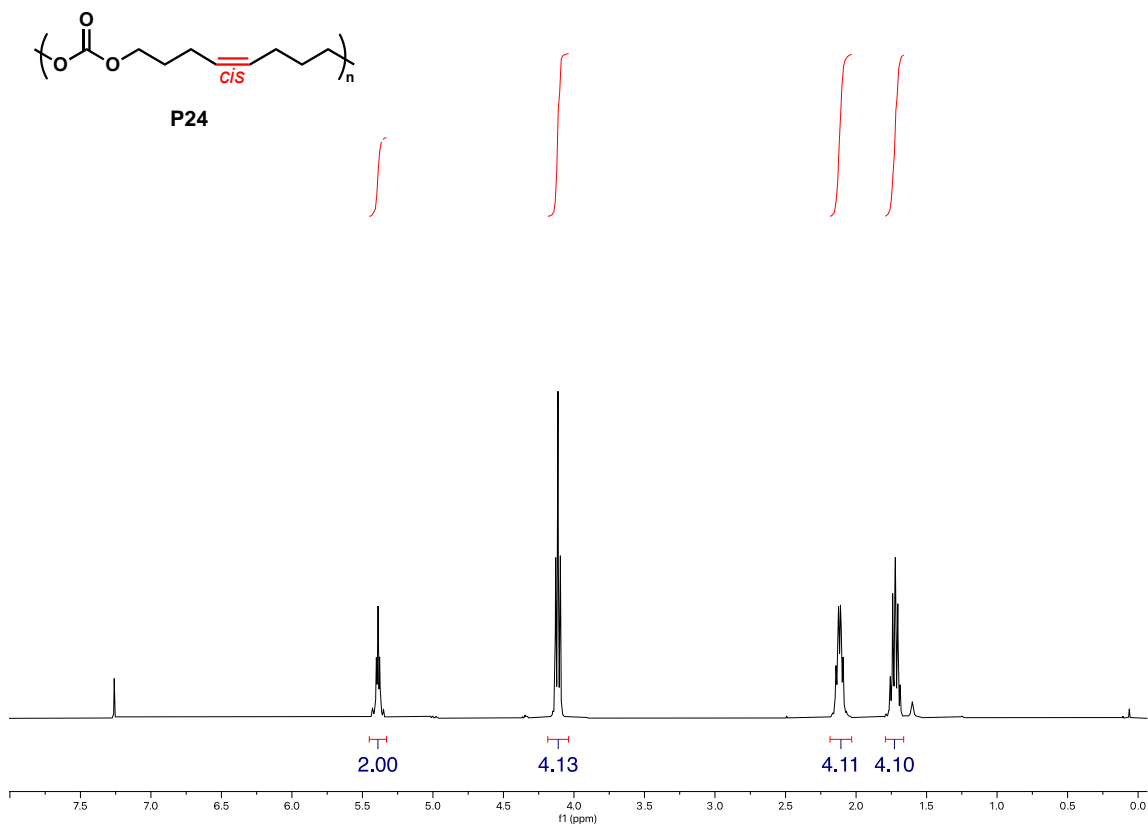
Figure V-61 ^{1}H NMR (400 MHz, CDCl$_3$) spectrum of *cis*-rich **P24**.
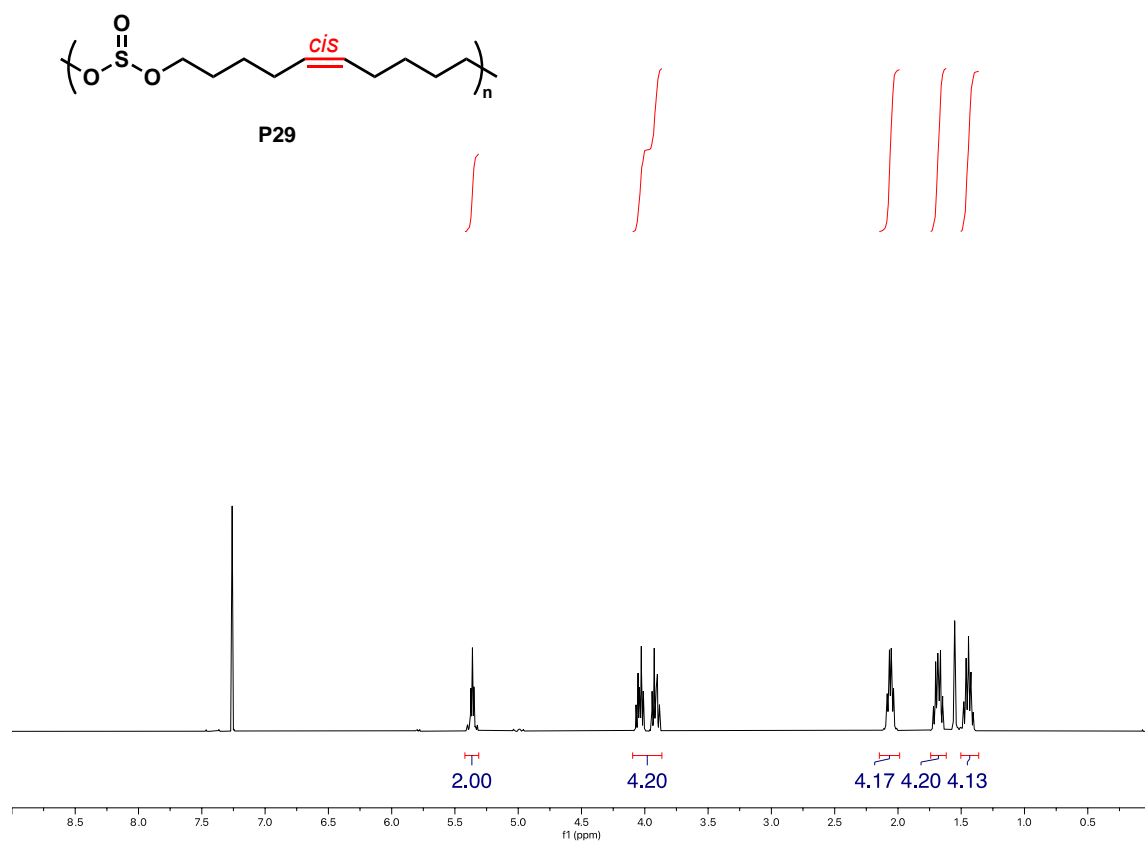
Figure V-62 ^{1}H NMR (400 MHz, CDCl3) spectrum of *cis*-rich **P29**.
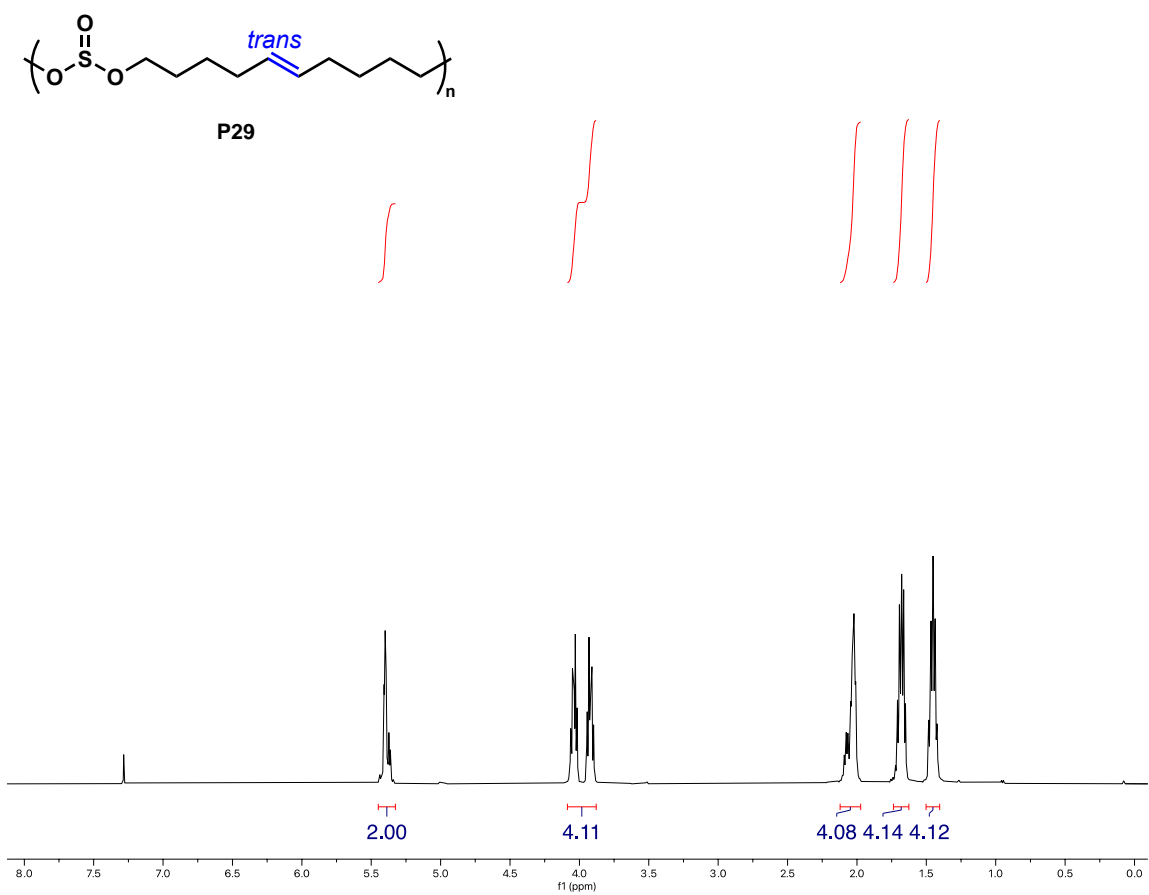
Figure V-63 ^{1}H NMR (400 MHz, CDCl$_3$) spectrum of *trans*-rich **P29**.

319
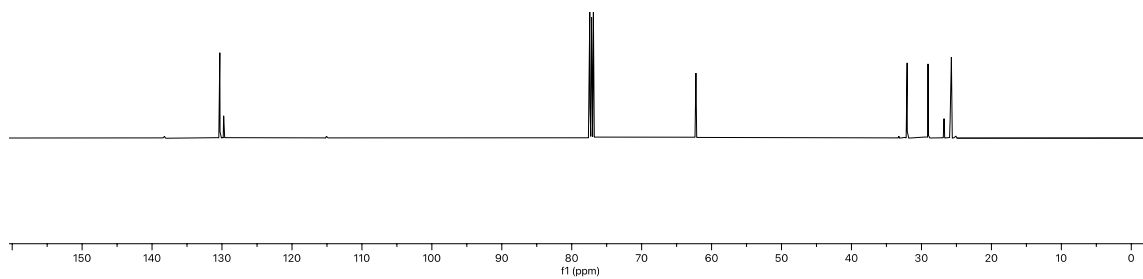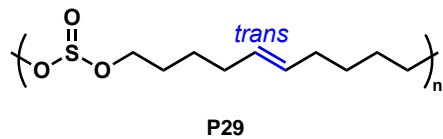
Figure V-64 ^{13}C NMR (125 MHz, CDCl$_3$) spectrum of *trans*-rich **P29**.
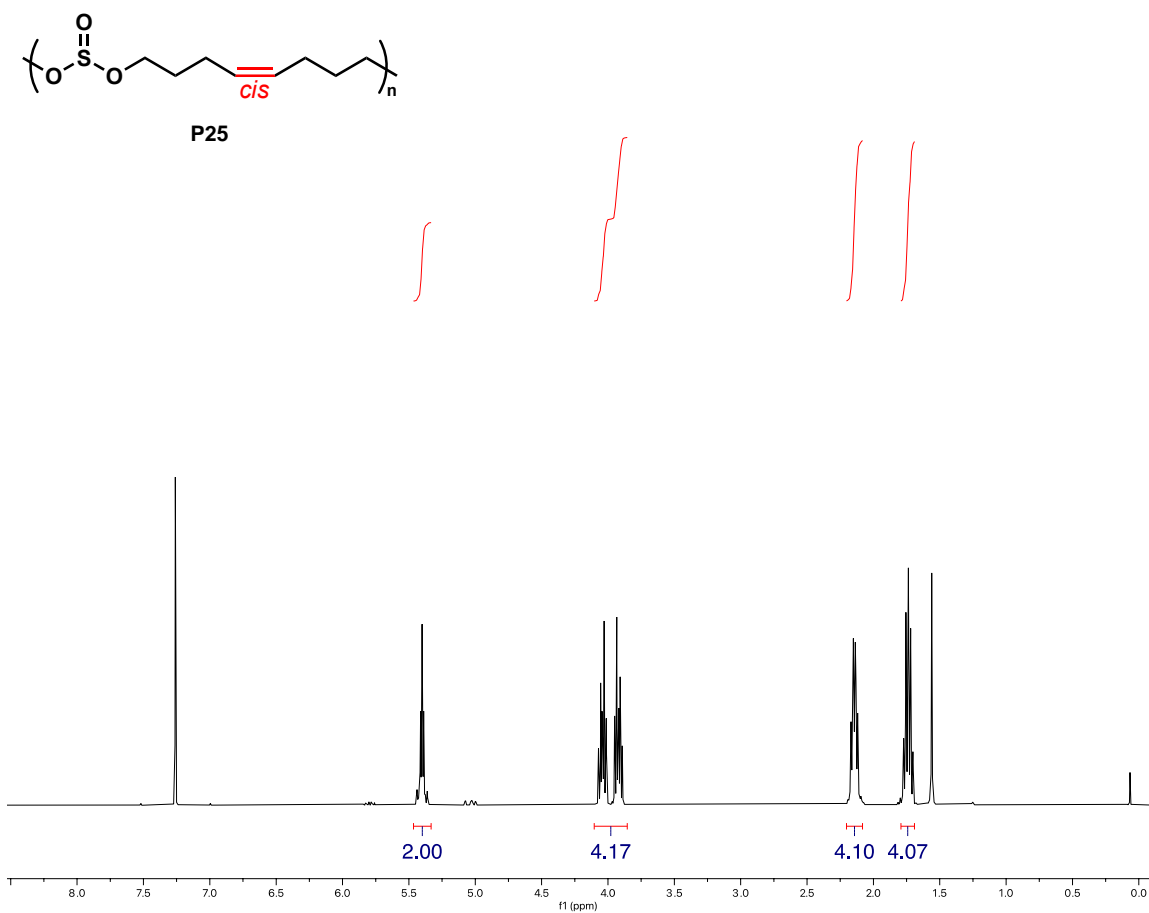
Figure V-65 ^{1}H NMR (400 MHz, CDCl$_3$) spectrum of *cis*-rich **P25**.
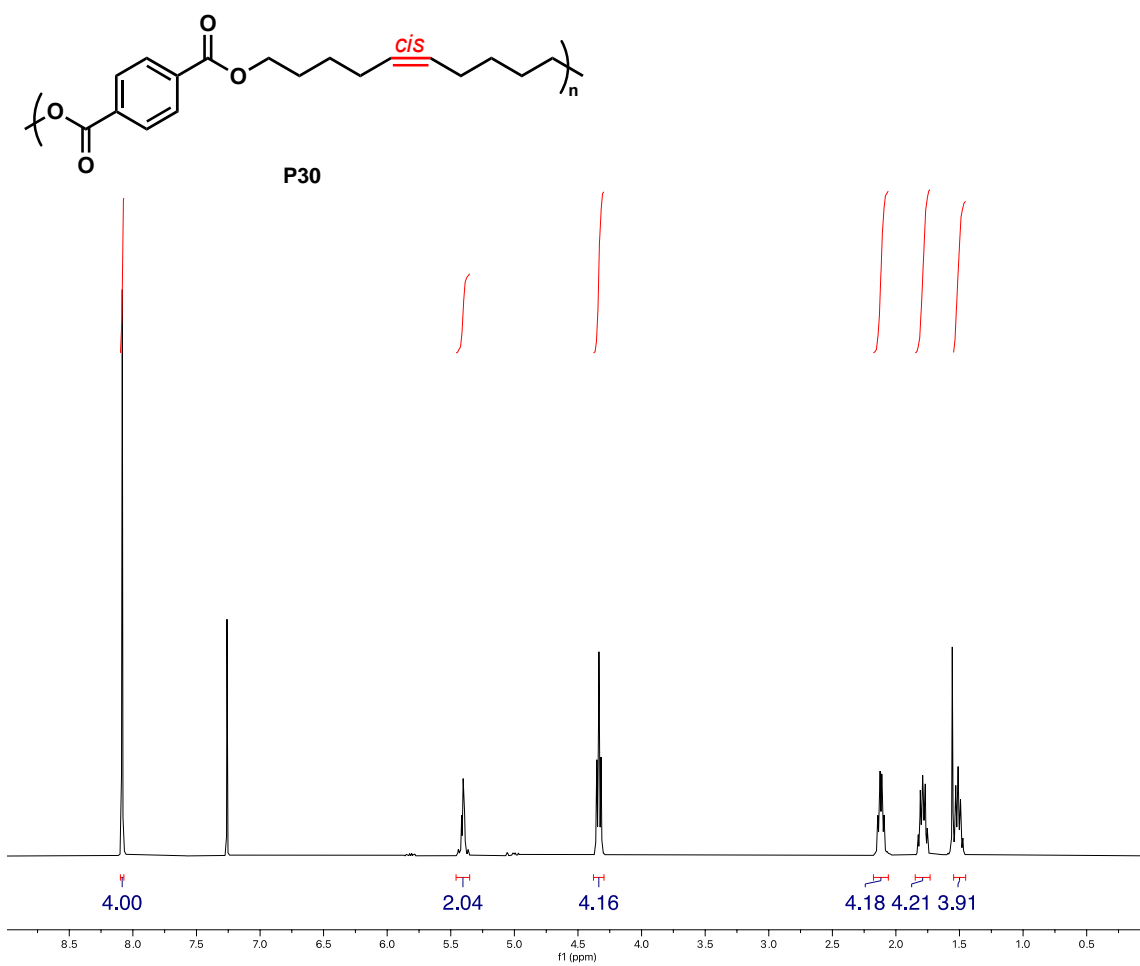
Figure V-66 ^{1}H NMR (400 MHz, CDCl$_3$) spectrum of *cis*-rich **P30**.
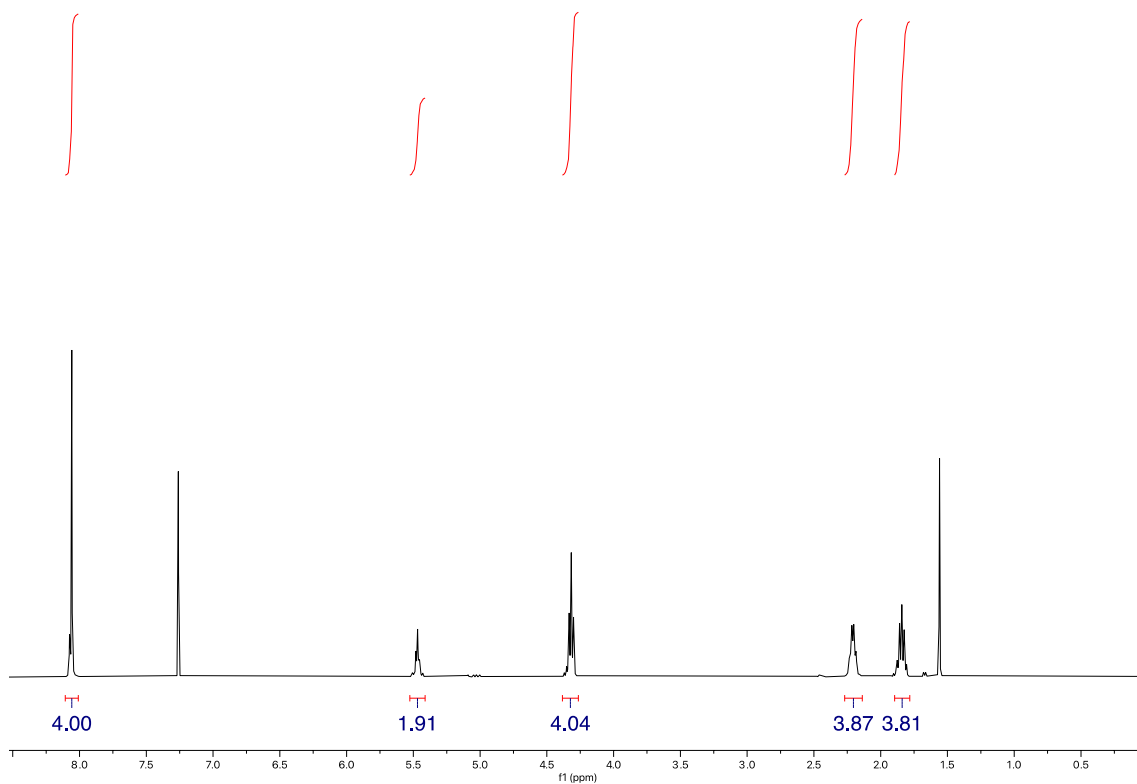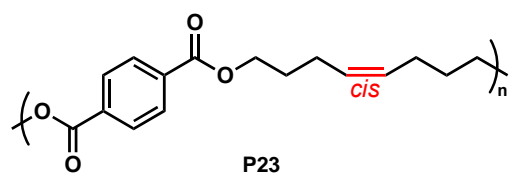
Figure V-67 ¹H NMR (400 MHz, CDCl₃) spectrum of *cis*-rich **P23**.
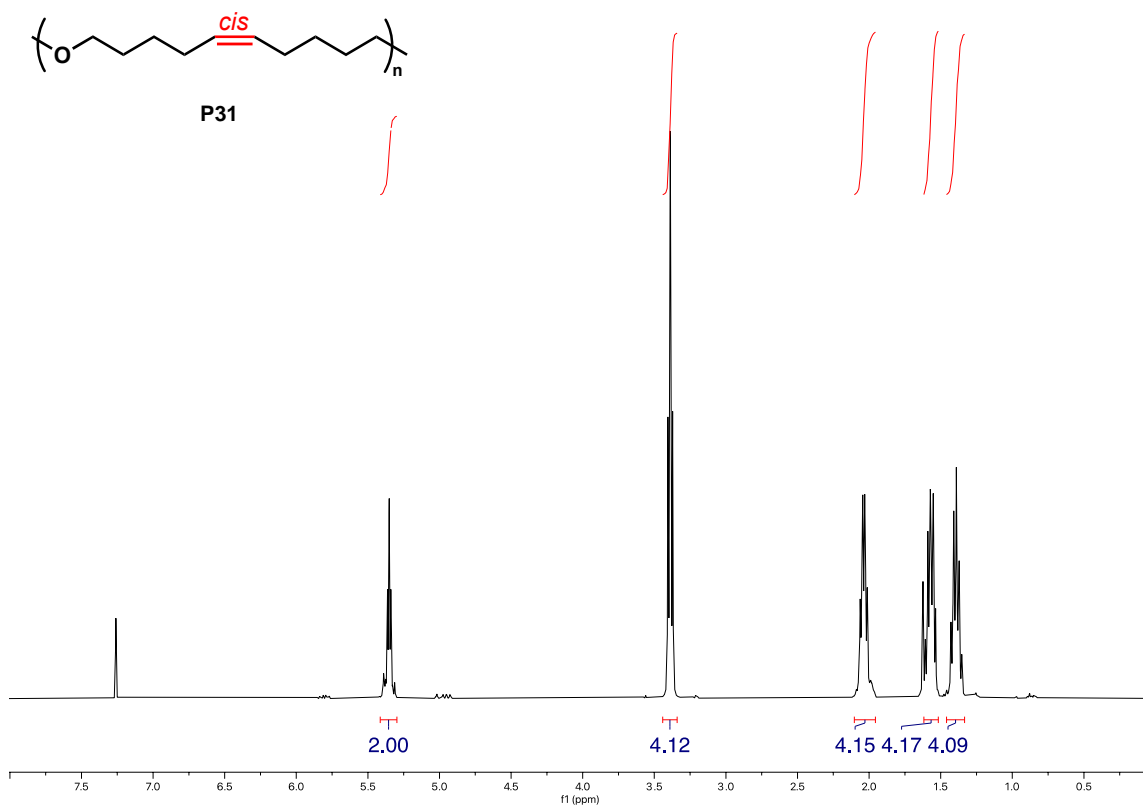
Figure V-68 ^{1}H NMR (400 MHz, CDCl$_3$) spectrum of *cis*-rich **P31**.
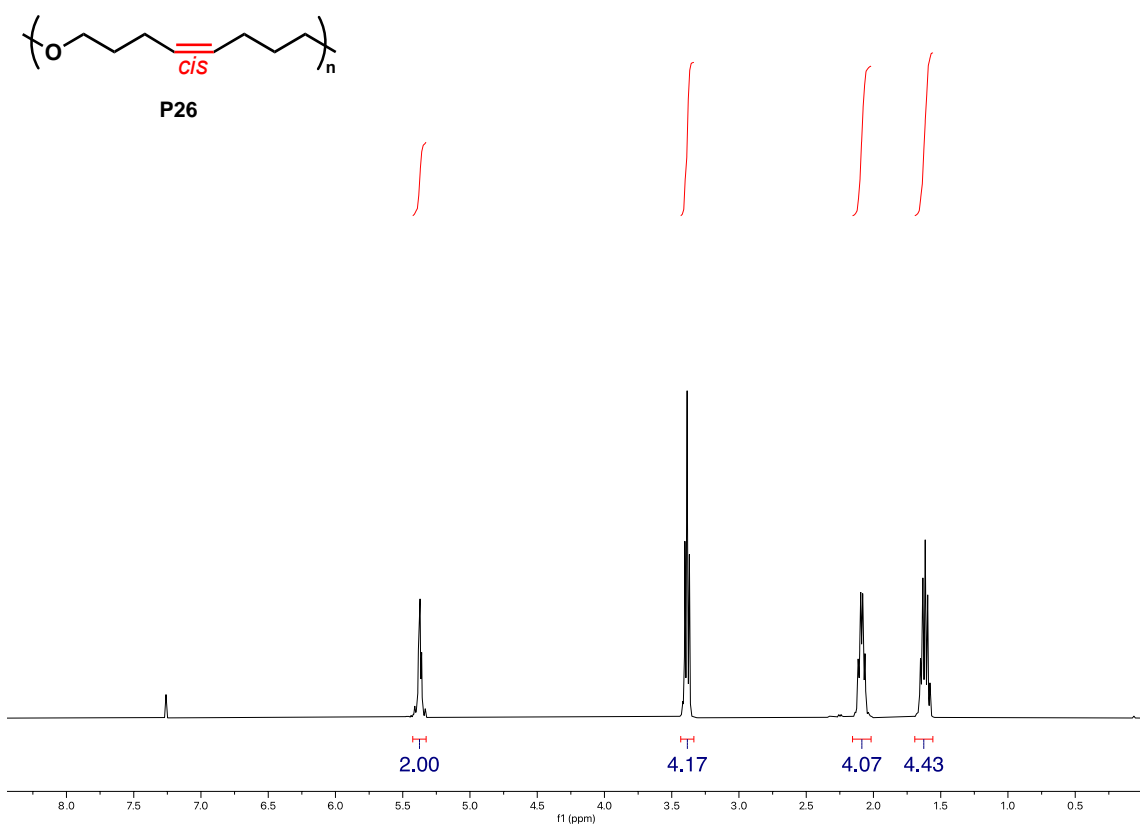
Figure V-69 ^{1}H NMR (400 MHz, CDCl$_3$) spectrum of *cis*-rich **P26**.
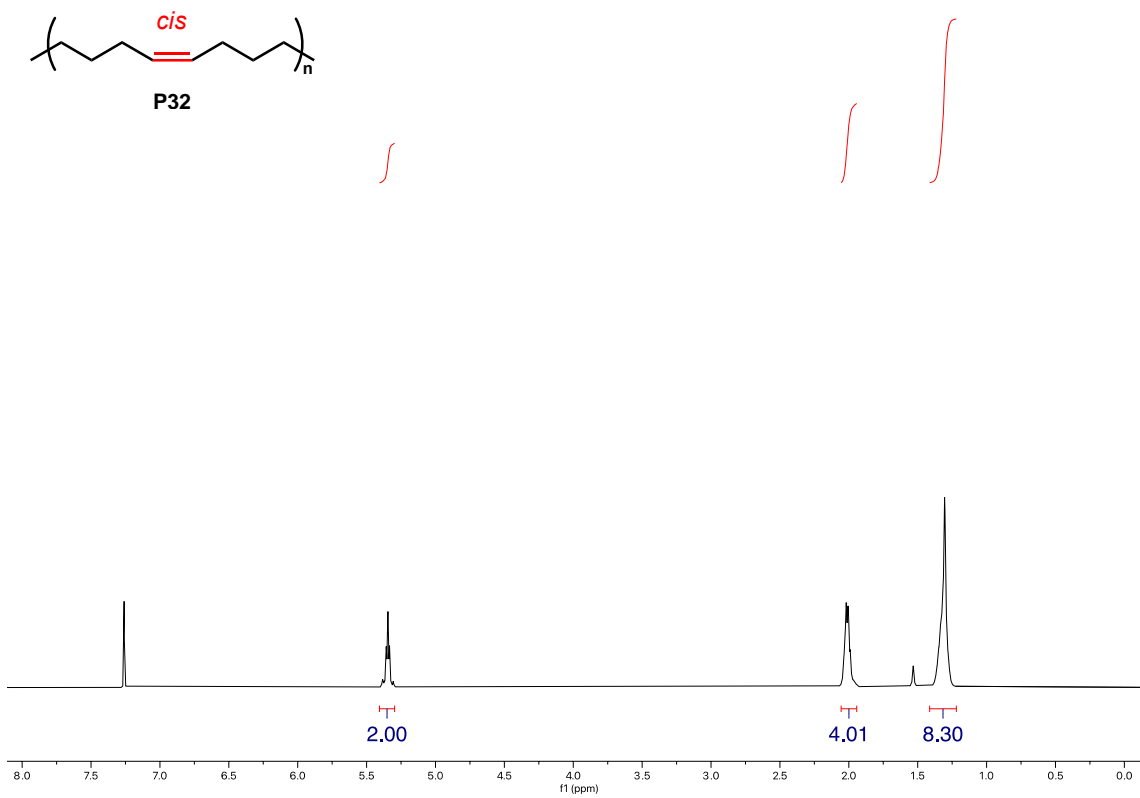
Figure V-70 ^{1}H NMR (400 MHz, CDCl$_3$) spectrum of *cis*-rich **P32**.
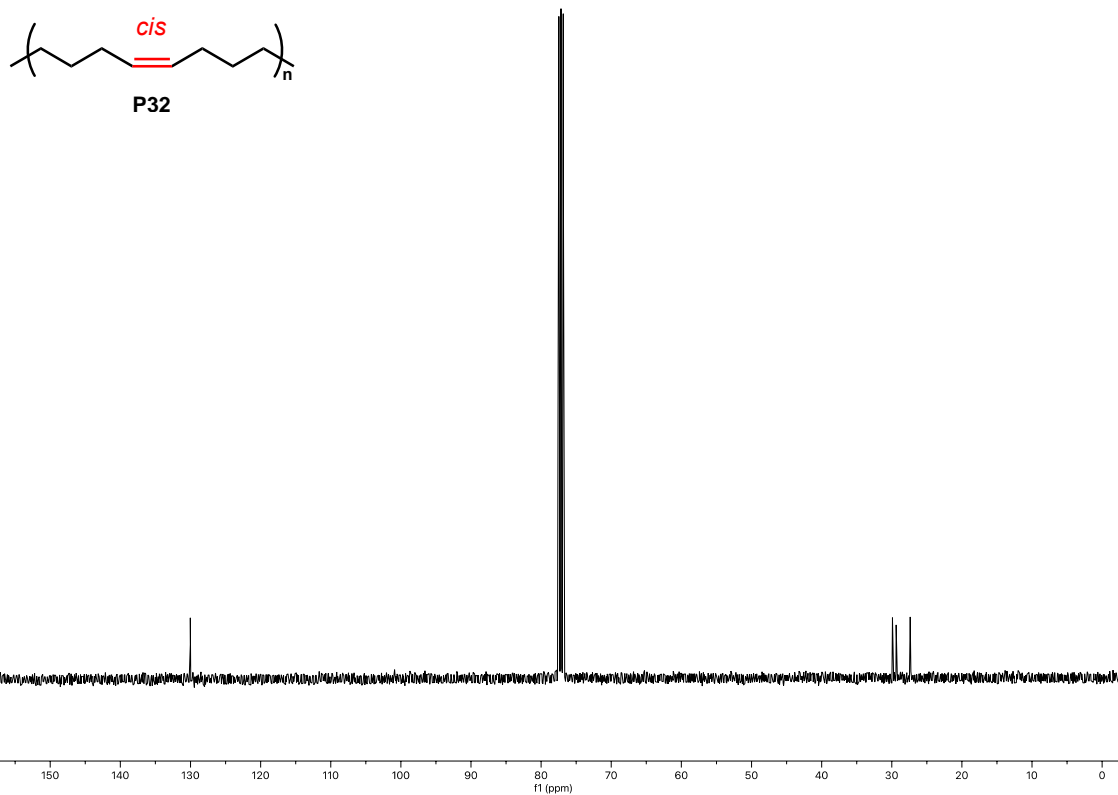
Figure V-71 ^{13}C NMR (101 MHz, CDCl$_3$) spectrum of *cis*-rich **P32**.
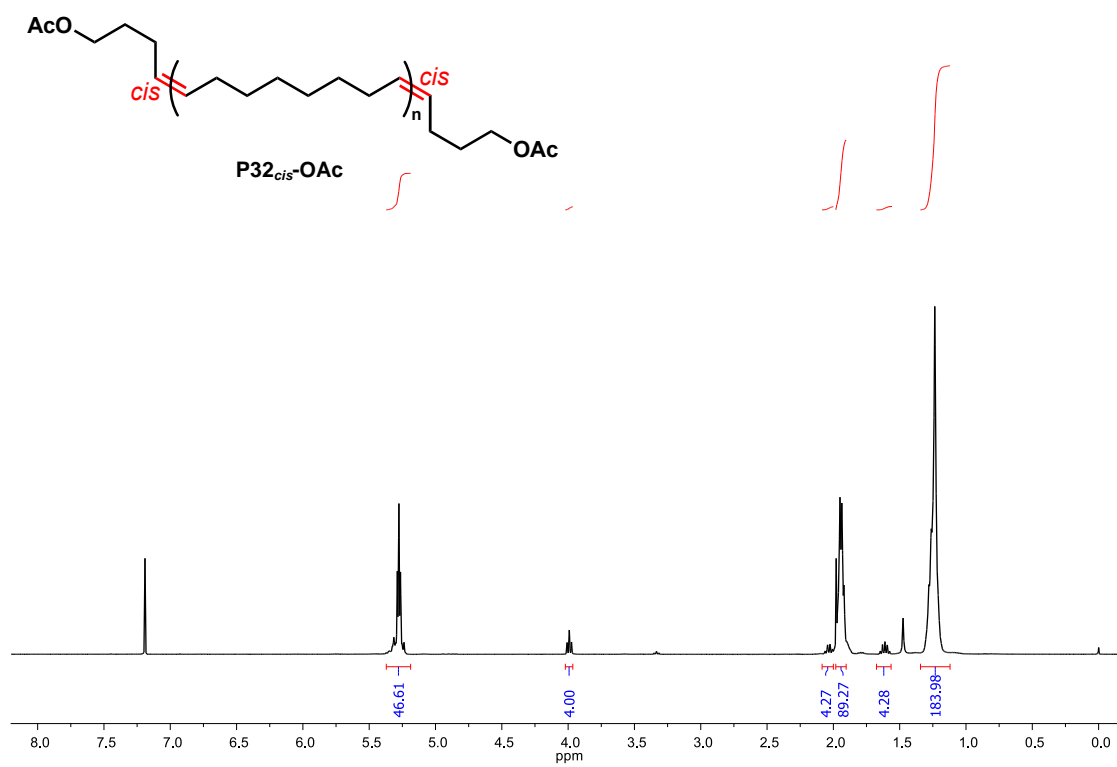
Figure V-72 ^{1}H NMR (400 MHz, CDCl$_3$) spectrum of **P32$_{cis}$-OAc**.
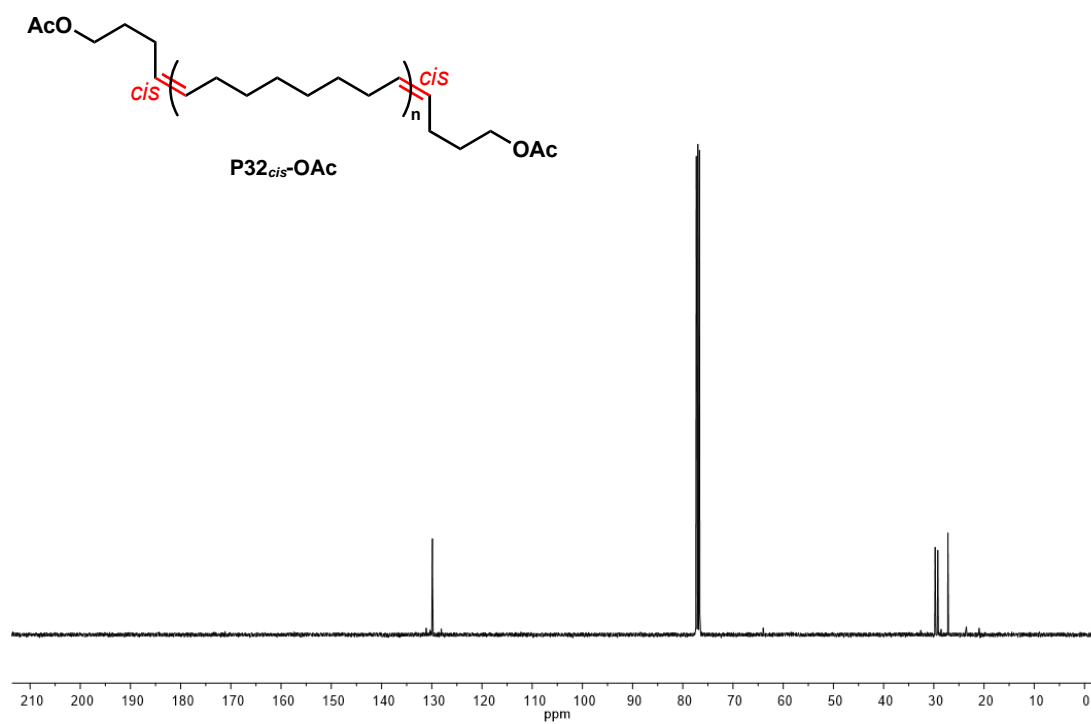
Figure V-73 ^{13}C NMR (101 MHz, CDCl$_3$) spectrum of **P32$_{cis}$-OAc**.
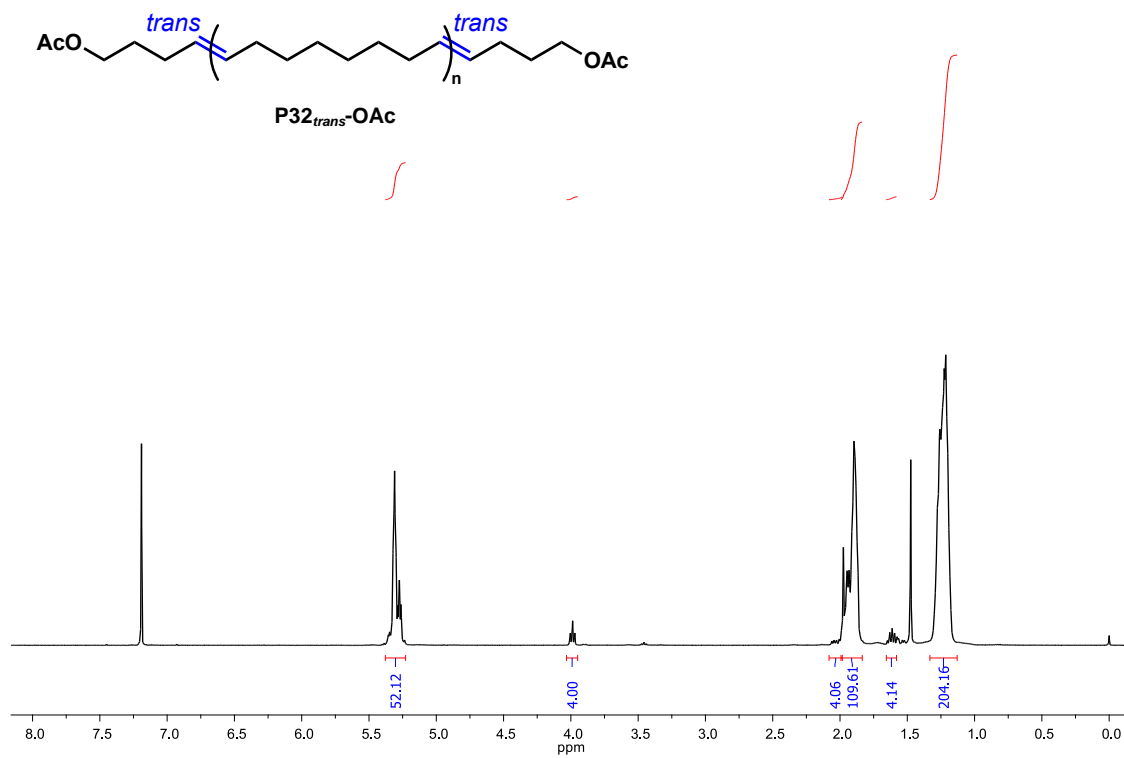
Figure V-74 ^{1}H NMR (400 MHz, CDCl$_3$) spectrum of **P32$_{trans}$-OAc**.
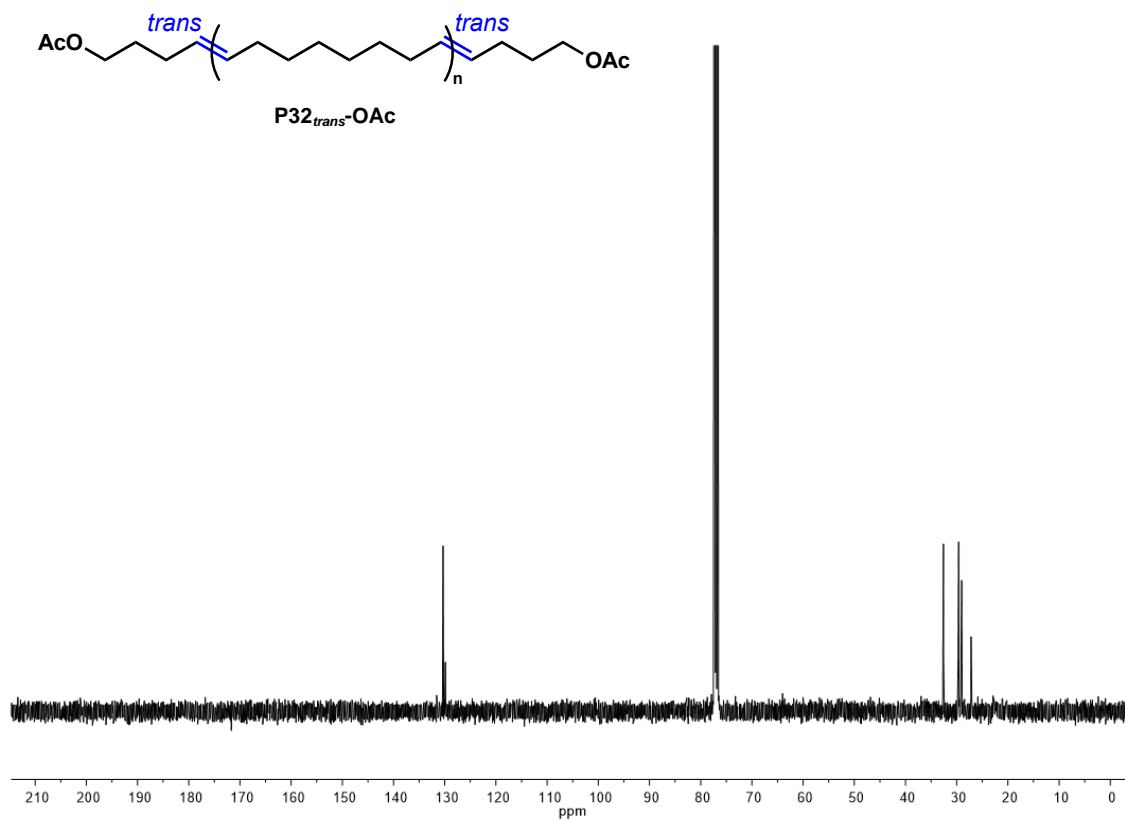
Figure V-75 ^{13}C NMR (101 MHz, CDCl$_3$) spectrum of **P32$_{trans}$-OAc**.
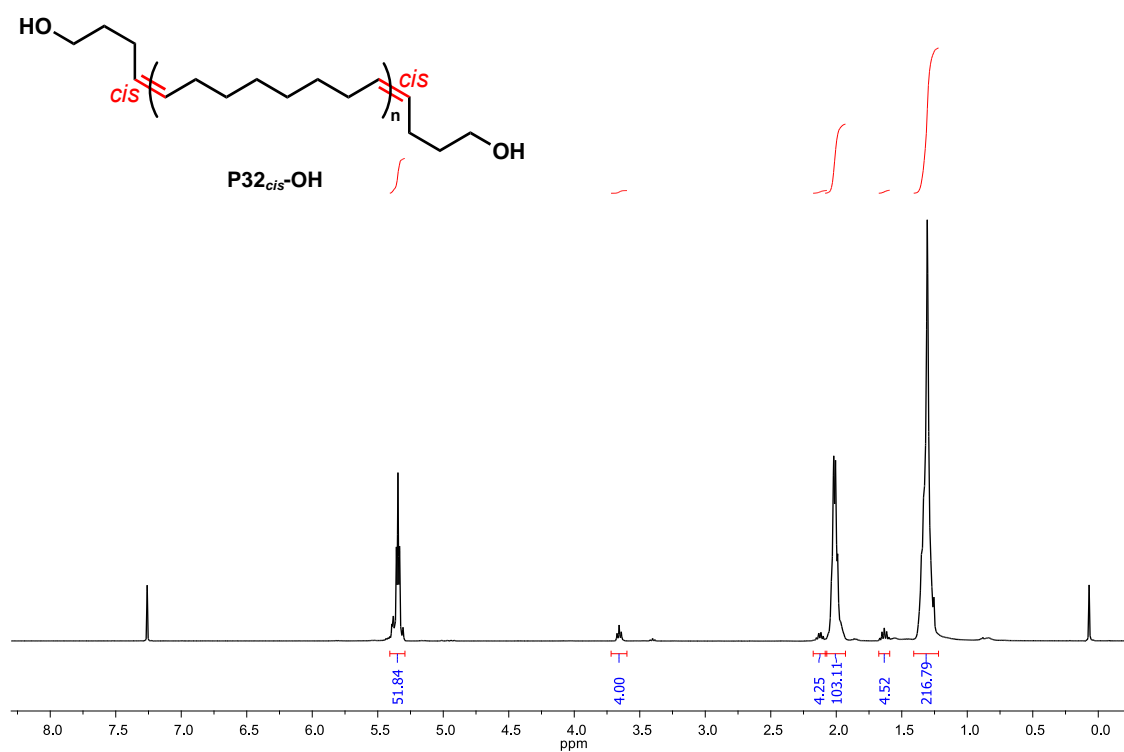
Figure V-76 ^{1}H NMR (400 MHz, CDCl$_3$) spectrum of **P32$_{cis}$-OH**.
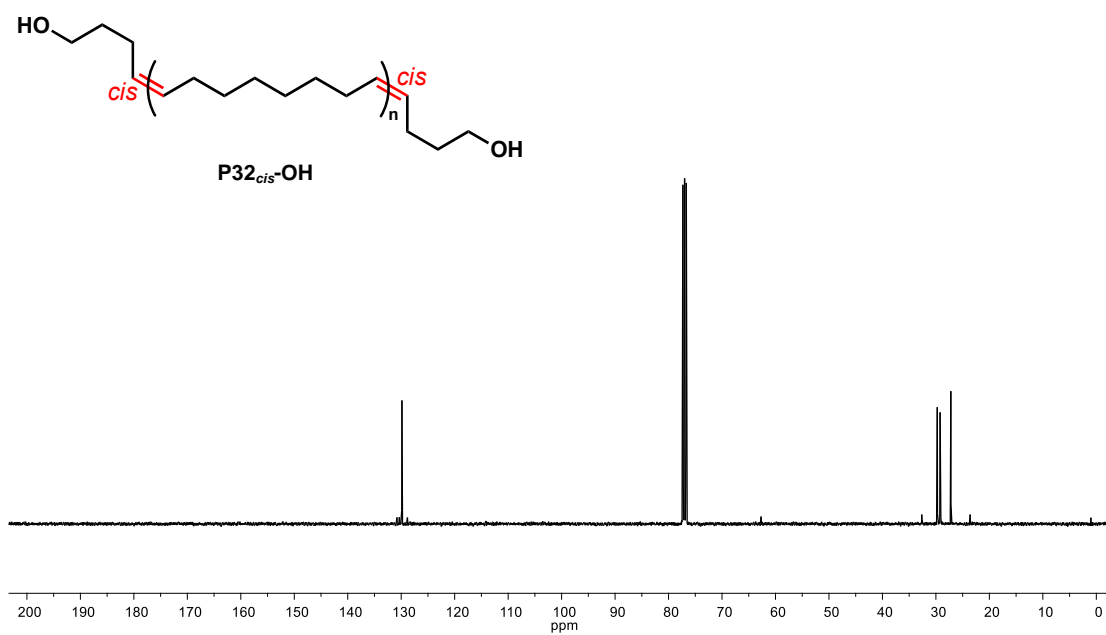
Figure V-77 ^{13}C NMR (101 MHz, CDCl$_3$) spectrum of **P32$_{cis}$-OH**.
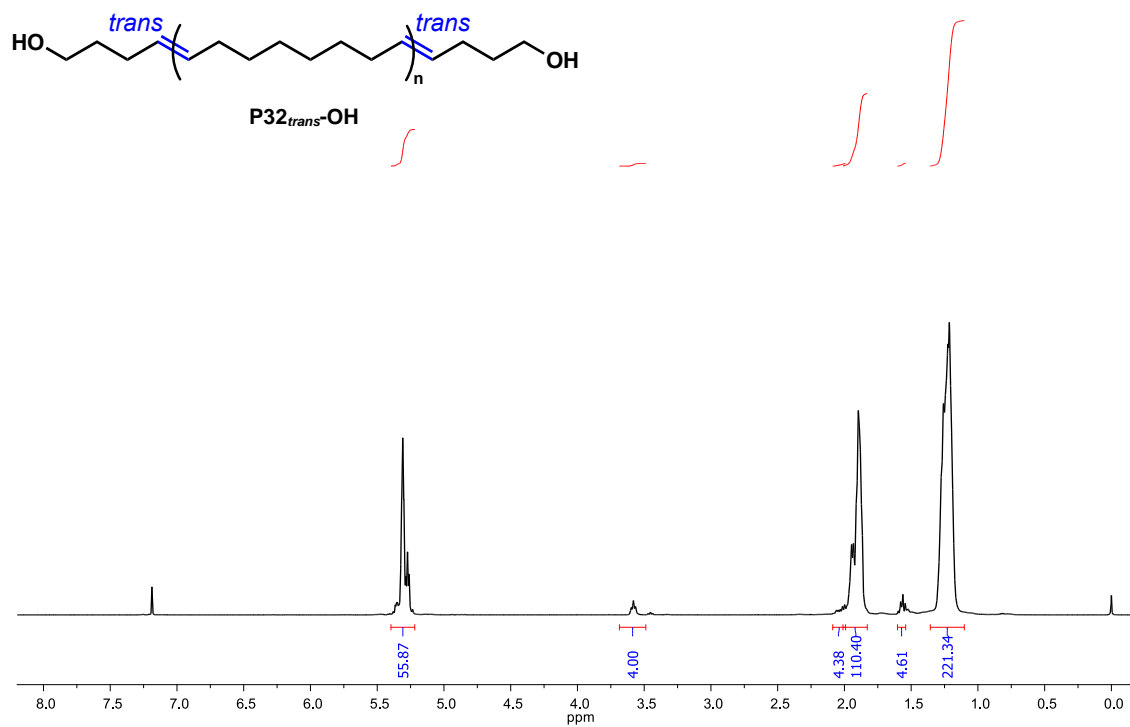
Figure V-78 ^{1}H NMR (400 MHz, CDCl$_3$) spectrum of **P32$_{trans}$-OH**.
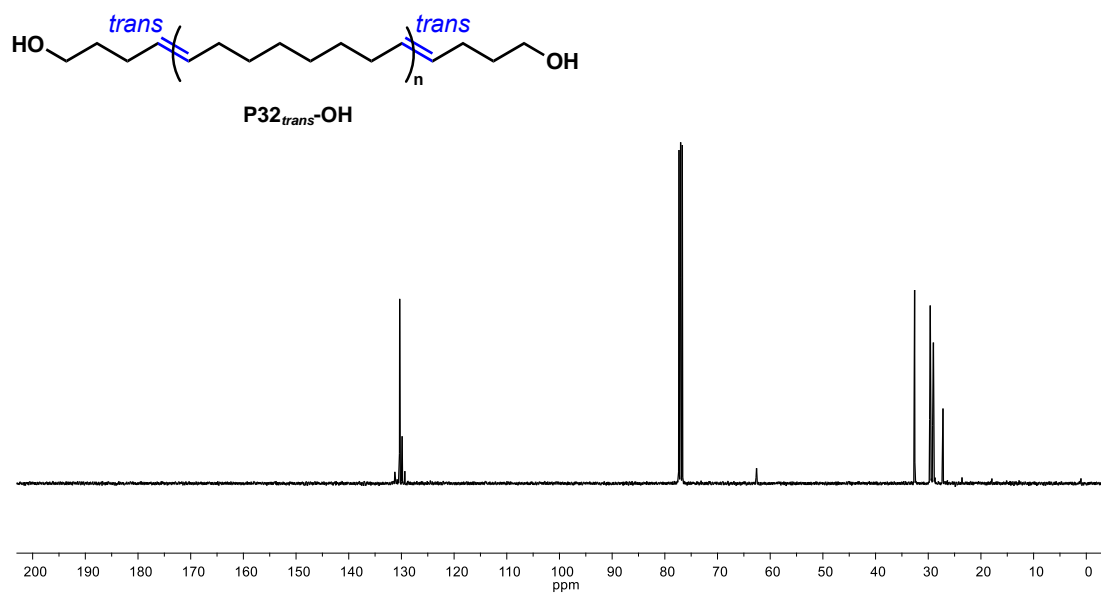
Figure V-79 ^{13}C NMR (101 MHz, $CDCl_3$) spectrum of **P32$_{trans}$-OH**.
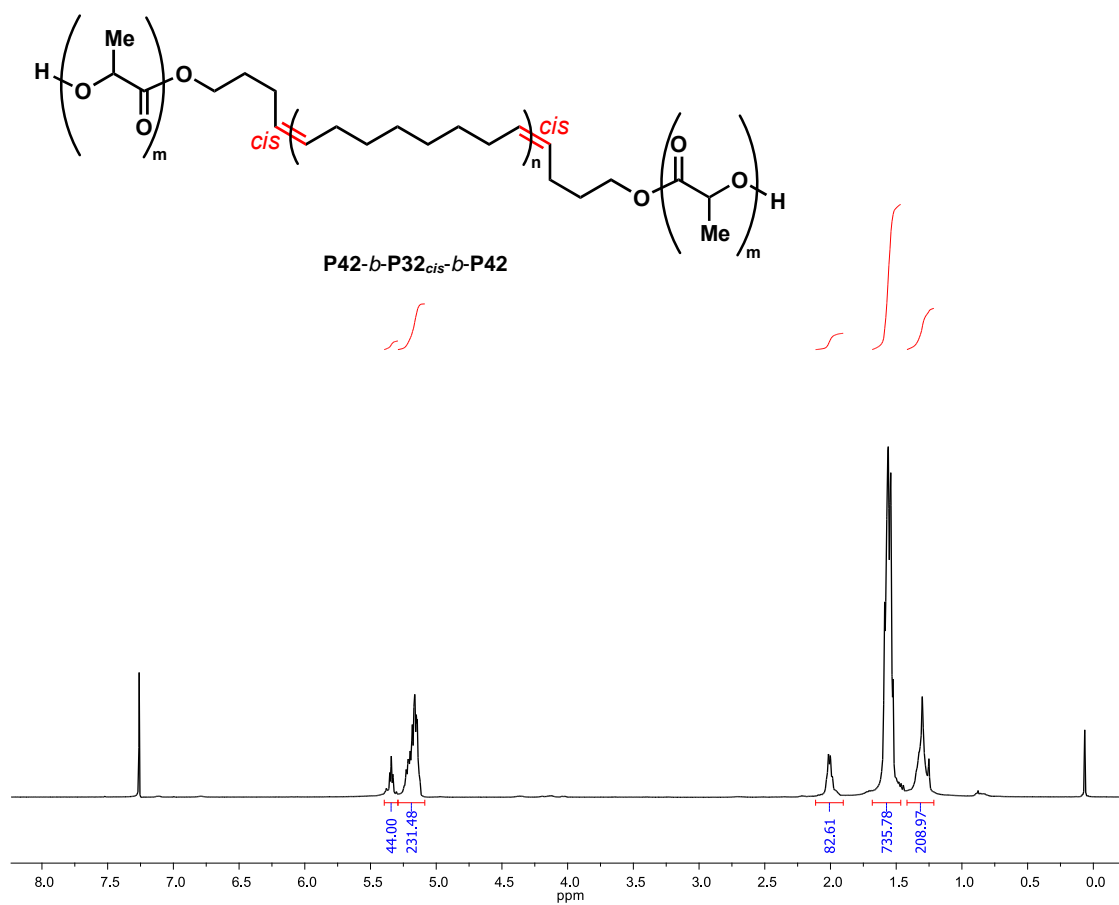
Figure V-80 ^{1}H NMR (400 MHz, CDCl$_3$) spectrum of **P42**-*b*-**P32**$_{cis}$-*b*-**P42**.
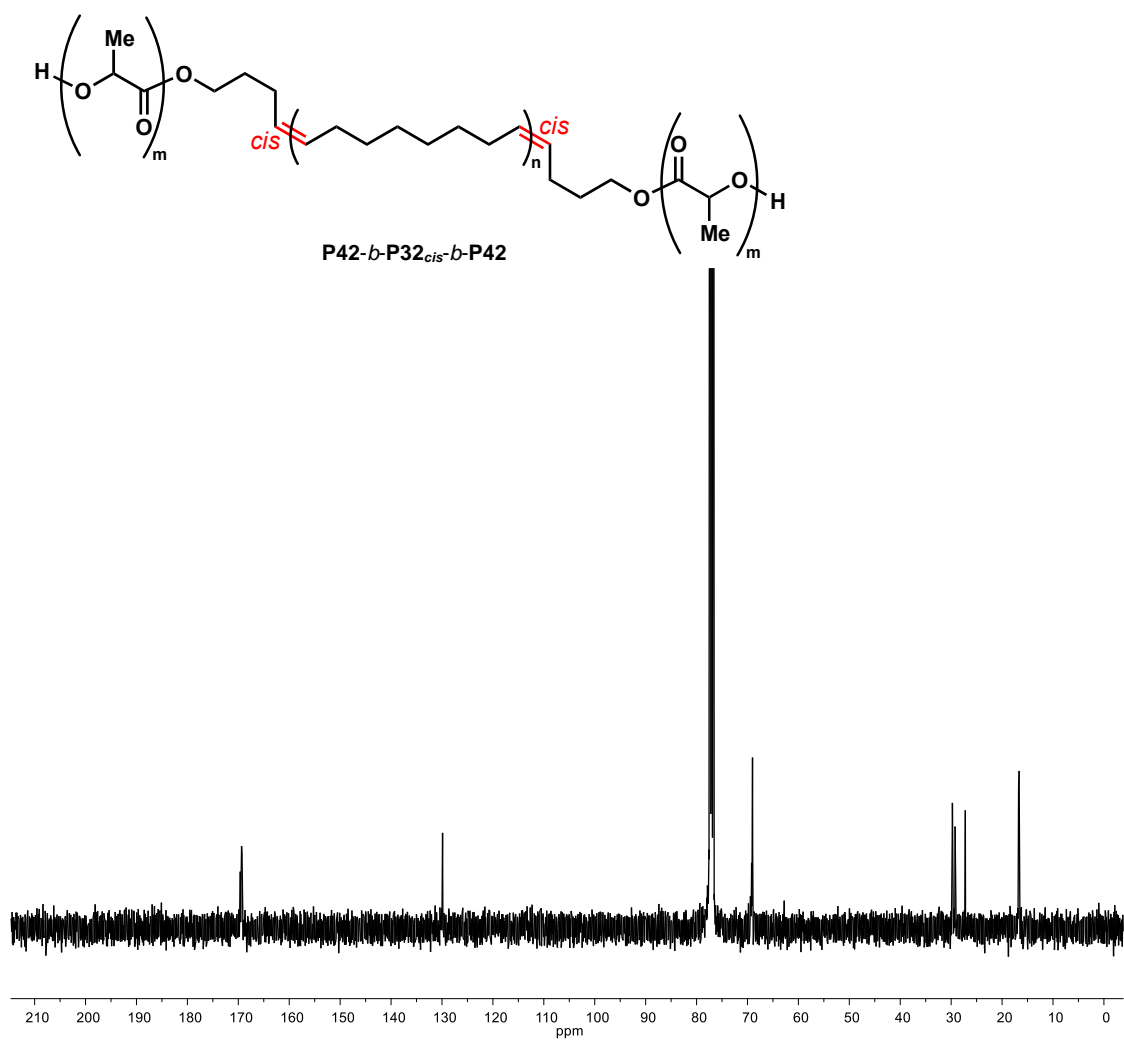
Figure V-81 ^{13}C NMR (101 MHz, CDCl$_3$) spectrum of **P42**-*b*-**P32$_{cis}$**-*b*-**P42**.
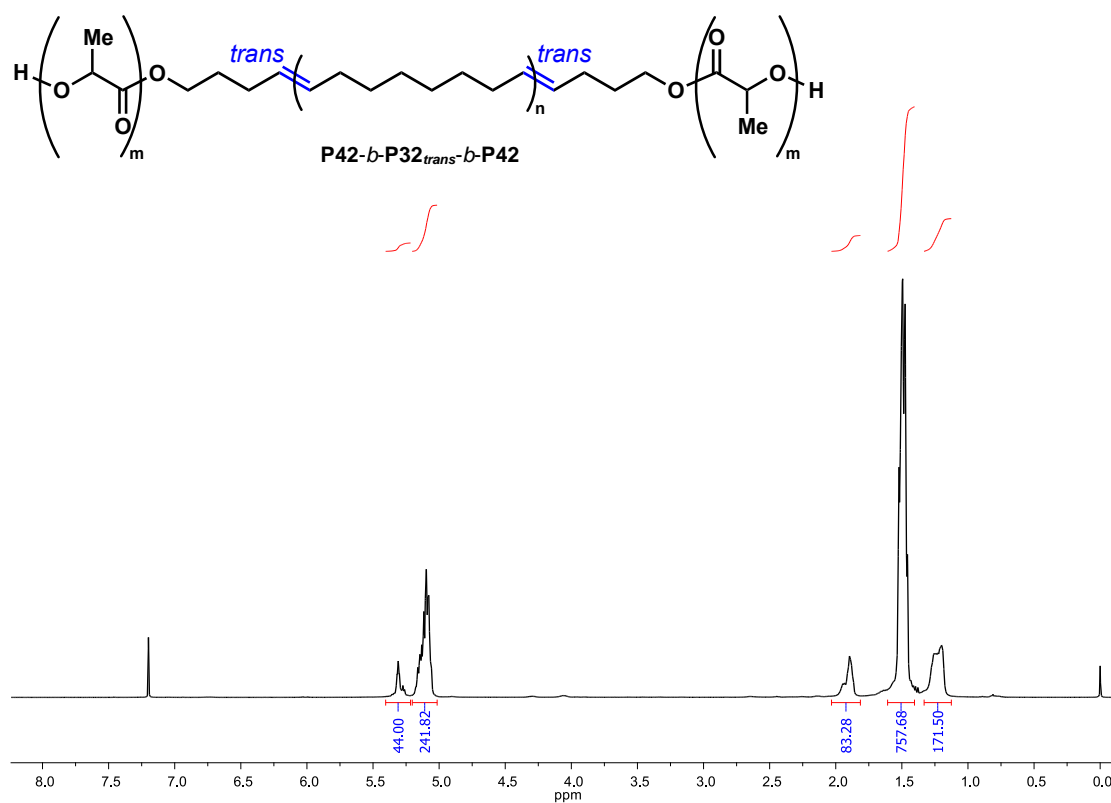
Figure V-82 ^{1}H NMR (400 MHz, CDCl$_3$) spectrum of **P42**-*b*-**P32**$_{trans}$-*b*-**P42**.
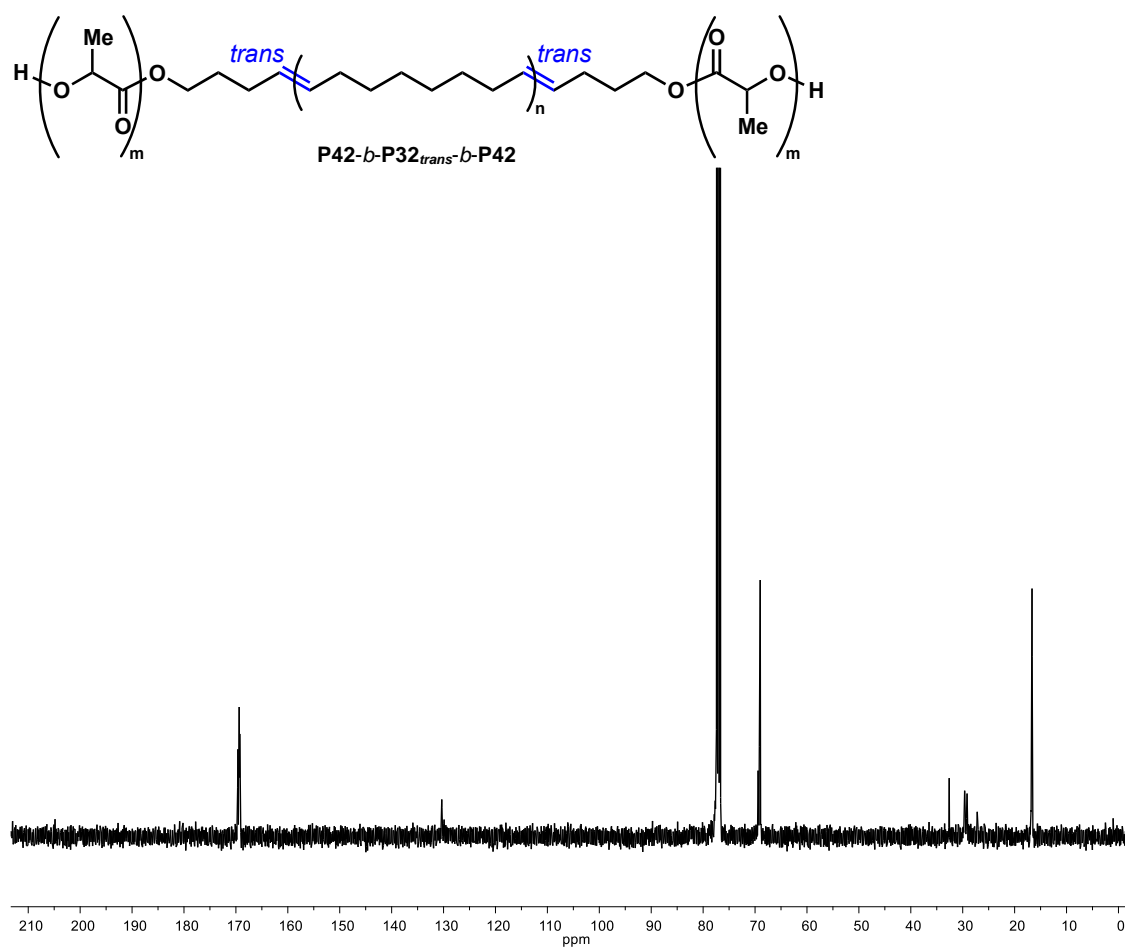
Figure V-83 ^{13}C NMR (101 MHz, CDCl$_3$) spectrum of **P42**-*b*-**P32**$_{trans}$-*b*-**P42**.
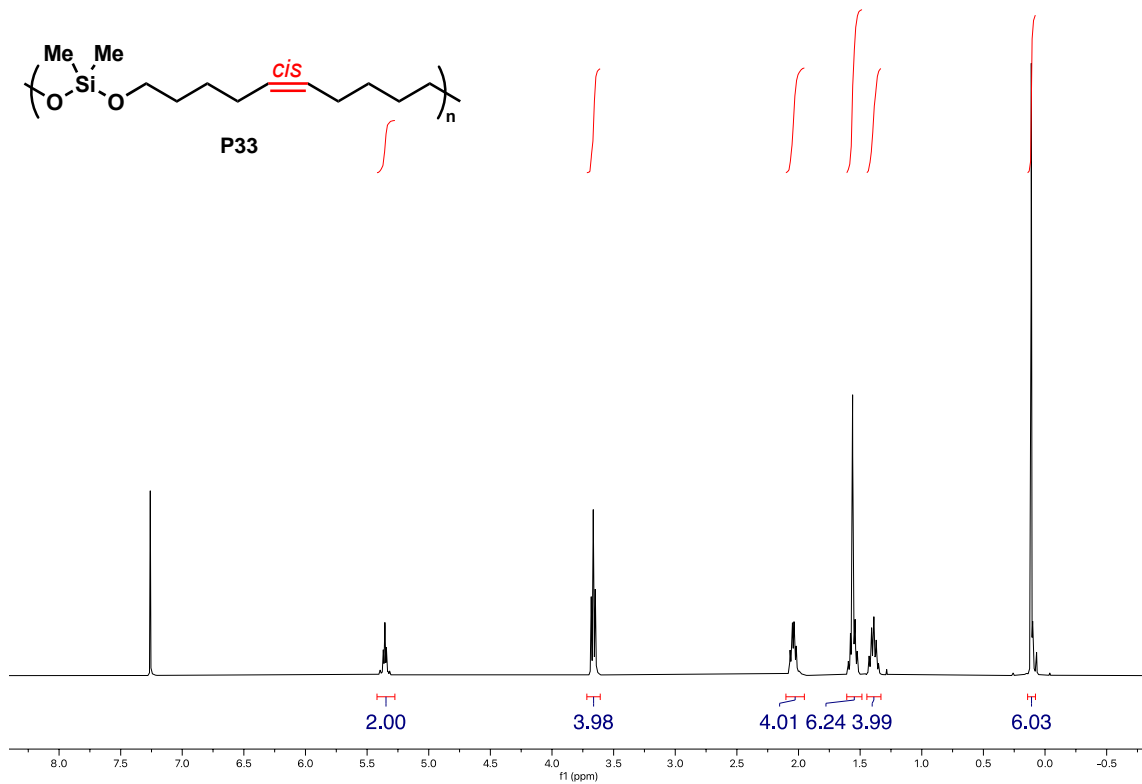
Figure V-84 [^1]H NMR (400 MHz, CDCl₃) spectrum of *cis*-rich compound **P33**.
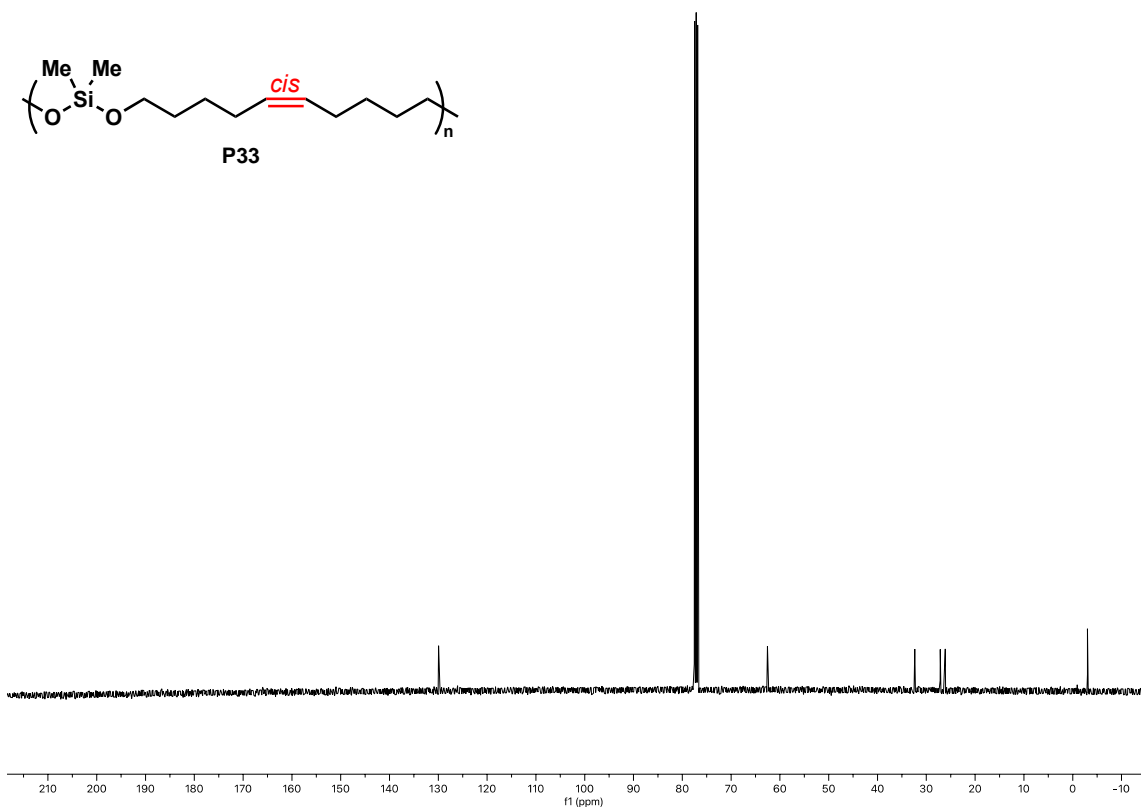
Figure V-85 ^{13}C NMR (101 MHz, CDCl$_3$) spectrum of *cis*-rich compound **P33**.
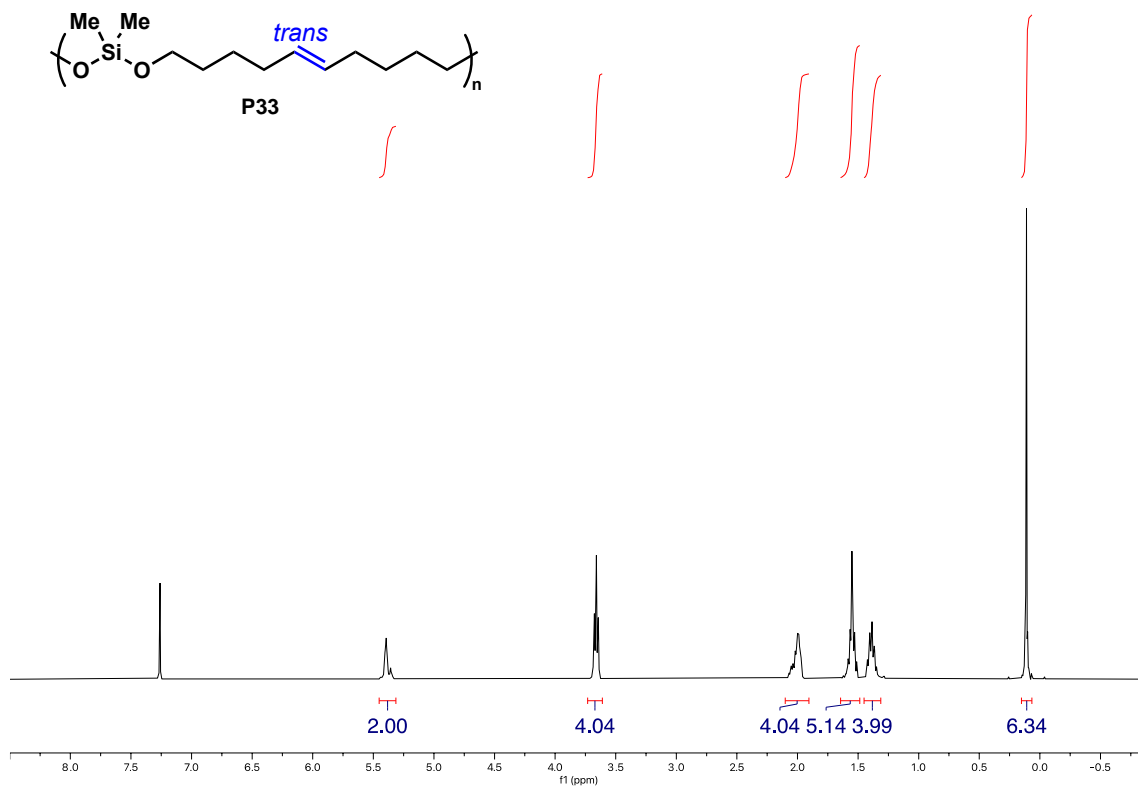
Figure V-86 ^{1}H NMR (400 MHz, CDCl$_3$) spectrum of *trans*-rich compound **P33**.
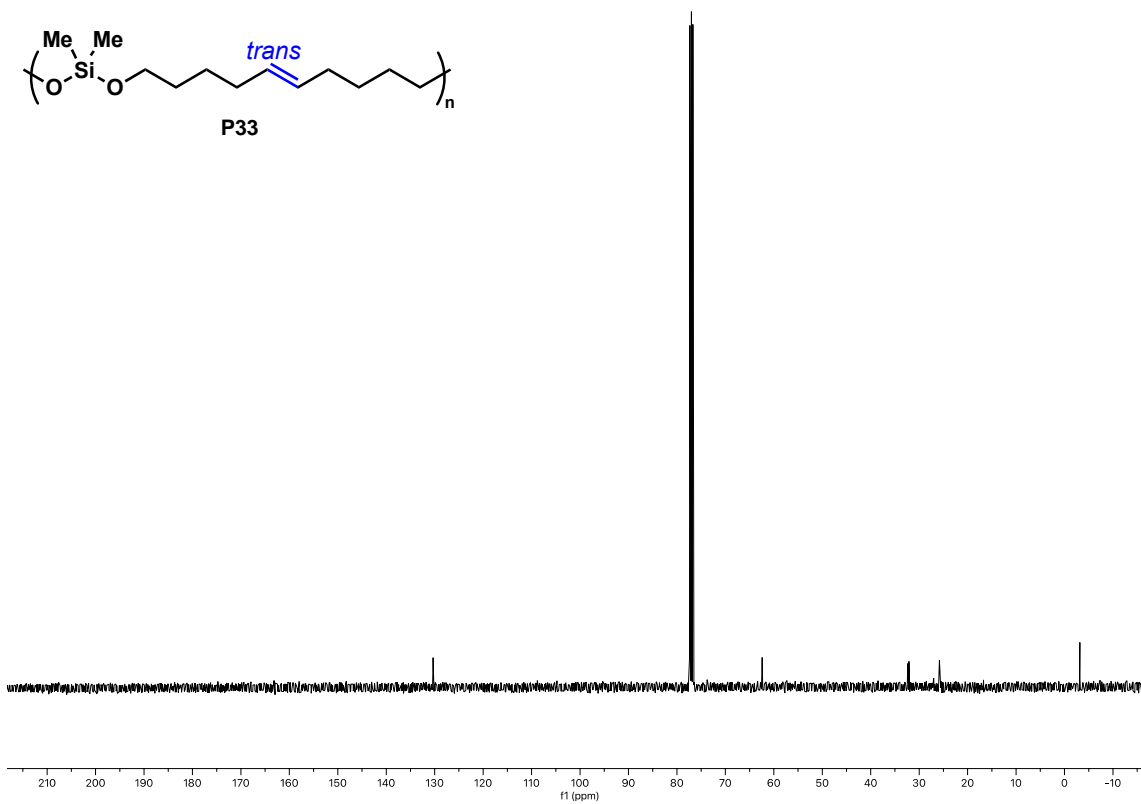
Figure V-87 ^{13}C NMR (101 MHz, CDCl$_3$) spectrum of *trans*-rich compound **P33**.
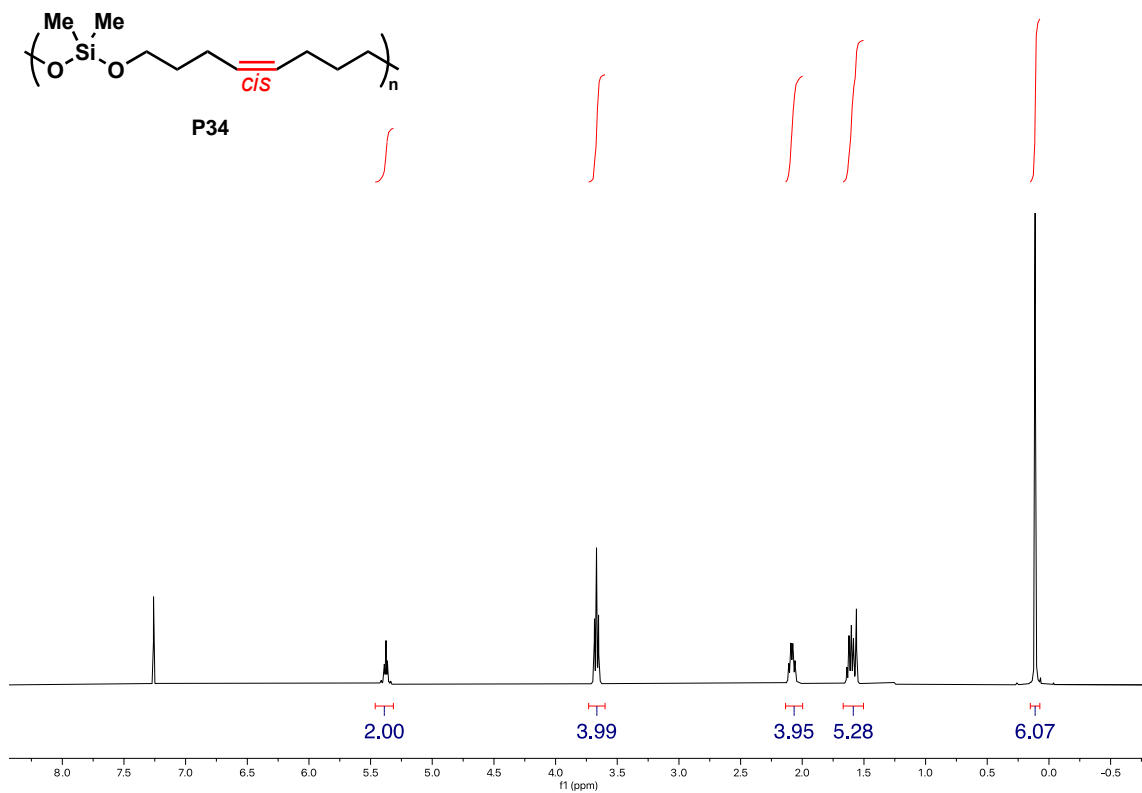
Figure V-88 ^{1}H NMR (400 MHz, CDCl$_3$) spectrum of *cis*-rich compound **P34**.
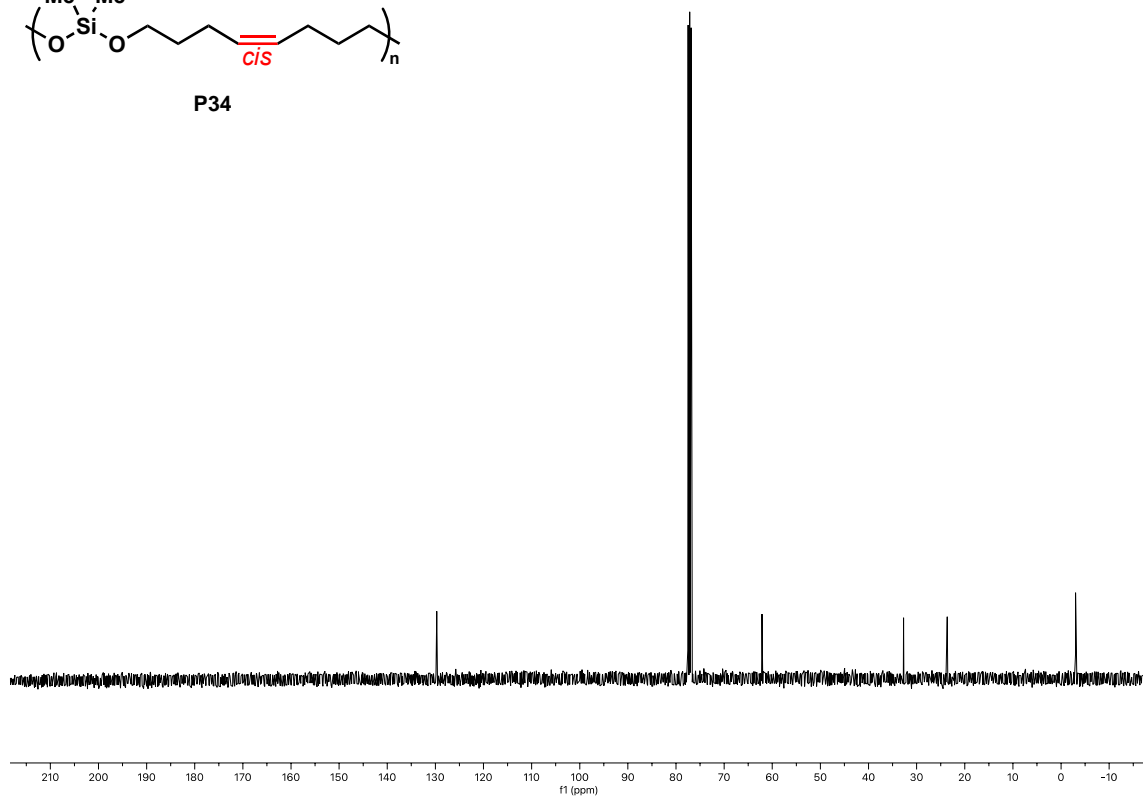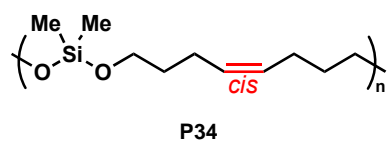
Figure V-89 ^{13}C NMR (101 MHz, CDCl$_3$) spectrum of *cis*-rich **P34**.
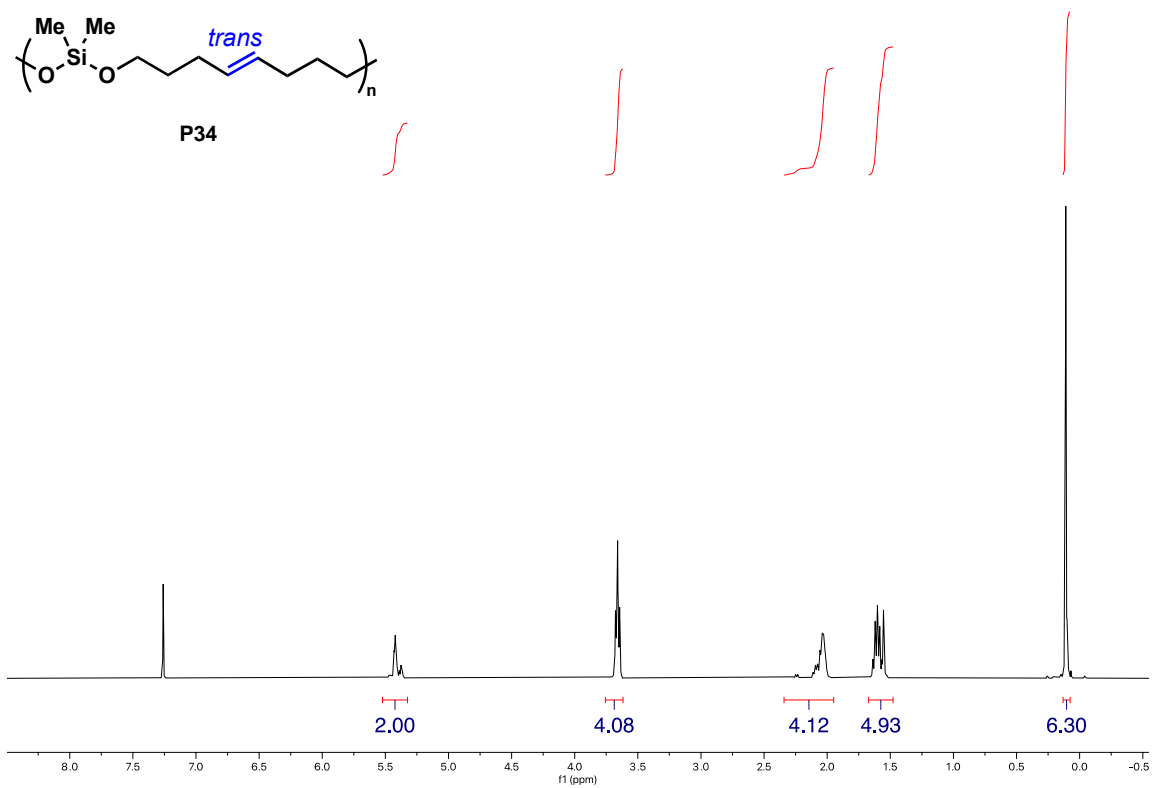
Figure V-90 ^{1}H NMR (400 MHz, CDCl$_3$) spectrum of *trans*-rich compound **P34**.
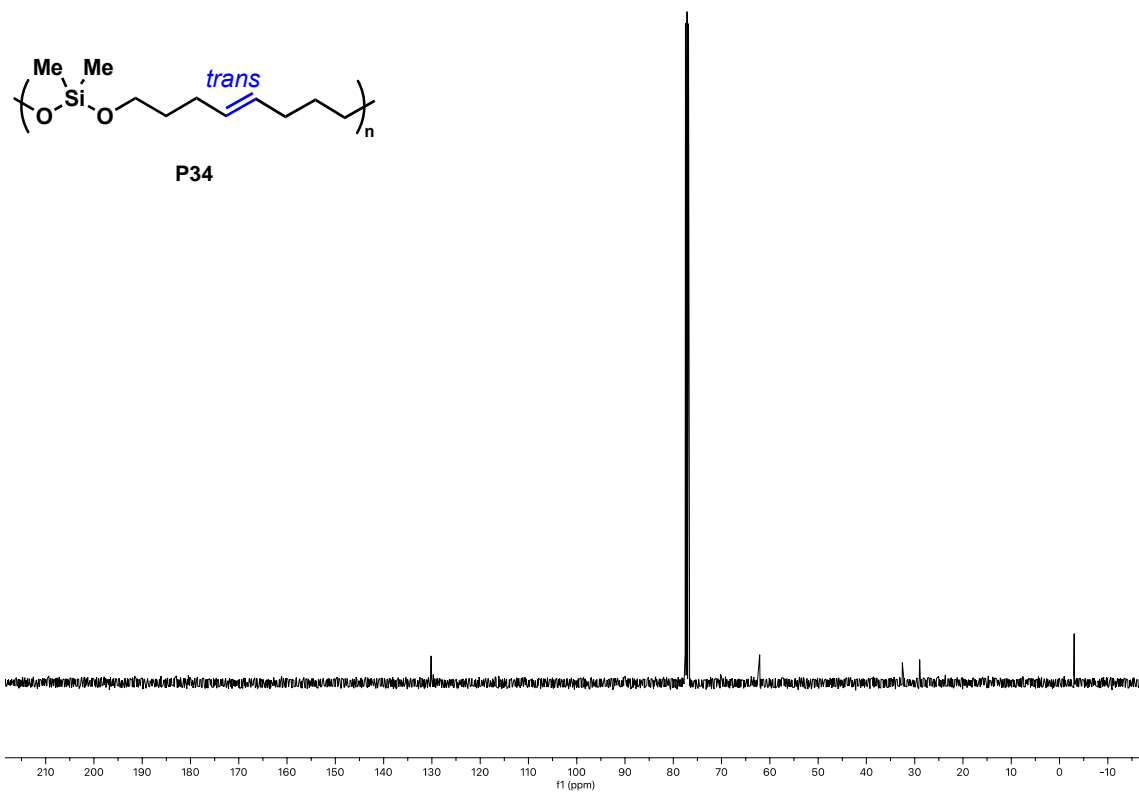
Figure V-91 ^{13}C NMR (101 MHz, CDCl$_3$) spectrum of *trans*-rich **P34**.
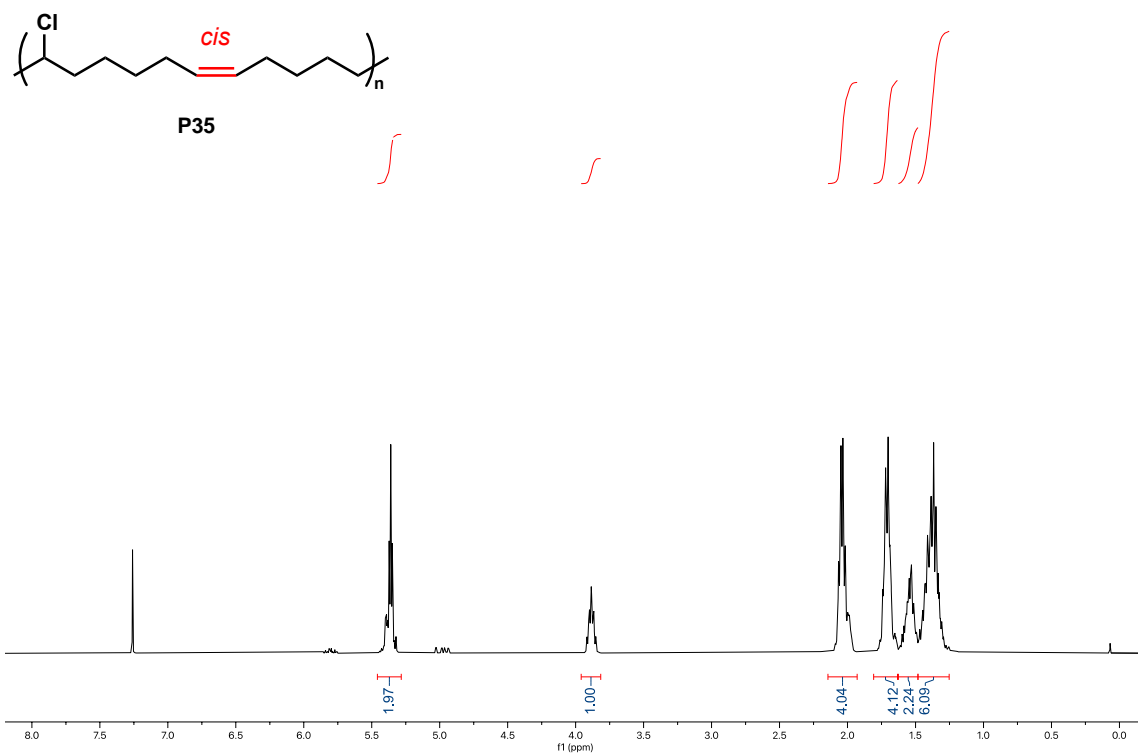
Figure V-92 ^{1}H NMR (400 MHz, CDCl$_3$) spectrum of *cis*-rich compound **P35**.
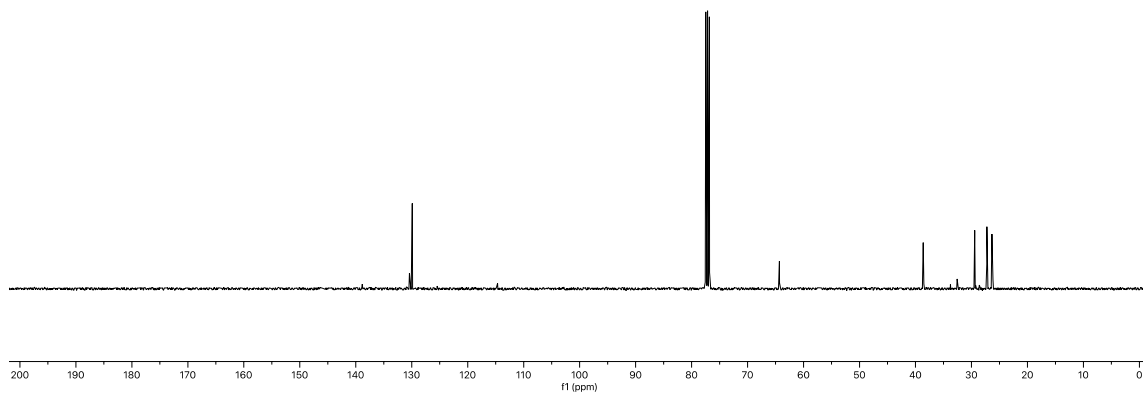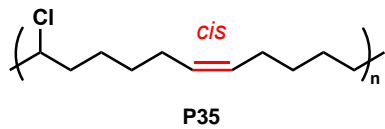
Figure V-93 ^{13}C NMR (101 MHz, CDCl$_3$) spectrum of *cis*-rich **P35**.
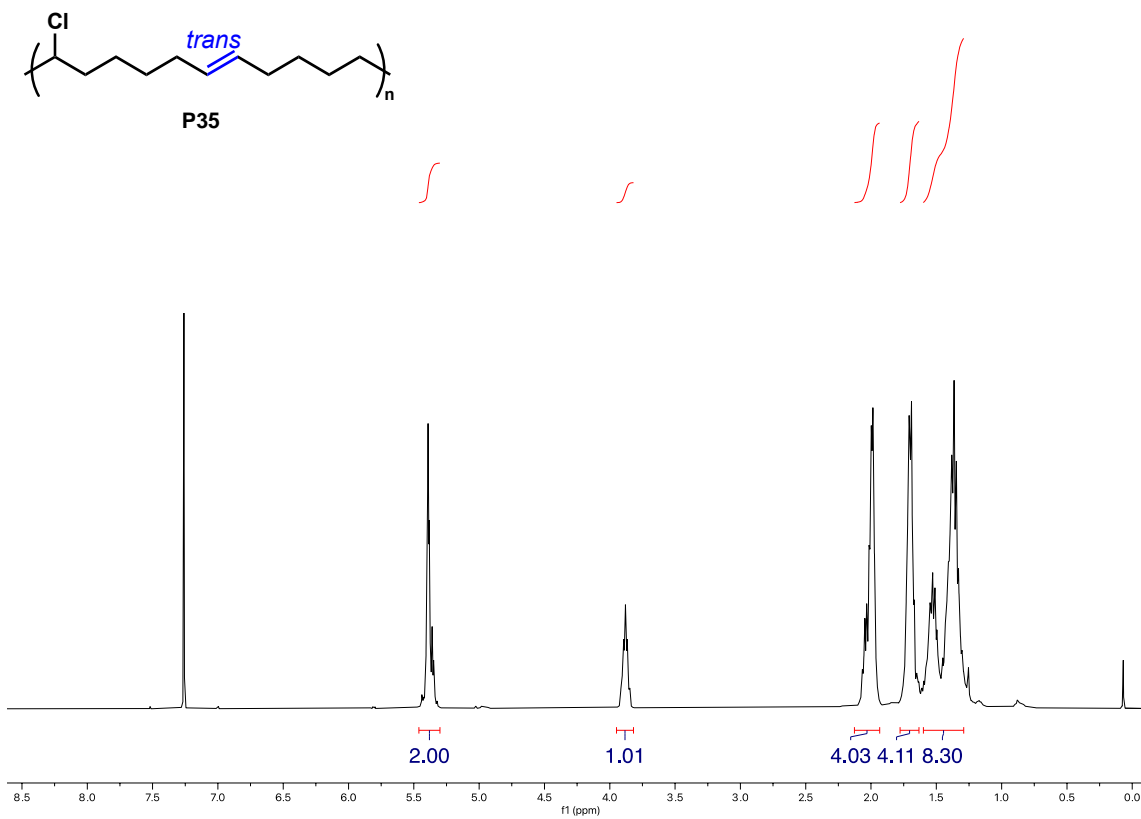
Figure V-94 ^{1}H NMR (400 MHz, CDCl$_3$) spectrum of *trans*-rich compound **P35**.
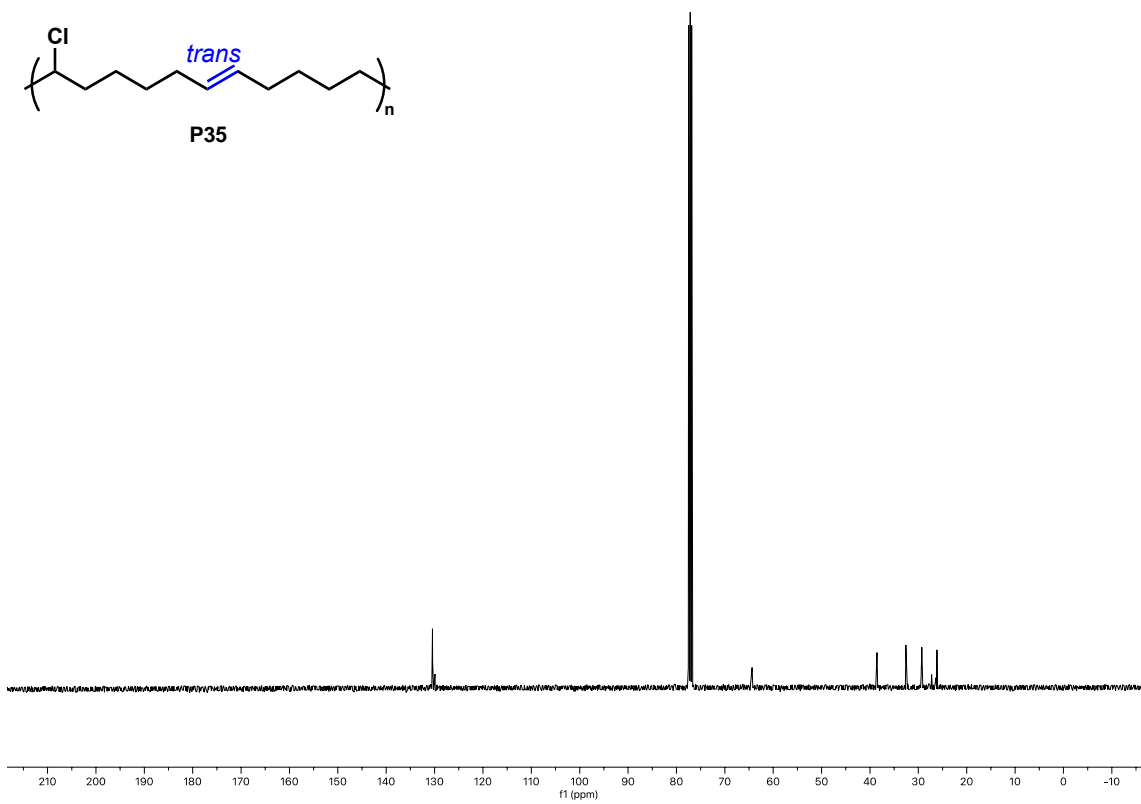
Figure V-95 ^{13}C NMR (101 MHz, CDCl$_3$) spectrum of *trans*-rich **P35**.
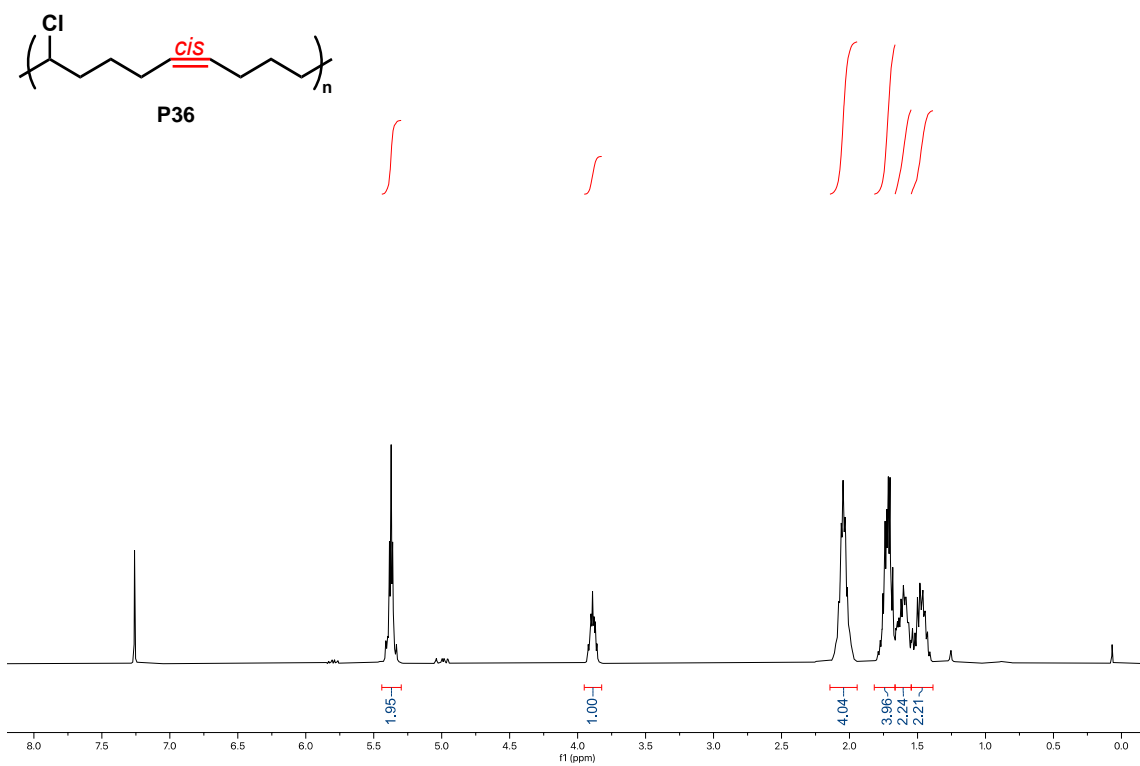
Figure V-96 ^{1}H NMR (400 MHz, CDCl$_3$) spectrum of *cis*-rich compound **P36**.
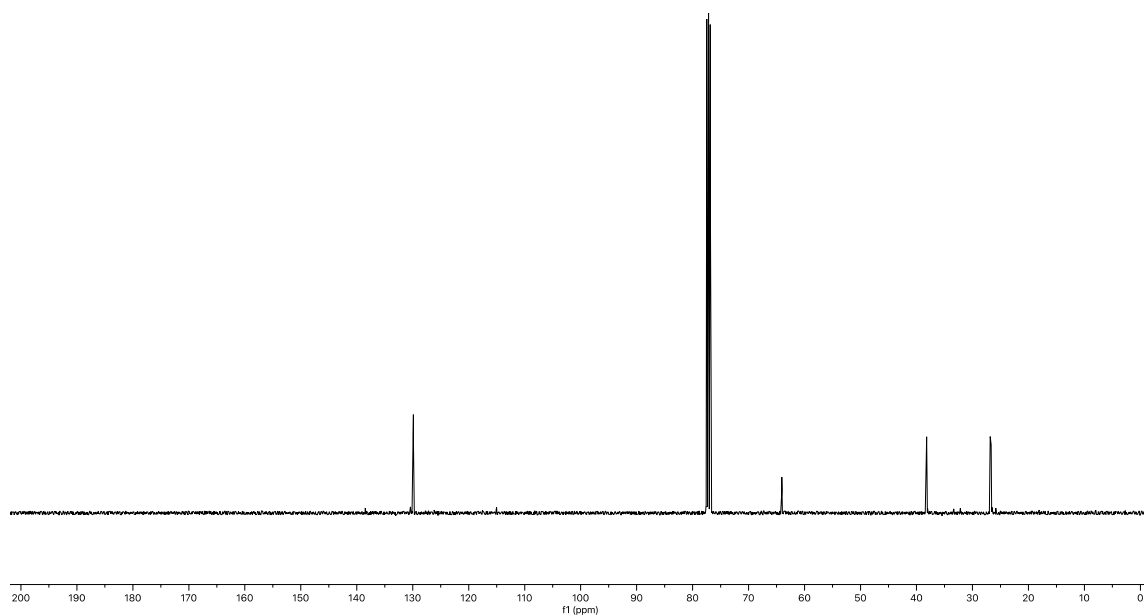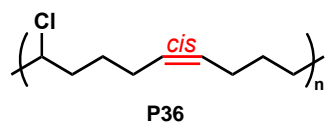
Figure V-97 ^{13}C NMR (101 MHz, CDCl$_3$) spectrum of *cis*-rich **P36**.
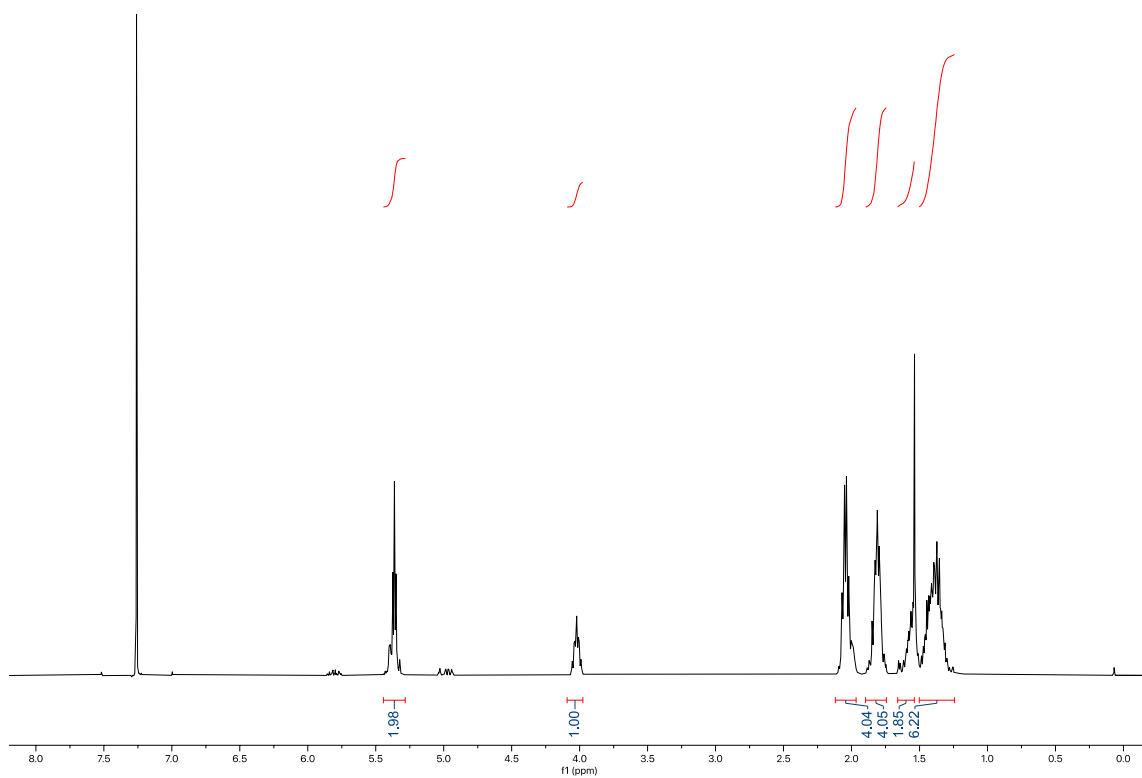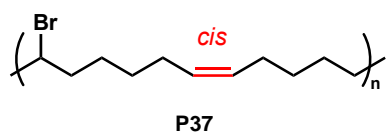
Figure V-98 ^{1}H NMR (400 MHz, CDCl$_3$) spectrum of *cis*-rich compound **P37**.
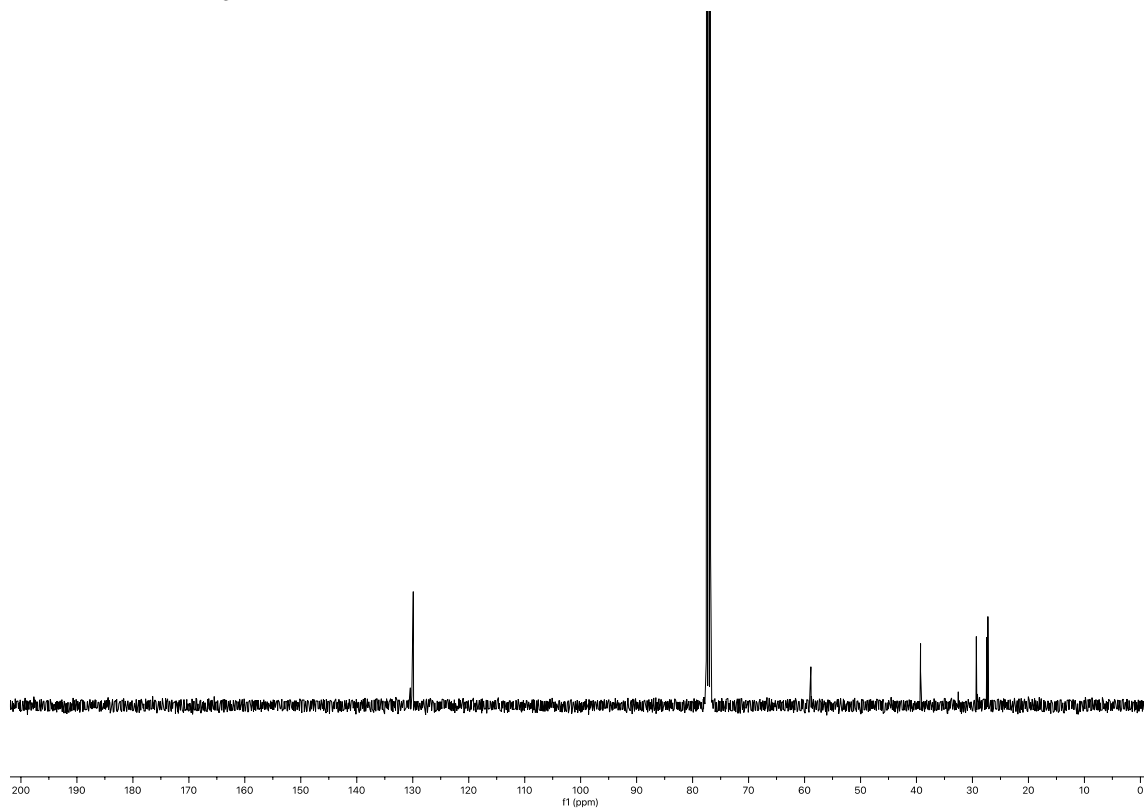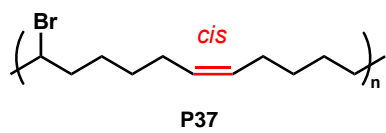
Figure V-99 ^{13}C NMR (101 MHz, CDCl$_3$) spectrum of *cis*-rich **P37**.
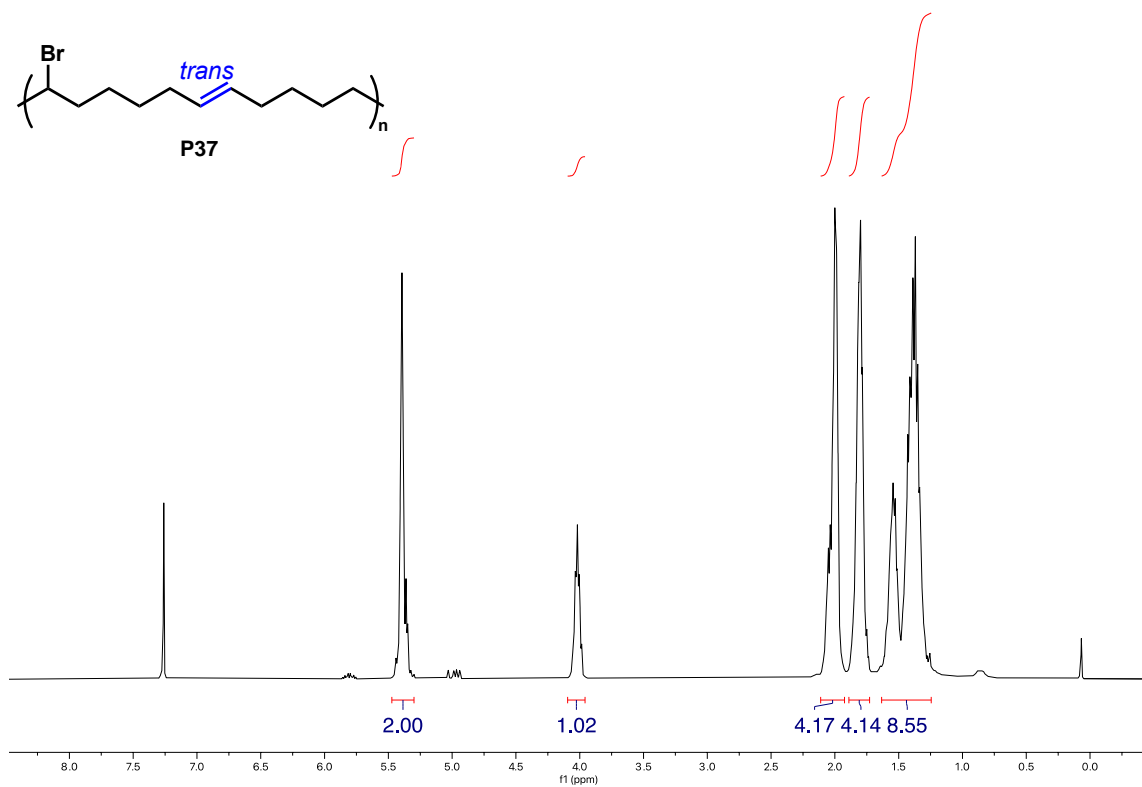
Figure V-100 ^{1}H NMR (400 MHz, CDCl$_3$) spectrum of *trans*-rich compound **P37**.
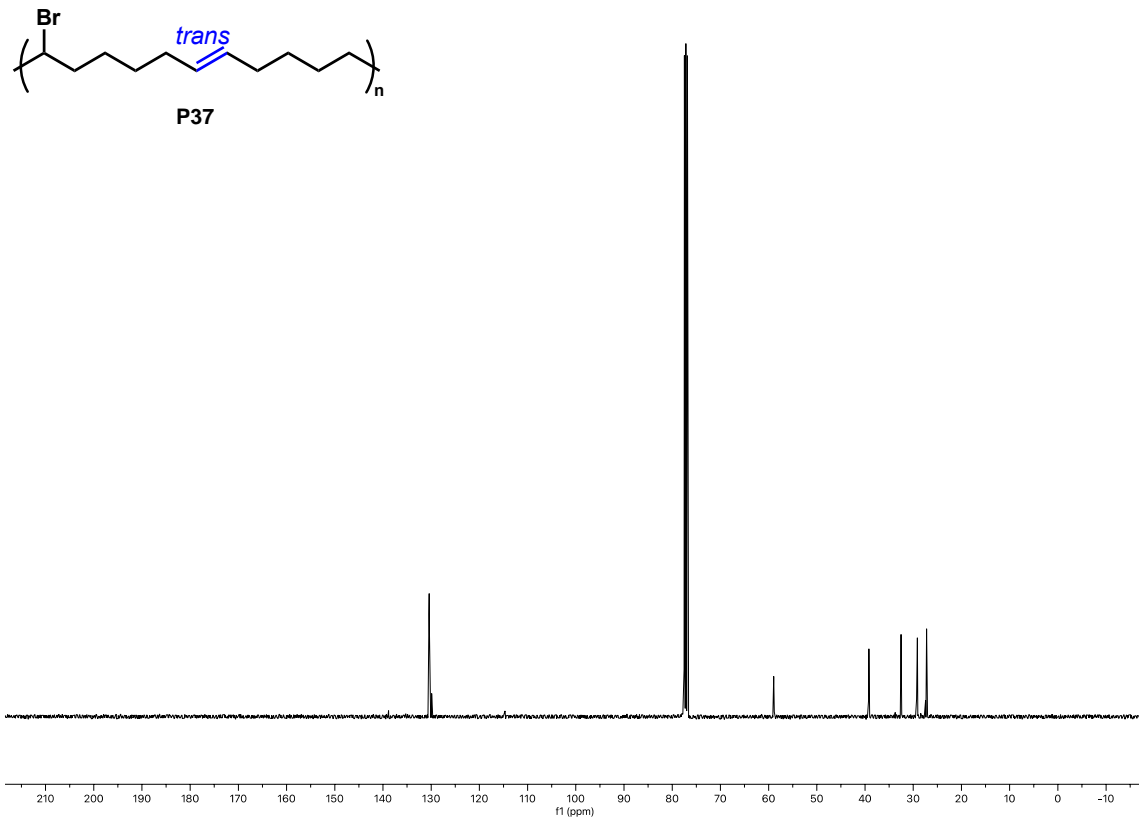
Figure V-101 ^{13}C NMR (101 MHz, CDCl$_3$) spectrum of *trans*-rich **P37**.
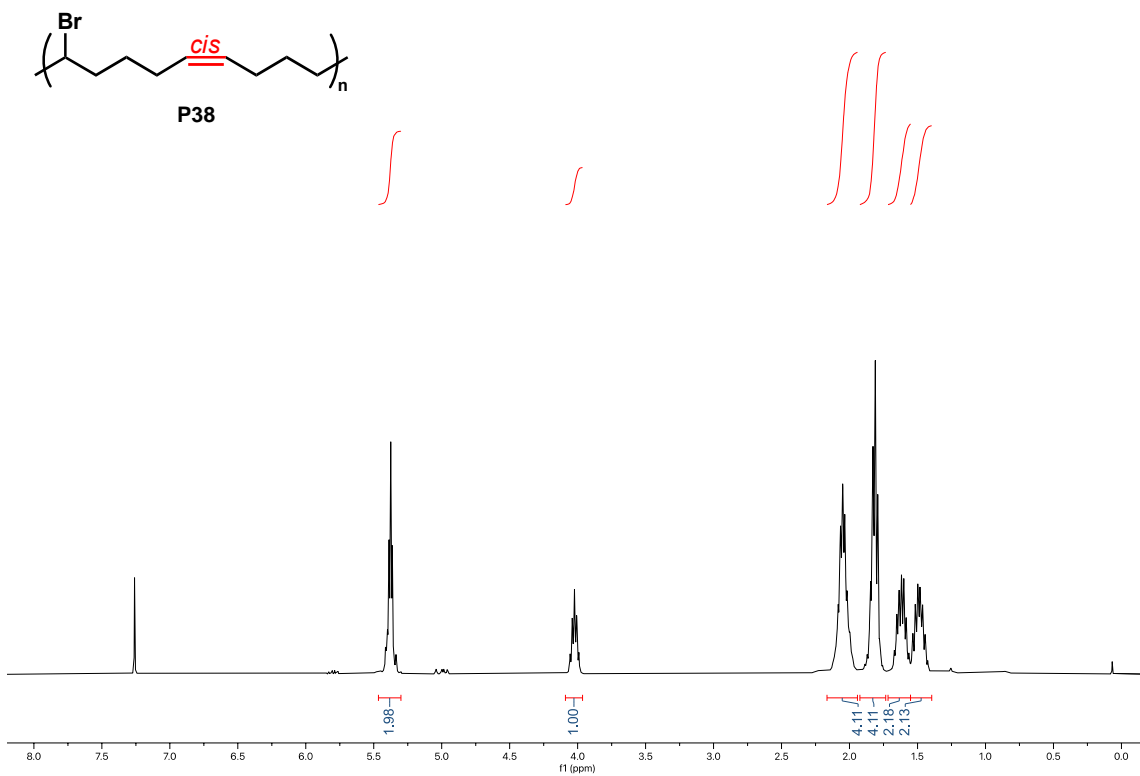
Figure V-102 ^{1}H NMR (400 MHz, CDCl$_3$) spectrum of *cis*-rich compound **P38**.
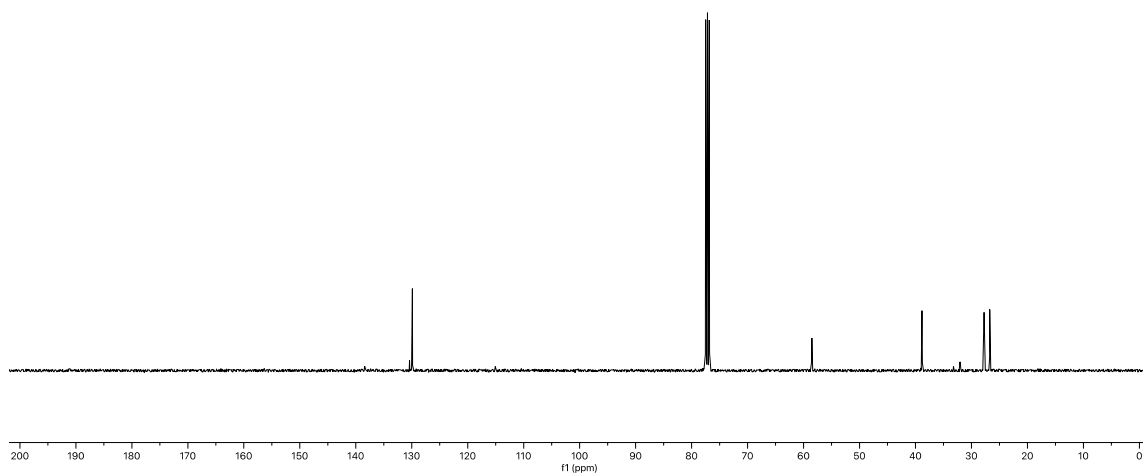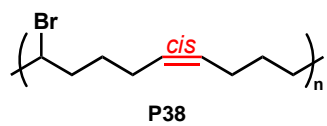
Figure V-103 ^{13}C NMR (101 MHz, CDCl$_3$) spectrum of *cis*-rich **P38**.
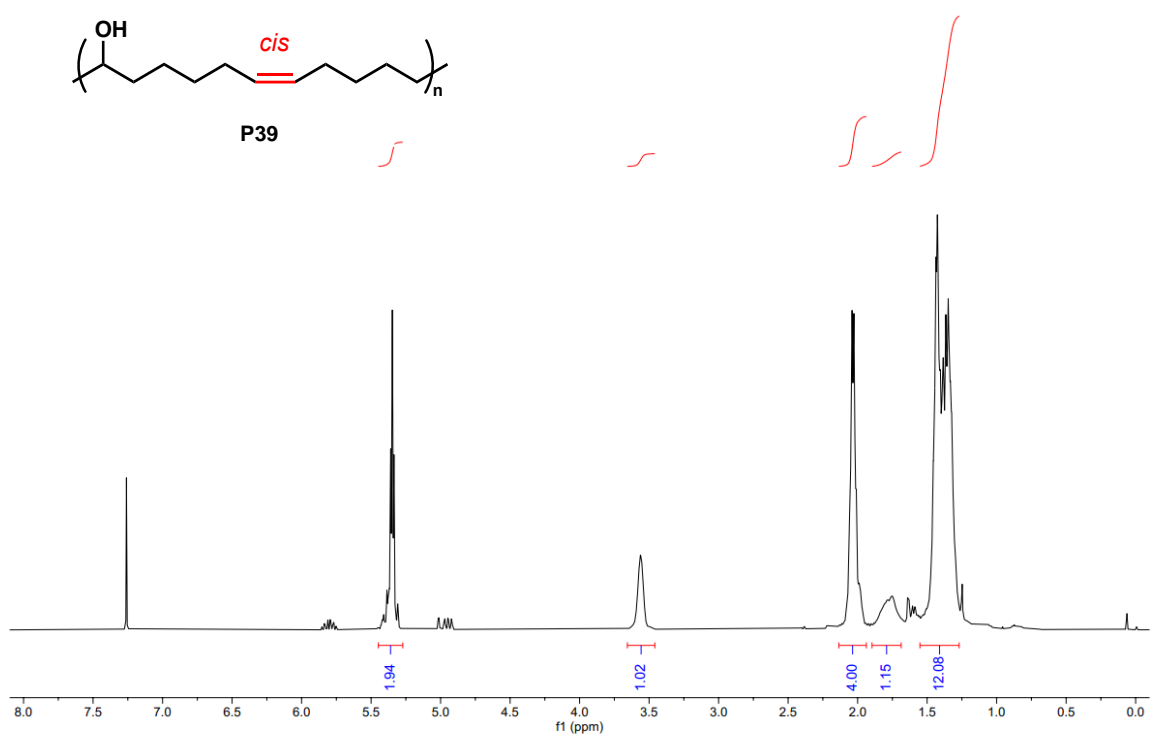
Figure V-104 ^{1}H NMR (400 MHz, CDCl$_3$) spectrum of *cis*-rich compound **P39**.
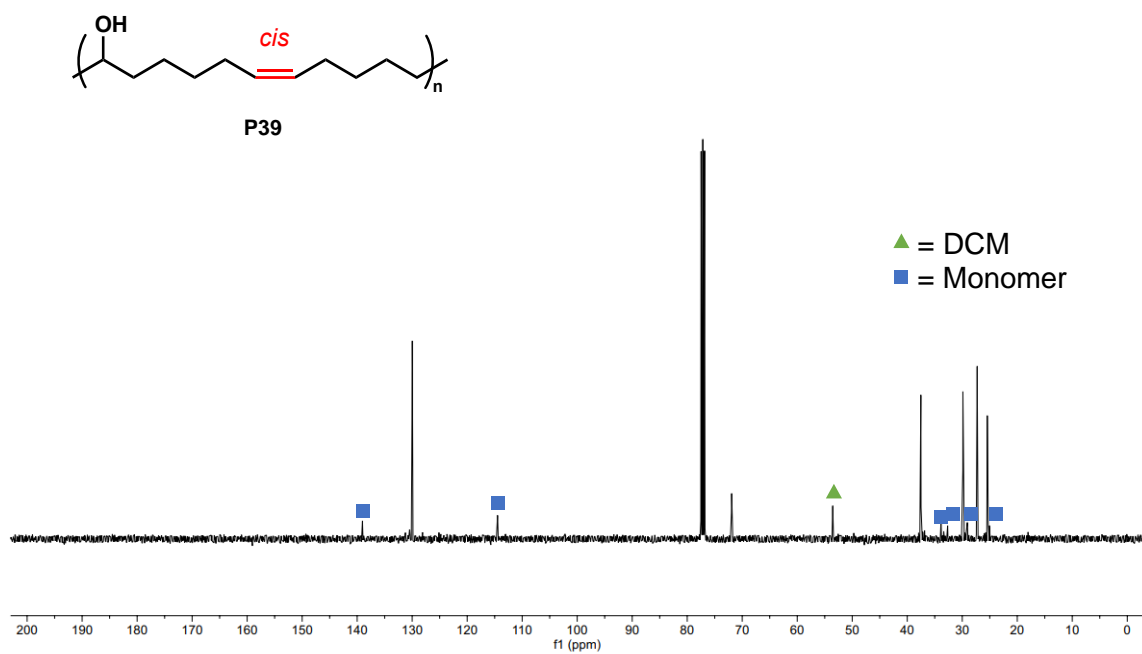
Figure V-105 ^{13}C NMR (101 MHz, CDCl$_3$) spectrum of *cis*-rich **P39** (NOTE: oligomer *cis*-**P39** could not be precipitated and separated from unreacted monomer **39** (blue square labels).
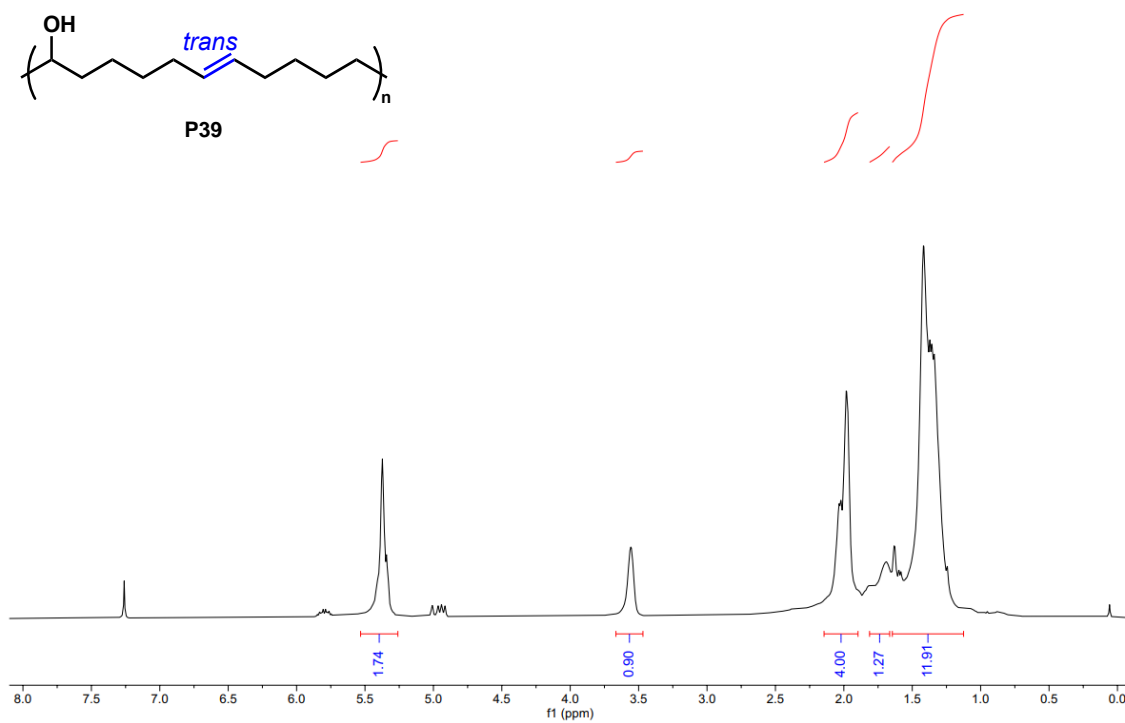
Figure V-106 ^{1}H NMR (400 MHz, CDCl$_3$) spectrum of *trans*-rich compound **P39**.
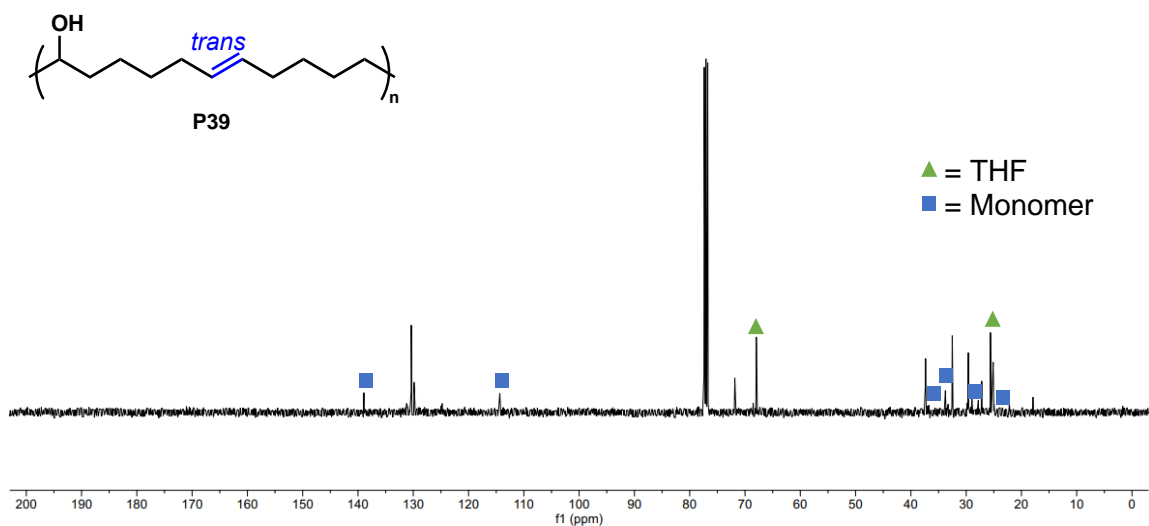
Figure V-107 ^{13}C NMR (101 MHz, CDCl$_3$) spectrum of *trans*-rich **P39** (NOTE: oligomer *trans*-**P39** could not be precipitated and separated from unreacted monomer **39** (blue square labels).
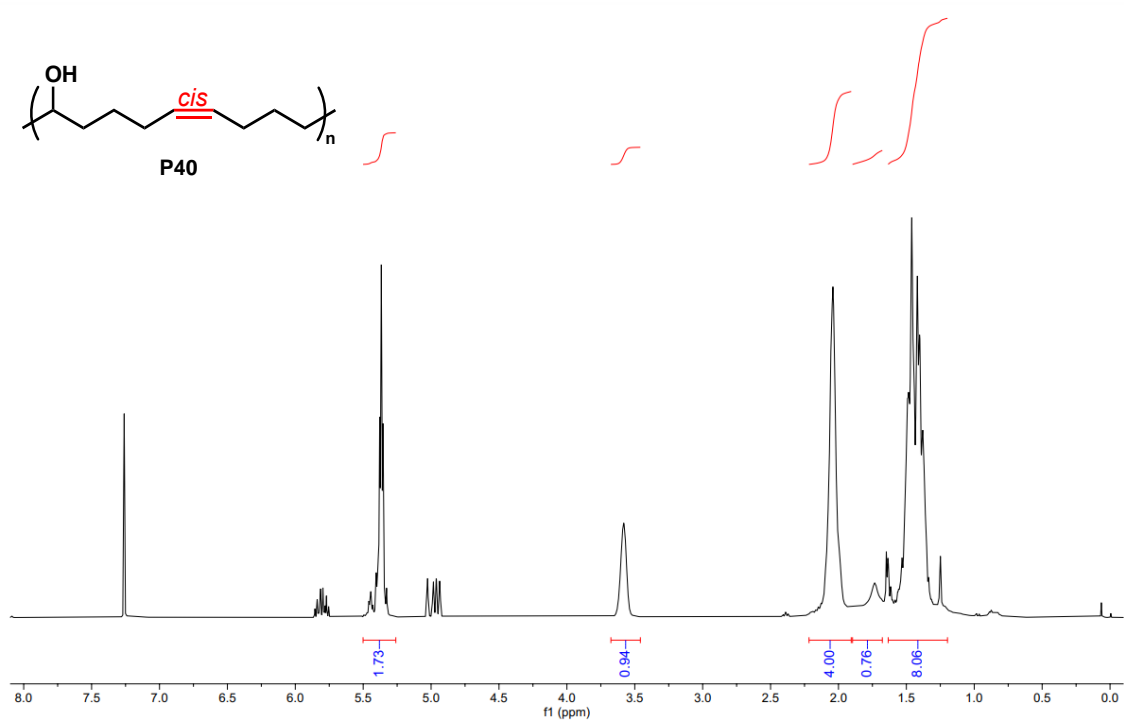
Figure V-108 ^{1}H NMR (400 MHz, CDCl$_3$) spectrum of *cis*-rich compound **P40**.
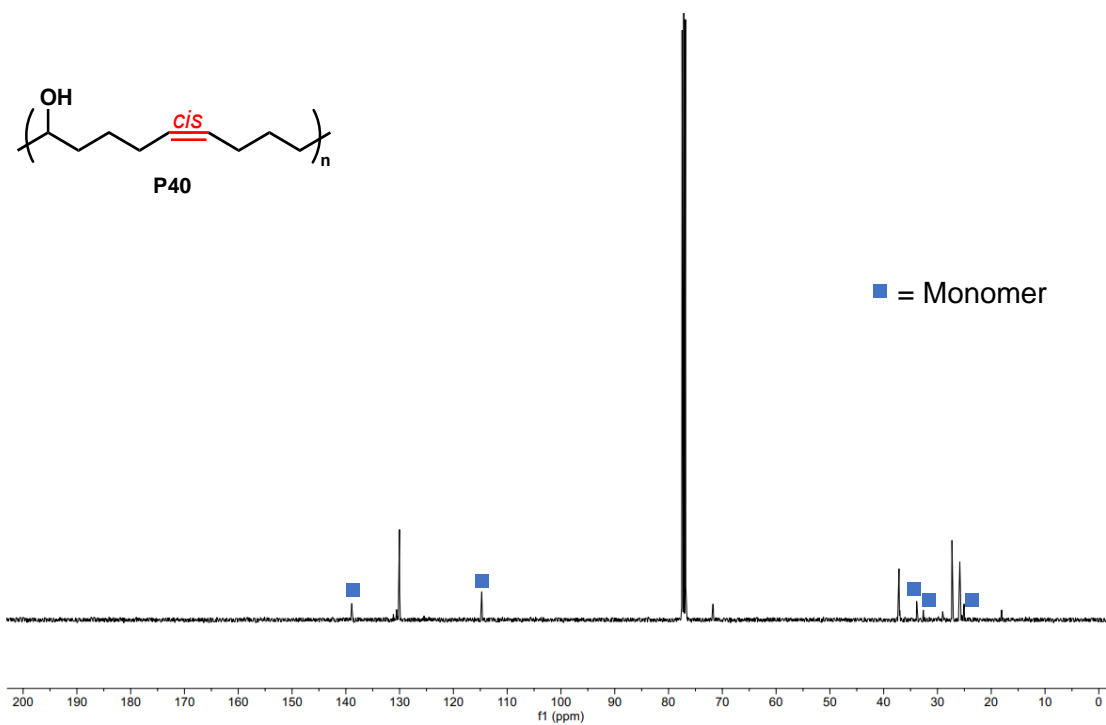
Figure V-109 ^{13}C NMR (101 MHz, CDCl$_3$) spectrum of *cis*-rich **P40** (NOTE: oligomer *cis*-**P40** could not be precipitated and separated from unreacted monomer **40** (blue square labels).

CHAPTER VI

CONCLUDING REMARKS AND OUTLOOK

Stereoselective Ru-catalysts for olefin metathesis are very promising, not only for the synthesis of small molecules, but also for the preparation of stereodefined polymers. We successfully leveraged the reactivity of dithiolate Ru catalysts for the synthesis of all-*cis* PPVs and of a broad range of *cis* polyalkenamers through either stereoselective ROMP or ADMET polymerization.

The development of a stereoretentive ROMP of [2,2] paracyclophane-1,9-dienes allowed access to all-*cis* PPVs with living characteristics and also permitted the construction of intricate polymeric architectures containing all-*cis* PPV segments. It also provided a strategy to obtain all-*trans* PPV with high molar masses and uniform chain size via a mild and efficient photoisomerization of the more soluble all-*cis* counterpart. The substituents on the paracyclophane diene framework was shown to impact the kinetics of both polymerization and isomerization processes significantly. Moreover, the *cis*/*trans* ratio of PPV can be regulated by the UV irradiation of all-*cis* PPV which was found to follow first-order kinetics on the concentration of *cis* linkage, serving as a powerful tool to customize PPV with specific *cis* and *trans* composition.

In parallel to our development of stereoretentive ROMP, we implemented stereoretention into the ADMET process using readily accessible *cis*,*cis*-diene monomers and dithiolate Ru catalysts, which led to a variety of *cis* polymers without the requirement of highly strained structures. Modulation of the reaction temperature and duration further enabled a stereocontrol of the ADMET process, which delivered an array of degradable

366

polyalkenamers with predictable *cis*/*trans* ratio, further allowing the modulation of polymer properties, such as crystallinity.

Meanwhile, we have also developed a *cis*-selective ADMET polymerization of readily available α,ω-dienes monomers. Exquisite *cis* selectivity was achieved for most monomers through kinetic control of the olefin metathesis process enabled by a robust cyclometalated Ru catalyst. This diversity-oriented polymerization allowed us to compare the thermal properties of a variety of *cis* polyalkenamers containing different polar functional groups with their *trans* congeners. High *cis*-content was found to generally correlate with better thermal stability, a lower glass transition temperature, and typically amorphous behavior. Furthermore, an ABA triblock copolymer with polyoctenamer as a rubbery middle segment and PLA as end blocks was synthesized. Nanoindentation measurements revealed that the *cis* stereochemistry led to a greater decrease in stiffness when compared to the ABA copolymer containing a *trans* middle block.

The development of these synthetic methods has enabled the precise synthesis of diverse alkene-containing polymers, paving the way for investigating the influence of stereochemistry on material properties. Despite decades of research in polymer science, this relationship remains poorly understood. Our ultimate goal is to unravel the influence of olefin geometry on polymer properties, which would enable the design and synthesis of soft materials with desirable properties for a wide range of applications through modulation of the *cis*/*trans* ratio.

REFERENCES

1. Hsu, T.-W.; Kim, C.; Michaudel, Q. Stereoretentive Ring-Opening Metathesis Polymerization to Access All-*cis* Poly(*p*-phenylenevinylene)s with Living Characteristics. *J. Am. Chem. Soc.* **2020**, *142*, 11983–11987.

2. Hsu, T.-W.; Kempel, S. J.; Michaudel, Q. All-*cis* poly(*p*-phenylene vinylene)s with high molar masses and fast photoisomerization rates obtained through stereoretentive ring-opening metathesis polymerization of [2,2]paracyclophane dienes with various aryl substituents. *J. Polym. Sci.* **2022**, *60*, 569–578.

3. Hsu, T.-W.; Kempel, S. J.; Felix Thayne, A. P.; Michaudel, Q. Stereocontrolled acyclic diene metathesis polymerization. *Nat. Chem.* **2023**, *15*, 14–20.

4. Kempel, S. J.; Hsu, T.-W.; Nicholson, J. L.; Michaudel, Q. *cis*-Selective Acyclic Diene Metathesis Polymerization of α,ω-Dienes. *J. Am. Chem. Soc.* **2023**, *145*, 12459–12464.

5. Worch, J. C.; Prydderch, H.; Jimaja, S.; Bexis, P.; Becker, M. L.; Dove, A. P. Stereochemical enhancement of polymer properties. *Nat. Rev. Chem.* **2019**, *3*, 514–535.

6. Coates, G. W.; Waymouth, R. M. Oscillating Stereocontrol: A Strategy for the Synthesis of Thermoplastic Elastomeric Polypropylene. *Science* **1995**, *267*, 217–219.

7. Wang, C.; Lin, C.-C.; Tseng, L.-C. Miscibility, crystallization and morphologies of syndiotactic polystyrene blends with isotactic polystyrene and with atactic polystyrene. *Polymer* **2006**, *47*, 390–402.

8. Bhowmick, A. K.; Kuo, C. C.; Manzur, A.; Arthur, A. M.; Intyre, D. M. Properties of *cis*-and *trans*-polyisoprene blends. *J. Macromol. Sci., Part B: Phys.* **1986**, *25*, 283–306.

9. Baboo, M.; Dixit, M.; Sharma, K.; Saxena, N. S. Mechanical and thermal characterization of *cis*-polyisoprene and *trans*-polyisoprene blends. *Polym. Bull.* **2011**, *66*, 661–672.

10. Kent; Kent, E. G.; Swinney, F. B. Properties and Applications of *trans*-1,4-Polyisoprene. *I & EC Product Research and Development* **1966**, *5*, 134–138.

11. Ricci, G.; Pampaloni, G.; Sommazzi, A.; Masi, F. Dienes Polymerization: Where We Are and What Lies Ahead. *Macromolecules* **2021**, *54*, 5879–5914.

12. Wang, F.; He, F.; Xie, Z. Q.; Li, Y. P.; Hanif, M.; Li, M.; Ma, Y. Poly(*p*-phenylene vinylene) Derivatives with Different Contents of *cis*-Olefins and their Effect on the Optical Properties. *Macromol. Chem. Phys.* **2008**, *209*, 1381–1388.

13. Wang, F.; He, F.; Xie, Z.; Li, M.; Hanif, M.; Gu, X.; Yang, B.; Zhang, H.; Lu, P.; Ma, Y. A solution-processable poly(*p*-phenylene vinylene) without alkyl substitution: Introducing the *cis*-vinylene segments in polymer chain for improved solubility, blue emission, and high efficiency. *J. Polym. Sci., Part A: Polym. Chem.* **2008**, *46*, 5242–5250.

14. Jean-Louis Hérisson, P.; Chauvin, Y. Catalyse de transformation des oléfines par les complexes du tungstène. II. Télomérisation des oléfines cycliques en présence d'oléfines acycliques. *Die Makromolekulare Chemie* **1971**, *141*, 161–176.

15. Michaudel, Q.; Kempel, S. J.; Hsu, T.-W.; deGruyter, J. N., 13.07 - *E* vs *Z* Selectivity in Olefin Metathesis Through Catalyst Design. In *Comprehensive Organometallic Chemistry IV*, Parkin, G.; Meyer, K.; O'hare, D., Eds. Elsevier: Oxford, 2022; pp 265–338.

16. Endo, K.; Grubbs, R. H. Chelated Ruthenium Catalysts for *Z*-Selective Olefin Metathesis. *J. Am. Chem. Soc.* **2011**, *133*, 8525–8527.

17. Keitz, B. K.; Endo, K.; Patel, P. R.; Herbert, M. B.; Grubbs, R. H. Improved Ruthenium Catalysts for *Z*-Selective Olefin Metathesis. *J. Am. Chem. Soc.* **2012**, *134*, 693–699.

18. Khan, R. K. M.; Torker, S.; Hoveyda, A. H. Readily Accessible and Easily Modifiable Ru-Based Catalysts for Efficient and *Z*-Selective Ring-Opening Metathesis Polymerization and Ring-Opening/Cross-Metathesis. *J. Am. Chem. Soc.* **2013**, *135*, 10258–10261.

19. Montgomery, T. P.; Ahmed, T. S.; Grubbs, R. H. Stereoretentive Olefin Metathesis: An Avenue to Kinetic Selectivity. *Angew. Chem. Int. Ed.* **2017**, *56*, 11024–11036.

20. Müller, D. S.; Baslé, O.; Mauduit, M. A tutorial review of stereoretentive olefin metathesis based on ruthenium dithiolate catalysts. *Beilstein J. Org. Chem.* **2018**, *14*, 2999–3010.

21. Liu, P.; Xu, X.; Dong, X.; Keitz, B. K.; Herbert, M. B.; Grubbs, R. H.; Houk, K. N. *Z*-Selectivity in Olefin Metathesis with Chelated Ru Catalysts:

Computational Studies of Mechanism and Selectivity. *J. Am. Chem. Soc.* **2012**, *134*, 1464–1467.

22. Johns, A. M.; Ahmed, T. S.; Jackson, B. W.; Grubbs, R. H.; Pederson, R. L. High *trans* Kinetic Selectivity in Ruthenium-Based Olefin Cross-Metathesis through Stereoretention. *Org. Lett.* **2016**, *18*, 772–775.

23. Grandner, J. M.; Shao, H.; Grubbs, R. H.; Liu, P.; Houk, K. N. Origins of the Stereoretentive Mechanism of Olefin Metathesis with Ru-Dithiolate Catalysts. *The Journal of Organic Chemistry* **2017**, *82*, 10595-10600.

24. Keitz, B. K.; Fedorov, A.; Grubbs, R. H. *cis*-Selective Ring-Opening Metathesis Polymerization with Ruthenium Catalysts. *J. Am. Chem. Soc.* **2012**, *134*, 2040–2043.

25. Song, J.-A.; Peterson, G. I.; Bang, K.-T.; Ahmed, T. S.; Sung, J.-C.; Grubbs, R. H.; Choi, T.-L. Ru-Catalyzed, *cis*-Selective Living Ring-Opening Metathesis Polymerization of Various Monomers, Including a Dendronized Macromonomer, and Implications to Enhanced Shear Stability. *J. Am. Chem. Soc.* **2020**, *142*, 10438–10445.

26. Blayney, A. J.; Perepichka, I. F.; Wudl, F.; Perepichka, D. F. Advances and Challenges in the Synthesis of Poly(*p*-phenylene vinylene)-Based Polymers. *Isr. J. Chem.* **2014**, *54*, 674–688.

27. Burroughes, J. H.; Bradley, D. D. C.; Brown, A. R.; Marks, R. N.; Mackay, K.; Friend, R. H.; Burns, P. L.; Holmes, A. B. Light-emitting diodes based on conjugated polymers. *Nature* **1990**, *347*, 539–541.

28. Yu, G.; Gao, J.; Hummelen, J. C.; Wudl, F.; Heeger, A. J. Polymer Photovoltaic Cells: Enhanced Efficiencies via a Network of Internal Donor-Acceptor Heterojunctions. *Science* **1995**, *270*, 1789–1791.

29. Grimsdale, A. C.; Leok Chan, K.; Martin, R. E.; Jokisz, P. G.; Holmes, A. B. Synthesis of Light-Emitting Conjugated Polymers for Applications in Electroluminescent Devices. *Chem. Rev.* **2009**, *109*, 897–1091.

30. Junkers, T.; Vandenbergh, J.; Adriaensens, P.; Lutsen, L.; Vanderzande, D. Synthesis of poly(*p*-phenylene vinylene) materials via the precursor routes. *Polym. Chem.* **2012**, *3*, 275–285.

31. Zaquen, N.; Lutsen, L.; Vanderzande, D.; Junkers, T. Controlled/living polymerization towards functional poly(*p*-phenylene vinylene) materials. *Polym. Chem.* **2016**, *7*, 1355–1367.

32. Arai, T.; Tokumaru, K. Photochemical one-way adiabatic isomerization of aromatic olefins. *Chem. Rev.* **1993**, *93*, 23–39.

33. Katayama, H.; Nagao, M.; Nishimura, T.; Matsui, Y.; Umeda, K.; Akamatsu, K.; Tsuruoka, T.; Nawafune, H.; Ozawa, F. Stereocontrolled Synthesis and Optical Properties of All-*cis* Poly(phenylene vinylenes) (PPVs): A Method for Direct Patterning of PPVs. *J. Am. Chem. Soc.* **2005**, *127*, 4350–4353.

34. Shin, S.; Gu, M.-L.; Yu, C.-Y.; Jeon, J.; Lee, E.; Choi, T.-L. Polymer Self-Assembly into Unique Fractal Nanostructures in Solution by a One-Shot Synthetic Procedure. *J. Am. Chem. Soc.* **2018**, *140*, 475–482.

35. Shin, S.; Menk, F.; Kim, Y.; Lim, J.; Char, K.; Zentel, R.; Choi, T.-L. Living Light-Induced Crystallization-Driven Self-Assembly for Rapid Preparation of Semiconducting Nanofibers. *J. Am. Chem. Soc.* **2018**, *140*, 6088–6094.

36. Yang, Z.; Hu, B.; Karasz, F. E. Polymer Electroluminescence Using ac or Reverse dc Biasing. *Macromolecules* **1995**, *28*, 6151–6154.

37. Pfeiffer, S.; Hörhold, H.-H. Investigation of poly(arylene vinylene)s, 41. Synthesis of soluble dialkoxy-substituted poly(phenylene alkenylidene)s by applying the Horner-reaction for condensation polymerization. *Macromol. Chem. Phys.* **1999**, *200*, 1870–1878.

38. Morin, J.-F.; Drolet, N.; Tao, Y.; Leclerc, M. Syntheses and Characterization of Electroactive and Photoactive 2,7-Carbazolenevinylene-Based Conjugated Oligomers and Polymers. *Chem. Mater.* **2004**, *16*, 4619–4626.

39. Katayama, H.; Nagao, M.; Nishimura, T.; Matsui, Y.; Fukuse, Y.; Wakioka, M.; Ozawa, F. Stereocontrolled Synthesis and Characterization of *cis*-Poly(arylenevinylene)s. *Macromolecules* **2006**, *39*, 2039–2048.

40. Moslin, R. M.; Espino, C. G.; Swager, T. M. Synthesis of Conjugated Polymers Containing *cis*-Phenylenevinylenes by Titanium-Mediated Reductions. *Macromolecules* **2009**, *42*, 452–454.

41. Yu, C.-Y.; Turner, M. L. Soluble Poly(*p*-phenylenevinylene)s through Ring-Opening Metathesis Polymerization. *Angew. Chem. Int. Ed.* **2006**, *45*, 7797–7800.

42. Lidster, B. J.; Behrendt, J. M.; Turner, M. L. Monotelechelic poly(*p*-phenylenevinylene)s by ring opening metathesis polymerisation. *Chem. Commun.* **2014**, *50*, 11867–11870.

43. Lidster, B. J.; Kumar, D. R.; Spring, A. M.; Yu, C.-Y.; Turner, M. L. Alkyl substituted poly(*p*-phenylene vinylene)s by ring opening metathesis polymerisation. *Polym. Chem.* **2016**, *7*, 5544–5551.

44. Herbert, M. B.; Grubbs, R. H. *Z*-Selective Cross Metathesis with Ruthenium Catalysts: Synthetic Applications and Mechanistic Implications. *Angew. Chem. Int. Ed.* **2015**, *54*, 5018–5024.

45. Wang, T.; Wu, B.; Guo, W.; Wu, S.; Zhang, H.; Dang, Y.; Wang, J. Synthesis, catalysis, and DFT study of a ruthenium carbene complex bearing a 1,2-dicarbadodecaborane (12)-1,2-dithiolate ligand. *Dalton Trans.* **2019**, *48*, 2646–2656.

46. Mikus, M. S.; Torker, S.; Hoveyda, A. H. Controllable ROMP Tacticity by Harnessing the Fluxionality of Stereogenic-at-Ruthenium Complexes. *Angew. Chem. Int. Ed.* **2016**, *55*, 4997–5002.

47. Jung, H.; Jung, K.; Hong, M.; Kwon, S.; Kim, K.; Hong, S. H.; Choi, T.-L.; Baik, M.-H. Understanding the Origin of the Regioselectivity in Cyclopolymerizations of Diynes and How to Completely Switch It. *J. Am. Chem. Soc.* **2018**, *140*, 834–841.

48. Jung, K.; Kim, K.; Sung, J.-C.; Ahmed, T. S.; Hong, S. H.; Grubbs, R. H.; Choi, T.-L. Toward Perfect Regiocontrol for β-Selective Cyclopolymerization Using a Ru-Based Olefin Metathesis Catalyst. *Macromolecules* **2018**, *51*, 4564–4571.

49. Conticello, V. P.; Gin, D. L.; Grubbs, R. H. Ring-opening metathesis polymerization of substituted bicyclo[2.2.2]octadienes: a new precursor route to poly(1,4-phenylenevinylene). *J. Am. Chem. Soc.* **1992**, *114*, 9708–9710.

50. Miao, Y.-J.; Bazan, G. C. Paracyclophene Route to Poly(*p*-phenylenevinylene). *J. Am. Chem. Soc.* **1994**, *116*, 9379–9380.

51. Wagaman, M. W.; Grubbs, R. H. Synthesis of Organic and Water Soluble Poly(1,4-phenylenevinylenes) Containing Carboxyl Groups: Living Ring-Opening Metathesis Polymerization (ROMP) of 2,3-Dicarboxybarrelenes. *Macromolecules* **1997**, *30*, 3978–3985.

52. Lidster, B. J.; Kumar, D. R.; Spring, A. M.; Yu, C.-Y.; Helliwell, M.; Raftery, J.; Turner, M. L. Alkyl substituted [2.2]paracyclophane-1,9-dienes. *Org. Biomol. Chem.* **2016**, *14*, 6079–6087.

53. Johns, A.M. Synthesis and characterization of metathesis catalysts. Patent WO2018038928 A1, August 10, 2017.

54. Kumar, D. R.; Lidster, B. J.; Adams, R. W.; Turner, M. L. Mechanistic investigation of the ring opening metathesis polymerisation of alkoxy and alkyl substituted paracyclophanedienes. *Polym. Chem.* **2017**, *8*, 3186–3194.

55. Menk, F.; Mondeshki, M.; Dudenko, D.; Shin, S.; Schollmeyer, D.; Ceyhun, O.; Choi, T.-L.; Zentel, R. Reactivity Studies of Alkoxy-Substituted

[2.2]Paracyclophane-1,9-dienes and Specific Coordination of the Monomer Repeating Unit during ROMP. *Macromolecules* **2015**, *48*, 7435–7445.

56. Matson, J. B.; Grubbs, R. H. Synthesis of Fluorine-18 Functionalized Nanoparticles for use as in vivo Molecular Imaging Agents. *J. Am. Chem. Soc.* **2008**, *130*, 6731–6733.

57. Cole, J. P.; Lessard, J. J.; Lyon, C. K.; Tuten, B. T.; Berda, E. B. Intra-chain radical chemistry as a route to poly(norbornene imide) single-chain nanoparticles: structural considerations and the role of adventitious oxygen. *Polym. Chem.* **2015**, *6*, 5555–5559.

58. Mäker, D.; Bunz, U. H. F. Fourfold Alkoxy-Substituted [2.2.2]Paracyclophane-1,9,17-trienes–ROMP into PPVs with Unusual Topologies. *Macromol. Rapid Commun.* **2014**, *35*, 2096–2100.

59. Elacqua, E.; Weck, M. Fabrication of Supramolecular Semiconductor Block Copolymers by Ring-Opening Metathesis Polymerization. *Chem. Eur. J.* **2015**, *21*, 7151–7158.

60. Elacqua, E.; Gregor, M. Poly(arylenevinylene)s through Ring-Opening Metathesis Polymerization of an Unsymmetrical Donor-Acceptor Cyclophane. *Angew. Chem. Int. Ed.* **2019**, *58*, 9527–9532.

61. Lynch, P. J.; O'Neill, L.; Bradley, D.; Byrne, H. J.; McNamara, M. Systematic Study of the Effects of Naphthalene and Anthracene Substitution on the Properties of PPV Derivative Conjugated Systems. *Macromolecules* **2007**, *40*, 7895–7901.

62. Murugan, P.; Raghavendra, V.; Chithiravel, S.; Krishnamoorthy, K.; Mandal, A. B.; Subramanian, V.; Samanta, D. Experimental and Theoretical Investigations of Different Diketopyrrolopyrrole-Based Polymers. *ACS Omega* **2018**, *3*, 11710–11717.

63. Elacqua, E.; Manning, K. B.; Lye, D. S.; Pomarico, S. K.; Morgia, F.; Weck, M. Supramolecular Multiblock Copolymers Featuring Complex Secondary Structures. *J. Am. Chem. Soc.* **2017**, *139*, 12240–12250.

64. Nallasivam, J. L.; Fernandes, R. A. A Cascade Aza-Cope/Aza-Prins Cyclization Leading to Piperidine Derivatives. *Eur. J. Org. Chem.* **2015**, *2015*, 2012–2022.

65. Cangelosi, V. M.; Zakharov, L. N.; Crossland, J. L.; Franklin, B. C.; Johnson, D. W. A Surprising "Folded-In" Conformation of a Self-Assembled Arsenic-Thiolate Macrocycle. *Crystal Growth & Design* **2010**, *10*, 1471–1473.

66. Halls, J. J. M.; Walsh, C. A.; Greenham, N. C.; Marseglia, E. A.; Friend, R. H.; Moratti, S. C.; Holmes, A. B. Efficient photodiodes from interpenetrating polymer networks. *Nature* **1995**, *376*, 498–500.

67. Z. R. Li, Organic Light-Emitting Materials and Devices, CRCPress, Boca Raton, FL 2015.

68. Shaked, S.; Tal, S.; Roichman, Y.; Razin, A.; Xiao, S.; Eichen, Y.; Tessler, N. Charge Density and Film Morphology Dependence of Charge Mobility in Polymer Field-Effect Transistors. *Adv. Mater.* **2003**, *15*, 913–916.

69. Koynov, K.; Bahtiar, A.; Ahn, T.; Cordeiro, R. M.; Hörhold, H.-H.; Bubeck, C. Molecular Weight Dependence of Chain Orientation and Optical Constants of Thin

Films of the Conjugated Polymer MEH-PPV. *Macromolecules* **2006**, *39*, 8692–8698.

70. Elacqua, E.; Geberth, G. T.; Vanden Bout, D. A.; Weck, M. Synthesis and folding behaviour of poly(*p*-phenylene vinylene)-based β-sheet polychromophores. *Chemical Science* **2019**, *10*, 2144–2152.

71. Liu, C.-J.; Wang, C.-C.; Kuo, D.-L.; Yu, C.-Y. Carbazolevinylene and phenylenevinylene polymers by ring-opening metathesis polymerization and their characterization, nanoaggregates and optical and electrochemical properties. *Polymer* **2019**, *181*, 121770.

72. Kempel, S. J.; Hsu, T.-W.; Michaudel, Q. Stereoretentive Olefin Metathesis: A New Avenue for the Synthesis of All-*cis* Poly(*p*-phenylene vinylene)s and Stereo-defined Polyalkenamers. *Synlett* **2021**, *32*, 851–857.

73. Gorman; Gorman, C.; Ginsburg, E.; Grubbs, R. H. Soluble, highly conjugated derivatives of polyacetylene from the ring-opening metathesis polymerization of monosubstituted cyclooctatetraenes: synthesis and the relationship between polymer structure and physical properties. *J. Am. Chem. Soc.* **1993**, *115*, 1397–1409.

74. Burkhart, B.; Khlyabich, P. P.; Thompson, B. C. Influence of the Ethylhexyl Side-Chain Content on the Open-Circuit Voltage in *rr*-Poly(3-hexylthiophene-*co*-3-(2-ethylhexyl)thiophene) Copolymers. *Macromolecules* **2012**, *45*, 3740–3748.

75. CDCl$_3$ used for NMR characterization to facilitate comparison to previously reported spectra of all-*trans* poly-**1b** and poly-**1d**.

76. Yao, J. H.; Chen, Y.; Pang, Y. Application of sonochemistry in the isomerization of carbon-carbon double bonds. *J. Polym. Sci., Part A: Polym. Chem.* **2010**, *48*, 5254–5257.

77. Liu; Liu, Z.; Morigaki, K.; Enomoto, T.; Hashimoto, K.; Fujishima, A. Kinetic studies on the thermal cis-trans isomerization of an azo compound in the assembled monolayer film. *J. Phys. Chem.* **1992**, *96*, 1875–1880.

78. Salaita, G. N. Kinetic study of *cis-trans* stilbene isomerization with SbCl$_3$ by nuclear magnetic resonance spectroscopy. *J. Inorg. Nucl. Chem.* **1974**, *36*, 875–879.

79. Smith, S.; Bou-Abdallah, F. The Kinetics of the *cis*-to-*trans* Thermal Isomerization of 4-Anilino-4'-Nitroazobenzene are Highly Influenced by Solvent Polarity. *Journal of Thermodynamics and Catalysis* **2017**, *8*, 1–6.

80. Würth, C.; Grabolle, M.; Pauli, J.; Spieles, M.; Resch-Genger, U. Relative and absolute determination of fluorescence quantum yields of transparent samples. *Nat. Protoc.* **2013**, *8*, 1535–1550.

81. Roman, D.; Sauer, M.; Beemelmanns, C. Applications of the Horner–Wadsworth–Emmons Olefination in Modern Natural Product Synthesis. *Synthesis* **2021**, *53*, 2713–2739.

82. Bell, C. A.; Yu, J.; Barker, I. A.; Truong, V. X.; Cao, Z.; Dobrinyin, A. V.; Becker, M. L.; Dove, A. P. Independent Control of Elastomer Properties through Stereocontrolled Synthesis. *Angew. Chem. Int. Ed.* **2016**, *55*, 13076–13080.

83. Yang, X.; Gitter, S. R.; Roessler, A. G.; Zimmerman, P. M.; Boydston, A. J. An Ion-Pairing Approach to Stereoselective Metal-Free Ring-Opening Metathesis Polymerization. *Angew. Chem. Int. Ed.* **2021**, *60*, 13952–13958.

84. Liu, J.; Lam, J. W. Y.; Jim, C. K. W.; Ng, J. C. Y.; Shi, J.; Su, H.; Yeung, K. F.; Hong, Y.; Faisal, M.; Yu, Y.; Wong, K. S.; Tang, B. Z. Thiol−Yne Click Polymerization: Regio- and Stereoselective Synthesis of Sulfur-Rich Acetylenic Polymers with Controllable Chain Conformations and Tunable Optical Properties. *Macromolecules* **2011**, *44*, 68–79.

85. Schrock, R. R. Synthesis of Stereoregular Polymers through Ring-Opening Metathesis Polymerization. *Acc. Chem. Res.* **2014**, *47*, 2457–2466.

86. Koh, M. J.; Khan, R. K. M.; Torker, S.; Yu, M.; Mikus, M. S.; Hoveyda, A. H. High-value alcohols and higher-oxidation-state compounds by catalytic *Z*-selective cross-metathesis. *Nature* **2015**, *517*, 181–186.

87. Montgomery, T. P.; Johns, A. M.; Grubbs, R. H. Recent Advancements in Stereoselective Olefin Metathesis Using Ruthenium Catalysts. *Catalysts* **2017**, *7*, 87.

88. Benedikter, M. J.; Ziegler, F.; Groos, J.; Hauser, P. M.; Schowner, R.; Buchmeiser, M. R. Group 6 metal alkylidene and alkylidyne *N*-heterocyclic carbene complexes for olefin and alkyne metathesis. *Coord. Chem. Rev.* **2020**, *415*, 213315.

89. Dawood, K. M.; Nomura, K. Recent Developments in Z-Selective Olefin Metathesis Reactions by Molybdenum, Tungsten, Ruthenium, and Vanadium Catalysts. *Adv. Synth. Catal.* **2021**, *363*, 1970–1997.

90. Grandner, J. M.; Shao, H.; Grubbs, R. H.; Liu, P.; Houk, K. N. Origins of the Stereoretentive Mechanism of Olefin Metathesis with Ru-Dithiolate Catalysts. *The Journal of Organic Chemistry* **2017**, *82*, 10595–10600.

91. Caire da Silva, L.; Rojas, G.; Schulz, M. D.; Wagener, K. B. Acyclic diene metathesis polymerization: History, methods and applications. *Prog. Polym. Sci.* **2017**, *69*, 79–107.

92. Pribyl, J.; Wagener, K. B.; Rojas, G. ADMET polymers: synthesis, structure elucidation, and function. *Mater. Chem. Front.* **2021**, *5*, 14–43.

93. Wagener; Wagener, K. B.; Boncella, J. M.; Nel, J. G. Acyclic diene metathesis (ADMET) polymerization. *Macromolecules* **1991**, *24*, 2649–2657.

94. Rojas, G.; Inci, B.; Wei, Y.; Wagener, K. B. Precision Polyethylene: Changes in Morphology as a Function of Alkyl Branch Size. *J. Am. Chem. Soc.* **2009**, *131*, 17376–17386.

95. Aitken, B. S.; Lee, M.; Hunley, M. T.; Gibson, H. W.; Wagener, K. B. Synthesis of Precision Ionic Polyolefins Derived from Ionic Liquids. *Macromolecules* **2010**, *43*, 1699–1701.

96. Weychardt, H.; Plenio, H. Acyclic Diene Metathesis Polymerization of Divinylarenes and Divinylferrocenes with Grubbs-Type Olefin Metathesis Catalysts. *Organometallics* **2008**, *27*, 1479–1485.

97. Xu, C.; Shen, X.; Hoveyda, A. H. In Situ Methylene Capping: A General Strategy for Efficient Stereoretentive Catalytic Olefin Metathesis. The Concept, Methodological Implications, and Applications to Synthesis of Biologically Active Compounds. *J. Am. Chem. Soc.* **2017**, *139*, 10919–10928.

98. Guoshun, Y.; Keda, H.; Yang, Q. *cis*/*cis*-2,5-dipropenylthiophene monomers for high-molecular-weight poly(2,5-thienylene vinylene)s through acyclic diene metathesis polymerization. *J. Polym. Sci., Part A: Polym. Chem.* **2014**, *52*, 591–595.

99. Patton, J. T.; Boncella, J. M.; Wagener, K. B. Acyclic diene metathesis (ADMET) polymerization: the synthesis of unsaturated polyesters. *Macromolecules* **1992**, *25*, 3862–3867.

100. Wagener, K. B.; Patton, J. T. Acyclic diene metathesis (ADMET) polymerization. Synthesis of unsaturated polycarbonates. *Macromolecules* **1993**, *26*, 249–253.

101. Wagener, K. B.; Brzezinska, K. Acyclic diene metathesis (ADMET) polymerization: synthesis of unsaturated polyethers. *Macromolecules* **1991**, *24*, 5273–5277.

102. Gaines, T. W.; Nakano, T.; Chujo, Y.; Trigg, E. B.; Winey, K. I.; Wagener, K. B. Precise Sulfite Functionalization of Polyolefins via ADMET Polymerization. *ACS Macro Lett.* **2015**, *4*, 624–627.

103. Fokou, P. A.; Meier, M. A. R. Studying and Suppressing Olefin Isomerization Side Reactions During ADMET Polymerizations. *Macromol. Rapid Commun.* **2010**, *31*, 368–373.

104. Engel, J.; Smit, W.; Foscato, M.; Occhipinti, G.; Törnroos, K. W.; Jensen, V. R. Loss and Reformation of Ruthenium Alkylidene: Connecting Olefin Metathesis, Catalyst Deactivation, Regeneration, and Isomerization. *J. Am. Chem. Soc.* **2017**, *139*, 16609–16619.

105. Courchay, F. C.; Sworen, J. C.; Ghiviriga, I.; Abboud, K. A.; Wagener, K. B. Understanding Structural Isomerization during Ruthenium-Catalyzed Olefin Metathesis: A Deuterium Labeling Study. *Organometallics* **2006**, *25*, 6074–6086.

106. Qin, H.; Chakulski, B. J.; Rousseau, I. A.; Chen, J.; Xie, X.-Q.; Mather, P. T.; Constable, G. S.; Coughlin, E. B. Synthesis and Characterization of Unsaturated Thermotropic Polyesters Prepared via Acyclic Diene Metathesis Polymerization. *Macromolecules* **2004**, *37*, 5239–5249.

107. McGuire, T. M.; Pérale, C.; Castaing, R.; Kociok-Köhn, G.; Buchard, A. Divergent Catalytic Strategies for the *cis/trans* Stereoselective Ring-Opening Polymerization of a Dual Cyclic Carbonate/Olefin Monomer. *J. Am. Chem. Soc.* **2019**, *141*, 13301–13305.

108. Stubbs, C. J.; Worch, J. C.; Prydderch, H.; Becker, M. L.; Dove, A. P. Unsaturated Poly(ester-urethanes) with Stereochemically Dependent Thermomechanical Properties. *Macromolecules* **2020**, *53*, 174–181.

109. Lodge, T. P. Celebrating 50 Years of Macromolecules. *Macromolecules* **2017**, *50*, 9525–9527.

110. Kim, J. G.; Jeon, J. Y.; Chun, J.; Kim, C. S.; Lee, P. C.; Lee, B. Y. Efficient synthesis of organic carbonates and poly(1,4-butylene carbonate-*co*-terephthalate)s. *J. Appl. Polym. Sci.* **2017**, *134*.

111. Polic, V.; Cheong, K. J.; Hammerer, F.; Auclair, K. Regioselective Epoxidations by Cytochrome P450 3A4 Using a Theobromine Chemical Auxiliary to Predictably Produce N-Protected β- or γ-Amino Epoxides. *Adv. Synth. Catal.* **2017**, *359*, 3983–3989.

112. Mancheno, D. E.; Thornton, A. R.; Stoll, A. H.; Kong, A.; Blakey, S. B. Copper-Catalyzed Olefin Aminoacetoxylation. *Org. Lett.* **2010**, *12*, 4110–4113.

113. Ganesh, N. V.; Fujikawa, K.; Tan, Y. H.; Nigudkar, S. S.; Stine, K. J.; Demchenko, A. V. Surface-Tethered Iterative Carbohydrate Synthesis: A Spacer Study. *The Journal of Organic Chemistry* **2013**, *78*, 6849–6857.

114. Wagener, K. B.; Brzezinska, K.; Anderson, J. D.; Younkin, T. R.; Steppe, K.; DeBoer, W. Kinetics of Acyclic Diene Metathesis (ADMET) Polymerization. Influence of the Negative Neighboring Group Effect. *Macromolecules* **1997**, *30*, 7363–7369.

115. Akbulatov, S.; Tian, Y.; Boulatov, R. Force–Reactivity Property of a Single Monomer Is Sufficient To Predict the Micromechanical Behavior of Its Polymer. *J. Am. Chem. Soc.* **2012**, *134*, 7620–7623.

116. Qin, D.; Sullivan, R.; Berkowitz, W. F.; Bittman, R.; Rotenberg, S. A. Inhibition of Protein Kinase Cα by Dequalinium Analogues: Dependence on Linker Length and Geometry. *J. Med. Chem.* **2000**, *43*, 1413–1417.

117. Worch, J. C.; Dove, A. P. Click Step-Growth Polymerization and *E/Z* Stereochemistry Using Nucleophilic Thiol–yne/–ene Reactions: Applying Old Concepts for Practical Sustainable (Bio)Materials. *Acc. Chem. Res.* **2022**, *55*, 2355–2369.

118. Khalfa, A. L.; Becker, M. L.; Dove, A. P. Stereochemistry-Controlled Mechanical Properties and Degradation in 3D-Printable Photosets. *J. Am. Chem. Soc.* **2021**, *143*, 17510–17516.

119. Grobelny, J. N.m.r. study of maleate (*cis*)—fumarate (*trans*) isomerism in unsaturated polyesters and related compounds. *Polymer* **1995**, *36*, 4215–4222.

120. Yu, Y.; Wei, Z.; Leng, X.; Li, Y. Facile preparation of stereochemistry-controllable biobased poly(butylene maleate-*co*-butylene fumarate) unsaturated copolyesters: a chemoselective polymer platform for versatile functionalization via aza-Michael addition. *Polym. Chem.* **2018**, *9*, 5426–5441.

121. Rojas, G.; Wagener, K.B.; Pribyl, J., ADMET Polymerization. In *Encyclopedia of Polymer Science and Technology*; Wiley, 2022.

122. Bielawski, C. W.; Grubbs, R. H. Living ring-opening metathesis polymerization. *Prog. Polym. Sci.* **2007**, *32*, 1–29.

123. Ogba, O. M.; Warner, N. C.; O'Leary, D. J.; Grubbs, R. H. Recent advances in ruthenium-based olefin metathesis. *Chem. Soc. Rev.* **2018**, *47*, 4510–4544.

124. Rosebrugh, L. E.; Herbert, M. B.; Marx, V. M.; Keitz, B. K.; Grubbs, R. H. Highly Active Ruthenium Metathesis Catalysts Exhibiting Unprecedented Activity and Z-Selectivity. *J. Am. Chem. Soc.* **2013**, *135*, 1276–1279.

125. Xu, Y.; Wong, J. J.; Samkian, A. E.; Ko, J. H.; Chen, S.; Houk, K. N.; Grubbs, R. H. Efficient *Z*-Selective Olefin-Acrylamide Cross-Metathesis Enabled by Sterically Demanding Cyclometalated Ruthenium Catalysts. *J. Am. Chem. Soc.* **2020**, *142*, 20987–20993.

126. Xu, Y.; Gan, Q.; Samkian, A. E.; Ko, J. H.; Grubbs, R. H. Bulky Cyclometalated Ruthenium Nitrates for Challenging *Z*-Selective Metathesis: Efficient One-Step Access to α-Oxygenated *Z*-Olefins from Acrylates and Allyl Alcohols. *Angew. Chem. Int. Ed.* **2022**, *61*, e202113089.

127. Dumas, A.; Tarrieu, R.; Vives, T.; Roisnel, T.; Dorcet, V.; Baslé, O.; Mauduit, M. A Versatile and Highly *Z*-Selective Olefin Metathesis Ruthenium Catalyst Based on a Readily Accessible *N*-Heterocyclic Carbene. *ACS Catalysis* **2018**, *8*, 3257–3262.

128. Because of the volatility of the monomer, nitrogen purging was used instead of vacuum to remove ethylene (Figure S4). See the following review for more information on N_2 purging in ADMET: Schwendeman, J. E.; Church, A. C.; Wagener, K. B., Synthesis and Catalyst Issues Associated with ADMET Polymerization. Adv. Synth. Catal. 2002, 344, 597–613.

129. Vestenamer. https://www.vestenamer.com/en (accessed: April 13, 2023).

130. Abe, Y.; Gunji, T. Oligo- and polysiloxanes. *Prog. Polym. Sci.* **2004**, *29*, 149–182.

131. Husted, K. E. L.; Brown, C. M.; Shieh, P.; Kevlishvili, I.; Kristufek, S. L.; Zafar, H.; Accardo, J. V.; Cooper, J. C.; Klausen, R. S.; Kulik, H. J.; Moore, J. S.; Sottos, N. R.; Kalow, J. A.; Johnson, J. A. Remolding and Deconstruction of

Industrial Thermosets via Carboxylic Acid-Catalyzed Bifunctional Silyl Ether Exchange. *J. Am. Chem. Soc.* **2023**, *145*, 1916–1923.

132. Boz, E.; Wagener, K. B.; Ghosal, A.; Fu, R.; Alamo, R. G. Synthesis and Crystallization of Precision ADMET Polyolefins Containing Halogens. *Macromolecules* **2006**, *39*, 4437–4447.

133. Navarro, R.; Perrino, M. P.; García, C.; Elvira, C.; Gallardo, A.; Reinecke, H. Opening New Gates for the Modification of PVC or Other PVC Derivatives: Synthetic Strategies for the Covalent Binding of Molecules to PVC. *Polymers* **2016**, *8*, 152.

134. Moulay, S. Chemical modification of poly(vinyl chloride)—Still on the run. *Prog. Polym. Sci.* **2010**, *35*, 303–331.

135. Blanco, C. O.; Fogg, D. E. Water-Accelerated Decomposition of Olefin Metathesis Catalysts. *ACS Catalysis* **2023**, *13*, 1097–1102.

136. Esteruelas, M. A.; González, F.; Herrero, J.; Lucio, P.; Oliván, M.; Ruiz-Labrador, B. Thermal properties of polynorbornene (*cis-* and *trans-*) and hydrogenated polynorbornene. *Polym. Bull.* **2007**, *58*, 923–931.

137. Ban, H. T.; Kase, T.; Kawabe, M.; Miyazawa, A.; Ishihara, T.; Hagihara, H.; Tsunogae, Y.; Murata, M.; Shiono, T. A New Approach to Styrenic Thermoplastic Elastomers: Synthesis and Characterization of Crystalline Styrene−Butadiene−Styrene Triblock Copolymers. *Macromolecules* **2006**, *39*, 171–176.

138. Auras, R.; Harte, B.; Selke, S. An Overview of Polylactides as Packaging Materials. *Macromol. Biosci.* **2004**, *4*, 835–864.

139. Pitet, L. M.; Hillmyer, M. A. Combining Ring-Opening Metathesis Polymerization and Cyclic Ester Ring-Opening Polymerization To Form ABA Triblock Copolymers from 1,5-Cyclooctadiene and d,l-Lactide. *Macromolecules* **2009**, *42*, 3674–3680.

140. Schwendeman, J. E.; Wagener, K. B. Synthesis of Amorphous Hydrophobic Telechelic Hydrocarbon Diols via ADMET Polymerization. *Macromol. Chem. Phys.* **2009**, *210*, 1818–1833.

141. Oliver, W. C.; Pharr, G. M. An improved technique for determining hardness and elastic modulus using load and displacement sensing indentation experiments. *J. Mater. Res.* **1992**, *7*, 1564–1583.

142. Poth, D.; Wollenberg, K. C.; Vences, M.; Schulz, S. Volatile Amphibian Pheromones: Macrolides from Mantellid Frogs from Madagascar. *Angew. Chem. Int. Ed.* **2012**, *51*, 2187–2190.

143. Boz, E.; Nemeth, A. J.; Ghiviriga, I.; Jeon, K.; Alamo, R. G.; Wagener, K. B. Precision Ethylene/Vinyl Chloride Polymers via Condensation Polymerization. *Macromolecules* **2007**, *40*, 6545–6551.

144. Boz, E.; Nemeth, A. J.; Alamo, R. G.; Wagener, K. B. Precision Ethylene/Vinyl Bromide Polymers. *Adv. Synth. Catal.* **2007**, *349*, 137–141.

145. Valenti, D. J.; Wagener, K. B. Direct Synthesis of Well-Defined Alcohol-Functionalized Polymers via Acyclic Diene Metathesis (ADMET) Polymerization. *Macromolecules* **1998**, *31*, 2764–2773.

146. Flook, M. M.; Jiang, A. J.; Schrock, R. R.; Müller, P.; Hoveyda, A. H. Z-Selective Olefin Metathesis Processes Catalyzed by a Molybdenum Hexaisopropylterphenoxide Monopyrrolide Complex. *J. Am. Chem. Soc.* **2009**, *131*, 7962–7963.